

HABILITATION PARIS VI

Michel CAFFAREL

Laboratoire de Chimie Théorique, UMR 7616
Université Pierre et Marie Curie, Paris.

Titre: “Méthodes Monte Carlo quantique en Chimie Théorique
et simulations numériques pour les fermions fortement corrélés”

Octobre 2000

SOMMAIRE

I	Présentation du document	5
II	Synthèse de mes travaux	7
A	Rappel de mes travaux de thèse	7
B	Depuis la thèse	9
1	Propriétés dynamiques	9
2	Forces intermoléculaires	10
3	Problème du signe pour les fermions	11
4	Spectres ro-vibrationnels	12
5	Propriétés des noeuds des fonctions d'onde	13
6	Meilleures fonctions d'onde d'essai	13
7	Méthode de reconfiguration stochastique	14
8	Principe de zéro-variance généralisé	15
9	Etude des modèles effectifs de la physique du solide	18
10	Modèle de Hubbard en dimension infinie	19
11	Modèle de paires unidimensionnel.	19
12	Modèle de Hubbard sur les hypercubes. Quelques résultats exacts.	20
13	Modèle de Hubbard $SU(N)$ unidimensionnel.	21
14	Modèle de Hubbard bosonique à deux dimensions	23
15	Systèmes de spin classiques	23
III	Encadrement d'étudiants	27
A	Thèses de doctorat	27
B	Stages de DEA	27
C	Stages de maîtrise	28
IV	Liste des publications	29
V	Méthodes Monte Carlo quantique en chimie théorique	33
A	Les méthodes Monte Carlo quantique en quelques mots	33
1	Méthodes Monte Carlo variationnelles	33
2	Méthodes Monte Carlo exactes	36
3	Contraintes associées au principe de Pauli: le problème du signe	38
B	Monte Carlo quantique en chimie théorique: où en est-on?	40
1	Problème du signe.	40

2	Choix de la fonction d'essai	42
3	Problème des électrons de cœur.	43
VI	Perspectives. Mon projet de recherche	49
VII	Papiers principaux	53
A	M. Caffarel and P. Claverie, "Development of a pure diffusion quantum Monte Carlo method using a full generalized Feynman-Kac formula. I. Formalism", J. Chem. Phys. 88 , 1088 (1988)	53
B	M. Caffarel and P. Claverie, "Development of a pure diffusion quantum Monte Carlo method using a full generalized Feynman-Kac formula. II. Application to simple systems", J. Chem. Phys. 88 , 1100 (1988)	65
C	M. Caffarel, P. Claverie, C. Mijoule, J. Andzelm, and D.R. Salahub, "Quantum Monte Carlo method for some model and realistic coupled anharmonic oscillators", J. Chem. Phys. 90 , 990 (1989)	77
D	O. Hess, M. Caffarel, C. Huiszoon, and P. Claverie, "Second-order exchange effects in intermolecular interactions. The water dimer", J. Chem. Phys. 92 , 6049 (1990)	93
E	M. Caffarel and O. Hess, "Quantum Monte Carlo-Perturbation Calculations of Interaction Energies", Phys. Rev. A 43 , 2139 (1991)	107
F	M. Caffarel, F.X. Gadea, and D.M. Ceperley, "Lanczos-type Algorithm for Quantum Monte Carlo Data", Europhys. Lett. 16 249 (1991)	123
G	W. Krauth, M. Caffarel and J.P. Bouchaud, "Gutzwiller Wave Function for a Model of Strongly Interacting Bosons", Phys. Rev B 45 , 3137 (1992)	131
H	M. Caffarel, X. Krokidis, and C. Mijoule, "On the Nonconservation of the Number of Nodel Cells of Eigenfunctions", Europhys. Lett. 20 , 581 (1992)	137
I	M. Caffarel and D.M. Ceperley, "A Bayesian Analysis of Green's Function Monte Carlo Correlation Functions", J. Chem. Phys. 97 , 8415 (1992) . . .	147
J	M. Caffarel, M. Rérat, and C. Pouchan, "Evaluating Dynamic Multipole Polarizabilities and van Der Waals Dispersion Coefficients of two-electron Systems with a Quantum Monte Carlo Calculation: A Comparison with some <i>Ab Initio</i> Calculations", Phys. Rev. A 47 , 3704 (1993)	159
K	M. Rérat, M. Caffarel, and C. Pouchan, "Dynamic Polarizabilities and van der Waals Coefficients of the 2^1S and 2^3S Metastable States of Helium", Phys. Rev A 48 , 161 (1993)	175

L	M. Caffarel and W. Krauth, “Exact Diagonalization Approach to Correlated Fermions in Infinite Dimensions: Mott Transition and Superconductivity”, <i>Phys. Rev. Lett.</i> 72 , 1545 (1994)	183
M	M. Caffarel, P. Azaria, B. Delamotte, and D. Mouhanna, “Monte Carlo Calculation of the Spin-stiffness of the two-dimensional Heisenberg Model”, <i>Europhys. Lett.</i> 26 , 493 (1994)	189
N	J. Langlet, J. Caillet, and M. Caffarel, “A Perturbational Study of some Hydrogen-Bonded Dimers”, <i>J. Chem. Phys.</i> 103 , 8043 (1995)	197
O	C. Huiszoon and M. Caffarel, “A quantum Monte Carlo perturbational study of the He-He interaction”, <i>J. Chem. Phys.</i> 104 , 4621 (1996)	215
P	M. van den Bossche and M. Caffarel, “One-dimensional pair-hopping and attractive Hubbard models: A comparative study”, <i>Phys. Rev. B</i> 54 , 17414 (1996)	229
Q	M. Caffarel and R. Mosseri, “Hubbard model on d-dimensional hypercubes: Exact solution for the two-electron case”, <i>Phys. Rev. B</i> , 12651 (1998)	239
R	R. Assaraf, P. Azaria, M. Caffarel, and P. Lecheminant, “Metal-insulator transition in the one-dimensional SU(N) Hubbard model”, <i>Phys. Rev. B</i> 60 , 2299 (1999)	245
S	R. Assaraf and M. Caffarel, “Zero-variance principle for Monte Carlo algorithms”, <i>Phys. Rev. Lett.</i> 83 , 4682 (1999)	267
T	R. Assaraf, M. Caffarel, and A. Khelif, “Diffusion Monte Carlo Methods with a fixed-number of walkers”, <i>Phys. Rev. E.</i> 61 4566 (2000)	273
U	R. Assaraf and M. Caffarel “Computing forces with quantum Monte Carlo” <i>J. Chem. Phys.</i> 113 4028 (2000)	285

I. PRÉSENTATION DU DOCUMENT

Ce document est organisé de la manière suivante. Dans une première partie (Section II) je présente la synthèse de mes travaux. Dans le cadre de cette habilitation, j'insiste plus particulièrement sur les travaux effectués après ma thèse. J'ai été amené à diriger ou à co-diriger un certain nombre d'étudiants en maîtrise, DEA ou thèse. J'en donne la liste dans la Section III. La liste complète de mes travaux publiés se trouve dans la Section IV. Comme je le soulignerai dans mon projet de recherche les méthodes Monte Carlo quantique (MCQ) appliquées à l'étude de la structure électronique des molécules sont à un moment important de leur développement: elles deviennent en effet compétitives vis à vis des méthodes *ab initio* plus traditionnelles [Density Functional Theory (DFT) et/ou méthodes Hartree-Fock + traitement de la corrélation électronique]. Afin d'illustrer ce point important je consacre la Section V à une discussion des "Méthodes Monte Carlo quantique en Chimie Théorique". J'y présente les méthodes MCQ en quelques mots, je discute ensuite les difficultés théoriques et pratiques, et je donne enfin l'"Etat de l'Art" concernant les applications. Dans la dernière partie (Section VI), je présente mon projet de recherche. Enfin, pour faciliter l'accès à mes résultats principaux je fournis en fin de document (Section VII) une copie de mes papiers les plus significatifs.

II. SYNTHÈSE DE MES TRAVAUX

L'essentiel de mon activité de recherche porte sur le développement et l'application de méthodes nouvelles pour la résolution de l'équation de Schrödinger (problème à N-corps quantique). Les problèmes que j'ai abordés sont les suivants. Etude de la structure électronique des atomes et des molécules: calcul des énergies totales, des énergies de liaison, des observables autres que l'énergie (moments dipolaires, valeurs moyennes diverses), des propriétés dynamiques (polarisabilités multipolaires, coefficients de van der Waals, etc.); détermination des forces intermoléculaires; calcul des spectres ro-vibrationnels (énergies de point-zéro, excitations fondamentales), et, finalement, étude des propriétés électroniques ou magnétiques des systèmes étendus modélisés par des Hamiltoniens effectifs (modèle de Hubbard, modèle de Heisenberg, etc.).

Le point fort de mon activité concerne les approches stochastiques connues sous le nom de méthodes Monte Carlo quantique (quantum Monte Carlo, QMC). Cependant, j'ai également utilisé et développé la plupart des méthodes usuelles pour le traitement du problème à N-corps quantique. En Chimie Théorique, il s'agit principalement des méthodes dites *ab initio* que j'ai utilisées pour le calcul des forces intermoléculaires par méthode de perturbation à symétrie forcée (Symmetry Adapted Perturbation Theory, SAPT). En matière condensée, j'ai eu recours aux méthodes dites de Diagonalisation Exacte (méthode de Lanczos), aux méthodes du groupe de renormalisation basée sur la matrice-densité (DMRG), aux méthodes Monte Carlo quantique à température finie (Path Integral Monte Carlo), et aux méthodes Monte Carlo classiques -algorithmes locaux et non-locaux- pour les systèmes de spins. Enfin, chaque fois que cela est possible, j'essaie d'analyser les résultats numériques à l'aide de solutions exactes connues ou construites pour l'occasion (système d'oscillateurs exactement intégrable, systèmes à faible nombre d'électrons, *ansatz* de Bethe) ou de modèles effectifs à fort pouvoir prédictif: méthodes du groupe de renormalisation perturbatif ou bosonisation pour les systèmes d'électrons à une dimension.

A. Rappel de mes travaux de thèse

Réf: Voir papiers A et B en Annexe.

Dans un premier temps il me semble utile de rappeler brièvement le point essentiel de ma thèse. Pendant cette période nous avons développé une approche originale de résolution de l'équation de Schrödinger par méthode stochastique. Au centre de cette approche est

l'expression de la solution de l'équation de Schrödinger sous la forme d'une intégrale fonctionnelle à la Feynman (intégrale de chemin). Plus précisément, nous avons généralisé la formule de Feynman-Kac (FK) définie sur un processus stochastique Gaussien (diffusion libre) à une nouvelle formule basée sur un processus non-Gaussien définie à partir d'une fonction d'onde d'essai pour l'état fondamental. Dans cette dernière formule, l'intégrand usuel $e^{-\int V}$, où V est le potentiel total et où l'intégrale est prise le long d'un chemin, est remplacé par un nouvel intégrand "écrané" de la forme $e^{-\int E_L}$ où E_L est un potentiel construit à partir de la fonction d'essai, $E_L = H\psi_T/\psi_T$ (le potentiel V correspond au cas particulier, $\psi_T = 1$). En effectuant ce changement de mesure fonctionnelle, les trajectoires browniennes libres de la formule de FK sont remplacées par des trajectoires browniennes dans un champ de dérive extérieur dépendant de la fonction d'essai (terme dit de dérive). Grâce à cette formule généralisée des simulations numériques précises sont possibles. En effet, si ψ_T est choisie suffisamment "proche" de la solution exacte, les fluctuations de l'intégrand, $e^{-\int E_L}$, le long des trajectoires browniennes peuvent être rendues suffisamment faibles pour permettre la convergence du calcul numérique de l'intégrale fonctionnelle dans un temps réaliste. Pendant ma thèse j'ai illustré sur des exemples simple la faisabilité pratique d'une telle approche (He, H₂, systèmes d'oscillateurs 1D très simples). Il est important de noter que dans un contexte plus général une telle méthode doit être vue comme une variante des méthodes dites méthodes Monte Carlo quantique (quantum Monte Carlo, QMC). Sans entrer dans les détails (pour cela voir partie V) la méthode QMC la plus répandue est la méthode dite Diffusion Monte Carlo, DMC. Développée d'une manière indépendante de notre approche, elle contient en fait les mêmes ingrédients: utilisation d'une fonction d'essai ψ_T , définition d'un mouvement brownien avec terme de dérive, définition du même potentiel écrané $H\psi_T/\psi_T$, appelé "énergie locale", et calcul de valeurs moyennes statistiques. La seule différence importante réside dans le traitement de l'intégrand de Feynman-Kac. Dans notre approche, il s'agit d'un poids "porté" le long des trajectoires. Dans les approches dites DMC ce terme est traité par l'intermédiaire d'un processus de mort-naissance (terme dit de "branching") simulé à l'aide de règles de création/disparition appliquées à une population assez grande de répliques du système. A chaque pas Monte Carlo chaque configuration est supprimée ou dupliquée un certain nombre de fois proportionnel en moyenne à l'amplitude du poids de FK local. On peut montrer que les valeurs moyennes obtenues sont essentiellement les mêmes. Notre approche, qui n'introduit pas de processus de branching, est connue sous le nom de méthode "Pure Diffusion Monte Carlo", PDMC. Notons que, contrairement à la méthode DMC, la méthode PDMC est parfaitement bien définie mathématiquement (le processus avec branchement ne conserve pas la probabilité totale et ceci pose un cer-

tain nombre de difficultés théoriques). Cette propriété nous a permis de généraliser assez facilement la méthode PDMC à des situations variées (voir plus loin). Contrairement aux méthodes avec branchement, le nombre de marcheurs utilisé est constant (à la limite on peut n'utiliser qu'un seul marcheur) et aucun biais associé au contrôle de population n'existe. Malheureusement, la méthode PDMC n'est pas parfaite. A grands temps de projection [temps imaginaire t qui permet d'extraire les quantités exactes grâce à l'opérateur e^{-tH}] les fluctuations statistiques peuvent croître de manière incontrôlée. Toutefois, si l'on dispose d'une fonction d'essai d'une qualité suffisante on peut montrer que ce problème ne pose pas de difficultés pratiques (la convergence en temps est atteinte très vite) et la méthode PDMC apparaît comme la méthode de choix (pas de biais systématique et contrôle des fluctuations statistiques). De nombreuses applications ont été menées au laboratoire et par d'autres groupes dans le monde en utilisant cette approche. Néanmoins, quand la fonction d'onde n'est pas de qualité suffisante les fluctuations statistiques croissent trop vite et la méthode PDMC devient inefficace. Cette difficulté est particulièrement présente dans les simulations des modèles de la matière condensée. En effet, il est très difficile de construire des fonctions d'essai de qualité constante lorsque la taille du système étudié augmente (problème de consistance en taille, "size-consistency"). Il est alors impératif d'avoir recours aux méthodes DMC avec branchement qui, elles, demeurent stables mais sont biaisées.

B. Depuis la thèse

Après ce rappel concernant mon travail de thèse je résume mes différentes contributions depuis cette époque.

1. Propriétés dynamiques

Réf: Voir papiers E, J et O en Annexe.

Comme je viens de le mentionner dans la partie précédente, la méthode PDMC est d'une grande souplesse mathématique. Ceci nous a permis de l'étendre facilement au calcul de propriétés autres que l'énergie. Notre contribution essentielle dans cette direction a été le calcul des propriétés dynamiques. Nous avons montré comment il était possible d'écrire les termes de perturbation Rayleigh-Schrödinger à un ordre quelconque, sous la forme de fonctions de corrélations à N -point (cumulants) du processus stochastique sous-jacent (variante stochastique du fameux "linked-cluster theorem", [1], [2]). Ce formalisme a été appliqué au

problème du calcul des polarisabilités atomiques et moléculaires et des coefficients de van der Waals [1], [2], [3], [4]. Ces quantités, dont la connaissance est importante dans de nombreuses applications en optique et en matière condensée, sont difficiles à évaluer avec les méthodes traditionnelles. Par exemple, dans le cadre de notre formalisme, les polarisabilités dipolaires peuvent se réécrire sous la forme d’une intégrale temporelle de la fonction de corrélation à deux points de l’opérateur dipolaire le long des trajectoires browniennes. Contrairement aux méthodes traditionnelles de la physique moléculaire qui reposent sur une évaluation explicite du terme de perturbation du second-ordre correspondant, notre méthode ne fait intervenir aucune représentation des états excités ou du continuum. C’est évidemment un point très intéressant. Nous avons effectué des calculs systématiques pour l’atome d’Hélium et la molécule d’hydrogène (polarisabilités multipolaires statiques et dynamiques). Nous avons également évalué les coefficients de van der Waals régissant l’interaction des différentes espèces à longues distances. Nos résultats, qui ont été comparés aux meilleurs résultats de la littérature, sont excellents. Pour des quantités comme les polarisabilités multipolaires dynamiques (dépendant de la fréquence du champ extérieur), certains de nos résultats sont les seuls disponibles. Nous avons également appliqué ces idées au problème du calcul des forces intermoléculaires par méthode de perturbation. Ce travail est présenté dans la partie suivante consacrée aux forces intermoléculaires. Malheureusement, l’extension de ces résultats à des systèmes à grand nombre d’électrons n’est pas facile, à cause du fameux “problème du signe” inhérent aux simulations Monte Carlo quantique pour les fermions (voir la sous-section 3: “Problème du signe pour les fermions”).

2. Forces intermoléculaires

Réf: Voir papiers D,E,N en Annexe

Une connaissance précise des forces intermoléculaires est essentielle pour les simulations de la matière condensée. Deux classes de méthode sont employées pour déterminer les champs de force: les méthodes supermoléculaires qui calculent l’interaction comme différence des énergies totales des espèces en interaction et les méthodes perturbatives qui décomposent l’énergie d’interaction sous la forme d’une série de termes de perturbation dans le potentiel intermoléculaire (formalisme SAPT, Symmetry-Adapted Perturbation Theory). Les défauts et les avantages des deux méthodes sont bien connus. J’ai essentiellement travaillé sur la seconde approche qui a un contenu plus physique car l’énergie d’interaction est effectivement petite et un calcul de perturbation est naturel. De plus, cette méthode permet de construire

de manière cohérente des représentations simplifiées de qualité pour le champs de force [5]. Dans un calcul SAPT l'énergie d'interaction est décomposée en une somme de contributions qui, à leur tour, sont décomposées en une composante champ moyen (Hartree-Fock) et une composante résiduelle due à la corrélation électronique intramonomère. En pratique, les calculs sont généralement limités au premier ordre complet (électrostatique et contribution d'échange du premier ordre) et au deuxième ordre Rayleigh-Schrödinger (termes d'induction et de dispersion), les contributions étant calculées au niveau Hartree-Fock. Nous avons développé une méthode originale pour évaluer les termes d'échange du second-ordre dans le cadre des méthodes *ab initio* sur base au niveau Hartree-Fock [6]. En accord avec d'autres groupes nous avons trouvé que ces contributions sont loin d'être négligeables. Des calculs ont été effectués pour plusieurs dimères par liaison hydrogène fortement ou faiblement liés [7]. Des comparaisons systématiques avec la méthode supermoléculaire et la méthode mixte (calcul supermoléculaire Hartree-Fock + énergie de dispersion calculée par perturbation) ont été effectuées. Afin d'avoir une description complète de l'interaction, il est nécessaire d'évaluer l'effet de la corrélation électronique intramonomère sur les composantes de perturbation, ainsi que l'importance des composantes d'ordre supérieur à deux. En utilisant le formalisme Monte Carlo quantique présenté précédemment (voir sous-section 4: "Propriétés dynamiques") nous avons pu évaluer pour la première fois ces contributions dans le cas de l'interaction He-He [4]. Les résultats ont mis en valeur le rôle important joué par la corrélation intra-atomique et le troisième ordre de perturbation. Nous avons montré que, dans la région d'équilibre, le développement de l'énergie d'interaction limité au troisième ordre est suffisant pour représenter correctement l'interaction. Au-delà de l'application particulière à l'interaction He-He, cette étude met en lumière dans un système non-trivial le rôle respectif de chacune des contributions intervenant dans une liaison de type van der Waals. C'est évidemment un point très important pour la compréhension générale des liaisons de ce type.

3. Problème du signe pour les fermions

Réf: Voir papiers F,I en Annexe

Nous avons proposé deux méthodes pour atténuer le fameux "problème du signe" pour les fermions (pour une présentation de ce problème, voir la section "Méthodes Monte Carlo quantiques en quelques mots" de la partie V).

Première tentative: Accélération de la convergence des estimateurs en fonction du "temps

de projection” [8]. Dans ce travail nous avons adapté l’algorithme de Lanczòs à nos données Monte Carlo. Il en résulte une convergence bien plus rapide de l’estimateur de l’énergie (et des autres estimateurs). Nous avons appliqué cette approche au cas de la molécule LiH. Malheureusement, nous nous sommes rendus compte que la méthode n’était bien conditionnée que si le bruit statistique sur les éléments de matrice calculés était suffisamment petit. L’augmentation exponentielle de l’erreur statistique pour les fermions est trop brutale pour que cette méthode soit vraiment efficace pour les systèmes de taille importante (notons cependant que cette méthode est maintenant utilisée par plusieurs groupes dans le contexte des simulations des modèles effectifs de la matière condensée théorique)

Deuxième tentative: Application de la méthode du maximum de l’entropie aux données Monte Carlo quantiques [9]. Cette approche permet en principe un contrôle rationnel (à partir de principes généraux de statistique, approche dite “Bayésienne”) de l’effet du bruit statistique sur les données pures. Son application à la molécule LiH (à la distance d’équilibre) nous a permis de calculer une des valeurs les plus précises de la littérature pour l’énergie totale de cette molécule. Une fois encore, le caractère exponentiellement croissant de l’erreur statistique pour les fermions limite les possibilités pratiques de cette approche pour les systèmes plus gros.

4. Spectres ro-vibrationnels

Réf: Voir papier C en Annexe

Il est important de rappeler que les méthodes Monte Carlo quantiques peuvent être appliquées à tout problème décrit par une équation de type Schrödinger. Nous avons ainsi appliqué notre méthode générale de résolution de l’équation de Schrödinger au problème de la détermination du spectre ro-vibrationnel des molécules [10]. Pour cela nous avons généralisé notre formalisme au calcul des excitations fondamentales d’un système de vibrateurs anharmoniques couplés de manière quelconque (aucune approximation, régime non perturbatif). Nous nous sommes concentrés sur les excitations fondamentales qui sont les excitations les plus intenses dans l’infrarouge, et qui sont celles que mesurent les expérimentateurs. Afin de déterminer ces excitations nous avons introduit un *ansatz* pour leurs hypersurfaces nodales. Nous avons illustré le fait remarquable que cet *ansatz* semble donner essentiellement la solution exacte pour des problèmes réalistes. Nous avons appliqué cette approche à des systèmes modèles et à des systèmes d’intérêt physique (molécule CO adsorbée sur une surface de Palladium). A l’occasion de ce travail nous avons découvert un certain nombre de propriétés

topologiques des régions nodales des fonctions d’onde (voir sous-section suivante).

5. Propriétés des noeuds des fonctions d’onde

Réf: Voir papier H en Annexe

Dans ce travail nous avons voulu comprendre la validité de l’ansatz que nous avons proposé pour les hypersurfaces nodales des fonctions d’onde des excitations fondamentales d’un ensemble d’oscillateurs couplés arbitrairement [11]. Notre hypothèse de travail est que le nombre de sous-volumes nodaux est toujours égal à deux pour ces états excités particuliers. Nous avons donné un ensemble d’arguments généraux qui semblent montrer que ceci est vrai dans le cas où les oscillateurs peuvent être découplés à l’aide d’un seul paramètre, ce qui est généralement possible avec des oscillateurs réalistes. Dans le cas d’oscillateurs plus généraux, nous avons pu construire explicitement un contre-exemple ne vérifiant pas notre hypothèse. Ce contre-exemple est non trivial et n’a pu être obtenu qu’en ayant recours à un programme de calcul symbolique (MAPLE). Le problème général des conditions précises de validité de notre ansatz reste encore ouvert.

6. Meilleures fonctions d’onde d’essai

De nombreux efforts ont été produits pour développer des fonctions d’onde d’essai de qualité. Les fonctions d’onde utilisées sont essentiellement monoconfigurationnelles. Nous avons effectué une étude portant sur l’utilisation de fonctions d’onde multiconfigurationnelles dans l’approche dite des noeuds-fixés (fonctions d’onde issues du programme MOLPRO). Les résultats obtenus sont bons, mais un peu décevants. En effet, de cette étude ne ressort pas un critère bien défini qui nous permettrait de sélectionner efficacement les configurations à retenir dans la simulation (nos résultats sont présentés dans la publication [12]). Je pense que des formes beaucoup plus physiques pour ces fonctions peuvent encore être exploitées. Une première contribution dans ce sens a été effectuée lors d’un travail exploratoire que j’ai mené avec une étudiante de deuxième cycle (Séverine Zirah), [13]. Nous avons étudié les résultats obtenus avec des formes issues de calculs de type valence-bond (VB) pour des petites molécules (LiH et Li₂). Les fonctions VB sont très attrayantes. Elles ont l’avantage d’être à la fois compactes et très physiques (description des structures de Lewis). Elles permettent une “lecture” simple des processus en jeu. Notons, en passant, que contrairement aux approches sur base, la non-orthogonalité des orbitales ne pose pas

de problèmes techniques particuliers pour les méthodes Monte Carlo. Afin de bien décrire chacune des composantes de la fonction VB (structures neutres et ioniques) et de bien séparer les différents effets, nous avons introduit un terme de Jastrow différent pour chacune d’elles. Nos résultats sont intéressants : après optimisation des paramètres il est possible de “lire” sur les paramètres associés à la corrélation électronique dynamique les différents types de réorganisation électronique qui ont lieu pour chacune des contributions physiques. Malheureusement, avec ces formes VB les fluctuations statistiques restent encore trop importantes (les structures VB contiennent la bonne information globale, mais pas les détails). Je crois que ce type de fonction d’onde mérite d’être réexaminé dans un formalisme où les fluctuations statistiques inessentiels de haute énergie (électrons de coeur) sont évacuées par d’autres moyens (utilisation de pseudo-potentiels ou, mieux, du principe de zéro-variance discuté dans la sous-section 8: “Principe de zéro-variance généralisé”).

7. Méthode de reconfiguration stochastique

Réf: Voir papier T en Annexe

Comme je l’ai expliqué précédemment (Sous-section II.A), la méthode PDMC est une méthode très générale et d’une très grande souplesse. Malheureusement, à grands temps de projection [temps imaginaire t qui permet d’extraire les quantités exactes grâce à l’opérateur e^{-tH}] les fluctuations statistiques peuvent croître de manière incontrôlée. En collaboration avec Anatole Khelif, mathématicien à Paris VII, nous avons regardé en détail les fondements mathématiques des algorithmes QMC de type Diffusion Monte Carlo, avec et sans branchement [14]. Dans un premier temps, nous avons étudié le comportement à grands temps de projection de la méthode PDMC. Nous avons montré rigoureusement que la “probabilité effective” associée à un état, telle qu’elle est construite par la méthode PDMC, ne converge pas vers une valeur déterministe quand le temps de projection tend vers l’infini. Notre analyse mathématique conclut donc à ce qu’on a appelé la “divergence du PDMC”. Notons que ce mauvais comportement à grands temps est une chose connue dans la communauté, souvent sous le vocable “explosion de la variance”, mais aucune preuve rigoureuse n’en avait été donnée. Insistons sur le fait que malgré cette difficulté, et comme nous l’avons déjà dit, la méthode reste malgré tout une méthode précieuse lorsque des fonctions d’onde de qualité suffisante sont disponibles (en particulier, ceci est le cas pour les molécules). Après ce premier résultat nous avons essayé de construire un algorithme Diffusion Monte Carlo qui concilie les avantages des méthodes avec et sans branchement, c’est à dire qui soit sta-

ble, comme l’approche DMC, et non-biaisé, comme l’approche PDMC. Nous avons montré que c’était possible et nous avons élaboré une méthode mixte qui emprunte des éléments aux deux approches. En quelques mots, la méthode consiste à effectuer un calcul de type PDMC, non pas avec un seul marcheur ayant un poids individuel w_i (poids de Feynman-Kac), mais avec une population de M marcheurs ayant un poids total donné par la moyenne des poids individuels. Comme les fluctuations du poids total sont beaucoup plus faibles que les fluctuations des poids élémentaires (méthode PDMC standard) le temps de projection à partir duquel le mauvais conditionnement de la méthode apparaît, est rejeté à des temps beaucoup plus grands. Afin de récupérer le résultat exact on montre qu’un terme supplémentaire analogue au terme de branchement doit être introduit. C’est l’étape dite de reconfiguration stochastique de la population de marcheurs. Aux étapes usuelles de diffusion et de dérive des M marcheurs, on rajoute une étape supplémentaire consistant à choisir M nouveaux marcheurs parmi les M marcheurs constituant la population courante avec une probabilité donnée par $p_i = w_i / \sum_{j=1}^M w_j$ (certains marcheurs sont donc choisis plusieurs fois, d’autres ne sont pas choisis). Utilisant ces deux ingrédients fondamentaux (PDMC pour une *population* de marcheurs, reconfiguration de la population) nous avons proposé une méthode optimale qui minimise les fluctuations statistiques (méthode DMC dite avec reconfiguration stochastique optimale). Cette méthode optimale est construite de manière à ce que l’algorithme tende à la fois vers la méthode DMC et la méthode PDMC, quand le nombre de marcheurs tend vers l’infini et/ou les poids individuels deviennent constants. Il est important de souligner que la méthode de reconfiguration n’est en fait pas nouvelle. L’idée fondamentale a été proposée il y a plus d’une quinzaine d’années par Hetherington [15] et semble avoir été oubliée. Très récemment (en 1998) Sorella et collaborateurs l’ont réintroduite et appliquée à quelques problèmes de la matière condensée. Pour notre part, nous avons développé notre algorithme indépendamment. Notons cependant que, comme nous l’avons montré, notre algorithme est plus général et plus efficace, il constitue une version optimale des approches de type reconfiguration stochastique.

8. Principe de zéro-variance généralisé

Réf: voir papiers S,U en Annexe

Les méthodes Monte Carlo quantique présentent une propriété dite de variance-zéro pour l’énergie. Disposant d’une fonction d’onde d’essai approchée, notée ψ_T , l’énergie est évaluée comme valeur moyenne d’une quantité appelée “énergie locale” sous la forme

$$\langle E \rangle = \frac{1}{N} \sum_{i=1}^N E_L[x^{(i)}] \quad (1)$$

où l'énergie locale est donnée par:

$$E_L \equiv H\psi_T/\psi_T \quad (2)$$

et $\{x^{(i)}\}_{i=1,N}$ représente un ensemble de N tirages Monte Carlo de configurations du système avec une distribution qui peut différer d'une méthode QMC à l'autre (pour une présentation plus détaillée se reporter à la section V.A "Méthodes Monte Carlo quantiques en quelques mots"). Le point important est que les fluctuations statistiques sur l'estimateur de l'énergie [formule (1)] dépendent directement des fluctuations de l'énergie locale, Eq.(2). Pour un nombre de pas MC fixé N (et donc un effort numérique donné) plus la fonction d'onde d'essai est "proche" de la fonction d'onde exacte inconnue plus les fluctuations statistiques (et donc l'erreur finale sur notre estimateur) sont faibles. A la limite d'une fonction d'essai exacte l'estimateur ne fluctue plus du tout. Cette propriété est la propriété dite de variance-zéro. Elle joue un rôle fondamental pour calculer avec précision les énergies totales de systèmes complexes.

Dans ce travail nous avons étendu la propriété de variance-zéro à n'importe quelle observable physique du système. Soit O une observable quelconque, on a montré qu'il est toujours possible de construire une observable \tilde{O} dite "renormalisée" qui possède la même valeur moyenne:

$$\langle O \rangle = \langle \tilde{O} \rangle \quad (3)$$

mais dont les fluctuations peuvent être beaucoup plus faibles que celles de O [16]. L'observable renormalisée peut être construite assez simplement. Elle dépend essentiellement d'une fonction que l'on a appelée "fonction auxiliaire". On a montré qu'il existe une équation qui détermine complètement cette fonction. La solution exacte correspond à une annulation totale des fluctuations (principe de zéro-variance généralisé).

Il est important de souligner que notre principe de zéro-variance est en fait très général et s'applique à tout type d'algorithme Monte Carlo. La seule condition requise est l'existence d'une densité stationnaire connue. Nous avons appliqué cette idée à quelques calculs Monte Carlo classiques (algorithme de Metropolis standard pour le modèle d'Ising) et quantiques (méthode DMC pour l'atome Hélium) Nous avons montré sur ces exemples simples qu'il est possible de gagner un à plusieurs ordres de grandeur en temps de calcul.

La première application réaliste, c'est à dire pour un problème réellement difficile, a concerné le calcul des forces par méthode Monte Carlo quantique. Un des objectifs centraux

de la chimie théorique est la prédiction des structures spatiales des édifices moléculaires (géométrie d'équilibre correspondant à l'annulation des forces) et à la structure des forces internes entre atomes en fonction de la géométrie (calcul des modes propres, dynamique des noyaux, etc.). Toute méthode de calcul électronique se doit donc d'être capable d'évaluer avec précision non seulement les énergies totales et les propriétés élémentaires (distribution des charges, moments multipolaires, etc.) mais aussi les forces entre atomes au sein d'une molécule. Jusqu'à ce jour, et malgré des efforts importants, le calcul des forces par méthode Monte Carlo quantique est resté un problème très difficile. Notons que très récemment, Filippi et Umrigar ont proposé un formalisme QMC pour les forces, qui semble donner pour la première fois des résultats stables pour quelques molécules diatomiques [17]. Néanmoins, leur formalisme -basé sur un principe d'échantillonnage corrélé et une transformation spéciale de coordonnées- ne permet pas de converger vers le résultat exact et il n'est pas encore très clair comment contrôler cette erreur. En utilisant le principe de variance-zéro il est possible de proposer une méthode simple et très stable de calcul des forces. Plus précisément, grâce à la fonction auxiliaire liée au principe de variance-zéro, il est possible de diminuer de manière drastique les fluctuations associées à la force locale ($\frac{\partial V}{\partial R}$). La diminution obtenue est très importante car la variance associée à la force nue est en fait infinie! (au voisinage d'une collision électron-noyau $f \sim 1/r^2$ où r est la distance entre particules et $\langle f^2 \rangle = \infty$). Le principe de variance-zéro permet sans difficulté de ramener cette variance infinie à une quantité finie. La figure suivante présente l'amélioration spectaculaire obtenue pour le calcul de la force à la distance d'équilibre de la molécule C_2 [18]. En abscisse, j'ai porté une quantité proportionnelle au nombre total de pas Monte Carlo effectués (et donc à l'effort numérique). La courbe principale avec de grandes fluctuations correspond à un calcul standard avec la force nue (non-renormalisée). On observe une très mauvaise convergence en fonction du temps de simulation et, surtout, la présence de discontinuités importantes liées à l'apparition de configurations électroniques comprenant des rapprochements d'électrons et de noyaux (variance infinie). En pratique, il n'y a aucun espoir de faire converger un tel calcul. La deuxième courbe obtenue avec une expression renormalisée pour la force montre un comportement extrêmement satisfaisant. A l'échelle de la figure la courbe est en fait totalement convergée. Insistons sur le fait que les deux calculs sont faits de front et que le deuxième calcul convergé ne nécessite pas d'effort numérique supplémentaire par rapport au premier.

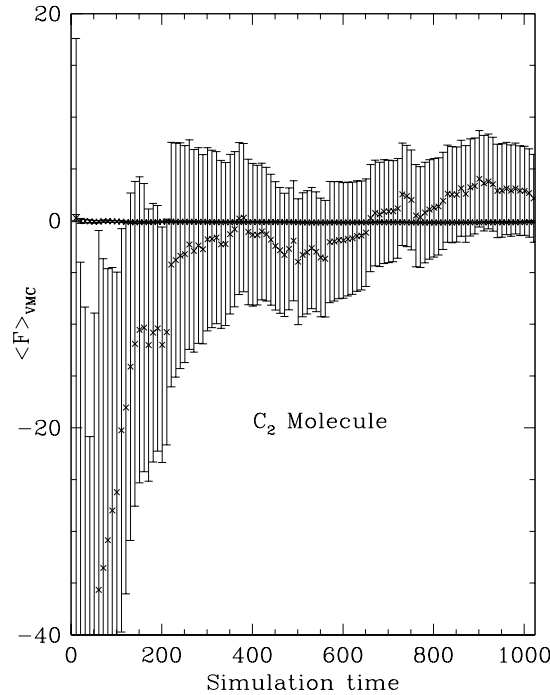


FIG. 1. Convergence en fonction du temps calcul (nombre N de pas Monte Carlo pour chaque marcheur) de l'estimateur de la force $F(R)$ à la distance d'équilibre pour la molécule C_2 . La courbe associées aux grandes variations correspond à l'utilisation d'un estimateur "nu" (non-renormalisé) de la force, la courbe convergée à un estimateur "renormalisé" (utilisation du principe de variance-zéro).

9. Etude des modèles effectifs de la physique du solide

Je me suis également intéressé aux propriétés des électrons dans les solides. De manière générale, il s'agit de déterminer la nature de l'état fondamental du système, l'existence ou non de transition de phase à température nulle, ainsi que les propriétés thermodynamiques. Nous nous intéressons plus particulièrement au régime dit de corrélation forte pour les électrons (répulsion coulombienne grande devant la largeur de bande), régime pertinent pour les nouveaux supraconducteurs à haute température critique. Les Hamiltoniens utilisés pour modéliser les systèmes considérés sont les Hamiltoniens effectifs de la physique du solide: modèle de Hubbard à une ou plusieurs bandes, modèles de spins de Heisenberg, etc. Au-delà de l'intérêt évident du problème en soi (comprendre le mécanisme à l'origine de la supraconductivité à haute température critique), il est important de souligner que le problème fondamental qui consiste en la détermination des propriétés de l'état fondamental d'un ensemble d'électrons dans un régime non-perturbatif, est tout à fait similaire à celui rencontré

pour les atomes et les molécules (problème à N-corps quantique). Il est donc important de développer et de confronter les techniques utilisées dans les deux domaines. Je présente maintenant plusieurs applications réalisées.

10. Modèle de Hubbard en dimension infinie

Réf: Voir papier L en Annexe

Dans ce travail nous nous sommes intéressés au modèle de Hubbard lorsque la dimension spatiale D tend vers l'infini [19], [20], [21]. Cette limite, qui peut paraître au premier abord assez académique, est en fait très féconde. En effet, elle permet de simplifier énormément le problème tout en conservant une partie de la richesse de comportements issue de la corrélation électronique. Notons que cette limite de dimension infinie est également utilisée en physique moléculaire depuis quelques années. Nous avons développé une méthode originale pour la résolution des équations du modèle de Hubbard en dimension infinie. Nous avons étudié la transition de Mott à demi-remplissage (transition métal-isolant due à la corrélation) et la possibilité d'apparition de la supraconductivité dans un modèle de Hubbard à deux bandes (par exemple, une bande d pour les atomes de cuivre et une bande p pour les oxygènes dans CuO). Notre méthode est maintenant utilisée couramment par différents groupes travaillant sur les modèles sur réseau en dimension infinie.

11. Modèle de paires unidimensionnel.

Réf: Voir papier P en Annexe

Il s'agit d'une seconde application portant sur un modèle d'électrons décrivant l'appariement de paires d'électrons de spins opposés sur un même site [22]. L'intérêt de ce modèle est qu'il décrit la formation de paires d'électrons d'extension spatiale très faible, une des caractéristiques originales des paires impliquées dans les nouveaux supraconducteurs. Ce modèle a donné lieu ces dernières années à une controverse sur la nature de l'état fondamental à demi-remplissage et à faible intensité de saut des paires sur le réseau. Certains auteurs ont prédit un comportement assez conventionnel, d'autres prédisent l'existence d'une phase exotique. Afin de comprendre l'origine de cette controverse, nous avons mis en œuvre plusieurs techniques. Nous avons effectué des calculs de diagonalisations exacts par

méthode Lanczòs, avec des conditions aux limites variées afin de comprendre comment le système répond à une perturbation, et également des calculs basés sur la méthode dite du groupe de renormalisation numérique utilisant la matrice densité [DMRG, White (1991)]. Cette dernière méthode est extrêmement puissante et permet de calculer l'état fondamental d'un système 1D étendu avec grande précision. En utilisant toutes nos données et en faisant appel aux prédictions à tailles finies des systèmes critiques (invariance conforme) nous avons montré que les effets de taille finie pour le modèle de paires sont très singuliers, et que le modèle ne semble pas présenter de phase exotique. De plus, dans le cadre de la théorie de Luttinger pour les fermions unidimensionnels nous avons proposé un scénario expliquant pourquoi certains auteurs ont cru déceler une phase exotique dans ce modèle.

12. Modèle de Hubbard sur les hypercubes. Quelques résultats exacts.

Réf: Voir papier Q en Annexe

Dans ce travail nous avons présenté un certain nombre de résultats exacts pour le modèle de Hubbard usuel défini sur les hypercubes [23], [24]. L'hypercube à D dimensions est défini comme l'ensemble des 2^D sites de coordonnées 0 ou 1 dans les D directions d'espace. En $D=1$ il s'agit d'un segment à deux sites, en $D=2$ du carré usuel, en $D=3$ du cube (8 sommets), etc. Le modèle de Hubbard est un modèle central de la matière condensée. Il contient les éléments minimaux requis pour décrire la compétition qui existe entre la tendance à la délocalisation des électrons (énergie cinétique) et la localisation due à la répulsion électronique (effet de l'interaction). De plus, c'est un candidat potentiel pour l'existence d'une phase supraconductrice d'origine purement électronique sans couplage extérieur (type phonons). Bien sûr, ce dernier point est controversé et reste à vérifier. De nombreux travaux ont été effectués ces dernières années pour comprendre les différentes phases de ce modèle. Très peu de résultats exacts sont connus. Essentiellement, il existe la célèbre solution de Lieb et Wu en dimension 1 [25] et quelques résultats quasi-exacts en dimension infinie [26]. Pour les dimensions intermédiaires de nombreux calculs numériques ou approximations plus ou moins contrôlées ont été présentées, mais il n'existe pratiquement pas de résultats exacts. En utilisant les très grandes propriétés de symétrie des hypercubes nous avons pu obtenir plusieurs résultats intéressants pour les systèmes à faibles remplissages. Dans le cas de deux électrons nous avons présenté la solution analytique complète du modèle. Nous avons montré que le spectre de l'Hamiltonien (2^{2D} niveaux d'énergie) est constitué d'une partie composée de niveaux indépendants de l'interaction coulombienne et d'une partie non-triviale

dépendante de l'interaction. Chaque niveau, ainsi que sa dégénérescence, a été calculé. Au-delà des propriétés énergétiques, nous avons également donné une expression exacte sous forme explicite de la fonction de Green à une particule du modèle. Cette fonction permet de calculer les propriétés dynamiques les plus importantes du modèle. Finalement, en introduisant un formalisme de variables de spin adapté aux remplissages plus importants, nous avons pu montrer comment le modèle de Hubbard peut se réécrire sous forme d'un Hamiltonien de spin assez simple tenant compte des symétries de l'hypercube. Dans le cas du remplissage ($N_{\uparrow} = N, N_{\downarrow} = 1$) nous avons montré que l'espace de Hilbert associé à la partie "dure" du problème (dépendant de l'interaction) peut être dans certains cas réduit de manière très importante.

13. *Modèle de Hubbard $SU(N)$ unidimensionnel.*

Réf: Voir papier R en Annexe

Dans ce travail nous avons présenté une étude très complète du modèle de Hubbard " $SU(N)$ " à une dimension [27]. Ce modèle est une généralisation très simple et très naturelle du modèle de Hubbard usuel. Au lieu de considérer deux types d'électrons ("up", "down" ou électrons α et β) ayant une symétrie $SU(2)$ dans l'espace de spin, nous avons généralisé au cas de N types ou "couleurs" avec une symétrie $SU(N)$. Nous savons, grâce à la solution exacte par ansatz de Bethe de Lieb et Wu [25], que pour le cas usuel $N = 2$ et à demi-remplissage, il n'y a pas de transition métal-isolant pour une valeur non-nulle ($U \neq 0$) de l'interaction coulombienne. A $U = 0$ les électrons libres forment un métal parfait, et dès que l'interaction est branché le système devient isolant. Nous avons montré que pour le cas $N > 2$ ceci n'est plus vrai. Nous avons démontré qu'il existe une transition de Mott métal-isolant à demi-remplissage (un "électron" par site) à une valeur non nulle [$U_c \sim \frac{\pi}{2} \frac{N^2-4}{N-1} \sin \frac{\pi}{N}$]. Ceci est un résultat remarquable: les systèmes possédant une transition métal-isolant provoquée par la compétition subtile entre la délocalisation électronique (phase métallique) et l'interaction sont actuellement énormément étudiés. Ce modèle représente à mon avis le système le plus simple et le moins artificiel qui possède une telle transition. Il s'agit d'un cas d'"école" qui devrait être beaucoup étudié dans la suite. Pour démontrer l'existence d'une telle transition nous avons confronté deux types d'approches complémentaires pour les systèmes électroniques unidimensionnels. Le cadre théorique dans lequel nous nous sommes placés est l'approche par bosonisation pour les fermions 1D. En collaboration avec deux spécialistes de ce type d'approche (P. Azaria et P. Lecheminant) nous avons pu prédire non seulement

l'existence de cette transition mais aussi nombre de prédictions qualitatives et quantitatives sur le comportement en fonction de l'interaction U et du nombre de couleurs N de plusieurs quantités physiques. L'approche par bosonisation est une approche extrêmement puissante. Elle permet de donner un contenu physique aux excitations collectives de basse-énergie et à leurs interactions. Malheureusement, bien qu'il s'agisse intrinsèquement d'une méthode non-perturbative, il subsiste un aspect perturbatif dans l'évaluation de certains paramètres caractérisant l'Hamiltonien effectif de basse-énergie (paramètres dits de Luttinger). Afin de contrôler totalement le scénario de la théorie, il est impératif d'estimer ces paramètres de manière non-perturbative et indépendante. C'est ce que nous avons fait en étudiant par méthode Monte Carlo quantique le comportement basse-énergie de systèmes finis de taille croissante (jusqu'à 32 sites). Sans entrer dans les détails, nous avons pu montrer d'une manière extrêmement convaincante que le scénario prévu par la bosonisation est tout à fait correct. L'évolution de l'Hamiltonien effectif basse-énergie est compatible avec une phase métallique à petites valeurs de U et une phase isolante à grands U . De plus, nous avons pu localiser de manière très précise la valeur critique de l'interaction où la transition a lieu. Dans le cas $SU(3)$ on trouve par exemple $U_c \sim 2.2$ et $U_c \sim 2.8$ pour $SU(4)$. Notons qu'à l'occasion de ce travail nous avons proposé plusieurs améliorations importantes pour les approches Monte Carlo quantique sur réseau. Une des améliorations les plus notables a été de montrer qu'il était possible d'intégrer exactement l'évolution temporelle du système quand celui-ci est bloqué dans une configuration donnée. Ceci permet de réduire de significativement les fluctuations statistiques des calculs, particulièrement à grands U où la répulsion coulombienne limite l'espace de phase des électrons. Cette amélioration est de portée tout à fait générale pour les systèmes sur réseau (matrice Hamiltonienne finie). Un autre point important a été de montrer comment calculer les paramètres de Luttinger de l'Hamiltonien effectif basse-énergie. Dans la littérature ces paramètres sont en général calculés par diagonalisation exacte (méthode de Lanczos). Malheureusement, de tels calculs sont limités à de petites tailles pour des chaînes finies. En introduisant des Hamiltoniens intermédiaires appropriés nous avons montré comment calculer exactement ces paramètres dans une formalisme Monte Carlo quantique. En particulier, nous avons trouvé un procédé pour s'affranchir des termes oscillants, liés aux conditions aux bords "twistés", qui sont si difficiles à calculer par méthode Monte Carlo.

14. *Modèle de Hubbard bosonique à deux dimensions*

Réf: Voir papier G en Annexe

Dans ce travail nous nous sommes intéressés au problème des systèmes de bosons en interaction forte modélisés par un Hamiltonien de Hubbard sur réseau bidimensionnel [28]. A température nulle, il est connu que deux types de transition de phase, connectant une phase superfluide et une phase isolant de Mott, existent pour ce modèle. A densité entière constante, une première transition apparaît lorsque le paramètre de répulsion du modèle approche une valeur critique. A répulsion suffisamment grande, on observe également une transition quand la densité passe par des valeurs entières. Ce problème a été étudié dans le cadre d'une approximation variationnelle de type Gutzwiller. On a montré qu'il est alors possible de décrire de manière analytique la transition superfluide-isolant de Mott du système. Cet ansatz pour la fonction d'onde reproduit correctement le diagramme de phase du système. Des calculs Monte Carlo quantique nous ont également permis d'étudier le comportement de la densité superfluide du système au-delà de l'approximation de Gutzwiller.

15. *Systèmes de spin classiques*

Réf: Voir papier M en Annexe

Dans cette étude [29], [30] nous nous sommes intéressés aux propriétés thermodynamiques des systèmes de spin représentés par des modèles effectifs de type Heisenberg. Différentes techniques Monte Carlo ont été appliquées ou développées pour comprendre la nature du fondamental et des transitions de phase de ces systèmes. Une de nos premières applications a concerné le modèle d'Heisenberg bidimensionnel. Dans ce modèle de base de la physique des systèmes de spin, nous avons illustré comment le calcul de la raideur de spin (spin-stiffness) pouvait être un outil précieux pour la compréhension de la nature de l'état fondamental et de ses excitations. La raideur de spin est liée à la réponse du système de spins à une rotation des spins de bords (twist). La manière dont la raideur de spin évolue avec la taille du système est directement liée aux types d'excitations élémentaires présents dans le système. Nous avons vérifié avec très grande précision que la raideur de spin suit exactement le comportement prévu par le groupe de renormalisation appliqué à un modèle décrivant le système comme un ensemble d'ondes de spin en interaction. Afin d'obtenir ces résultats, nous avons proposé de simuler le modèle à l'aide d'une méthode de Monte Carlo non-locale

(adaptation de l’algorithme de Swendsen-Wang), c’est à dire une méthode qui construit des agrégats de spins de taille importante à basse température (suppression du phénomène de “ralentissement critique” au voisinage d’une transition de phase continue). Nous avons montré qu’il est essentiel d’utiliser une telle approche pour obtenir des résultats raisonnables. Un deuxième développement entrepris a été de généraliser ces résultats aux systèmes de spins frustrés [30]. La physique des spins frustrés est riche et donne lieu à de nombreuses polémiques. En particulier, le rôle des excitations topologiques est mal compris. Afin d’étudier les effets nous nous sommes proposés de comparer les prédictions des modèles effectifs basse-energie des systèmes frustrés bidimensionnels (modèle σ -nonlinéaire) aux simulations numériques dans les cas avec et sans topologie. Nous avons montré qu’une fois encore à basse température les prédictions du groupe de renormalisation sont en accord avec les données. A des températures intermédiaires, nous avons mis en valeur les effets provoqués par les défauts. Il est important de souligner qu’il est bien connu que la simulation des systèmes classiques frustrés à l’aide d’algorithmes non-locaux est difficile. Nous avons proposé une généralisation de ces algorithmes qui permet de conserver les performances des systèmes non-frustrés.

- [1] M. Caffarel and O. Hess, “Quantum Monte Carlo-Perturbation Calculations of Interaction Energies”, *Phys. Rev. A* **43**, 2139 (1991).
- [2] M. Caffarel and O. Hess “Computing Response Properties with Quantum Monte Carlo” in *AIP Conference Proceedings No 239, Advances in Biomolecular Simulations Obernai, France 1991* pp. 20-32.
- [3] M. Caffarel, M. Rérat, and C. Pouchan, “Evaluating Dynamic Multipole Polarizabilities and van Der Waals Dispersion Coefficients of two-electron Systems with a Quantum Monte Carlo Calculation: A Comparison with some *Ab Initio* Calculations”, *Phys. Rev. A* **47**, 3704 (1993).
- [4] C. Huiszoon and M. Caffarel, “A quantum Monte Carlo perturbational study of the He-He interaction”, *J. Chem. Phys.* **104**, 4621 (1996).
- [5] O. Hess, M. Caffarel, J. Langlet, J. Caillet, C. Huiszoon, and P. Claverie, “The water dimer. Comparison of results obtained by both *ab initio* supermolecule and SAPT methods. Derivation of simplified formulas” in *Modeling of Molecular Structures and Properties Studies in Physical and Theoretical Chemistry*, Vol. 71, pp.323-335.

- [6] O. Hess, M. Caffarel, C. Huiszoon, and P. Claverie, “Second-order exchange effects in intermolecular interactions. The water dimer”, *J. Chem. Phys.* **92**, 6049 (1990).
- [7] J. Langlet, J. Caillet, and M. Caffarel, “A Perturbational Study of some Hydrogen-Bonded Dimers”, *J. Chem. Phys.* **103**, 8043 (1995).
- [8] M. Caffarel , F.X. Gadea, and D.M. Ceperley, “Lanczòs-type Algorithm for Quantum Monte Carlo Data”, *Europhys. Lett.* **16** 249 (1991).
- [9] M. Caffarel and D.M. Ceperley, “A Bayesian Analysis of Green’s Function Monte Carlo Correlation Functions”, *J. Chem. Phys.* **97**, 8415 (1992).
- [10] M. Caffarel, P. Claverie, C. Mijoule, J. Andzelm, and D.R. Salahub, “Quantum Monte Carlo method for some model and realistic coupled anharmonic oscillators”, *J. Chem. Phys.* **90**, 990 (1989)
- [11] M. Caffarel, X. Krokidis, and C. Mijoule, “On the Nonconservation of the Number of Nodel Cells of Eigenfunctions”, *Europhys. Lett.* **20**, 581 (1992).
- [12] H.J. Flad, M. Caffarel, and A. Savin, “Quantum Monte Carlo calculations with multi-reference trial wave functions”, *Recent Advances in Quantum Monte Carlo Methods*, ed.: W.A. Lester Jr., World Scientific Publishing p.73 (1997)
- [13] S. Zirah, “Méthodes Monte Carlo quantiques pour les molécules. Utilisation de formes Valence Bond”, Stage de Maîtrise-Licence, Université Paris-Sud (1998).
- [14] R. Assaraf, M. Caffarel, and A. Khelif, “ Diffusion Monte Carlo Methods with a fixed-number of walkers”, *Phys. Rev. E.* **61**, 4566 (2000).
- [15] J.H. Hetherington, *Phys. Rev. A* **30**, 2713 (1984).
- [16] R. Assaraf and M. Caffarel, “Zero-variance principle for Monte Carlo algorithms”, *Phys. Rev. Lett.* **83** , 4682 (1999).
- [17] C. Filippi and C.J. Umrigar, “Correlated sampling in quantum Monte Carlo: a route to forces”, preprint cond-mat/9911326 (1999).
- [18] R. Assaraf and M. Caffarel, “Computing forces with quantum Monte Carlo”, *J. Chem. Phys.* **113** ,4028 (2000).
- [19] M. Caffarel and W. Krauth, “Exact Diagonalization Approach to Correlated Fermions in Infinite Dimensions: Mott Transition and Superconductivity”, *Phys. Rev. Lett.* **72**, 1545 (1994)

- [20] M. Caffarel and W. Krauth, “Exact Diagonalization Approach for the infinite D Hubbard Model”, 7 pages, cond-mat/9306057, version étendue du papier [19] (première partie)
- [21] M. Caffarel and W. Krauth, “Superconductivity in the Two-Band Hubbard Model in Infinite D: an Exact Diagonalization Study”, 7 pages, cond-mat/9306056, version étendue du papier [19] (deuxième partie)
- [22] M. van den Bossche and M. Caffarel, “One-dimensional pair-hopping and attractive Hubbard models: A comparative study”, *Phys. Rev. B* **54**, 17414 (1996).
- [23] M. Caffarel and R. Mosseri, “Hubbard model on d-dimensional hypercubes: Exact solution for the two-electron case”, *Phys. Rev. B* , 12651 (1998).
- [24] R. Assaraf, M. Caffarel, and R. Mosseri, “Hubbard model on hypercubes”, *Physica B* **259-261**, 787 (1999).
- [25] E.H. Lieb and F.Y. Wu, *Phys. Rev. Lett* **20**, 1445 (1968).
- [26] See, e.g., A. Georges, G. Kotliar, W. Krauth, and M.J. Rozenberg, *Rev. Mod. Phys.* **68**, 13 (1996).
- [27] R. Assaraf, P. Azaria, M. Caffarel, and P. Lecheminant, “Metal-insulator transition in the one-dimensional SU(N) Hubbard model”, *Phys. Rev. B* **60**, 2299 (1999).
- [28] W. Krauth, M. Caffarel and J.P. Bouchaud, “Gutzwiller Wave Function for a Model of Strongly Interacting Bosons”, *Phys. Rev B* **45**, 3137 (1992).
- [29] M. Caffarel, P. Azaria, B. Delamotte, and D. Mouhanna, “Monte Carlo Calculation of the Spin-stiffness of the two-dimensional Heisenberg Model”, *Europhys. Lett.* **26**, 493 (1994).
- [30] M. Caffarel, P. Azaria, B. Delamotte, and D. Mouhanna, “Role of topological defects in two-dimensional frustrated spin systems”, (soumis)

III. ENCADREMENT D'ÉTUDIANTS

A. Thèses de doctorat

- Direction d'une thèse de doctorat. Sujet: "Approche perturbative des interactions intermoléculaires. Calcul *ab initio* et Monte Carlo quantique des composantes de l'énergie d'interaction" Olivier Hess, Université Paris VI, soutenue le 03 Novembre 1989. Jury: M. Allavena (Paris), M. van der Avoird (Hollande), M. Caffarel (Paris), J.P. Daudey (Toulouse), C. Lhuillier (Paris), J.L. Rivail (Nancy).
- Direction d'une thèse de doctorat. Sujet: "Méthodes Monte Carlo quantique pour les atomes et les molécules" , Piere Siccardi (DEA "Champs, Particules, Matière", Orsay) (Mai 1994-Juin 1995) Arrêt de la thèse pour entrer comme directeur de l'informatique dans une entreprise privée spécialisée dans la sécurité.
- Co-direction (avec Prof. K. Penson, Paris VI) d'une thèse de doctorat. Sujet: "Fermions à une dimension: Etude du modèle à interaction par sauts de paire", Mathias van den Bossche, Univ. Paris VI, soutenue le 09 Décembre 1996. Jury: M. Caffarel (Paris), D. Förster (Bordeaux), C. Lhuillier (Paris), K. Penson (Paris), D. Poilblanc (Toulouse), T. Schneider (Zurich), T. Ziman (Toulouse).
- Direction d'une thèse de doctorat. Sujet: "Méthodes de Monte-Carlo quantique. Développements et applications à quelques problèmes quantiques fortement corrélés." Roland Assaraf, Université Paris VI, thèse soutenue le 13 Juiller 1999. Jury: A. Beswick (Toulouse), M. Caffarel (Paris), T. Giamarchi (Orsay), C. Lhuillier (Paris), D. Poilblanc (Toulouse), J.C. Rayez (Bordeaux).

B. Stages de DEA

- Direction d'un stage de DEA: DEA "Atomes, Molécules, Photons et leurs interactions", Toulouse III, Francis Beaubois, "Méthode Monte Carlo quantique variationnelle: application à la molécule H₂" (Mars 1993-Juin 1993).
- Direction d'un stage de DEA: DEA "Physique des Particules, Mathématiques et Modélisation", Marseille, Roland Assaraf, "Développements à couplage fort (strong coupling) pour les systèmes de spins bidimensionnels" (Mars 1994-Juin 1994).

C. Stages de maîtrise

- Direction d'un stage de maîtrise: Maîtrise de physique fondamentale, Toulouse III, Unité de valeur UM6 (Méthodes et Pratique du calcul scientifique). Roland Assaraf et Stéphane Guérin "Méthode Monte Carlo variationnelle pour l'étude de systèmes quantiques" (Mars 1993-Juin 1993).
- Direction d'un stage de maîtrise: Maîtrise de physique fondamentale, Paris VI, Xénophon Krokidis "Construction d'une fonction d'onde de qualité pour l'atome de Lithium" (Mars 1994-Juin 1994).
- Direction d'un stage de Licence-Maîtrise, Séverine Zirah, Université Paris-Sud, "Méthodes Monte Carlo quantique pour les molécules. Utilisation de formes Valence Bond", Juin-Juillet 1998.

IV. LISTE DES PUBLICATIONS

- (1) M. Caffarel and P. Claverie, "Treatment of the Schrödinger Equation Through a Monte Carlo Method Based upon the Generalized Feynman-Kac Formula", *J. Stat. Phys.* **43**, 797 (1986).
- (2) M. Caffarel, "Méthodes d'intégration fonctionnelle et méthodes stochastiques pour le traitement de problèmes quantiques. Application à la physique atomique et moléculaire", Doctorat de l'Université Paris VI, 27 Mars 1987.
- (3) M. Caffarel and P. Claverie, "Development of a pure diffusion quantum Monte Carlo method using a full generalized Feynman-Kac formula. I. Formalism", *J. Chem. Phys.* **88**, 1088 (1988).
- (4) M. Caffarel and P. Claverie, "Development of a pure diffusion quantum Monte Carlo method using a full generalized Feynman-Kac formula. II. Application to simple systems", *J. Chem. Phys.* **88**, 1100 (1988).
- (5) M. Caffarel, P. Claverie, C. Mijoule, J. Andzelm, and D.R. Salahub, "Quantum Monte Carlo method for some model and realistic coupled anharmonic oscillators", *J. Chem. Phys.* **90**, 990 (1989).
- (6) M. Caffarel, "Stochastic methods in quantum mechanics" in *Numerical Determination of the Electronic Structure of Atoms, Diatomic and Polyatomic Molecules* (Kluwer Academic Publishers, 1989), pp.85-105.
- (7) O. Hess, M. Caffarel, C. Huiszoon, and P. Claverie, "Second-order exchange effects in intermolecular interactions. The water dimer", *J. Chem. Phys.* **92**, 6049 (1990).
- (8) O. Hess, M. Caffarel, J. Langlet, J. Caillet, C. Huiszoon, and P. Claverie, "The water dimer. Comparison of results obtained by both *ab initio* supermolecule and SAPT methods. Derivation of simplified formulas" in *Modeling of Molecular Structures and Properties Studies in Physical and Theoretical Chemistry*, Vol. 71, pp.323-335.
- (9) M. Caffarel and O. Hess, "Quantum Monte Carlo-Perturbation Calculations of Interaction Energies", *Phys. Rev. A* **43**, 2139 (1991).
- (10) M. Caffarel and O. Hess "Computing Response Properties with Quantum Monte Carlo" in *AIP Conference Proceedings No 239, Advances in Biomolecular Simulations Obernai, France 1991* pp. 20-32
- (11) M. Caffarel, F.X. Gadea, and D.M. Ceperley, "Lanczos-type Algorithm for Quantum Monte Carlo Data", *Europhys. Lett.* **16** 249 (1991).
- (12) W. Krauth, M. Caffarel and J.P. Bouchaud, "Gutzwiller Wave Function for a Model of Strongly Interacting Bosons", *Phys. Rev B* **45**, 3137 (1992).

- (13) M. Caffarel, X. Krokidis, and C. Mijoule, “On the Nonconservation of the Number of Nodel Cells of Eigenfunctions”, *Europhys. Lett.* **20**, 581 (1992)
- (14) M. Caffarel and D.M. Ceperley, “A Bayesian Analysis of Green’s Function Monte Carlo Correlation Functions”, *J. Chem. Phys.* **97**, 8415 (1992).
- (15) M. Caffarel, M. Rérat, and C. Pouchan, “Evaluating Dynamic Multipole Polarizabilities and van Der Waals Dispersion Coefficients of two-electron Systems with a Quantum Monte Carlo Calculation: A Comparison with some *Ab Initio* Calculations”, *Phys. Rev. A* **47**, 3704 (1993).
- (16) M. Rérat, M. Caffarel, and C. Pouchan, “Dynamic Polarizabilities and van der Waals Coefficients of the 2^1S and 2^3S Metastable States of Helium”, *Phys. Rev A* **48**, 161 (1993).
- (17) M. Caffarel, D.M. Ceperley, and M.H. Kalos, “Comment on Feynman-Kac Path-Integral Calculation of the Ground-State Energies of Atoms”, *Phys. Rev. Lett.* **71**, 2159 (1993).
- (18) M. Caffarel and W. Krauth, “Exact Diagonalization Approach to Correlated Fermions in Infinite Dimensions: Mott Transition and Superconductivity”, *Phys. Rev. Lett.* **72**, 1545 (1994)
- (19) M. Caffarel, P. Azaria, B. Delamotte, and D. Mouhanna, “Monte Carlo Calculation of the Spin-stiffness of the two-dimensional Heisenberg Model”, *Europhys. Lett.* **26**, 493 (1994)
- (20) J. Langlet, J. Caillet, and M. Caffarel, “A Perturbational Study of some Hydrogen-Bonded Dimers”, *J. Chem. Phys.* **103**, 8043 (1995)
- (21) C. Huiszoon and M. Caffarel, “A quantum Monte Carlo perturbational study of the He-He interaction”, *J. Chem. Phys.* **104**, 4621 (1996)
- (22) H.J. Flad, M. Caffarel, and A. Savin, “Quantum Monte Carlo calculations with multi-reference trial wave functions”, *Recent Advances in Quantum Monte Carlo Methods*, ed.: W.A. Lester Jr., World Scientific Publishing p.73 (1997)
- (23) M. van den Bossche and M. Caffarel, “One-dimensional pair-hopping and attractive Hubbard models: A comparative study”, *Phys. Rev. B* **54**, 17414 (1996)
- (24) M. Caffarel and R. Mosseri, “Hubbard model on d-dimensional hypercubes: Exact solution for the two-electron case”, *Phys. Rev. B* , 12651 (1998)
- (25) R. Assaraf, M. Caffarel, and R. Mosseri, “Hubbard model on hypercubes”, *Physica B* **259-261**, 787 (1999).
- (26) R. Assaraf, P. Azaria, M. Caffarel, and P. Lecheminant, “Metal-insulator transition in the one-dimensional SU(N) Hubbard model”, *Phys. Rev. B* **60**, 2299 (1999).
- (27) R. Assaraf and M. Caffarel, “Zero-variance principle for Monte Carlo algorithms”, *Phys. Rev. Lett.* **83** , 4682 (1999).

- (28) R. Assaraf, M. Caffarel, and A. Khelif, “ Diffusion Monte Carlo Methods with a fixed-number of walkers”, *Phys. Rev. E.* **61**, 4566 (2000).
- (29) M. Caffarel, R. Assaraf, “A pedagogical introduction to quantum Monte Carlo”, à paraître in “Mathematical models and methods for *ab initio* Quantum Chemistry” in *Lecture Notes in Chemistry* (Springer).
- (30) R. Assaraf and M. Caffarel, “Computing forces and observables with quantum Monte Carlo”, *J. Chem. Phys.* **113** , 4028 (2000).
- (31) M. Caffarel, P. Azaria, B. Delamotte, and D. Mouhanna, “Role of topological defects in two-dimensional frustrated spin systems”, (soumis).

V. MÉTHODES MONTE CARLO QUANTIQUE EN CHIMIE THÉORIQUE

A. Les méthodes Monte Carlo quantique en quelques mots

Ramenées à leur plus simple expression, les méthodes Monte Carlo quantique consistent à faire évoluer une population de marcheurs à l'aide d'un ensemble de règles probabilistes et à évaluer les valeurs moyennes quantiques au moyen d'estimateurs statistiques appropriés sur l'ensemble de toutes les positions obtenues pour les marcheurs. Par marcheur on entend un point \mathbf{x} dans l'espace de configuration complet du système. Par exemple, si on considère une molécule comprenant N électrons, il s'agira de l'ensemble des $3N$ coordonnées spatiales $\mathbf{x} = (\mathbf{r}_1, \dots, \mathbf{r}_N)$ des électrons (on suppose ici les noyaux fixes, mais on peut également traiter les noyaux). Dans la littérature on parle de marcheurs, de répliques, de points, voire de ψ particles). Notons que les degrés de liberté de spin n'apparaissent pas explicitement mais sont pris en compte en imposant l'antisymétrie sous l'échange des coordonnées spatiales des électrons α et β séparément. Les règles stochastiques définissent les "règles du jeu" de la simulation. On peut définir plusieurs ensembles de règles et plusieurs sortes d'estimateurs qui donnent les mêmes valeurs moyennes. Cette variété de choix explique les nombreuses variantes QMC existant dans la littérature. Pour ne citer que les principales: Diffusion Monte Carlo, Pure Diffusion Monte Carlo, Projector Monte Carlo, Green's function Monte Carlo, Lattice Green's function Monte Carlo, etc.

Afin de clarifier la situation on peut définir deux grandes classes de méthodes Monte Carlo quantique: les méthodes Monte Carlo dites variationnelles (Variational Monte Carlo, VMC) et les méthodes Monte Carlo dites "exactes". Signalons qu'il existe aussi des approches Monte Carlo dites à température finie permettant d'évaluer les moyennes thermodynamiques (Path Integral Monte Carlo, World-line MC, etc.) mais je n'en parlerai pas ici.

1. Méthodes Monte Carlo variationnelles

Dans ce type d'approches on se propose de calculer les valeurs moyennes quantiques associées à une fonction d'onde d'essai $\psi_T(\mathbf{x}, \mathbf{p})$ supposée connue et donnée sous forme analytique. Ici, \mathbf{x} représente l'ensemble des coordonnées spatiales et \mathbf{p} un jeu de paramètres permettant de faire varier la fonction d'essai. Par exemple, dans le cas de l'énergie on cherche à évaluer l'énergie variationnelle suivante:

$$E_V(\mathbf{p}) = \frac{\int d\mathbf{x} \psi_T(\mathbf{x}, \mathbf{p}) H \psi_T(\mathbf{x}, \mathbf{p})}{\int d\mathbf{x} \psi_T(\mathbf{x}, \mathbf{p})^2} \quad (4)$$

Cette expression peut facilement se réécrire sous la forme:

$$E_V(\mathbf{p}) = \langle\langle E_L(\mathbf{x}, \mathbf{p}) \rangle\rangle \quad (5)$$

où le symbole $\langle\langle \dots \rangle\rangle$ représente la valeur moyenne définie relativement à la densité de probabilité de présence associée à ψ_T :

$$\pi(\mathbf{x}, \mathbf{p}) = \psi_T^2 / \int d\mathbf{x} \psi_T^2 \quad (6)$$

et

$$\langle\langle \dots \rangle\rangle = \int d\mathbf{x} \pi(\mathbf{x}, \mathbf{p}) \dots \quad (7)$$

Dans la formule (5) la quantité moyennée est appelée “énergie locale”. Elle est définie par l’expression:

$$E_L(\mathbf{x}, \mathbf{p}) \equiv H\psi_T(\mathbf{x}, \mathbf{p})/\psi_T(\mathbf{x}, \mathbf{p}) \quad (8)$$

Cette quantité joue un rôle central dans les méthodes MC quantique. C’est une fonction locale (elle ne dépend que du point courant \mathbf{x}) et qui est homogène à une énergie. Lorsque la fonction d’essai est exacte, elle se réduit à l’énergie exacte. Si on est capable de construire un ensemble de configurations qui se distribuent dans l’espace avec la densité π , alors un estimateur de l’énergie est donné par la valeur moyenne arithmétique des valeurs de l’énergie locale:

$$E_V(\mathbf{p}) = \lim_{P \rightarrow \infty} \frac{1}{P} \sum_{i=1}^P E_L[\mathbf{x}^{(i)}]. \quad (9)$$

Construire des configurations dans un espace de grande dimension qui soient distribuées selon une densité non-triviale -mais donnée analytiquement- est un problème bien connu des simulations. Pour cela on a recours à l’algorithme de Metropolis ou à l’une de ses variantes [1], [2]. Les règles du jeu sont alors les suivantes:

1^{ere} règle: Etape de déplacement. Pour un marcheur donné situé en \mathbf{x} on propose une nouvelle position \mathbf{y} à l’aide d’une densité de probabilité de transition choisie préalablement, $p(\mathbf{x} \rightarrow \mathbf{y})$.

2^{eme} règle: Etape d’acceptation-refus. La nouvelle position \mathbf{y} est acceptée avec probabilité $q(\mathbf{x}, \mathbf{y})$ donnée par:

$$q(\mathbf{x}, \mathbf{y}) = \text{Min}[1, \pi(\mathbf{y})p(\mathbf{y} \rightarrow \mathbf{x})/\pi(\mathbf{x})p(\mathbf{x} \rightarrow \mathbf{y})] \quad (10)$$

Dans le cas où la position \mathbf{y} est refusée, on considère que la nouvelle position est donnée par \mathbf{x} (on fait du “sur place”).

On peut montrer que, quelle que soit la configuration initiale de la population de marcheurs et quelle que soit la probabilité de transition choisie, pourvue quelle soit ergodique -une condition assez simple à réaliser [2]- l’ensemble des positions successives construites avec ces règles simples se distribuent selon la densité π (pour une démonstration mathématique, voir mes notes de cours [2]).

Afin d’accélérer l’échantillonnage de l’espace de configuration, on choisit une probabilité de transition qui admet comme distribution stationnaire une densité proche de π . De plus, il faut que cette densité soit facile à échantillonner. La solution communément utilisée a la forme suivante:

$$p(\mathbf{x} \rightarrow \mathbf{y}, \tau) = \left[\frac{1}{\sqrt{2\pi\tau}} \right]^{3N} \exp \left[-\frac{(\mathbf{y} - \mathbf{x} - \mathbf{b}(\mathbf{x})\tau)^2}{2\tau} \right] \quad (11)$$

où τ joue le rôle d’un pas de temps et \mathbf{b} est un vecteur appelé vecteur dérive (“drift vector”) et qui est donné par

$$\mathbf{b} = \nabla\psi_T/\psi_T. \quad (12)$$

On peut montrer que, dans la limite d’un pas de temps infinitésimal, cette probabilité de transition admet ψ_T^2 comme densité stationnaire. De plus, elle s’écrit comme un produit de $3N$ gaussiennes indépendantes (une gaussienne pour chaque coordonnée) et est donc très facile à échantillonner. La partie “diffusive” de la probabilité de transition permet aux marcheurs de visiter l’ensemble des configurations possibles du système; la partie dite “déterministe” associée au vecteur dérive permet, quant à elle, de “pousser” les marcheurs vers les régions de grande probabilité (échantillonnage selon l’importance ou “importance sampling”).

Ce premier exemple simple de méthode Monte Carlo quantique permet d’appréhender les aspects essentiels des méthodes stochastiques. Les règles à appliquer sont simples et très faciles à programmer sur machine. Les quantités à calculer sont locales et il n’y a pas de calculs d’intégrales à effectuer. L’essentiel de l’effort numérique consiste à évaluer la dérivée première (vecteur dérive) et seconde (énergie locale) de la fonction d’essai. L’avantage principale de ces méthodes est donc de permettre le calcul des valeurs moyennes associées à une fonction d’onde variationnelle de forme *a priori* quelconque. Ceci est évidemment un avantage important par rapport aux méthodes *ab initio* plus traditionnelles définies à partir d’un développement de la fonction d’onde restreint à des produits de fonctions à un électron et qui nécessitent le calcul de nombreuses intégrales élémentaires.

2. Méthodes Monte Carlo exactes

Dans cette partie je montre comment s'affranchir de l'approximation variationnelle, c'est à dire calculer les quantités exactes du système. Différentes règles du jeu permettent d'atteindre cet objectif. Nous présentons ici les deux principales approches:

α . Méthode introduisant un poids dans les valeurs moyennes: Pure Diffusion Monte Carlo

Cette méthode est l'approche que j'ai plus particulièrement développée pendant mon travail de thèse [3], [4], [5], [6]. Sans entrer dans les détails on peut montrer qu'en utilisant les mêmes règles que précédemment, et au prix de l'introduction d'un produit de poids élémentaires dans les moyennes, on peut construire des estimateurs pour les propriétés exactes. Par exemple pour le cas important de l'énergie totale, on a la formule suivante:

$$E_0 = \frac{E_L[\mathbf{x}^{(1)}] + E_L[\mathbf{x}^{(2)}]w[\mathbf{x}^{(2)}] + E_L[\mathbf{x}^{(3)}]w[\mathbf{x}^{(2)}]w[\mathbf{x}^{(3)}] + E_L[\mathbf{x}^{(4)}]w[\mathbf{x}^{(2)}]w[\mathbf{x}^{(3)}]w[\mathbf{x}^{(4)}] + \dots}{1 + w[\mathbf{x}^{(2)}] + w[\mathbf{x}^{(2)}]w[\mathbf{x}^{(3)}] + w[\mathbf{x}^{(2)}]w[\mathbf{x}^{(3)}]w[\mathbf{x}^{(4)}] + \dots} \quad (13)$$

où le poids $w(\mathbf{x})$ est donné par:

$$w(\mathbf{x}) = \exp[-\tau(E_L(\mathbf{x}) - E_T)] \quad (14)$$

où E_T est une énergie de référence arbitraire et les $\mathbf{x}^{(i)}$ représentent la suite des configurations engendrées. La formule précédente pour l'énergie est l'analogie de la formule (9). Le cas variationnel est obtenu en prenant les poids tous égaux à un, $w = 1$. Notons, qu'en pratique, la formule (13) précédente est loin d'être optimale, nous n'entrerons pas dans ce genre de considérations ici.

β .Méthode avec processus de mort-naissance (branching): Diffusion Monte Carlo

La méthode QMC la plus populaire est certainement la méthode dite Diffusion Monte Carlo où le poids w est introduit dans les règles probabilistes plutôt que dans les estimateurs comme précédemment. Pour ce faire, on rajoute aux règles 1. et 2. du cas variationnel une nouvelle étape qui consiste à détruire ou faire un certain nombre de répliques des marcheurs en fonction du poids local w (processus dit de branching). En pratique:

3^{eme} règle: Etape de branching. Pour chaque marcheur le nombre de copies effectué est pris égal à:

$$m \equiv \text{int}(w + \eta) \quad (15)$$

où η est un nombre aléatoire uniforme compris entre 0 et 1.

Notons que dans cette approche où le nombre de marcheurs n'est plus constant il est nécessaire d'introduire une étape de contrôle de population (il faut éviter que le nombre total de marcheurs diverge ou s'annule...). Ceci peut être réalisé assez simplement de différentes manières, nous n'entrerons pas dans ces détails. Le point important est qu'on peut démontrer que la nouvelle densité stationnaire obtenue avec cette étape de branchement supplémentaire est maintenant égale à:

$$\pi^*(\mathbf{x}) = \psi_T(\mathbf{x})\phi_0(\mathbf{x}) / \int d\mathbf{x}\psi_T(\mathbf{x})\phi_0(\mathbf{x}) \quad (16)$$

au lieu du carré de la fonction d'onde d'essai comme dans le cas variationnel ou la méthode PDMC. Ici, $\phi_0(\mathbf{x})$ représente la fonction d'onde exacte inconnue. En prenant la moyenne de l'énergie locale sur cette nouvelle densité on obtient un estimateur très simple de l'énergie exacte:

$$E_0 = \langle\langle E_L \rangle\rangle_{\pi^*} = \lim_{P \rightarrow \infty} \frac{1}{P} \sum_{i=1}^P E_L[\mathbf{x}^{(i)}] \quad (17)$$

Nous venons de donner les éléments-clefs des méthodes Monte Carlo quantique. Il nous suffiront pour la suite. Pour une présentation complète on peut se reporter par exemple à [7], [8], ou [9]. Faisons toutefois quelques remarques importantes:

- Il existe une propriété dite de variance-zéro pour l'énergie totale. Plus la fonction d'essai est "proche" de la fonction d'onde exacte, plus les fluctuations de l'énergie locale sont faibles. A la limite d'une fonction d'essai exacte, le résultat exact est obtenu quel que soit le nombre de pas Monte Carlo. La conséquence de cette propriété est qu'il est extrêmement important d'utiliser les "meilleures" fonctions d'essai possibles pour réduire l'effort numérique. Notons également que nous avons très récemment généralisé cette propriété de variance-zero au calcul de n'importe quelle observable physique. (voir section II.B.8, "Principe de zéro-variance généralisé").
- Nous avons présenté dans ce qui précède des estimateurs pour l'énergie totale. On peut également écrire des expressions analogues pour toutes les propriétés autres que l'énergie (observables, forces, polarisabilités, etc.), même si leur calcul n'est pas toujours aussi facile que celui de l'énergie.
- Nous avons limité notre présentation au calcul des propriétés de l'état fondamental. En théorie, les états excités peuvent également être abordés. En pratique, les calculs sont en fait beaucoup plus instables que pour l'état fondamental.

- Il existe deux sources de biais systématiques dans les calculs: l'approximation à temps court Eq.(11) associée au choix d'un pas de temps τ non-infinitésimal, et l'erreur de contrôle de population dans le cas des méthodes avec branching. La première erreur peut être supprimée en utilisant une version un peu plus sophistiquée des méthodes DMC (méthodes Green's function MC, [10]). On peut également, et c'est la solution généralement adoptée, faire plusieurs calculs avec des valeurs différentes du pas de temps et extrapoler à zéro. En ce qui concerne l'erreur de contrôle de population on peut également réduire l'erreur en prenant des populations suffisamment grandes et en extrapolant à population infinie (en pratique, cette erreur décroît très vite avec le nombre de marcheurs).
- Les approches Monte Carlo quantique sont extrêmement bien adaptées au calcul sur ordinateur. On peut très facilement vectoriser ou paralléliser les codes (simplement en considérant des marcheurs indépendants sur des processeurs indépendants). De plus, les besoins en mémoire centrale sont extrêmement limités. Ce sont des méthodes de simulation assez idéale du point de vue informatique.

Avant de terminer cette partie il est important de discuter le traitement pratique des contraintes résultant du principe de Pauli pour les électrons.

3. Contraintes associées au principe de Pauli: le problème du signe

Le fait que les électrons soient des fermions et donc obéissent au principe de Pauli implique que la fonction d'onde électronique ait des propriétés d'antisymétrie bien spécifiques par rapport aux échanges d'électrons. Dans un formalisme purement spatial, comme celui présenté ici, on peut montrer que la fonction d'onde doit être antisymétrique dans l'échange des coordonnées spatiales des électrons de même spin (sans contrainte particulière pour les électrons de spin différents). Une telle contrainte implique que pour plus de deux électrons la fonction d'onde ait un signe non-constant. Dans un calcul variationnel ceci ne pose aucune difficulté particulière: la densité π donnée par l'équation (6) est positive et peut être construite sans difficulté particulière. En revanche, dans le cas des méthodes exactes la densité stationnaire $\pi^* = \psi_T \phi_0$, Eq. (16), n'a plus un signe constant puisqu'en général les domaines de l'espace de configuration (domaines nodaux) où la fonction d'onde d'essai et la fonction d'onde exacte ont le même signe, diffèrent. Deux grandes classes d'approche ont été proposées pour résoudre cette difficulté. Elles correspondent aux deux solutions naturelles

qui s’offrent à nous: soit introduire le signe dans les estimateurs comme un poids, soit incorporer le signe directement dans le processus stochastique lui-même.

α .Signe dans les estimateurs: les méthodes exactes mais instables

En théorie, il n’y a aucune difficulté à tenir compte de l’antisymétrie de la fonction d’onde exacte en l’introduisant dans les estimateurs à l’aide d’un projecteur. Pour cela il suffit de prendre comme fonction d’essai une fonction essentiellement égale à la valeur absolue d’une fonction fermionique et d’introduire le signe fermionique dans les estimateurs. Sans entrer dans les détails, on parle alors soit de méthodes “transientes” (transient methods), soit de méthodes avec “relâchement des nœuds” (nodal-release methods). En opérant de la sorte aucune erreur systématique n’est introduite. Malheureusement, en pratique, de telles approches sont très difficiles à faire converger. La raison fondamentale réside dans le fait qu’à grands temps de simulation la partie positive et la partie négative des estimateurs signés deviennent essentiellement égales, et c’est la différence exponentiellement négligeable qui nous intéresse! Comme l’erreur statistique est proportionnelle à la somme, et non à la différence des parties positives et négatives, le rapport signal sur bruit devient excessivement mauvais. Plus précisément, on peut montrer que l’erreur statistique croît exponentiellement avec le temps calcul T de la manière suivante:

$$\delta E = c \frac{\exp [K(E_{0F} - E_{0B})T]}{\sqrt{T}} \quad (18)$$

où c et K sont deux constantes positives et E_{0F} et E_{0B} sont respectivement les énergies fondamentales fermioniques (celle qui nous intéresse) et bosoniques (essentiellement, l’énergie qui correspondrait à des électrons qui auraient tous le droit de se condenser dans le niveau le plus bas). On peut également montrer que la différence $\Delta E = (E_{0F} - E_{0B})$ qui commande l’exposant de l’exponentiel croît également très rapidement avec le nombre de particules! Ce problème sévère est connu sous le nom de “problème du signe”. En trouver une solution est considéré comme un des problèmes les plus importants de la physique numérique. Remarquons tout de même qu’une telle formule ne signifie pas que tout calcul exact pour des électrons soit désespéré. Elle signifie seulement, qu’à ce jour, tout algorithme QMC exact est intrinsèquement instable. Des procédés astucieux ont été développés pour amoindrir les difficultés liées au problème du signe et des calculs “exacts” sur des systèmes réalistes ont pu être menés à bout malgré ces difficultés. Nous reviendrons sur ce point dans la section suivante: “Monte Carlo quantique en Chimie Théorique: où en est-on?”).

β .Signe dans le processus: approximation des nœuds fixés (fixed-node QMC)

Afin de contourner la difficulté du signe dans les estimateurs il est naturel d’essayer de construire des règles probabilistes qui incorporent directement l’antisymétrie. Ceci peut être réalisé très simplement en utilisant l’algorithme usuel présenté précédemment et une fonction d’onde d’essai correctement antisymétrisée. Le point nouveau par rapport au cas d’une fonction d’essai à signe constant est que les lieux (hypersurfaces) où la fonction d’essai s’annule (on parle des zéros ou des nœuds de la fonction d’onde) deviennent des barrières infranchissables pour les marcheurs (le terme de dérive donné par l’équation (12) correspond à un terme infiniment répulsif près des nœuds). En pratique, les marcheurs restent donc piégés dans les sous-volumes nodaux découpés par les nœuds de la fonction d’essai. Ceci revient à résoudre l’équation de Schrödinger avec de nouvelles conditions aux limites (annulation de la fonction d’onde exacte aux nœuds de la fonction d’essai). L’instabilité liée au signe disparaît alors complètement. Malheureusement, le prix à payer est l’introduction d’une erreur systématique (l’erreur dite “fixed-node”), résultant de la position approximative des nœuds de la fonction d’essai. Cependant, et c’est un point important, on peut démontrer qu’un calcul “fixed-node” est un calcul variationnel, c’est à dire qu’on a la propriété:

$$E_0(\text{Fixed - Node}) \geq E_0(\text{Exact}) \quad (19)$$

B. Monte Carlo quantique en chimie théorique: où en est-on?

En nous appuyant sur les quelques éléments présentés dans la section précédente on peut maintenant discuter l’“état de l’art” en chimie théorique des calculs électroniques par méthode Monte Carlo quantique.

1. Problème du signe.

Le premier point qu’il s’agit de commenter est la nature des difficultés associées au problème du signe pour les atomes et les molécules. Comme nous venons de le dire, il existe deux grandes classes de méthodes pour traiter ce problème: les méthodes exactes mais instables (“transient” ou “nodal-release” methods) et les méthodes stables mais approchées de type nœuds fixés (fixed-node). La première classe de méthodes a été appliquée avec succès à des systèmes comportant des atomes très légers. On peut citer le calcul de la surface de potentiel complète $H + H_2 \rightarrow H_2 + H$ qui joue un rôle important dans les calculs

de dynamique quantique [11] ainsi que quelques calculs “tous-electrons” pour des petits systèmes (LiH, Li₂ ..., voir par exemple la revue récente d’Anderson [8]). Notons que pour des systèmes homogènes en densité, comme les liquides et les solides quantiques, des calculs à très grand nombre d’électrons sont également possibles. On peut citer le célèbre calcul du gaz électronique uniforme par Ceperley et Alder [12] qui sert à calibrer les méthodes de type Density Functional Theory (DFT). Ce calcul correspond à une résolution exacte par méthode Monte Carlo quantique de l’équation de Schrödinger pour un grand nombre d’électrons (jusqu’à 246 électrons) à l’aide d’un schéma exact avec relâchement des nœuds. On peut également citer le calcul du diagramme de phase de l’hydrogène en fonction de la pression qui a été effectué sous différentes conditions [13]. Dans ce type de calculs, les auteurs se sont même affranchis de l’approximation de Born-Oppenheimer en résolvant l’équation de Schrödinger complète pour un grand nombre de protons et d’électrons (jusqu’à plusieurs centaines). Dans ces exemples, les quantités c , K et $\Delta E = E_{0F} - E_{0B}$ de la formule fondamentale (18) sont suffisamment petites pour que l’estimateur de l’énergie “converge” dans un temps raisonnable. Physiquement, ceci est relié au fait que le système simulé a une densité électronique relativement homogène sans grandes variations d’échelle en son sein. Dans le cas des molécules, ceci n’est absolument pas le cas. A cause du principe de Pauli et du caractère très inhomogène de l’attraction coulombienne des noyaux (avec charge éventuellement élevée), on doit décrire une densité électronique très structurée. Il y a des régions de cœur à haute densité d’énergie et des régions de valence beaucoup plus homogènes. Les zones où les liaisons chimiques s’établissent doivent être décrites avec précision. Il faut également être à un niveau de précision très grand pour espérer retrouver les effets subtils à longues distances (par exemple, les forces de van der Waals). Mathématiquement, cela se traduit par le fait que le préfacteur c de la formule (18) (relié à la qualité de la fonction d’onde d’essai utilisée) doit absolument être réduit le plus possible et que l’écart énergétique $\Delta E = E_{0F} - E_{0B}$ entre le fondamental physique et le fondamental “bosonique” (tous les électrons dans l’orbitale la plus basse) est très grand à cause de la structure en couche très prononcée.

Pour conclure, imaginer des calculs exacts pour des systèmes moléculaires lourds et structurés n’est actuellement pas réaliste à cause du comportement pathologique, Eq.(18). Cependant, et c’est le point fondamental, l’expérience numérique a montré que la méthode à nœuds fixés représente une très bonne approximation pour les molécules. Ceci est particulièrement vrai pour l’énergie mais cela semble aussi être vrai pour un certain nombre de propriétés au prix de développements spécifiques (voir, par exemple, le calcul très récent du dipôle de la molécule CO par Schautz et Flad [14]). Comme nous l’avons déjà mentionné une

propriété très intéressante des calculs fixed-node est le fait qu’il existe un principe variationnel pour l’énergie, Eq.(19). L’expérience montre qu’en choisissant, par exemple, les nœuds d’une fonction d’onde de type Hartree-Fock l’erreur fixed-node est déjà très petite. Pour fixer les idées, nous présentons dans le tableau I quelques résultats obtenus pour l’énergie totale de petits atomes et molécules (calcul “tous-électrons”). On voit que l’erreur fixed-node ne représente pour ces systèmes que quelques pourcents de l’énergie de corrélation totale. En d’autres mots, l’approximation fixed-node est tout à fait satisfaisante. Notons qu’on obtient également ce type de précision pour les calculs QMC avec pseudo-potentiels (voir plus loin).

TABLE I. Energies totales (“tous-électrons”) calculées par méthode Monte Carlo variationnelle (VMC) et par méthode QMC dans l’approximation des nœuds fixés (fixed-node). L’énergie de corrélation (EC) totale obtenue dans chaque cas est donnée en pourcentage. L’erreur statistique sur le dernier chiffre est donnée entre parenthèses.

Atome ou Molécule	$E_0(\text{HF})$	$E_0(\text{VMC})$	EC(%)	$E_0(\text{Fixed-Node})$	EC(%)	$E_0(\text{Exact})$
He (pas de nœuds)	-2.86168	-2.9037244(1) ^a	100.0000(2)			-2.90372437
LiH	-7.987	-8.06973(26) ^b	99.4(3)	-8.0699(10) ^c	100(1)	-8.07021
Li ₂	-14.87152	-14.98850(4)	94.43(4)	-14.9938(1) ^d	98.7(1)	-14.9954
Ne	-128.54705	-128.9011(1)	90.56(2)	-128.9236(2) ^a	96.32(4)	-128.93755
H ₂ O	-76.0675	-76.20(3) ^e	36(8)	-76.430(20) ^f	90.5(7)	-76.4376
N ₂	-108.9928	-109.4376(5)	80.94(8)	-109.505(1) ^d	93.1(2)	-109.5423
F ₂	-198.7701	-199.4101(6)	84.23(8)	-199.487(1) ^d	94.3(1)	-199.5299

^a Réf. [15]; ^b Réf. [16] ^c Réf. [17]; ^d Réf. [18]; ^e Réf. [10] ^f Réf. [19]

2. Choix de la fonction d’essai

Comme nous l’avons déjà mentionné, un aspect fondamental qui détermine la qualité des simulations est le choix de la fonction d’essai utilisée, ψ_T . Plus cette fonction d’onde est “proche” de la solution inconnue plus les fluctuations statistiques sur l’énergie totale sont faibles. De nombreux efforts ont été faits pour choisir les meilleures approximations possibles. Il est important d’insister sur le fait que le choix des formes possibles est très large puisque, contrairement aux méthodes sur base, aucune intégration de la fonction n’est effectuée au cours de la simulation. Seule la dérivée première [vecteur dérive, Eq.(12)] et la dérivée seconde [énergie locale, Eq.(8)] par rapport aux $3N$ variables sont requises. Sans entrer dans les détails des nombreux travaux effectués, on peut dire que les formes les plus élaborées considérées à ce jour s’écrivent essentiellement de la manière suivante:

$$\psi_T = \exp \left[\sum_{i < j} \sum_{\alpha} U_{\alpha}(r_{i\alpha}, r_{j\alpha}, r_{ij}) \right] \sum_K c_K \text{Det}_{\alpha}^K \text{Det}_{\beta}^K \quad (20)$$

La partie déterminantale est constituée d’une somme sur un ensemble de configurations au sens des méthodes *ab initio* traditionnelles. Les orbitales moléculaires utilisées proviennent généralement d’un programme *ab initio* sur base et sont le plus souvent réoptimisées dans le cadre de la méthode Monte Carlo quantique. Le nombre de configurations utilisées ne peut pas être très important car le Laplacien de la fonction d’essai doit être calculé à chaque pas Monte Carlo, et on effectue des millions de pas. Le préfacteur qui est écrit sous une forme exponentielle est habituellement désigné sous le vocable “terme de Jastrow”. C’est une partie qui dépend explicitement des coordonnées interelectroniques r_{ij} et de leur couplage avec les distances electrons-noyaux $r_{i\alpha}$ (l’indice grec porte ici sur les coordonnées nucléaires). Ce terme joue un rôle très important : il permet d’incorporer dans la fonction d’onde les comportements corrects de la fonction d’onde quand les électrons sont très proches (conditions dites de CUSP) ainsi que la réorganisation du nuage électronique quand la corrélation explicite entre électrons est prise en compte. En introduisant des paramètres variationnels dans les fonctions U_{α} et la partie déterminantale, il est possible de chercher des représentations optimales. Il est important de noter que cette étape d’optimisation des paramètres (éventuellement en grand nombre) peut être effectuée relativement aisément dans un formalisme QMC grâce à la méthode dite de “l’échantillonnage corrélée” introduite il y a une dizaine d’années par Umrigar et collaborateurs [20]. Les résultats obtenus avec de telles représentations sont déjà très bons. Suivant les systèmes, on peut récupérer assez facilement entre 40 et 90 % de l’énergie de corrélation au niveau variationnel. Quelques exemples illustratifs sont présentés dans le tableau I (calculs VMC).

Notons que le développement de fonctions d’onde d’essai de qualité constitue encore à mon avis un thème d’étude crucial pour les méthodes Monte Carlo quantique. En particulier, des formes beaucoup plus physiques pour ces fonctions peuvent encore être exploitées. Nous avons déjà discuté cet aspect dans la section II.B.6: “Meilleures fonction d’essai”.

3. Problème des électrons de cœur.

En utilisant les fonctions d’essai que nous venons de présenter on peut calculer l’énergie totale électronique pour des systèmes moléculaires comprenant au maximum une vingtaine d’électrons. Comme nous l’avons déjà discuté, le nombre maximal d’électrons qui peut être traité dépend en fait très fortement de la distribution des charges nucléaires. Définir un tel nombre sans faire référence aux propriétés du potentiel extérieur n’a pas réellement de

sens. La raison principale de l'existence de cette limite réside dans la difficulté de maîtriser les fluctuations internes dues aux électrons de cœur des atomes. De nombreuses tentatives ont été faites pour résoudre ou contourner cette difficulté. L'idée la plus naturelle qui vient à l'esprit est évidemment de geler les électrons de cœur d'une façon ou d'une autre comme cela est effectué dans les méthodes *ab initio* sur base. Plusieurs propositions ont été faites dans cette direction (Hamiltoniens modèles, pseudo-Hamiltoniens, "damped-core" approches, etc.). On ne détaillera pas ici ces différentes tentatives (pour cela, se reporter au livre de Hammond et collaborateurs, [7]) mais on notera que ce n'est qu'assez récemment qu'un algorithme stable et de portée générale a été mis au point [22]. Le résultat-clef a été de montrer que l'utilisation de projecteurs de type "potentiels de cœur effectifs" (Effective Core Potentials) et de fonctions d'onde d'essai de grande qualité pour les électrons de valence permet d'obtenir en pratique des résultats de grande qualité. L'Hamiltonien des électrons de valence est écrit sous la forme:

$$H_{val} = \sum_i -\frac{1}{2}\vec{\nabla}_i^2 + \sum_{i\alpha} V_{loc}(r_{i\alpha}) + \sum_{\alpha<\beta} Z_\alpha Z_\beta / R_{\alpha\beta} + \sum_{i<j} 1/r_{ij} + W_{nonloc} \quad (21)$$

où V_{loc} décrit l'attraction électron-noyau usuelle et W_{nonloc} est l'opérateur non-local qui projette sur les états de cœur:

$$W_{nonloc} = \sum_{i\alpha} \sum_{lm} v_l(r_{i\alpha}) Y_{lm}(\Omega_{i\alpha}) \int d\Omega'_{i\alpha} Y_{lm}^*(\Omega'_{i\alpha}) \quad (22)$$

où v_l représente le pseudo-potentiel radial et Y_{lm} les harmoniques sphériques usuelles. L'expérience montre que, si l'opérateur est rendu local de la manière suivante (la non-localité est *a priori* difficile à implémenter dans un schéma Monte Carlo)

$$W_{localise}(\mathbf{x}) = W_{nonloc}\psi_T(\mathbf{x})/\psi_T(\mathbf{x}) \quad (23)$$

et qu'une fonction ψ_T de qualité suffisante (c'est un point important) est utilisée, alors la méthode donne des résultats très satisfaisants. Pour illustrer le type de résultats obtenus nous présentons dans la tableau II quelques énergies de liaison d'agrégats et de molécules organiques, calculées avec des pseudo-potentiels dans l'approximation des nœuds fixés. Les résultats comparés aux résultats expérimentaux sont toujours très bons.

TABLE II. Quelques énergies de liaison calculées par méthode Monte Carlo quantique (QMC) dans l’approximation des nœuds fixés et utilisation de pseudo-potentiels. L’erreur statistique sur le dernier chiffre est donnée entre parenthèses

Energies de liaison(eV) de quelques molécules organiques ^a	HF	LDA	QMC	Exp.
Méthane (CH ₄)	14.20	20.59	18.28(5)	18.19
Acétylène (C ₂ H ₂)	12.70	20.49	17.53(5)	17.59
Ethane (C ₂ H ₆)	23.87	35.37	31.10(5)	30.85
Benzène (C ₆ H ₆)	44.44	70.01	59.2(1)	59.24

Energies de liaison (eV/atome) de qqes agrégats de Si ^b	HF	LDA	QMC	Exp.
Si ₂ (D _{2h})	0.85	1.98	1.580(7)	1.61(4)
Si ₃ (C _{3v})	1.12	2.92	2.374(8)	2.45(6)
Si ₇ (D _{5h})	1.91	4.14	3.43(2)	3.60(4)
Si ₁₀ (C _{3v})	1.89	4.32	3.48(2)	...
Si ₂₀ (C _{3v})	1.55	4.28	3.43(3)	...

^a Réf. [23]; ^b Réf. [24];

En conclusion, en utilisant les fonctions d’essai actuellement disponibles et l’approximation des nœuds fixés, on peut mener des calculs QMC “tous-électrons” de grande qualité pour des systèmes moléculaires ayant des charges nucléaires pas trop élevées et un nombre d’électrons relativement limité (disons une vingtaine d’électrons). Pour des systèmes plus gros, il est possible depuis peu d’éliminer de manière efficace les électrons de cœur responsables de la majeure partie de l’erreur statistique en utilisant des potentiels de cœur effectifs. Cette approche, couplée à l’utilisation de fonctions d’onde d’essai de qualité pour les électrons de valence, permet de traiter des systèmes de tailles comparables à celles traitées par les méthodes *ab initio* traditionnelles. Ce dernier point est extrêmement important car il rend les méthodes QMC compétitives. Il est donc prévisible que dans les années qui viennent les méthodes stochastiques se développent dans le milieu de la chimie théorique.

Terminons cette partie en présentant un travail très récent qui illustre le fait que les méthodes QMC sont sur le point de devenir des méthodes tout à fait compétitives vis à vis des méthodes *ab initio*. La figure qui suit présente quelques résultats obtenus par le groupe de Cambridge sur des système de type fullèrenes [25]. Le système étudié est la molécule C₂₄. Les deux électrons de cœur 1s ont été gelés par la technique présentée ci-dessus et les 24×4=96 électrons de valence sont traités dans l’approximation des nœuds fixés. Différentes structures (anneau, feuille, boule, cage, etc.) ont été calculées par QMC et par plusieurs

variantes des méthodes de type DFT. Sans entrer dans les détails, on voit que les résultats Monte Carlo quantique (DMC) sont très bons et, d'après les auteurs, d'une qualité supérieure à celle des résultats DFT.

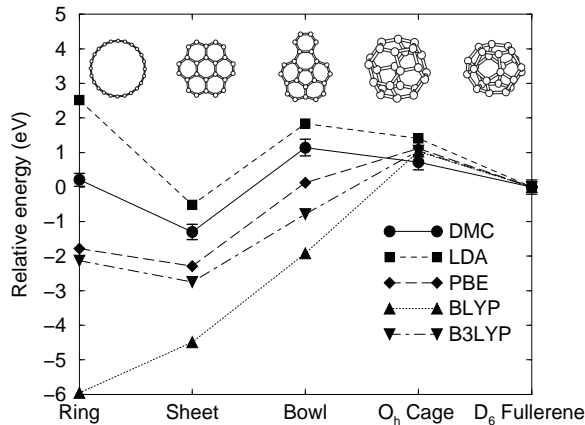


FIG. 2. Structures et énergies des isomères C_{24} relativement au fullérène D_6 . Les résultats Monte Carlo quantique sont indiqués sous le nom de DMC (Diffusion Monte Carlo)

-
- [1] N. Metropolis, A.W. Rosenbluth, M.N. Rosenbluth, A.H Teller, and E. Teller, *J. Chem. Phys.* **21**, 1097 (1953).
 - [2] M. Caffarel, "Introduction aux simulations numériques", support de cours de DEA, document disponible sur le serveur: <http://www.lpthe.jussieu.fr/DEA/>
 - [3] M. Caffarel, "Méthodes d'intégration fonctionnelle et méthodes stochastiques pour le traitement de problèmes quantiques. Application à la physique atomique et moléculaire", Doctorat de l'Université Paris 6, 27 Mars 1987.
 - [4] M. Caffarel and P. Claverie, "Treatment of the Schrödinger Equation Through a Monte Carlo Method Based upon the Generalized Feynman-Kac Formula", *J. Stat. Phys.* **43**, 797 (1986).
 - [5] M. Caffarel and P. Claverie, "Development of a pure diffusion quantum Monte Carlo method using a full generalized Feynman-Kac formula. I. Formalism", *J. Chem. Phys.* **88**, 1088 (1988).
 - [6] M. Caffarel and P. Claverie, "Development of a pure diffusion quantum Monte Carlo method using a full generalized Feynman-Kac formula. II. Application to simple systems", *J. Chem. Phys.* **88**, 1100 (1988).

- [7] B.L. Hammond, W.A. Lester, Jr., and P.J. Reynolds in *Monte Carlo Methods in Ab Initio Quantum Chemistry*, World Scientific Lecture and course notes in chemistry Vol.1 (1994).
- [8] J.B. Anderson in *Reviews in Computational Chemistry*, Vol.13, edited by K.B. Lipkowitz and D.B. Boyd (Wiley, 1999).
- [9] M. Caffarel, R. Assaraf, “A pedagogical introduction to quantum Monte Carlo”, à paraître in “Mathematical models and methods for *ab initio* Quantum Chemistry” in *Lecture Notes in Chemistry* (Springer).
- [10] D.M. Ceperley and B.J. Alder, *J. Chem. Phys.* **64**, 5833 (1984).
- [11] D.L. Diedrich and J.B. Anderson, *Science* **258**, 786 (1992); D.L. Diedrich and J.B. Anderson, *J. Chem. Phys.* **100**, 8089 (1994).
- [12] D.M. Ceperley and B.J. Alder, *Phys. Rev. Lett.* **45**, 566 (1980).
- [13] D.M. Ceperley and B.J. Alder, *Physica B* **108**, 876 (1981); D.M. Ceperley and B.J. Alder, *Phys. Rev. B* **36**, 2092 (1987); V. Natoli, R.M. Martin, and D.M. Ceperley, *Phys. Rev. Lett.* **70**, 1952 (1993).
- [14] F. Schautz and H.J. Flad, *J. Chem. Phys.* **110** 11700 (1999).
- [15] M.P. Nightingale and C.J. Umrigar in *Recent Advances in Computational Chemistry* Vol.2, edited by W.A. Lester Jr., World Scientific (1997).
- [16] K. Iguchi in *Recent Advances in Computational Chemistry* Vol.2, edited by W.A. Lester Jr., World Scientific (1997).
- [17] R.P. Subramanian, M.A. Lee, K.E. Schmidt, and J.W. Moskowitz, *J. Chem. Phys.* **97**, 2600 (1992).
- [18] C. Filippi and C.J. Umrigar, *J. Chem. Phys.* **105**, 213 (1996).
- [19] P.J. Reynolds, D.M. Ceperley, B.J. Alder and W.A. Lester, Jr., *J. Chem. Phys.* **77**, 5593 (1982).
- [20] C. J. Umrigar, K. G. Wilson, and J. W. Wilkins, *Phys. Rev. Lett.* **60**, 1719 (1988).
- [21] S. Zirah, “Méthodes Monte Carlo quantiques pour les molécules. Utilisation de formes Valence Bond”, Stage de Maîtrise-Licence, Université Paris-Sud (1998).
- [22] L. Mitas, E.L. Shirley, and D.M. Ceperley, *J. Chem. Phys.* **95**, 3467 (1991) et références dans: L. Mitas et J.C. Grossman in *Recent Advances in Computational Chemistry* Vol.2, edited by

- W.A. Lester Jr., World Scientific (1997).
- [23] J.C. Grossman, L. Mitas, and K. Raghavachari, *Phys. Rev. Lett.* **75**, 3870 (1995).
- [24] J.C. Grossman, and L. Mitas, *Phys. Rev. Lett.* **74**, 1323 (1995).
- [25] P.R.C. Kent, M.D. Towler, R.J. Needs, and G. Rajagopal, preprint physics/9909037 (1999).
- [26] R. Assaraf and M. Caffarel, “Zero-variance principle for Monte Carlo algorithms”, *Phys. Rev. Lett.* **83** , 4682 (1999).
- [27] R. Assaraf and M. Caffarel, “Computing observables with quantum Monte Carlo”, en préparation.
- [28] M. Caffarel and O. Hess, “Quantum Monte Carlo-Perturbation Calculations of Interaction Energies”, *Phys. Rev. A* **43**, 2139 (1991).
- [29] M. Caffarel and O. Hess “Computing Response Properties with Quantum Monte Carlo” in *AIP Conference Proceedings No 239, Advances in Biomolecular Simulations Obernai, France 1991* pp. 20-32.
- [30] M. Caffarel, M. Rérat, and C. Pouchan, “Evaluating Dynamic Multipole Polarizabilities and van Der Waals Dispersion Coefficients of two-electron Systems with a Quantum Monte Carlo Calculation: A Comparison with some *Ab Initio* Calculations”, *Phys. Rev. A* **47**, 3704 (1993).
- [31] C. Huiszoon and M. Caffarel, “A quantum Monte Carlo perturbational study of the He-He interaction”, *J. Chem. Phys.* **104**, 4621 (1996).
- [32] C. Filippi and C.J. Umrigar, “Correlated sampling in quantum Monte Carlo: a route to forces”, preprint cond-mat/9911326 (1999).
- [33] R. Assaraf and M. Caffarel, “Computing forces with quantum Monte Carlo”, *J. Chem. Phys.* **113** ,4028 (2000).
- [34] R. Assaraf, M. Caffarel, and A. Khelif, “Diffusion Monte Carlo Methods with a fixed-number of walkers”, *Phys. Rev. E.* **61**, 4566 (2000).
- [35] J.H. Hetherington, *Phys. Rev. A* **30**, 2713 (1984).

VI. PERSPECTIVES. MON PROJET DE RECHERCHE

Dans les années qui viennent je vais m'employer à développer les deux idées importantes que nous avons introduites récemment, à savoir le principe de zéro-variance et l'introduction de processus de reconfiguration stochastique. Ces deux idées vont permettre de diminuer de manière très significative les fluctuations statistiques et donc l'efficacité des méthodes Monte Carlo quantique. C'est un point très important que ce soit pour le calcul des propriétés électroniques des molécules ou pour la détermination des diagrammes de phase des systèmes de fermions fortement corrélés. Dans le domaine de la physique du solide, les méthodes QMC sont des méthodes bien établies et abondamment utilisées. Augmenter leur efficacité est essentiel car la plupart des effets subtils liés à la corrélation électronique n'apparaissent clairement qu'à des tailles, ou des nombres d'électrons, exigeant des simulations assez volumineuses. En Chimie Théorique les méthodes QMC sont d'utilisation plus limitée; nous en avons expliqué les raisons dans la section V. Toutefois, comme nous l'avons déjà souligné ces méthodes sont sur le point de devenir compétitives vis à vis des méthodes *ab initio* plus traditionnelles (Density Functional Theory (DFT) et/ou méthodes Hartree-Fock + traitement de la corrélation électronique) et nous vivons donc une période charnière de leur développement. Ceci a été rendu possible grâce à un ensemble d'améliorations méthodologiques qui se sont échelonnés sur les vingt dernières années: développement de fonctions d'essai de qualité, approche des nœuds-fixés, introduction d'une méthodologie de type pseudo-potentiels stable et efficace. Depuis peu, des applications sur des systèmes moléculaires réalistes incluant jusqu'à une centaine d'électrons actifs ont été effectués (agrégats d'atomes de Silicium ou de Carbone, molécules organiques, etc.). La raison essentielle pour laquelle les méthodes Monte Carlo sont encore trop peu utilisées dans la communauté de la Chimie Théorique est que, pour une édifice moléculaire complexe, il n'existe pas encore de procédure automatisée pour calculer efficacement n'importe quelle propriété (en particulier pour les forces et la plupart des observables). De plus, les volumes de calcul restent encore importants, quoique comparables à ceux des calculs *ab initio* les plus poussés ("grandes" interactions de configuration, calculs Coupled-Cluster de précision, etc.). Il est donc très important de remédier à ces limitations.

Comme nous l'avons déjà dit notre première direction de travail est la mise en pratique de notre principe de variance-zéro de portée très générale. Nous avons déjà montré qu'un tel principe permet le calcul des forces entre atomes au sein d'une molécule. C'est un résultat important puisque le calcul des forces est un des objectifs centraux de la chimie calculatoire et qu'il n'existait pas de moyen effectif pour le calcul de telles quantités dans les

approches QMC. Le principe de variance-zéro devrait également nous permettre d’aborder des quantités aussi délicates que les petites différences d’énergie et les propriétés de réponse sous champs. Le problème des fluctuations importantes associées aux électrons de cœur devrait également être abordé sous un angle nouveau. Comme nous l’avons déjà remarqué, ce sont les fluctuations de cœur qui sont responsables de la limitation des méthodes QMC “tous-électrons” aux systèmes ayant des petites charges nucléaires. La définition d’un formalisme QMC basé sur les pseudo-potentiels a constitué une étape importante: on peut maintenant aborder des systèmes assez complexes. Néanmoins, il est évident que les difficultés associées à l’utilisation de potentiels de cœur (contrôle de l’approximation effectuée, problème de l’interaction cœur-valence, polarisation du cœur, etc.) subsistent comme dans les méthodes *ab initio* sur base. A terme, il est donc souhaitable de rester dans une approche “tous-électrons”. L’objectif à atteindre est de réduire les fluctuations de cœur au niveau de celles des électrons de valence. Ceci semble tout à fait possible en “renormalisant” la partie très fluctuante de l’énergie locale associée aux électrons de cœur. J’ai commencé ce projet en collaboration avec R. Assaraf et P. Reinhardt au laboratoire. Ce travail comprend une partie exploratoire assez importante (partition de l’énergie locale, choix de la représentation pour la fonction d’essai associée au principe de variance zéro, etc.) mais je ne doute pas qu’il soit possible d’atténuer grandement les fluctuations de cœur.

Le deuxième axe de recherche est l’exploitation du processus dit de reconfiguration stochastique en vue d’accélérer la convergence des simulations Monte Carlo quantique (réduction des volumes de calcul pour une précision donnée). En effet, nous nous sommes aperçus que, grâce au processus de reconfiguration d’une population de marcheurs, il était possible de réaliser une idée très intéressante du point de vue mathématique. A savoir, l’introduction de corrélation entre marcheurs sans changement de la densité stationnaire associée à chaque marcheur individuellement. En jouant sur la nature des corrélations entre marcheurs, on peut modifier de manière importante la vitesse de convergence d’une observable donnée calculée à partir des populations successives sans changer sa valeur moyenne. Pour illustrer les potentialités d’une telle approche je présente dans le tableau suivant quelques calculs préliminaires effectués en collaboration avec R. Assaraf et A. Khelif. Il s’agit du calcul d’une observable pour un système modèle de taille finie (matrice 200 par 200). Je donne les résultats obtenus avec différents niveaux de corrélation entre marcheurs. La population considérée comprend 4096 marcheurs et un million de pas Monte Carlo pour chaque marcheur. J’insiste sur le fait que chaque résultat nécessite (à des variations négligeables près) le même effort numérique. Le premier résultat (Monte Carlo standard) correspond à l’approche habituelle sans corrélation entre marcheurs. Les trois autres résultats correspon-

dent à des niveaux différents de corrélation. On voit que l’amélioration de convergence peut être spectaculaire. Dans le meilleur des cas (Reconfiguration avec choix alterné) on obtient un rapport d’erreur statistique égal à $0.1100/0.0068$, ce qui correspond à un gain de l’ordre de 300 en temps calcul (l’erreur se comporte en $1/\sqrt{N}$). Evidemment, il s’agit d’être prudent et de ne pas généraliser trop vite des résultats obtenus sur un système modèle simple à des systèmes réalistes. Toutefois, nos premiers résultats sur des atomes légers indiquent qu’il y a en effet une amélioration sensible de la convergence. Il reste encore beaucoup d’aspects à élucider (en particulier, la détermination des corrélations optimales) mais l’idée doit être développée.

TABLE III. Calcul d’une valeur moyenne pour un système modèle à 200 états. Le nombre de marcheurs est 4096, le nombre de pas Monte Carlo pour chaque marcheur est de 10^6 . L’erreur statistique sur le dernier chiffre est donnée entre parenthèses

Méthode	$\langle O \rangle$
Monte Carlo standard	320.86(0.11)
Reconfiguration standard	320.98(0.039)
Reconfiguration avec choix aléatoire	320.935(0.010)
Reconfiguration avec choix alterné	320.953(0.0068)
Valeur exacte	320.944181...

On peut imaginer généraliser cette idée aux corrélations spatiales et temporelles des marcheurs sur le processus. Ceci permettrait de réaborder le problème si important du signe sous un angle nouveau. Par exemple, en cherchant à déterminer quelles sont les corrélations spatio-temporelles entre marcheurs qui permettraient d’asservir les fluctuations du signe fermionique et donc de réduire (supprimer?) le fameux “problème du signe” qui surgit quand on cherche à s’affranchir de l’approximation des nœuds fixés.

VII. PAPIERS PRINCIPAUX

- A. M. Caffarel and P. Claverie, "Development of a pure diffusion quantum Monte Carlo method using a full generalized Feynman-Kac formula. I. Formalism", *J. Chem. Phys.* 88, 1088 (1988)

Development of a pure diffusion quantum Monte Carlo method using a full generalized Feynman–Kac formula. I. Formalism

Michel Caffarel and Pierre Claverie

Dynamique des Interactions Moléculaires, Université Pierre et Marie Curie, Paris VI, Tour 22, 4 Place Jussieu, 75252 Paris, Cedex 05, France

(Received 26 January 1987; accepted 15 September 1987)

This paper presents systematic developments in the previously initiated line of research concerning a quantum Monte Carlo (QMC) method based on the use of a pure diffusion process corresponding to some reference function and a generalized Feynman–Kac path integral formalism. Not only mean values of quantum observables, but also response properties are expressed using suitable path integrals involving the diffusion measure of the reference diffusion process. Moreover, by relying on the ergodic character of this process, path integrals may be evaluated as time-averages along any sample trajectory of the process. This property is of crucial importance for the computer implementation of the method. As concerns the treatment of many-fermion systems, where the Pauli principle must be taken into account, we can use the fixed-node approximation, but we also discuss the potentially exact release-node procedure, whereby some adequate symmetry is imposed on the integrand (of the generalized Feynman–Kac formula), associated with a possibly refined choice of the reference function.

I. INTRODUCTION

This paper deals with the treatment of the time-independent Schrödinger equation using a Monte Carlo method. Essentially, the purpose of this method is to obtain values of observables pertaining to the lowest eigenstate(s) of any given symmetry type. The “observables” are the usual quantum averages associated with the eigenstate under consideration (e.g., energy, dipole moment,...) or response properties which are usually written as second-order perturbation expressions (e.g., static and dynamic polarizabilities).

Monte Carlo methods have been used with success in treating many-body boson systems.^{1–6} Unfortunately, due to the Pauli principle requirements for fermion systems, atoms and molecules are much less easy to manage. A basic reason for this is the nonconstant sign of Fermi wave functions, a property which implies unavoidable numerical difficulties. Nevertheless, for about 15 years specific Monte Carlo schemes for dealing with molecular systems have been developed. A few approaches have resulted^{7–14} and very accurate results for total energies on systems involving a number of 2–10 electrons have been obtained.^{9,14–17} Further methodological developments are presently under investigation, particularly to calculate excited state energies and ground state properties other than energy.¹⁸

The basic common idea of these different approaches, called quantum Monte Carlo (QMC) methods, rests on the similarity between the time-dependent Schrödinger equation in imaginary time and a generalized diffusion equation. These methods have important advantages:

(i) The exact resolution of the Schrödinger equation within the statistical errors due to the finite simulation time (no “truncation error” as occurs unavoidably in the framework of variational methods due to the use of finite basis sets).

(ii) The computational complexity of the code increases slowly with the number of particles. An increase proportion-

al to n^3 at most is expected for fermionic problems with two-body potentials as explained in Ref. 9 (see note 20) for systems of given density. However, if we consider systems with a density increasing with n such as atoms with higher and higher Z , then a more rapid increase of the computation time as a function of n could happen.¹⁹

(iii) Memory requirements remain perfectly bounded (as opposed to the very fast increase of memory required in variational approaches).

(iv) The short and simple codes are very well suited for vector computing and more specifically for multitasking proper.

A new quantum Monte Carlo method is presented here. We have developed the line of investigation initiated by Soto and Claverie²⁰ aiming at the design of a Monte Carlo method based on the use of a generalized Feynman–Kac formula applied to a pure diffusion process. More precisely, we have further extended here the previous generalized Feynman–Kac (GFK) formula^{20,21} into a so-called full generalized Feynman–Kac (FGFK) formula. The former (GFK) formula expresses as a functional integral the matrix elements of the (imaginary-time) evolution operator $\exp(-tH)$ and thus gives access essentially to energy eigenvalues of H . Now, the latter (FGFK) formula expresses matrix elements of operator products such as

$\exp(-\tau_1 H)A_1 \exp(-\tau_2 H)A_2 \cdots A_q \exp(-\tau_{q+1} H)$, where $\sum_{i=1}^q \tau_i = t$ and the A_i 's are q scalar multiplicative operators. This enables us to evaluate not only *mean values* of such operators A_i (so-called “first-order” properties in perturbation-theoretic language), but also n -time “quantum correlation functions” (in terms of the Heisenberg picture, cf. e.g., Ref. 22), which are related to *response properties*: e.g., for $n = 2$ we get second-order response properties such as polarizabilities (static and dynamic as well). These various matrix elements involve the evolution operator $\exp(-tH)$ with t arbitrary but fixed. They will be ultimately evaluated as suitable time-averages over sample trajector-

ies for a long enough simulation time T (theoretically we should take the limit $T \rightarrow +\infty$ for fixed t). The clear distinction between t and T is of overwhelming importance and will be emphasized at appropriate places below.

The underlying stochastic process (with respect to which our functional integrals are defined) is a *pure diffusion* process, associated with some reference function $\varphi_0^{(0)}$: no branching is involved, in contrast with most proposals of quantum Monte Carlo schemes presented so far.^{7,9,14} Some connection with these methods can be established by noticing that their branching term plays a role which is analogous with the role played in our own approach by the ‘‘Feynman–Kac integrand’’ $\exp\{-\int V_p[X(s)]ds\}$ which appears in the FGFK formula (cf. Sec. III). This point has been noticed by Ceperley and Alder¹⁴ [see their Eq. (11)] and Pollock and Ceperley²³ [see Eq. (A5) in their Appendix A]. Details about the correspondence with our present formalism are provided in the Appendix. Another point which deserves to be mentioned is the fact that in previous Monte Carlo methods the simulation time T is also the imaginary time appearing in the evolution operator. In our notation this amounts to putting $t = T$. We shall see below how the possibility of distinguishing t and T may be advantageous, especially in order to keep variance under control.

As recalled above, a serious challenge for all Monte Carlo methods is the treatment of many-fermion systems due to the specific constraints imposed by the Pauli principle. We therefore paid due attention to this problem, and we discuss several ways of solving it.

The full mathematical details are reported elsewhere in previous papers.²⁰ However, in order to make the present paper self-contained, all that is necessary to understand the theory is briefly recalled at each appropriate place.

The contents of this paper are as follows. In Sec. II we present the basic similarity transformation which permits mathematically connecting the quantum formalism with the stochastic processes. The essential idea is to associate a diffusion process with some given reference function $\varphi_0^{(0)}$ (to which a ‘‘reference Hamiltonian’’ $H^{(0)}$ is also associated). Section III is devoted to the presentation and derivation of the full generalized Feynman–Kac formula alluded to above. In Sec. IV we describe how this FGFK formula can be used for expressing quantum observables (mean values and response properties). In Sec. V we give an outline of the theoretical algorithm (further details concerning its computer implementation are deferred to a companion paper). Section VI deals with the Pauli principle requirements and with some directions for treating this problem. Finally, Sec. VII presents some conclusions and perspectives.

II. DIFFUSION PROCESS ASSOCIATED WITH AN ARBITRARY REFERENCE FUNCTION

We are interested in the nonrelativistic quantum problem of N particles interacting via a potential $V(x)$ (x denotes the $3N$ space-coordinates r_1, r_2, \dots, r_N). For the sake of simplicity atomic units will be used throughout the paper and the same electronic mass $m_e = 1$ is chosen for the N particles. The Hamiltonian operator is written

$$H = -\frac{1}{2}\nabla^2 + V. \quad (2.1)$$

Following previous authors²⁴ this Hamiltonian operator H may be changed through a similarity transformation into the Fokker–Planck operator L of a diffusion process. With φ_i denoting an arbitrary eigenstate of H and E_i the associated energy, it can be proven after simple algebra that²⁰

$$\varphi_i(E_i - H)1/\varphi_i = L, \quad (2.2)$$

where L is a Fokker–Planck operator:

$$L = \frac{1}{2}\mathcal{D}\nabla^2 - \nabla(\mathbf{b}) \quad (2.3)$$

The ‘‘drift’’ vector \mathbf{b} and the diffusion coefficient \mathcal{D} are given by

$$\mathbf{b} = \nabla\varphi_i/\varphi_i, \quad (2.4a)$$

$$\mathcal{D} = 1. \quad (2.4b)$$

From equality (2.2) it follows the expression of the eigenfunctions and eigenvalues of the Fokker–Planck operator L :

$$L\varphi_i\varphi_k = (E_i - E_k)\varphi_i\varphi_k. \quad (2.5)$$

In this last expression (E_k, φ_k) are the eigensolutions of the usual eigenproblem, namely

$$H\varphi_k = E_k\varphi_k \quad (2.6a)$$

but with the *unusual boundary conditions*

$$\varphi_k = 0 \quad \text{at any point where } \varphi_i = 0. \quad (2.6b)$$

Because of these possibly unusual boundary conditions, it is clear that the previous eigensolutions may differ from the usual ones. As a particular case, if φ_i is chosen to be the nodeless bosonic ground state, φ_0 , no extra boundary conditions are introduced (since φ_0 does not vanish at finite distances) and the previous eigenvalues E_k are the usual eigenvalues of H obtained from the usual boundary conditions. This possible modification of the spectrum due to the nodal hypersurfaces of φ_i is responsible for the so-called ‘‘fixed-node’’ approximation (for more details see Sec. VI dealing with the Pauli principle). In addition, note that the wavefunction φ_i is now a ground state in the new eigenvalue problem (2.6). From equality (2.5) we deduce that the stationary probability density $p(x)$ of the diffusion process (which is defined as the eigenfunction of L corresponding to the zero eigenvalue) is nothing but the probability density associated with the wave function, namely

$$p(x) = \varphi_i^2(x). \quad (2.7)$$

Now, it is possible to generalize this construction, that is, to associate a diffusion process with any arbitrary function. The generalization rests on the fact that any given function can always be considered as an eigenstate of a Hamiltonian built from it. We decided to note as $\varphi_0^{(0)}$ this arbitrary function and $H^{(0)}$ the associated Hamiltonian. The expression of $H^{(0)}$ in terms of the function $\varphi_0^{(0)}$ is given by

$$H^{(0)} = -\frac{1}{2}\nabla^2 + V^{(0)}, \quad (2.8a)$$

where

$$V^{(0)} = E_0^{(0)} + \frac{1}{2}\nabla^2\varphi_0^{(0)}/\varphi_0^{(0)}. \quad (2.8b)$$

Throughout the paper, the function $\varphi_0^{(0)}$ will be called ‘‘reference function’’ and $H^{(0)}$ ‘‘reference Hamiltonian.’’ In order to avoid any risk of confusion, the superscript (0) will

always be used to label quantities related to $H^{(0)}$. Note that only derivations have to be performed to determine $H^{(0)}$ and that the constant $E_0^{(0)}$ in Eq. (2.8b) may be chosen arbitrarily. Now, we can apply to this Hamiltonian $H^{(0)}$ the similarity transformation exactly in the same way as done in Eq. (2.2). We get the following basic relations:

$$\varphi_0^{(0)}(E_0^{(0)} - H_0^{(0)})1/\varphi_0^{(0)} = L^{(0)}, \quad (2.9)$$

where $L^{(0)}$ is the "reference" Fokker-Planck operator

$$L^{(0)} = \frac{1}{2} \mathcal{D} \nabla^2 - \nabla(\mathbf{b}) \quad (2.10)$$

with

$$\mathbf{b} = \nabla \varphi_0^{(0)}/\varphi_0^{(0)}, \quad (2.11a)$$

$$\mathcal{D} = 1. \quad (2.11b)$$

Of course, if the reference function $\varphi_0^{(0)}$ is chosen to be one of the eigenstates of H and $E_0^{(0)}$ the corresponding energy, we are led to the previous particular case where $H^{(0)} = H$.

Finally, let us now present a fundamental relation derived from the basic similarity transformation (2.9). A stationary diffusion process is entirely determined by its transition probability density defined as

$$p^{(0)}(x|y,t) = \langle y|e^{tL^{(0)}}|x\rangle, \quad (2.12)$$

where $L^{(0)}$ is the Fokker-Planck operator of the diffusion process. Note that we use a bracket enclosing the conditioning variable x instead of a simple bar as usual. Now, from Eq. (2.9) we get

$$p^{(0)}(x|y,t) = \varphi_0^{(0)}(y)/\varphi_0^{(0)}(x)e^{tE_0^{(0)}}G^{(0)}(x,y;t), \quad (2.13)$$

where $G^{(0)}(x,y;t)$ is the quantum time-dependent Green's function (in imaginary time) defined as

$$G^{(0)}(x,y;t) = \langle x|e^{-tH^{(0)}}|y\rangle. \quad (2.14)$$

The fundamental relation (2.13) between the quantum Green's function of $H^{(0)}$ and the Green's function of $L^{(0)}$, i.e., the transition probability density of the process, will permit us to express quantum quantities related to $H^{(0)}$ in terms of suitable averages pertaining to the diffusion process and conversely. However, we are interested in quantum properties related to H and not to $H^{(0)}$ and, except for a few very simple systems for which eigenstates of H are known, these two Hamiltonians will be different. The aim of the next Section is to present a possible way of escaping from this difficulty using a so-called "full generalized Feynman-Kac formula."

III. THE FULL GENERALIZED FEYNMAN-KAC FORMULA

Let us decompose the Hamiltonian into two parts:

$$H = H^{(0)} + V_p, \quad (3.1)$$

where $H^{(0)}$ is the reference Hamiltonian built from the reference function $\varphi_0^{(0)}$ and V_p the "perturbing" potential defined as the difference $H - H^{(0)}$. From Eqs. (2.1) and (2.8) we get the expression of the perturbing potential in terms of the reference function:

$$V_p = V - V^{(0)} = V - E_0^{(0)} - \frac{1}{2}\nabla^2\varphi_0^{(0)}/\varphi_0^{(0)}. \quad (3.2)$$

The usual Feynman-Kac formula expresses the quantum time-dependent Green's function (in imaginary time) in terms of a functional integral^{25,26}:

$$G(x,y;t) = \int_{\Omega(x,-t/2;y,t/2)} \times \exp \left[- \int_{-t/2}^{t/2} V_p[X(s)]ds \right] D^W X, \quad (3.3)$$

where $\Omega(x,-t/2;y,t/2)$ denotes the set of continuous trajectories starting from x at time $-t/2$ and ending at y at time $t/2$. In this formula V_p is defined by $H = -\frac{1}{2}\nabla^2 + V_p$, which is of the form (3.1) with $H^{(0)} = -\frac{1}{2}\nabla^2$ (free-particle Hamiltonian). The functional measure $D^W X$ is the usual Wiener measure. It is well known that it can be reinterpreted as a diffusion measure, namely the diffusion measure associated with the free Brownian process (see e.g., Sec. I.3.1 in Ref. 27, see also Ref. 28). Note that this later process is the diffusion process obtained from the similarity transformation (2.9) with $H^{(0)} = -\frac{1}{2}\nabla^2$, $\varphi_0^{(0)} = 1$ and $E_0^{(0)} = 0$.

Glimm and Jaffe (Sec. I.3 in Ref. 27) have given a first generalization of this formula. Using the decomposition

$$H = -\frac{1}{2}\nabla^2 + \frac{1}{2}x^2 - \frac{1}{2} + V_p(x), \quad (3.4)$$

they derived a generalized Feynman-Kac formula written in the form:

$$G(x,y;t) = \int_{\Omega(x,-t/2;y,t/2)} \times \exp \left[- \int_{-t/2}^{t/2} V_p[X(s)]ds \right] D^{GJ} X. \quad (3.5)$$

In their derivation they introduced explicitly a diffusion process associated with the harmonic oscillator (the Ornstein-Uhlenbeck process) which corresponds in our language to the diffusion process obtained from the similarity transformation (2.9) with $H^{(0)} = -\frac{1}{2}\nabla^2 + \frac{1}{2}x^2 - \frac{1}{2}$, $\varphi_0^{(0)} = e^{-x^2/2}$ and $E_0^{(0)} = 0$. In formula (3.5) above, we denote as $D^{GJ} X$ the diffusion measure associated with the diffusion process built from the Gaussian reference function²⁷ (the superscript GJ in $D^{GJ} X$ stands for Glimm and Jaffe).

A generalization of this approach has been made by Soto and Claverie²⁰ to the more general case of an arbitrary non-perturbed Hamiltonian $H^{(0)}$, thus encompassing the two previous trivial cases of the free particle (Feynman-Kac formula with $H^{(0)} = -\frac{1}{2}\nabla^2$) and of the harmonic oscillator (Glimm and Jaffe with $H^{(0)} = -\frac{1}{2}\nabla^2 + \frac{1}{2}x^2 - \frac{1}{2}$). This generalized Feynman-Kac formula corresponding to $H = H^{(0)} + V_p$ is written

$$G(x,y;t) = \int_{\Omega(x,-t/2;y,t/2)} \times \exp \left[- \int_{-t/2}^{t/2} V_p[X(s)]ds \right] D^{\varphi_0^{(0)}} X, \quad (3.6)$$

where the measure $D^{\varphi_0^{(0)}} X$ is the diffusion measure²⁹ associated with the diffusion process built from the reference function $\varphi_0^{(0)}$.

We shall now derive a very general formula including all the previous ones and allowing to evaluate all quantum mean values we are interested in. This formula is written

$$\begin{aligned}
 & I_{A_1 \dots A_q}(t; t_1, \dots, t_q) \\
 &= \langle f\varphi_0^{(0)} | e^{-(t_1+t/2)(H-E_0^{(0)})} A_1 e^{-(t_2-t_1)(H-E_0^{(0)})} \\
 &\quad \times A_2 \dots A_q e^{-(t/2-t_q)(H-E_0^{(0)})} | g\varphi_0^{(0)} \rangle \\
 &= \int_{\Omega(-t/2, t/2)} f[X(-t/2)] \\
 &\quad \times A_1[X(t_1)] \dots A_q[X(t_q)] g[X(t/2)] \\
 &\quad \times \exp \left[- \int_{-t/2}^{t/2} V_p[X(s)] ds \right] D^{\varphi_0^{(0)}} X \quad (3.7)
 \end{aligned}$$

with $-t/2 < t_1 \leq t_2 \dots \leq t_q < t/2$. The A_i 's are q scalar multiplicative operators and f, g two arbitrary functions verifying

$$\int f\varphi_0^{(0)2} dx < \infty \text{ and } \int g\varphi_0^{(0)2} dx < \infty.$$

$\Omega(-t/2, t/2)$ is the set of continuous trajectories defined in the time interval $(-t/2, t/2)$.

Proof

Let us note $\tau_1 = t_1 + t/2, \tau_2 = t_2 - t_1, \dots, \tau_{i+1} = t_{i+1} - t_i, \dots, \tau_{q+1} = t/2 - t_q$:

$$R^{(0)} = E_0^{(0)} - H^{(0)} \quad (3.8)$$

and $I = I_{A_1 \dots A_q}(t; t_1, \dots, t_q)$.

We then have

$$\begin{aligned}
 I &= \langle f\varphi_0^{(0)} | e^{\tau_1 R^{(0)}} A_1 e^{-\tau_1 V_p} A_1 \dots A_i e^{\tau_{i+1} R^{(0)}} A_{i+1} e^{-\tau_{i+1} V_p} A_{i+1} \\
 &\quad \times \dots A_q e^{\tau_{q+1} R^{(0)}} A_q e^{-\tau_{q+1} V_p} | g\varphi_0^{(0)} \rangle.
 \end{aligned}$$

Using the usual following Trotter formula

$$e^{A+B} = \lim_{n \rightarrow +\infty} [e^{A/n} e^{B/n}]^n \quad (3.9)$$

$$\begin{aligned}
 I &= \lim_{n \rightarrow +\infty} \int \prod_{j=1}^{q+1} \prod_{i=0}^n dX_{2i}^{(j)} \langle f\varphi_0^{(0)} | X_0^{(1)} \rangle \varphi_0^{(0)}(X_0^{(1)}) \prod_{j=1}^q \frac{\varphi_0^{(0)}(X_0^{(j+1)})}{\varphi_0^{(0)}(X_{2n}^{(j)})} \prod_{i=0}^{2n-2,2} p^{(0)}(X_i^{(j)}) X_{i+2}^{(j)}, \epsilon_j e^{-\epsilon_j V_p(X_{i+2}^{(j)})} \\
 &\quad \times \prod_{j=1}^q \langle X_{2n}^{(j)} | A_j | X_0^{(j+1)} \rangle \prod_{i=0}^{2n-2,2} p^{(0)}(X_i^{(q+1)}) X_{i+2}^{(q+1)}, \epsilon_{q+1} e^{-\epsilon_{q+1} V_p(X_{i+2}^{(q+1)})} \frac{1}{\varphi_0^{(0)}(X_{2n}^{(q+1)})} \langle X_{2n}^{(q+1)} | g\varphi_0^{(0)} \rangle.
 \end{aligned}$$

The A_i 's are scalar multiplicative operators, we then have

$$\langle X_{2n}^{(j)} | A_j | X_0^{(j+1)} \rangle = \delta(X_{2n}^{(j)} - X_0^{(j+1)}) A_j(X_0^{(j+1)}). \quad (3.12)$$

Inserting Eq. (3.12) into the expression of I and integrating over $X_{2i}^{(j)}$ (for $j = 1$ to q), we get, after the change of notation $X_{2i}^{(j)} \rightarrow X_i^{(j)}$:

$$\begin{aligned}
 I &= \lim_{n \rightarrow +\infty} \int \prod_{j=1}^{q+1} \prod_{i=0}^{n-1} dX_i^{(j)} dX_n^{(q+1)} f(X_0^{(1)}) \\
 &\quad \times \prod_{j=1}^q A_j(X_0^{(j+1)}) g(X_n^{(q+1)}) \prod_{j=1}^{q+1} \prod_{i=0}^{n-1} e^{-\epsilon_j V_p(X_{i+1}^{(j)})}
 \end{aligned}$$

we obtain

$$\begin{aligned}
 I &= \lim_{n \rightarrow +\infty} \langle f\varphi_0^{(0)} | [e^{\epsilon_1 R^{(0)}} e^{-\epsilon_1 V_p}]^n A_1 \\
 &\quad \times \dots A_i [e^{\epsilon_{i+1} R^{(0)}} e^{-\epsilon_{i+1} V_p}]^n A_{i+1} \\
 &\quad \times \dots A_q [e^{\epsilon_{q+1} R^{(0)}} e^{-\epsilon_{q+1} V_p}]^n | g\varphi_0^{(0)} \rangle,
 \end{aligned}$$

where $\epsilon_i = \tau_i/n$.

Introducing the spectral resolution of operator X , namely

$$1 = \int dX |X\rangle \langle X| \quad (3.10)$$

between each operator involved in the above matrix element we get

$$\begin{aligned}
 I &= \lim_{n \rightarrow +\infty} \int \prod_{j=1}^{q+1} \prod_{i=0}^{2n} dX_i^{(j)} \langle f\varphi_0^{(0)} | X_0^{(1)} \rangle \\
 &\quad \times \prod_{j=1}^{q+1} \prod_{i=0}^{2n-2,2} \langle X_i^{(j)} | e^{\epsilon_j R^{(0)}} | X_{i+1}^{(j)} \rangle \langle X_{i+1}^{(j)} | e^{-\epsilon_j V_p} | X_{i+2}^{(j)} \rangle \\
 &\quad \times \prod_{j=1}^q \langle X_{2n}^{(j)} | A_j | X_0^{(j+1)} \rangle \langle X_{2n}^{(q+1)} | g\varphi_0^{(0)} \rangle,
 \end{aligned}$$

where $\prod_{i=0}^{n,m}$ means $\prod_{i=0}^n$ with steps of size m .

Using relations

$$\langle X_{i+1}^{(j)} | e^{-\epsilon_j V_p} | X_{i+2}^{(j)} \rangle = \delta(X_{i+1}^{(j)} - X_{i+2}^{(j)}) e^{-\epsilon_j V_p(X_{i+2}^{(j)})}, \quad (3.11a)$$

$$\begin{aligned}
 \langle X_i^{(j)} | e^{\epsilon_j R^{(0)}} | X_{i+1}^{(j)} \rangle &= \varphi_0^{(0)}(X_i^{(j)}) / \varphi_0^{(0)}(X_{i+1}^{(j)}) p^{(0)}(X_i^{(j)}) X_{i+1}^{(j)}, \epsilon_j, \\
 &\quad (3.11b)
 \end{aligned}$$

where relation (3.11b) results from Eqs. (2.13), (2.14), and (3.8), and after integrating over variables $X_{2i+1}^{(j)}$ (for $i = 0$ to $n-1$ and $j = 1$ to $q+1$), we obtain

$$\times \varphi_0^{(0)2}(X_0^{(1)}) \prod_{j=1}^{q+1} \prod_{i=0}^{n-1} p^{(0)}(X_i^{(j)}) X_{i+1}^{(j)}, \epsilon_j.$$

In the last formula and below, we use the convenient identity:

$$X_n^{(j)} \equiv X_0^{(j+1)} \quad (\text{for } j = 1 \text{ to } q).$$

Using the fundamental property for stationary Markovian processes, namely

$$\begin{aligned}
 p_n^{(0)}(X_1, t_1; \dots; X_n, t_n) &= p^{(0)}(X_1) \prod_{i=1}^{n-1} p^{(0)}(X_i | X_{i+1}, t_{i+1} - t_i), \\
 &\quad (3.13)
 \end{aligned}$$

where $p_n^{(0)}$ is the n -time probability density of the diffusion process, we get

$$\begin{aligned}
 I &= \lim_{n \rightarrow +\infty} \int f(X_0^{(1)}) \prod_{j=1}^q A_j(X_0^{(j+1)}) g(X_n^{(q+1)}) \\
 &\quad \times \prod_{j=1}^{q+1} \prod_{i=0}^{n-1} e^{-\epsilon_j V_p(X_i^{(j)})} \\
 &\quad \times p_{n(q+1)+1}^{(0)}(X_0^{(1)}, -t/2; \dots; X_n^{(q+1)}, t/2) \\
 &\quad \times \prod_{j=1}^{q+1} \prod_{i=0}^{n-1} dX_i^{(j)} dX_n^{(q+1)}. \quad (3.14)
 \end{aligned}$$

This expression is symbolically written as:

$$\int_{\Omega(-t/2; t/2)} f[X(-t/2)] A_1[X(t_1)] \dots A_q[X(t_q)] \\
 \times g[X(t/2)] \exp \left[- \int_{-t/2}^{t/2} V_p[X(s)] ds \right] D^{\varphi_0^{(0)}} X$$

Q.E.D.

We give to this equality the name of “full generalized Feynman–Kac (FGFK) formula.”

At this point, it is interesting to notice that the full generalized Feynman–Kac formula (3.7) is essentially based on the possibility of expressing the diffusion measure $D^{\varphi_0} X$ (associated with the exact eigenstate φ_0 of H) in terms of the diffusion measure $D^{\varphi_0^{(0)}} X$ (associated with the reference function $\varphi_0^{(0)}$) through a suitable “relative density” (the so-called Radon–Nikodym derivative: see Chap. III, Sec. 12 in Ref. 29), which can be noted $D^{\varphi_0} X / D^{\varphi_0^{(0)}} X$. This relative density (pertaining to function space!) is actually given (except for a normalization constant) by the “Feynman–Kac integrand” in the long time limit $\lim_{t \rightarrow +\infty} \exp \left\{ - \int_{-t/2}^{t/2} V_p[X(s)] ds \right\}$. The normalization factor actually appears explicitly in the expressions for operator mean values derived in the next section.

Now, it is of crucial importance to remark that the diffusion measure, $D^{\varphi_0^{(0)}} X$, involved in the path integrals may be chosen ergodic. A diffusion measure is said to be ergodic when any sample trajectory is recurrent in space. A theorem due to Has’minskii³⁰ shows that integrability of the stationary density $p^{(0)}(x)$, i.e., $\int p^{(0)}(x) dx < \infty$, is a sufficient condition for ergodicity. Accordingly, if the reference function $\varphi_0^{(0)}$ has been chosen such that $p^{(0)}(x) = \varphi_0^{(0)2}$ is integrable (and from now on it will be always the case), the following ergodic property may be invoked to evaluate functional integrals:

$$\begin{aligned}
 &\int_{\Omega(-t/2; t/2)} f[X(-t/2)] \prod_{i=1}^q A_i[X(t_i)] g[X(t/2)] \\
 &\quad \times \exp \left[- \int_{-t/2}^{t/2} V_p[X(s)] ds \right] D^{\varphi_0^{(0)}} X \\
 &= \lim_{T \rightarrow +\infty} \frac{1}{T} \int_0^T f[X^{(0)}(-t/2 + \tau)] \\
 &\quad \times \prod_{i=1}^q A_i[X^{(0)}(t_i + \tau)] g[X^{(0)}(t/2 + \tau)] \\
 &\quad \times \exp \left[- \int_{-t/2 + \tau}^{t/2 + \tau} V_p[X^{(0)}(s)] ds \right] d\tau, \quad (3.15)
 \end{aligned}$$

where $X^{(0)}(s)$ denotes an arbitrary sample trajectory of the diffusion process.

It must be emphasized that in the basic formula (3.7) (and in the formulas derived from it) we only have the time parameter t and functional integrals, the simulation time T appears only when these functional integrals are expressed as time-averages over sample trajectories according to the previous formula (3.15). Once this is done these formulas would exhibit $T \rightarrow +\infty$, while t remains fixed, and, therefore, the distinction between T and t remains perfectly clear.

We can now discuss with more detail the connection with other Monte Carlo methods based on the use of a branching term. The “trial wave function” ψ_T introduced in these methods corresponds exactly to our reference function $\varphi_0^{(0)}$,³¹ and accordingly the pure “drifting-diffusion” part of their process would be identical with our own diffusion process. Our Fokker–Planck equation (with drift term $\nabla \varphi_0^{(0)} / \varphi_0^{(0)}$) is actually identical with the evolution equation of the branching-diffusion process [see, e.g., Eq. (6) in Ref. 9] when the branching term is removed. Adding the branching term modifies the process and thus generates a new measure in function space (space of trajectories). Instead of directly sampling this new functional measure, as has been done in most previous work, it would be conceivable to use a Feynman–Kac type formula applied to the reference (pure drifting-diffusion) process. This second alternative has precisely been noticed by Ceperley and Alder [see their Eq. (11) in Ref. 14] and by Pollock and Ceperley [see their Appendix A, notably Eq. (A5) in Ref. 23]. It must be emphasized, however, that the branching-diffusion process is not identical with the pure diffusion process corresponding to the exact state φ_0 , if only because the former has the stationary density $\varphi_0 \psi_T$, while the latter has the stationary density φ_0^2 . In the Appendix, we present further discussion concerning the connection between the various approaches and, more specifically, between the possibly associated Feynman–Kac type formulas.

IV. EXPRESSIONS OF QUANTUM MEAN VALUES AND RESPONSE PROPERTIES USING THE FGFK FORMULA

A. Energy

Taking $A_i = 1$, for $i = 1$ to q in the FGFK formula, we obtain

$$\begin{aligned}
 I(t) &= \langle f \varphi_0^{(0)} | e^{-t(H - E_0^{(0)})} | g \varphi_0^{(0)} \rangle \\
 &= \int_{\Omega(-t/2; t/2)} f[X(-t/2)] g[X(t/2)] \\
 &\quad \times \exp \left[- \int_{-t/2}^{t/2} V_p[X(s)] ds \right] D^{\varphi_0^{(0)}} X. \quad (4.1)
 \end{aligned}$$

We now introduce on the left- and right-hand sides of operator $e^{-t(H - E_0^{(0)})}$ the resolution of the identity associated with the spectral resolution of H , namely

$$1 = \sum_i |\varphi_i\rangle\langle\varphi_i|. \quad (4.2)$$

The summation sign \sum_i here is a shorthand notation which may represent either a discrete summation or a continuous integration. This notation will be used throughout the paper. Using the orthogonality relation

$$\langle\varphi_i|\varphi_k\rangle = \delta_{ik} \quad (4.3)$$

we obtain

$$I(t) = \sum_i \langle f\varphi_0^{(0)}|\varphi_i\rangle\langle\varphi_i|g\varphi_0^{(0)}\rangle e^{-t(E_i - E_0^{(0)})}. \quad (4.4)$$

From Eq. (4.4) it is then easy to derive that

$$\begin{aligned} I_A(t;t_1) &= \langle f\varphi_0^{(0)}|e^{-(t_1+t/2)(H-E_0^{(0)})}Ae^{-(t/2-t_1)(H-E_0^{(0)})}|g\varphi_0^{(0)}\rangle \\ &= \int_{\Omega(-t/2;t/2)} f[X(-t/2)]A[X(t_1)]g[X(t/2)]\exp\left[-\int_{-t/2}^{t/2} V_p[X(s)]ds\right]D^{\varphi_0^{(0)}}X. \end{aligned} \quad (4.6)$$

By inserting the spectral expansion by Eq. (4.2) at each side of the three operators into the quantum matrix element we get

$$\begin{aligned} I_A(t;t_1) &= \sum_{i,j,k,l} \langle f\varphi_0^{(0)}|\varphi_i\rangle\langle\varphi_i|e^{-(t_1+t/2)(H-E_0^{(0)})}|\varphi_j\rangle\langle\varphi_j|A|\varphi_k\rangle\langle\varphi_k|e^{-(t/2-t_1)(H-E_0^{(0)})}|\varphi_l\rangle\langle\varphi_l|g\varphi_0^{(0)}\rangle \\ &= e^{-t(E_{i_0} - E_0^{(0)})} \langle f\varphi_0^{(0)}|\varphi_{i_0}\rangle\langle\varphi_{i_0}|g\varphi_0^{(0)}\rangle \\ &\quad \times \left[\langle\varphi_{i_0}|A|\varphi_{i_0}\rangle + \sum_{\substack{i,k \\ i>i_0, k>i_0}} \frac{\langle f\varphi_0^{(0)}|\varphi_i\rangle\langle\varphi_i|A|\varphi_k\rangle\langle\varphi_k|g\varphi_0^{(0)}\rangle}{\langle f\varphi_0^{(0)}|\varphi_{i_0}\rangle\langle\varphi_{i_0}|g\varphi_0^{(0)}\rangle} e^{-t_1(E_i - E_k) - \frac{t}{2}[(E_i - E_{i_0}) + (E_k - E_{i_0})]} \right] \end{aligned}$$

taking $A = 1$ in the last equality we obtain

$$I(t) = e^{-t(E_{i_0} - E_0^{(0)})} \langle f\varphi_0^{(0)}|\varphi_{i_0}\rangle\langle\varphi_{i_0}|g\varphi_0^{(0)}\rangle \left[1 + \sum_{i>i_0} \frac{\langle f\varphi_0^{(0)}|\varphi_i\rangle\langle\varphi_i|g\varphi_0^{(0)}\rangle}{\langle f\varphi_0^{(0)}|\varphi_{i_0}\rangle\langle\varphi_{i_0}|g\varphi_0^{(0)}\rangle} e^{-t(E_i - E_{i_0})} \right]$$

finally we find

$$\lim_{t \rightarrow +\infty} \frac{I_A(t;t_1)}{I(t)} = \langle\varphi_{i_0}|A|\varphi_{i_0}\rangle \quad \forall t_1 \in]-t/2, t/2[$$

or

$$\langle\varphi_{i_0}|A|\varphi_{i_0}\rangle = \lim_{t \rightarrow +\infty} \frac{\int_{\Omega(-t/2;t/2)} f[X(-t/2)]A[X(t_1)]g[X(t/2)]\exp\{-\int_{-t/2}^{t/2} V_p[X(s)]ds\}D^{\varphi_0^{(0)}}X}{\int_{\Omega(-t/2;t/2)} f[X(-t/2)]g[X(t/2)]\exp\{-\int_{-t/2}^{t/2} V_p[X(s)]ds\}D^{\varphi_0^{(0)}}X}. \quad (4.7)$$

C. Second-order mean values

We apply the FGFK formula to the case $A_1 = A, A_2 = B$. Using the same kind of arguments as in the both previous cases it is easy to be convinced that the following matrix element:

$$I_{AB}(t;t_1,t_2) = \langle f\varphi_0^{(0)}|e^{-(t_1+t/2)(H-E_0^{(0)})}Ae^{-(t_2-t_1)(H-E_0^{(0)})}Be^{-(t/2-t_2)(H-E_0^{(0)})}|g\varphi_0^{(0)}\rangle$$

may be written in the form

$$\begin{aligned} e^{-t(E_{i_0} - E_0^{(0)})} \langle f\varphi_0^{(0)}|\varphi_{i_0}\rangle\langle\varphi_{i_0}|g\varphi_0^{(0)}\rangle &\left\{ \sum_k \langle\varphi_{i_0}|A|\varphi_k\rangle\langle\varphi_k|B|\varphi_{i_0}\rangle e^{-(t_1-t_2)(E_{i_0} - E_k)} \right. \\ &\left. + \sum_{\substack{i>i_0 \\ m>i_0}} e^{-t/2[(E_i - E_{i_0}) + (E_m - E_{i_0})]} \frac{\langle f\varphi_0^{(0)}|\varphi_i\rangle\langle\varphi_m|g\varphi_0^{(0)}\rangle}{\langle f\varphi_0^{(0)}|\varphi_{i_0}\rangle\langle\varphi_{i_0}|g\varphi_0^{(0)}\rangle} \left[\sum_k \langle\varphi_i|A|\varphi_k\rangle\langle\varphi_k|B|\varphi_m\rangle e^{-t_1(E_i - E_k) - t_2(E_k - E_m)} \right] \right\}. \end{aligned}$$

We now extract the following quantity:

$$\begin{aligned} E_{i_0} &= E_0^{(0)} - \lim_{t \rightarrow +\infty} 1/t \\ &\quad \times \log \int_{\Omega(-t/2;t/2)} f[X(-t/2)]g[X(t/2)] \\ &\quad \times \exp\left[-\int_{-t/2}^{t/2} V_p[X(s)]ds\right]D^{\varphi_0^{(0)}}X, \end{aligned} \quad (4.5)$$

where E_{i_0} is the energy associated with the lowest state φ_{i_0} having nonzero overlap with the functions $f\varphi_0^{(0)}$ and $g\varphi_0^{(0)}$.

In actual fact more sophisticated schemes to extract the exponent of the leading real exponential will be considered in numerical calculations (see companion paper).

B. Expression of quantum averages

Taking $A_1 = A$ and $A_2 = \dots = A_q = 1$ in the FGFK formula, we obtain

$$C_{AB}(\tau) = \sum_k \langle \varphi_{i_0} | A | \varphi_k \rangle \langle \varphi_k | B | \varphi_{i_0} \rangle e^{-\tau(E_k - E_{i_0})},$$

where $\tau = t_2 - t_1$, in a way similar to that used for obtaining $\langle \varphi_{i_0} | A | \varphi_{i_0} \rangle$ in the previous derivation [Eq. (4.7)]. We thus obtain

$$C_{AB}(\tau) = \lim_{t \rightarrow +\infty} \frac{\int_{\Omega(-t/2; t/2)} f[X(-t/2)] A[X(t_1)] B[X(t_1 + \tau)] g[X(t/2)] \exp\{-\int_{-t/2}^{t/2} V_p[X(s)] ds\} D \varphi^{(0)} X}{\int_{\Omega(-t/2; t/2)} f[X(-t/2)] g[X(t/2)] \exp\{-\int_{-t/2}^{t/2} V_p[X(s)] ds\} D \varphi^{(0)} X} \quad \forall t_1, t_2 \in [-t/2, t/2]. \quad (4.8)$$

From the Laplace-transform of $C_{AB}(\tau)$ one obtains

$$\begin{aligned} \mathcal{L}[C_{AB}(\tau)] &= \int_0^{+\infty} e^{-\omega\tau} C_{AB}(\tau) d\tau \\ &= \sum_k \frac{\langle \varphi_{i_0} | A | \varphi_k \rangle \langle \varphi_k | B | \varphi_{i_0} \rangle}{\omega + (E_k - E_{i_0})}. \end{aligned} \quad (4.9)$$

Now, we can consider for example the dynamic dipole polarizability tensor $A(\omega)$ at frequency ω for an atomic or molecular system, which is given by the second-order perturbation formula³²:

$$A(\omega) = 2 \sum_{k \neq 0} \frac{\boldsymbol{\mu}_{k0} \otimes \boldsymbol{\mu}_{k0} E_{k0}}{E_{k0}^2 - \omega^2}, \quad (4.10)$$

where $E_{k0} = E_k - E_0$ and $\boldsymbol{\mu}_{k0} = \langle \varphi_k | \boldsymbol{\mu} | \varphi_0 \rangle$ denotes the matrix elements of the dipole operator $\boldsymbol{\mu} = \sum_{j=1}^N q_j \mathbf{r}_j$ and \otimes denotes the tensor product. Now, as remarked, e.g., by Tang and Karplus,³³ Eq. (4.10) may be written as

$$A(\omega) = A^+(\omega) + A^+(-\omega), \quad (4.11)$$

where

$$A^+(\omega) = \sum_{k \neq 0} \frac{\boldsymbol{\mu}_{k0} \otimes \boldsymbol{\mu}_{k0}}{\omega + E_{k0}}. \quad (4.12)$$

This last quantity may be evaluated with

$$\begin{aligned} \mathcal{L}[C_{AB}(\tau) - \langle A \rangle \langle B \rangle] \\ = \sum_{k \neq i_0} \frac{\langle \varphi_{i_0} | A | \varphi_k \rangle \langle \varphi_k | B | \varphi_{i_0} \rangle}{\omega + E_k - E_{i_0}}, \end{aligned} \quad (4.13)$$

where $A = B = \boldsymbol{\mu}$. Of course, the subscript i_0 used in Eq. (4.13) for labeling the fermionic quantities corresponds to the subscript 0 appearing in the standard Eqs. (4.10)–(4.12).

It must be emphasized here that all the formulas just derived (for energy, mean values, and second-order properties) are expressed in terms of one and same diffusion measure (corresponding to the reference function $\varphi_0^{(0)}$). Only the integrand changes from one functional integral to the other. Moreover, according to the ergodic property (3.15), these functional integrals may be reformulated as time-averages of the corresponding integrands over any given sample trajectory of the diffusion process (associated with $\varphi_0^{(0)}$). This use of one and the same trajectory for evaluating all quantities of interest is a very appealing feature, and deserves to be contrasted with the situation encountered in previous QMC methods.^{7–18} As a general rule, these methods introduce a branching process designed for generating a cloud of points asymptotically distributed according to the density $\varphi\psi_T$ (where φ denotes the exact eigenfunction of H and ψ_T

the so-called trial function). Now, such a density enables one to evaluate exactly the mean value of the energy, or more generally of any observable A commuting with H , but gives only an approximate mean value for other observables.¹⁸ If an exact mean value is wanted, a modified procedure has to be used in order to generate the exact density φ^2 . In the same way that in the previous Sec. III, we emphasize that our formulas (4.5), (4.7), and (4.8) involve only the time parameter t and functional integrals; only when expressing the latter integrals as time-averages [Eq. (3.15)] we would get a simulation time T systematically involved in a limit $T \rightarrow +\infty$ to be performed for each value of t . Then formulas (4.5), (4.7), and (4.8) would give rise to a double limit $t \rightarrow +\infty$ [$T \rightarrow +\infty$]. It is *a priori* allowed neither to interchange these two limits nor to collapse them into a single limit by putting $(t = T) \rightarrow +\infty$. Any such changes should be carefully justified. An illustrative and important case where even the collapse of the two limits is *not* justified will be encountered in the release-node treatment of the fermion problem (see Sec. VI).

Finally, as far as we know, no procedure aiming at evaluating *second-order* properties seems to have been proposed in the framework of these previous QMC methods, and our procedure offers in this respect an important potential advantage.

V. THEORETICAL ALGORITHM

We present here the basic ideas of the algorithm. The main steps are:

(i) Choose some suitable reference function $\varphi_0^{(0)}$ from which the reference diffusion is built [see Eqs. (2.9)–(2.11)].

(ii) Using the stochastic differential equation (SDE) associated with the reference diffusion process³⁴ generate through a step-wise procedure (with a time step Δt) a stochastic trajectory $\mathbf{X}^{(0)}(t)$. The SDE is written

$$d\mathbf{X}(t) = \mathbf{b}[\mathbf{X}(t)]dt + \mathcal{D}^{1/2}d\mathbf{W}, \quad (5.1)$$

where \mathbf{W} is the multidimensional Wiener process and \mathbf{b} , \mathcal{D} are given by Eqs. (2.11).

(iii) According to formula (3.15), evaluate the desired functional integrals as time-averages over the stochastic trajectory $\mathbf{X}^{(0)}(t)$.

In actual fact, it is appropriate to introduce, instead of a single very long trajectory, a set of shorter trajectories because the corresponding set of mean values enable us to evaluate the variance using standard statistical methods.³⁵

VI. THE PAULI PRINCIPLE AND ITS CONSTRAINTS

A. General framework

The quantum mechanics of fermionic systems with a spin-free Hamiltonian can be formulated independently of spin functions or spin operators. The requirements of the Pauli principle are then expressed as follows: among eigenfunctions of H only those belonging to irreducible representation (IR) of the symmetric group $S(N)$ (where N is the number of particles) with a Young diagram containing at most two columns are allowed. These states are referred to as the fermionic states. Moreover, for each of these allowed representation there corresponds a well-defined total spin S for the system. Further explanations concerning the formulation of the Pauli principle in a spin-free formalism may be found elsewhere (a convenient reference is the textbook by Landau and Lifshitz,³⁶ see also Hamermesh³⁷ and Matsen³⁸).

In Sec. IV above, the expressions of quantum mean values and response properties have been given for the lowest state (which was denoted as φ_{i_0}) having nonzero overlap with $f\varphi_0^{(0)}$ and $g\varphi_0^{(0)}$. Now, by choosing the functions f , g , and $\varphi_0^{(0)}$ such that the space-functions $\phi_f = f\varphi_0^{(0)}$ and $\phi_g = g\varphi_0^{(0)}$ belong to the desired IR, it is possible to determine quantum observables for the lowest fermionic state corresponding to a given total spin. The construction of such space-functions ϕ corresponding to a given type of symmetry is easily done (see, e.g., Chap. 7 in Ref. 37). Let us give here the most common choice for ϕ ^{9,39}:

$$\phi(\mathbf{r}_1, \dots, \mathbf{r}_N) = \det \left(\prod_{i=1}^{N/2+S} u_i(\mathbf{r}_i) \right) \times \det \left(\prod_{i=1}^{N/2-S} u_i(\mathbf{r}_{i+N/2+S}) \right), \quad (6.1)$$

where $\{u_i\}$ is a set of $(N/2 + S)$ different one-electron orbitals, N the number of electrons, and S the total spin determining the desired type of symmetry.

B. Some practical procedures

1. Fixed-node approximation (FNA)

In this approach, we take

$$f = g = 1 \quad (6.2)$$

and we introduce the symmetry into the diffusion process through the reference function $\varphi_0^{(0)}$:

$$\varphi_0^{(0)} = \phi_f = \phi_g = \phi. \quad (6.3)$$

According to its symmetry properties, such a reference function $\varphi_0^{(0)}$ must have some nodal hypersurfaces. These nodal hypersurfaces, where the drift $\mathbf{b} = \nabla\varphi_0^{(0)}/\varphi_0^{(0)}$ is infinite, are seen as infinite barriers for any sample trajectory. The diffusion process is then decomposed into a juxtaposition of subprocesses in subdomains delimited by the nodal hypersurfaces of the reference function $\varphi_0^{(0)}$. Now, as rightfully pointed out by Klein and Pickett,⁴⁰ the full nodal hypersurface of any space-function ϕ obeying the Pauli principle requirement cannot be completely determined by these symmetry requirements. In actual fact, the full nodal

hypersurface of any continuous function $\phi(\mathbf{r}_1, \dots, \mathbf{r}_N)$ of $3N$ variables is obviously of dimension $(3N - 1)$ and bifurcates the $3N$ -dimensional space. In contrast, the symmetry requirements determine only subhypersurfaces of lower dimension $(3N - 3)$ embedded in the full nodal hypersurface of ϕ .⁴⁰ We shall denote these subhypersurfaces as exchange or symmetry nodal hypersurfaces. The subset (also of dimension $3N - 1$) of the full nodal hypersurface, which complements the symmetry nodal hypersurface, will be referred to for definiteness as peculiar nodal hypersurface. For example, in the case of the lowest triplet state of helium-like systems,⁴⁰ the full nodal hypersurface (of dimension $6 - 1 = 5$) is defined by $|\mathbf{r}_1| = |\mathbf{r}_2|$, while the symmetry nodal subhypersurface (of dimension $6 - 3 = 3$) is defined by $\mathbf{r}_1 = \mathbf{r}_2$. Now, the exchange (symmetry) nodes are exact by their very definition (i.e., they may be taken identical for the exact solution φ_{i_0} of the Schrödinger equation and for the reference function $\varphi_0^{(0)} = \phi$): thus, they correspond to correct (but unfortunately incomplete) boundary conditions. In contrast, since the peculiar nodal hypersurface of ϕ has no reason to coincide with the exact peculiar nodal hypersurface (of the exact function φ_{i_0}) it will impose to the eigenfunctions of the Schrödinger Hamiltonian some wrong boundary conditions (i.e., boundary conditions different from those pertaining to the original problem of solving the genuine Schrödinger equation, where the only condition imposed to the eigenfunctions is in general vanishing at infinity). Consequently, the eigenvalues of the Schrödinger operator modified in this way will be somewhat different from those of the genuine Hamiltonian H , and some bias will be accordingly introduced. This is the well-known fixed-node approximation (see, e.g., Ref. 9).

2. Projection methods

In this case the reference function $\varphi_0^{(0)}$ is chosen nodeless and the symmetry is introduced via the functions f and g :

$$f = \phi_f / \varphi_0^{(0)}, \quad (6.4a)$$

$$g = \phi_g / \varphi_0^{(0)}. \quad (6.4b)$$

Since no extra boundary conditions are imposed to the eigenfunctions of the Schrödinger operator, the requirements concerning the Pauli principle are fulfilled here without any approximation.

We have distinguished two versions of the projection method:

(i) *Simple projection (SP) method.* In order to reduce the perturbing potential V_p , the reference function $\varphi_0^{(0)}$ is chosen as close as possible to the bosonic ground state φ_0 of H . In particular, no built-in structure akin to the exact wave function φ_{i_0} is introduced into $\varphi_0^{(0)}$.

(ii) *Release-node projection (RNP) method.* In this approach we use a more refined choice of the reference function. Choosing a symmetry-adapted ϕ close to the wave function φ_{i_0} and introducing a nonvanishing "connecting piece" function, noted $\text{cpf}(x)$, we construct the reference function in the following way:

$$\varphi_0^{(0)} = |\phi| \quad \text{when } |\phi| > \epsilon, \quad (6.5a)$$

$$\varphi_0^{(0)} = \text{cpf}(x) \quad \text{otherwise,} \quad (6.5b)$$

where ϵ is a threshold value. Continuity of $\varphi_0^{(0)}$ and its first derivative is imposed at the points where $\varphi_0^{(0)} = \epsilon$. This construction is illustrated in Fig. 1.

In these projection methods, and in contrast to the fixed-node approach, the product

$$f[X(-t/2 + \tau)] g[X(t/2 + \tau)]$$

may change sign. This change occurs when the trajectory goes through nodal surfaces of ϕ an odd number of times in the time interval $(-t/2 + \tau, t/2 + \tau)$. Note that our release-node projection method is essentially similar to the so-called nodal relaxation method of Ceperley and Alder (see Secs. III B and IV in Ref. 14).

C. Further remarks concerning the exact projection methods

1. Choice of $\varphi_0^{(0)}$, f , and g

Let us consider for definiteness the problem of evaluating $I(t)$ given by Eq. (4.1):

$$I(t) = \int_{\Omega(-t/2; t/2)} f[X(-t/2)] g[X(t/2)] \times \exp \left[- \int_{-t/2}^{t/2} V_p[X(s)] ds \right] D^{\varphi_0^{(0)}} X. \quad (6.6)$$

Numerical difficulties are essentially due to the non constant sign of $f[X(-t/2)] g[X(t/2)]$. We shall therefore write

$$I(t) = I_+(t) - I_-(t), \quad (6.7)$$

where $I_+(t)$ and $I_-(t)$ are the contributions coming respectively from the positive and negative values of the product $f[X(-t/2)] g[X(t/2)]$, namely

$$I_{\pm}(t) = \int_{\Omega(-t/2; t/2)} \frac{1}{2} \{ |f[X(-t/2)] \times g[X(t/2)] | \pm f[X(-t/2)] g[X(t/2)] \} \times \exp \left[- \int_{-t/2}^{t/2} V_p[X(s)] ds \right] D^{\varphi_0^{(0)}} X. \quad (6.8)$$

Using $|fg| = |f||g|$, we can also [according to Eq. (4.1)] express $I_{\pm}(t)$ as follows:

$$I_{\pm}(t) = \frac{1}{2} \left[\langle |f| \varphi_0^{(0)} | e^{-t(H-E_0^{(0)})} ||g| \varphi_0^{(0)} \rangle \pm \langle f \varphi_0^{(0)} | e^{-t(H-E_0^{(0)})} |g \varphi_0^{(0)} \rangle \right]. \quad (6.9)$$

We can now apply to each matrix element the same procedure as used in obtaining Eq. (4.4):

$$\langle |f| \varphi_0^{(0)} | e^{-t(H-E_0^{(0)})} ||g| \varphi_0^{(0)} \rangle = \langle |f| \varphi_0^{(0)} | \varphi_0 \rangle \langle \varphi_0 | |g| \varphi_0^{(0)} \rangle e^{-t(E_0 - E_0^{(0)})} + \dots, \quad (6.10a)$$

$$\langle f \varphi_0^{(0)} | e^{-t(H-E_0^{(0)})} |g \varphi_0^{(0)} \rangle = \langle f \varphi_0^{(0)} | \varphi_{i_0} \rangle \langle \varphi_{i_0} |g \varphi_0^{(0)} \rangle e^{-t(E_{i_0} - E_0^{(0)})} + \dots, \quad (6.10b)$$

where φ_{i_0} is the lowest state belonging to the symmetry type imposed by f and g . Note that in the previous matrix element (6.10a) the expansion actually begins with the bosonic ground state φ_0 of H , since $|f| \varphi_0^{(0)}$ and $|g| \varphi_0^{(0)}$ are nonnegative everywhere, as is φ_0 . Let us denote for brevity:

$$[f \varphi_0^{(0)}, g \varphi_0^{(0)}](t) = \langle f \varphi_0^{(0)} | e^{-t(H-E_0^{(0)})} |g \varphi_0^{(0)} \rangle. \quad (6.11)$$

We can rewrite Eq. (6.9) as

$$I_{\pm}(t) = \frac{1}{2} \{ [|f \varphi_0^{(0)}, |g \varphi_0^{(0)} |](t) \pm [f \varphi_0^{(0)}, g \varphi_0^{(0)}](t) \}. \quad (6.12)$$

We now notice the remarkable fact that $I_+(t)$ and $I_-(t)$, like $I(t)$ itself, depend only on $\phi_f = f \varphi_0^{(0)}$ and $\phi_g = g \varphi_0^{(0)}$, and *not* on f , g , and $\varphi_0^{(0)}$ separately. Consequently, the choice of $\varphi_0^{(0)}$ is not directly crucial at this stage, since it is always possible to compensate it through a suitable choice of f and g in such a way as to get prescribed functions

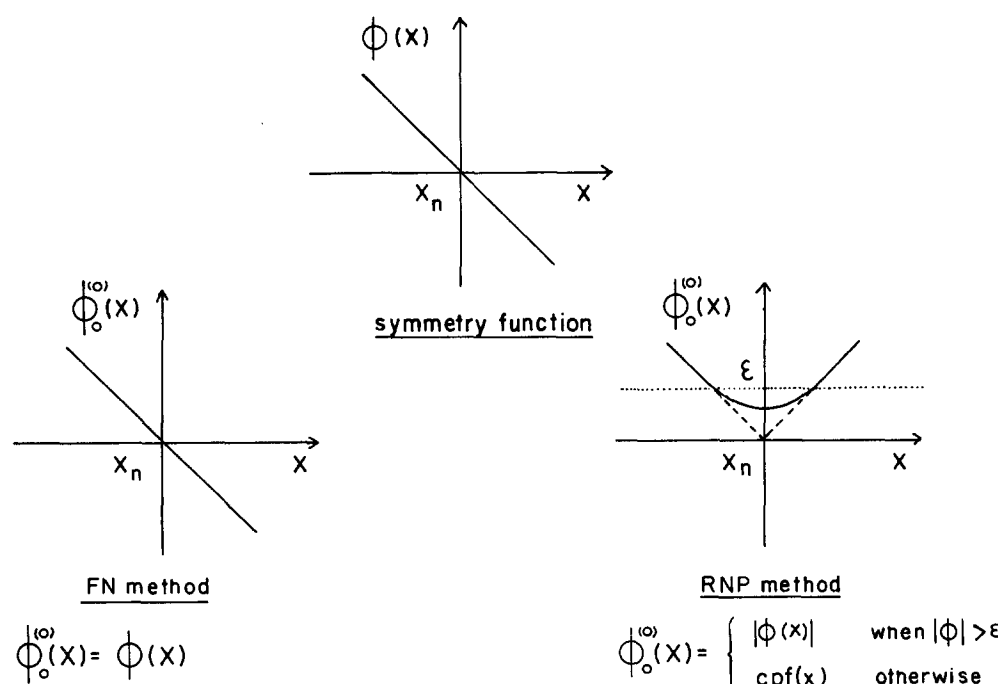


FIG. 1. Comparison between the fixed-node (FN) method and the release-node projection (RNP) method. In both cases, the behavior of the reference function $\varphi_0^{(0)}$ in the neighborhood of the node X_n is pictured. The continuous line — represents $\varphi_0^{(0)}(X)$. In the RNP case, the dashed line - - - represents $|\phi|(X)$.

$\phi_f = f\varphi_0^{(0)}$ and $\phi_g = g\varphi_0^{(0)}$. At this stage, it therefore appears convenient to proceed in two steps for our discussion:

(i) Choice of ϕ_f and ϕ_g (in actual practice, we generally take $\phi_f = \phi_g = \phi$).

(ii) Once ϕ_f and ϕ_g have been chosen, what role is left for the choice of $\varphi_0^{(0)}$?

As concerns the choice of ϕ_f and ϕ_g , it must first be emphasized that $I_+(t)$ and $I_-(t)$ contain unavoidably non-zero contributions from the unwanted bosonic states. These contributions are actually identical, since they are provided by the matrix element $[|\phi_f\rangle, |\phi_g\rangle](t)$, common to both $I_+(t)$ and $I_-(t)$. The other matrix element $[\phi_f, \phi_g](t) = I(t)$ contains no such bosonic contribution, according precisely to the *ad hoc* choice of ϕ_f and ϕ_g . According to Eqs. (6.10), it now appears that ϕ_f and ϕ_g should be chosen so as to maximize the overlap integrals $\langle \phi_f | \varphi_{i_0} \rangle$ and $\langle \varphi_{i_0} | \phi_g \rangle$, while also minimizing the overlap integrals $\langle \phi_f | \varphi_{i < i_0} \rangle$ and $\langle \varphi_{i < i_0} | \phi_g \rangle$. From these requirements, taking $\phi_f = \phi_g = \phi$ close to the desired (fermionic) state φ_{i_0} looks like a reasonable choice.

Once ϕ_f and ϕ_g have been so chosen, $I_+(t)$ and $I_-(t)$ are determined, and the choice of $\varphi_0^{(0)}$ now concerns the variance (for any given simulation time) in the Monte Carlo estimation of $I_+(t)$ and $I_-(t)$. Thus, the release-node projection method consists in choosing $\varphi_0^{(0)}$ close to $|\varphi_{i_0}\rangle$, and $f = g$ close to $\text{sign}(\varphi_{i_0})$, while the simple projection method chooses $\varphi_0^{(0)}$ close to the bosonic ground state φ_0 . Numerical experiment (see Ref. 14 and part II of the present work) so far indicates that the RNP method indeed exhibits lower variance.

2. On the role played by the distinction between the evolution time parameter t and the simulation time T

We are now in a position to discuss in a precise manner the difficulties associated with the Pauli principle requirements alluded to in the Introduction. As emphasized by other authors (see, e.g., Refs. 8, 14, and 41), the fermionic quantity of interest is obtained as the difference of two (bosonic type) larger quantities which have the same order of magnitude. This is a typically unfavorable situation from the numerical point of view. More precisely, in our formalism, the desired fermionic quantity is $I(t)$, and the two bosonic quantities are $I_+(t)$ and $I_-(t)$ [see Eq. (6.7)]. Then, according to Eqs. (6.9) and (6.10) we have, for large t :

$$I_+(t) \sim I_-(t) \sim [|f\varphi_0^{(0)}\rangle, |g\varphi_0^{(0)}\rangle](t) \sim e^{-t(E_0 - E_0^{(0)})}, \quad (6.13a)$$

$$I(t) = [f\varphi_0^{(0)}, g\varphi_0^{(0)}](t) \sim e^{-t(E_{i_0} - E_0^{(0)})}, \quad (6.13b)$$

hence

$$I(t)/I_{\pm}(t) \underset{t \rightarrow +\infty}{\sim} e^{-t(E_{i_0} - E_0)}. \quad (6.14)$$

Now the Monte Carlo simulation will provide the values of $I_+(t)$ and $I_-(t)$ with some statistical uncertainty (standard deviation) leading to a relative error of the form (for large T)

$$\delta I_{\pm}(t)/I_{\pm}(t) \sim C_{\pm}(t)T^{-1/2}, \quad (6.15)$$

where T denotes the simulation time, while $C_+(t)$ and $C_-(t)$ are independent of T (and in general increase with t). Since we have no reason to assume that the errors δI_+ and δI_- are correlated, the error δI should be of the same order of magnitude, and consequently the relative error pertaining to $I(t)$ would be of the form

$$\delta I/I \sim C(t)T^{-1/2}e^{t(E_{i_0} - E_0)}. \quad (6.16)$$

According to this formula, in order to keep $\delta I/I$ under control, it appears essential to vary t and T independently. Noticeably, when t increases, it will become necessary, sooner or later, to have T increasing *much faster*. Any method in which t and T are (possibly in an implicit way) taken of the same order of magnitude will fail to meet this requirement and will therefore become useless for large enough values of $t \approx T$. Such a method will be able to work for not too large values of $t \approx T$, and under the condition that $C(t)$ is small enough. Since $C(t)$ gives the (relative) variance for $T = 1$, we may expect to reduce it by improving the choice of the reference function $\varphi_0^{(0)}$. Apparently, the situation just described corresponds to the previous Monte Carlo procedures,^{8,14} where the simulation time T is also the evolution “imaginary” time t . In actual fact, a discussion similar to the above one has been given by Kalos⁴² in the framework of the Green’s function Monte Carlo method. This can be seen by comparing his Eq. (14) with our Eqs. (6.7) and (6.13). Kalos’s Eq. (14) involves only *one parameter* n , proportional to the total simulation time (that we denote T), a situation which reflects the implicit relationship $t = T$. By contrast, in our procedure, t and T remain perfectly distinct, which in principle offers the possibility of correctly evaluating $I(t)$ for fixed t by making T large enough. Now, in order to obtain the energy E_{i_0} , the straightforward procedure corresponding to formula (4.5) requires large values of t . This could result in a demand for unrealistically large values of the simulation time T . However, we could then still resort to more sophisticated procedures using only values of $I(t)$ for a set of values of t restricted to some reasonable interval (see the Padé-integral procedure in the companion paper).

VII. CONCLUSION

A basic feature of the Monte Carlo method developed in the present work is the definition of a reference diffusion process associated with some reference function $\varphi_0^{(0)}$, with the crucial property that the Fokker–Planck operator $L^{(0)}$ of this process is connected through a similarity transformation with some reference Hamiltonian $H^{(0)}$ itself easily defined from $\varphi_0^{(0)}$. By relying on this connection between $L^{(0)}$ and $H^{(0)}$, we showed that it is possible to express in an easy and systematic way quantum properties pertaining to any Hamiltonian $H = H^{(0)} + V_p$, in terms of functional integrals (involving the “perturbing” potential V_p) making use of the diffusion measure associated with the reference diffusion process. Its simple and systematic character makes this approach quite attractive. Thus, to our knowledge, the possibility of easily obtaining expressions for response properties (beyond usual mean values) is a specific advantage of our approach over the other Monte Carlo methods. Needless to say, this possibility is also a very attractive feature with re-

spect to standard methods based on the use of basis sets, since the evaluation of response properties then implies the introduction of basis sets augmented with suitable "polarization" functions (with little assurance concerning the quality of the results, beyond the simplest systems).

Similarly, it has been possible to discuss in a natural way some "hierarchy" of solutions concerning the problems posed by the Pauli principle requirements for many-fermion problems. First, as is the case in other Monte Carlo schemes, we could define a so-called *fixed-node* approximation, whereby approximate eigenfunctions of the Hamiltonian H are obtained, subject to the constraint that they vanish along the nodes of the reference function $\varphi_0^{(0)}$. But in order to give to the Monte Carlo approach its full power, it is of course essential to go beyond this approximation, and we therefore examined a theoretically rigorous procedure for getting access to eigenspaces belonging to some *prescribed symmetry type*. As done in previous work (see, e.g., Refs. 8 and 14) we further considered two variants for this procedure, based on different choices for the reference function $\varphi_0^{(0)}$. The first choice is a mere "bosonic" ground state, with no built-in structure akin to the desired symmetry type. The second choice, although being everywhere strictly positive (as it must), is required to remain close to $|\phi|$, where ϕ is some function belonging to the desired symmetry type, and, as far as possible, close to the desired exact function (in order to reduce the perturbing potential V_p). The latter choice, of course, looks more attractive than the former one, but adequate checking of both variants remains to be done.

In a companion paper, the computer implementation of the method will be considered in more detail. We shall describe a few illustrative examples, namely one-dimensional systems first, and then some simple systems of chemical interest (atoms and the H_2 molecule).

ACKNOWLEDGMENT

We would like to thank Dr. E. M. Evleth for his careful reading of the manuscript.

APPENDIX

In this Appendix, we present the rigorous relationship existing between our generalized Feynman-Kac formula and quite similar formulas written down without explicit derivation by Pollock and Ceperley [formula (A5) in Ref. 23] and Ceperley and Alder [formula (11) in Ref. 14].

For that purpose we start from our basic FGFK formula (3.7) with $A_i = 1$, $i = 1$ to q :

$$\begin{aligned} & \langle f \varphi_0^{(0)} | e^{-\iota(H - E_0^{(0)})} | g \varphi_0^{(0)} \rangle \\ &= \int_{\Omega(-\iota/2, \iota/2)} f[\mathbf{X}(-\iota/2)] g[\mathbf{X}(\iota/2)] \\ & \quad \times \exp \left[- \int_{-\iota/2}^{\iota/2} V_p[\mathbf{X}(s)] ds \right] D^{\varphi_0^{(0)}} \mathbf{X}. \end{aligned} \quad (\text{A1})$$

Choosing $f = \delta_r / \varphi_0^{(0)}$ and $g = \delta_{r'} / \varphi_0^{(0)}$ we get

$$\begin{aligned} & \langle \mathbf{r} | e^{-\iota H} | \mathbf{r}' \rangle \\ &= \frac{e^{-\iota E_0^{(0)}}}{\varphi_0^{(0)}(\mathbf{r}) \varphi_0^{(0)}(\mathbf{r}')} \int_{\Omega(-\iota/2, \iota/2)} \delta_r[\mathbf{X}(-\iota/2)] \delta_{r'} \\ & \quad \times [\mathbf{X}(\iota/2)] \exp \left[- \int_{-\iota/2}^{\iota/2} V_p[\mathbf{X}(s)] ds \right] D^{\varphi_0^{(0)}} \mathbf{X}. \end{aligned} \quad (\text{A2})$$

Note that $\langle \mathbf{r} | e^{-\iota H} | \mathbf{r}' \rangle$ is the usual time-dependent Green function (or density matrix). Using notations from Refs. 14 and 23 and the time-shifting invariance of the functional integral, equality (A2) may be rewritten in the form

$$\begin{aligned} \rho(\mathbf{r}, \mathbf{r}', \beta) &= \frac{e^{-\beta E_0^{(0)}}}{\varphi_0^{(0)}(\mathbf{r}) \varphi_0^{(0)}(\mathbf{r}')} \\ & \quad \times \int_{\Omega(0, \beta)} \delta_r[\mathbf{X}(0)] \delta_{r'}[\mathbf{X}(\beta)] \\ & \quad \times \exp \left[- \int_0^\beta V_p[\mathbf{X}(s)] ds \right] D^{\varphi_0^{(0)}} \mathbf{X}. \end{aligned} \quad (\text{A3})$$

Now, we express the previous functional integral under its constructive form, namely

$$\begin{aligned} & \lim_{n \rightarrow +\infty} \int d\mathbf{X}_0 \cdots d\mathbf{X}_n \delta_r(\mathbf{X}_0) \delta_{r'}(\mathbf{X}_n) \\ & \quad \times p_{n+1}^{(0)}(\mathbf{X}_0, 0; \mathbf{X}_1, \Delta\beta; \cdots; \mathbf{X}_n, n\Delta\beta) \\ & \quad \times \exp \left[- \Delta\beta \sum_{i=1}^n V_p(\mathbf{X}_i) \right] \end{aligned} \quad (\text{A4})$$

with $\Delta\beta = \beta/n$. Integrating over \mathbf{X}_0 and \mathbf{X}_n , using Eq. (3.13) and the property $p^{(0)} = \varphi_0^{(0)2}$, lead to the following expression for $\rho(\mathbf{r}, \mathbf{r}', \beta)$:

$$\begin{aligned} \rho(\mathbf{r}, \mathbf{r}', \beta) &= e^{-\beta E_0^{(0)}} \frac{\varphi_0^{(0)}(\mathbf{r})}{\varphi_0^{(0)}(\mathbf{r}')} \lim_{n \rightarrow +\infty} \int d\mathbf{X}_1 \cdots d\mathbf{X}_{n-1} \\ & \quad \times p^{(0)}(\mathbf{r} | \mathbf{X}_1, \Delta\beta) \cdots p^{(0)}(\mathbf{X}_{n-1} | \mathbf{r}', \Delta\beta) \\ & \quad \times \exp \left[- \Delta\beta \sum_{i=1}^n V_p(\mathbf{X}_i) \right]. \end{aligned} \quad (\text{A5})$$

Equality (2.13) gives

$$p^{(0)}(\mathbf{r} | \mathbf{r}', \beta) = \frac{\varphi_0^{(0)}(\mathbf{r}')}{\varphi_0^{(0)}(\mathbf{r})} e^{\beta E_0^{(0)}} \rho^{(0)}(\mathbf{r}, \mathbf{r}', \beta),$$

where $\rho^{(0)}$ is the time-dependent Green function (or density matrix) associated with $H^{(0)} = H - V_p$. Equality (A5) becomes

$$\begin{aligned} \rho(\mathbf{r}, \mathbf{r}', \beta) &= \rho^{(0)}(\mathbf{r}, \mathbf{r}', \beta) \lim_{n \rightarrow +\infty} \int d\mathbf{X}_1 \cdots d\mathbf{X}_{n-1} \\ & \quad \times \frac{p^{(0)}(\mathbf{r} | \mathbf{X}_1, \Delta\beta) \cdots p^{(0)}(\mathbf{X}_{n-1} | \mathbf{r}', \Delta\beta)}{p^{(0)}(\mathbf{r} | \mathbf{r}', \beta)} \\ & \quad \times \exp \left[- \Delta\beta \sum_{i=1}^n V_p(\mathbf{X}_i) \right]. \end{aligned} \quad (\text{A6})$$

Now, using Eq. (3.13) and the definition of the conditional probability densities, namely

$$\begin{aligned}
 & p_{p|n+p}(X_1, t_1; \dots; X_p, t_p | X_{p+1}, t_{p+1}; \dots; X_{p+n}, t_{p+n}) \\
 &= p_{p+n}(X_1, t_1; \dots; X_{p+n}, t_{p+n}) / p_p(X_1, t_1; \dots; X_p, t_p);
 \end{aligned}
 \tag{A7}$$

the infinitesimal probability

$$\frac{p^{(0)}(\mathbf{r} | \mathbf{X}_1, \Delta\beta) \cdots p^{(0)}(\mathbf{X}_{n-1} | \mathbf{r}', \Delta\beta)}{p^{(0)}(\mathbf{r} | \mathbf{r}', \beta)} d\mathbf{X}_1 \cdots d\mathbf{X}_{n-1}$$

may be rewritten as

$$p\left(\mathbf{r}, 0; \mathbf{r}', \beta | \mathbf{X}_1, \Delta\beta; \dots; \mathbf{X}_{n-1}, \Delta\beta \frac{n-1}{n}\right) d\mathbf{X}_1 \cdots d\mathbf{X}_{n-1},
 \tag{A8}$$

which leads to a conditioned measure over the space of trajectories, namely the measure associated with the drifting random walks satisfying the boundary conditions $\mathbf{X}(0) = \mathbf{r}$ and $\mathbf{X}(\beta) = \mathbf{r}'$. The corresponding functional integral has been denoted $\langle \cdots \rangle_{\text{DRW}}$ by Pollock and Ceperley. Finally, using this notation we have

$$\begin{aligned}
 \rho(\mathbf{r}, \mathbf{r}', \beta) &= \rho^{(0)}(\mathbf{r}, \mathbf{r}', \beta) \\
 &\times \left\langle \exp \left[- \int_0^\beta V_p[\mathbf{X}(s)] ds \right] \right\rangle_{\text{DRW}}.
 \end{aligned}
 \tag{A9}$$

This formula coincides with formulas (11) in Ref. 14 and (A5) in Ref. 23. In conclusion, expression (A5) of Ref. 23 appears to be a particular case of our more general FGFK formula.

¹M. H. Kalos, Phys. Rev. **128**, 1791 (1962).

²M. H. Kalos, Nucl. Phys. A **126**, 609 (1969).

³M. H. Kalos, D. Levesque, and L. Verlet, Phys. Rev. A **9**, 2178 (1974).

⁴P. A. Whitlock, D. M. Ceperley, G. V. Chester, and M. H. Kalos, Phys. Rev. B **19**, 5598 (1979).

⁵M. H. Kalos, M. A. Lee, P. A. Whitlock, and G. V. Chester, Phys. Rev. B **24**, 115 (1981).

⁶D. M. Ceperley and M. H. Kalos, *Monte Carlo Methods in Statistical Physics*, edited by K. Binder (Springer, Berlin, 1979), Chap. 4.

⁷(a) J. B. Anderson, J. Chem. Phys. **63**, 1499 (1975); (b) F. Mentch and J. B. Anderson *ibid.* **80**, 2675 (1984).

⁸D. M. Arnow, M. H. Kalos, M. A. Lee, and K. E. Schmidt, J. Chem. Phys. **77**, 5562 (1982).

⁹P. J. Reynolds, D. M. Ceperley, B. J. Alder, and W. A. Lester, Jr., J. Chem. Phys. **77**, 5593 (1982).

¹⁰K. E. Schmidt and M. H. Kalos, *Monte Carlo Methods in Statistical Physics II*, edited by K. Binder (Springer, Berlin, 1984), Chap. 4.

¹¹I. Oksüz, J. Chem. Phys. **81**, 5005 (1984).

¹²H. R. Jauslin and T. Schneider, J. Stat. Phys. **43**, 865 (1986).

¹³D. M. Ceperley, J. Comp. Phys. **51**, 404 (1983).

¹⁴D. M. Ceperley and B. J. Alder, J. Chem. Phys. **81**, 5833 (1984).

¹⁵P. J. Reynolds, M. Dupuis, and W. A. Lester, Jr., J. Chem. Phys. **82**, 1983 (1985).

¹⁶R. J. Harrison and N. C. Handy, Chem. Phys. Lett. **113**, 257 (1985).

¹⁷R. N. Barnett, P. J. Reynolds, and W. A. Lester, Jr., J. Chem. Phys. **84**, 4992 (1986).

¹⁸P. J. Reynolds, R. N. Barnett, B. L. Hammond, and W. A. Lester, Jr., J. Stat. Phys. **43**, 1017 (1986).

¹⁹D. M. Ceperley, J. Stat. Phys. **43**, 815 (1986).

²⁰(a) F. Soto-Eguibar and P. Claverie, in *Stochastic Processes Applied to Physics and Other Related Fields*, edited by B. Gomez, S. M. Moore, A. M. Rodriguez-Vargas, and A. Rueda (World Scientific, Singapore, 1983), pp. 637–649; (b) P. Claverie and F. Soto (to be submitted); (c) F. Soto-Eguibar, Ph.D. thesis, Univ. Nac. Auton. de Mexico. Facultad de Ciencias, 1982.

²¹M. Caffarel and P. Claverie, J. Stat. Phys. **43**, 797 (1986).

²²J. T. Hynes, J. M. Deutch, C. H. Wang, and I. Oppenheim, J. Chem. Phys. **48**, 3085 (1968).

²³E. L. Pollock and D. M. Ceperley, Phys. Rev. B **30**, 2555 (1984).

²⁴(a) L. F. Favella, Ann. Inst. Henri Poincaré **7**, 77 (1967); (b) S. Albeverio and R. Hoegh-Krohn, J. Math. Phys. **15**, 1745 (1974); (c) G. Jonia-Lasinio, F. Martinelli, and E. Scoppola, Phys. Rep. **77**, 313 (1981).

²⁵I. M. Gelfand and A. M. Yaglom, J. Math. Phys. **1**, 48 (1960).

²⁶S. G. Brush, Rev. Mod. Phys. **33**, 79 (1961).

²⁷J. Glimm and A. Jaffé, *Quantum Physics. A Functional Integral Point of View* (Springer, New York, 1981).

²⁸J. Glimm, in *Local Quantum Theory, School of Physics Enrico Fermi, Course 45*, edited by R. Jost (Academic, New York, 1969).

²⁹I. I. Gikhman and A. V. Skorokhod, *Stochastic Differential Equations* (Springer, Berlin, 1972).

³⁰R. Z. Khas'minskii, Theory Probl. its Appl. (USSR) **5**, 179 (1960).

³¹For the sake of clarity it must be emphasized that the notations used in Ref. 14 differ from those used in previous works: the reference function (our $\varphi_0^{(0)}$) was denoted ψ_T (trial function) in previous works, and is renamed ψ_G (guiding function) in Ref. 14, while ψ_T now has a nonconstant sign and is just used for performing projection into a subspace with prescribed symmetry type; in our treatment (see Sec. VI) the role of this ψ_T is played by $f\varphi_0^{(0)}$ and $g\varphi_0^{(0)}$.

³²W. Kauzmann, *Quantum Chemistry* (Academic, New York, 1957), Chap. 16, Sect. A c, pp. 645–646.

³³K. T. Tang and M. Karplus, Phys. Rev. **171**, 70 (1968).

³⁴(a) L. Arnold, *Stochastic Differential Equations* (Wiley, New York, 1974); (b) C. W. Gardiner, *Handbook of Stochastic Methods* (Springer, Berlin, 1983).

³⁵H. Cramér, *Mathematical Methods of Statistics* (Princeton University, Princeton, 1966), Chap. 8.2.

³⁶L. D. Landau and E. Lifshitz, *Quantum Mechanics* (Pergamon, Oxford, 1965), Chap. 9.

³⁷M. Hamermesh, *Group Theory* (Addison-Wesley, Reading, MA, 1962).

³⁸F. A. Matsen, Adv. Quantum Chem. **1**, 60 (1964).

³⁹V. A. Fock, *Fundamentals of Quantum Mechanics* (Mir, Moscow, 1976), Part IV, p. 261.

⁴⁰D. J. Klein and H. M. Pickett, J. Chem. Phys. **64**, 4811 (1976).

⁴¹V. Elser, Phys. Rev. A **34**, 2293 (1986).

⁴²M. H. Kalos, *Monte Carlo Methods in Quantum Problems*, NATO ASI Series C (Reidel, Dordrecht, 1982).

B. M. Caffarel and P. Claverie, "Development of a pure diffusion quantum Monte Carlo method using a full generalized Feynman-Kac formula. II. Application to simple systems", J. Chem. Phys. 88, 1100 (1988)

Development of a pure diffusion quantum Monte Carlo method using a full generalized Feynman–Kac formula. II. Applications to simple systems

Michel Caffarel and Pierre Claverie

Dynamique des Interactions Moléculaires, Université Pierre et Marie Curie, Paris VI, Tour 22, 4 Place Jussieu, 75252 Paris, Cedex 05, France.

(Received 26 January 1987; accepted 15 September 1987)

We have described in part I of this work the theoretical basis of a quantum Monte Carlo method based on the use of a pure diffusion process and of the so-called full generalized Feynman–Kac (FGFK) formula. In this second part, we present a set of applications (one-dimensional oscillator, helium-like systems, hydrogen molecule) with the purpose of illustrating in a systematic way the various aspects pertaining to the practical implementation of this method. We thus show how energy and other observables can be obtained, and we discuss the various sources of biases occurring in the different procedures (notably the so-called short-time approximation pertaining to the generation of the sample trajectories of the diffusion process, and the numerical integration pertaining to the evaluation of the “Feynman–Kac factor”). After having thus considered the case of the genuine “bosonic” ground state, we illustrate the various proposals for dealing with some “relative” ground state (namely the lowest state belonging to some prescribed symmetry), one of the most important cases being obviously the physical ground state of many-fermion systems (owing to the Pauli principle requirements). More specifically, we consider the so-called fixed-node approximation (FNA), on one hand, and two variants of a potentially exact procedure, the so-called simple projection (SP) and release-node projection (RNP) methods, on the other hand. Finally, some perspectives concerning future developments are outlined.

I. INTRODUCTION

In paper I,¹ we have shown how quantum mechanical properties can be expressed in terms of functional integrals using our full generalized Feynman–Kac (FGFK) formula. More precisely, these functional integrals involve in their integrand the operators corresponding to the desired observables, and make use of the functional measure corresponding to a *pure diffusion* process, which is itself associated in a simple way with some reference function denoted $\varphi_0^{(0)}$.

When $\varphi_0^{(0)}$ is chosen to be square integrable (which is always the case in our applications), this associated diffusion process is ergodic (recurrent, actually), and accordingly the functional integrals may be rigorously expressed as time-averages along any single sample trajectory (or any finite number of sample trajectories) of the process. From the practical point of view, this feature sharply contrasts with the situation encountered when dealing with the Feynman path integral (in imaginary time) or the Wiener integral (involved in the usual Feynman–Kac formula). Indeed, in the two latter cases, no ergodic property holds, and consequently the numerical evaluation of the functional integrals would require summing over an unlimited number of trajectories.

As concerns the generation of the trajectories themselves, we use the Langevin equation associated with the diffusion process, with a suitable time discretization. In earlier stages of our work, we contented ourselves with a constant time step, but later on we were led to improve our procedure by using a variable time step, noticeably for avoiding so-called “overshooting” effects (see e.g., Ref. 2) near hypersurfaces where the drift vector of the Langevin equation becomes infinite.

An important problem consists in evaluating quantities pertaining to the lowest state belonging to some prescribed symmetry type, rather than the “absolute” lowest state only. Perhaps the most important special case is that of N -fermion systems (with $N > 2$), since the Pauli principle requires that the physical states belong to some *restricted* set of representations of the permutation group, thereby excluding the absolute (bosonic) ground state, which belongs to the (fully symmetric) identity representation. In order to illustrate the various possibilities of treating this problem, we put into application the three procedures examined in part I, namely the simple projection (SP) method, the fixed-node approach (FNA), and the release-node projection (RNP) method.

The contents of the paper are as follows. In sec. II, we consider several one-dimensional problems of increasing complexity with the purpose of illustrating in a stepwise way the essential properties of the method and its different versions. More specifically, we consider first (Sec. II A) for $H^{(0)}$ a harmonic oscillator Hamiltonian and we take $H = H^{(0)}$ (i.e., $V_p = 0$); this case will enable us to check some basic features of the algorithms (noticeably the so-called short-time approximation). Then (Sec. II B), using the same $H^{(0)}$ but now $V_p = x^2$ (so that H is still harmonic), we can study the error due to the numerical integration of the “Feynman–Kac factor” $\exp\{-\int V_p[X(s)]ds\}$. In Sec. II C, we consider as total Hamiltonian: $H = -\frac{1}{2}d^2/dx^2 + \frac{1}{2}x^2 + x^4$, but we now study successively *two* choices for $\varphi_0^{(0)}$, from which we build two different reference Hamiltonian $H^{(0)}$'s, with corresponding potential V_p 's having qualitatively different magnitudes (varying like x^4 or x^2 , respectively for $|x| \rightarrow +\infty$). We also introduce here the use of the Padé–integral transform for extracting the first excitation energies from a set of sampled values of $I(t)$, the matrix element of the “evolution

operator" (in imaginary time) $\exp(-tH)$. In Sec. II D we consider (for the same Hamiltonian H as in Sec. II C) the problem of obtaining the lowest state of some *prescribed symmetry* (odd parity here) different from the one of the genuine ground state (even parity here). For that purpose, we introduce the simple projection (SP) method and the fixed-node approximation (FNA), which turns out to be exact in this case. Finally, in Sec. II E we return to the harmonic oscillator Hamiltonian, but we now focus our attention on the *second* excited state φ_2 , whose "peculiar nodes" are *not* imposed by any symmetry (see part I). We can then study a genuine case of fixed-node *approximation*, and also the release-node projection (RNP) method for reaching the exact result. It must be emphasized that the cases treated in Secs. II D and II E illustrate the methods which will be necessary for dealing with the N -fermion systems ($N > 2$). In Sec. III, we describe our first applications to the simplest atomic and molecular systems. In Sec. III A we deal with bosonic ground state properties (*energies and mean values of other observables*) for two-electron systems: helium atom and helium-like ions and the hydrogen molecule. These cases enable us to illustrate efficient choices of $\varphi_0^{(0)}$ (from which result nontrivial $H^{(0)}$ and V_p operators). In Sec. III B, we consider, as a preliminary step towards the study of N -fermion systems, the problem of obtaining the energy of the lowest helium triplet, both with the simple projection and fixed-node approach (which can still be made exact here). Finally we present in Sec. IV some perspectives about the treatment of larger systems, concerning the evaluation of energies, mean values of other observables, and response properties.

II. ONE-DIMENSIONAL SYSTEMS

A. Harmonic oscillator

The Hamiltonian is written

$$H = -\frac{1}{2} \frac{d^2}{dx^2} + \frac{1}{2} x^2. \quad (2.1)$$

According to the general theory presented in part I, the Hamiltonian is decomposed into two parts:

$$H = H^{(0)} + V_p, \quad (2.2)$$

where $H^{(0)}$ is the so-called reference Hamiltonian built from a given reference function $\varphi_0^{(0)}$ and V_p the perturbing potential defined as the difference $H - H^{(0)}$. In this simple case, the reference function may be chosen as the exact ground state φ_0 of H , namely

$$\varphi_0^{(0)}(x) = \varphi_0(x) = e^{-x^2/2}. \quad (2.3)$$

The perturbing potential V_p which is expressed in terms of the reference function as [see Eq. (3.2) of part I]

$$V_p = V - E_0^{(0)} - \frac{1}{2} \nabla^2 \varphi_0^{(0)} / \varphi_0^{(0)}, \quad (2.4)$$

where V is the potential energy of H and $E_0^{(0)}$ an arbitrary constant, becomes here

$$V_p = 1/2 - E_0^{(0)}. \quad (2.5)$$

Note that the arbitrary reference energy $E_0^{(0)}$ may be chosen so that $V_p = 0$.

Now, the full generalized Feynman-Kac (FGFK) for-

mula permits to express the following matrix element of the (imaginary-time) evolution operator $\exp(-tH)$:

$$I(t) = \langle f \varphi_0^{(0)} | e^{-t(H - E_0^{(0)})} | g \varphi_0^{(0)} \rangle \quad (2.6)$$

as a functional integral [see Eq. (4.1) of part I]. Using the ergodic property of the reference diffusion process built from $\varphi_0^{(0)}$ [cf. Eq. (3.15) of part I], this functional integral may be expressed as a time-average over the stochastic trajectories of this process. In the present case where $V_p = 0$, we obtain

$$I(t) = \lim_{T \rightarrow +\infty} \frac{1}{T} \int_0^T f[X^{(0)}(-t/2 + \tau)] \times g[X^{(0)}(t/2 + \tau)] d\tau, \quad (2.7)$$

where $X^{(0)}(s)$ denotes an arbitrary trajectory of the reference diffusion process. It must be pointed out that the ergodic property may be invoked here since $\varphi_0^{(0)}$ has been chosen square integrable (cf. Sec. III of part I).

On the other hand, using the well-known equality

$$\varphi_n(n) = \varphi_0(n) (2^n n!)^{-1/2} H_n(x), \quad (2.8)$$

where $H_n(x)$ are the Hermite polynomials, and choosing the functions f and g as follows

$$f(x) = g(x) = (2^n n!)^{-1/2} H_n(x), \quad (2.9)$$

the matrix element [Eq. (2.6)] takes on the simpler form

$$I(t) = e^{-t(E_n - E_0^{(0)})} \quad (2.10)$$

and from Eqs. (2.10) and (2.7) we obtain the basic equality

$$e^{-t(E_n - E_0^{(0)})} = \lim_{T \rightarrow +\infty} \frac{1}{T} \int_0^T \frac{1}{2^n n!} H_n[X^{(0)}(-t/2 + \tau)] \times H_n[X^{(0)}(t/2 + \tau)] d\tau. \quad (2.11)$$

Then, by evaluating numerically the right-hand side of Eq. (2.11) above, the excited energies of the system can be calculated.

As concerns the construction of the arbitrary stochastic trajectory $X^{(0)}(s)$, a discretized form of the stochastic differential equation (SDE), suitable for computer simulation, is introduced (see e.g., Ref. 3, Sec. 3.6)

$$X(t + \Delta t) = X(t) + b[X(t)]\Delta t + (\Delta t)^{1/2} \eta, \quad (2.12)$$

where the η 's denote successive samples of a Gaussian random variable with zero mean and variance 1. The drift function $b(x)$ above may be evaluated from the general expression of the drift vector given in terms of the reference function [see Eq. (2.11a) of part I]:

$$\mathbf{b} = \nabla \varphi_0^{(0)} / \varphi_0^{(0)}. \quad (2.13)$$

Using expression (2.3) for the reference function, we obtain

$$b(x) = -x. \quad (2.14)$$

As a second step, the numerical integration involved in the right-hand side of Eq. (2.11) is performed over the stochastic trajectory $X^{(0)}(s)$ for large but finite T . In fact, by using a suitable updating scheme, the two operations (construction of the trajectory and integration) are performed simultaneously.

The numerical realization has put three points into evi-

dence: (1) The pseudorandom generator used for generating Gaussian numbers must have a very good quality in order to prevent the apparition of biases and artificial oscillations in the results. (2) The statistical fluctuations are significantly decreased when a large number of trajectories starting from points distributed according to the stationary probability density $p^{(0)}(x) = \varphi_0^{(0)2}$ are used, rather than a single one only. Furthermore, by decomposing this set of trajectories into a few subsets (typically about ten) and by evaluating the functional integral *independently* for each of these subsets, it is possible to obtain an evaluation of the variance using standard statistical methods.⁴ (3) Time-discretization of the SDE (with a time step Δt) introduces a systematic bias in the results: this is the well-known "short-time approximation" (see, e.g., Refs. 2 and 5). More precisely, by using the discretized form [Eq. (2.12)] of the SDE, the exact transition probability density $p^{(0)}(x|y, \Delta t)$ corresponding to the exact continuous form of the SDE is approximated by the following transition density:

$$P_{\text{approx}}^{(0)}(x|y, \Delta t) = (2\pi\Delta t)^{-1/2} \exp\left\{-\frac{[y-x-b(x)\Delta t]^2}{2\Delta t}\right\}. \quad (2.15)$$

In the particular case of the diffusion process associated with the Gaussian reference function (2.3) (the so-called "Ornstein-Uhlenbeck" process) $p^{(0)}(x|y, \Delta t)$ is exactly known (see e.g., Sec. 5.3 of Ref. 3):

$$P^{(0)}(x|y, \Delta t) = [\pi(1-\gamma^2)]^{-1/2} \times \exp\left[-\frac{(y-\gamma x)^2}{(1-\gamma^2)}\right], \quad (2.16)$$

where $\gamma = \exp(-\Delta t)$.

As it must be, the two expressions [Eqs. (2.15) and (2.16)] coincide when Δt goes to zero. Thus, in the special case under consideration, we can avoid the short-time approximation by generating the stochastic trajectories from the transition probability [Eq. (2.16)] instead of Eq. (2.15).

In Table I, results for some of the lowest excited energies

TABLE I. First excited energies for the harmonic oscillator.^a

	E_1	E_2	E_3
Biased results ^b			
$\Delta t = 0.04$	1.518(7)	2.54(2.6)	3.58(6)
$\Delta t = 0.03$	1.514(8)	2.53(3)	3.55(7.5)
$\Delta t = 0.02$	1.510(9)	2.51(3.3)	3.51(11)
$\Delta t = 0.01$	1.504(15)	2.50(5.4)	3.45(17)
Nonbiased results ^c			
$\Delta t = 0.04$	1.499(7)	2.50(2.6)	3.52(6)
Exact results			
	1.5	2.5	3.5

^a Calculations have been performed using 100 trajectories (divided in 10 subsets of 10 trajectories each for the purpose of evaluating the standard deviation, and hence the confidence interval corresponding to some prescribed level of accuracy). 500 000 elementary time steps have been used for each trajectory. Energies are derived from formula (2.11) with $t = 0.4$. Statistical uncertainties (99% confidence interval) are indicated in parentheses.

^b Using Eq. (2.15).

^c Using Eq. (2.16).

are presented. Expressions (2.15) and (2.16), above, for the transition probability density have been used to generate trajectories. The bias resulting from the short-time approximation appears clearly. The improvement resulting from the removal of this approximation is clearly evidenced when using the *exact* transition probability density. As concerns the biased results, no procedure of extrapolation to $\Delta t = 0$ has been used since the statistical fluctuations are of the same order of magnitude as the biases. Results for $\Delta t = 0.01$ may be considered as satisfactory.

B. Harmonic oscillator with a harmonic perturbation

The Hamiltonian is written

$$H = -\frac{1}{2} \frac{d^2}{dx^2} + \frac{1}{2} x^2 + \lambda x^2. \quad (2.17)$$

The reference function and energy are chosen as follows

$$\varphi_0^{(0)}(x) = e^{-x^2/2}, \quad (2.18a)$$

$$E_0^{(0)} = \frac{1}{2}. \quad (2.18b)$$

Using Eqs. (2.4), (2.2), and (2.18), we thus obtain

$$H^{(0)} = -\frac{1}{2} \frac{d^2}{dx^2} + \frac{1}{2} x^2, \quad (2.19a)$$

$$V_p = \lambda x^2. \quad (2.19b)$$

In this example, we use a high-quality generator of pseudorandom numbers, a large number of trajectories (about 100) and the exact transition probability density (no short-time approximation). We are then in a position to test the numerical effectiveness of our generalized Feynman-Kac formula [Eq. (4.1) of part I] in a case where the perturbing potential V_p is not zero. Using as usual the ergodic property, the quantum matrix element (2.6) (with $f = g = 1$) may be rewritten as

$$I(t) = \lim_{T \rightarrow +\infty} \frac{1}{T} \int_0^T \exp\left[-\int_{-t'/2+\tau}^{t'/2+\tau} V_p[X^{(0)}(s)] ds\right] d\tau. \quad (2.20)$$

Now, if we want to extract the ground state energy E_0 of H , the following formula valid for large but finite t could be used [see Eqs. (4.4) and (4.5) of part I]:

$$-\frac{1}{t} \log I(t) = E_0 - E_0^{(0)} - \frac{1}{t} \log |\langle \varphi_0^{(0)} | \varphi_0 \rangle|^2 + O(e^{-t}). \quad (2.21)$$

In actual fact, the error $O(1/t)$ due to the second term may be very easily suppressed by considering the slope of $\log I(t)$ at infinity:

$$-\frac{[\log I(t_2) - \log I(t_1)]}{(t_2 - t_1)} = E_0 - E_0^{(0)} + O(e^{-t_1}) \quad t_2 > t_1 \quad (2.22)$$

which now involves, for large t_2 and t_1 , an exponentially small error.

On the other hand, using the eigensolutions for $H^{(0)}$ and H , that is, respectively,

$$\varphi_n^{(0)}(x) = \pi^{-1/4} (2^n n!)^{-1/2} H_n(x) e^{-x^2/2} \quad (2.23a)$$

$$E_n^{(0)} = n + 1/2 \quad (2.23b)$$

and

$$\begin{cases} \varphi_n(x) = \omega^{1/4} \pi^{-1/4} (2^n n!)^{-1/2} H_n(\omega^{1/2} x) e^{-\omega x^2/2} & \text{with } \omega = (1 + 2\lambda)^{1/2} \\ E_n = (n + 1/2)\omega \end{cases} \quad (2.24a)$$

$$(2.24b)$$

and inserting these expressions into the expanded expression for $I(t)$ in terms of the complete set of eigenstates of H given in Eq. (4.4) of part I, it is possible to obtain after a few algebraic manipulations the analytical value of $I(t)$:

$$I(t) = \frac{2\omega^{1/2}}{1 + \omega} e^{-t/2(\omega - 1)} \times \left[1 + \sum_{n=1}^{\infty} \frac{(2n-1)!!}{2^n n!} \left(\frac{\omega - 1}{\omega + 1} \right)^{2n} e^{-2\omega t n} \right]. \quad (2.25)$$

The numerical realization (with $\lambda = 1$, i.e., $\omega = 3^{1/2}$) shows the existence of a bias for $I(t)$ when $\Delta t = 0.2$ (see Table II). This bias is due to use of a finite Riemann sum for evaluating the integral $\int V_p ds$ appearing in Eq. (2.20). However, as we can see in Table II, it seems that this bias is very small compared with previous biases due to the short-time approximation.

C. Quartic oscillator. Evaluation of the ground state energy E_0

The Hamiltonian is written

$$H = -\frac{1}{2} \frac{d^2}{dx^2} + \frac{1}{2} x^2 + x^4. \quad (2.26)$$

In this example we illustrate a basic feature of the method namely, the importance of choosing a "good" reference function $\varphi_0^{(0)}$. As already noticed above, if $\varphi_0^{(0)}$ were chosen as the exact function φ_0 , the perturbing potential defined by Eq. (2.4) would be zero ($E_0^{(0)}$ is arbitrary and may be chosen so that $V_p = 0$) and the variance would vanish. In the general case, the numerical experience has shown that the importance of the statistical fluctuations is directly related to the "importance" of this perturbing potential. Two cases have been treated here. In the first one, we make the natural choice:

$$\varphi_0^{(0)} = e^{-x^2/2} \quad (2.27)$$

which leads to

TABLE II. Harmonic oscillator with a harmonic perturbation.^a

	E_0
QMC ($\Delta t = 0.02$)	0.8660(14)
Exact ^b	0.86603
	$I(t = 3)$
QMC:	
$\Delta t = 0.2$	0.3227(4)
$\Delta t = 0.1$	0.3214(4)
$\Delta t = 0.075$	0.3213(4)
Exact ^c	0.32131

^a Calculations have been performed using 100 trajectories, 500 000 elementary time steps for each trajectory. Energy is derived from formula (2.22) with $t_2 = 9$ and $t_1 = 8$. Statistical uncertainties are indicated in parentheses.

^b From formula (2.24b).

^c Calculated from formula (2.25).

$$V_p = x^4 + \frac{1}{2} - E_0^{(0)}. \quad (2.28)$$

By contrast, in the second case, the behavior for $|x| \rightarrow +\infty$ of the exact eigenfunction φ_0 is incorporated into $\varphi_0^{(0)}$. The asymptotic form of φ_0 is easily deduced from the asymptotic form of the Schrödinger equation. We obtain:

$$\varphi_0(x) \underset{|x| \rightarrow +\infty}{\sim} e^{-2^{1/2}/3 |x|^3}. \quad (2.29)$$

Consequently, our second choice will be

$$\varphi_0^{(0)}(x) = e^{-2^{1/2}/3 |x|^3} \quad (2.30)$$

and from Eq. (2.4) above it then follows that

$$V_p = \frac{1}{2} x^2 + 2^{1/2} |x| - E_0^{(0)}. \quad (2.31)$$

With this choice, the quartic part of V_p has been removed. The ground state energy E_0 has been evaluated using the two forms for $\varphi_0^{(0)}$ and for different values of the time step Δt . Results are displayed in Table III. The important point is that with the expression (2.30) for $\varphi_0^{(0)}$, the variance is actually smaller than with the expression (2.27). From now on, this strategy of variance reduction will be systematically used.

From the expanded form [Eq. (4.4)] of part I it is clear that $I(t)$ may be written in the following form:

$$I(t) = \sum_t c_t e^{-\lambda t}. \quad (2.32)$$

TABLE III. Ground state and second excited state energies for the quartic oscillator.

E_0^a	
First choice for $\varphi_0^{(0)b}$	
$\Delta t = 0.01^c$	0.8037(20)
Second choice for $\varphi_0^{(0)d}$	
$\Delta t = 0.1$	0.8199(5)
$\Delta t = 0.075$	0.8156(6)
$\Delta t = 0.05$	0.8114(7)
$\Delta t = 0.025$	0.8079(8)
Extrapolation ^e	0.8037(10)
Exact ^f	0.80377
Excited energies ^g	
E_0	
QMC	0.8033(30)
Exact ^f	0.80377
E_2	
QMC	5.18(2)
Exact ^f	5.179

^a Energy is derived from formula (2.22) with $t_2 = 4$ and $t_1 = 3$. Calculations have been performed using 1000 trajectories with 75 000 elementary time steps for each trajectory.

^b Expression (2.27).

^c Using Eq. (2.16).

^d Expression (2.30).

^e A least-squares fit to a straight line has been performed.

^f Reference 15.

^g A Padé z -transform analysis of $I(t)$ has been done with 40 regularly sampled values $I(t_i)$ with t_i ranging from 0 to 4. The calculation has been performed using 100 trajectories, 200 000 elementary time steps for each trajectory and $\Delta t = 0.1$.

The expression (2.22) enables us to extract the smallest exponent λ_0 using the behavior of $I(t)$ for large t . Now, we would like to extract more information about $I(t)$. More precisely, we are faced with the general problem of the analysis of functions expressed as sum of real exponentials. We used here the Padé-integral transform method recently developed.⁶ This method enables us to evaluate excited energies. However, the main point appears to be the possibility to perform an analysis of $I(t)$ without using large values of t . The importance of such a possibility has been already emphasized in part I (Sec. VI C 2). A Padé- z transform analysis of $I(t)$ has been performed here. Results are displayed in Table III.

D. Quartic oscillator. Evaluation of the first excited energy E_1

The first excited energy E_1 of the quartic oscillator may be viewed as the ground state energy of the *odd* symmetry subspace. Since this subspace is *not* the symmetry subspace of the genuine ground state E_0 , this example may be considered as a *model problem* for illustrating the constraints due to the Pauli principle requirements (see part I, Sec. VI). Two of the procedures designed for dealing with such a situation are presented here.

1. Simple projection (SP) method

Two projection functions f and g are used in order to impose the odd symmetry. We have chosen the simplest form, namely

$$f(x) = g(x) = x. \quad (2.33)$$

In order to avoid the short-time approximation the Gaussian nodeless reference function $\varphi_0^{(0)}$ defined in Eq. (2.27) is chosen. Now, using the odd character of the functions $f\varphi_0^{(0)}$ and $g\varphi_0^{(0)}$, the expanded form [Eq. (4.4)] of part I for $I(t)$ reduces to the following form:

$$I(t) = \sum_{k=0}^{+\infty} |\langle n\varphi_0^{(0)} | \varphi_{2k+1} \rangle|^2 e^{-t(E_{2k+1} - E_0^{(0)})}, \quad (2.34)$$

where half of the terms (corresponding to even levels) have disappeared. In fact, due to the numerical nature of the evaluation of $I(t)$, the scalar products $\langle n\varphi_0^{(0)} | \varphi_{2k} \rangle$ could be not exactly zero. Then, residual exponentials associated with even levels may appear with a small amplitude. The numerical experience has shown that such amplitudes were small enough so that no practical trouble results when performing the analysis of $I(t)$. As usual, using the ergodic property we write

$$I(t) = \lim_{T \rightarrow +\infty} \frac{1}{T} \int_0^T X^{(0)}(-t/2 + \tau) X^{(0)}(t/2 + \tau) \times \exp\left[-\int_{-t/2 + \tau}^{t/2 + \tau} X^{(0)4}(s) ds\right] d\tau. \quad (2.35)$$

Now, an important point related to the numerical evaluation of the quantity above must be pointed out. By using expression (2.27) for $\varphi_0^{(0)}$, we have built a reference diffusion process with a stationary density $p^{(0)}(x) = \varphi_0^{(0)2}$ strongly peaked with a symmetric shape around zero. Accordingly, the trajectory will go through zero very often and the sign of

the product $X^{(0)}(-t/2 + \tau)X^{(0)}(t/2 + \tau)$ will change rapidly. Moreover, the values of the position at two very different times being almost independent (the correlation function of the diffusion process falls exponentially as a function of time) the sign of the previous product will change with a very high rate for large t . The consequence is a large increase of variance in calculations when non small values of t are considered, a situation which contrasts sharply with the one encountered in the calculations for which $f=g=1$. With such variances for large t , formula (2.22), which requires two large values of t for evaluating E_1 , is inadequate, and the Padé-integral transform method for analyzing $I(t)$ becomes essential. We have performed a Padé- z transform analysis of $I(t)$. The results are displayed in Table IV and show a relatively important variance in this approach.

2. Fixed-node (FN) method

In this approach, no problems related to some change of sign as in the expression (2.35) occur since no projection functions are used. The symmetry requirements are directly introduced into the reference function. Here $\varphi_0^{(0)}$ must be odd and is chosen as follows:

$$\varphi_0^{(0)} = xe^{-2^{1/2/3}|x|^3}. \quad (2.36)$$

Note that in this particular one-dimensional case the node of the exact solution φ_1 is known and consequently the fixed-node procedure actually introduces no approximation.

At this point, it seems important to make a practical remark concerning the use of a variable time step scheme for calculations involving a reference function endowed with nodal hypersurfaces. Let us be more precise. The discretized form of the SDE with $\Delta t \neq 0$ enables us to generate successive points on a trajectory through finite jumps but not infinitesimal ones as would be required by the exact continuous SDE. A finite jump may lead the current point to the other side of a nodal hypersurface (through essentially the free diffusion part of the SDE) or very far in a domain of very low probability when the drift vector becomes too large (the "overshooting" effect near the nodes). In order to avoid the important biases associated with these two artificial effects which disappear for really infinitesimal time steps, we used a variable time step scheme. When the magnitude of the drift

TABLE IV. First excited energy E_1 of the quartic oscillator.

I. Simple projection (SP) method ^a	
QMC	2.74(2)
Exact ^b	2.738
II. Fixed-node approach (FNA) ^c	
QMC ($\Delta t = 0.005$)	2.738(4)
Exact ^b	2.738

^a Calculations have been performed using 1000 trajectories, 20 000 elementary time steps for each trajectory with $\Delta t = 0.1$. A Padé z -transform analysis of $I(t)$ has been done with 30 regularly sampled values $I(t_i)$ with t_i ranging from 0 to 3.

^b Reference 15.

^c Calculations have been performed using 100 trajectories, 500 000 elementary time steps for each trajectory. Energy is derived from formula (2.22) with $t_2 = 2.5$ and $t_1 = 2$. Statistical uncertainties are indicated in parentheses.

becomes too important (larger than some threshold value), we take Δt such that the product $|b|\Delta t$ remains small enough. Thus, the trajectory is slowed down near nodal surfaces and large jumps are avoided. Now, the variance becomes sufficiently low to permit the use of formula (2.22) to obtain E_1 .

Results are displayed in Table IV and it clearly appears that the fixed-node (FN) method (Sec. II D 2) actually performs better than the simple projection (SP) method (Sec. II D 1).

E. Harmonic oscillator. Evaluation of the second excited energy E_2

In the previous example illustrating the fixed-node approach, we used a reference function having the right symmetry and the exact node of the solution. Unfortunately, the complete nodal hypersurfaces of exact solutions for more complex systems are generally not known. For atoms or molecules we will use a reference function having the desired symmetry [i.e., belonging to the corresponding irreducible representation of the symmetric group $S(N)$] but *approximate nodes*. At this point, it must be emphasized that, due to the degeneracy of the physical ground state (the “exchange” degeneracy), there is not a single nodal hypersurface associated with the ground state but a (continuous) set of such surfaces. “Approximate” means here that the nodal hypersurface of $\varphi_0^{(0)}$ does not belong to this set. A fixed-node approach with approximate nodes leads to approximate results and in order to remove this approximation the release-node projection (RNP) method presented in part I is examined here. To evaluate the second excited energy of the one-dimensional harmonic oscillator is a simple model problem which gives us the opportunity to introduce in a simple way the main features of this RNP method. In this model problem, the exact solution is known:

$$\varphi_2(x) = (2\pi^{1/2})^{-1/2}(2x^2 - 1)e^{-x^2/2}, \quad (2.37a)$$

$$E_2 = 5/2. \quad (2.37b)$$

$$\varphi_0^{(0)}(x) = |[2x^2 - (1 + d)]e^{-x^2/2}|$$

$$\varphi_0^{(0)}(x) = \text{cpf}(x) = A(x \pm x_n)^3 + B(x \pm x_n)^2 + C(x \pm x_n) + D$$

where $\pm x_n$ denote the two nodes of the function (2.39a) above. Note that, instead of using a threshold value for the reference function as we did in part I, we directly define here the interval where the connecting piece function is used. Both procedures are essentially equivalent and ϵ' now plays a role similar to that of the quantity ϵ introduced in part I. The coefficients (A, B, C, D) are determined so that the reference function and its first derivative are continuous at the points $\mp x_n - \epsilon'$ and $\mp x_n + \epsilon'$. Expressions of the coefficients (A, B, C, D) in terms of (d, ϵ') are then given as solutions of a linear system of four equations.

As already noticed, φ_2 is not the lowest eigenfunction in the subspace of even symmetry. Consequently the first non-vanishing component of $I(t)$, namely $\langle f \varphi_0^{(0)} | \varphi_0 \rangle \langle \varphi_0 | g \varphi_0^{(0)} \rangle \times e^{-t(E_0 - E_0^{(0)})}$ could be important enough to trouble the analysis (in particular if large values of

1. Fixed-node (FN) method

As a first step, we consider a fixed-node approach where the reference function $\varphi_0^{(0)}$ has the right symmetry (here $\varphi_0^{(0)}$ must be an even function) and approximate nodes. The reference function is chosen as follows:

$$\varphi_0^{(0)}(x) = [2x^2 - (1 + d)]e^{-x^2/2}, \quad (2.38)$$

where d is related to the “distance” between approximate nodes and exact ones.

Now, the fixed-node ground-state energy E_2^{FN} can be evaluated for different values of d using, as usual, formula (2.22) and using the variable time step procedure required by the existence of nodes for $\varphi_0^{(0)}$ (see Sec. II D 2 above). Results for $E_2^{\text{FN}}(d)$ are displayed in Table V and illustrate very clearly the existence of the fixed-node approximation. We may notice that the values of $E_2^{\text{FN}}(d)$ lie *below* the exact energy $E_2^{\text{FN}}(0)$. At first sight, this result could appear contradictory with the so-called “variational principle for fixed-node process” considered by Reynolds *et al.*⁵ and by Ceperley.⁷ The contradiction disappears, however, when we notice that the above variational principle was derived for the following specific situation: (1) to consider the lowest state belonging to some prescribed type of symmetry and (2) to use a reference function belonging to this type of symmetry, so that its nodes are invariant under the corresponding symmetry operations. Failure to fulfill these conditions invalidates the proof. In our present case, assumption (1) is not fulfilled, since the lowest *even* state is E_0 rather than E_2 .

2. Release-node projection (RNP) method

Now, we want to remove the fixed-node approximation by using the RNP procedure described in our part I. A non-vanishing third-order polynomial is chosen as “connecting piece” function $\text{cpf}(x)$. The reference function is written

$$x \in (\mp x_n - \epsilon', \mp x_n + \epsilon'), \quad (2.39a)$$

$$x \in (\mp x_n - \epsilon', \mp x_n + \epsilon'), \quad (2.39b)$$

t are used) and this situation would require the use of the Padé-integral transform to evaluate E_2 . This complication does not occur in the case of atoms or molecules where the true wave function is a lowest state in a given symmetry subspace. Now, in order not to introduce artificial problems in this model problem, we have decided to use functions f and g not only to impose the right symmetry (as it must be in the general case) but also to impose the orthogonality of $f \varphi_0^{(0)}$ and $g \varphi_0^{(0)}$ with φ_0 . For that reason we choose

$$f = g = \varphi_2 / \varphi_0^{(0)} \quad (2.40)$$

which leads to

$$I(t) = e^{-t(E_2 - E_0^{(0)})}. \quad (2.41)$$

Obviously, in the general case, only the symmetry of the desired state has to be known even if for convenience we have

TABLE V. Harmonic oscillator. Evaluation of E_2 .

I. Fixed-node approximation (FNA) ^a	
$d = 0.1$	2.346(21)
$d = 0.075$	2.401(20)
$d = 0.05$	2.451(16)
$d = 0.025$	2.484(8)
$d = 0$	2.5
II. Release-node projection (RNP) ^b	
$d = 0.1 \quad \epsilon' = 0.45$	2.49(3)
Exact	2.5

^aCalculations have been performed using 50 trajectories, 10 000 elementary time steps for each trajectory and $\Delta t = 0.001$. Energy is derived from formula (2.22) with $t_2 = 8$ and $t_1 = 7.5$.

^bCalculations have been performed using 50 trajectories, 800 000 elementary time steps for each trajectory and $\Delta t = 0.001$. Energy is derived from formula (2.41) with $t = 0.4$. Statistical uncertainties are indicated in parentheses.

introduced here its analytical expression through the functions f and g . Now, when ϵ' goes to zero, two phenomena occur. On one hand, since the value of the reference function at the points $\pm x_n$ goes to zero with ϵ' , passages from one domain to another one become rare and the variance related to the change of sign of the integrand decreases. On the other hand, $V_p(x)$ in the neighborhood of $\pm x_n$ goes to infinity when ϵ' goes to zero and the sampling of this domain, responsible for the removal of the nodes, becomes more and more difficult (we try to sample rare events associated with a high value of V_p or, equivalently, we attempt to sample a δ function!). Therefore some compromise has to be found. We present in Fig. 1 the curve giving the variance of calculations versus ϵ' . Clearly an optimal choice for ϵ' may be found in such an approach. The energy for $d = 0.1$ is presented in Table V. The difference $E_2^{\text{FN}} - E_2$ being recovered, we conclude that the RNP works for this simple case.

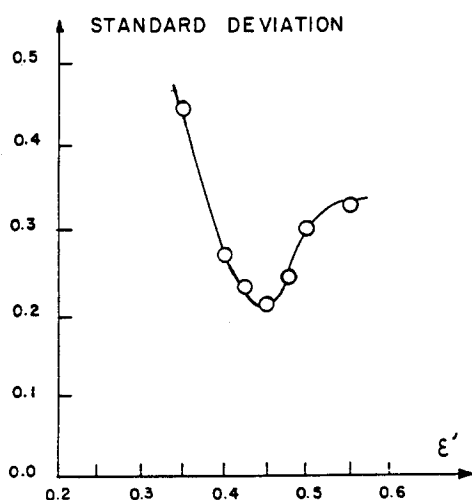


FIG. 1. Standard deviation of the energy as a function of the threshold parameter ϵ' appearing in the RNP method. These values have been obtained for rather short runs. In order to obtain an accurate value of the energy, a 100 times longer run has been performed for the value $\epsilon' = 0.45$ which gives the optimal choice of the reference function. The corresponding result is presented in Table V (the standard deviation is actually divided by about $100^{1/2} = 10$).

III. SIMPLE ATOMIC AND MOLECULAR SYSTEMS

Molecules are represented in the framework of the Born–Oppenheimer approximation. The potential energy of the molecule is written as

$$V = \sum_{i>j} 1/r_{ij} - \sum_{i,\alpha} Z_\alpha/r_{i\alpha} + \sum_{\alpha>\beta} Z_\alpha Z_\beta/r_{\alpha\beta}, \quad (3.1)$$

where $r_{ab} = |\mathbf{r}_a - \mathbf{r}_b|$. Roman indices label electronic coordinates and Greek indices label nuclear coordinates. Z_α is the charge number of nucleus α .

A. Bosonic properties

The purpose of this first subsection is to evaluate energy and observables pertaining to the ground state of two-electron systems. Since no constraints are introduced by the Pauli principle for two-electron systems (see Sec. VI of part I), this ground state is the nodeless mathematical ground state of the Hamiltonian. This is the reason why the properties evaluated in this subsection may be viewed as bosonic properties.

1. Helium-like systems

Before treating helium-like systems, let us give a general expression of a nodeless reference function suitable for an arbitrary atomic system:

$$\varphi_0^{(0)} = \exp \left[\sum_{i,\alpha} a_{i\alpha} r_{i\alpha} + \sum_{i<j} a_{ij} r_{ij} \right]. \quad (3.2)$$

The important point is that this expression includes all the cusp conditions. Note that such a representation has been already discussed in detail in the framework of previous QMC methods (see, e.g., Ref. 5). Obviously, for atomic systems with more than two electrons, this function can be used only in the SP method where a nodeless reference function is needed (see Sec. VI B 2 in part I). The coefficients a_{ab} are chosen in order to reduce as much as possible the perturbing potential V_p . Let us now evaluate the two basic quantities of our algorithm, namely the perturbing potential V_p and the drift vector \mathbf{b} . The perturbing potential is evaluated as usual from formula (2.4). After a few algebraic manipulations we obtain

$$\begin{aligned} V_p &= \sum_{i>j} 1/r_{ij} - \sum_{i,\alpha} Z_\alpha/r_{i\alpha} + \sum_{\alpha>\beta} Z_\alpha Z_\beta/r_{\alpha\beta} \\ &- E_0^{(0)} - \sum_{i>j} 2a_{ij}/r_{ij} - \sum_{i,\alpha} a_{i\alpha}/r_{i\alpha} \\ &- \frac{1}{2} \sum_{\alpha,\beta,i} a_{i\alpha} a_{i\beta} (\nabla_i r_{i\alpha}) \cdot (\nabla_i r_{i\beta}) \\ &- \sum_{i,j \neq i,\alpha} a_{ij} a_{i\alpha} (\nabla_i r_{i\alpha}) \cdot (\nabla_i r_{ij}) \\ &- \frac{1}{2} \sum_{i,j \neq i,k \neq i} a_{ij} a_{ik} (\nabla_i r_{ij}) \cdot (\nabla_i r_{ik}). \end{aligned} \quad (3.3)$$

Let us introduce the directional vectors

$$\mathbf{u}_{ij} = \frac{1}{2} \nabla_i r_{ij}, \quad (3.4a)$$

$$\mathbf{u}_{i\alpha} = -Z_\alpha \nabla_i r_{i\alpha}. \quad (3.4b)$$

Choosing coefficients a_{ij} and $a_{i\alpha}$ such that

$$a_{ij} = a_{ji} = \frac{1}{2}, \quad (3.5a)$$

$$a_{k\alpha} = -Z_{\alpha}, \quad (3.5b)$$

the Coulomb singularities may be entirely suppressed. Finally, we have

$$V_p = \sum_{\alpha>\beta} Z_{\alpha} Z_{\beta} / r_{\alpha\beta} - E_0^{(0)} - \frac{1}{2} \sum_{i,\alpha,\beta} \mathbf{u}_{i\alpha} \cdot \mathbf{u}_{i\beta} - \sum_{i,j \neq i,\alpha} \mathbf{u}_{i\alpha} \cdot \mathbf{u}_{ij} - \frac{1}{2} \sum_{i,j \neq i,k \neq i} \mathbf{u}_{ij} \cdot \mathbf{u}_{ik}. \quad (3.6)$$

Now, V_p is a nonsingular bounded function expressed as a sum of bounded scalar products. At this point, it seems appropriate to mention that this result illustrates clearly the necessity of including explicit interelectronic coordinates when a good approximate wave function is wanted. In particular, as noticed by a few authors (see, e.g., Ref. 8), the poor convergence of CI expansions is mainly due to the absence of such r_{ij} -dependent terms in the wave function. Now, a major advantage of all Monte Carlo schemes appears in the possibility of using correlated wave functions without dealing with the complicated integrals that occur in variational methods.

The expression for the drift vector is derived from Eq. (2.13):

$$\mathbf{b} = (\mathbf{b}_1, \mathbf{b}_2, \dots, \mathbf{b}_N) \quad (3.7a)$$

with

$$\mathbf{b}_i = \sum_{\alpha} \mathbf{u}_{i\alpha} + \sum_{j \neq i} \mathbf{u}_{ij}. \quad (3.7b)$$

For two-electron systems, energy and mean value $\langle r_1^2 + r_2^2 \rangle$ have been evaluated using expression (3.2) for the reference function. The constant time step scheme have been used since $\varphi_0^{(0)}$ is nodeless and calculations have been performed for different values of the elementary time step Δt ranging from $\Delta t = 0.02$ to $\Delta t = 0.12$. For each quantity evaluated, a quasiparabolic behavior for the curve representing this quantity vs Δt has been obtained. We therefore systematically performed a least-squares fit to a parabola to determine the extrapolated value at $\Delta t = 0$. We give in Table VI the results concerning the He atom ($Z = 2$) and the Be^{++} ion ($Z = 4$).

As concerns the calculation of the quantity $\langle r_1^2 + r_2^2 \rangle$, the formula (4.7) of part I is written here:

$$\langle \varphi_0 | r_1^2 + r_2^2 | \varphi_0 \rangle = \lim_{t \rightarrow +\infty} \frac{\int_{\Omega(-t/2; t/2)} (r_1^2 + r_2^2) [X(t_1)] \exp[-\int_{-t/2}^{t/2} V_p [X(s)] ds] D^{\varphi_0^{(0)}} X \forall t_1 \in]-t/2, t/2[}{\int_{\Omega(-t/2; t/2)} \exp[-\int_{-t/2}^{t/2} V_p [X(s)] ds] D^{\varphi_0^{(0)}} X} \quad (3.8)$$

and using the ergodic property this formula may be rewritten as

$$\langle \varphi_0 | r_1^2 + r_2^2 | \varphi_0 \rangle = \lim_{T \rightarrow +\infty} \frac{\lim_{t \rightarrow +\infty} \frac{1}{T} \int_0^T (r_1^2 + r_2^2) [X^{(0)}(t_1 + \tau)] \exp[-\int_{-t/2+\tau}^{t/2+\tau} V_p [X^{(0)}(s)] ds] d\tau}{\lim_{T \rightarrow +\infty} \frac{1}{T} \int_0^T \exp[-\int_{-t/2+\tau}^{t/2+\tau} V_p [X^{(0)}(s)] ds] d\tau}. \quad (3.9)$$

Results after extrapolation are given in Table VI. It is important to note that E_0 and $\langle r_1^2 + r_2^2 \rangle$ are evaluated simultaneously from the same realization of the process (i.e., from the same set of stochastic trajectories).

2. H_2 molecule

The potential energy of the molecule is

$$V = 1/r_{12} - 1/r_{1A} - 1/r_{1B} - 1/r_{2A} - 1/r_{2B} + 1/R, \quad (3.10)$$

where R is the internuclear distance. Two different reference functions have been used, namely

$$\varphi_0^{(0)} = e^{\frac{\alpha}{2} r_{12}} u(\mathbf{r}_1) u(\mathbf{r}_2) \quad (3.11a)$$

$$\text{with } u(\mathbf{r}_i) = e^{-\xi r_{iA}} + e^{-\xi r_{iB}} \quad (3.11b)$$

and

$$\varphi_0^{(0)} = \exp[-r_{1A} - r_{2B}] + \exp[-r_{2A} - r_{1B}]. \quad (3.12)$$

The first case corresponds to the usual molecular orbital point of view well suited for the equilibrium geometry while the second choice, where $\varphi_0^{(0)}$ is written as a symmetrized product of atomic wave functions, is supposed to be better for large values of R .

In order to illustrate the simplicity of the procedure for

evaluating different quantities pertaining to the same eigenstate, we have evaluated from the same basic set of trajectories, not only the energy but also 15 mean values corresponding to multiplicative operators. We have simply chosen the same operators considered by Kolos and Wolniewicz⁹ in

TABLE VI. Helium-like systems. Ground state properties.*

	He	Be^{++}
	E_0	
SCF	-2.8617	-13.611 3
QMC	-2.903 8(10)	-13.655(11)
"Exact" value	-2.903 72 ^a	-13.655 6 ^b
	$\langle r_1^2 + r_2^2 \rangle$	
QMC	2.37(2)	0.464(2)
Exact value	2.386 9 ^c	0.464 14 ^d

* Calculations have been performed using 400 trajectories, 40 000 elementary time steps for each trajectory. Energies are derived from formula (2.22) with $t_2 = 10$ and $t_1 = 9$. Mean values are derived from formula (3.9) with $t/2 = 5$ and $t_1 = 0$. Each quantity has been extrapolated to $\Delta t = 0$. All quantities are given in atomic units and statistical uncertainties are indicated in parentheses.

^b Reference 16.

^c Reference 17.

^d Reference 18.

their benchmark calculations concerning the H_2 molecule. In order to appreciate the powerful simplicity of the Monte Carlo approach, it must be pointed out that, for each such observable A , we have just to insert in the program the evaluation of $A[X(t)]$ and to calculate the corresponding accumulator (which, in the present case, amounts merely to inserting in the computer program one single statement per observable!). Calculations have been performed for two values of R corresponding to the two choices of $\varphi_0^{(0)}$. Results are displayed in Table VII, and are very satisfactory.

B. Fermionic properties

In this subsection, the first excited energy E_1 of the helium atom is evaluated. The corresponding eigenstate φ_1 is antisymmetric in the exchange of electron labels and corresponds to the ground state of the antisymmetric representation. In Sec. II D we have shown that the different methods to evaluate properties of the lowest state in a given symmetry subspace do work for simple one-dimensional cases. Here, the aim is to illustrate the validity of those different procedures for atomic and molecular systems.

1. Simple projection (SP) method

We choose

$$\varphi_0^{(0)} = \exp[-2r_1 - 2r_2 + \frac{1}{2}r_{12}] \quad (3.13)$$

and

$$f = g = \frac{1}{4}[(1 - r_1)e^{r_1} - (1 - r_2)e^{r_2}]. \quad (3.14)$$

TABLE VII. H_2 molecule. Ground state properties.^a

	$R = 1.4^c$		$R = 4^d$	
	QMC	Exact ^b	QMC	Exact ^b
E_0	-1.175(1.7)	-1.1745	-1.0167(7)	-1.016 37
$\langle r_{12}^{-1} \rangle$	0.587(2.6)	0.5874	0.263(1.5)	0.263 0
$\langle r_{12} \rangle$	2.169(9)	2.1690	4.33(1.5)	4.327
$\langle r_{12}^2 \rangle$	5.63(4.5)	5.632	20.6(1.3)	20.569
$\langle r_A \rangle$	1.550(6)	1.5499	2.86(1.3)	2.863
$\langle r_A^{-1} \rangle$	0.908(4)	0.9128	0.610(3.5)	0.613 6
$\langle r_A^2 \rangle$	3.04(2)	3.036	10.79(8.5)	10.815
$\langle r_A r_B \rangle$	2.71(2)	2.704	6.68(2.3)	6.663
$\langle r_{1A} r_{2A} \rangle$	2.33(1.5)	2.321	6.57(3)	6.551
$\langle r_{1A} r_{2B} \rangle$	2.39(1.5)	2.385	9.82(3)	9.806
$\langle z_1 z_2 \rangle$	-0.156(5.5)	-0.1596	-3.39(6)	-3.392
$\langle x_1 x_2 \rangle$	-0.055(3.5)	-0.0551	-0.039(4.5)	-0.038 4
$\langle z^2 \rangle$	1.02(2)	1.023	4.74(4)	4.708
$\langle x^2 \rangle$	0.76(2)	0.762	1.05(1.5)	1.054
$\langle r^2 \rangle$	2.55(4)	2.546	6.85(5.5)	6.815
Q	0.9(1)	0.91	1.3(1.5)	1.38

^aCalculations have been performed using 50 trajectories and about 10^6 elementary time steps for each trajectory with $\Delta t = 0.01$. Energies are derived from formula (2.22) with $t_2 = 20$ and $t_1 = 19$. Each mean value is derived from formula (4.7) of part I with $t/2 = 10$ and $t_1 = 0$. Q denotes the electric quadrupole moment of the molecule defined as $Q = R^2 - 2(3\langle z^2 \rangle - \langle r^2 \rangle)$. All quantities are given in atomic units and statistical uncertainties are indicated in parentheses.

^bReference 9.

^cUsing Eq. (3.11) for $\varphi_0^{(0)}$ with $\alpha = 0.56$ and $\xi = 1.285$.

^dUsing Eq. (3.12) for $\varphi_0^{(0)}$.

As it must be, $f\varphi_0^{(0)}$ and $g\varphi_0^{(0)}$ are antisymmetric in the exchange of electron labels. Moreover, by using the atomic orbital model, f and g have been chosen such that $f\varphi_0^{(0)}$ and $g\varphi_0^{(0)}$ have a maximum overlap with φ_1 . This last point simplifies the analysis of $I(t)$ as sum of real exponentials by giving an important weight to the first nonvanishing exponential associated with E_1 .

As already noticed in Sec. II D 1, the nonconstant sign of f and g prevents any attempt to use formula (2.22) for calculating E_1 . Thus a Padé- z transform analysis must be performed. A very predominant real exponential associated with E_1 appeared and then the first Padé approximant⁶ was sufficient to extract E_1 . The results are displayed in Table VIII.

2. Fixed-node (FN) approach

In this case, the complete nodal hypersurface of φ_1 is known (its equation is $r_1 = r_2$).^{10,11} However, even if there is no fixed-node approximation here, the aim is to verify that our scheme works for atomic systems.

The following reference function is chosen:

$$\varphi_0^{(0)} = (1 - r_1)e^{-r_1}e^{-2r_2} - (1 - r_2)e^{-r_2}e^{-2r_1} \quad (3.15)$$

and the same algorithm as in Sec. II D 2 is used. Conclusions are identical with those obtained in this previous case: due to the constant sign of the integrand, the variance is markedly smaller than in the previous (SP) method, and formula (2.22) for evaluating the energy may be used. The variable time step procedure permits to avoid undesirable effects. Results are displayed in Table VIII.

IV. CONCLUSIONS

While part I of the present work was devoted to the theoretical description of our Monte Carlo method, the purpose of the present part II was to consider with some detail the various practical and numerical aspects pertaining to its computer implementation.

It appeared convenient to organize the discussion around three main points:

- (1) The convergence problem (time-length of each

TABLE VIII. First excited energy E_1 of the helium atom (triplet state).

I. Simple projection (SP) method ^a	
QMC	-2.175(10)
Exact ^b	-2.1752
II. Fixed-node (FN) method ^c	
QMC	-2.175(3)
Exact ^b	-2.1752

^aCalculations have been performed using 400 trajectories, 15 000 elementary time steps for each trajectory. A Padé z -transform analysis of $I(t)$ has been done with about 30 regularly sampled values $I(t_i)$ with t_i ranging from 0 to about 3. Four calculations with $\Delta t = 0.04, 0.03, 0.02$, and 0.01 have been done and a least-squares fitting to a parabola was performed to extrapolate to $\Delta t = 0$.

^bReference 17.

^cCalculations have been performed using 50 trajectories, 100 000 elementary time steps for each trajectory with $\Delta t = 0.01$. Energy is derived from formula (2.22) with $t_2 = 40$ and $t_1 = 36$. Statistical uncertainties are indicated in parentheses.

sample trajectory, number of such trajectories, choice of the reference function $\varphi_0^{(0)}$.

(2) The sources of systematic biases: the quality of the random number generator, the time-discretization error in the generation of the sample trajectories (the so-called "short-time approximation") and the time-discretization error pertaining to the evaluation through a finite Riemann sum of the integral appearing as the exponent in the Feynman-Kac factor [see, e.g., Eq. (3.7) of part I].

(3) The specific problems related to the problem of obtaining states belonging to some prescribed symmetry, the most important case corresponding to the Pauli principle requirements in many-fermion systems.

We have first treated a number of one-dimensional examples [involving harmonic (x^2) and quartic (x^4) potentials] in order to illustrate the various points listed above and to propose some solutions when necessary. As a conclusion of this first step, we found it is possible to keep under control all the above listed sources of error. Second, with the purpose of moving towards the study of more interesting physical systems, we considered the simplest (two-electron) atomic and molecular systems, namely helium-like systems (He, Be^{++}) and hydrogen molecule. For these systems, our results are of comparable quality with those obtained within the framework of the other QMC methods (see, e.g., Refs. 5 and 12–14). We did not content ourselves with the (bosonic) ground state energy, since this would not at all be a typical representative for many-electron atomic and molecular systems, where the Pauli principle becomes really involved: we also considered the lowest triplet state (antisymmetric space function) as a model of the symmetry requirements to be taken into account for these larger systems. On the other hand, we also evaluated a number of observables other than the energy, in order to illustrate how easily such evaluations can be performed in the framework of the present Monte Carlo method.

As concerns the perspectives for future developments, two steps may appropriately be distinguished. A first step would rely (as many previous Monte Carlo computations did) on the fixed-node approximation for evaluating energy and observables (including now, response properties). According to the experience borrowed from other QMC com-

putations, we may expect that such calculations could be achieved with reasonable accuracy for systems having a number of electrons ranging up to about ten. The second step, would consist in applying to many-electron systems the release-node projection (RNP) method, the results of which appeared rather encouraging for the one-dimensional system to which it was applied in the present work. Investigation concerning these two steps is presently in progress.

ACKNOWLEDGMENTS

We would like to thank the "Conseil Scientifique du Centre de Calcul Vectoriel pour la Recherche" for providing us with computer facilities from which the major part of previous calculations have been done. We are also indebted to the "Centre Inter Régional de Calcul Electronique" (CIRCE) for allowing us to make use of facilities on NAS 9080 and IBM 3090/200 computers and to the "Centre de Calcul Recherche (Paris VI)" for facilities on its GOULD PN9050.

¹M. Caffarel and P. Claverie, *J. Chem. Phys.* **88**, 1088 (1988), referred to as part I.

²J. Vrbik and S. M. Rothstein, *J. Comp. Phys.* **63**, 130 (1986).

³H. Risken, *The Fokker-Planck Equation* (Springer, Berlin, 1984).

⁴H. Cramér, *Mathematical Methods of Statistics* (Princeton University, Princeton, 1966), Chap. 8.2.

⁵P. J. Reynolds, D. M. Ceperley, B. J. Alder, and W. A. Lester, Jr., *J. Chem. Phys.* **77**, 5593 (1982).

⁶(a) E. Yeramian and P. Claverie, *Nature* **326**, 169 (1987); (b) P. Claverie, A. Denis, and E. Yeramian, *Comp. Phys. Rep.* (submitted); (c) J. Aubard, P. Levoir, A. Denis, and P. Claverie, *Comp. Chem.* **11**, 163 (1987).

⁷D. M. Ceperley, in *Recent Progress in Many-Body Theories*, edited by J. Zabolitzky, M. de Llano, M. Fortes, and J. W. Clark (Springer, Berlin, 1981), pp. 262–269.

⁸W. Kutzelnigg, *Theor. Chim. Acta* **68**, 445 (1985).

⁹W. Kolos and L. Wolniewicz, *J. Chem. Phys.* **43**, 2429 (1965).

¹⁰D. J. Klein and H. M. Pickett, *J. Chem. Phys.* **64**, 4811 (1976).

¹¹M. D. Kostin and K. Steighitz, *Phys. Rev.* **159**, 27 (1967).

¹²J. B. Anderson, *J. Chem. Phys.* **73**, 3897 (1980).

¹³J. B. Anderson, *J. Chem. Phys.* **65**, 4121 (1976).

¹⁴J. B. Anderson, *Int. J. Quantum Chem.* **15**, 109 (1979).

¹⁵F. T. Hioe, D. MacMillen, and E. W. Montroll, *Phys. Rep.* **43**, 305 (1978).

¹⁶K. Frankowski and C. L. Pekeris, *Phys. Rev.* **146**, 46 (1966).

¹⁷C. L. Pekeris, *Phys. Rev.* **115**, 1216 (1959).

¹⁸W. A. Sanders and J. O. Hirschfelder, *J. Chem. Phys.* **42**, 2904 (1965).

C. M. Caffarel, P. Claverie, C. Mijoule, J. Andzelm, and D.R. Salahub, “Quantum Monte Carlo method for some model and realistic coupled anharmonic oscillators”,
J. Chem. Phys. 90, 990 (1989)

Quantum Monte Carlo method for some model and realistic coupled anharmonic oscillators

M. Caffarel, P. Claverie,^{a)} and C. Mijoule

Dynamique des Interactions Moléculaires, Université Pierre et Marie Curie, Paris VI, Tour 22, 4 Place Jussieu, Paris Cedex 05, France

J. Andzelm^{b)} and D. R. Salahub

Département de Chimie, Université de Montréal, C. P. 6128, Succ. A, Montréal, Québec, H3C 3J7, Canada

(Received 27 October 1987; accepted 23 September 1988)

A new quantum Monte Carlo (QMC) method of evaluating low lying vibrational levels for coupled modes is presented. We use a modified fixed-node (FN) approach in which an extremum principle for energy levels is invoked. In this way, the nodal hypersurfaces of the nuclear wave function are parametrized and then optimized for each excited state. The method is tested on the fundamental excitations of some two-dimensional model potentials and is applied to the case of realistic coupled modes of the CO molecule adsorbed on a palladium cluster. The effect of an external electric field is also examined. The quantum Monte Carlo results are compared with those obtained in the conventional variational treatment of the nuclear Schrödinger equation for coupled vibrations. The QMC results give the exact values with an error which is in general less than 1 cm^{-1} . In all cases (even in the case of strong coupling) the use of our procedure leads to "optimal" nodal lines (in the sense of the extremum principle used in this work) which are practically undistorted. A salient feature of the Monte Carlo method presented here is that it readily permits the evaluation of the fundamental excitations of an arbitrary number of coupled vibrations. Furthermore, the potential energy surface may be represented by any analytical form without practical difficulties.

INTRODUCTION

In this paper a new method of evaluating vibrational energy levels is presented. Our goal is to overcome the limitations of the usual variational approaches. Two important limitations must be pointed out. The first is related to the difficulty of taking into account strong anharmonicity of the potential energy surface. Strong anharmonicity generally yields too slow convergence of the variational calculation.¹ A second limitation occurs when a large number of interacting vibrations has to be treated. Indeed, the rapid increase of memory and CPU time requirements limits realistic calculations to a small number of vibrations (typically not more than three). Problems related to the quality of the fitting procedure of the potential may also be troublesome in variational approaches.

The new approach is developed within the very general framework of a pure diffusion quantum Monte Carlo (QMC) method using a full generalized Feynman-Kac (FGFK) formula.²⁻⁵ This method is referred to in the following as the FGFK-QMC method. That method, originally designed² for treating the electronic structure of atoms and molecules, is here adapted to the multimode vibrational problem. A widely used approach for treating molecular vibrations is the well-known "normal mode approximation" using an approximate Hamiltonian.⁶ However, if accurate results are desired this description must be abandoned and

the entire potential energy hypersurface must be considered. In this situation a new difficulty arises, namely the loss of any kind of symmetry for the Hamiltonian. We are then led to the problem of evaluating some "genuine" excited levels, i.e., excited states which cannot be considered as the ground state in a given symmetry subspace. This problem is not a trivial one for Monte Carlo schemes. In order to take it into account, we present here a generalization of the well-known fixed-node approximation.^{4,5,7} This approach is currently used to determine properties of the ground state in a symmetry subspace (the so-called "fermionic" ground states corresponding to a given total spin for atoms and molecules⁴). In this paper the method is first tested on some model potentials including intermediate or strong anharmonic coupling terms. Then the first applications are presented which are drawn from a realistic potential surface involving the vibrations of a chemisorbed molecule. Both cases illustrate the efficiency and the simplicity of the method. In particular, in light of the results, it now seems reasonable to hope for solutions of the vibrational problem for an "arbitrary" surface and an arbitrary number of coupled (even strongly coupled) vibrations accurate to about 1 cm^{-1} for the ground state energy (or zero point energy) and for some of the lower-lying excited levels.

The organization of the paper is as follows. We first summarize the main features of the basic quantum Monte Carlo method used here. The detailed theory including mathematical derivations may be found elsewhere.²⁻⁵ Second, we present the fixed-node approximation in the framework of the FGFK-QMC method and our generalization to

^{a)}Deceased, January 24, 1988.

^{b)}Present address: Cray Research Inc., 1333 Northland Drive, Mendota Heights, Minnesota 55120.

the case of the determination of genuine excited levels. Third, the method is tested on some numerically solvable problems. Finally, we present some realistic numerical applications. The preliminary results presented here should be understood primarily as a comparison between the two methods, the classical variational and our new QMC approach. Their physical implications and comparisons with various experiments will, in due course, be treated separately.

II. OUTLINE OF THE QUANTUM MONTE CARLO METHOD

The method is based on the use of a pure diffusion process and a generalized Feynman–Kac formula. The underlying diffusion process is built from a so-called “reference function” $\varphi_0^{(0)}$ which is chosen as close as possible to the exact wave function to reduce the statistical error (see, e.g., Refs. 5 and 7).

The reference diffusion process is completely determined by its drift vector \mathbf{b} and diffusion constant \mathcal{D} . These quantities are written in terms of the reference function as follows (atomic units $\hbar = 1$, $e = 1$, $m_e = 1$ are used throughout the paper):

$$\mathbf{b} = \nabla \varphi_0^{(0)} / \varphi_0^{(0)}, \quad (1a)$$

$$\mathcal{D} = 1. \quad (1b)$$

From the Langevin equation associated with the reference diffusion process, stochastic trajectories may be generated using a step-wise procedure (see, e.g., Ref. 9 Sec. 3.6)

$$d\mathbf{X}(t) = \mathbf{b}[\mathbf{X}(t)]dt + \mathcal{D}^{1/2}d\mathbf{W} \quad (2a)$$

with the discretized version corresponding to the time step Δt :

$$\Delta\mathbf{X}(t) = \mathbf{b}[\mathbf{X}(t)]\Delta t + \mathcal{D}^{1/2}\Delta\mathbf{W}(\Delta t), \quad (2b)$$

where \mathbf{W} represents the multidimensional Wiener process and \mathbf{b} and \mathcal{D} the drift vector and diffusion constant defined in Eqs. (1) [$\Delta\mathbf{W}(\Delta t)$ is a multidimensional Gaussian random vector whose components verify $\langle \Delta W_i \rangle = 0$ and $\langle \Delta W_i \Delta W_j \rangle = \delta_{ij} \Delta t$].

In this work we use a simplified form of the full generalized Feynman–Kac formula presented elsewhere,⁴ namely

$$I(t) = \langle \varphi_0^{(0)} | e^{-t(H - E_0^{(0)})} | \varphi_0^{(0)} \rangle \\ = \int_{\Omega(t)} \exp \left[- \int_{-t/2}^{t/2} V_p[X(s)] ds \right] D^{\varphi_0^{(0)}} X. \quad (3)$$

This formula expresses a quantum matrix element of the evolution operator (in imaginary time) $\exp(-tH)$ as a functional integral involving the diffusion measure of the reference diffusion process. $\Omega(t)$ denotes the set of continuous trajectories defined in the time interval $(-t/2, +t/2)$, while the diffusion measure is noted $D^{\varphi_0^{(0)}} X$. The function V_p is the so-called perturbing potential given by

$$V_p = V - E_0^{(0)} - (1/2)\nabla^2 \varphi_0^{(0)} / \varphi_0^{(0)}, \quad (4)$$

where V is the potential energy of the system to be studied

and $E_0^{(0)}$ an arbitrary constant [in actual fact, V_p is nothing but $V - V^{(0)}$, where $V^{(0)}$ denotes the “reference potential energy” of the reference Hamiltonian $-\nabla^2/2 + V^{(0)}$, associated with the reference function $\varphi_0^{(0)}$ as described in Refs. 4 and 5].

If the reference function is chosen square integrable (and this will always be the case in the following), then the associated diffusion process is ergodic⁴ and the functional integral appearing in Eq. (3) may be evaluated as a time average along any stochastic trajectory $X^{(0)}(s)$ of the process. We thus write

$$I(t) = \int_{\Omega(t)} \exp \left[- \int_{-t/2}^{t/2} V_p[X(s)] ds \right] D^{\varphi_0^{(0)}} X \\ = \lim_{T \rightarrow +\infty} (1/T) \\ \times \int_0^T \exp \left[- \int_{-t/2+\tau}^{t/2+\tau} V_p[X^{(0)}(s)] ds \right] d\tau. \quad (5)$$

Note that, according to the ergodic property of the diffusion process, it is possible, instead of a single, very long stochastic trajectory, to use a set of shorter trajectories. In practice, this possibility enables us to obtain an evaluation of the variance using standard statistical methods.

In fact, as concerns the ergodic property, two different cases must be properly distinguished. If the reference function does not vanish at any finite distance, the property readily holds and any arbitrary stochastic trajectory may be used. If not, it is necessary to take account of consequences resulting from divergence of the drift vector [Eq. (1a)] at nodes of $\varphi_0^{(0)}$. Indeed, nodal hypersurfaces of $\varphi_0^{(0)}$ play the role of infinitely repulsive barriers for stochastic trajectories. There then results a decomposition of the diffusion process into a juxtaposition of subprocesses in subdomains delimited by the nodes of the reference function. In other words, an arbitrary stochastic trajectory cannot leave a subdomain in which it is trapped and accordingly, cannot visit everywhere. Property (5) must then be applied, not by using a single trajectory, but a set of trajectories consisting of at least one trajectory trapped in each subdomain. The whole space is accordingly sampled.

Now, the quantum matrix element $I(t)$ may be written in terms of the spectral expansion of H thus leading to

$$I(t) = \langle \varphi_0^{(0)} | e^{-t(H - E_0^{(0)})} | \varphi_0^{(0)} \rangle \\ = \sum |\langle \varphi_0^{(0)} | \varphi_i \rangle|^2 e^{-t(E_i - E_0^{(0)})}. \quad (6)$$

E_i and φ_i denote, respectively, the eigenvalues and eigenfunctions of H .

The summation sign Σ is here a shorthand notation which may represent either a discrete summation or a continuous integration. The spectrum of H can be obtained by analyzing $I(t)$ into a sum of real exponentials. Let us denote as E_{i_0} the lowest energy associated with a nonvanishing overlap integral $\langle \varphi_0^{(0)} | \varphi_i \rangle$. Extracting E_{i_0} may be done as follows:

$$E_{i_0} = E_0^{(0)} - \lim_{t \rightarrow +\infty} (1/t) \log I(t). \quad (7)$$

A much more efficient way consists in considering the slope at infinity of $\log I(t)$:

$$E_{i_1} = E_0^{(0)} - [\log I(t_2) - \log I(t_1)] / (t_2 - t_1) + O(e^{-\Delta E t_1}) \quad (8)$$

with $t_2 > t_1$. ΔE denotes the energy difference between E_{i_1} and the first excited energy associated with a nonvanishing overlap $\langle \varphi_0^{(0)} | \varphi_{i_1} \rangle$. The residual error may be made arbitrarily small by using a large enough value of t_1 .

Finally, the complete algorithm is as follows:

- choose some good representation of the exact wave function as reference function $\varphi_0^{(0)}$;
- generate stochastic trajectories using the Langevin equation (2);
- evaluate $I(t)$ expressed as a time average along the previous trajectories using the basic formula (5);
- extract the desired energy according to formula (8).

At this stage, it is of interest to note that the present quantum Monte Carlo method differs from other similar methods (e.g., Refs. 7 and 8) essentially because no branching is introduced. Indeed, the reference diffusion process used here coincides with their branching-diffusion process when the branching term is removed [see, e.g., Eq. (6) in Ref. 7] and if our reference function $\varphi_0^{(0)}$ is identified to their “trial wave function” Ψ_T . In addition, our perturbing potential V_p [Eq. (4)] may be rewritten in the equivalent form

$$V_p = H\Psi_T / \Psi_T$$

which corresponds exactly to the “local energy” used in these methods.

III. EVALUATION OF VIBRATIONAL ENERGY LEVELS

A. Zero-point energy (ZPE)

Ground state energies are very simply and accurately evaluated by all Monte Carlo schemes. This salient feature is directly related to the lack of nodes in the ground state wave function (see, e.g., Ref. 10). As a consequence, the algorithm presented in the previous section may be readily used. A few excellent results for zero-point energies are presented below.

B. Fixed-node approximation and excited levels

In this section we are interested in evaluating energies of excited levels. We will denote as φ_{i_1} the corresponding excited-state wave functions. By contrast with the previous case, we are now dealing with wave functions with nodes. It can be shown that the algorithm defined above may be used in the same way as for the ground state energy.⁴ The basic difference concerns the drift vector of the reference diffusion process which may now diverge. Accordingly, eigensolutions determined by the Monte Carlo scheme correspond to eigensolutions of the Schrödinger equation constrained to vanish everywhere the reference function vanishes. This must be understood as a change in boundary conditions for the Schrödinger equation. Consequently, the energies obtained in this way may differ from the exact ones. This is the well-known fixed-node approximation.^{4,5,7}

Let \mathbf{v}_α denote the hypervolumes delimited by the nodes of the reference function $\varphi_0^{(0)}$ and S_α the corresponding boundary hypersurfaces. From the continuity of $\varphi_0^{(0)}$ it follows that

$$\mathbf{R}^N = \bigcup_{\alpha=1}^l \mathbf{v}_\alpha, \quad (9)$$

where N is the dimension of the relevant space. In what follows, N will represent the number of coupled modes. l is the number of hypervolumes.

As explained above, the Schrödinger equation is solved (through the Monte Carlo procedure) *independently* in each volume \mathbf{v}_α . Let us denote as Φ_α the different nodeless solutions in subdomains \mathbf{v}_α and as ϵ_α the corresponding energy:

$$H\Phi_\alpha = \epsilon_\alpha \Phi_\alpha \quad \mathbf{r} \in \mathbf{v}_\alpha, \quad (10a)$$

$$\Phi_\alpha = 0 \quad \mathbf{r} \in \mathbf{v}_\alpha. \quad (10b)$$

Note that Φ_α may have a discontinuous gradient at the nodal hypersurface S_α .

The functional integral involved in the Feynman–Kac formula may be decomposed into a sum of functional integrals defined over the set of continuous trajectories $\Omega_\alpha(t)$ trapped in a given subdomain \mathbf{v}_α . We thus write

$$I(t) = \sum_{\alpha} w_\alpha I_\alpha(t), \quad (11)$$

where the w_α 's denote the relative statistical weights of the different subdomains \mathbf{v}_α which are immediately obtained from the stationary density $(\varphi_0^{(0)})^2$ associated with the reference function $\varphi_0^{(0)}$:

$$w_\alpha = \int_{\mathbf{v}_\alpha} (\varphi_0^{(0)})^2 d^N \mathbf{x} / \int_{\mathbf{R}^N} (\varphi_0^{(0)})^2 d^N \mathbf{x} \quad (12)$$

and $I_\alpha(t)$ denotes the “partial” functional integral

$$I_\alpha(t) = \int_{\Omega_\alpha(t)} \exp \left[- \int_{-t/2}^{t/2} V_p[X(s)] ds \right] D^{\varphi_0^{(0)}} X. \quad (13)$$

Using the Feynman–Kac formula $I_\alpha(t)$ may also be expressed as a quantum matrix element. The spectral expansion (6) for $I_\alpha(t)$ combined with the expression (11) for $I(t)$ leads to the following expression for the fixed-node energy E_{FN} :

$$E_{\text{FN}} = E_0^{(0)} - \lim_{t \rightarrow +\infty} (1/t) \log I(t) = \min_{\alpha} \epsilon_\alpha. \quad (14)$$

If exact nodes were known, the fixed-node approximation would be exact and we should thus obtain

$$E_{\text{FN}} = \epsilon_1 = \dots = \epsilon_\alpha = \dots = \epsilon_l = E_{i_1}. \quad (15)$$

In the general case of approximate nodes, E_{FN} is different from the exact result E_{i_1} .

In previous work, the fixed-node approach has been introduced in order to evaluate energies corresponding to ground states in subspaces of given symmetry. It is then possible to show that a variational property holds,^{7,11} namely

$$E_{\text{FN}} = \min(\epsilon_\alpha) \geq E_{i_1}. \quad (16)$$

As already mentioned, the excited levels of multivibrational systems are generally *true* excited energies. No symmetry holds and the upper-bound property is no longer valid.

We have therefore developed a generalization of the fixed-node approach for such true excited levels. This generalization rests on the extremum property associated with *all* eigenvalues of the Schrödinger Hamiltonian. This property states that^{12,13}

$$E(\varphi_k + \delta\varphi) = E(\varphi_k) + O(\delta\varphi^2), \quad (17)$$

where $E(\varphi)$ is the usual energy mean value

$$E(\varphi) = \langle \varphi | H | \varphi \rangle / \langle \varphi | \varphi \rangle \quad (18)$$

and φ_k is an arbitrary eigenstate of H . Note that the widely used property of *minimum* energy is valid only for the ground state energy E_0 . Now, in order to use this extremum property we must establish an *a priori* nontrivial connection between the quantum mean value $E(\varphi)$ and the fixed-node energy E_{FN} evaluated in the Monte Carlo scheme. As emphasized above, the resolution of the Schrödinger equation is done *independently* in each volume. As a consequence the relative magnitude of the different solutions Φ_α in different subdomains is *not* determined by the fixed-node procedure. More precisely, the set of coefficients $\{c_\alpha\}$ such that the function φ defined as

$$\varphi = \sum_\alpha c_\alpha \Phi_\alpha \quad (19)$$

is close to the desired exact wave function φ_{i_0} is unknown. From Eqs. (18) and (19) we obtain the following energy mean value for φ :

$$E(\varphi) = \frac{\sum_\alpha c_\alpha^2 \epsilon_\alpha \langle \Phi_\alpha | \Phi_\alpha \rangle}{\sum_\alpha c_\alpha^2 \langle \Phi_\alpha | \Phi_\alpha \rangle}. \quad (20)$$

Note that delta functions due to the possibly discontinuous gradient of Φ_α do not contribute to the numerator (because these discontinuities of the gradient can occur only on the boundaries, where the Φ_α 's just vanish themselves). The important point now is that the coefficients c_α do not have to be known if the Monte Carlo energies ϵ_α have a common value. More precisely, we obtain from Eq. (20) in this particular case:

$$E(\varphi) = E_{\text{FN}} = \epsilon_1 = \epsilon_2 = \dots = \epsilon_l. \quad (21)$$

Consequently, if Eq. (21) is verified it is possible to apply the extremum principle to the fixed-node energy. The method presented in this paper is essentially based on this latter remark and thus consists in extremizing the fixed-node energy with respect to some deformations of nodes with the constraint that the energies have a common value. In what follows, the reference function will be written in the general form

$$\varphi_0^{(0)} = f(x_1, \dots, x_N; p_1, \dots, p_q) e^{-\phi(x_1, \dots, x_N)}, \quad (22)$$

where ϕ is a bounded function at any finite distance and $f=0$ defines the $(N-1)$ -dimensional nodal hypersurface which is parametrized by p_1, \dots, p_q . In order to apply the constrained extremum principle, the set of parameters $\{p_i\}_{i=1,q}$ is decomposed into two subsets $\{p_i\}_{i=1,r}$ and $\{p_i\}_{i=r+1,q}$. The variation of the fixed-node energy is performed with respect to the subset $\{p_i\}_{i=r+1,q}$ while for each given $\{p_i\}_{i=r+1,q}$ the parameters $\{p_i\}_{i=1,r}$ are only used to

fulfill the constraint (21). The theoretical algorithm of the method is then as follows: (1) For a given subset of fixed parameters $\{p_i\}_{i=r+1,q}$ vary parameters $\{p_i\}_{i=1,r}$ to obtain equality of energies $\{\epsilon_\alpha\}_{1,l}$. Each of energies ϵ_α may be evaluated by Monte Carlo according to Eq. (14) from a set of trajectories trapped in the corresponding subdomain v_α so that $I(t) = I_\alpha(t)$ and $E_{\text{FN}} = \epsilon_\alpha$. The common value for the energies will be denoted as $\epsilon(p_{r+1}, \dots, p_q)$. According to Eq. (21), this step assures that $\epsilon(p_{r+1}, \dots, p_q) = E(\varphi)$ where φ is a function close to the exact wave function φ_{i_0} . (2) Repeat step 1 for different subsets $\{p_i\}_{i=r+1,q}$. (3) According to the extremum principle [Eq. (17)], deduce E_{i_0} as a local extremum of $\epsilon(p_{r+1}, \dots, p_q)$.

Although such a theoretical algorithm is simple and general, its practical implementation may lead to serious difficulties. In fact, the most important problem consists in constructing a reference function whose nodes are close enough to the exact ones to justify the use of the extremum property [Eq. (17)]. Such a construction is by no means a trivial task since the nodal hypersurface of the exact wave function cannot be known *a priori* and may be obtained only by solving the Schrödinger equation. In general, the topological structure of the nodal hypersurfaces is complicated and may be difficult to reproduce, particularly when arbitrarily high energy levels are considered. Even the number of subdomains delimited by nodes is generally unknown. If exact nodes were known, the constraint (21) would be automatically fulfilled. It is natural to think that for very good nodes this is still possible. In contrast, if parametrized nodes are not close to the exact nodes, as is the case in general, it may be very difficult to fulfill this constraint even by using a large number of parameters. In addition, if Eq. (21) is satisfied, there can be several extrema for the energy and the problem of choosing between them arises. Such unwanted additional extrema may correspond to other physical levels or, perhaps, to artificial extrema in functional space. All the problems listed above illustrate the difficulty in applying the previous theoretical algorithm to an arbitrary multimode problem. However, in this paper we will restrict ourselves to the problem of evaluating the so-called fundamental energies of the system. A convenient way of defining fundamental energies is to introduce the Hamiltonian consisting of the noncoupled part of the total Hamiltonian, namely

$$H^{\text{NC}} = \sum_{i=1}^N h_i(x_i) = \sum_{i=1}^N -\frac{1}{2} \frac{\partial^2}{\partial x_i^2} + V_i(x_i) \quad (23)$$

while the total Hamiltonian will be written in the form

$$H = H^{\text{NC}} + \lambda W(x_1, \dots, x_N). \quad (24)$$

Eigenfunctions and eigenvalues of H^{NC} are given by

$$\phi_{k_1 \dots k_N}(x) = \prod_{j=1}^N \varphi_{k_j}^{(j)}(x_j) \quad (25)$$

and

$$E_{k_1 \dots k_N} = \sum_{j=1}^N \epsilon_{k_j}^{(j)}, \quad (26)$$

where $\varphi_{k_j}^{(j)}$ and $\epsilon_{k_j}^{(j)}$ denote the eigensolutions of the one-dimensional oscillators defined by h_j . The fundamental ener-

gies of the noncoupled Hamiltonian are defined as the energies corresponding to $k_j = 1$, all other k 's being zero. The energy levels of H which are connected to the previous ones as the perturbation parameter λ goes to zero are called fundamental energies of H . In what follows, these energies will be denoted as $E_{(0,\dots,1,\dots,0)}$. Denoting by $E_{(0,\dots,0,\dots,0)}$ the ground state energy (or zero-point energy), the differences: $E_{(0,\dots,1,\dots,0)} - E_{(0,\dots,0,\dots,0)}$ will be referred to as the fundamental excitations of the system. Now, it is important to point out that these excitations play a central role in spectroscopy because they are generally the more intense. Due to the inherent limitations of the variational approach, it would be valuable to be able to compute them accurately for problems in which many modes are involved. For that, we apply the previous theoretical algorithm by using a basic assumption concerning the nodal structure of wave functions corresponding to fundamental excitations. More precisely, it will be assumed here that nodes of such functions may be correctly approximated by a hypersurface dividing the N -dimensional space into exactly *two* subdomains. It is known that such a representation of nodes is exact for the first excited state of H^{19} (which corresponds here to one of the fundamental energies) but is generally wrong for other levels. As concern the true fundamental energies, we have seen that they are connected to the fundamental energies of the non-coupled Hamiltonian by their very definition. But it is clear that fundamental energies of H^{NC} correspond to wave functions which verify the basic assumption. It is then assumed here that adding a coupling potential [such as $W(x)$ given in Eq. (24)] does not destroy in an abrupt way the nodal pattern of fundamental wave functions. In what follows, this assumption is tested by treating some two-dimensional model problems in which the magnitude of $W(x)$ (the coupling potential) may be very important and for fundamental energies which do not necessarily correspond to a first excited state. Let us denote the "excited" mode as x_1 . Invoking our basic assumption the nodal function f is represented as follows:

$$f(x_1, \dots, x_N, p_1, \dots, p_q) = x_1 + p_1 + g(x_2, \dots, x_N, p_2, \dots, p_q). \quad (27)$$

Clearly, the function f divides the N -dimensional space into two subdomains. Let us denote ϵ_1 and ϵ_2 the two corresponding energies. In what follows, p_1 will correspond to the single parameter used to fulfill the constraint of Eq. (21), that is here $\epsilon_1 = \epsilon_2$. Parameters p_2, \dots, p_q are introduced to extremize the common value $\epsilon(p_2, \dots, p_q)$. As concerns the function g , it may be developed as increasing powers of the x_i and then successive improvements of g may be made. For instance

$$g^{(0)} = 0, \quad (28a)$$

$$g^{(1)} = \sum_i p_i x_i, \quad (28b)$$

$$g^{(2)} = g^{(1)} + \sum_{i,j} p_{ij} x_i x_j, \quad (28c)$$

and so on. Increasing the order of g should yield a "better" representation of the nodes and, finally, a converged optimized energy. In contrast to the theoretical algorithm pre-

sented above for a very general energy level, it is important to note that no basic difficulties arise from such an algorithm in which only two subdomains are introduced. Its practical implementation may thus be considered.

IV. APPLICATION TO TWO-DIMENSIONAL SYSTEMS

In order to test the theoretical algorithm described above, the fundamental excited states of some two-dimensional model potentials have been investigated. They were chosen in such a way that the exact solutions may be reached by the variational method. Both intermediate and strong coupling potentials are studied.

Furthermore, the method has been applied to some surface science problems involving vibrations of the CO molecule adsorbed on palladium. In the first instance adsorption on the bridge site of a 14-atom cluster model of Pd (100) was considered.^{14,15} A second example involves the bridge-bonded Pd₂CO cluster in the presence of an external electric field.¹⁶ In each case the coupling of two modes has been considered.

Throughout the paper the $|N_1, N_2\rangle$ normal mode notation is used, where N_1, N_2 refer to the harmonic oscillator quantum numbers of the first and second vibrations, respectively. In this paper we are interested in the fundamental excitations for the system. We are then led to evaluate $E_{(0,0)}$, $E_{(0,1)}$, and $E_{(1,0)}$ for each couple. In each case both variational and QMC methods are applied.

A. Model potentials

First we have to compare the QMC calculations with energies which may be reached exactly by numerical calculations. Polynomial forms of potentials have therefore been chosen, where the ground and excited energies may be readily obtained by a variational calculation. In order to study both symmetrical and unsymmetrical excited states, the first kind of potentials we chose have the following analytical form:

$$V_{I,II}(x,y) = x^2 + y^2 + \lambda(-xy^2 + y^4). \quad (29)$$

The shape of the nodal line of the $|1,0\rangle$ excited state is unknown, whereas that of the symmetrical $|0,1\rangle$ level is given by $y = 0$. The coupling between x and y is governed by the parameter λ . Two values of λ have been considered, $\lambda = 1$ (V_I) and $\lambda = 3.5$ (V_{II}). In any case, λ is chosen so that the potential has only one minimum and no unbound states to assure the convergency of the variational treatment. It is straightforward to show that these two properties are fulfilled for $0 < \lambda < 4.0$. Furthermore, in order to study the effect of long-range coupling on the shape of the nodal line of the unsymmetrical excited state $|1,0\rangle$, the following form of V has also been studied:

$$V_{III}(x,y) = x^2 + y^2 + \lambda(-xy^2 + x^2y^2 + y^4). \quad (30)$$

Indeed, although the two oscillators associated with V_I and V_{II} are decoupled for large values of x and y , they remain strongly coupled in the case of V_{III} .

As discussed below, the potentials V_I , V_{II} , and V_{III} have their unsymmetrical $|1,0\rangle$ state as the lowest excited level. In order to investigate the accuracy of Eq. (27) for higher excited unsymmetrical states, the last model example we treated is the following potential:

$$V_{IV}(x,y) = 4x^2 + 0.1y^2 + \lambda(-xy^2 + y^4) \quad (31)$$

with $\lambda = 3.5$. In this more general case, the intrinsic properties associated with a first excited state (i.e., the partitioning of the space into two subdomains) are eventually removed.

B. Realistic potentials

For the Pd_{14}CO study, the first mode involves the beating of the rigid CO molecule against the surface (denoted h on Fig. 1). The second coordinate is a surface mode of the metal cluster, either the out-of-plane Pd_2 -bulk stretch (z on Fig. 1) or the in-plane Pd - Pd stretch (r on Fig. 1). In the electric field study we have focused on the CO stretch (coordinate d on Fig. 2) and its coupling with the surface-CO beating vibration (h). We calculated total energy surfaces as a function of h,r , h,z , and h,d , respectively. In each case the potential surface was evaluated on a two-dimensional grid of about 40 points using the LCGTO-MP-LSD method developed elsewhere.^{14,17} The points were chosen to bracket the ground and first excited vibrational levels. Furthermore, for large values of h , the asymptotic form of the potential was taken into account by adding to the grid, four or five points at distances beyond 10 Å, derived from the known experimental chemisorption energy of CO on the Pd (100) surface. The supplementary points are introduced to prevent an unphysical asymptotic behavior of the polynomial fit to the potential, namely a fourth-order polynomial using a least-squares fit method¹⁸:

$$V(x_1, x_2) = \sum_{i+j < 4} a_{ij} x_1^i x_2^j. \quad (32)$$

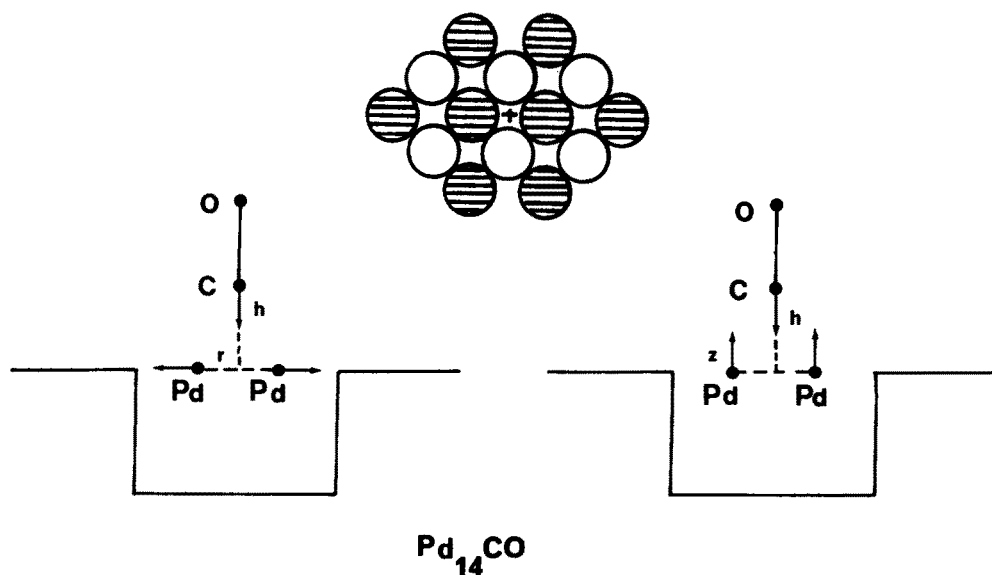


FIG. 1. Representation of the Pd_{14}CO cluster and couples h,r and h,z . The dashed Pd atoms belong to the first layer. The CO chemisorption site is indicated by the cross.

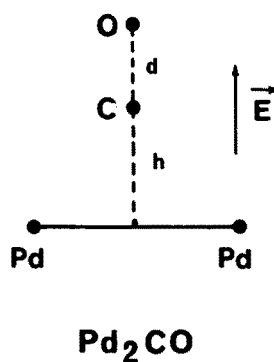


FIG. 2. Representation of the couple h,d . The study of this coupling is performed in presence of an external electric field E .

C. Variational treatment

The variational equations are solved explicitly using a Hermite polynomial expansion as described elsewhere.¹⁸ The effect of the basis size is studied. The polynomial representation of the potential allows easy calculations of the matrix elements of the nuclear Hamiltonian. However, concerning realistic potentials, such a mathematical expansion, suitable for small displacements, may lead to nonphysical behavior of the potential at large distances. This is the case for the h,z system where the coupling is significant. As a consequence, large basis set calculations using very delocalized Hermite polynomials are prohibited. Consequently, we are led to contract the basis set significantly in order to assure that the process converges in the region of space where the potential is physically well described. Since the QMC method does not involve the evaluation of matrix elements over a basis, the computational constraints on the form of the potential are much less severe. More precisely, according to formulas (4) and (5) only the successive values of the potential V along the trajectory are needed and then an arbitrary analytical form of V may be chosen. It is then possible to introduce more physical expressions for V with the right

asymptotic behavior (i.e., Morse functions for stretching modes, Fourier expansions for multiple-wells potentials, etc.). However, as the purpose of this paper is to compare both variational and QMC methods, the form (32) above is used in all cases. Concerning the h,z potential, the reference functions are chosen so that the nonphysical part of the potential cannot be visited by the stochastic trajectories during the Monte Carlo simulation. This is accomplished by using reference functions nearly vanishing in these pathological regions of the potential fit. In this way, a “local convergency” may be reached. By local convergency it is meant here that we obtain the energy corresponding to a new problem represented by the physical potential surface around the potential well and infinite repulsive barriers at large distances. If very long Monte Carlo runs would be performed, these pathological regions would, in fact, be visited and the energy would converge to a nonphysical value (which can be equal to $-\infty$ if the nonphysical part of the potential is not bounded from below). It is very important to emphasize that these difficulties occur only because an inadequate polynomial fit is used. Such difficulties do not occur for more physical potentials. As remarked above, reasonable physical potentials may be readily used, without practical difficulties, in the Monte Carlo approach since no complicated matrix elements have to be evaluated. This is one of the main advantages of QMC methods. In the following a unitary transformation $(x_1, x_2) \rightarrow (x'_1, x'_2)$ is performed on the three realistic potentials such that the a_{11} coefficient in Eq. (32) vanishes. These new coordinates will be called “pseudonormal coordinates” (PNC).

D. QMC treatment

Concerning the nodeless vibrational ground states $|0,0\rangle$ the choice of the reference function $\varphi_0^{(0)}$ is rather flexible, the statistical fluctuations becoming rapidly small. $\varphi_0^{(0)}$ is written in the following form:

$$\varphi_0^{(0)}(x_1, x_2) = e^{-k_1 x_1^2 - k_2 x_2^2}, \quad (33)$$

where (x_1, x_2) stands for h', r' , h', z' , or h', d' . The reference function for excited states $|0,1\rangle$ and $|1,0\rangle$ is chosen as follows:

$$\varphi_0^{(0)}(x_1, x_2) = f(x_1, x_2) e^{-k_1 f^2(x_1, x_2) - k_2 x_2^2}, \quad (34)$$

where x_1 refers to the excited vibration. When choosing the function f the boundary conditions of $\varphi_0^{(0)}$ at infinity must be satisfied. $f(x_1, x_2) = 0$ is the equation defining the nodal structure of the reference function. As explained in Sec. III B, in the following the nodes of the states $|0,1\rangle$ and $|1,0\rangle$ are represented by a line dividing the two-dimensional space into two domains. As a general rule, this representation, which is exact for the first excited state of the Hamiltonian, is wrong for the higher excited states.¹⁹ Nevertheless, the approximation associated with this representation is expected to be good when excited states under consideration correspond to the first excitation of a given vibration (denoted as $|0,1\rangle$ and $|1,0\rangle$). Note that the function f appears in the exponential part and allows the maximum of $\varphi_0^{(0)}$ to keep a

constant distance from the nodal line when it is moved. At the beginning of our investigation, in order to describe as well as possible the nodal surface with the generalized fixed-node approximation, only small deformations and displacements of the nodal line about the straight line $x_1 = 0$ have been performed. The approximate form for $f(x_1, x_2)$ is chosen by expanding the development given in Eqs. (28) to the second order. We may then write f as

$$f(x_1, x_2) = x_1 - \alpha x_2^2 - x_N, \quad (35)$$

where x_N is related to the translation of the nodal line while αx_2^2 corresponds to a small parabolic deformation. Linear terms (rotation of the nodal line) corresponding to $g^{(1)}$ [Eq. (28b)] are zero for the model potentials and are negligible in the PNC representation of the realistic h,r and h,z potentials.

In order to apply the generalized fixed-node (GFN) algorithm described in Sec. III B to our examples the following steps are performed: (i) for each value of α the equality $\epsilon_1 = \epsilon_2 = \epsilon(\alpha)$ is obtained by varying x_N , (ii) the extremum principle is used for optimizing $\epsilon(\alpha)$ with respect to α .

In order to reduce as much as possible the variance of the QMC procedure, at each step described above the k_1 and k_2 parameters in Eq. (34) are adjusted to minimize the variance by performing short-time preliminary runs using a common underlying sequence of random numbers.

V. RESULTS OF THE VARIATIONAL AND QMC CALCULATIONS

A. Model potentials

The analytical form of the model potentials studied are summarized in Table I. The potential map of V_{II} is represented in Fig. 3 as an example. In Table II, different approaches of the ground and fundamental excited states of V_{II} are compared with QMC, namely, the crude harmonic approximation and the variational procedure. The effect of the basis set size for the latter is also reported. All the calculated energies as well as the optimized nodal lines at the second-order level are reported in Table III for all studied potentials. Concerning the ground state energies, it is clear that they are very well reached by variational calculations and that QMC runs converge rapidly as a function of the simulation time T as shown in Fig. 4. An accuracy better than 1 cm^{-1} is very easy to obtain. Such results will allow the method to be extended without difficulties to physical problems where a good evaluation of the zero-point energy (ZPE) for a high dimensional system is necessary.

TABLE I. Polynomial model potentials for which the ground state and fundamental excitations have been investigated.^a

Coefficients ^b	V_I	V_{II}	V_{III}	V_{IV}
a_{20}	1.0	1.0	1.0	4.0
a_{02}	1.0	1.0	1.0	0.1
a_{12}	-1.0	-3.5	-3.5	-3.5
a_{22}	0.0	0.0	3.5	0.0
a_{04}	1.0	3.5	3.5	3.5

^aMass normalized coordinates are used.

^bAtomic units. All the missing coefficients are set to zero.

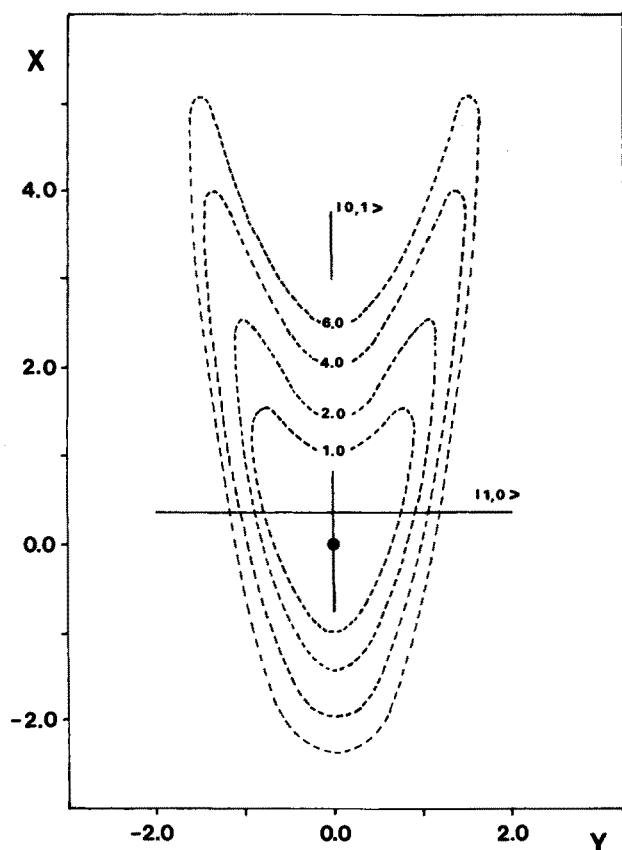


FIG. 3. Potential map of the V_{II} potential as a function of x and y . The nodal lines of the fundamental excited states $|1,0\rangle$ and $|0,1\rangle$ are represented. Distances are mass normalized coordinates, energies in a.u.

Concerning the excited states $|1,0\rangle$ and $|0,1\rangle$, the variational process converges less rapidly than for the $|0,0\rangle$ (see, e.g., Table II). Although convergence is, nevertheless, reached easily with a two-dimensional potential, serious difficulties of memory size may arise for problems of higher dimension. In our case, the convergence has been extended enough (10^{-2} cm^{-1}) to consider our results as exact numerical solutions. Now we can deduce, in the framework of the QMC solutions, the following important properties concerning the nodal lines of fundamental excited states; first we may note that all the energies of the $|1,0\rangle$ and $|0,1\rangle$ states of the studied model potentials are very well reproduced by the QMC calculations. This shows that the choice of the analytical form given in Eq. (27) for the nodal line of a fundamental excited state is appropriate. We may conclude that such states may be reached by partitioning the full space into two subdomains. A more surprising result concerns the shape of the node of the nonsymmetrical $|1,0\rangle$ states: in each case where it is the lowest excited state of the spectrum the parameter α is found to be zero and therefore the node is a straight line, translated from the origin by x_N . We give on Fig. 3 the potential map associated to V_{II} together with the nodal lines of the excited state wave functions $|0,1\rangle$ and $|1,0\rangle$. As explained above, in order to see if this particularity is also true for higher excited (though fundamental) states, we calculated the $|1,0\rangle$ energy of the potential V_{IV} whose lowest excited state is the symmetrical $|0,1\rangle$ level. In that

TABLE II. Energies (cm^{-1}) of the ground and fundamental excited states for the model potential $V_{II}(x,y)$.^a

State $ x,y\rangle$	$ 0,0\rangle$	$ 1,0\rangle$	$ 0,1\rangle$
Harmonic	169.0	338.1	338.1
Variational			
$n^b = 2$	288.5	532.5	930.4
4	221.1	387.4	531.8
6	213.1	373.2	485.3
8	211.7	367.5	478.0
10	211.0	365.5	475.1
12	210.6	365.0	473.0
14	210.4	364.9	471.9
16	210.3	364.8	471.4
18	210.3	364.7	471.3
20	210.3	364.7	471.2
22	210.3	364.7	471.2
QMC ^c	210.0 ± 1.0	364.7 ± 1.3	472.1 ± 1.1
Parameters ^d		$\alpha = 0.0$	$\alpha = 0.0$
		$x_N = 0.37$	$x_N^e = 0.0$

^aQMC calculations have been performed using 40 trajectories with 500 000 elementary time steps. The time step used is 0.01 a.u.

^bThe size of the basis set is $n \times n$.

^cOur results.

^dOptimized parameters of the nodal line defined in Eq. (35).

^eThe notation y_N would be better. However, our convention here is to denote x_N the translation parameter associated with the excited vibration (y in this case).

case, there may be a very weak distortion of the nodal line. We give in Table III the QMC energy values for this state corresponding to $\alpha = 0.0$ and -0.02 , respectively. In that case, even if the nodal line is slightly distorted, we show that the straight line approximation is good. From Table III, we can see that the increase of the coupling between V_I and V_{II} leads, as expected, to an increased value of x_N . Concerning the symmetrical $|0,1\rangle$ states, the predicted values of the pa-

TABLE III. Vibrational energies of the ground and fundamental excited states of some model and realistic potentials.^a

Potential	State	Var.	QMC	α	x_N^b
I	$ 0,0\rangle$	192.8	192.8 ± 0.3
	$ 1,0\rangle$	359.8	359.8 ± 0.2	0.0	0.125
	$ 0,1\rangle$	436.6	437.1 ± 0.5	0.0	0.0
II	$ 0,0\rangle$	210.3	210.0 ± 1.0
	$ 1,0\rangle$	364.7	364.6 ± 1.5	0.0	0.368
	$ 0,1\rangle$	471.2	472.1 ± 2.2	0.0	0.0
III	$ 1,0\rangle$	447.4	448.3 ± 1.1	0.0	0.164
IV	$ 1,0\rangle$	618.1	619.0 ± 0.9 619.3 ± 0.9	-0.02 0.0	0.093 0.088
	h,r	$ 0,0\rangle$	356.7	356.7 ± 0.1	...
h,z	$ 1,0\rangle$	877.8	877.3 ± 0.1	0.0	0.053
	$ 0,1\rangle$	548.7	548.7 ± 0.2	0.0	0.044
	$ 0,0\rangle$	247.5	247.9 ± 0.5
h,z	$ 1,0\rangle^c$	648.4	645.0 ± 0.6	0.0	0.067
	$ 0,1\rangle$	312.7	313.6 ± 1.1	0.0	-0.072

^aAll energy values are in cm^{-1} .

^bIn atomic units with mass normalized coordinates.

^cSee Fig. 7.

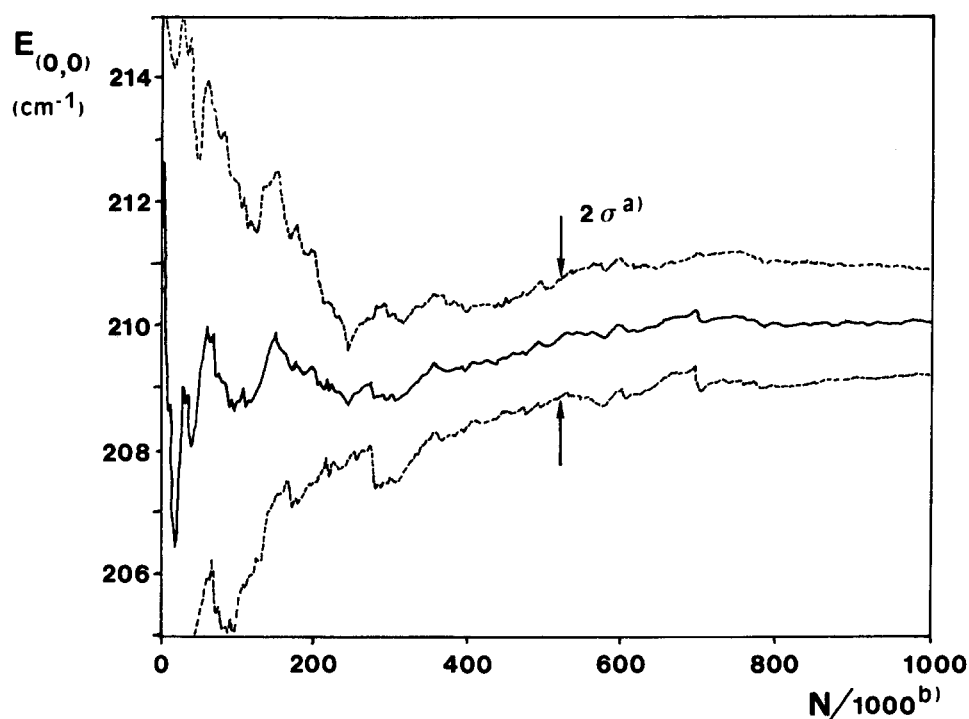


FIG. 4. Estimator of the ground state energy as a function of the simulation time for the V_{II} model potential. σ is the standard deviation. A set of 40 trajectories is divided into 10 subsets of 4 trajectories and σ is evaluated from the dispersion of the ten corresponding energies calculated for each subset. N is the number of time steps for each trajectory. The CPU simulation time is directly proportional to N .

parameters α and x_N (zero) are reproduced. Finally, to illustrate our algorithm, we present in Fig. 5 the dependency of $E_{FN} = \min(\epsilon_1, \epsilon_2)$ with respect to x_N for symmetrical ($|0,1\rangle$ state of V_I) and unsymmetrical ($|1,0\rangle$ state of V_{II}) states. Clearly, E_{FN} is very dependent on the partitioning of the space and then the desired equality $\epsilon(\alpha) = \epsilon_1 = \epsilon_2$ is obtained very easily. Note that the asymptote of the curve $E_{FN}(x_N)$ gives the ZPE since $\lim_{x_N \rightarrow \infty} \varphi_0^{(0)}$ is a nodeless function. Finally, the extremum principle is represented in Fig. 6 for the unsymmetrical $|1,0\rangle$ state of V_{II} . It shows clearly that the minimum is obtained for $\alpha = 0.0$. Furthermore, the correlation between the two parameters is clear: as α increases (from -0.5 to $+0.5$ on Fig. 6) and tends to unbalance the two subdomains, x_N decreases to compensate this effect.

B. Pd₁₄CO

Calculated energies of vibrational states for the two types of coupling are presented in Tables III and IV. Different approaches are compared with QMC, namely, the crude harmonic approximation (one-dimensional approximation) the PNC representation and the variational procedure. The effect of the basis set size on the $|1,0\rangle$ excited state energy is also illustrated by Fig. 7 for the h,z coupling. The ground state energies in these simple two-dimensional cases are very well reached by variational calculations whereas harmonic approximations (crude and PNC) may give significant errors (see Table IV). For $|0,0\rangle$ states the QMC runs converge very rapidly as a function of the simulation time T . An accuracy better than 1 cm^{-1} is very easy to obtain.

Concerning the first excited state $|0,1\rangle$ of the cluster vibration, the variational convergence is also satisfactory for both couplings, less than 1.0 cm^{-1} from the value given by

QMC. In the case of the h,r coupling the optimization of α and x_N shows that the nodal line is slightly translated. This reflects the slight difference between PNC and exact QMC results (about 1 cm^{-1}) which results from both anharmonic and coupling terms of the potential. In the case of the $|0,1\rangle$ state of the h,z coupling, the nodal line is a little more translated. Hence, the difference between PNC and exact QMC results (about 20 cm^{-1}) is larger.

The variational treatment of the $|1,0\rangle$ excited state of the h,z coupling (the adsorbate-surface vibration) is more difficult. A few comments on the rather erratic behavior of the variational results for $|1,0\rangle$ may be in order. The first concerns the lack of monotonic convergence seen for the h,z calculations (Fig. 7) upon increasing the size of the basis set. In fact the Hylleraas–Undheim–MacDonald theorem^{20–22} ensures that in a linear variational calculation the m th lowest root is never lower than the m th exact eigenvalue of the Hamiltonian. This theorem is of course satisfied for our calculations. The fact that the energy of the $|1,0\rangle$ state (identified by its eigenvector) sometimes increases when basis functions are added reflects the existence of lower lying states (overtone $|0,\nu\rangle$ of the z vibration). If the added basis functions can better describe these overtones than the $|1,0\rangle$ state then a change in the order of the approximate excited-state energies can occur and the accuracy of the $|1,0\rangle$ level can deteriorate. This is the case for the h,z coupling when the basis set size goes from 10×10 to 12×12 (see Fig. 7). In that case the overtone $|0,4\rangle$ reaches an energy lower than the $|1,0\rangle$ fundamental excited state whose energy increases. If the convergence of the $|1,0\rangle$ state associated with the h,r potential is obtained easily (both QMC and variational treatments lead to very close results), that is not the case for h,z. The explanation involves the fact that the potential has been fitted by a polynomial and hence does not have the correct asymptotic form. The eigenvalues of this fit to the

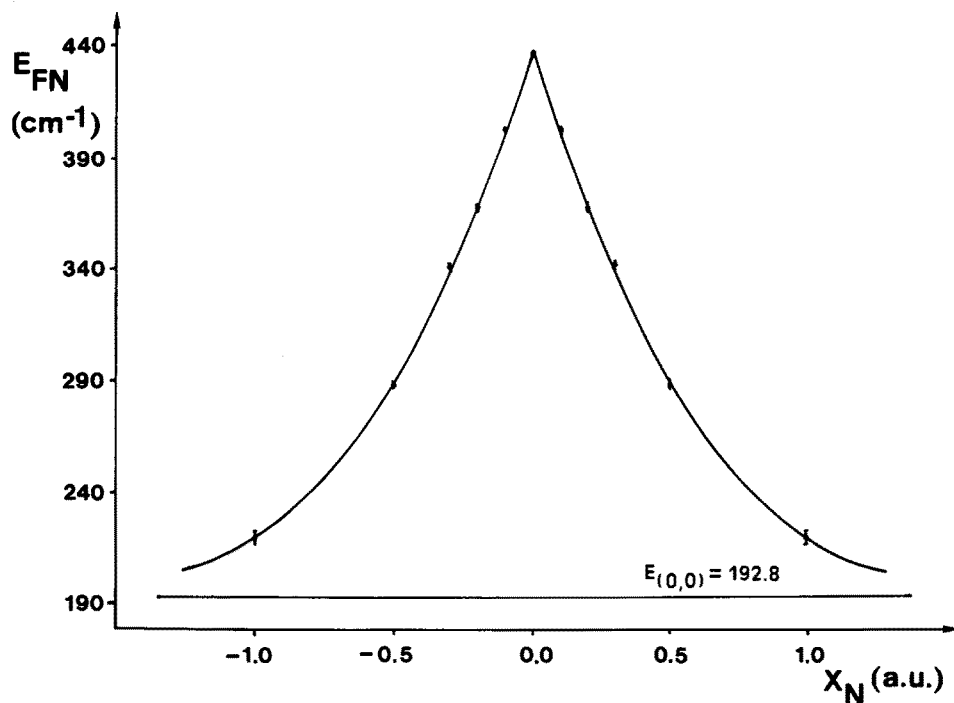
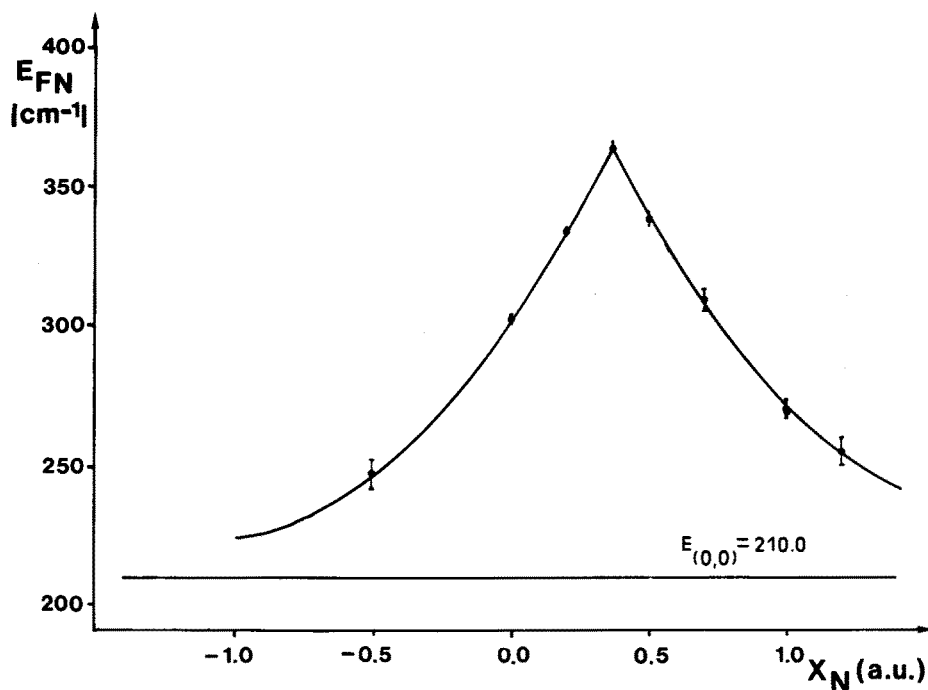


FIG. 5. Fixed-node energy of (a) the $|0,1\rangle$ state of the V_I potential (symmetrical case, optimized value of x_N is 0.0) and (b) the $|1,0\rangle$ state of the V_{II} potential (unsymmetrical case, optimized value of x_N is 0.368), vs the translational parameter x_N .



potential are determined by the arbitrary tail as well as by the physically interesting region near the minimum. If only low-order functions are included in the variational calculation (say $n = 5, 7$), functions which have negligible weight in the pathological region of the potential fit, then an upper bound to the physical eigenvalue will be attained. Adding higher-order, more long-range basis functions eventually allows convergence to the exact (but unphysical) eigenvalue of the fitted potential. In order to improve the physical eigenvalue, we chose to contract sufficiently the basis set functions in the physical region of the potential in order to extend the convergence process as far as possible. In that case, the long-range

effects are avoided, but on the other hand, the convergence is slow as shown in Fig. 7. By contrast, the QMC procedure using only local behavior of the potential around the equilibrium position works well in this case and then illustrates its efficiency. To summarize, we can say that in the variational process, a large extension of the basis set is needed to describe as well as possible the wave function in the neighborhood of the physical potential, but at the same time it would increase the contribution of the "nonphysical" region of V ; on the other hand, it is always possible with the QMC to choose the reference function to prevent the trajectories (through the drift vector) from visiting the wrong region of

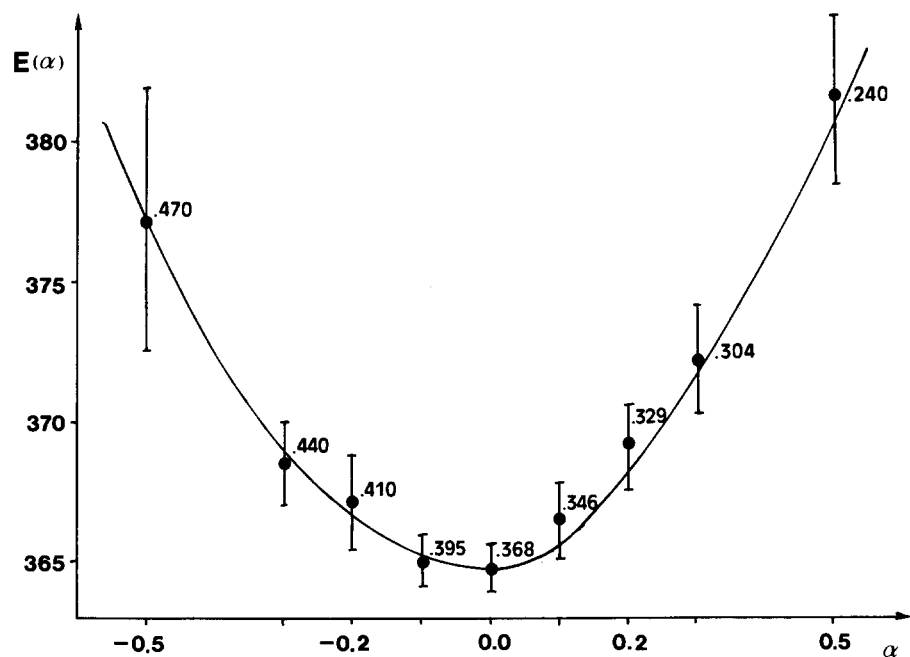


FIG. 6. Illustration of the extremum principle for the $|1,0\rangle$ state of the V_{11} potential. At each point of the curve, we give the value of the translational parameter x_N which assures the equality $\epsilon_1 = \epsilon_2 = \epsilon(\alpha)$ (see Figs. 5).

V during the simulation time. It is then possible to satisfactorily describe the metastable states of the whole potential. However, as already emphasized, a much more satisfactory approach would consist in using a physical representation for V having the correct asymptotic behavior, instead of a polynomial fit. This nonphysical fit is used only because the purpose of this paper is to compare both variational and Monte Carlo treatments. In our example (see Table III), we deduce that the QMC improves the $|1,0\rangle$ energy by 3.4 cm^{-1} on the best variational result. The QMC value is presented in Fig. 7 as the asymptote of the variational process. For both couplings the nodal line is a straight line ($\alpha = 0$). Finally,

each of the nodal lines of the excited states of the two realistic potentials studied here are “undistorted” as was also found for the model potentials. In Table IV, the corresponding vibrational frequencies are quoted.

C. Pd_2CO

As a second example where the accuracy and stability of the QMC approach have proven crucial, we briefly present a few results from a preliminary study of the effect of an external electric field on the CO stretch vibration of the Pd_2CO cluster. We have studied the coupling of this d mode with the

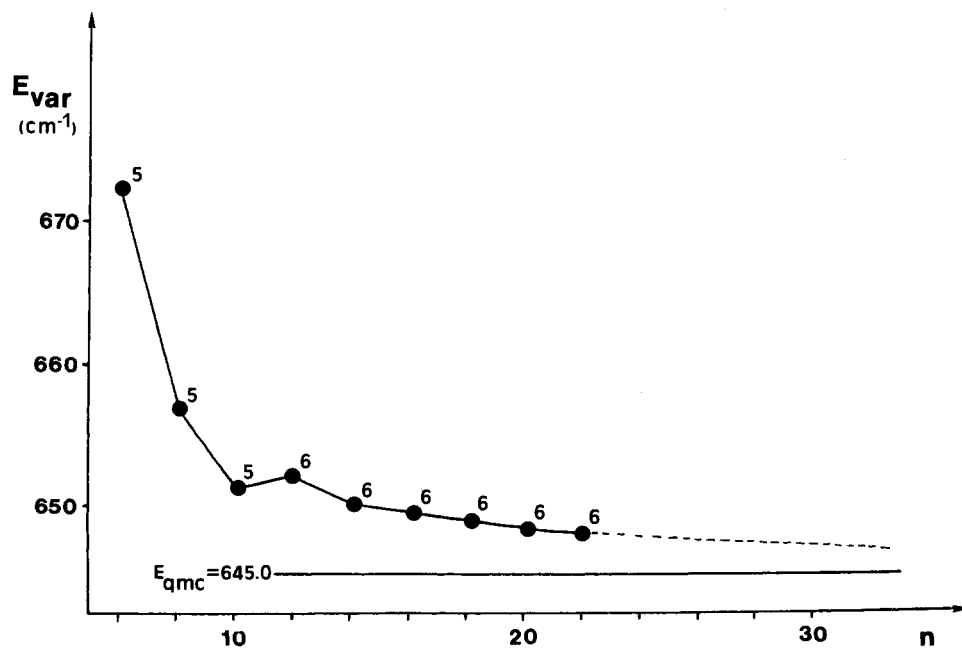


FIG. 7. Convergence of the variational process with respect to the basis set size, $n \times n$, for the $|1,0\rangle$ state of the h,z coupling. At each point, we give the sequence number of the $|1,0\rangle$ root.

TABLE IV. Vibrational frequencies^a (cm⁻¹) of the two coupled modes h,r and h,z.

Method	Harmonic	PNC	Variational ^b	QMC ^c
Coupling				
ω_r^d	240.0	192.8	192.0	192.0 ± 0.3
ω_h^d	498.0	504.9	521.1	520.6 ± 0.2
ω_z^d	195.7	86.7	65.2	65.7 ± 1.6
ω_h^d	498.0	544.4	400.9	397.1 ± 1.1

^aEvaluated from Tables III.^bThe size of the basis set is 22 × 22.^cOur results.

$$^d\omega_h = E_{(1,0)} - E_{(0,0)} \cdot \omega_{r/z} = E_{(0,1)} - E_{(0,0)}$$

adsorbate-surface h mode. Table V shows the results of a convergence study for variational calculations in the field-free case. The overall variations of the frequencies as a function of $2 < l < 6$ (l is the polynomial order) and of $6 < n < 20$ (the size of the basis set) are about 50 cm⁻¹ for the d vibration and about 10 cm⁻¹ for h. Although this could be a useful level of accuracy in many contexts, the frequency shifts as a function of field in which we are interested are of the same order of magnitude.²³ We are in a case where the convergence of the variational treatment seems satisfactory. However, the results show the sensitivity of the excitation energies to the polynomial order. It is another example of the necessity to fit the potential by a more physical analytical form. As already noticed, this may be done straightforwardly with the QMC procedure. In order to compare the two methods we decided to use a polynomial fitting at the fourth order ($l = 4$) and the variational results obtained with $n = 20$. Variational and QMC results are shown in Table VI for values of an external electric field appropriate for an electrochemical study. Although the differences in frequencies between the variational and QMC approaches are at most about 10 cm⁻¹ ($\approx 0.5\%$) and the qualitative trend as a function of electric field is the same in both cases, there are significant quantitative differences. In particular the variational calculations yield quite different results for fields of the same

TABLE V. Excitation energies (cm⁻¹) ($v = 0 \rightarrow v = 1$) for the C-O (d) (top numbers) and Pd₂-CO (h) (bottom numbers) vibrations of Pd₂CO in absence of electric field.

Polynomial order ^a / n^b	6	10	16	20
l				
2	1923	1923	1907	1908
	505	504	505	505
3	1899	1888	1874	1875
	501	500	499	499
4	1898	1890	1873	1873
	495	495	495	495
5	1894	1881	1866	1866
	500	500	500	500
6	1920	1915	1911	1913
	498	497	497	497

^aPotential fit with $V(x_1, x_2) = \sum_{i+j \leq l} a_{ij} x_1^i x_2^j$.^bThe size of the basis set is $n \times n$.TABLE VI. C-O stretching frequency (cm⁻¹) vs electric field (V/cm × 10⁷) for Pd₂CO calculated by variational and by quantum Monte Carlo (QMC) methods.

Method	ω_{CO}			$\Delta\omega_{CO}/\Delta E^a$		
	PNC	Var.	QMC ^b	PNC	Var	QMC ^b
Electric field (V/cm × 10⁷)						
- 5.0	1871	1833	1833	28	26	22
- 2.5	1899	1859	1855	15	14	23
0.0	1914	1873	1878	35	35	22
2.5	1949	1908	1900	20	19	20
5.0	1969	1927	1920	15.5	17	14.5
10.0	2000	1961	1949			

^a ΔE is taken as 2.5 V/cm × 10⁷.^bFor each QMC value, the variance is lower than 0.5 cm⁻¹.

magnitude but opposite sign whereas the QMC frequency shifts are nearly symmetrical. In fact, the experimental electrochemical curves, frequency vs voltage, have a symmetrical sigmoid shape. Given the uncertainties of the cluster model and of the electrochemical double layer, etc., this does not in itself prove the superiority of QMC; however, taken together with the convergence difficulties of the variational approach we believe that QMC affords clear advantages for this type of problem.

VI. CONCLUSIONS

The results presented here show the efficiency of the FGFK-QMC method applied to two-mode vibrational problems when considering zero-point energy and fundamental excitations. The extension to many-mode problems is straightforward. Furthermore the results emphasize the difficulty of obtaining convergence for variational calculations when the coupling and anharmonicity parts of the interaction are nonnegligible. In that case a large number of basis states is required; however it is clear that if the number of coupled vibrations increases, variational solutions become unfeasible due to the size of the basis set needed. No such limitation arises with the QMC approach; the essential condition in this case is to find a fair reference function in order to reduce the computer time. This last point appears to be made easier by the remarkable properties of the approximate nodal surfaces associated with the fundamental excited states: (i) The partition of space into two and only two subdomains (independently of the sequence number of the state) seems to lead to satisfactory results. (ii) Their distortion seems to reduce to nearly a translation. If such strong assumptions always lead to very good results, then a potentially important criticism of the method, namely the more or less complicated parametrization of the nodal surface, disappears. Nevertheless, this point needs to be verified for larger systems. Another aspect of the difficulties encountered with the variational treatment is related to the analytical representation of the potential. In practice, the only analytical forms used are polynomial expansions which permit straightforward evaluation of Hamiltonian matrix elements. Unfortunately, such expansions can efficiently represent

only potentials where anharmonicity and coupling are weak. Furthermore, the wrong asymptotic behavior of these fitted analytical potentials does not allow the use of large delocalized basis sets. QMC entirely avoids these problems, since no specific constraints resulting from the potential are introduced. Furthermore, it is even possible to introduce a locally interpolated numerical form of the potential into the numerical process. Consequently, this method appears well-adapted for studying strongly coupled interactions as well as multiple-well potentials.

ACKNOWLEDGMENTS

This work was partially supported by grants from NSERC (Canada, operating and supercomputer access), FCAR (Québec), and the Institut Français du Pétrole for which we are grateful. D.R.S. wishes to acknowledge a stimulating conversation with Mark Wrighton. M.C., P.C., and C.M. thank the "Conseil Scientifique du Centre de Calcul Vectoriel pour la Recherche" for providing them with computer facilities and are indebted to the "Centre de calcul d'Orsay" for allowing them to make use of facilities on the NAS 9080 and the IBM 3090/200.

¹R. J. Whitehead and N. C. Handy, *J. Mol. Spectrosc.* **55**, 356 (1975).

²F. Soto-Eguibar and P. Claverie, in *Stochastic Processes Applied to Physics and Other Related Fields*, edited by B. Gomez, S. M. Moore, A. M. Rodriguez-Vargas, and A. Rueda (World Scientific, Singapore, 1983), p. 637-649.

³M. Caffarel and P. Claverie, *J. Stat. Phys.* **43**, 797 (1986).

⁴M. Caffarel and P. Claverie, *J. Chem. Phys.* **88**, 1088 (1988).

⁵M. Caffarel and P. Claverie, *J. Chem. Phys.* **88**, 1101 (1988).

⁶E. B. Wilson, J. C. Decius, and P. C. Cross, *Molecular Vibrations* (Dover, New York, 1955).

⁷P. J. Reynolds, D. M. Ceperley, B. J. Alder, and W. A. Lester Jr., *J. Chem. Phys.* **77**, 5593 (1982).

⁸D. M. Ceperley and B. J. Adler, *J. Chem. Phys.* **81**, 5833 (1984).

⁹H. Risken, *The Fokker-Planck Equation* (Springer, Berlin, 1984).

¹⁰M. H. Kalos, *Monte Carlo Methods in Quantum Problems*, NATO ASI Series C (Reidel, Dordrecht, 1982), pp. 19-31.

¹¹D. M. Ceperley, in *Recent Progress in Many-Body Theories*, edited by J. G. Zabolitzky, M. deLlano, M. Fortes, and J. W. Clark (Springer, Berlin, 1981), p. 262.

¹²L. D. Landau and E. Lifshitz, *Quantum Mechanics* (Pergamon, Oxford, 1965), Chap. 3, Sec. 20.

¹³M. Caffarel, Thèse de Doctorat de l'Université Paris VI, 1987.

¹⁴J. Andzelm and D. R. Salahub, *Int. J. Quantum. Chem.* **29**, 1091 (1986).

¹⁵J. Andzelm and D. R. Salahub, in *Physics and Chemistry of Small Clusters*, edited by P. Jena, B. K. Rao, and S. N. Khamma, NATO ASI Series B158 (Plenum, New York, 1987), p. 867.

¹⁶J. Andzelm, D. R. Salahub, M. Caffarel, P. Claverie, and C. Mijoule (unpublished).

¹⁷J. Andzelm, E. Radzio, and D. R. Salahub, *J. Chem. Phys.* **83**, 4573 (1985).

¹⁸C. Mijoule, M. Allavena, J. M. Leclercq, and Y. Bouteiller, *Chem. Phys.* **109**, 207 (1986).

¹⁹For one-dimensional systems it is known (see Ref. 12, Chap. 3, Sec. 21) that the k th excited state has just k nodes which divide the configuration space (the real line) into just $(k + 1)$ subdomains. This property admits a weaker generalization for an N -dimensional configuration space proved by Zhislin [G. M. Zhislin, *Usp. Mat. Nauk* **16**, 149 (1961)]. This theorem states that the nodal hypersurfaces of the k th excited state divide the N -dimensional configuration space into at most $(k + 1)$ subdomains.

²⁰E. A. Hylleraas and B. Undheim, *Z. Phys.* **65**, 759 (1930).

²¹J. K. L. MacDonald, *Phys. Rev.* **43**, 830 (1933).

²²J. P. Lowe, *Quantum Chemistry* (Academic, New York, 1978), Appendix 4.

²³K. Kunimatsu, *J. Phys. Chem.* **88**, 2195 (1984).

D. O. Hess, M. Caffarel, C. Huiszoon, and P. Claverie, "Second-order exchange effects in intermolecular interactions. The water dimer", *J. Chem. Phys.* **92**, 6049 (1990)

Second-order exchange effects in intermolecular interactions. The water dimer

O. Hess, M. Caffarel, C. Huiszoon,^{a)} and P. Claverie^{b)}

*Dynamique des Interactions Moléculaires, Université Pierre et Marie Curie, Paris VI,
Tour 22, 4 Place Jussieu, 75252 Paris Cedex 05, France*

(Received 21 September 1989; accepted 30 January 1990)

A new method of deriving explicit formulas for the calculation of second-order exchange contributions (induction as well as dispersion) within the framework of symmetry-adapted perturbation theories is presented. It is shown how exchange contributions can be expressed as a combination of electrostatic interaction energies between suitably generalized charge distributions (overlap intermolecular charge distributions). Each of these contributions are derived within the Hartree-Fock approximation (neglect of all electron correlation effects within the noninteracting molecules) and by considering only single-electron exchange between interacting molecules. Numerical calculations for the interaction of two water molecules are presented. In the region of the equilibrium geometry, it is found that the complete second-order exchange contribution accounts for about 20% of the total intermolecular interaction energy. This contribution is essentially dominated by the exchange induction component which is found to represent approximately 1 kcal/mol (using a basis set containing 94 orbitals). To our knowledge, this is the first example of calculation of exchange induction interaction energy for a molecular system. Concerning the less important, but non-negligible, exchange dispersion component, our result is found to agree with a very recent calculation for the water dimer.

I. INTRODUCTION

Calculating intermolecular interaction energies in the important region around the equilibrium configuration with a high level of accuracy (say with an error less than 10% of the experimental interaction energy) is known to be a difficult task. As an illustrative example, Szalewicz *et al.* pointed out in a recent paper¹ that for a relatively simple system as the water dimer, the calculated values of the interaction energy range from -4.1 to -6.1 kcal/mol, even after having rejected results obtained with too small basis sets or based on low-quality theoretical methods. In particular, the spread on the calculated values is larger than the commonly accepted experimental range of -5.4 ± 0.7 kcal/mol.² Obviously, the situation generally becomes worse when more complex systems are considered.

In the field of theoretical evaluations of interaction energies, two types of approach are generally distinguished. The first approach (certainly the most commonly employed) is the so-called supermolecule method³ in which the interaction energy is obtained by subtracting from the total energy of the interacting molecules (the supermolecule) the sum of the total energies of each monomer, all energies being calculated by using the same method. A major difficulty inherent to this type of approach is that a particularly high level of accuracy on calculated energies is required. The basic reason is that interaction energies represent only an extremely small fraction of the total energy of the supermolecule (about 5×10^{-5} for the favorable case of the water dimer). In addition,

it is, in general, difficult to know whether errors made in calculating total energies for interacting and noninteracting molecules are of comparable magnitude or not, which may lead to an important relative error for the interaction energy (basically one is dealing with the very general problem associated with the evaluation of a small quantity expressed as a difference of two large and approximately evaluated quantities). As an important example, let us mention calculations done at the self-consistent-field (SCF) level for which it is not at all clear *a priori* whether a favorable cancellation of the errors due to the lack of electron correlation contributions for monomers and dimer may occur or not. In fact, it is known that the intermolecular electron correlation effects (dispersion contributions) cannot be, in general, neglected. Accurate values for electron correlation contributions can be, in principle, obtained by application of some form of configuration interaction (CI), but in practice this may lead to prohibitively large computer time and memory requirements. Another well-known difficulty one has to cope with is the occurrence of the so-called basis-set superposition error (BSSE). A great amount of work dealing with this difficulty has been done (see, e.g., Refs. 4–6). However, it should be emphasized that the most commonly used solution to this problem, namely the so-called counterpoise method proposed by Boys and Bernardi,⁷ is still in discussion. In the second approach, which will be followed in the present study, the intermolecular interaction energy is calculated from perturbation theory using the intermolecular potential as the perturbing operator. When the intermolecular distance R is large, one is dealing with the Rayleigh-Schrödinger perturbation theory in which only simple products of monomer wave functions are used. Due to the large separation between monomers no antisymmetrization of the

^{a)} Permanent address: Chemical Physics Laboratory, Twente University of Technology, P. O. Box 217, 7500 AE Enschede, The Netherlands.

^{b)} Deceased, January 24, 1988.

factorized wave functions is necessary. Also, in this particular case, the multipole expansion⁸ for the interaction operator can be applied to obtain the interaction energy as a series of inverse powers of R (such terms being, in general, orientationally dependent). For shorter distances, e.g., distances corresponding to the region around the equilibrium configuration, the usual Rayleigh–Schrödinger perturbation theory must be abandoned,⁹ and in order to take into account, at least to some extent, the exchange of electrons between the interacting molecules, some form of exchange perturbation theory [the so-called symmetry-adapted perturbation theories (SAPT), see, e.g., Refs. 10 and 11] must be used. Before entering into the details of SAPT, it is important to emphasize two general features of perturbation theory which make this approach particularly attractive with regard to the usual supermolecular approach. First, the difficult problem just discussed above of evaluating the interaction energy as a difference of two large and approximate quantities is avoided since a direct evaluation of the interaction energy is done. Second, the interaction energy is decomposed into a sum of terms for each of which it is possible to give some physical interpretation (at least for terms up to and including second-order terms). This is a very appealing feature for a qualitative understanding of the interaction and can be very helpful for the development of simplified formulas for intermolecular interactions.

To our knowledge, the first example of an exchange-perturbation-theory calculation is due to Jeziorski and van Hemert (JvH) in their pioneering work on the water dimer.¹² Neglecting all intramonomer correlation effects, they evaluated the complete first-order interaction energy $E^{(1)} = E_{\text{RS}}^{(1)} + E_{\text{exch}}^{(1)}$ (explicitly, the sum of the Rayleigh–Schrödinger and first-order exchange energies) and the Rayleigh–Schrödinger second-order interaction energy which is known to decompose into the induction $E_{\text{ind}}^{(2)}$ and dispersion $E_{\text{disp}}^{(2)}$ components. In particular, no calculations of second-order exchange contributions were done. One of their major results was that the dispersion contribution was found to greatly stabilize the water dimer. More precisely, the dispersion energy turned out to amount to 50% of the SCF binding energy at the equilibrium geometry. This result is important since, as a part of the intermolecular correlation energy, the dispersion contribution cannot be obtained in a SCF calculation of the interaction energy. In other words, an extensive CI calculation would be necessary to recover this important contribution in a supermolecular approach. A second major result of JvH was that, for interoxygen distances greater than 5.0 a.u. (5.67 a.u. being the equilibrium distance) the SCF binding energy was found to be very well represented by the sum of the complete first-order energy and the second-order induction energy, thus leading to the approximate equality:

$$E_{\text{int}}^{\text{SCF}} \simeq E^{(1)} + E_{\text{ind}}^{(2)}. \quad (1)$$

On the other hand, it is known that besides the first-order and the second-order induction energies, the SCF binding energy contains some part of the second-order exchange induction contribution, and of the third- and higher-order “induction” energies as well as some intramonomer electron

correlation contributions due to the self-consistency at the dimer level.¹³ Accordingly, the preceding equality (1) was interpreted by supposing that, at least for interoxygen distances greater than 5.0 a.u., the three effects just quoted did not contribute significantly to the interaction energy. In fact, further calculations done by Chalasinski and Jeziorski for atomic van der Waals dimers such as He₂, Be₂, and Ne₂ failed to confirm this assertion.^{14–17} More precisely, in contrast to JvH, they observed that the SCF binding energy was poorly represented by Eq. (1). A number of reasons have been given to explain this result (see, e.g., the discussion in Ref. 18). Actually, one of these reasons (not the only one) is the non-negligible role of second-order exchange terms. In order to study quantitatively the importance of these contributions, Chalasinski and Jeziorski developed a method of evaluating second-order exchange energies (induction as well as dispersion) for the interaction of closed-shell atoms or molecules.¹⁵ In practice, they performed calculations on atomic van der Waals systems such as He₂, Be₂, and Ne₂.^{14–17} One of their main conclusions is that, as a general rule, the second-order exchange energy is repulsive and quenches a significant fraction of the interaction energy, at least for the van der Waals dimers studied. Concerning molecular interactions, no systematic calculations have been performed that would show the importance of second-order induction and dispersion exchange effects. To our knowledge, the first calculation for a molecular system is due to Chalasinski.¹⁹ He showed that for the HF dimer at the equilibrium geometry, $E_{\text{exch-disp}}^{(2)}$ represents about 10% of $E_{\text{disp}}^{(2)}$. Very recently, Rybak^{20,21} found a similar contribution for the water dimer. Finally, it seems that no calculations exist concerning the exchange induction energy for molecular systems.

The main purpose of this paper is to present a new method of deriving explicit formulas for the calculation of second-order exchange contributions. Following Claverie’s point of view,²² the strategy adopted in this work is essentially to express exchange contributions as a combination of formal electrostatic interaction energies between suitably generalized charge distributions (so-called overlap intermolecular charge distributions). To do that, two basic ingredients are used: (1) the so-called Longuet–Higgins representation of the intermolecular interaction operator in terms of molecular charge distributions,²³ and (2) the possibility of reducing the action of the intersystem antisymmetrizer (appearing in SAPT, see Sec. II) on factorized SCF wave functions to a sum of simple products of SCF determinants pertaining to each subsystem. These determinants are formally “charge-transfer” determinants corresponding to a certain number of opposite transfers (depending on the number of exchange of electrons between interacting molecules which are considered) between all possible pairs of spin orbitals of each monomer.

In order to demonstrate the applicability of the present approach, some numerical results on the interaction between two water molecules are presented.

The organization of the present paper is as follows. In Sec. II, we present the formal development of second-order exchange contributions. In order to make as far as possible

the present paper self-contained, the theory is presented in a systematic and comprehensive way. Section III is devoted to the presentation of numerical calculations for the two water molecules. Results for the different components of the interaction energy as a function of the interoxygen distance are presented and the importance of second-order exchange contributions are discussed. The role of the basis set used is also investigated. Finally, some concluding remarks are given in Sec. IV.

II. THEORY

Let us consider two interacting systems A and B . The total Hamiltonian H of the complex is written as

$$H = H_0 + V^{AB}, \quad (2)$$

with

$$H_0 = H^A + H^B, \quad (3)$$

where H^M ($M = A, B$) denotes the Hamiltonian of the non-interacting systems and V^{AB} is the intermolecular interaction potential

$$V^{AB} = \sum_{\alpha \in A} \sum_{\beta \in B} \frac{Z_\alpha Z_\beta}{r_{\alpha\beta}} - \sum_{\alpha \in A} \sum_{j \in B} \frac{Z_\alpha}{r_{\alpha j}} - \sum_{\beta \in B} \sum_{i \in A} \frac{Z_\beta}{r_{\beta i}} + \sum_{i \in A} \sum_{j \in B} \frac{1}{r_{ij}}, \quad (4)$$

where $r_{ab} = |\mathbf{r}_a - \mathbf{r}_b|$. Italic indices label electronic coordinates and Greek indices label nuclear coordinates. Z_μ is the charge number of nucleus μ belonging to molecule M ($M = A, B$). The eigenfunctions of the Hamiltonian H^M of molecule M ($M = A, B$) are denoted Ψ_i^M with the corresponding energies E_i^M . Then, the eigenfunctions of $H_0 = H^A + H^B$ are merely the products $\Psi_i^A \Psi_j^B$ with the corresponding energies $E_i^A + E_j^B$.

Following standard symmetry-adapted perturbation theories,^{10,11} the complete first- and second-order interaction energies are written in the form^{24,25}

$$E^{(1)} = \frac{\langle \Psi_0^A \Psi_0^B | V^{AB} \mathbf{A} | \Psi_0^A \Psi_0^B \rangle}{\langle \Psi_0^A \Psi_0^B | \mathbf{A} | \Psi_0^A \Psi_0^B \rangle}, \quad (5)$$

$$E^{(2)} = - \frac{\langle \Psi_0^A \Psi_0^B | V^{AB} R_0 \mathbf{A} (V^{AB} - E^{(1)}) | \Psi_0^A \Psi_0^B \rangle}{\langle \Psi_0^A \Psi_0^B | \mathbf{A} | \Psi_0^A \Psi_0^B \rangle}, \quad (6)$$

where R_0 denotes the reduced resolvent of H_0 given by

$$R_0 = \sum'_{ij} \frac{|\Psi_i^A \Psi_j^B\rangle \langle \Psi_i^A \Psi_j^B|}{(E_i^A + E_j^B) - (E_0^A + E_0^B)} \quad (7)$$

(the prime in Σ' means as usual that the term corresponding to $i = 0$ and $j = 0$ is excluded from the summation) and \mathbf{A} is the intersystem antisymmetrizer which we shall write in the form²²

$$\mathbf{A} = 1 - \mathbf{A}' = 1 - P_{(1)} + P_{(2)} - \dots + (-1)^{N_{\text{inf}}} P_{(N_{\text{inf}})}, \quad (8)$$

where $P_{(1)} = \sum_i^A \sum_j^B P_{ij}$ denotes the sum of all permutations exchanging (space and spin) coordinates of electron i of molecule A with coordinates of electron j of molecule B , and similar definitions hold for $P_{(2)}, P_{(3)}, \dots$ (N_{inf} denotes the

smallest value of N_A and N_B , the numbers of electrons of molecule A and B , respectively).

Remark that a number of definitions of \mathbf{A} differing from one another by the normalization factor have been given elsewhere (see Appendix A in Ref. 22). However, this is of no importance since \mathbf{A} appears in both numerator and denominator of Eqs. (5) and (6) and therefore the normalization of \mathbf{A} is immaterial.

Now, by using the decomposition $\mathbf{A} = 1 - \mathbf{A}'$, where $\mathbf{A}' = P_{(1)} - P_{(2)} + \dots$, the second-order perturbation energy $E^{(2)}$ [Eq. (6)] may be decomposed into the usual second-order Rayleigh–Schrödinger (RS) perturbation energy $E_{\text{RS}}^{(2)}$ [obtained by setting $\mathbf{A} = 1$ in Eq. (6)] and into the so-called second-order exchange energy $E_{\text{exch}}^{(2)}$ in which we are interested here.

After elementary algebra, the complete second-order exchange term is found to be

$$E_{\text{exch}}^{(2)} = E^{(2)} - E_{\text{RS}}^{(2)} = - \frac{\langle \Psi_0^A \Psi_0^B | (V^{AB} - E^{(1)}) (\mathbf{A}' - \langle \mathbf{A}' \rangle) | \Phi^{(1)} \rangle}{\langle \mathbf{A} \rangle}, \quad (9)$$

where $\langle \mathbf{A}' \rangle$ and $\langle \mathbf{A} \rangle$ are the expectation values of \mathbf{A}' and \mathbf{A} calculated with the ground-state wave function $\Psi_0^A \Psi_0^B$ and $\Phi^{(1)}$ stands for the first-order correction to the wave function in the perturbation theory¹¹

$$\Phi^{(1)} = -R_0 V^{AB} \Psi_0^A \Psi_0^B. \quad (10)$$

Now, since multiple exchanges are supposed to contribute weakly in the region around the equilibrium geometry,^{13,14} here we shall limit ourselves to the calculation of the leading contribution to $E_{\text{exch}}^{(2)}$ corresponding to a single exchange of electrons between molecules A and B . Thus, setting $\mathbf{A}' = P_{(1)}$ in Eq. (9) and neglecting terms which will correspond to contributions of order higher than S^2 (where S stands for overlap integrals between orbitals of monomers A and B) within the Hartree–Fock formalism used below, the following expression of $E_{\text{exch}}^{(2)}$ is obtained:

$$E_{\text{exch}}^{(2)} = - \langle \Psi_0^A \Psi_0^B | (V^{AB} - \langle V^{AB} \rangle) \times (P_{(1)} - \langle P_{(1)} \rangle) | \Phi^{(1)} \rangle, \quad (11)$$

where $\langle V^{AB} \rangle$ is the first-order Rayleigh–Schrödinger interaction energy obtained by setting $\mathbf{A} = 1$ in Eq. (5).

Note that our formula (11) seems to differ from those given in other works (see, e.g., Refs. 14–17) by a minus sign. In fact, this is not true because the convention of sign we have adopted for the decomposition of the antisymmetrizer \mathbf{A} is different [compare, e.g., Eq. (5) in Ref. 15 with our definition (8)].

For our purposes it is convenient to rewrite $\Phi^{(1)}$ [Eq. (10)] as follows:

$$\Phi^{(1)} = \Psi_0^A \Phi_{\text{ind}}^B + \Phi_{\text{ind}}^A \Psi_0^B + \Phi_{\text{disp}}^{AB}, \quad (12a)$$

with

$$\Phi_{\text{ind}}^B = \sum_{i \neq 0} \Psi_i^B \frac{\langle \Psi_0^A \Psi_0^B | V^{AB} | \Psi_0^A \Psi_i^B \rangle}{E_0^B - E_i^B}, \quad (12b)$$

$$\Phi_{\text{ind}}^A = \sum_{i \neq 0} \Psi_i^A \frac{\langle \Psi_0^A \Psi_0^B | V^{AB} | \Psi_i^A \Psi_0^B \rangle}{E_0^A - E_i^A}, \quad (12c)$$

$$\Phi_{\text{disp}}^{AB} = \sum_{\substack{i \neq 0 \\ j \neq 0}} \Psi_i^A \Psi_j^B \frac{\langle \Psi_0^A \Psi_0^B | V^{AB} | \Psi_i^A \Psi_j^B \rangle}{(E_0^A - E_i^A) + (E_0^B - E_j^B)}. \quad (12d)$$

When inserting the previous decomposition of $\Phi^{(1)}$ into Eq. (11), the second-order exchange energy decomposes into three terms

$$E_{\text{exch}}^{(2)} = E_{\text{exch-ind}}^{(2)}(A \rightarrow B) + E_{\text{exch-ind}}^{(2)}(B \rightarrow A) + E_{\text{exch-disp}}^{(2)}. \quad (13)$$

The sum of the first two terms in Eq. (13) will be referred to in the following as the exchange induction energy, while $E_{\text{exch-disp}}^{(2)}$ will be referred to as the exchange dispersion energy.

Evaluating such quantities requires expressions of Ψ_i^A and Ψ_j^B , the exact eigenfunctions of monomers *A* and *B*. Unfortunately, it is well known that exact or even accurate correlated eigenfunctions for atomic or molecular systems are, in general, not available, except for very simple systems. As a consequence, approximate wave functions are generally used. However, it should be remarked that such an approximation is not inherent to the perturbation theory but is rather related to the way adopted in *ab initio* frameworks for evaluating perturbation quantities which consists in performing explicitly the infinite summation involved in the reduced resolvent of H_0 . As an example, it is possible by using a Monte Carlo path integral formalism to calculate *exactly* perturbation quantities without doing such a summation. The problem of finding good approximations of *all* exact eigenfunctions of H_0 [needed for evaluating R_0 ; see Eq. (7)] is then avoided.^{26,27}

Here, we shall limit ourselves to the use of approximate eigenfunctions obtained from a SCF calculation, thus neglecting the internal electron correlation of monomers. By denoting $a_i = a_i(\mathbf{r})\sigma_i^A$ and $b_i = b_i(\mathbf{r})\sigma_i^B$ as the SCF orthonormalized spin orbitals of monomers *A* and *B* (occupied as well as virtual), the approximate (normalized) eigenfunctions of H^A and H^B constructed from these spin orbitals will be the following determinants:

$$\Psi^A = \frac{1}{\sqrt{N_A!}} \mathbf{A}^A [a_1(1) \cdots a_{N_A}(N_A)], \quad (14a)$$

$$\Psi^B = \frac{1}{\sqrt{N_B!}} \mathbf{A}^B [b_1(1) \cdots b_{N_B}(N_B)], \quad (14b)$$

where \mathbf{A}^M ($M = A, B$) is the intrasystem antisymmetrizer for the electrons belonging to the monomer *M* [intrasystem antisymmetrizer in contrast with the intersystem antisymmetrizer defined above in Eq. (8)].

In order to avoid any risk of confusion, we shall systematically use different types of indices for labeling occupied and virtual spin orbitals. More precisely, occupied and virtual spin orbitals will be indexed by using subscripts *i, j, k, l* and *p, q, r, s*, respectively.

A. Second-order exchange induction energy

By using Eqs. (11), (12a), and (13), $E_{\text{exch-ind}}^{(2)}(A \rightarrow B)$ may be written as

$$E_{\text{exch-ind}}^{(2)}(A \rightarrow B) = - \langle \Psi_0^A \Psi_0^B | (V^{AB} - \langle V^{AB} \rangle) \times (P_{(1)} - \langle P_{(1)} \rangle) | \Psi_0^A \Phi_{\text{ind}}^B \rangle, \quad (15)$$

with a similar formula for $E_{\text{exch-ind}}^{(2)}(B \rightarrow A)$. Because of symmetry, only the expression for $E_{\text{exch-ind}}^{(2)}(A \rightarrow B)$ will be considered in the following.

For our purposes let us introduce the quantity $\Psi_0^B(b_r)$ defined as the Slater determinant obtained by replacing in Ψ_0^B the occupied spin orbital b_k by the virtual spin orbital b_r . A similar definition holds for monomer *A*.

Let us define c_k^r as

$$c_k^r = \frac{\langle \Psi_0^A \Psi_0^B | V^{AB} | \Psi_0^A \Psi_0^B(b_r) \rangle}{E_0^B - E_0^B(k \rightarrow r)}, \quad (16)$$

where $E_0^B(k \rightarrow r)$ are eigenvalues of the Fock operator associated with monoexcited wave functions $\Psi_0^B(b_k)$.

Using this notation and Eq. (12b), Φ_{ind}^B may be rewritten in the form

$$\Phi_{\text{ind}}^B = \sum_{k \in B} \sum_{r \in B} c_k^r \Psi_0^B(b_r), \quad (17)$$

where summations run over all occupied and virtual spin orbitals b_k and b_r , respectively. Note that Eq. (17) involves only single excitations since the interaction operator V^{AB} is a mono-electronic operator with respect to each of the interacting subsystems.

Now, defining the so-called "induction functions" f_k^B (see Ref. 15) associated with the occupied spin orbital b_k ,

$$f_k^B = \sum_{r \in B} c_k^r b_r, \quad (18)$$

and using standard properties of determinants, Eq. (17) takes the following form:

$$\Phi_{\text{ind}}^B = \sum_{k \in B} \Psi_0^B \left(\begin{matrix} f_k^B \\ b_k \end{matrix} \right), \quad (19)$$

where $\Psi_0^B \left(\begin{matrix} f_k^B \\ b_k \end{matrix} \right)$ is an obvious generalization of the previous notation indicating the replacement of the occupied spin orbital b_k by the associated induction function f_k^B . By inserting Eq. (19) into Eq. (15), the exchange induction energy is written

$$E_{\text{exch-ind}}^{(2)}(A \rightarrow B) = - \sum_{k \in B} \left\langle \Psi_0^A \Psi_0^B \left| (V^{AB} - \langle V^{AB} \rangle) \times \left(P_{(1)} - \langle P_{(1)} \rangle \right) \Psi_0^A \Psi_0^B \left(\begin{matrix} f_k^B \\ b_k \end{matrix} \right) \right\rangle. \quad (20)$$

In order to make our notation more compact, the following convention is introduced

$$[O]_k \equiv \left\langle \Psi_0^A \Psi_0^B \left| O \left| \Psi_0^A \Psi_0^B \left(\begin{matrix} f_k^B \\ b_k \end{matrix} \right) \right\rangle, \quad (21)$$

where O stands for an arbitrary operator. Thus, $E_{\text{exch-ind}}^{(2)}(A \rightarrow B)$ may be written in the expanded form

$$E_{\text{exch-ind}}^{(2)}(A \rightarrow B) = - \sum_{k \in B} \left([V^{AB}P_{(1)}]_k - \langle V^{AB} \rangle [P_{(1)}]_k - \langle P_{(1)} \rangle [V^{AB}]_k \right). \quad (22)$$

Note that the contribution associated with $\langle V^{AB} \rangle \langle P_{(1)} \rangle$ vanishes because of orthogonality between spin orbitals.

Before expliciting further the three basic contributions $[V^{AB}P_{(1)}]_k$, $[P_{(1)}]_k$, and $[V^{AB}]_k$, involved in Eq. (22), let us present the very important formula expressing the action of the permutation operator $P_{(1)}$ on a product of two determinants Ψ^A and Ψ^B in terms of a linear combination of simple products of determinants pertaining to subsystems A and B (see Sec. III B in Ref. 22):

$$P_{(1)}[\Psi^A\Psi^B] = \sum_{i \in A} \sum_{j \in B} \Psi^A \begin{pmatrix} b_j \\ a_i \end{pmatrix} \Psi^B \begin{pmatrix} a_i \\ b_j \end{pmatrix}, \quad (23)$$

where the summation is over the spin orbitals of determinants Ψ^A (here labeled by i) and Ψ^B (labeled by j). Let us emphasize that no subscript 0 has been used for denoting Ψ^A and Ψ^B since they must be viewed as rather arbitrary determinants and, in particular, are not necessarily constructed from a set of occupied spin orbitals. Using Eq. (23), all integrals involving functions of the type $P_{(1)}[\Psi^A\Psi^B]$ are reduced to sums of integrals involving simple products $\Psi^A \begin{pmatrix} b_j \\ a_i \end{pmatrix} \Psi^B \begin{pmatrix} a_i \\ b_j \end{pmatrix}$ of "opposite transfer" determinants.

1. Expression of $[V^{AB}P_{(1)}]_k$

By applying the property just presented $[V^{AB}P_{(1)}]_k$ is written as

$$[V^{AB}P_{(1)}]_k = \sum_{i \in A} \sum_{j \in B} \left\langle \Psi_0^A \Psi_0^B \left| V^{AB} \right| \Psi_0^A \begin{pmatrix} b_j \\ a_i \end{pmatrix} \Psi_0^B \begin{pmatrix} f_k^B a_i \\ b_k b_j \end{pmatrix} \right\rangle + \sum_{i \in A} \left\langle \Psi_0^A \Psi_0^B \left| V_{AB} \right| \Psi_0^A \begin{pmatrix} f_k^B \\ a_i \end{pmatrix} \Psi_0^B \begin{pmatrix} a_i \\ b_k \end{pmatrix} \right\rangle, \quad (24)$$

where $\Psi_0^B \begin{pmatrix} f_k^B a_i \\ b_k b_j \end{pmatrix}$ denotes the Slater determinant of molecule B in which the occupied spin orbital b_k has been replaced by f_k^B (sum of virtual spin orbitals of B) and the occupied spin orbital b_j ($b_j \neq b_k$) has been replaced by the occupied spin orbital a_i of molecule A . Indices i and j in summations of Eq. (24) run over occupied spin orbitals of A and B , respectively.

Our next step consists of the use of the so-called Longuet-Higgins representation of the interaction operator V^{AB} in terms of the molecular charge distributions ρ^M ($M = A, B$), namely,²³

$$V^{AB} = \iint \frac{\rho^A(\mathbf{r}^A)\rho^B(\mathbf{r}^B)}{|\mathbf{r}^A - \mathbf{r}^B|} d\mathbf{r}^A d\mathbf{r}^B, \quad (25)$$

with

$$\begin{aligned} \rho^M(\mathbf{r}) &= \rho_{\text{nuclear}}^M(\mathbf{r}) + \rho_{\text{electronic}}^M(\mathbf{r}) \\ &= \sum_{\mu \in M} Z_{\mu} \delta(\mathbf{r} - \mathbf{r}_{\mu}) - \sum_{i \in M} \delta(\mathbf{r} - \mathbf{r}_i), \\ M &= A, B. \end{aligned} \quad (26)$$

By using this representation, $[V^{AB}P_{(1)}]_k$ is written as

$$[V^{AB}P_{(1)}]_k = \sum_{i \in A} \sum_{j \in B} \int \int \frac{f_{00}^A \begin{pmatrix} b_j \\ a_i \end{pmatrix} f_{00}^B \begin{pmatrix} f_k^B a_i \\ b_k b_j \end{pmatrix}}{|\mathbf{r}^A - \mathbf{r}^B|} d\mathbf{r}^A d\mathbf{r}^B + \sum_{i \in A} \int \int \frac{f_{00}^A \begin{pmatrix} f_k^B \\ a_i \end{pmatrix} f_{00}^B \begin{pmatrix} a_i \\ b_k \end{pmatrix}}{|\mathbf{r}^A - \mathbf{r}^B|} d\mathbf{r}^A d\mathbf{r}^B, \quad (27)$$

with the definitions

$$f_{00}^A \begin{pmatrix} b_j \\ a_i \end{pmatrix} = \left\langle \Psi_0^A \left| \rho^A(\mathbf{r}^A) \right| \Psi_0^A \begin{pmatrix} b_j \\ a_i \end{pmatrix} \right\rangle, \quad (28a)$$

$$f_{00}^B \begin{pmatrix} f_k^B a_i \\ b_k b_j \end{pmatrix} = \left\langle \Psi_0^B \left| \rho^B(\mathbf{r}^B) \right| \Psi_0^B \begin{pmatrix} f_k^B a_i \\ b_k b_j \end{pmatrix} \right\rangle \quad (j \neq k), \quad (28b)$$

$$f_{00}^A \begin{pmatrix} f_k^B \\ a_i \end{pmatrix} = \left\langle \Psi_0^A \left| \rho^A(\mathbf{r}^A) \right| \Psi_0^A \begin{pmatrix} f_k^B \\ a_i \end{pmatrix} \right\rangle, \quad (28c)$$

$$f_{00}^B \begin{pmatrix} a_i \\ b_k \end{pmatrix} = \left\langle \Psi_0^B \left| \rho^B(\mathbf{r}^B) \right| \Psi_0^B \begin{pmatrix} a_i \\ b_k \end{pmatrix} \right\rangle. \quad (28d)$$

Note that the quantities of Eqs. (28a)–(28d) can be viewed as generalizations of the usual intramolecular charge density associated with the ground-state wave function of molecule M ($M = A, B$)

$$\begin{aligned} f_{00}^M(\mathbf{r}^M) &= \langle \Psi_0^M | \rho^M(\mathbf{r}^M) | \Psi_0^M \rangle \\ &= \sum_{\mu \in M} Z_{\mu} \delta(\mathbf{r}^M - \mathbf{r}_{\mu}) - \sum_{i \in M} |c_i(\mathbf{r}^M)|^2, \end{aligned} \quad (28e)$$

where $c \equiv a$ for $M = A$ and $c \equiv b$ for $M = B$, and thus may be referred to as "overlap intermolecular charge densities." Using this terminology, $[V^{AB}P_{(1)}]_k$, as given by Eq. (27), may be interpreted as a combination of electrostatic interactions between these various overlap intermolecular charge densities.

In order to write down simple formulas for these formal charge densities it is convenient to rewrite the determinantal wave functions in terms of orthogonal spin orbitals. Let Ψ be a determinant constructed from a set of N orthonormal spin orbitals $\{u_k\}_{k=1, N}$ and let v_j be an arbitrary spin orbital (that is with no particular orthogonality relations with respect to $\{u_k\}$), then the following property holds:

$$\Psi \begin{pmatrix} v_j \\ u_i \end{pmatrix} = \Psi \begin{pmatrix} v_j' \\ u_i \end{pmatrix} + \langle u_i | v_j \rangle \Psi, \quad (29)$$

where v_j' is constructed to be orthogonal on the set $\{u_k\}_{k=1, N}$, namely,

$$v_j' = v_j - \sum_{k=1}^N \langle u_k | v_j \rangle u_k. \quad (30)$$

Applying this property and denoting S_{ij}^{AB} and $S_{if_k^B}^{AB}$ as the spin-orbital overlaps

$$S_{ij}^{AB} = \langle a_i | b_j \rangle = \int d\mathbf{r} a_i(\mathbf{r}) b_j(\mathbf{r}) \langle \sigma_i^A | \sigma_j^B \rangle, \quad (31a)$$

and

$$S_{if_k^B}^{AB} = \langle a_i | f_k^B \rangle = \int d\mathbf{r} a_i(\mathbf{r}) f_k^B(\mathbf{r}) \langle \sigma_i^A | \sigma_{f_k^B}^B \rangle, \quad (31b)$$

we obtain the following relations:

$$\Psi_0^A(b_j) = \Psi_0^A(b'_j) + S_{ij}^{AB}\Psi_0^A$$

with $b'_j = b_j - \sum_{i \in A} S_{ij}^{AB}a_i$,

$$\Psi_0^A(f_k^B) = \Psi_0^A(f_{k'}^B) + S_{if_k}^{AB}\Psi_0^A$$

with $f_{k'}^B = f_k^B - \sum_{i \in A} S_{if_k}^{AB}a_i$,

and

$$\Psi_0^B(a_i) = \Psi_0^B(a'_i) + S_{ik}^{AB}\Psi_0^B$$

with $a'_i = a_i - \sum_{i \in B} S_{il}^{AB}b_l$.

For convenience, the expression of $\Psi_0^B(f_k^B a'_i)$ will be written down by using a slightly generalized version of property (29). Direct application of (29) would require constructing a spin orbital a'_i orthogonal with the set $\{b_j\}_{j \neq k}$ and f_k^B . In particular, a'_i would have no particular orthogonality relation with respect to the spin orbital b_k . However, as will become evident below, it is very convenient to impose also the orthogonality between these two spin orbitals. We thus define the new primed orbital a'_i as

$$a'_i = a_i - \sum_{i \in B} S_{il}^{AB}b_l - S_{if_k}^{AB}f_k^B,$$

which leads to the following expression:

$$\begin{aligned} \Psi_0^B(f_k^B a_i) &= \Psi_0^B(f_k^B a'_i) + S_{ij}^{AB}\Psi_0^B(f_k^B) \\ &\quad - S_{ik}^{AB}\Psi_0^B(f_k^B) \quad (j \neq k), \end{aligned}$$

which contains an extra term resulting from our new additional constraint.

Now, to evaluate matrix elements of Eqs. (28a)–(28d) we take advantage of the previous expressions and of the mono-electronic character of operators $\rho^A(\mathbf{r}^A)$ and $\rho^B(\mathbf{r}^B)$ (nonzero matrix elements only when evaluated between two determinants differing by at most one spin orbital). Note that this property holds here merely because we have introduced new spin orbitals (labeled with a prime) constructed to be orthogonal with original spin orbitals.

Thus, after some algebra we obtain

$$\begin{aligned} f_{00}^A(b_j) &= -a_i(\mathbf{r}^A) \left[b_j(\mathbf{r}^A) \langle \sigma_i^A | \sigma_j^B \rangle \right. \\ &\quad \left. - \sum_{i \in A} S_{ij}^{AB} a_i(\mathbf{r}^A) \langle \sigma_i^A | \sigma_i^A \rangle \right] + S_{ij}^{AB} f_{00}^A(\mathbf{r}^A), \end{aligned} \quad (32a)$$

$$\begin{aligned} f_{00}^B(f_k^B a_i) &= -b_k(\mathbf{r}^B) f_k^B(\mathbf{r}^B) \langle \sigma_k^B | \sigma_{f_k}^B \rangle S_{ij}^{AB} \\ &\quad + b_j(\mathbf{r}^B) f_k^B(\mathbf{r}^B) \langle \sigma_j^B | \sigma_{f_k}^B \rangle S_{ik}^{AB} \quad (j \neq k), \end{aligned} \quad (32b)$$

$$\begin{aligned} f_{00}^A(f_k^B) &= -a_i(\mathbf{r}^A) \left[f_k^B(\mathbf{r}^A) \langle \sigma_i^A | \sigma_{f_k}^B \rangle \right. \\ &\quad \left. - \sum_{i \in A} S_{if_k}^{AB} a_i(\mathbf{r}^A) \langle \sigma_i^A | \sigma_i^A \rangle \right] + S_{if_k}^{AB} f_{00}^A(\mathbf{r}^A), \end{aligned} \quad (32c)$$

$$\begin{aligned} f_{00}^B(a_i) &= -b_k(\mathbf{r}^B) \left[a_i(\mathbf{r}^B) \langle \sigma_i^A | \sigma_i^B \rangle \right. \\ &\quad \left. - \sum_{i \in B} S_{il}^{AB} b_l(\mathbf{r}^B) \langle \sigma_i^B | \sigma_i^B \rangle \right] + S_{ik}^{AB} f_{00}^B(\mathbf{r}^B), \end{aligned} \quad (32d)$$

where $f_{00}^M(\mathbf{r})$ ($M = A, B$) stands for the usual molecular charge density at \mathbf{r} , Eq. (28e). Finally, $[V^{AB}P_{(1)}]_k$ given by expression (27) can be written as a sum of mono- and bielectronic integrals involving spin orbitals a_i , b_j , and f_k^B .

2. Expression of $\langle V^{AB} \rangle [P_{(1)}]_k$

The quantity $\langle V^{AB} \rangle$ is nothing but the electrostatic energy of interaction between the systems A and B which may be expressed as usual in terms of mono- and bielectronic integrals involving occupied spin orbitals $\{a_i\}$ and $\{b_j\}$ of the two monomers.²²

Now, to evaluate $[P_{(1)}]_k$, we simply set $V^{AB} = 1$ in Eq. (24),

$$\begin{aligned} [P_{(1)}]_k &= \sum_{i \in A} \sum_{j \in B} \left\langle \Psi_0^A \Psi_0^B \left| \Psi_0^A(b_j) \Psi_0^B(f_k^B a_i) \right. \right. \\ &\quad \left. \left. + \sum_{i \in A} \left\langle \Psi_0^A \Psi_0^B \left| \Psi_0^A(f_k^B) \Psi_0^B(a_i) \right. \right. \right. \end{aligned} \quad (33)$$

Due to the orthogonality of the spin orbitals f_k^B with the occupied spin orbitals of B , only the second contribution in Eq. (33) does not vanish, and we obtain

$$[P_{(1)}]_k = \sum_{i \in A} \left\langle \Psi_0^A \left| \Psi_0^A(f_k^B) \right. \right\rangle \left\langle \Psi_0^B \left| \Psi_0^B(a_i) \right. \right\rangle, \quad (34)$$

which may be expressed in terms of overlaps between spin orbitals as follows:

$$[P_{(1)}]_k = \sum_{i \in A} S_{if_k}^{AB} S_{ik}^{AB}. \quad (35)$$

3. Expression of $\langle P_{(1)} \rangle [V^{AB}]_k$

Using Eq. (23), $\langle P_{(1)} \rangle$ is written as

$$\langle P_{(1)} \rangle = \sum_{i \in A} \sum_{j \in B} \left\langle \Psi_0^A \Psi_0^B \left| \Psi_0^A(b_j) \Psi_0^B(a_i) \right. \right\rangle, \quad (36)$$

which leads to

$$\langle P_{(1)} \rangle = \sum_{i \in A} \sum_{j \in B} |S_{ij}^{AB}|^2. \quad (37)$$

On the other hand, $[V^{AB}]_k$ is written

$$[V^{AB}]_k = \left\langle \Psi_0^A \Psi_0^B \left| V^{AB} \left| \Psi_0^A \Psi_0^B(f_k^B) \right. \right. \right\rangle.$$

We shall not make explicit this latter expression further since, when the summation over k is performed, it corre-

sponds to the usual second-order Rayleigh–Schrödinger induction energy of A on B .¹²

B. Second-order exchange dispersion energy

The derivation of the second-order exchange dispersion energy is actually very similar to the derivation just presented for the induction term. Introducing the following coefficients

$$c_{kl}^{rs} = \frac{\langle \Psi_0^A \Psi_0^B | V^{AB} | \Psi_0^A(a_r) \Psi_0^B(b_s) \rangle}{(E_0^A + E_0^B) - [E_0^A(k \rightarrow r) + E_0^B(l \rightarrow s)]} \quad (38)$$

and defining the so-called “dispersion pair functions” (which play a role here similar to the “induction functions” f_k^B introduced for the induction term) as follows:¹⁵

$$u_{kl}^{AB}(1,2) = \sum_{r \in A} \sum_{s \in B} c_{kl}^{rs} a_r(1) b_s(2), \quad (39)$$

the expression of Φ_{disp}^{AB} may be rewritten as [using Eqs. (12d) and (14)]

$$\Phi_{\text{disp}}^{AB} = \sum_{k \in A} \sum_{l \in B} \mathbf{A}^A \mathbf{A}^B \left[u_{kl}^{AB}(k,l) \prod_{i \neq k} a_i(i) \prod_{j \neq l} b_j(j) \right]. \quad (40)$$

Now, by inserting Φ_{disp}^{AB} into formula (11) [Φ_{disp}^{AB} is the dispersion part of $\Phi^{(1)}$ according to Eq. (12a)] it is possible to express $E_{\text{exch-disp}}^{(2)}$ in terms of the previous dispersion pair functions.¹⁵ However, we shall not follow this method. In the present work we shall prefer to show how the exchange dispersion energy may also be formally written as a sum of contributions which may be interpreted as the electrostatic interaction between suitable “overlap intermolecular charge distributions” localized on monomers A and B , respectively, thus pursuing what has been done for the exchange induction term. It should be remarked that such a point of view is no longer possible when introducing the dispersion pair functions since such functions connect explicitly variables of monomers A and B [Eq. (39)]. The two ways of writing down expressions for the exchange dispersion energy are of course equivalent but the latter approach will be particularly simple to handle.

By using Eqs. (11), (12a), (12d), (13), and (38) the following form for $E_{\text{exch-disp}}^{(2)}$ is obtained:

$$E_{\text{exch-disp}}^{(2)} = - \sum_{k \in A} \sum_{l \in B} \sum_{r \in A} \sum_{s \in B} c_{kl}^{rs} \left\langle \Psi_0^A \Psi_0^B \left| (V^{AB} - \langle V^{AB} \rangle) \times (P_{(1)} - \langle P_{(1)} \rangle) \right| \Psi_0^A(a_r) \Psi_0^B(b_s) \right\rangle, \quad (41)$$

where the two first summations are performed over the set of occupied spin orbitals of A and B , while the two last ones run over the virtual spin orbitals of A and B . Here also, $E_{\text{exch-disp}}^{(2)}$ is expressed as a sum of three nonzero contributions resulting from the expansion of the bracketed product. For future use, the following compact notation is defined:

$$[O]_{kl}^{rs} \equiv \left\langle \Psi_0^A \Psi_0^B \left| O \right| \Psi_0^A(a_r) \Psi_0^B(b_s) \right\rangle, \quad (42)$$

where O stands for an arbitrary operator.

1. Expression of $[V^{AB}P_{(1)}]_{kl}^{rs}$

In order to write down the expression of $[V^{AB}P_{(1)}]_{kl}^{rs}$, the permutation operator $P_{(1)}$ must be applied to the product of determinants $\Psi_0^A(a_r) \Psi_0^B(b_s)$. To do this, our basic formula (23) is used. When performing the double summation involved in (23), four different cases must be distinguished, depending on whether the spin orbitals a_r and/or b_s are considered in the summations or not. Next, the Longuet–Higgins representation of the interaction operator is used and then the quantity $[V^{AB}P_{(1)}]_{kl}^{rs}$ takes the form

$$\begin{aligned} [V^{AB}P_{(1)}]_{kl}^{rs} &= \sum_{i \in A} \sum_{j \in B} \int \int \frac{f_{00}^A(a_r, b_j) f_{00}^B(b_s, a_i)}{|\mathbf{r}^A - \mathbf{r}^B|} d\mathbf{r}^A d\mathbf{r}^B \\ &+ \sum_{i \in A} \int \int \frac{f_{00}^A(a_r, b_s) f_{00}^B(b_i, a_i)}{|\mathbf{r}^A - \mathbf{r}^B|} d\mathbf{r}^A d\mathbf{r}^B \\ &+ \sum_{j \in B} \int \int \frac{f_{00}^A(b_j, a_i) f_{00}^B(b_s, a_r)}{|\mathbf{r}^A - \mathbf{r}^B|} d\mathbf{r}^A d\mathbf{r}^B \\ &+ \int \int \frac{f_{00}^A(b_s, a_i) f_{00}^B(b_i, a_r)}{|\mathbf{r}^A - \mathbf{r}^B|} d\mathbf{r}^A d\mathbf{r}^B. \quad (43) \end{aligned}$$

Now, to calculate the “overlap intermolecular charge distributions” the same method as that used in the derivation of the exchange induction is employed. In fact, it is not difficult to convince oneself that calculations are identical with those accomplished for obtaining Eqs. (32). Let us just give the results in the following compact form:

$$\begin{aligned} f_{00}^M \begin{pmatrix} c_p & d_k \\ c_i & c_j \end{pmatrix} &= -c_i(\mathbf{r}^M) c_p(\mathbf{r}^M) \langle \sigma_i^M | \sigma_p^M \rangle S_{jk}^{AB} \\ &+ c_j(\mathbf{r}^M) c_p(\mathbf{r}^M) \langle \sigma_j^M | \sigma_p^M \rangle S_{ik}^{AB}, \quad (44) \end{aligned}$$

with $c \equiv a$, $d \equiv b$ for $M = A$ and $c \equiv b$, $d \equiv a$ for $M = B$.

Note that c_i , c_j , and d_k are occupied spin orbitals and $c_i \neq c_j$. With the same notations, we have

$$\begin{aligned} f_{00}^M \begin{pmatrix} d_\beta \\ c_i \end{pmatrix} &= -c_i(\mathbf{r}^M) \left[d_\beta(\mathbf{r}^M) \langle \sigma_i | \sigma_\beta \rangle \right. \\ &\left. - \sum_{j \in M} S_{j\beta}^{AB} c_j(\mathbf{r}^M) \langle \sigma_i | \sigma_j \rangle \right] + S_{i\beta}^{AB} f_{00}^M(\mathbf{r}^M). \quad (45) \end{aligned}$$

Note that c_i denotes an occupied spin orbital of one of the two monomers, while d_β may represent either an occupied or a virtual spin orbital of the other monomer.

2. Expression of $\langle V^{AB} \rangle [P_{(1)}]_{kl}^{rs}$

As already noticed, the quantity $\langle V_{AB} \rangle$ is nothing but the usual electrostatic interaction energy between monomers A and B . Expression of $[P_{(1)}]_{kl}^{rs}$ in terms of spin orbital overlaps is as usual obtained by making use of our basic property (23). One obtains

$$\begin{aligned} [P_{(1)}]_{kl}^{rs} &= \left\langle \Psi_0^A \Psi_0^B \left| P_{(1)} \right| \Psi_0^A(a_r) \Psi_0^B(b_s) \right\rangle \\ &= S_{ks}^{AB} S_{rl}^{AB}. \quad (46) \end{aligned}$$

3. Expression of $\langle P_{(1)} \rangle [V^{AB}]_{kl}^{rs}$

We shall not make explicit the expression of $[V^{AB}]_{kl}^{rs}$ further since, when summations over the indices are performed, it corresponds to the usual second-order Rayleigh–Schrödinger dispersion energy.¹² On the other hand, $\langle P_{(1)} \rangle$ has already been given in Eqs. (36) and (37).

C. Hylleraas variational procedure

Now, when performing the practical evaluation of the quantities written above, we are faced with the well-known problem of summing expressions defined over the infinite set of unoccupied orbitals of the Fock operator belonging to the continuous spectrum. As pointed out by Jeziorski and van Hemert,¹² such summations are practically inexecutable integration. To overcome this difficulty, here we will use the variational-perturbation method proposed by JvH. This method, which is essentially based on the minimization of a Hylleraas-type functional, has been already described in detail (see, e.g., Refs. 12 and 16) and therefore only its main features are summarized here. When applying the variational procedure, it is possible to show^{12,16} that expressions of induction and dispersion may be rewritten in a form identical with that obtained by the direct procedure, except that expressions are expressed in a new basis set donated by JvH as a *molecular* (or dimer) basis set. This new basis set consists of the occupied spin orbitals of monomers *A* and *B* ($\{a_i\}$ and $\{b_j\}$) with the corresponding orbital energies ϵ_i^A and ϵ_j^B) and of a new set of virtual spin orbitals obtained by diagonalizing the one-electron Fock operator of *A* (respectively, *B*) within the space spanned by the basis set of the whole dimer *AB* (denoted as $\{\tilde{a}_r\}$ and $\{\tilde{b}_s\}$ with the corresponding orbital energies $\tilde{\epsilon}_r^A$ and $\tilde{\epsilon}_s^B$). Note that the symbols *a* and *b* do not indicate at which center the orbital is located (basis set delocalized on the whole dimer). It should be emphasized that $\{\tilde{a}_r\}$ and $\{\tilde{b}_s\}$ are sets of square-integrable functions whereas $\{a_r\}$ and $\{b_s\}$ form continuous sets of unnormalizable functions. When using the molecular basis set, the induction and dispersion pair functions f_k^B and u_{kl}^{AB} [defined by Eqs. (18) and (39), respectively] must be replaced by the following new functions:

$$\tilde{f}_k^B = \sum_{r \in B} \tilde{c}_k^r \tilde{b}_r, \quad (47a)$$

$$\tilde{u}_{kl}^{AB}(1,2) = \sum_{r \in A} \sum_{s \in B} \tilde{c}_{kl}^{rs} \tilde{a}_r(1) \tilde{b}_s(2), \quad (47b)$$

where

$$\tilde{c}_k^r = \langle b_k | \omega^A | \tilde{b}_r \rangle / (\epsilon_k^B - \tilde{\epsilon}_r^B), \quad (48a)$$

with

$$\omega^A(\mathbf{r}) = \int \frac{f_{00}^A(\mathbf{r}')}{|\mathbf{r} - \mathbf{r}'|} d\mathbf{r}'$$

and

$$\tilde{c}_{kl}^{rs} = \left\langle a_k b_l \left| \frac{1}{r_{12}} \right| \tilde{a}_r \tilde{b}_s \right\rangle (\epsilon_k^A + \epsilon_l^B - \tilde{\epsilon}_r^A - \tilde{\epsilon}_s^B). \quad (48b)$$

The practical evaluation of expressions of second-order exchange contributions derived in the preceding sections

(II A) and (II B) are performed by using the dimer basis set $\{\tilde{a}, \tilde{b}\}$ instead of the monomer basis set $\{a, b\}$ and by employing formulas (47a) and (48a) for the induction functions \tilde{f}_k^B and formula (48b) for the coefficient \tilde{c}_{kl}^{rs} . Note that, in contrast with other works,^{12,14–17} the new dispersion pair functions \tilde{u}_{kl}^{AB} are not directly used (see discussion above, Sec. II B).

III. NUMERICAL RESULTS AND DISCUSSION

The implementation of the preceding expressions has been performed by modifying and extending an original program written by JvH. Since the main purpose of this work is to study the importance of the second-order exchange effects rather than to make a detailed investigation of the complete potential-energy surface, all numerical calculations have been done for a fixed relative orientation of the two interacting water molecules and by varying only the distance, R_{OO} , between the two oxygen atoms. In order to facilitate comparisons, the fixed orientation has been chosen to be identical with that used by JvH in their original work on the water dimer.¹² The nuclear coordinates of the water dimer are listed in Table I.

Second-order exchange induction and dispersion energies have been calculated by using the same basis set as JvH, namely a Gaussian basis (11,7,2/6,1) contracted into (4,3,2/2,1). This means 35 contracted basis functions for the monomer and 70 functions for the dimer. By employing this basis set, the total energy of the monomer and the binding energy of the water dimer are found to be -76.0576 a.u. and -3.87 kcal/mol, respectively.

Calculations with R_{OO} ranging from 4.40 to 9.00 a.u. have been performed. Numerical results for each individual component of the interaction energy are listed in Table II. No particular comments on results obtained for the commonly calculated contributions $E_{RS}^{(1)}$, $E_{\text{exch}}^{(1)}$, $E_{\text{ind}}^{(2)}$, and $E_{\text{disp}}^{(2)}$ will be made here: for a discussion concerning these terms the interested reader is referred to the work of JvH.¹²

Before discussing our results, let us briefly present the few calculations performed so far for second-order exchange contributions. Most of calculations have been done for atomic van der Waals dimers (He_2 , Be_2 , Ne_2).^{14–17} For distances around the equilibrium separation, two general features seem to emerge when treating inert gas dimers.

(1) There exists a large and systematic cancellation of $E_{\text{ind}}^{(2)}$ by the exchange induction contribution, $E_{\text{exch-ind}}^{(2)}$.

(2) The exchange dispersion energy cannot be considered as negligible and typically may represent a few percent

TABLE I. Nuclear coordinates for the water dimer (atomic units are used).

Atom	X	Y	Z
O	0.0	0.0	0.0
H	1.8088	0.0	0.0
H	-0.4641	1.7483	0.0
O	R_{OO}	0.0	0.0
H	$0.9551 + R_{OO}$	-0.5514	1.4338
H	$0.9551 + R_{OO}$	-0.5514	-1.4338

TABLE II. Particular contributions to the interaction energy of water dimer (in kcal/mol).

R_{OO} ^a	$E_{RS}^{(1)}$	$E_{exch}^{(1)}$	$E_{ind}^{(2)}$	$E_{disp}^{(2)}$	$E_{exch-ind}^{(2)}$	$E_{exch-disp}^{(2)}$
4.40	-27.10	51.59	-21.22	-8.42	14.31	3.11
4.80	-17.06	25.11	-9.30	-4.89	6.05	1.44
5.20	-11.10	12.03	-4.12	-2.86	2.45	0.67
5.67	-7.11	4.89	-1.63	-1.54	0.80	0.27
7.00	-2.79	0.30	-0.18	-0.31	0.03	0.02
9.00	-1.12	0.00	-0.02	-0.05	0.00	0.00

^a Atomic units.

of the dispersion energy $E_{disp}^{(2)}$ [up to 10% for Be_2 (Ref. 15)].

With regard to molecular interactions, no systematic calculations have been performed that would show the importance of second-order induction and dispersion exchange effects. Indeed, it has been recommended¹⁴⁻¹⁷ to calculate the interaction energy by using the following decomposition:

$$E_{int} \simeq E_{int}^{SCF} + E_{disp}^{(2)} + E_{exch-disp}^{(2)}, \quad (49)$$

and therefore attention has been focused on the evaluation of the intermolecular correlation effects represented by $E_{disp}^{(2)} + E_{exch-disp}^{(2)}$ and not on the evaluation of the exchange induction contribution which is supposed to be correctly taken into account in the SCF binding energy. To our knowledge the first calculation for a molecular system is due to Chalasinski.¹⁹ He showed that for the HF dimer at the equilibrium geometry, $E_{exch-disp}^{(2)}$ represents about 10% of $E_{disp}^{(2)}$ which corresponds to a slightly more important contribution than for inert-gas dimers. His observation has been very recently confirmed by Rybak and co-workers,^{20,21} who found a similar contribution for the water dimer. To our knowledge no calculations exist concerning the exchange induction energy for molecular systems.

Our results for second-order exchange contributions are presented in the two last columns of Table II. It should be noted that, in order to study basis-set size effects, we have performed an additional calculation with a substantially larger basis set than that employed by JvH.¹² The results presented in Tables IV and V will be discussed in detail below. However, anticipating our conclusions it is important

to note that results are, in fact, not qualitatively changed. Therefore, the following discussion and conclusions based on results obtained by employing the JvH basis set will remain valid. A first remark would concern the magnitude of the second-order exchange dispersion energy which is found to represent about 20% of the dispersion energy, thus confirming the non-negligible role of this contribution.^{14-17,20,21}

Note that our result for $E_{exch-disp}^{(2)}$ is 0.27 kcal/mol while Rybak's result is 0.19 kcal/mol.^{20,21} This difference may be interpreted as resulting from a basis-set size effect. Indeed, we observed a systematic lowering of our result when we repeated our calculation with basis sets of various smaller sizes (results not presented here). A particularly interesting result concerns the second-order exchange induction energy which is found to be quite important. At the equilibrium geometry, it compensates for approximately 50% of the induction energy. The importance of this contribution, which has been already noticed for inert-gas dimers,¹⁴⁻¹⁷ is therefore confirmed for the water dimer. When combining both second-order exchange components a contribution of about 1 kcal/mol is obtained at the equilibrium geometry. Comparing this contribution to the estimated interaction energy of about 5.4 kcal/mol,¹² the importance of second-order exchange effects is clearly illustrated. It is therefore quite obvious that such an exchange contribution cannot be neglected when doing high-quality evaluations of intermolecular interactions (exactly or by means of high-quality simplified representations).

Having calculated the exchange induction energy, it is interesting to compare the SCF binding energy to the sum of the complete first-order and second-order induction energies (displayed in columns 2 and 1 of Table III, respectively). Except at large distances, results displayed in Table III clearly demonstrate the noncoincidence of these two quantities. As a consequence, it is concluded that the additional terms present in the SCF binding energy (induction part of third- and higher-order Rayleigh-Schrödinger terms, some intramolecular correlation contribution introduced when doing a SCF supermolecule calculation¹³) contribute in a non-negligible way, even in the neighborhood of the equilibrium geometry. It is seen that these additional contributions become more important as the intermolecular distance is decreased. It may be expected that the difference between

TABLE III. Comparison of the SCF and perturbation-theory interaction energies for the water dimer (in kcal/mol).

R_{OO} ^a	$E_{ind}^{(1)} + E_{exch-ind}^{(2)}$	E_{int}^{SCF}	E_{int}^{pert} ^b	$E_{int}^{SCF} + E_{disp}^{(2)}$	$E_{int}^{SCF} + E_{disp}^{(2)} + E_{exch-disp}^{(2)}$
4.40	17.57	10.72	12.27	2.30	5.41
4.80	4.79	0.92	1.35	-3.97	-2.53
5.20	-0.75	-2.77	-2.93	-5.62	-4.95
5.67	-3.05	-3.87	-4.32	-5.41	-5.14
7.00	-2.65	-2.69	-2.93	-3.00	-2.98
9.00	-1.14	-1.14	-1.19	-1.19	-1.19

^a Atomic units.

^b Pure perturbational interaction energy calculated as $E_{int}^{pert} = E_{RS}^{(1)} + E_{exch}^{(1)} + E_{ind}^{(2)} + E_{disp}^{(2)} + E_{exch-ind}^{(2)} + E_{exch-disp}^{(2)}$.

$E_{\text{int}}^{\text{SCF}}$ and $E^{(1)} + E_{\text{ind}}^{(2)}$ would be partly cancelled if in the perturbational approach the induction part of third- and higher-order contributions would be considered. At this point, let us recall that JvH (Ref. 12) obtained at $R_{\text{OO}} = 5.67$ a.u. a good agreement between the SCF binding energy $E_{\text{int}}^{\text{SCF}}$ (-3.87 kcal/mol) and $E^{(1)} + E_{\text{ind}}^{(2)}$ (-3.85 kcal/mol). Accordingly, their approximate equality

$$E_{\text{int}}^{\text{SCF}} \approx E^{(1)} + E_{\text{ind}}^{(2)} \quad (50)$$

results essentially from a cancellation between $E_{\text{exch-ind}}^{(2)}$ and high-order contributions. Such a cancellation must be considered as fortuitous and cannot be generalized without further theoretical investigations. In conclusion, it does not seem justifiable to approximate the SCF binding energy by a sum of perturbation terms limited to second-order contributions, even at intermediate distances (including the equilibrium geometry).

Now, in order to compare calculations with experimentally predicted values of the total interaction energy, it is necessary to take into account intermolecular correlation effects, that is, dispersion contributions. We present in Table III values of the total interaction energy as calculated by our pure perturbational approach (third column) and by the most commonly used approach consisting of supplementing the SCF binding energy with the dispersion contributions (fifth column). Both potential-energy curves reveal a minimum which is approximately located at the same intermolecular separation, namely, $R_{\text{OO}} = 5.67$ a.u. As is known, the experimental evaluation of the total interaction energy at the equilibrium geometry is not easy to perform,¹ in what follows we shall use the most commonly accepted value of -5.4 kcal/mol with an estimated error of ± 0.7 kcal/mol.² It is very interesting to note that supplementing the sum $E_{\text{int}}^{\text{SCF}} + E_{\text{disp}}^{(2)}$ with the exchange dispersion contribution noticeably deteriorates the very good value of -5.41 kcal/mol obtained at the equilibrium geometry (without inclusion of the exchange dispersion term). Once again, such a result must be interpreted as a consequence of a fortuitous cancellation of terms which are not evaluated. To be more precise, it is expected that the sum $E_{\text{int}}^{\text{SCF}} + E_{\text{disp}}^{(2)} + E_{\text{exch-disp}}^{(2)}$ cannot fit the exact interaction energy. Indeed, it is well known that the difference between the SCF and correlated dipole moments of the water molecule are non-negligible (relative error of 10%; see Ref. 28), thus indicating a large electron

correlation contribution to the electrostatic interaction energy. Concerning the pure perturbational approach, it is clear that, besides intracorrelation contributions, high-order contributions must also be incorporated if a high accuracy is needed.

Now, we will pay some attention to the important problem of the quality of the basis set used. There exists a large amount of calculations performed with various basis sets at the supermolecular SCF level. All these studies indicate that basis sets involving a very large number of basis functions are needed to accurately reproduce the total interaction energy. However, except in a very recent extensive study of Szalewicz *et al.*¹ in which the problem of the basis-set dependency of the dispersion energy for the water dimer is addressed, to date no systematic study has been performed that shows the dependence of each particular perturbational contribution on the quality of the basis set employed. Here, we shall not do such an extensive work. In order to test the sensitivity of our results to the basis set we shall limit ourselves to the use of one substantially larger basis set. The so-called isotropic part of our basis (functions describing orbitals occupied in the ground states of the atoms; see Ref. 28) has been taken from Ref. 29 and consists of a set of (13s8p) and (6s) functions on the oxygens and hydrogens, respectively. This basis set has been extended with a set of (2d) and (2p) polarization functions on oxygen and hydrogen, respectively. The exponents were chosen to minimize the dispersion as well as the complementary exchange energies (see Ref. 22). Exponents $\alpha_d = 1$ and 0.3, $\alpha_p = 0.6$ and 0.15 have been obtained. The complete contracted basis represents 94 basis functions for the water dimer.

The energy of the water monomer calculated by using this basis set equals -76.06004 a.u. The SCF binding energies obtained for the water dimer are -3.96 and -3.73 kcal/mol without and with the counterpoise correction (CP), respectively. The latter value agrees very well with the SCF limit of -3.73 ± 0.05 kcal/mol (including CP correction) recently estimated by Szalewicz *et al.*¹ using a very large basis set containing 212 contracted orbitals. The values of the particular contributions to the interaction energy are listed in Tables IV and V. The essential result to point out is that the total interaction energy calculated as $E^{(1)} + E_{\text{RS}}^{(2)} + E_{\text{exch}}^{(2)}$ or as $E_{\text{int}}^{\text{SCF}} + E_{\text{disp}}^{(2)} + E_{\text{exch-disp}}^{(2)}$ with both basis sets (see Tables III and V) is not very different at the

TABLE IV. Particular contributions to the interaction energy of the water dimer (in kcal/mol) calculated with a 94 AO basis set.^a

R_{OO}^b	$E_{\text{RS}}^{(1)}$	$E_{\text{exch}}^{(1)}$	$E_{\text{ind}}^{(2)}$	$E_{\text{disp}}^{(2)}$	$E_{\text{exch-ind}}^{(2)}$	$E_{\text{exch-disp}}^{(2)}$
4.40	-23.66	50.31	-21.25	-8.90	14.28	3.32
4.80	-16.68	24.19	-9.42	-5.27	6.19	1.51
5.20	-10.81	11.61	-4.37	-3.18	2.70	0.75
5.67	-6.89	4.85	-1.82	-1.79	0.99	0.32
7.00	-2.67	0.39	-0.22	-0.46	0.06	0.03
9.00	-1.05	0.01	-0.03	-0.09	0.00	0.00

^a Basis set described in the text.

^b Atomic units.

TABLE V. Comparison of the SCF and perturbation-theory interaction energies for the water dimer (in kcal/mol) calculated with the 94 AO basis set.

R_{OO} ^a	$E^{(1)} + E_{ind}^{(2)}$ $+ E_{exch-ind}^{(2)}$	E_{int}^{SCF}	E_{int}^{pert} ^b	$E_{int}^{SCF} + E_{disp}^{(2)}$	$E_{int}^{SCF} + E_{disp}^{(2)}$ $+ E_{exch-disp}^{(2)}$
4.40	16.68	10.97	11.10	2.07	5.39
4.80	4.28	1.08	0.52	-4.19	-2.68
5.20	-0.87	-2.62	-3.30	-5.80	-5.05
5.67	-2.87	-3.73	-4.34	-5.52	-5.20
7.00	-2.44	-2.55	-2.87	-3.01	-2.98
9.00	-1.07	-1.08	-1.15	-1.16	-1.16

^a Atomic units.

^b Pure perturbational interaction energy calculated as $E_{int}^{pert} = E_{RS}^{(1)} + E_{exch}^{(1)} + E_{ind}^{(2)} + E_{disp}^{(2)} + E_{exch-ind}^{(2)} + E_{exch-disp}^{(2)}$.

equilibrium geometry and for large intermolecular separations. In addition, it should be noted that for these intermediate and large distances individual components appear to be more sensitive to the basis-set extension than the total sum. The two contributions to the total first-order interaction energy, namely, the electrostatic and first-order exchange terms, are not seriously affected when the size of the basis set is increased. However, the dipole moment of the water monomer calculated with the 94 atomic-orbital (AO) basis set (1.98 D) is in a better agreement with the experimental value³⁰ (1.85 D) than the value obtained with the JvH basis set (2.06 D).

With regard to the total second-order energy, it is interesting to note that the appreciable change of the RS contribution (-3.61 kcal/mol vs -3.17 kcal/mol with the JvH basis set) is partly compensated by a quite important increase of the exchange contribution (1.31 kcal/mol vs 1.07 kcal/mol with the JvH basis set). The total interaction energies calculated with the 70 and 94 AO basis set as the sum $E_{int} = E_{int}^{SCF} + E_{disp}^{(2)} + E_{exch-disp}^{(2)}$ equal -5.14 and -5.20 kcal/mol, respectively, and are consistent with the experimental value -5.4 ± 0.7 kcal/mol.² However, as already noticed above, non-negligible contributions to the interaction energy must be expected from intramolecular correlation effects which are known to decrease the dipole moment of the monomers and therefore are expected to modify noticeably the electrostatic contribution.

Szalewicz *et al.* pointed out that the use of f functions improved considerably their dispersion energy.¹ This observation is consistent with the results of Chalasinski for the neon dimer.¹⁶ However, although no f functions are present in our calculations, our 94 AO basis set leads to a value for the dispersion energy of -1.79 kcal/mol, close enough to the exact value of -2 kcal/mol estimated by Szalewicz *et al.*¹ In addition, as just noticed, our SCF binding energy of the water dimer coincides with the SCF limit estimated by these authors. Accordingly, we do not think that inclusion of f orbitals should change the qualitative nature of our conclusions.

IV. CONCLUSIONS

In the present paper new expressions for the exchange induction and dispersion energies have been derived within

the framework of symmetry-adapted perturbation theories. These expressions are valid for atomic and molecular systems having an arbitrary number of electrons. They have been derived by neglecting all electron correlation effects within the noninteracting molecules and by considering only single-electron exchange between interacting molecules. Within these approximations, numerical evaluation of second-order exchange contributions for the water dimer have been performed. Our major conclusion is that for such a polar system, second-order exchange effects are essentially dominated by the exchange induction energy and account for 20% of the total intermolecular interaction energy. As a conclusion, such contributions must be considered in any accurate calculation of the interaction energy. On the other hand, if a high accuracy on calculated interaction energies is needed, it is clear that going beyond the SCF approximation for the noninteracting systems is essential. In the case of the water molecule, it is known that the Hartree-Fock ground-state wave function overestimates the molecular dipole moment by about 10%, thus leading to an error of about 20% in the electrostatic contribution due to the lack of intramonomer electron correlation effects (let us recall that the electrostatic contribution is the leading component of the interaction energy at the equilibrium geometry). In addition, as already pointed out in our discussion of results, third-order (and higher-order) Rayleigh-Schrödinger contributions should be evaluated since they are expected not to be negligible in the region of the equilibrium geometry (see calculations of Jeziorski *et al.* in Ref. 21).

At this point, it is important to emphasize that the goal of the present work was not to obtain a very accurate value of the interaction energy between two water molecules. Indeed, it is clear that for a relatively simple system such as the water dimer, standard supermolecule approaches based on a very large CI calculation (or some form of it) are preferable (see, e.g., calculations of Diercksen, Kraemer, and Roos³¹ and of Matsuoka, Clementi, and Yoshimine).³² Actually, one of the basic motivations of our work was to put into evidence the non-negligible role of the complete second-order exchange contribution (exchange induction as well as exchange dispersion components). To be able to determine *quantitatively* the importance of each of these components opens the way towards representing second-order exchange contributions through simple analytical functions fitted on

calculated values. Knowledge of these functions will be required to derive high-quality parametrized formulas which describe quantitatively the interaction between molecules of arbitrary size.

ACKNOWLEDGMENTS

The authors are grateful to B. Jeziorski and M. van Hemert for making available to us their original program. Two of us (O.H. and M.C.) wish to thank the Groupement Scientifique "Modélisation Moléculaire" IBM-CNRS for providing us with computer facilities on IBM 3090/600E. This work was partly supported by the Ministère de l'Education Nationale of France (Grant No. P6.86016).

- ¹K. Szalewicz, S. J. Cole, W. Kolos, and R. J. Bartlett, *J. Chem. Phys.* **89**, 3662 (1988).
- ²L. A. Curtiss, D. J. Frurip, and M. Blander, *J. Chem. Phys.* **71**, 2703 (1979).
- ³See, e.g., K. Morokuma and K. Kitaura, in *Molecular Interactions*, edited by H. Ratajczak and W. J. Orville-Thomas (Wiley, New York, 1980), Vol. 1.
- ⁴N. R. Kestner, *J. Chem. Phys.* **48**, 252 (1968).
- ⁵A. Pullman, H. Berthold, and N. Gresh, *Int. J. Quantum Chem. Symp.* **10**, 56 (1976).
- ⁶W. Kolos, *Theor. Chim. Acta* **51**, 219 (1979).
- ⁷S. F. Boys and F. Bernardi, *Mol. Phys.* **19**, 553 (1970).
- ⁸J. O. Hirschfelder and W. J. Meath, in *Intermolecular Forces*, edited by J. O. Hirschfelder (Interscience, New York, 1967), Vol. XII, p. 3; see also A. D. Buckingham, *ibid.*, p. 107; and A. Dalgarno, *ibid.*, p. 143.
- ⁹P. Claverie, *Int. J. Quantum Chem.* **5**, 273 (1971).
- ¹⁰B. Jeziorski and W. Kolos, in *Molecular Interactions*, edited by H. Ratajczak and W. J. Orville-Thomas (Wiley, New York, 1982), Vol. 3.
- ¹¹I. G. Kaplan, in *Theory of Molecular Interactions* (Elsevier, Amsterdam, 1986), Vol. 42.
- ¹²B. Jeziorski and M. van Hemert, *Mol. Phys.* **31**, 713 (1976).
- ¹³G. Chalasinski and B. Jeziorski, *Int. J. Quantum Chem.* **7**, 63 (1973).
- ¹⁴G. Chalasinski and B. Jeziorski, *Mol. Phys.* **32**, 81 (1976).
- ¹⁵G. Chalasinski and B. Jeziorski, *Theor. Chim. Acta* **46**, 277 (1977).
- ¹⁶G. Chalasinski, *Mol. Phys.* **49**, 1353 (1983).
- ¹⁷G. Chalasinski, *Chem. Phys.* **82**, 207 (1983).
- ¹⁸M. Jeziorska, B. Jeziorski, and J. Cizek, *Int. J. Quantum Chem.* **32**, 149 (1987).
- ¹⁹G. Chalasinski, *Chem. Phys. Lett.* **86**, 165 (1982).
- ²⁰S. Rybak, Ph.D. thesis, University of Warsaw, Warsaw, 1988.
- ²¹B. Jeziorski, R. Morzynski, S. Rybak, and K. Szalewicz, in *Proceedings of the Symposium on Many-Body Methods, Tel-Aviv, Israël, 1988* edited by U. Kaldor (Springer-Verlag, Berlin, 1989).
- ²²P. Claverie, in *Intermolecular Interactions: From Diatomics to Biopolymers*, edited by B. Pullman (Wiley, New York, 1978).
- ²³H. C. Longuet-Higgins, *Proc. R. Soc. London* **235**, 537 (1956).
- ²⁴There exist a number of symmetrized perturbation treatments which differ from one another in the way of forcing the symmetry. A detailed discussion of the advantages and limitations of each approach may be found, for example, in Refs. 10 and 25. In the present work expressions of the first- and second-order perturbation terms common to the three exchange perturbation treatments MSMA, JK, and SRS (see Ref. 25) are used.
- ²⁵B. Jeziorski, K. Szalewicz, and G. Chalasinski, *Int. J. Quantum Chem.* **14**, 271 (1978).
- ²⁶M. Caffarel and O. Hess (preprint).
- ²⁷M. Caffarel, Ph.D thesis, University Paris VI, 1987.
- ²⁸J. G. C. M. van Duijneveldt-van de Rijdt and F. B. van Duijneveldt, *J. Mol. Struct. Theochem.* **89**, 185 (1982).
- ²⁹R. Poirier, R. Kari, and I. G. Csizmadia, *Handbook of Gaussian Basis Sets* (Elsevier, New York, 1985), Vol. 24, Tables 8.76.2 and 1.41.2.
- ³⁰S. A. Clough, Y. Beers, G. P. Klein, and L. S. Rothman, *J. Chem. Phys.* **59**, 2254 (1973).
- ³¹G. H. F. Diercksen, W. P. Kraemer, and B. O. Roos, *Theor. Chim. Acta* **36**, 249 (1975).
- ³²O. Matsuoka, E. Clementi, and M. Yoshimine, *J. Chem. Phys.* **64**, 1351 (1976).

E. M. Caffarel and O. Hess, “Quantum Monte Carlo-Perturbation Calculations of Interaction Energies”, *Phys. Rev. A* 43, 2139 (1991)

Quantum Monte Carlo perturbation calculations of interaction energies

M. Caffarel

*Dynamique des Interactions Moléculaires, Université Pierre et Marie Curie, Paris VI Tour 22, 4 place Jussieu,
75252 Paris CEDEX 05, France*

and National Center for Supercomputing Applications and Department of Physics, University of Illinois, Champaign, Illinois 61820

O. Hess

*Dynamique des Interactions Moléculaires, Université Pierre et Marie Curie, Paris VI Tour 22, 4 place Jussieu,
75252 Paris CEDEX 05, France*

and IBM France, Academic Information System, Service 3393, 94-96 rue Réaumur, 75002 Paris, France

(Received 24 September 1990)

A method of evaluating perturbational components of intermolecular interaction energies by using quantum Monte Carlo (QMC) techniques is presented. It is shown how the n th-order Rayleigh-Schrödinger (RS) perturbation term may be expressed in a very compact way in terms of suitably defined stochastic autocorrelation functions of the perturbing operator (the intermolecular interaction potential). The resulting formula is very general (not restricted to intermolecular interactions) and corresponds in fact to an alternative way of expressing RS perturbation theory in any order. As concerns the exchange contribution responsible for repulsion at small distances, an approximate expression for the first-order exchange interaction energy (by far the leading component) is given. Both advantages and drawbacks of the proposed QMC approach with respect to more conventional *ab initio* perturbational treatments are discussed. Some test calculations for the interaction of two helium atoms at small distances are presented. Results are systematically compared to those obtained with *ab initio* perturbation calculations using large Gaussian basis sets.

I. INTRODUCTION

Evaluating interaction energies between atoms and molecules is an important goal of molecular physics. Today, the most commonly employed method for such calculations is certainly the so-called supermolecule method¹ in which the interaction energy is obtained by subtracting from the total energy of the interacting molecules (the supermolecule) the sum of the total energies of each monomer, all energies being calculated by using the same method, generally some form of the configuration-interaction (CI) method. Difficulties associated with such an approach are well known and have been discussed in many places.¹ They can be summarized as follows.

(1) The problem of evaluating a very small quantity, the interaction energy, as a difference of two large and approximately evaluated quantities. Generally, it is very difficult to know whether errors made in calculating the total energies of the monomers and of the dimers are of comparable quality or not.

(2) Difficulties associated with the occurrence of the basis-set superposition error (BSSE), see, e.g., Refs. 2–5.

(3) Rapid increase of memory and CPU time requirements as a function of the size of the system studied.

An alternative approach to the supermolecule method consists in calculating interaction energies from perturbation theory using the intermolecular potential as perturbing operator. When the intermolecular distance R is large, one is dealing with the usual Rayleigh-Schrödinger perturbation theory. In this case, the complete set of excited states of the unperturbed Hamiltonian involved in

perturbational components is simply chosen to be the products of monomer wave functions: due to the large separation between monomers no antisymmetrization of the factorized wave functions is necessary. In contrast, for shorter distances, such as, for example, distances corresponding to the region around the equilibrium configuration, the usual Rayleigh-Schrödinger theory must be generalized⁶ in order to take into account the exchange of electrons between the interacting monomers (the introduction of exchange terms). This may be done by making use of one of the versions of the so-called symmetry-adapted perturbation theories (SAPT) in which the fermionic antisymmetry of the whole dimer is imposed within the perturbational expansion through the use of intersystem antisymmetrizers (see, e.g., Refs. 7 and 8). By using perturbation theory the basic difficulties of the supermolecule method listed above are essentially avoided: a direct evaluation of the small interaction energy is done, the BSSE is avoided, and calculations are generally much less expensive (the problem of having a high level of accuracy on total energies of each system is removed). However, a number of difficulties are still present. First, in order to perform the infinite summations over intermediate states involved in perturbational quantities, exact eigensolutions of monomers are required. Unfortunately, it is known that exact or even accurate correlated wave functions for atomic and molecular systems are in general not available. Consequently, approximate wave functions must be used. Generally, they are obtained from a self-consistent-field (SCF) calculation, so that the intramonomer electron correlation of monomers is neglected. However, it should be pointed

out that by using the decomposition of the exact Hamiltonian of each monomer into the complete Fock operator and into the residual two-electron operator accounting for the electron correlation (Moller-Plesset-type decomposition), and by applying the usual Rayleigh-Schrödinger perturbation theory, one can express in principle each perturbation contribution (with respect to the intermolecular interaction potential) as an infinite series of perturbation corrections due to internal correlation.⁹ In practice, such a procedure is generally limited to the calculation of leading corrections (e.g., up to second order in the internal correlation) and/or to some partial infinite-order summation corresponding to specific classes of diagrams (see, e.g., Ref. 10). Another difficulty associated with *ab initio* perturbation theory is the problem of summing efficiently infinite sums involved in perturbational expressions. In particular, as pointed out by Jeziorski and van Hemert¹¹ summations defined over the infinite set of unoccupied orbitals belonging to the continuous spectrum are practically inexecutable integrations. To overcome this difficulty, suitable variation-perturbation schemes have been proposed.¹¹ In practice, the achievement of a complete basis set is an obvious shortcoming of such procedures. An additional well-known difficulty common to any *ab initio* framework (supermolecular as well as perturbational approaches) is the problem of adequately choosing the basis set to use for a given physical problem. Due to the great sensitivity of perturbation quantities with basis set, the use of judiciously chosen basis sets turns out in fact to be essential. Finally, it is known that computational aspects of *ab initio* techniques are not favorable. Codes are important, complex, and many practical difficulties arise from calculation, storage, and manipulation of huge numbers of bi-electronic integrals (with a very fast increase of the number of these integrals with the number of electrons treated).

In the present work, a method of evaluating perturbation quantities by using quantum Monte Carlo (QMC) techniques (e.g., Refs. 12–17 and references therein) is presented. The basic idea of this approach is to express perturbational quantities of interest in terms of suitably defined stochastic averages. The underlying stochastic process from which averages are taken is a pure diffusion process (a generalized Brownian process) constructed in a simple way from some reference wave function (a detailed presentation of this aspect may be found in Ref. 17). It is demonstrated how the n th-order Rayleigh-Schrödinger (RS) term $\Delta E_{\text{RS}}^{(n)}$ can be expressed as an $(n-1)$ -time integral of the connected (cumulant) n -time autocorrelation function of the perturbing potential (the intermolecular interaction potential) with respect to the diffusion process constructed from the exact ground-state wave function of the unperturbed Hamiltonian (the Hamiltonian describing noninteracting dimer). It should be remarked that this formula is very general (not restricted to intermolecular interactions) and corresponds in fact to an alternative way of expressing RS perturbation theory in any order.¹⁸ In addition, this new formulation appears to be particularly compact, in contrast with the usual Bloch-Brückner formulation of the RS perturbation theory.¹⁹

By expressing stochastic averages defined from the generally unknown exact ground-state wave function of the unperturbed Hamiltonian in terms of stochastic averages defined from an approximate trial wave function, and by resorting to standard Langevin simulation techniques, it is shown how practical calculations of $\Delta E_{\text{RS}}^{(n)}$ may be performed. As concerns the exchange contribution responsible for intermolecular repulsion at small distances an approximate formula for the first-order exchange interaction energy $\Delta E_{\text{exch}}^{(1)}$ (by far the leading contribution of the total exchange interaction energy) is given.

An essential feature of the method presented here is that no basis-set expansions are used. Resulting difficulties described above are therefore avoided. Another remarkable point is that infinite summations involved in usual perturbational expressions do not appear in our QMC formalism (in fact, they only appear *implicitly*, see below). Accordingly, no approximate expressions for eigenfunctions of each monomer are required. In practice, the only quantity needed for making exact calculations of perturbational quantities is an *approximate* ground-state wave function for each monomer (e.g., a Hartree-Fock wave function or better an explicitly correlated wave function). Another basic point which deserves to be mentioned is that intramonomer correlation contributions to perturbational quantities may be exactly taken into account without basic practical difficulties. Finally, we would like to emphasize that the computational aspects of the method are quite favorable²⁰ (in fact, this is a very general feature of all Monte Carlo approaches): (1) memory requirements remain perfectly bounded (no calculation and storage of bi-electronic integrals) and (2) codes are short, simple, and very well suited for vector and parallel computing.

In a more general perspective, let us mention that a recent proposal based on the renormalization-group approach for electronic structure^{40,41} could lead to an alternative way of computing interaction energies. However, no realistic calculations (done at the level of the chemical accuracy) have been performed so far.

The contents of this paper are as follows. In Sec. II we present the basic theoretical elements of the method. Section II A is devoted to the derivation of the basic formula expressing $\Delta E_{\text{RS}}^{(n)}$ in terms of stochastic averages. In Sec. II B we present our approximate formula for calculating $\Delta E_{\text{exch}}^{(1)}$. How to compute the stochastic averages involved in both formulas is presented in Sec. II C. The detailed theory including mathematical derivations may be found elsewhere.¹⁷ Section II D briefly discusses how to correctly introduce Fermi statistics for monomers within the framework of the proposed method. Section III is devoted to the presentation of some numerical results for the interaction of two helium atoms at short distances (ranging from 1.5 to 2 a.u.). The essential motivation of such numerical application is to demonstrate the applicability of theoretical expressions derived in Sec. II and not to make a quantitative study of He-He interaction. In any case, at the short distances studied corresponding to a nonperturbative region of interaction, perturbational treatments for describing He-He interaction would fail (note that an exact treatment of this region of

interaction has been made by Ceperley and Partridge²¹ using a QMC supermolecular approach). Some calculations for $\Delta E_{\text{RS}}^{(1)}$, $\Delta E_{\text{exch}}^{(1)}$, and $\Delta E_{\text{RS}}^{(2)}$ are presented. In order to check the validity of the method our calculations have been systematically compared to calculations performed with an *ab initio* perturbational program based on the Jeziorski–van Hemert approach.^{11,22} The role of the intra-atomic correlation contribution on perturbational quantities (known to be particularly difficult to evaluate within *ab initio* frameworks) is briefly discussed. Finally, some concluding remarks are presented in Sec. IV.

II. THEORY

Consider two interacting systems A and B (atom or molecule). The total Hamiltonian of the complex, denoted as H , is decomposed as usual into three different parts

$$H = H^A + H^B + V^{AB}, \quad (1)$$

where H^M denotes the Hamiltonian of the noninteracting system M ($M = A, B$) and V^{AB} is the intermolecular interaction potential (atomic units are used)

$$V^{AB} = \sum_{\alpha \in A} \sum_{\beta \in B} \frac{Z_\alpha Z_\beta}{r_{\alpha\beta}} - \sum_{\alpha \in A} \sum_{j \in B} \frac{Z_\alpha}{r_{\alpha j}} - \sum_{\beta \in B} \sum_{i \in A} \frac{Z_\beta}{r_{\beta i}} + \sum_{i \in A} \sum_{j \in B} \frac{1}{r_{ij}}, \quad (2)$$

where $r_{ab} = |\mathbf{r}_a - \mathbf{r}_b|$. Roman indices label electronic coordinates and Greek indices label nuclear coordinates. Z_μ is the charge number of nucleus μ belonging to molecule M ($M = A, B$). The normalized eigenfunctions of the Hamiltonian H^M of isolated system M ($M = A, B$) are denoted ϕ_i^M with the corresponding energies E_i^M , thus we write

$$H^M \phi_i^M = E_i^M \phi_i^M, \quad M = A, B. \quad (3)$$

The intermolecular interaction energy is defined as the difference between the total ground-state energy E_0^{AB} of the complex described by the Hamiltonian H and the total ground-state energy of the two noninteracting subsystems A and B ,

$$\Delta E = E_0^{AB} - (E_0^A + E_0^B). \quad (4)$$

As usual, the interaction energy is decomposed into two contributions corresponding to the so-called Rayleigh-Schrödinger and exchange parts of the interaction energy

$$\Delta E = \Delta E_{\text{RS}} + \Delta E_{\text{exch}}. \quad (5)$$

The Rayleigh-Schrödinger interaction energy corresponds to the interaction energy obtained when antisymmetry constraints on wave functions associated with the possibility of exchanging electrons between each subsystem are not considered. When full antisymmetry constraints are taken into account, the resulting increase in energy is given by the exchange part ΔE_{exch} . Let us first focus our attention on the Rayleigh-Schrödinger part of the interaction energy.

A. n th-order Rayleigh-Schrödinger interaction energy

Within the framework of perturbational treatments, ΔE_{RS} is expressed as an infinite perturbation series of the form

$$\Delta E_{\text{RS}} = \sum_{n=1}^{+\infty} \Delta E_{\text{RS}}^{(n)}, \quad (6)$$

where n corresponds to the order in V^{AB} . Let us show how the n th-order RS interaction energy $\Delta E_{\text{RS}}^{(n)}$ may be expressed in terms of a suitably defined stochastic time-correlation function of the intermolecular interaction potential V^{AB} . For that purpose, it is first noticed that the RS interaction energy may be expressed in the following form:

$$\Delta E_{\text{RS}} = - \lim_{t \rightarrow +\infty} \frac{\partial}{\partial t} \ln \langle \phi_0^A \phi_0^B | e^{-t(H - E_0^A - E_0^B)} | \phi_0^A \phi_0^B \rangle. \quad (7)$$

The validity of this expression is easily checked by making use of the spectral representation of operator e^{-tH} . It should be noted that the eigenvalue of H extracted by making the long-time limit is the lowest eigenvalue of H whose corresponding eigenfunction has a nonzero overlap with $\phi_0^A \phi_0^B$. This wave function obeys the same antisymmetry properties as $\phi_0^A \phi_0^B$ and the interaction energy obtained in Eq. (7) is therefore the RS interaction energy and not the true physical one as defined by Eq. (4).

Now, our essential step consists in invoking the so-called generalized Feynman-Kac (GFK) formula presented elsewhere.^{17,20} Basically, this formula expresses the quantum matrix element of the right-hand side of Eq. (7) (actually, a slightly generalized version of the imaginary time-dependent Green's function associated with H) as an expectation value with respect to a suitable diffusion process. This basic formula is written here in the form

$$\langle \phi_0^A \phi_0^B | e^{-t(H - E_0^A - E_0^B)} | \phi_0^A \phi_0^B \rangle = \left\langle \exp \left[- \int_{-t/2}^{t/2} V^{AB}(\mathbf{X}(s)) ds \right] \right\rangle_{\phi_0^A \phi_0^B}, \quad (8)$$

where $\langle \rangle_{\phi_0^A \phi_0^B}$ denotes the stochastic average over the infinite set of stochastic continuous trajectories $\mathbf{X}(s)$ [defined in the time interval $(-t/2, t/2)$] of the underlying diffusion process constructed from the wave function $\phi_0^A \phi_0^B$ (Refs. 17 and 20). Here, $\mathbf{X}(s)$ is a compact notation for representing a point (at time s) in the $3(N_A + N_B)$ -dimensional configuration space, that is $\mathbf{X} = (\mathbf{r}_1^A, \dots, \mathbf{r}_{N_A}^A, \mathbf{r}_1^B, \dots, \mathbf{r}_{N_B}^B)$, where N_A and N_B are the numbers of electrons of molecule A and B , respectively. At this stage, we shall not define the exact meaning of this stochastic average and the way of computing it in a Monte Carlo simulation. This will be done in detail in Sec. II C.

Our next step consists in taking advantage of the fact that the previous stochastic average is a genuine average operation (in the Kubo sense, see Ref. 23) so that it is possible to resort to standard cumulant expansion methods. Applying a theorem due to Kubo (theorem II in Ref. 23), the averaged exponential in the right-hand side of formula (8) may be rewritten as the exponential of a cumulant expansion

$$\left\langle \exp \left[- \int_{-t/2}^{t/2} V^{AB}(\mathbf{X}(s)) ds \right] \right\rangle_{\phi_0^A \phi_0^B} = \exp \left[\sum_{n=1}^{+\infty} (-1)^n \int_{-t/2}^{t/2} dt_n \int_{-t/2}^{t_n} dt_{n-1} \cdots \int_{-t/2}^{t_2} dt_1 \langle V^{AB}(\mathbf{X}(t_1)) \cdots V^{AB}(\mathbf{X}(t_n)) \rangle_{\phi_0^A \phi_0^B}^c \right], \quad (9)$$

where $\langle \rangle_{\phi_0^A \phi_0^B}^c$ are the usual cumulant averages which are known to be expressed as some well-defined linear combination of products of same and lower-order moments (as pointed out by Kubo,²³ c may be as well understood as connected in the sense given to this word in the techniques of graphical representation). Note that for the sake of clarity a superscript notation for c is employed here instead of the more commonly used subscript notation. By making use of Eqs. (7), (8), and (9), the RS interaction energy takes the form

$$\Delta E_{\text{RS}} = - \lim_{t \rightarrow +\infty} \frac{\partial}{\partial t} \sum_{n=1}^{+\infty} (-1)^n \int_{-t/2}^{t/2} dt_n \int_{-t/2}^{t_n} dt_{n-1} \cdots \int_{-t/2}^{t_2} dt_1 \langle V^{AB}(\mathbf{X}(t_1)) \cdots V^{AB}(\mathbf{X}(t_n)) \rangle_{\phi_0^A \phi_0^B}^c. \quad (10)$$

Now, it is important to note that, due to the stationarity property of the diffusion process, all the cumulants involved in the preceding expression are only functions of the time differences $t_i - t_{i-1}$. It is therefore possible to perform a time-shift of length $t/2$ on each variable of integration and then to make the time derivative, one obtains

$$\Delta E_{\text{RS}} = - \lim_{t \rightarrow +\infty} \sum_{n=1}^{+\infty} (-1)^n \int_0^t dt_{n-1} \int_0^{t_{n-1}} dt_{n-2} \cdots \int_0^{t_2} dt_1 \langle V^{AB}(\mathbf{X}(t_i)) \cdots V^{AB}(\mathbf{X}(t_{n-1})) V^{AB}(\mathbf{X}(t)) \rangle_{\phi_0^A \phi_0^B}^c. \quad (11)$$

By making the following change of variables: $u_{i-1} - u_{i-2} = t_i - t_{i-1}$ ($i=2$ to n with $t_n \equiv t$ and $u_0 \equiv 0$) and by invoking once more the stationarity property, the n th-order contribution of Eq. (11), $\Delta E_{\text{RS}}^{(n)}$, may be finally written in the form

$$\Delta E_{\text{RS}}^{(n)} = (-1)^{n+1} \int_0^{+\infty} du_{n-1} \int_0^{u_{n-1}} du_{n-2} \cdots \int_0^{u_2} du_1 \langle V^{AB}(\mathbf{X}(0)) V^{AB}(\mathbf{X}(u_1)) \cdots V^{AB}(\mathbf{X}(u_{n-1})) \rangle_{\phi_0^A \phi_0^B}^c. \quad (12)$$

This is our final form for the n th-order RS perturbation term as a function of the n -time connected (cumulant) auto-correlation function of the intermolecular interaction operator with respect to the underlying diffusion process. It should be emphasized that this form is very compact, in contrast with the standard Bloch-Brückner formulation of the RS perturbation theory in any order (see, e.g., Ref. 19).

Let us briefly explain how to recover standard expression for $\Delta E_{\text{RS}}^{(n)}$ from our formula (12). In order to make explicit the n th-order cumulant, k th-order correlation functions of the perturbing potential are needed ($k=1$ to n). Using the very basic definition of stochastic averages in terms of the underlying probability densities, the k th-order correlation function of V^{AB} is written

$$\langle V^{AB}(\mathbf{X}(0)) \cdots V^{AB}(\mathbf{X}(u_{k-1})) \rangle_{\phi_0^A \phi_0^B} = \int d\mathbf{x}_0 \cdots d\mathbf{x}_{k-1} p(\mathbf{x}_0) V^{AB}(\mathbf{x}_0) \prod_{i=1}^{k-1} p(\mathbf{x}_{i-1} \rightarrow \mathbf{x}_i, u_i - u_{i-1}) V^{AB}(\mathbf{x}_i), \quad (13)$$

with $u_0 \equiv 0$ and where $p(\mathbf{x})$ and $p(\mathbf{x} \rightarrow \mathbf{y}, u)$ denote the stationary and transition probability densities of the diffusion process, respectively. These densities may be expressed in terms of the eigenfunctions $\phi_i^A \phi_j^B$ (with corresponding energies $E_i^A + E_j^B$) of the unperturbed Hamiltonian $H_0 = H^A + H^B$ as follows [see Eqs. (2.7) and (2.13) in Ref. 17]:

$$p(\mathbf{x}) = (\phi_0^A \phi_0^B)^2(\mathbf{x}) \quad (14a)$$

and

$$p(\mathbf{x} \rightarrow \mathbf{y}, u) = \frac{(\phi_0^A \phi_0^B)(\mathbf{y})}{(\phi_0^A \phi_0^B)(\mathbf{x})} \sum_{i,j} (\phi_i^A \phi_j^B)(\mathbf{x}) (\phi_i^A \phi_j^B)(\mathbf{y}) \times e^{-u(E_i^A + E_j^B - E_0^A - E_0^B)}. \quad (14b)$$

After having inserted expressions (13) and (14) into Eq. (12) time integrals may be easily performed. Once this is done, standard expanded expressions of Rayleigh-

Schrödinger perturbational components in terms of combination of multiple summations over the complete set of eigenfunctions of the unperturbed Hamiltonian $H^A + H^B$ are recovered. Let us derive the two first perturbational contributions. The first-order interaction energy is readily obtained; one has

$$\Delta E_{\text{RS}}^{(1)} = \langle V^{AB} \rangle_{\phi_0^A \phi_0^B}^c = \langle V^{AB} \rangle_{\phi_0^A \phi_0^B}. \quad (15)$$

Now, since the stationary density of the diffusion process is nothing but the quantum-mechanical probability density associated with $\phi_0^A \phi_0^B$ [Eq. (14a)], the usual expression for $\Delta E_{\text{RS}}^{(1)}$ is recovered:

$$\Delta E_{\text{RS}}^{(1)} = \langle \phi_0^A \phi_0^B | V^{AB} | \phi_0^A \phi_0^B \rangle. \quad (16)$$

Applying the general formula (12) to the case $n=2$ and using expression of the second-order cumulant²³

$$\langle X_1 X_2 \rangle^c = \langle (X_1 - \langle X_1 \rangle)(X_2 - \langle X_2 \rangle) \rangle, \quad (17)$$

the second-order RS interaction energy takes the form

$$\Delta E_{\text{RS}}^{(2)} = - \int_0^{+\infty} du \langle (V^{AB} - \langle V^{AB} \rangle_{\phi_0^A \phi_0^B})(\mathbf{X}(0))(V^{AB} - \langle V^{AB} \rangle_{\phi_0^A \phi_0^B})(\mathbf{X}(u)) \rangle_{\phi_0^A \phi_0^B}. \quad (18)$$

Using the basic definition of stochastic averages in terms of probability densities, one obtains

$$\Delta E_{\text{RS}}^{(2)} = - \int_0^{+\infty} du \int \int d\mathbf{x}_0 d\mathbf{x}_1 p(\mathbf{x}_0) [V^{AB}(\mathbf{x}_0) - \langle V^{AB} \rangle_{\phi_0^A \phi_0^B}] p(\mathbf{x}_0 \rightarrow \mathbf{x}_1, u) [V^{AB}(\mathbf{x}_1) - \langle V^{AB} \rangle_{\phi_0^A \phi_0^B}]. \quad (19)$$

By using Eqs. (14) and performing the time integral, expression (19) is finally found to be

$$\Delta E_{\text{RS}}^{(2)} = \sum'_{ij} \frac{|\langle \phi_0^A \phi_0^B | V^{AB} | \phi_i^A \phi_j^B \rangle|^2}{E_0^A + E_0^B - (E_i^A + E_j^B)}, \quad (20)$$

which is nothing but the usual expression for the second-order term (here, the prime in \sum' means as usual that the term corresponding to $i=0$ and $j=0$ is excluded from the summation). Higher-order perturbational terms would be recovered in the same way.

B. Exchange interaction energy

In this work, we shall limit ourselves to the calculation of the first-order exchange contribution which is by far the leading contribution of the exchange interaction energy. Following standard symmetry-adapted perturbation theories,^{7,8} the complete first-order interaction energy is written

$$\Delta E^{(1)} = \frac{\langle \Phi_0^A \Phi_0^B | V^{AB} \underline{A} | \Phi_0^A \Phi_0^B \rangle}{\langle \Phi_0^A \Phi_0^B | \underline{A} | \Phi_0^A \Phi_0^B \rangle}, \quad (21)$$

where \underline{A} is the full antisymmetrizer of the interacting supersystem (intra- and intersystem permutations are both considered) and where Φ_0^M ($M=A, B$) denotes the complete exact wave function of system M (depending on *both* space and spin coordinates). Now, especially because \underline{A} is a nonlocal operator mixing coordinates of each subsystem, to derive an *exact* expression of $\Delta E^{(1)}$ suitable for Monte Carlo simulation is not a trivial task (it involves off-diagonal matrix elements). In the present work, we did not investigate such a possibility. We shall content ourselves with giving a high-quality approximate expression for $\Delta E^{(1)}$. To do that, some approximate trial wave function Ψ_0^M ($M=A, B$) for representing each monomer will be employed. Note that such an approximation is similar to that used when doing variational quantum Monte Carlo simulation for calculating total energies (see, e.g., Ref. 24). However, it should be emphasized that no variational property holds here for such a perturbational component. A well-known feature of any QMC approach is that no basic limitations on the form of the trial wave function to be used are required. Here, following previous works (e.g., Refs. 12–17), we shall use an explicitly correlated wave function for describing monomers:

$$\Psi_0^M = \underline{A}_N^M (\exp U_{\text{LS}}^M \exp U_{\text{US}}^M X_\alpha^M X_\beta^M), \quad M=A, B \quad (22)$$

where $X_\alpha^M = \prod_i \phi_i^M \alpha$ and $X_\beta^M = \prod_i \phi_i^M \beta$. The symbol \underline{A}_N^M stands for the intramonomer antisymmetrizer acting on space and spin coordinates of the N electrons of system M ; functions U_{LS}^M and U_{US}^M are some fully symmetric

Jastrow-like pair-correlation factors introduced to allow explicitly for electron correlation in the wave function, subscripts LS and US being introduced in order to distinguish between like spin (LS) and unlike spin (UL) electron-electron correlation factors (for more details on wave functions see, e.g., Refs. 14, 15, and 24–26). Finally, $\{\phi_i^M\}$ is some set of one-particle atomic or molecular space orbitals and α and β represent usual spin functions. For the sake of clarity only expressions for two interacting closed-shell systems having the same number of electrons (here denoted N) will be derived. Generalizations to different numbers of electrons $N_A \neq N_B$ and/or to non-closed-shell systems do not involve particular difficulties. Now, since our Monte Carlo approach is defined within a spin-free framework, spin variables in Eq. (21) must be integrated out. Once this has been done, $\Delta E^{(1)}$ may be rewritten in the following form:

$$\Delta E^{(1)} = \frac{\langle \psi_0^A \psi_0^B | V^{AB} \bar{A} | \psi_0^A \psi_0^B \rangle}{\langle \psi_0^A \psi_0^B | \bar{A} | \psi_0^A \psi_0^B \rangle}, \quad (23)$$

where only space-dependent functions and space integrations are involved. Here, ψ_0^M ($M=A, B$) denotes the space-dependent part of the trial wave function (22) and \bar{A} is an effective local operator depending only on space coordinates of monomers A and B [expression (27b) below]. To show this, we take advantage of the following equalities:

$$\underline{A}^2 = \underline{A} \quad (24a)$$

and

$$\underline{A} \underline{A}_N^A \underline{A}_N^B = \underline{A}, \quad (24b)$$

and then rewrite $\Delta E^{(1)}$ in the form

$$\Delta E^{(1)} = \frac{\langle \underline{A} \Phi^{AB} | V^{AB} | \underline{A} \Phi^{AB} \rangle}{\langle \underline{A} \Phi^{AB} | \underline{A} \Phi^{AB} \rangle}, \quad (25a)$$

where

$$\Phi^{AB} = \exp(U_{\text{LS}}^A + U_{\text{US}}^A) \exp(U_{\text{LS}}^B + U_{\text{US}}^B) X_\alpha^A X_\beta^B X_\alpha^A X_\beta^B. \quad (25b)$$

Now, let us remark that $\Delta E^{(1)}$ as written in the form (25a) is nothing but the average of a spin-independent operator V^{AB} with respect to a properly antisymmetrized wave function for the dimer, $\underline{A} \Phi^{AB}$. Spin integrations may be easily performed and the resulting expression includes only space antisymmetrizations over α and β electrons separately. More precisely, we have

$$\Delta E^{(1)} = \frac{\langle A_{N_\alpha} A_{N_\beta} \phi^{AB} | V^{AB} | A_{N_\alpha} A_{N_\beta} \phi^{AB} \rangle}{\langle A_{N_\alpha} A_{N_\beta} \phi^{AB} | A_{N_\alpha} A_{N_\beta} \phi^{AB} \rangle}, \quad (26a)$$

where ϕ^{AB} (depending only on space coordinates) is given by

$$\begin{aligned} \phi^{AB} = & \exp(U_{LS}^A + U_{US}^A) \exp(U_{LS}^B + U_{US}^B) \\ & \times \prod_{i=1}^{N_\alpha} \phi_i^A \phi_i^B \prod_{i=1}^{N_\beta} \phi_i^A \phi_i^B. \end{aligned} \quad (26b)$$

Quantities A_{N_γ} ($\gamma = \alpha, \beta$) refer here to *space-* antisymmetrizers with respect to the N_γ electrons of spin γ (belonging to *both* A and B monomers). Finally, $\Delta E^{(1)}$ may be written in the form (23) where ψ_0^M ($M = A, B$) are usual space-dependent trial wave functions for monomers A and B :

$$\psi_0^M = \exp(U_{LS}^M + U_{US}^M) A_{N/2}^M \prod_{i=1}^{N/2} \phi_i^M A_{N/2}^M \prod_{i=1}^{N/2} \phi_i^M, \quad M = A, B \quad (27a)$$

and \tilde{A} the effective function is given by

$$\Delta E_{\text{exch}}^{(1)} = \frac{\langle \psi_0^A \psi_0^B | \tilde{A}' | \psi_0^A \psi_0^B \rangle \langle \psi_0^A \psi_0^B | V^{AB} | \psi_0^A \psi_0^B \rangle - \langle \psi_0^A \psi_0^B | V^{AB} \tilde{A}' | \psi_0^A \psi_0^B \rangle}{1 - \langle \psi_0^A \psi_0^B | \tilde{A}' | \psi_0^A \psi_0^B \rangle}. \quad (29)$$

By rewriting quantum averages involved in Eq. (29) as one-time stochastic averages with respect to the approximate diffusion process constructed from $\psi_0^A \psi_0^B$ [admitting $(\psi_0^A \psi_0^B)^2$ as stationary density, see details of Sec. II C], $\Delta E_{\text{exch}}^{(1)}$ takes the final following form suitable for Monte Carlo simulation:

$$\Delta E_{\text{exch}}^{(1)} = \frac{\langle \tilde{A}' \rangle_{\psi_0^A \psi_0^B} \langle V^{AB} \rangle_{\psi_0^A \psi_0^B} - \langle V^{AB} \tilde{A}' \rangle_{\psi_0^A \psi_0^B}}{1 - \langle \tilde{A}' \rangle_{\psi_0^A \psi_0^B}}. \quad (30)$$

C. The calculation of stochastic averages

In this section the problem of computing stochastic averages introduced in the preceding sections [more precisely, k th-order correlation functions involved in Eq. (12) and one-time averages of Eq. (30)] is addressed. Let us first focus our attention on the computation of k th-order correlation functions as defined in Eq. (13). In principle, the computation of such quantities may be easily performed by merely averaging successive values of the product $V^{AB}(\mathbf{X}(0)) \cdots V^{AB}(\mathbf{X}(u_{k-1}))$ along any stochastic trajectory of the underlying diffusion process constructed from the reference unperturbed Hamiltonian $H^A + H^B$,¹⁷ that is

$$\tilde{A} = \left[\frac{A_{N_\alpha} A_{N_\beta} \phi^{AB}}{\psi_0^A \psi_0^B} \right]^2. \quad (27b)$$

In Eq. (27a) $A_{N/2}^M$ stands for the intramonomer antisymmetrizer acting on space coordinates of the $N/2$ electrons of system M with the same spin. It should be emphasized that in contrast with expression (27a) in which the total Jastrow factor is invariant under the action of $A_{N/2}^M A_{N/2}^M$ and then can be factorized out, the Jastrow factor involved in ϕ^{AB} [Eq. (26b)] is not invariant under $A_{N_\alpha} A_{N_\beta}$ (because of exchanges between electrons of same spin of systems A and B) and then cannot be factorized out when this operator is applied to ϕ^{AB} .

Now, by using the decomposition

$$\tilde{A} = 1 - \tilde{A}', \quad (28)$$

the total first-order energy given by Eq. (23) may be expressed as a sum of two contributions corresponding to some approximate Rayleigh-Schrödinger first-order interaction energy and to the approximate first-order exchange interaction energy resulting from \tilde{A}' in which we are interested here:

$$\begin{aligned} & \langle V^{AB}(\mathbf{X}(0)) \cdots V^{AB}(\mathbf{X}(u_{k-1})) \rangle_{\phi_0^A \phi_0^B} \\ & = \lim_{T \rightarrow +\infty} \frac{1}{T} \int_0^T V^{AB}(\mathbf{X}(\tau)) \cdots V^{AB}(\mathbf{X}(u_{k-1} + \tau)) d\tau, \end{aligned} \quad (31)$$

where the infinite length stochastic trajectory $\mathbf{X}(s)$ is generated by using the Langevin equation associated with the underlying diffusion process, namely,

$$d\mathbf{X}(t) = \mathbf{b}(\mathbf{X}(t)) dt + d\mathbf{W}(t), \quad (32)$$

where \mathbf{W} represents the multidimensional Wiener process and \mathbf{b} , the drift vector, depends only on the ground-state wave function of the unperturbed Hamiltonian $\phi_0^A \phi_0^B$ as follows:¹⁷

$$\mathbf{b} = \nabla \phi_0^A \phi_0^B / \phi_0^A \phi_0^B. \quad (33)$$

In practice, such a scheme is impossible to perform since the ground-state wave function of monomer M ($M = A, B$) is generally unknown. To escape this difficulty we introduce a new diffusion process defined from a *known* trial wave function ψ_0^M ($M = A, B$) for each monomer. For that purpose, let us construct a new reference Hamiltonian $H^{(0)M}$ admitting ψ_0^M as ground-state wave function. This may be trivially done as follows:

$$H^{(0)M} = -\frac{1}{2}\Delta + V^{(0)M} \quad (34a)$$

with

$$V^{(0)M} = \frac{1}{2}\Delta\psi_0^M/\psi_0^M + E_0^{(0)M}, \quad M = A, B \quad (34b)$$

where Δ denotes the $3N_M$ -dimensional Laplacian operator, N_M being the number of electrons of monomer M , and $E_0^{(0)M}$ some arbitrary reference energy associated with $H^{(0)M}$. It is elementary to verify that

$$H^{(0)M}\psi_0^M = E_0^{(0)M}\psi_0^M, \quad M = A, B. \quad (35)$$

The complete Hamiltonian H^M of monomer M ($M = A, B$) may now be written in the form

$$H^M = H^{(0)M} + H^M\psi_0^M/\psi_0^M - E_0^{(0)M}, \quad M = A, B. \quad (36)$$

The basic quantity $H^M\psi_0^M/\psi_0^M$ is referred to in the follow-

ing as the intramonomer local energy E_L^M associated with ψ_0^M :

$$E_L^M = H^M\psi_0^M/\psi_0^M, \quad M = A, B. \quad (37)$$

Roughly speaking, the magnitude of this quantity (actually, a function of all particle coordinates) is a measure of how much the unknown exact wave function ϕ_0^M and the used trial wave function ψ_0^M are different. Note that when the trial wave function is chosen to be identical with ϕ_0^M , the intramonomer local energy reduces to a constant (namely, the exact energy E_0^M) and one obtains $H^M = H^{(0)M}$. Now, by constructing the reference diffusion process from the trial wave function $\psi_0^A\psi_0^B$ and by making use of the GFK formula as explained in Ref. 17, the previously defined stochastic averages can be expressed as stochastic averages with respect to this new diffusion process. Let us write the quantity in which we are interested here, namely, the k -time autocorrelation function of the intermolecular interaction operator

$$\langle V^{AB}(\mathbf{X}(0)) \cdots V^{AB}(\mathbf{X}(u_{k-1})) \rangle_{\phi_0^A\phi_0^B}$$

$$= \lim_{t \rightarrow +\infty} \frac{\left\langle V^{AB}(\mathbf{X}(0)) \cdots V^{AB}(\mathbf{X}(u_{k-1})) \exp \left[-\int_{-t/2}^{t/2} (E_L^A + E_L^B - E_0^{(0)A} - E_0^{(0)B})(\mathbf{X}(s)) ds \right] \right\rangle_{\psi_0^A\psi_0^B}}{\left\langle \exp \left[-\int_{-t/2}^{t/2} (E_L^A + E_L^B - E_0^{(0)A} - E_0^{(0)B})(\mathbf{X}(s)) ds \right] \right\rangle_{\psi_0^A\psi_0^B}}, \quad (38)$$

with $-t/2 < 0 \leq u_1 \leq \cdots \leq u_{k-1} < t/2$.

The main steps of our approach for practical computations of $\Delta E_{RS}^{(n)}$ may be then summarized as follows.

(1) Use formula (12) to express $\Delta E_{RS}^{(n)}$ in terms of a suitable combination of time-correlation functions with respect to the diffusion process constructed from $\phi_0^A\phi_0^B$.

(2) Resort to formula (38) to express stochastic averages defined over the diffusion process built from the generally unknown ground-state wave function $\phi_0^A\phi_0^B$ in terms of stochastic averages defined over the diffusion process built from the chosen trial wave function $\psi_0^A\psi_0^B$.

(3) Calculate stochastic averages involved in the right-hand side of Eq. (38) by resorting to the ergodic formula (31) (merely add the Feynman-Kac exponential weight), the stochastic trajectory being generated using a discretized version of the Langevin equation (32) in which the drift vector is constructed from $\psi_0^A\psi_0^B$. In actual fact, it is appropriate to introduce, instead of a single very long trajectory, a set of shorter trajectories since the corresponding set of time averages may be used for evaluating the variance using standard statistical methods.²⁷

As concerns the computation of the first-order exchange interaction energy, it is readily done by taking one-time averages of the integrand involved in formula (30) along stochastic trajectories of the diffusion process constructed from the trial wave function $\psi_0^A\psi_0^B$.

D. Fermi statistics for monomers

Up to now, we did not pay attention to the problem of imposing fermion statistics for each monomer. In the preceding sections, formulas have been derived by implicitly assuming that a fixed-node approach for monomers was employed. Indeed, the trial wave function $\psi_0^A\psi_0^B$ was supposed to obey the correct antisymmetry properties with respect to internal exchange of electrons within each monomer (no intermonomer exchanges of electrons). In practice, such a condition may be fulfilled by antisymmetrizing independently electrons of spin up and down for each monomer (see Ref. 17 and references therein). When computing first-order observables (that is, mere one-time averages of local operators with respect to the trial wave function, the total energy for example), it is well known that such an approach generally introduces a bias in results due to an eventual error in the fixed location of the nodes of the trial wave function. The resulting approximation, known as the fixed-node approximation, has been extensively described in many works.^{14,16,17} Here, it is important to realize that we are in somewhat different situation. In contrast with the usual case where only a very good approximation of the unknown ground-state wave function is needed, the computation of the k -time correlation functions implicitly requires the *com-*

plete set of eigenfunctions of the reference Hamiltonian constructed from the trial wave function [Hamiltonian defined by Eq. (34)]. To be more precise, let us write which transition probability density is introduced when a fixed-node framework for each monomer is used:

$$p(\mathbf{x} \rightarrow \mathbf{y}, \tau) = \frac{\phi_0^{\text{FN}}(\mathbf{y})}{\phi_0^{\text{FN}}(\mathbf{x})} \sum_i \phi_i^{\text{FN}}(\mathbf{x}) \phi_i^{\text{FN}}(\mathbf{y}) e^{-\tau(E_i^{\text{FN}} - E_0^{\text{FN}})} \quad (39)$$

where $(\phi_i^{\text{FN}}, E_i^{\text{FN}})$ denote the fixed-node eigensolutions of the reference Hamiltonian (34). These eigensolutions are those obtained by imposing *all* eigenfunctions of $H^{(0)M}$ to vanish wherever the ground-state wave function $\phi_0^{\text{FN}} = \psi_0^M$ vanishes. In particular, excited states obtained in that way may be very different from the correct ones which actually have no reason to vanish at the same locations as ϕ_0^{FN} . Accordingly, a *wrong* dynamics for the underlying

diffusion process is introduced and an *a priori* uncontrolled error for correlation functions is made. It is quite important to stress that such an error *does* exist, even if *exact* nodes for the trial wave function would be used. As a consequence, it is never *a priori* justified to use a fixed-node framework for computing multiple-time correlation functions.²⁸ To escape this difficulty, projection methods or some form of them^{15,17,29,30} (simple projection method, release-node projection, or nodal relaxation methods) must be used. This type of approach has already been described elsewhere.^{17,29} In a few words, the essence of these methods consists in using a bosonic-type nonvanishing wave function as trial wave function and to remove bosonic components by making use of projection functions having correct fermionic antisymmetry properties. Let us denote as f and g two such projection functions; the exact nonbiased autocorrelation function of V^{AB} is then written

$$\begin{aligned} & \langle V^{AB}(\mathbf{X}(0)) \cdots V^{AB}(\mathbf{X}(u_{k-1})) \rangle_{\psi_0^A \psi_0^B} \\ &= \lim_{t \rightarrow +\infty} \frac{\langle f(\mathbf{X}(-t/2)) V^{AB}(\mathbf{X}(0)) \cdots V^{AB}(\mathbf{X}(u_{k-1})) g(\mathbf{X}(t/2)) \exp - \int_{-t/2}^{t/2} (E_L^A + E_L^B - E_0^{(0)A} - E_0^{(0)B})(\mathbf{X}(s)) ds \rangle_{\psi_0^A \psi_0^B}}{\langle f(\mathbf{X}(-t/2)) g(\mathbf{X}(t/2)) \exp - \int_{-t/2}^{t/2} (E_L^A + E_L^B - E_0^{(0)A} - E_0^{(0)B})(\mathbf{X}(s)) ds \rangle_{\psi_0^A \psi_0^B}} \quad (40) \end{aligned}$$

where $\psi_0^A \psi_0^B$ is a bosonic (nonvanishing) trial wave function. From a practical point of view, it is important to recall that Monte Carlo procedures based on projection methods are much less stable than those based on a fixed-node approach. We shall return to this point in our final discussion of the concluding section.

III. NUMERICAL APPLICATIONS

In order to demonstrate the applicability of formulas derived in the preceding sections, some test calculations for the interaction of two helium atoms at small distances have been performed. Results have been systematically compared to those obtained by using standard *ab initio* techniques. In what follows, two different trial wave functions for the helium atom are employed. The first trial wave function is the Hartree-Fock wave function proposed by Clementi and Roetti,³¹

$$\psi_0^M(\mathbf{r}_1, \mathbf{r}_2) = 1s_M(r_1)1s_M(r_2), \quad M = A, B \quad (41)$$

where the optimized $1s_M$ orbital (centered at nucleus M) is built as a linear combination of five Slater orbitals, namely,

$$1s_M(r) = \sum_{i=1}^5 c_i e^{-\lambda_i r}, \quad M = A, B. \quad (42)$$

Coefficients and exponents may be found in the tables of Clementi and Roetti.³¹ Our second trial wave function is a more sophisticated wave function which explicitly contains the interelectron coordinate r_{12} to properly describe the electron-electron interaction at small distances. It is

written in the form

$$\begin{aligned} \psi_0^{(M)}(\mathbf{r}_1, \mathbf{r}_2) &= \exp \left[\frac{0.5r_{12}}{1+ar_{12}} \right] \exp \left[- \left[\frac{2+br_1^M}{1+b_1^M} \right] r_1^M \right] \\ &\times \exp \left[- \left[\frac{2+br_2^M}{1+br_2^M} \right] r_2^M \right], \quad M = A, B \quad (43) \end{aligned}$$

where r_i^M denotes the distance between electron i ($i=1,2$) and nucleus M ($M=A,B$). By employing this form, it should be remarked that all two-particle cusp conditions are fulfilled, namely $(1/\psi)(\partial\psi/\partial r_{12})|_{r_{12}=0} = \frac{1}{2}$ (electron-electron cusp condition for unlike spins) and $(1/\psi)(\partial\psi/\partial r_i)|_{r_i=0} = -Z$ (electron-nucleus cusp condition for an infinite mass nucleus of charge number Z). In addition, a Padé form for both correlated and Slater parts of the trial wave function has been chosen. Parameters involved in Eq. (43) have been adjusted in an exact QMC calculation of total energy of the He atom so as to achieve the lowest variance on the estimator of the ground-state energy. Some features of both trial wave functions are presented in Table I. In the following, electrons labeled 1 and 2 (respectively, 3 and 4) are arbitrarily assigned to atom A (respectively atom B). Using this convention, the intermolecular interaction operator V^{AB} is written

$$\begin{aligned} V^{AB}(\mathbf{r}_1, \mathbf{r}_2, \mathbf{r}_3, \mathbf{r}_4) &= \frac{4}{r_{AB}} - \frac{2}{r_{1B}} - \frac{2}{r_{2B}} - \frac{2}{r_{3A}} - \frac{2}{r_{4A}} \\ &+ \frac{1}{r_{13}} + \frac{1}{r_{14}} + \frac{1}{r_{23}} + \frac{1}{r_{24}}. \quad (44) \end{aligned}$$

TABLE I. Some features of trial wave functions used.^a

Properties	Hartree-Fock wave function ^b	Correlated wave function ^c
E_0	-2.861 68	-2.8983(1)
Correlation energy ^d	0%	87%
$\langle r_{12} \rangle$	1.362(1)	1.4247(6)

^aAll quantities are given in atomic units. Statistical uncertainties on QMC results are indicated in parentheses.

^bEquations (41) and (42), see Ref. 31.

^cEquation (43) with $a=0.3$ and $b=0.1$.

^dDefined as the difference between the exact nonrelativistic and Hartree-Fock total energies.

A. First-order interaction energy

Let us first present some approximate calculations of first-order Rayleigh-Schrödinger and exchange interaction energies. For that we shall set the intramonomer local energies [Eq. (37)] to zero. Such an approximation consists in neglecting internal fluctuations due to the nonexactness of the trial wave function $\psi_0^A \psi_0^B$ used. As already pointed out, this approximation is similar to the approximation made when doing variational quantum Monte Carlo simulations for calculating total energies, except that no variational property holds here for such variational components. Rewriting Eq. (15) by replacing the exact ground-state wave function by the approximate trial wave function, and Eq. (30), the following expressions for $\Delta E_{\text{RS}}^{(1)}$ and $\Delta E_{\text{exch}}^{(1)}$ are obtained:

$$\Delta E_{\text{RS}}^{(1)} = \langle V^{AB} \rangle_{\psi_0^A \psi_0^B}, \quad (45a)$$

$$\Delta E_{\text{exch}}^{(1)} = \frac{\langle \tilde{A}' \rangle_{\psi_0^A \psi_0^B} \langle V^{AB} \rangle_{\psi_0^A \psi_0^B} - \langle V^{AB} \tilde{A}' \rangle_{\psi_0^A \psi_0^B}}{1 - \langle \tilde{A}' \rangle_{\psi_0^A \psi_0^B}}. \quad (45b)$$

Expectation values involved in Eqs. (45) may be evaluated as one-time averages with respect to the diffusion process constructed from $\psi_0^A \psi_0^B$. It should be remarked that they are simply six-dimensional integrals and therefore it would be possible here to resort to any efficient integration procedure to calculate them. However, let us emphasize that such procedures would no longer be useful when considering calculation of exact quantities (such as the exact first- and second-order RS interaction energies). A practical difficulty encountered when using a finite time step for integrating the Langevin equation (32) is the occurrence of the well-known short-time approximation.^{14,16,17,32} Indeed, the transition probability density used to generate stochastic trajectories (corresponding to a discretized form of the Langevin equation) is only an approximate version of the exact one, for example, in the simple Gaussian approximation,

$$p(\mathbf{x} \rightarrow \mathbf{y}, \Delta t) = \frac{1}{(2\pi\Delta t)^{1/2}} \exp \left[-\frac{[\mathbf{y} - \mathbf{x} - \mathbf{b}(\mathbf{x})\Delta t]^2}{2\Delta t} \right], \quad (46)$$

TABLE II. Hartree-Fock first-order RS interaction energy.^a

R^b	$\Delta E_{\text{RS}}^{(1)}$ (QMC) ^c	$\Delta E_{\text{RS}}^{(1)}$ (<i>ab initio</i>) ^d	$\Delta E_{\text{RS}}^{(1)}$ (exact) ^e
1.5	-0.0805(4)	-0.0807	-0.0806
1.6	-0.0686(4)	-0.0688	-0.0686
1.7	-0.0575(5)	-0.0577	-0.0575
1.8	-0.0477(4)	-0.0478	-0.0476
1.9	-0.0390(3)	-0.0392	-0.0391
2.0	-0.0318(2)	-0.0319	-0.0318

^aAll quantities are given in atomic units.

^bInteratomic separation.

^cUsing Eq. (45a). Statistical uncertainties are indicated in parentheses.

^d*Ab initio* calculation using ten Gaussian functions for representing 1s orbital (42).

^eExact analytical evaluation of Eq. (45a).

and therefore calculated stationary averages are subject to a finite time-step error. One possible way of removing this error consists in imposing the detailed balance condition in the Monte Carlo simulation. Doing that, a non-biased stationary density is constructed. In practice, detailed balancing is ensured by accepting moves from \mathbf{x} to \mathbf{y} with a probability P_{accept} given by³³

$$P_{\text{accept}} = \min \left[1, \frac{(\psi_0^A \psi_0^B)^2(\mathbf{y})p(\mathbf{y} \rightarrow \mathbf{x}, \Delta t)}{(\psi_0^A \psi_0^B)^2(\mathbf{x})p(\mathbf{x} \rightarrow \mathbf{y}, \Delta t)} \right], \quad (47)$$

where $p(\mathbf{x} \rightarrow \mathbf{y}, \Delta t)$ is the short-time Gaussian approximation (46) of the exact unknown transition probability density. This procedure may be viewed as a generalized version of the well-known Metropolis algorithm in which the usual initial random displacement is replaced by a Langevin move generated through Eq. (46).

Tables II and III present Hartree-Fock calculations performed by using form (41) of the trial wave function. Quantum Monte Carlo results for $\Delta E_{\text{RS}}^{(1)}$ and $\Delta E_{\text{exch}}^{(1)}$ (second column of Tables II and III, respectively) are compared to *ab initio* calculations performed with a large Gaussian basis set (ten Gaussian functions for represent-

TABLE III. Hartree-Fock first-order exchange interaction energy.^a

R^b	$\Delta E_{\text{exch}}^{(1)}$ (QMC) ^c	$\Delta E_{\text{exch}}^{(1)}$ (<i>ab initio</i>) ^d
1.5	0.508(11)	0.513
1.6	0.412(6)	0.415
1.7	0.334(8)	0.335
1.8	0.268(4)	0.270
1.9	0.215(4)	0.218
2.0	0.172(5)	0.175

^aAll quantities are given in atomic units.

^bInteratomic separation.

^cUsing Eq. (45b). Statistical uncertainties are indicated in parentheses.

^d*Ab initio* calculation using ten Gaussian functions for representing 1s orbital (42).

TABLE IV. First-order RS interaction energy using different wave functions.^a

R^b	HF wave function ^c	Correlated wave function ^d	Exact wave function ^e
1.5	-0.0805(4)	-0.0818(4)	-0.080(4)
1.6	-0.0686(4)	-0.0693(4)	-0.068(3)
1.7	-0.0575(5)	-0.0578(3)	-0.057(3)
1.8	-0.0477(4)	-0.0476(2)	-0.048(3)
1.9	-0.0390(3)	-0.0388(2)	-0.039(2)
2.0	-0.0318(2)	-0.0314(2)	-0.032(2)

^aAll quantities are given in atomic units. Statistical uncertainties are indicated in parentheses.

^bInteratomic separation.

^cEquations (41) and (42), see Ref. 31.

^dEquation (43) with $a=0.3$ and $b=0.1$.

^eEquation (48).

ing 1s orbital taken from the van Duijneveldt tables³⁴. Gaussian basis-set calculations are presented in the third columns of Tables II and III. In addition, exact results for $\Delta E_{\text{RS}}^{(1)}$ obtained by performing space integrals involved in Eq. (45a) are given (last column of Table II). Of course, such exact integrations are possible only because the Hartree-Fock wave function (41) has a very simple structure. Agreement between exact and/or *ab initio* results and QMC results is excellent (within statistical errors). Calculations of first-order RS and exchange interaction energies with the explicitly correlated wave function (43) are displayed in Tables IV and V, respectively. It is seen that using a highly correlated wave function for describing each monomer does not change significantly the Hartree-Fock results obtained for $\Delta E_{\text{RS}}^{(1)}$,

TABLE V. First-order exchange interaction energy using different wave functions.^a

R^b	HF wave function ^c	Correlated wave function ^d
1.5	0.508(11)	0.566(12)
1.6	0.412(6)	0.450(10)
1.7	0.334(8)	0.358(10)
1.8	0.268(4)	0.284(9)
1.9	0.215(5)	0.226(8)
2.0	0.172(5)	0.178(7)

^aAll quantities are given in atomic units. Statistical uncertainties are indicated in parenthesis.

^bInteratomic separation.

^cEquations (41) and (42), see Ref. 31.

^dEquation (43) with $a=0.3$ and $b=0.1$.

at least for the small distances studied. Such a conclusion will be confirmed below from exact calculations of $\Delta E_{\text{RS}}^{(1)}$. In contrast, $\Delta E_{\text{exch}}^{(1)}$ appears to be slightly more sensitive to intra-atomic correlation. For all distances, the effect of correlation seems to be to increase Hartree-Fock results. It should be noted that a similar conclusion has been obtained within the framework of *ab initio* calculations using CI wave functions,^{35,36} for larger distances (R ranging from 3.0 to 7.0 a.u.).

Let us now present some exact calculations of the first-order RS interaction energy. The basic expression for practical calculation of $\Delta E_{\text{RS}}^{(1)}$ is obtained by rewriting expression (15) in terms of stochastic averages with respect to the diffusion process built from $\psi_0^A \psi_0^B$ [Eq. (38)] and by resorting to the property of ergodicity of the diffusion process [Eq. (31)]. One gets

$$\Delta E_{\text{RS}}^{(1)} = \lim_{t \rightarrow +\infty} \lim_{T \rightarrow +\infty} \frac{\frac{1}{T} \int_0^T V^{AB}(\mathbf{X}(\tau)) \exp \left[- \int_{-t/2+\tau}^{t/2+\tau} (E_L^A + E_L^B - E_0^{(0)A} - E_0^{(0)B})(\mathbf{X}(s)) ds \right] d\tau}{\frac{1}{T} \int_0^T \exp \left[- \int_{-t/2+\tau}^{t/2+\tau} (E_L^A + E_L^B - E_0^{(0)A} - E_0^{(0)B})(\mathbf{X}(s)) ds \right] d\tau}, \quad (48)$$

where $\mathbf{X}(s)$ is an arbitrary stochastic trajectory of the diffusion process built from $\psi_0^A \psi_0^B$. In contrast with preceding approximate evaluations of $\Delta E_{\text{RS}}^{(1)}$ which were based only on the use of the stationary density, formula (48) also makes use of the dynamical properties of the diffusion process. Accordingly, exact calculations of $\Delta E_{\text{RS}}^{(1)}$ [using Eq. (48)] are subject to the short-time error resulting from the nonexact form of the transition probability density used. The usual way of handling this problem is to repeat calculations for different values of the time step Δt and then to extrapolate results to zero time step by using a more or less sophisticated extrapolation procedure (see, e.g., Refs. 14, 17, and 32). Exact calculations of $\Delta E_{\text{RS}}^{(1)}$ displayed in the last column of Table IV have been obtained with $\Delta t=0.01$ a.u. For such a time step, the short-time error turned out to be smaller than statistical fluctuations. Accordingly, results of Table IV may be essentially considered as exact within the statisti-

cal noise. It is seen by comparing the second and last columns of Table IV that for distances ranging from $R=1.5$ to 2.0 a.u., no differences appear between Hartree-Fock and exact results (up to statistical fluctuations). It is therefore concluded that intra-atomic correlation contribution to $\Delta E_{\text{RS}}^{(1)}$ is certainly negligible at these small distances.

B. Second-order Rayleigh-Schrödinger interaction energy

Calculation of the second-order RS interaction energy is based on Eq. (18):

$$\Delta E_{\text{RS}}^{(2)} = - \int_0^{+\infty} C^c(u) du, \quad (49)$$

where $C^c(u)$ is the connected two-time autocorrelation function of V^{AB} with respect to the diffusion process constructed from $\phi_0^A \phi_0^B$, namely,

$$C^c(u) = \langle \overline{V^{AB}}(\mathbf{X}(0)) \overline{V^{AB}}(\mathbf{X}(u)) \rangle_{\phi_0^A \phi_0^B}, \quad (50)$$

$$C^c(u) = \lim_{t \rightarrow +\infty} \lim_{T \rightarrow +\infty} \frac{\frac{1}{T} \int_0^T \overline{V^{AB}}(\mathbf{X}(\tau)) \overline{V^{AB}}(\mathbf{X}(\tau+u)) \exp \left[- \int_{-t/2+\tau}^{t/2+\tau} (E_L^A + E_L^B - E_0^{(0)A} - E_0^{(0)B})(\mathbf{X}(s)) ds \right] d\tau}{\frac{1}{T} \int_0^T \exp \left[- \int_{-t/2+\tau}^{t/2+\tau} (E_L^A + E_L^B - E_0^{(0)A} - E_0^{(0)B})(\mathbf{X}(s)) ds \right] d\tau}, \quad (51)$$

and the numerical evaluation of this expression is performed as usual. On the other hand, by using the basic definition of stochastic averages in terms of probability densities [Eq. (13)] and by resorting to expressions (14) for these densities, the following form for $C^c(u)$ is obtained:

$$C^c(u) = \sum_{i,j} |\langle \phi_0^A \phi_0^B | (V^{AB} - \langle V^{AB} \rangle) | \phi_i^A \phi_j^B \rangle|^2 \times e^{-u(E_i^A + E_j^B - E_0^A - E_0^B)}. \quad (52)$$

Accordingly, it is seen that $C^c(u)$ is written as an infinite sum of real exponentials with true excitation energies of the noninteracting systems as exponents, and squared centered transition moments of V^{AB} as amplitudes. Due to this form, it is natural to fit the calculated function C^c by a function expressed as a sum of a finite number of real exponentials, namely,

$$C^c(u) = \sum_{i=1}^N c_i e^{-\lambda_i u}. \quad (53)$$

At the distance studied ($R=2$ a.u.), this fit was performed from a set of 50 calculated values of C^c uniformly distributed in the time interval (0,2). The method used to perform the fit is a recently proposed method based on a Padé analysis of the Laplace transform (or eventually other integral transforms) of the function to analyze. This method is presented in detail elsewhere (see Ref. 37). We found out that a three-real-exponentials description was sufficient to correctly describe our data. The following amplitudes and exponents have been obtained:

$$\begin{aligned} c_1 &= 0.03377, & \lambda_1 &= 1.7539, \\ c_2 &= 0.08087, & \lambda_2 &= 5.4948, \\ c_3 &= 0.06304, & \lambda_3 &= 19.025. \end{aligned}$$

Having an analytical expression of the autocorrelation function, $\Delta E_{RS}^{(2)}$ is readily obtained from Eqs. (49) and (53); one obtains

$$\Delta E_{RS}^{(2)} = - \sum_{i=1}^N \frac{c_i}{\lambda_i}. \quad (54)$$

where $\overline{V^{AB}} \equiv V^{AB} - \langle V^{AB} \rangle_{\phi_0^A \phi_0^B}$. By expressing the stochastic average in terms of stochastic averages with respect to the diffusion process constructed from $\psi_0^A \psi_0^B$ [Eq. (38)] and by making use of the ergodic property (31), the following expression suitable for computational purposes is obtained:

The autocorrelation function obtained for the intratomic distance $R=2$ a.u. is presented in Fig. 1. Note that the statistical fluctuations for all data are rather small, except at the initial time value $u=0$. This feature is explained as follows. From expression (52) of $C^c(u)$, it is seen that $C^c(0)$ is nothing but the average of the squared centered potential $C^c(0) = \langle \phi_0^A \phi_0^B | (V^{AB})^2 | \phi_0^A \phi_0^B \rangle$. When a particle of A (respectively, B) is close to a particle of B (respectively, A), this latter quantity is essentially given by $\langle 1/r^2 \rangle$, where r is the interparticle distance. This average has a well-defined value but an infinite variance. Special techniques for handling this difficulty could be used (such as the introduction of a cutoff as made in Ref. 38). However, it should be noted that this difficulty occurs only for $u=0$. Accordingly, in order not to bias our analysis, we decided to remove the initial point from the set of data used to perform the fit. However, it should be noted that the initial value was correctly recovered by the fit function (53). The result obtained for $\Delta E_{RS}^{(2)}$ at $R=2$ is presented in Table VI and is compared with an *ab initio* SCF perturbational calculation of the same quantity (method presented

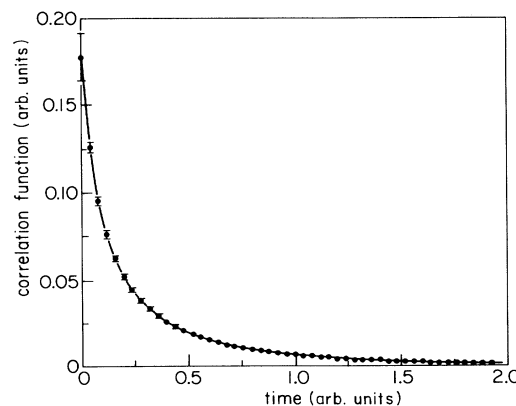


FIG. 1. The autocorrelation function of the intermolecular potential computed by Monte Carlo simulation vs the time u [Eq. (50)].

TABLE VI. Second-order RS interaction energy.^a

R^b	$\Delta E_{\text{RS}}^{(2)}$ (QMC) ^c	$\Delta E_{\text{RS}}^{(2)}$ (SCF) ^d
2	-0.0375(11)	-0.030

^aAll quantities are given in atomic units.

^bInteratomic separation.

^cEquations (49) and (51). Statistical uncertainties are indicated in parentheses.

^d*Ab initio* SCF calculation, see text.

in Refs. 11 and 22). The numerical calculation was carried out by using an $(8s, 3p, 2d)$ Gaussian basis set. The major conclusion resulting from comparison between exact and Hartree-Fock calculations of $\Delta E_{\text{RS}}^{(2)}$ is that intratomic correlation contribution to $\Delta E_{\text{RS}}^{(2)}$ is important. At the distance studied ($R = 2$ a.u.), it accounts for more than 20% of the exact value. It is therefore essential to take account of such a contribution in any accurate calculation of interaction energies.

IV. DISCUSSION

Let us summarize what has been done in the present work. First, a very compact expression for the n th-order Rayleigh-Schrödinger perturbational energy has been derived within the framework of diffusion processes [Eq. (12)]. This formula expresses the n th-order component of the energy as an $(n-1)$ -time integral of a connected correlation function of the perturbing operator. It should be stressed that it is a very general formula which can be used in any problem for which a perturbational approach is desired. However, in the present work we focused our attention on a specific application: the calculation of perturbational components in intermolecular interactions. In order to be able to compute the main part of the exchange interaction energy (a contribution resulting from the change of antisymmetry properties between the monomer and the interacting dimer), a high-quality approximate expression for this quantity (defined beyond the commonly used Hartree-Fock approximation) has been derived. In order to demonstrate the feasibility of our new approach we have carried out some test calculations for the interaction of two helium atoms at small distances. For this small system comparisons with more standard calculations using *ab initio* techniques are very satisfactory. Potential advantages of this new approach with respect to commonly employed *ab initio* methods may be summarized as follows.

(1) No basis-set expansions are used. Accordingly, well-known difficulties associated with basis-set calculations are avoided.

(2) Infinite summations appearing in the usual Bloch-Brücker formulation of perturbational components are not performed. Consequently, good representations of the infinite (continuous) set of excited wave functions and calculations of transition matrix elements of the perturbing operator between all intermediate states are not needed. Actually, the resolvent of the unperturbed Hamiltonian (responsible for the occurrence of infinite sets of inter-

mediate wave functions in the usual formalism) is implicitly taken into account through the transition probability density [see Eq. (14b)] of the underlying diffusion process. In practice, the transition probability density may be easily simulated [from Langevin equation (32)] only by using an approximate expression of the ground-state wave function of the unperturbed Hamiltonian.

(3) Quantities difficult to evaluate within *ab initio* frameworks, such as intramonomer correlation contributions or high-order perturbational terms (third order, for example) are in principle easy to evaluate.

However, a number of potential difficulties may also exist.

(1) When applying formula (12) to systems involving fermions, it has been seen that the fixed-node procedure must be avoided, whatever the quality of the nodes of the trial wave function used. By making use of a projection approach, this problem may be in principle solved. However, it is known that such approaches are in general quite unstable numerically due to the sign problem. Only realistic calculations on bigger systems will permit one to give a precise answer about the feasibility of such a proposal. However, let us once more emphasize that this problem disappears when bosonic-type systems (or more generally when no change of symmetry between the unperturbed and total Hamiltonian occurs) are treated.

(2) It is not clear at this stage what the dependency is of statistical fluctuations on the order of the perturbational component considered. Here also the importance of such a difficulty could be very dependent on the system treated and on the quality of the trial wave function used.

The next step of this work will be to make calculations for interaction of bigger systems [such as $(\text{LiH})_2$, Be_2 , or $(\text{H}_2\text{O})_2$, for example]. Expected practical limitations of the method result essentially from present limitations of QMC methods for treating monomers. Indeed, it is known that a serious increase of statistical fluctuations with the number of electrons treated is observed for atomic and molecular systems (see, e.g., discussion in Ref. 39). In the present method, this means that an increase of statistical fluctuations on intramonomer local energies must be expected when treating systems of increasing size. In practice, calculating interaction of systems having up to ten electrons should be considered as a reasonable limit at the present time. However, it is clear that any future improvement in the efficiency of quantum Monte Carlo methods for treating electronic structure would directly improve the practical possibilities of the present method.

ACKNOWLEDGMENTS

We would like to acknowledge many helpful discussions with Professor D. M. Ceperley and Professor A. van der Avoird. One of us (M.C.) is grateful to the NCSA and the Department of Physics at Urbana-Champaign for their kind hospitality. We thank the "Conseil Scientifique du Centre de Calcul Vectoriel

pour la Recherche" for providing us with computer facilities on its Cray 2, the Groupement Scientifique "Modélisation Moléculaire" IBM-Centre National de la Recherche Scientifique for facilities on IBM 3090/600E and the "Center Inter Régional de Calcul Electronique"

(CIRCE) for generous technical support. This work was partly supported by the Ministère de l'Education Nationale of France (Grants No. P6.86016) and No. NSF-DMR-8808126.

- ¹See, e.g., K. Morokuma and K. Kitaura, in *Molecular Interactions*, edited by H. Ratajczak and W. J. Orville-Thomas (Wiley, New York, 1980), Vol. 1.
- ²N. R. Kestner, *J. Chem. Phys.* **48**, 252 (1968).
- ³F. S. Boys and D. Bernardi, *Mol. Phys.* **19**, 553 (1970).
- ⁴A. Pullman, H. Berthold, and N. Gresh, *Int. J. Quantum Chem. Symp.* **10**, 56 (1976).
- ⁵W. Kolos, *Theor. Chim. Acta* **51**, 219 (1979).
- ⁶P. Claverie, *Int. J. Quantum Chem.* **5**, 273 (1971).
- ⁷B. Jeziorski and W. Kolos, in *Molecular Interactions*, edited by H. Ratajczak and W. J. Orville-Thomas (Wiley, New York, 1982), Vol. 3.
- ⁸I. G. Kaplan, in *Theory of Molecular Interactions*, Studies in Physical and Theoretical Chemistry (Elsevier, Amsterdam, 1986), Vol. 42.
- ⁹K. Szalewicz and B. Jeziorski, *Mol. Phys.* **38**, 191 (1979).
- ¹⁰B. Jeziorski, R. Moszynski, S. Rybak, and K. Szalewicz, *Lect. Notes Chem.* **52**, 65 (1989).
- ¹¹B. Jeziorski and M. van Hemert, *Mol. Phys.* **32**, 713 (1976).
- ¹²J. B. Anderson, *J. Chem. Phys.* **63**, 1499 (1975).
- ¹³D. M. Arnou, M. H. Kalos, M. A. Lee, and K. E. Schmidt, *J. Chem. Phys.* **77**, 5562 (1982).
- ¹⁴P. J. Reynolds, D. M. Ceperley, B. J. Alder, and W. A. Lester, Jr., *J. Chem. Phys.* **77**, 5593 (1982).
- ¹⁵D. M. Ceperley and B. J. Alder, *J. Chem. Phys.* **81**, 5833 (1984).
- ¹⁶B. H. Wells, in *Methods in Computational Chemistry*, edited by S. Wilson (Plenum, New York, 1987), Vol. 1.
- ¹⁷M. Caffarel and P. Claverie, *J. Chem. Phys.* **88**, 1088 (1988); **88**, 1100 (1988).
- ¹⁸M. Caffarel, Ph.D. thesis, University of Paris, 1987, Appendix I.
- ¹⁹R. Huby, *Proc. Phys. Soc. London* **78**, 529 (1961).
- ²⁰M. Caffarel and P. Claverie, *J. Stat. Phys.* **43**, 797 (1986).
- ²¹D. M. Ceperley and H. Partridge, *J. Chem. Phys.* **84**, 820 (1986).
- ²²O. Hess, M. Caffarel, C. Huiszoon, and P. Claverie, *J. Chem. Phys.* **92**, 6049 (1990).
- ²³R. Kubo, *J. Phys. Soc. Jpn.* **17**, 1100 (1962).
- ²⁴J. W. Moskowitz and M. H. Kalos, *Int. J. Quantum Chem.* **20**, 1107 (1981).
- ²⁵Z. Sun, P. J. Reynolds, R. K. Owen, and W. A. Lester, Jr., *Theor. Chim. Acta* **75**, 353 (1989).
- ²⁶C. J. Umrigar, K. G. Wilson, and J. W. Wilkins, *Phys. Rev. Lett.* **60**, 1719 (1988); *Computer Simulation Studies in Condensed Matter Physics: Recent Developments* (Springer-Verlag, New York, 1988), pp. 185–194.
- ²⁷H. Cramér, *Mathematical Methods of Statistics* (Princeton University Press, Princeton, 1966), Chap. 8.2.
- ²⁸We are indebted to Professor D. M. Ceperley for having pointed out this difficulty to us.
- ²⁹M. Caffarel, in *Numerical Determination of the Electronic Structure of Atoms, Diatomic and Polyatomic Molecules* (Kluwer Academic, Dordrecht, 1989), pp. 85–105.
- ³⁰M. H. Kalos, in *Monte Carlo Methods in Quantum Problems*, Vol. 125 of *NATO Advanced Study Institute, Series C*, edited by M. H. Kalos (Reidel, Dordrecht, 1984).
- ³¹E. Clementi and C. Roetti, *Atomic Data and Nuclear Data Tables* (Academic, New York, 1974), Vol. 14.
- ³²J. Vrbik and S. M. Rothstein, *J. Comput. Phys.* **63**, 130 (1986).
- ³³E. L. Pollock and D. M. Ceperley, *Phys. Rev. B* **30**, 2555 (1984).
- ³⁴F. B. van Duijneveldt, IBM Technical Report No. RJ 945, 1971 (unpublished).
- ³⁵G. Chalasinski, S. van Smaalen, and F. B. van Duijneveldt, *Mol. Phys.* **45**, 1113 (1982).
- ³⁶G. Chalasinski and M. Gutowski, *Mol. Phys.* **54**, 1173 (1985).
- ³⁷E. Yeramian and P. Claverie, *Nature (London)* **326**, 169 (1987); J. Aubard, P. Levoir, A. Denis, and P. Claverie, *Comput. Chem.* **11**, 163 (1987).
- ³⁸J. Vrbik, D. A. Legare, and S. M. Rothstein, *J. Chem. Phys.* **92**, 1221 (1990).
- ³⁹D. M. Ceperley, *J. Stat. Phys.* **43**, 815 (1986).
- ⁴⁰S. R. White, J. W. Wilkins, and K. G. Wilson, *Phys. Rev. Lett.* **56**, 412 (1986).
- ⁴¹A. Koutselos and U. Mohanty, *Physica A* **166**, 99 (1990).

F. M. Caffarel , F.X. Gadea, and D.M. Ceperley, “Lanczos-type Algorithm for Quantum Monte Carlo Data”, *Europhys. Lett.* 16 249 (1991)

Lanczós-Type Algorithm for Quantum Monte Carlo Data

This article has been downloaded from IOPscience. Please scroll down to see the full text article.

1991 Europhys. Lett. 16 249

(<http://iopscience.iop.org/0295-5075/16/3/005>)

View [the table of contents for this issue](#), or go to the [journal homepage](#) for more

Download details:

IP Address: 86.221.86.45

The article was downloaded on 24/09/2010 at 18:03

Please note that [terms and conditions apply](#).

Lanczós-Type Algorithm for Quantum Monte Carlo Data.

M. CAFFAREL(*)(**), F. X. GADEA(***) and D. M. CEPERLEY(**)

(*) *Laboratoire Dynamique des Interactions Moléculaires, Université Paris VI
75252 Paris Cedex 05, France*

(**) *Department of Physics and NCSA, University of Illinois at Urbana-Champaign
Urbana, IL 61801*

(***) *Laboratoire de Physique Quantique, Université Paul Sabatier
31062 Toulouse Cedex, France*

(received 11 March 1991; accepted 11 July 1991)

PACS. 31.15 – General mathematical and computational developments.

PACS. 31.50 – Molecular solids.

PACS. 05.30F – Fermion systems and electron gas.

Abstract. – A method for accelerating the rate of convergence of the long-time (or small-temperature) limit of quantum Monte Carlo approaches is presented. To do that, a variation of the Lanczós algorithm suitable for QMC data is introduced. This algorithm allows one to extract more information from correlation functions at small times, thus avoiding large statistical fluctuations associated with large times. It is first applied to an exactly soluble system and then to the LiH molecule. Calculations using both the fixed-node and nodal-release approaches are discussed.

Quantum Monte Carlo (QMC) methods have proved to be powerful techniques for solving the Schrödinger equation. They have been applied to a variety of problems [1] such as the study of quantum liquids and solids, the electron gas or the electronic structure of small molecules. In each case, very accurate results for some properties of these systems have been obtained. Although there exists a number of variants of QMC methods, the common idea in the approaches we consider here consists in projecting out the ground-state component of a known trial wave function, Ψ_T , by applying a suitable projection operator to this function ($\exp[-tH]$ in diffusion Monte Carlo (DMC) or $1/(H-E)^n$ in Green's function Monte Carlo (GFMC) methods, H denoting the Hamiltonian operator) and then letting the projecting parameter (t or n) go to infinity. Within the framework of DMC methods used in this work, this projection procedure takes the form

$$\exp[-tH] \Psi_T \rightarrow \Psi_0 + O(\exp[-t\Delta E]), \quad \text{as } t \rightarrow \infty, \quad (1)$$

where Ψ_0 denotes the ground-state wave function and ΔE is the gap in energy between the first two eigenstates having a nonzero overlap with the trial wave function.

This long-time limit may be difficult to perform. Certainly the most well-known illustration of such a difficulty is the so-called sign problem occurring in exact simulations of

fermion systems. This problem has been discussed in detail in many places (see, *e.g.*, [2-4]). It can be summarized as follows. Fermion matrix elements of the operator $\exp[-tH]$ decompose as a difference of two boson contributions corresponding to even and odd permutations of the particle labels. At large times t (or low temperatures), the two boson contributions nearly cancel and the resulting fermion contribution becomes rapidly exponentially smaller than the statistical fluctuations. Accordingly, only reasonably small values of t may be used in eq. (1) in a fermionic simulation and convergence of the limit may not be possible in practice. Even in bosonic-type calculations the long-time limit can be difficult to handle for quantities other than the energy, particularly for systems involving a large number of bosons. For example, to compute ground-state expectations of operators not commuting with H requires a similar projection at large time (see, for instance, the discussion in [5]).

In this work we propose a new procedure for taking advantage of the information contained in data at small values of the projecting time t , thus minimizing the effect of statistical fluctuations at large times. We shall present this procedure within the framework of a variant of the DMC approach—the pure diffusion Monte Carlo method [6]—although any other Monte Carlo scheme could be employed without essential changes. Consider the projected trial wave function at time t :

$$\tilde{\Psi}_T(t) \equiv \exp[-tH] \Psi_T. \quad (2)$$

With quantum Monte Carlo techniques, quantum averages with respect to $\tilde{\Psi}_T$ may be computed. In what follows the norm $n(t)$ of $\tilde{\Psi}_T(t/2)$ and the average $h(t)$ of H over $\tilde{\Psi}_T(t/2)$ will be used:

$$n(t) \equiv \langle \tilde{\Psi}_T(t/2) | \tilde{\Psi}_T(t/2) \rangle = \langle \Psi_T | \exp[-tH] | \Psi_T \rangle \quad (3a)$$

and

$$h(t) \equiv \langle \tilde{\Psi}_T(t/2) | H | \tilde{\Psi}_T(t/2) \rangle = \langle \Psi_T | H \exp[-tH] | \Psi_T \rangle. \quad (3b)$$

These matrix elements of $\exp[-tH]$ may be computed as stochastic averages over a set of drifting random walks generated by using a Langevin equation. Denoting $\langle \dots \rangle_{\text{DRW}}$ the stochastic average, $n(t)$ and $h(t)$ may be written in the following form:

$$n(t) = \langle \Psi_G | \Psi_G \rangle \left\langle w(R(0)) w(R(t)) \exp \left[- \int_0^t E_L^G(R(s)) ds \right] \right\rangle_{\text{DRW}} \quad (4a)$$

and

$$h(t) = \langle \Psi_G | \Psi_G \rangle \cdot \left\langle w(R(0)) w(R(t)) \frac{1}{2} (E_L^T(R(0)) + E_L^T(R(t))) \exp \left[- \int_0^t E_L^G(R(s)) ds \right] \right\rangle_{\text{DRW}}. \quad (4b)$$

Here $w = \Psi_T/\Psi_G$ is a weight factor involving the trial wave function, Ψ_T , and the guiding function, Ψ_G , a strictly positive function responsible for importance sampling; $E_L^T = H\Psi_T/\Psi_T$ is the local energy associated with Ψ_T , $E_L^G = H\Psi_G/\Psi_G$ is the local energy associated with Ψ_G , and $R(s)$ stands for the drifting random walk in the $3N$ -dimensional configuration space. The normalization factor appearing on the right-hand side of each expression will be immaterial in what follows. Equations (4) are a generalization of the well-known Feynman-Kac formula.

For a detailed presentation and derivation of these formulae, the reader is referred to previous works [6]. At this point, we would like to emphasize two situations that will be encountered in what follows. When Ψ_G is chosen to be $|\Psi_T|$, random walks generated by the Langevin equation are trapped in subdomains of the configuration space delimited by the $(3N - 1)$ -dimensional nodes of the trial wave function Ψ_T and no change of sign for the weight factor occurs. This stable approach is called fixed-node approximation, since the nodes are in general approximate. On the other hand, when Ψ_G is chosen to be strictly positive everywhere, no approximation is made but weights have no longer a definite sign for fermions. This exact but unstable method will be referred to as the nodal-release approach. More details about both approaches may be found elsewhere [3, 6].

The standard way of extracting the exact energy from a set of QMC data $\{n(t_i), h(t_i)\}_{i=1,N}$ consists in looking at the ratio

$$\frac{h(t)}{n(t)} \rightarrow E_0 \quad \text{as } t \rightarrow \infty. \quad (5)$$

To do that, matrix elements are computed up to values of t necessary to reach the convergence. The main point of this work is to use information contained in h, n at smaller t . This is important due to the increase of statistical fluctuations as t goes to infinity. This idea, which in fact takes its origin in the somewhat different context of effective Hamiltonian theory [7], is implemented here in a quite simple way.

Let us define the following basis set of size n consisting of the projected trial wave function evaluated at n different times:

$$\{\tilde{\Psi}_T(t_1), \tilde{\Psi}_T(t_2), \dots, \tilde{\Psi}_T(t_n)\} \equiv \{t_1, t_2, \dots, t_n\}.$$

For finite n , such a basis set is in general linearly independent and may be used to diagonalize H . To perform the diagonalization, the matrix elements H_{ij} of H and N_{ij} of the unity operator between two arbitrary functions of the basis set are needed. It is easy to check that such matrix elements may be in fact trivially expressed in terms of the matrix elements (3) as follows:

$$H_{ij} \equiv \langle \tilde{\Psi}_T(t_1) | H | \tilde{\Psi}_T(t_2) \rangle = h(t_1 + t_2) \quad (6a)$$

and

$$N_{ij} \equiv \langle \tilde{\Psi}_T(t_1) | \tilde{\Psi}_T(t_2) \rangle = n(t_1 + t_2). \quad (6b)$$

This is important since it means that no extra quantities beyond the usual matrix elements (eq. (3)) are required. Then once H and N are estimated with QMC, the generalized eigenvalue problem is solved by standard numerical methods. At this point, it is important to emphasize that the algorithm proposed here is nothing but a variation of the well-known Lanczós algorithm with Ψ_T playing the role of the initial vector and $\exp[-tH]$ playing the role of H . Using the terminology of Krylov spaces [8], this can be rephrased by saying that H is diagonalized within the Krylov subspace $\{\Psi_T, \exp[-t_1 H] \Psi_T, \dots, \exp[-t_n H] \Psi_T\}$ instead of the Krylov subspace $\{\Psi_T, H\Psi_T, \dots, H^{n-1} \Psi_T\}$ as in the Lanczós algorithm. Note that the standard method described by (5) may be viewed as a rather trivial case for which H is diagonalized within the one-dimensional subspace defined by $\tilde{\Psi}_T(t/2)$.

Let us first present the application of this approach to an exactly solvable problem, namely the harmonic oscillator described by the Hamiltonian $H = -(1/2)(d^2/dx^2) + (1/2)Kx^2$. The trial wave function is chosen to be Gaussian (different from the exact solution) and since the kernel of $\exp[-tH]$ is also Gaussian, exact expressions for matrix elements (3) may be

TABLE I. - Comparison between the Lanczós-type algorithm and the standard method for the harmonic oscillator. Hamiltonian corresponding to $K = 3.0$, trial wave function^(a) with $k = 1$.

This work		Standard method ^(b)		Exact
Basis set ^(c)	Eigenvalues	Basis set ^(c)	Eigenvalues	
{0.0}	$\lambda_0 = 1.0$	{0.0}	$\lambda_0 = 1.0$	
{0.0, 0.02}	$\lambda_0 = 0.88$ $\lambda_1 = 5.1$	{0.02}	$\lambda_0 = 0.98$	
{0.0, 0.02, 0.04}	$\lambda_0 = 0.8668$ $\lambda_1 = 4.4$ $\lambda_2 = 9.4$	{0.04}	$\lambda_0 = 0.96$	
{0.0, 0.02, 0.04, 0.06}	$\lambda_0 = 0.8661$ $\lambda_1 = 4.34$ $\lambda_2 = 7.86$ $\lambda_3 = 13.9$	{0.06}	$\lambda_0 = 0.95$	
{0.0, 0.02, 0.04, 0.06, 0.08}	$\lambda_0 = 0.86603$ $\lambda_1 = 4.331$ $\lambda_2 = 7.80$ $\lambda_3 = 12.0$ $\lambda_4 = 18.4$	{0.08}	$\lambda_0 = 0.94$	$\lambda_0 = 0.8666025\dots$ $\lambda_1 = 4.3301\dots$ $\lambda_2 = 7.794\dots$ $\lambda_3 = 11.258\dots$ $\lambda_4 = 14.72\dots$

(a) $\Psi_T = (k/\pi)^{1/4} \exp[-(\sqrt{k}/2)x^2]$.

(b) Equation (5).

(c) Basis set defined as $\{t_1, t_2, \dots, t_n\} \equiv \{\exp[-t_1 H] \Psi_T, \exp[-t_2 H] \Psi_T, \dots, \exp[-t_n H] \Psi_T\}$, see text.

obtained. Table I presents results obtained when using a basis set of increasing size and compared to those resulting from (5) using only the last component of the set. For the case of the Lanczós-type algorithm all the eigenvalues are given. A few remarks are in order. First, it is clear that the lowest eigenvalue in the Lanczós approach converges quite rapidly toward the exact energy. This is in sharp contrast with the standard method which would require much larger times to achieve the convergence. A way of understanding this may be put as follows. Diagonalizing H within the subspace $\{t_1, t_2, \dots, t_n\}$ may be viewed as constructing the best wave function written in the form of a linear combination of the projected trial wave function defined at different times, $\sum_k c_k \Psi_T(t_k)$. This combination has much more variational freedom than the one-state approach using only $\{t_n\}$ and therefore the resulting improvement in energy may be important.

A second point worth mentioning is that excited-state energies may also be obtained in principle. Results presented in table I show a good convergence of excited-state eigenvalues toward their respective limit, at least for the first two. Note that, according to the MacDonal variational theorem applying for linear variational calculations [9], all the eigenvalues $\lambda_i(t)$ are always greater than the corresponding exact eigenvalue of the Hamiltonian, the equality would be obtained by letting t go to infinity. How far $\lambda_i(t)$ is from $E_i = \lambda_i(\infty)$ for a given time t depends essentially on the overlap between the exact excited-state and the trial wave function. The problem of evaluating excited-state energies will not be discussed further, since the obtained results are not representative of the typical case where matrix elements have statistical errors. However, note that this approach may be readily generalized to the multiple-state method for computing excited-state properties of Ceperley and Bernu [10].

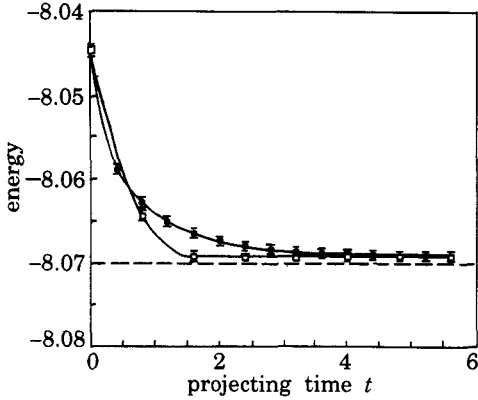


Fig. 1.

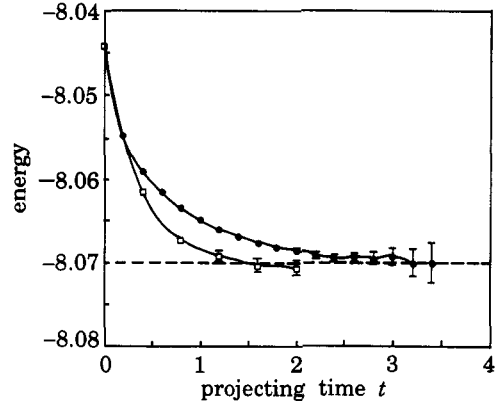


Fig. 2.

Fig. 1. – Fixed-node energy as a function of the projecting time t for the LiH molecule for both the standard method (\bullet) and the proposed Lanczós-type method (\square). The dashed line indicates the exact energy. The small difference between the energy obtained for large times and the exact energy is due to the fixed-node error. Energy and time in atomic units. The curves are only a guide to the eye.

Fig. 2. – Nodal-release energy as a function of the projecting time t for the LiH molecule for both the standard method (\bullet) and the proposed Lanczós-type method (\square). The dashed line indicates the exact energy. Large fluctuations at large times in the standard method result from the fermion sign problem. Energy and time in atomic units. The curves are only a guide to the eye.

Let us present a realistic application to the LiH molecule involving quantum Monte Carlo evaluation of matrix elements (3). In order to deal with the fermionic constraints, we have used both the approximate fixed-node and exact nodal-release approaches. Figure 1 presents the convergence of the fixed-node energy as a function of the projecting time t for both the standard method (5) (upper curve) and the proposed method (lower curve). With the Lanczós-type approach convergence is reached at times ~ 1.6 a.u., while the standard method requires times greater than 3 a.u. Statistical errors for both curves have been obtained by computing the dispersion of results over a set of independent calculations.

There is a serious numerical problem in applying this scheme to Monte Carlo results. When t goes to infinity the projected trial wave function $\tilde{\Psi}_T(t)$ converges exponentially fast to Φ_0 , eq. (1). Accordingly, projected trial wave functions at large times become almost identical. Hence the matrices become nearly singular and, because of the finite precision on machine, it is not possible to use basis sets of arbitrary size if there is any statistical error on the matrix elements. We circumvented this problem by employing basis sets small enough to lead to well-conditioned matrices. For the case presented in fig. 1, the successive basis sets employed are: $\{0,0\}$, $\{0,0,0.4\}$, $\{0,0,0.4,0.8\}$, $\{0,0,0.4,1.2\}$, ..., and $\{0,0,0.4,2.8\}$ with $\Delta t = 0.005$ a.u. as time step. The energy obtained in both calculations is $-8.0691(6)$ ((99 \pm 0.7)% of the correlation energy is recovered).

Figure 2 presents our calculations using the exact nodal-release procedure. The positive guiding function used here is of the form $\Psi_G = \sqrt{\Psi_T^2 + \theta \prod_i \rho(r_i)}$, where $\prod_i \rho$ denotes the

Hartree density corresponding to the trial wave function Ψ_T . The switching parameter θ has been chosen to have a value of 0.48 so as to minimize both statistical fluctuations on the local energy $E_L = H\Psi_G/\Psi_G$ and fluctuations arising from crossings and recrossings of nodes [3]. The upper curve of fig. 2 represents the variation of the energy *vs.* the projecting time as

obtained with the standard method (5). The fermion sign problem is evident as t becomes greater than 2.0 a.u. The lower curve has been obtained by applying our algorithm with the successive basis sets: $\{0.0\}$, $\{0.0, 0.2\}$, $\{0.0, 0.2, 0.4\}$, $\{0.0, 0.2, 0.6\}$, $\{0.0, 0.2, 0.8\}$, and $\{0.0, 0.2, 1.0\}$ with $\Delta t = 0.005$ a.u. Within statistical fluctuations the convergence is reached for $t \sim 2.0$ u.a., that is before statistical fluctuations arising from the sign problem become too pathological. The resulting energy is $E_0 = -8.070(1)$, compared with the exact nonrelativistic energy of -8.0699 [11].

These good results should be taken with caution. The main point to emphasize is that by using a linear variational calculation the energy is expressed as a lowest eigenvalue which is a nonlinear function of the matrix elements (3). The stability of the eigenvalue with respect to statistical errors has been obtained here at the expense of a high-quality evaluation of the matrix elements. It is not clear whether such a quality can be obtained for fermionic systems involving a large number of particles. However, the results presented here are important since they demonstrate that QMC data at small times, that is before the sign catastrophe occurs, may eventually contain enough information for computing exact fermionic ground-state properties. In a forthcoming work, a more stable and general method for taking advantage of this information will be presented [12].

* * *

One of us (MC) would like to thank W. KRAUTH for a number of helpful discussions. MC also wishes to thank the CNRS, the NATO and the Department of Physics at Urbana-Champaign for their financial support during his visit at the University of Illinois. The computations were done on the CRAY Y-MP of the National Center for Supercomputing Applications at Urbana-Champaign. DC is supported by the NSF under NSF-DMR-8808126.

REFERENCES

- [1] See, e.g., contributions in *J. Stat. Phys.*, **43** (1986). See also *Monte Carlo Methods in Statistical Physics*, edited by K. BINDER (Springer-Verlag, Berlin) 1977 and *ibid.*, Vol. II (1984). For applications to the electronic structure of atoms and molecules, see, e.g., LESTER jr. W. A. and HAMMOND B. L., *Annu. Rev. Phys. Chem.*, **41** (1990) 283 and references therein.
- [2] KALOS M. H., in *Monte Carlo Methods in Quantum Problems*, NATO ASI Series C (Reidel, Dordrecht) 1982.
- [3] CEPERLEY D. M. and ALDER B. J., *J. Chem. Phys.*, **64** (1984) 5833.
- [4] SCHMIDT K. E. and KALOS M. H., in *Monte Carlo Methods in Statistical Physics*, edited by K. BINDER (Springer-Verlag, Berlin) 1984.
- [5] RUNGE K. J. and RUNGE R. J., preprint (1990).
- [6] CAFFAREL M. and CLAVERIE P., *J. Stat. Phys.*, **43** (1986) 797; *J. Chem. Phys.*, **88** (1988) 1088, 1100.
- [7] GADEA F. X., Thèse d'Etat, Toulouse, 1987; *Phys. Rev. A*, **36** (1987) 2557.
- [8] PARLETT B. N., *The Symmetric Eigenvalue Problem*, Prentice-Hall Series in Computational Mathematics, 1980.
- [9] MACDONALD J. K. L., *Phys. Rev.*, **43** (1933) 830.
- [10] CEPERLEY D. M. and BERNU B., *J. Chem. Phys.*, **89** (1988) 6316.
- [11] LIE G. C. and CLEMENTI E., *J. Chem. Phys.*, **60** (1974) 1275.
- [12] CAFFAREL M. and CEPERLEY D. M., to be published.

G. W. Krauth, M. Caffarel and J.P. Bouchaud, "Gutzwiller Wave Function for a Model of Strongly Interacting Bosons", Phys. Rev B 45, 3137 (1992)

Gutzwiller wave function for a model of strongly interacting bosons

Werner Krauth

NCSA, University of Illinois at Urbana-Champaign, Urbana, Illinois 61801

Michel Caffarel

NCSA, University of Illinois at Urbana-Champaign, Urbana, Illinois 61801

and Laboratoire Dynamique des Interactions Moléculaires, Université Paris VI, F-75252 Paris CEDEX 05, France

Jean-Philippe Bouchaud

Laboratoire de Physique Statistique de l'École Normale Supérieure, 24, rue Lhomond, F-75231 Paris CEDEX 05, France

(Received 20 March 1991)

We study a model of strongly interacting lattice bosons with a Gutzwiller-type wave function that contains only on-site correlations. The variational energy and the condensate fraction associated with the variational wave function are exactly evaluated for both finite and infinite systems and compared with exact quantum Monte Carlo results in two dimensions. This ansatz for the wave function gives the correct qualitative picture of the phase diagram of this system; at commensurate densities, this system enters a Mott-insulator phase for large values of the interaction.

Strongly interacting boson systems have been extensively studied for a long time. Apart from the usual λ transition between the superfluid and the normal liquid at a given temperature, systems of bosons in an external potential may also undergo a superfluid-insulator transition at $T=0$ upon a change of strength in the interaction or the conditions of the environment. Such a phase transition has recently been studied in several works for a model of strongly interacting lattice bosons interacting with a repulsive on-site interaction. The model described by the Hamiltonian

$$H = \frac{-t}{2} \sum_{\langle i,j \rangle} (a_i^\dagger a_j + \text{H.c.}) + \frac{U}{2} \sum_i n_i(n_i - 1) \quad (1)$$

is the focus of the present Brief Report. It describes a system of M bosons on a lattice with N sites in d dimensions. This system exhibits a superfluid phase for all values of the interaction U and noncommensurate densities; i.e., $\rho = M/N$ not an integer. Indeed, some particles can always gain kinetic energy at no cost in potential energy by hopping to sites occupied by a smaller number of particles. At commensurate densities (i.e., integer ρ), the model also exhibits a superfluid phase at small U/t since the penalty in potential energy is not large enough to offset the gain in kinetic energy that delocalizes the particles. However, for large enough interaction, this is no longer true, and the system is trapped into a Mott-insulator state. Accordingly, there exist two transitions from the superfluid phase to the Mott-insulator phase: (i) when U/t approaches some critical value U_c/t at commensurate (integer) densities n_c and (ii) when the density ρ approaches n_c at large on-site repulsion U/t .

A scaling theory of these transitions has been worked out by Fisher *et al.*¹ They have shown that transition (i) is in the universality class of the $(d+1)$ -dimensional XY model, whereas (ii) is described correctly by mean-field

theory in any dimension.

Apart from considerations of universal quantities, the explicit phase diagram of this system is of interest. These questions have recently been addressed in exact path-integral Monte Carlo (PIMC) simulations in both one and two dimensions.^{2,3} More general, if approximate, information is provided by mean-field theory, in which the location of the phase boundaries can also be determined. A mean-field-theory treatment of this model has been indicated in the work by Fisher *et al.*¹

In this work we present an exact variational calculation with a Gutzwiller-type wave function

$$\Psi(n_1, n_2, \dots, n_N) = \prod_{i=1}^N f(n_i) \delta \left[\sum_{i=1}^N n_i - M \right], \quad (2)$$

for both finite and infinite lattices. This wave function does not incorporate any information on the geometry or dimensionality of the lattice and is therefore also mean field in nature. In particular, it does not include long-range correlations arising from zero-point phonons: These must be described by a Jastrow factor of the type $\exp[\sum_{i<j} g(r_i - r_j)]$ multiplying Eq. (2), with $g(r)$ decaying as r^{-2} for large r .⁴ This term would ensure a correct behavior of the structure factor $S(k)$ for small k and hence the correct spectrum for low-energy excitations. However, inclusion of this factor ruins the appealing feature of Eq. (2), namely, that it leads to an explicit solution for all values of the interaction U/t and density ρ .

We use two variational approaches: a *general* minimization with respect to the $\{f(n), n=0, 1, \dots\}$ and a simplified approach in which $f(n)$ is *parametrized* according to

$$f(n) \sim \exp(-\kappa n^2/2) / \sqrt{n!}, \quad (3)$$

and where the optimal parameter κ minimizing the ener-

gy is sought. This parametrization corresponds (in position representation) to a wave function with a contact term $\Psi(r_1, r_2, \dots, r_M) = \exp[-\kappa/2 \sum_{i < j} \delta(r_i - r_j)]$. As we shall see, the two approaches are equivalent for all intents and purposes: They give the same asymptotic behavior [$U/t \rightarrow U_c/t = d(\sqrt{n_c} + \sqrt{n_c + 1})^2$] for commensurate densities $\rho = n_c$ and at $U/t = \infty$ for incommensurate densities, and agree closely in the numerical values for the energy and momentum condensate. As the critical value U_c/t (at $\rho = n_c$) is approached from below, there is a second-order phase transition from the superfluid into a Mott insulator with an energy per particle, $E \sim -(U_c - U)^2$, below the transition and $E = 0$ above it. As the parameterized form of the wave function is considerably simpler to evaluate for the finite systems (which we can then compare to the exact numerical calculations), we shall base much of our detailed calculations on this version.

We are also able to calculate the condensate fraction associated with the wave function (the Fourier transform at $k = 0$ of the one-body density matrix), $n(k = 0)$. One obtains $n(k = 0) \sim U_c - U$ below the transition and $n(k = 0) = 0$ above it. For incommensurate densities the condensate fraction is strictly positive for any value of U , demonstrating that the system is always superfluid. We given an explicit formula for $n(k = 0)$ as a function of the density ρ .

We have in addition performed high-precision simulations of the two-dimensional model ($d = 2$) using a zero-temperature diffusion Monte Carlo scheme⁵ [it is for this reason that we use a canonical formulation in Eq. (2)]. This allows us to compare the variational energy (at finite N) with the exact energy at all values of the parameters, especially away from the critical point where the solution is expected to be accurate. The exact energy for a system

with 16 bosons ($\rho = 1$, $d = 2$), e.g., is found to be off by about 20% at $U/t = 6$, by 5% at $U/t = 4$, and by 1.5% at $U/t = 2$. The critical interaction $U_c/t = 6 + 4\sqrt{2} \sim 11.66$ (at density $\rho = 1$, in two dimensions) compares well with the value of $U_c/t \sim 8.5$ found in a previous work² from two-dimensional PIMC simulations.

We now present the calculations for this model. The norm of the wave function is given by

$$\langle \Psi | \Psi \rangle = \prod_{i=1}^N \left[\sum_{n_i} f^2(n_i) \right] \delta \left[\sum_{i=1}^N n_i - M \right]. \quad (4)$$

This can be written as

$$\langle \Psi | \Psi \rangle = \int_{-\pi}^{\pi} \frac{d\lambda}{2\pi} \exp Ng(f, \lambda), \quad (5)$$

$$g(f, \lambda) \equiv -i\lambda\rho + \ln \left[\sum_{n=0}^{\infty} f^2(n) \exp(i\lambda n) \right]. \quad (6)$$

Similarly, we find, for the potential and kinetic energies,

$$\langle \Psi | \begin{cases} E_{\text{pot}} \\ |\Psi\rangle \\ E_{\text{kin}} \end{cases} = N \int_{-\pi}^{\pi} \frac{d\lambda}{2\pi} \exp[Ng(f, \lambda)] \begin{cases} \tilde{E}_{\text{pot}}(f, \lambda) \\ \\ \tilde{E}_{\text{kin}}(f, \lambda) \end{cases}, \quad (7)$$

with

$$\tilde{E}_{\text{pot}}(f, \lambda) = \frac{U}{2} \frac{\sum n(n-1) f^2(n) \exp(i\lambda n)}{\sum f^2(n) \exp(i\lambda n)} \quad (8)$$

and

$$\tilde{E}_{\text{kin}}(f, \lambda) = -dt \exp(i\lambda) \frac{[\sum \sqrt{n+1} f(n) f(n+1) \exp(i\lambda n)]^2}{[\sum f^2(n) \exp(i\lambda n)]^2}. \quad (9)$$

For the given wave function, the condensate fraction is proportional to the kinetic energy per particle. We find that $n(k = 0) = -1/(dN)E_{\text{kin}}$.

For finite systems the integrals [Eqs. (5) and (7)] have to be calculated explicitly. In the $N \rightarrow \infty$ limit, of course, the integrals are given by the values of the integrands at their saddle point $\bar{\lambda}$, which is located at $\bar{\lambda} = 0$, provided that $\rho = \sum_{n=0}^{\infty} n f^2(n) / \sum_{n=0}^{\infty} f^2(n)$ [cf. Eq. (6)]. Under this condition [and considering properly normalized wave functions $\sum_{n=0}^{\infty} f^2(n) = 1$], the energy per particle is given by

$$E = -\frac{dt}{\rho} \left[\sum_{n=0}^{\infty} \sqrt{n+1} f(n) f(n+1) \right]^2 + \frac{U}{2\rho} \sum_{n=0}^{\infty} n(n-1) f^2(n). \quad (10)$$

From this equation we can now obtain the optimal values

of the parameters $f(n)$, $n = 0, \dots, \infty$, by solving for $\partial E / \partial f(n) = 0$ (under the constraints stated above). This can easily be done by iteration.

Equation (10) can also be solved asymptotically in the limit $U/t \rightarrow U_c/t$, for commensurate densities n_c , and $U/t \rightarrow \infty$ (for incommensurate densities). In fact, we can show that a self-consistent ansatz for $f(n)$ close to the transition is given by $f(n_c) = \sqrt{1 - 2\epsilon}$ and $f(n_c \pm 1) = \sqrt{\epsilon}$ with $\epsilon \ll 1$ and $f(n_c \pm 2) \ll \sqrt{\epsilon}$, etc. In this limit the energy [Eq. (10)] reduces to

$$E = -\frac{dt}{n_c} \epsilon(1 - 2\epsilon)(\sqrt{n_c} + \sqrt{n_c + 1})^2 + \frac{U}{2n_c} [2\epsilon + n_c(n_c - 1)]. \quad (11)$$

A simple derivation of E with respect to ϵ shows that the probability ϵ to have $n_c \pm 1$ particles on one site vanishes at the critical interaction $U_c/t = d(\sqrt{n_c}$

$+\sqrt{n_c+1}^2$. Close to the transition ($\Delta=U_c/t-U/t$), the energy is given by

$$E(\Delta) = \frac{-\Delta^2}{4n_c U_c}. \quad (12)$$

For $U > U_c$ we find that $E_{\text{kin}}=0$, $E_{\text{pot}}=U/2(n_c-1)$.

Our complete results for the commensurate case $\rho=1$ are presented in Figs. 1–3. In Fig. 1 we show the evolution of the probability to have a site occupied by n particles, $f^2(n)$, with U/t for $n=0,1,2,3,4$ [cf. Eq. (10)]. Note that $f^2(n)$ quickly becomes extremely small for $n \geq 3$.

In Fig. 2 we show the energy per particle of the system as a function of the variational parameter κ for different values of the interaction ($U/t=1,3,5,7$) for a finite lattice with size $N=16$ [from Eq. (7)] and for the infinite lattice [from Eqs. (8) and (9)]. The optimal value of the parameter, κ_{opt} , is marked also. The variational energy $E(\kappa_{\text{opt}})$ is on this scale indistinguishable from the one given by the more general $E[\{f(n)\}_{\text{opt}}]$.

The inset in Fig. 2 gives the value of κ_{opt} as a function of U , as determined numerically, both for the finite and infinite systems, where it diverges as $\kappa_{\text{opt}} \sim \ln(U_c/t - U/t)$.

Figure 2 contains one more important piece of information. The horizontal lines underneath each curve for the finite system give the *exact* value of the ground-state energy for the corresponding two-dimensional (2D) system (with $N=16$), as determined with a pure-diffusion Monte Carlo method.⁵ For example, we find a ground-state energy per particle of $E = -0.511 \pm 0.002$ at $U/t=6$ (in 2D), whereas the variational energy is $E_{\text{var}} = -0.401$ for the optimal solution $\{f(n)\}$ and $E_{\text{var}} = -0.388$ for the wave function parametrized according to Eq. (3). The agreement of the variational energy with the exact solution is good, considering the simplicity of the wave function.

In Fig. 3 we show the values of the momentum condensate for this case of $\rho=1$, both for the finite case $N=16$ and in the infinite system and compare them to the *exact* superfluid density at $N=16$ (cf. Ref. 2). The numerical calculation of the momentum condensate, although in principle possible,⁶ has not been carried out for this model, in contrast to the (more interesting) superfluid density.

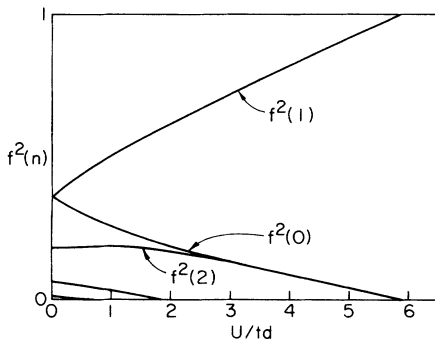


FIG. 1. Probability $f^2(n)$ of a site to be occupied by n particles vs interaction U/t for $n=0,1,2,3,4$.

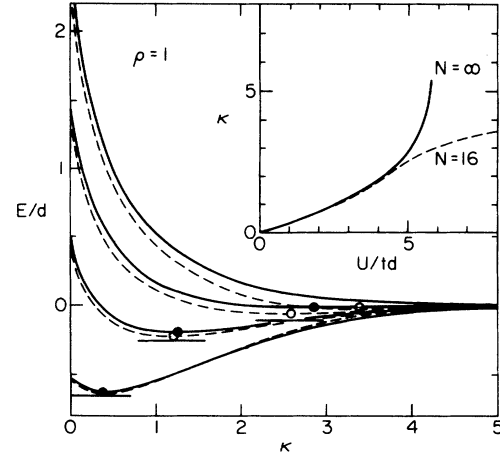


FIG. 2. Variational energy (scaled by the dimension of the lattice) E/d vs variational parameter κ at density $\rho=1$ for $U/t=1,3,5,7$ (from below). $N=\infty$ (solid line, solid circles) and $N=16$ (dashed line, open circles). The exact ground-state energies for $N=16$ in two dimensions are indicated by horizontal lines. The inset gives the optimal values of the variational parameter, κ_{opt} , as a function of U/t for both $N=16$ and ∞ .

As is well known,^{7,8} there is no direct relationship between the two quantities away from the small- U/t region, where the agreement is excellent. In general, the fact that $n(k) > 0$ only allows us to conclude that the trial wave function describes a superfluid. For $N=\infty$, $n(k)$ goes to zero as $(U_c - U)/4dtn_c$ at the transition into the insulating state. In two dimensions the transition takes place at an interaction strength of $U_c/t=11.66$, which compares well with the exact value from the PIMC simulations, which yield $U_c/t \sim 8.5$. The critical exponent, of course, coincides with the mean-field one and cannot be expected to coincide with that (~ 0.669) predicted by the scaling theory of Fisher *et al.*¹

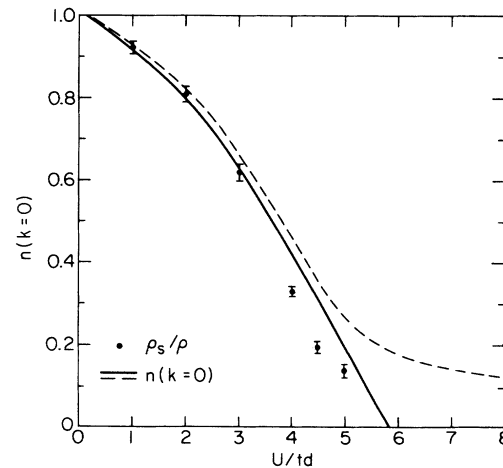


FIG. 3. Variationally calculated values of the momentum condensate $n(k=0)$ vs interaction (scaled by the dimension) U/t for density $\rho=1$. $N=\infty$ (solid line) and $N=16$ (dashed line). Also shown are the exact values of the superfluid density ρ_s/ρ for the system with $N=16$ in 2D.

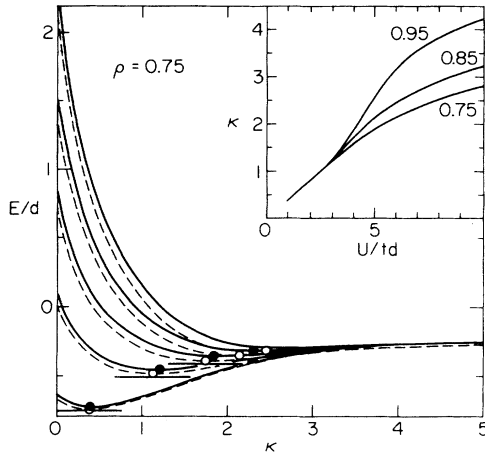


FIG. 4. Variational energy E/d vs κ at density $\rho=0.75$ for $U/td=1,3,5,7,9$ (from below). $N=\infty$ (solid line, solid circles) and $N=16$ (dashed line, open circles). The exact ground-state energies for $N=16$ in two dimensions are indicated by horizontal lines. The inset gives the optimal values of the variational parameter, κ_{opt} , as a function of U/td at $N=\infty$ for densities $\rho=0.75,0.85,0.95$.

At a general incommensurate density ρ ($n_c-1 < \rho < n_c$) and $U/t = \infty$, we can again perform an asymptotic analysis with a self-consistent ansatz $f(n_c-1)=a$ and $f(n_c)=(1-a^2)^{1/2}$. A calculation analogous to the one presented for the commensurate case now yields

$$\tilde{E}_{\text{pot}}(\kappa) \rightarrow \frac{U(n_c-1)(2\rho-n_c)}{2\rho}, \quad (13)$$

$$\tilde{E}_{\text{kin}}(\kappa) \rightarrow -dt \frac{n_c(n_c-\rho)[\rho-(n_c-1)]}{\rho}. \quad (14)$$

Complete results for the incommensurate case $\rho=0.75$ are given in Fig. 4. In the main picture we show again the energy per particle as a function of the variational parameter κ for different values of the interaction ($U/td=1,3,5,7,9$) for a finite lattice with size $N=16$ and for the infinite lattice. The optimal value of the parameter, κ_{opt} , and the *exact* ground-state energies for

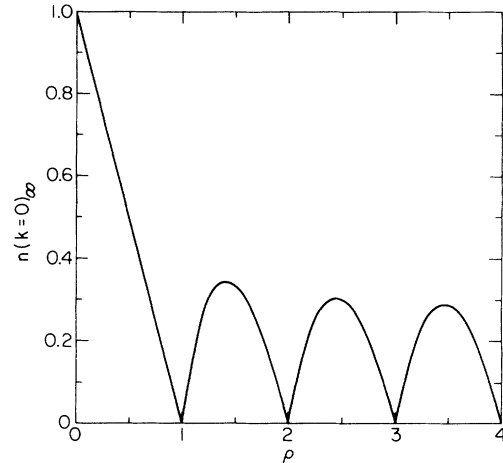


FIG. 5. Variationally calculated momentum condensate $n(k=0)$ vs density ρ .

$N=16$ (in 2D) are also marked. The inset in Fig. 4 gives the value of κ_{opt} as a function of U/td for the infinite system (the asymptotic behavior is $\kappa \sim -\ln[2d(1-\rho)] + \ln(U_c - 2d)$).

Finally, we show in Fig. 5 the variationally calculated momentum condensate $n(k=0)$ at $U/t = \infty$ as a function of ρ at $N=\infty$. From Eq. (14) we can see that $n(k=0) = n_c(n_c-\rho)[\rho-(n_c-1)]/\rho$. For large values of the density ($n_c-1 < \rho < n_c$, with $n \rightarrow \infty$), the momentum condensate is therefore given by the formula $n(k=0) \sim (n_c-\rho)[\rho-(n_c-1)]$, with a *finite* maximum value of $n(k=0) = \frac{1}{4}$ for $\rho = n_c - \frac{1}{2}$.

In conclusion, we have given a complete treatment of the problem of strongly interacting lattice bosons in terms of a Gutzwiller variational wave function. It will be interesting to see whether this approach can be extended successfully to provide a suitable starting point for calculations on more difficult problems, such as the one of disordered bosons.^{9,1}

J.P.B. wants to thank P. Nozières for discussions on the problem on interacting bosons.¹⁰

¹M. P. A. Fisher, P. B. Weichman, G. Grinstein, and D. S. Fisher, Phys. Rev. B **40**, 546 (1989).

²W. Krauth and N. Trivedi, Europhys. Lett. **14**, 627 (1991).

³G. G. Batrouni, R. T. Scalettar, and G. T. Zimanyi, Phys. Rev. Lett. **65**, 1765 (1990).

⁴L. Reatto and G. V. Chester, Phys. Lett. **22**, 276 (1966).

⁵M. Caffarel and P. Claverie, J. Stat. Phys. **43**, 797 (1986); M. Caffarel and P. Claverie, J. Chem. Phys. **88**, 1088 (1988).

⁶D. M. Ceperley and E. L. Pollock, Can. J. Phys. **65**, 1416 (1987).

⁷A. J. Leggett, Phys. Fennica **8**, 125 (1973).

⁸E. L. Pollock and D. M. Ceperley, Phys. Rev. B **36**, 8343 (1987).

⁹W. Krauth, N. Trivedi, and D. M. Ceperley, Phys. Rev. Lett. **67**, 2307 (1991).

¹⁰P. Nozières (unpublished).

H. M. Caffarel, X. Krokidis, and C. Mijoule, “On the Nonconservation of the Number of Nodel Cells of Eigenfunctions”, *Europhys. Lett.* **20**, 581 (1992)

On the Nonconservation of the Number of Nodal Cells of Eigenfunctions

This article has been downloaded from IOPscience. Please scroll down to see the full text article.

1992 Europhys. Lett. 20 581

(<http://iopscience.iop.org/0295-5075/20/7/002>)

View [the table of contents for this issue](#), or go to the [journal homepage](#) for more

Download details:

IP Address: 86.221.86.45

The article was downloaded on 24/09/2010 at 18:02

Please note that [terms and conditions apply](#).

On the Nonconservation of the Number of Nodal Cells of Eigenfunctions.

M. CAFFAREL, X. KROKIDIS and C. MIJOLE

*Laboratoire Dynamique des Interactions Moléculaires, Université Paris VI
75252 Paris Cedex 05, France*

(received 27 July 1992; accepted 29 September 1992)

PACS. 03.65G – Solutions of wave equations: bound state.

PACS. 33.10G – Vibrational analysis.

Abstract. – The theorem stating that the number of nodal cells of a pure eigenfunction of a Hamiltonian with a smooth and uniformly bounded potential may change as the potential is continuously varied, is illustrated by constructing a particular two-dimensional Hamiltonian (two coupled oscillators) of which one of the eigenfunctions exhibits the nonconservation property. The analytical form of both the potential (a six-order polynomial) and the eigenfunction is given.

Very little is known about the properties of the nodes of eigenfunctions of multidimensional systems. Paraphrasing Korsch [1] we may summarize the few established properties as follows (here n labels the nondegenerate eigenvalues, E_n , $n = 1, 2, 3, \dots$, ordered according to increasing magnitude; for simplicity, the properties are expressed for a two-dimensional case):

- 1) The only state having no nodes is the ground state, $n = 1$.
- 2) The number of nodal cells of the n -th eigenfunction is not larger than n [2].
- 3) The number of nodal cells does not necessarily increase with n .
- 4) The nodal set is generically a manifold; in particular it means that in most cases nodal lines do not cross in the interior of the domain of the Hamiltonian; however, crossings of nodal lines are expected at the boundary [3, 4].
- 5) If q nodal lines cross, the crossing occurs at equal angles π/q , in particular at right angles for $q = 2$ [5].
- 6) The total length of the nodal lines in state n is bounded from below and increases with n faster than $n^{1/2}$ [6].
- 7) For a Hamiltonian with a uniformly bounded potential and a given energy the volumes of the nodal cells are bounded from below [7] (strictly greater than zero).

An additional property which has been discussed is whether or not the number of nodal cells of a given eigenfunction is conserved when a parameter of the Hamiltonian is continuously varied. A proof that this number is conserved (adiabatic invariant) has been

given by Robnik [7], but was very soon later on criticized by him as containing a gap [8] (events such as the merging of two nodal cells along an $(N-2)$, $(N-3)$, ..., 0-dimensional boundary in an N -dimensional configuration space were not considered, and indeed we shall construct below our counterexample in that way). Numerical calculations performed by Korsch [1] for a rectangular «billiard» deformed into a parallelogram demonstrated that the number of nodal cells can change when deforming boundary conditions. A similar conclusion may be drawn from a number of numerical calculations done to study the connection between nodal patterns of nodal lines of eigenfunctions in the semi-classical regime and «quantum chaos» (see, *e.g.*, [9-11]). However, it is generally considered that the number of nodal cells in almost all cases is a conserved quantity, particularly when the energy spectrum is nondegenerate [8]. To our knowledge, no exact eigenfunction of a nontrivial system changing its number of nodal cells under a smooth variation of the potential has been exhibited so far.

The motivation of the present work takes its origin in a recent proposal [12] of computing the fundamental excitations of coupled oscillators with quantum Monte Carlo (QMC). In this scheme—relying essentially on a generalization of the fixed-node approach for excited states—a basic assumption on the nodal structure of eigenfunctions associated with fundamental excitations was made. More precisely it was assumed that their nodes divide the N -dimensional space (N oscillators) into exactly *two* domains. Such an assumption was considered as reasonable since, by their very definition, the fundamental excitations are connected continuously (when decreasing the coupled part of the potential) to the fundamental excitations of some N uncoupled oscillators which, indeed, have this property. However, although numerical calculations for some model and realistically coupled anharmonic oscillators (compared to the exact results obtained by diagonalizing H using a large enough Hermite-Gaussian basis set) have strongly supported our basic assumption, an eventual breakdown of the conservation property could occur. Let us now construct such a situation for a system of two coupled oscillators.

We consider the following wave function:

$$\psi(x, y, \lambda) = f(x, y, \lambda) \exp[-\Phi(x, y, \lambda)], \quad (1)$$

where Φ is a smooth and bounded function, f some function determining the nodes of ψ via the relation $f=0$, and λ a parameter controlling the deformation of the nodal pattern. The function Φ is chosen so that ψ describes a bound state, that is $\Phi \rightarrow +\infty$ when $|x|$ or $|y|$ tend to infinity (a polynomial form for f being used here, the large-distance behaviour of ψ is determined by Φ). Let us choose f as the simplest function exhibiting the nonconservation property when varying λ . We take

$$f = y^2 - x^3 - F(\lambda)x - \frac{2}{27}, \quad (2)$$

where $F(\lambda)$ is some function of λ . Regarding the nodal structure of f (or ψ) three different regimes have to be distinguished:

- i) When $F(\lambda) > -1/3$ the nodes of f divide the plane into two regions.
- ii) At the critical value $F(\lambda) = -1/3$ the nodal line crosses itself at the singular point $\Omega(1/3, 0)$. Note that f has been chosen so that the crossing is at right angles as required by the property 5) stated above.
- iii) For $F(\lambda) < -1/3$ the nodes divide the plane into three nodal cells.

The three different regimes are represented in fig. 1. It should be pointed out that condition (7) forbids the emergence of an extra nodal cell from an isolated point of the plane

(the volume of a nodal cell cannot be arbitrarily small at a given energy). Deforming a nodal line in the way just described above circumvents this problem. The next step consists in showing that the wave function (1) may be interpreted as an eigenfunction of a physical Hamiltonian H , namely

$$H\psi = E\psi, \tag{3}$$

where

$$H = -\frac{1}{2} \left(\frac{\partial^2}{\partial x^2} + \frac{\partial^2}{\partial y^2} \right) + V(x, y, \lambda) \tag{4}$$

and V is a bounded potential function to be determined. Using eqs. (1), (3) and (4) V may be written as follows:

$$V = E + \frac{1}{2} \{(\nabla\Phi)^2 - \nabla^2\Phi\} + \frac{1}{2} \frac{\nabla^2 f}{f} - \frac{\nabla f}{f} \cdot \nabla\Phi. \tag{5}$$

The first three terms of the r.h.s. of (5) are bounded at any finite distances and therefore do not introduce any difficulty (the imposition of the adequate large-distance behaviour of V and ψ will be treated later). In contrast, dividing by f in the last two terms may lead to unphysical divergencies in the potential at the nodes. Therefore, we shall seek a solution for Φ verifying

$$\frac{1}{2} \frac{\nabla^2 f}{f} - \frac{\nabla f}{f} \cdot \nabla\Phi = K(x, y), \tag{6}$$

where K is any bounded function well behaved at large distances. Equation (6) may be rewritten under the form

$$\frac{\partial\Phi}{\partial x} Q(x) + \frac{\partial\Phi}{\partial y} R(y) = S(x, y) \tag{7}$$

with

$$Q(x) = -3x^2 - F, \quad R(y) = 2y, \quad S(x, y) = -Kf + 1 - 3x.$$

It turns out that there exists a polynomial solution of eq. (7) when K is also chosen to be polynomial. The simplest (lowest-order) form for K is

$$K(x, y) = K_0 + K_1 x + K_2 x^2 + K_3 y^2, \tag{8}$$

the solution Φ having the form

$$\Phi(x, y) = \sum_{i+j \leq 4} a_{ij} x^i y^j. \tag{9}$$

The only nonzero coefficients a_{ij} are

$$a_{10} = -\frac{1}{F} \left(1 + \frac{2K_0}{27} \right), \quad (10a)$$

$$a_{20} = -\frac{1}{2F} \left(K_0 F + \frac{2K_1}{27} - 3 \right), \quad (10b)$$

$$a_{30} = -\frac{K_1}{9}, \quad (10c)$$

$$a_{40} = -\frac{K_2}{12}, \quad (10d)$$

$$a_{02} = -\frac{K_0}{4} - \frac{FK_1}{16} + \frac{(4 + 9F^2)}{216} K_3, \quad (10e)$$

$$a_{12} = -\frac{K_1}{4} + \frac{K_3 F}{6}, \quad (10f)$$

$$a_{22} = -\frac{K_3}{6}, \quad (10g)$$

$$a_{04} = -\frac{K_3}{8}. \quad (10h)$$

In addition, the coefficients K_0 , K_1 , and K_3 are related via the following equalities:

$$K_0 = \frac{F}{3} K_2 + \frac{27}{2} \left(\frac{F^2}{P} - 1 \right), \quad (11a)$$

$$K_1 = \frac{9}{2P}, \quad (11b)$$

$$K_2 = \frac{K_3}{2} \left(1 + \frac{1 + 27F^3}{27P} \right) - \frac{27}{8P}, \quad (11c)$$

where

$$P \equiv F^2 - \frac{F}{3} + \frac{1}{9} \quad (11d)$$

is a strictly positive function of λ . In order to get an eigenfunction describing a bound state, the higher-order coefficients a_{40} , a_{04} , and a_{22} determining the large-distance behaviour of ψ and V must all be strictly positive. From eqs. (10) it follows that coefficients K_2 and K_3 must be strictly negative. Finally, since no particular conditions hold for K_0 and K_1 , any choice of strictly negative coefficients K_2 and K_3 verifying eq. (11c) is a solution of our problem. We shall exemplify this by choosing K_3 so that coefficient a_{12} (eq. (10f)) vanishes, *i.e.* $K_3 = -3K_1/2F$. From eqs. (11b), (11c), and (11d) it is easy to check that this is a valid choice if F is taken to be negative. Note that the only requirement on F to obtain a wave function

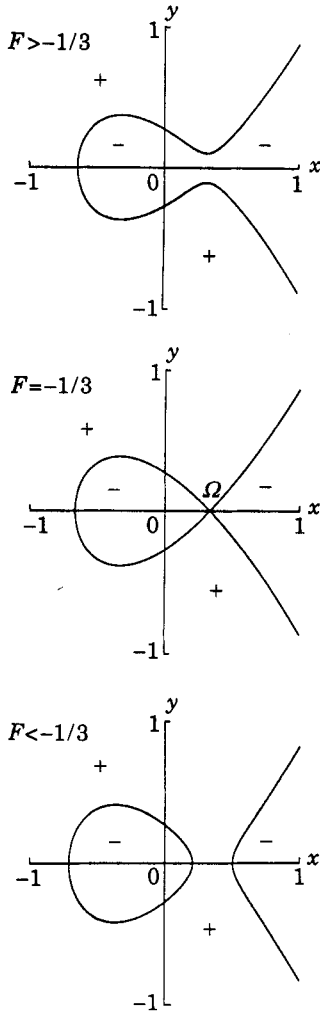


Fig. 1.

Fig. 1. - Nodal pattern of the wave function ψ , eq. (1). The three different regimes depending on parameter F are shown. Ω is the singular point where the two nodal cells separate.

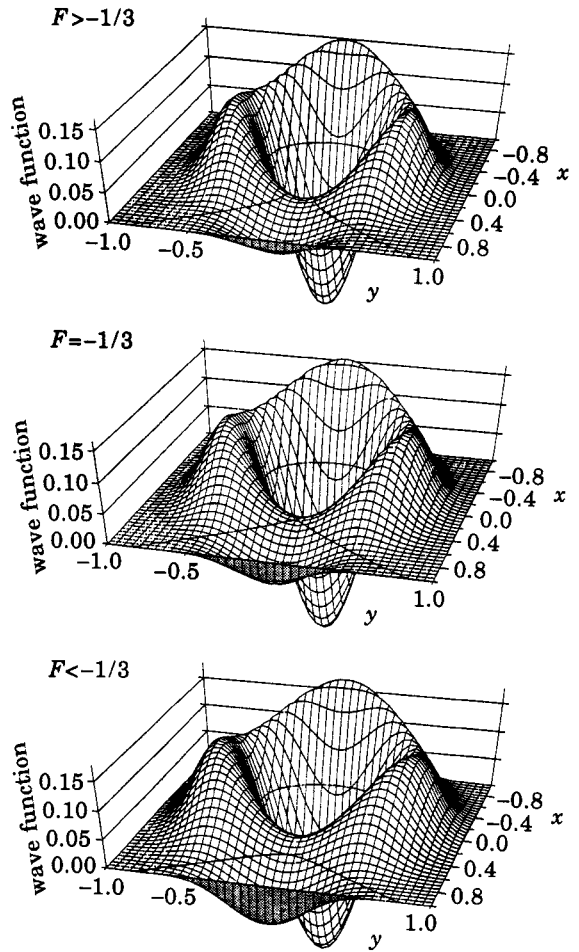


Fig. 2.

Fig. 2. - Plot of the wave function ψ (see table II). Note the zero contour line reproducing the nodes.

exhibiting the nonconservation property is that F , while varying λ , goes through the critical value of $-1/3$. To summarize, we present the potential energy function and its excited eigenfunction of energy E in tables I and II, respectively. In fig. 2 the wave function is drawn for the three different nodal regimes. Figure 3 presents the potential energy function at the critical value $F = -1/3$. No qualitative changes occur at other values of parameter F . Finally, we would like to point out that the solution obtained is a nondegenerate one. To see this, we have performed a careful variational calculation of the lowest eigenvalues by diagonalizing H using a large Hermite-Gaussian basis set. Results are presented in fig. 4. They indicate that the eigenfunction just constructed is nondegenerate (note that a crossing

TABLE I. - Potential energy function of the coupled anharmonic oscillators: $V(x, y) = \sum_{i+j \leq 6} c_{ij} x^i y^j$. Here $P \equiv F^2 - F/3 + 1/9$.

$$c_{00} = E + \frac{63F}{8P} + \frac{3}{8PF} - \frac{3}{2F} + \frac{1}{2F^2} + \frac{1}{18P^2}$$

$$c_{10} = \frac{21}{2P} + \frac{1}{3PF^2} - \frac{3}{F^2} + \frac{3F}{2P^2} + \frac{1}{9FP^2} - \frac{1}{PF}$$

$$c_{20} = \frac{75}{8PF} + \frac{2}{P^2} + \frac{81F^2}{8P^2} - \frac{27}{2P} + \frac{1}{18P^2F^2} - \frac{1}{PF^2} + \frac{9}{2F^2}$$

$$c_{30} = \frac{3}{2PF^2} + \frac{1}{FP^2} + \frac{27F}{4P^2} - \frac{9}{2PF}$$

$$c_{40} = \frac{63}{8P^2} + \frac{1}{2P^2F^2} - \frac{9}{2PF^2}$$

$$c_{50} = \frac{9}{4P^2F}$$

$$c_{60} = \frac{9}{8F^2P^2}$$

$$c_{02} = \frac{1}{32P^2F^2} - \frac{9}{16P^2} + \frac{81F^2}{32P^2} + \frac{207}{16PF}$$

$$c_{04} = \frac{243}{32P^2} - \frac{27}{32P^2F^2}$$

$$c_{06} = \frac{729}{128F^2P^2}$$

$$c_{12} = \frac{9}{4PF^2} + \frac{3}{4FP^2}$$

$$c_{22} = \frac{243}{16P^2} + \frac{3}{16P^2F^2} - \frac{27}{4PF^2}$$

$$c_{32} = \frac{27}{8P^2F}$$

$$c_{42} = \frac{189}{32F^2P^2}$$

$$c_{24} = \frac{81}{8F^2P^2}$$

of levels of different symmetry, V is invariant under $y \rightarrow -y$, occurs just before the critical value) and is the 4th excited state of H in the subspace of even symmetry.

TABLE II. - *Eigenfunction of the coupled anharmonic oscillators: $P \equiv F^2 - F/3 + 1/9$.*

$$\psi(x, y, \lambda) = \left(y^2 - x^2 - Fx - \frac{2}{27} \right) \exp[-a_{10}x - a_{20}x^2 - a_{30}x^3 - a_{40}x^4 - a_{02}y^2 - a_{22}x^2y^2]$$

with

$$a_{10} = -\frac{1}{F} - \frac{1}{3P}$$

$$a_{20} = -\frac{9F}{4P} - \frac{1}{6PF} + \frac{3}{2F}$$

$$a_{30} = -\frac{1}{2P}$$

$$a_{40} = -\frac{3}{8PF}$$

$$a_{02} = \frac{1}{8PF} - \frac{9F}{8P}$$

$$a_{04} = -\frac{27}{32PF}$$

$$a_{22} = -\frac{9}{8PF}$$

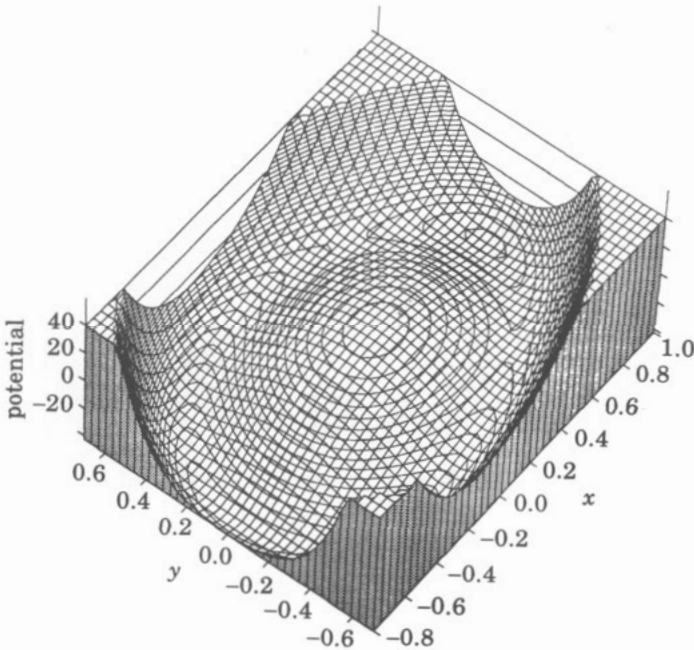


Fig. 3.

Fig. 3. - Plot of the potential energy function for $F = -1/3$. Other values of F give a similar shape.

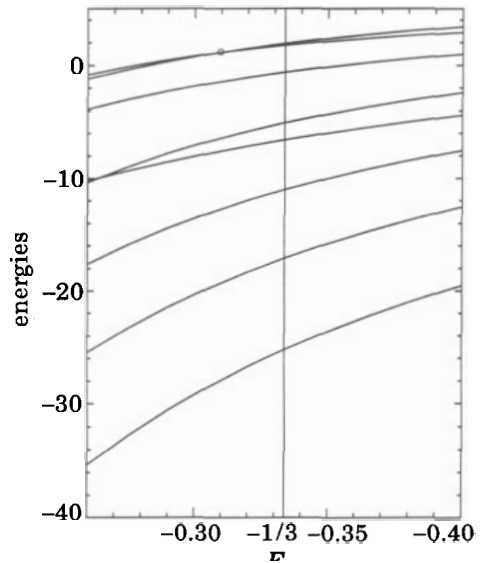


Fig. 4.

Fig. 4. - Low-lying energies of potential V (table I) vs. F (the arbitrary coefficient c_{00} of V being set to zero). The constructed wave function ψ is the 8th level when $F > -0.31$ and the 7th for smaller values. Crossing of the two energy curves (of different symmetries) is indicated by an open circle.

* * *

We would like to acknowledge a fruitful discussion with Prof. D. R. SALAHUB (Montreal) on how to get a new nodal cell by deforming a line. We are grateful to L.-H. JOLLY (Paris) for his valuable technical help at different stages of this work. Analytical calculations presented in this work have been performed by using the symbolic computation programme MAPLE (University of Waterloo, Canada). Finally, we would like to thank the «Centre National de la Recherche Scientifique» (CNRS) and the «Ministère de l'Éducation Nationale» (MEN) for their priceless support.

REFERENCES

- [1] KORSCH H. J., *Phys. Lett. A*, **97** (1983) 77.
- [2] COURANT R. and HILBERT D., *Methoden der mathematischen Physik I* (Springer, Berlin) 1930.
- [3] UHLENBECK K., *Am. J. Math.*, **98** (1976) 1059.
- [4] ALBERT J. H., *Trans. Am. Math. Soc.*, **238** (1978) 341.
- [5] PECHUKAS P., *J. Chem. Phys.*, **57** (1972) 5577.
- [6] BRÜNING J., *Math. Z.*, **124** (1972) 79.
- [7] ROBNIK M., *Phys. Lett. A*, **80** (1980) 117.
- [8] ROBNIK M., *J. Phys. A*, **14** (1981) 3195.
- [9] BERRY M. V. and WILKINSON M., *Proc. R. Soc. London, Ser. A*, **392** (1984) 15.
- [10] BERRY M. V., in *Chaotic Behaviour of Deterministic Systems, Les Houches Summer School Lectures*, edited by R. H. G. HELLEMAN and G. IOOSS, Vol. **36** (North-Holland, Amsterdam) 1983.
- [11] GUTZWILLER M. C., in *Chaos in Classical Mechanics* (Springer-Verlag) 1990, Chapt. 15.
- [12] CAFFAREL M., CLAVERIE P., MIJOLE C., ANDZELM J. and SALAHUB D. R., *J. Chem. Phys.*, **90** (1989) 990.

- I. M. Caffarel and D.M. Ceperley, "A Bayesian Analysis of Green's Function Monte Carlo Correlation Functions", *J. Chem. Phys.* **97**, 8415 (1992)

A Bayesian analysis of Green's function Monte Carlo correlation functions

M. Caffarel^(a) and D. M. Ceperley

Department of Physics and National Center for Supercomputing Applications, University of Illinois at Urbana-Champaign, Urbana, Illinois 61801

(Received 20 April 1992; accepted 18 August 1992)

Imaginary-time correlation functions calculated by quantum Monte Carlo (QMC) are analyzed using the maximum entropy method (MaxEnt) to determine the ground-state energy and spectral overlap function. In contrast to earlier applications of MaxEnt, the data is obtained from importance-sampled zero-temperature quantum Monte Carlo simulations. The analysis includes two steps. First, that spectral overlap function and ground state energy which maximizes the entropy and agrees with the QMC correlation functions is obtained. Then the errors in the energy are evaluated by averaging over all the possible images (average MaxEnt method), the multidimensional integrals being computed using the Metropolis algorithm. The central feature of this approach is that all the information present in the correlation functions is used in the only way consistent with fundamental probabilistic hypotheses. This allows us to fully exploit the information contained in the correlation functions at small imaginary times, thus avoiding large statistical fluctuations associated with large imaginary times. In addition, the computed errors include both the statistical errors and systematic extrapolation errors. The method is illustrated with a harmonic oscillator and the four-electron LiH molecule.

I. INTRODUCTION

It is known to be very difficult to solve the Schrödinger equation for fermion systems with a Monte Carlo procedure because of the "sign problem." This problem arises because Fermi averages decompose into a difference of contributions corresponding to even and odd permutations of the particle labels. At large imaginary times, these contributions nearly cancel and become exponentially smaller than the statistical error, but large times are needed to project out from the trial wave function excited state components. The increased variance coming from the cancellations at large times will be greatly reduced by exploiting more fully all the information present in data at small times. In any case, it is important to estimate not only the statistical errors, but the systematic errors resulting from stopping the calculation at a fixed projection time. These same issues are involved in computing the energy of any excited state, not just the Fermion ground state.

In a previous work,¹ we have shown that the usual methods of calculating the energy are not optimal. More specifically, using a variation of the Lanczós algorithm for QMC, we have shown that the ground-state energy could be recovered from fixed-node or released-node data computed at smaller imaginary times. However, there is no guarantee that the Lanczós method will use all the information present in the data and the stability of the algorithm with respect to statistical fluctuations is bad.

In this work, we present a general procedure for taking full advantage of the QMC data. In addition, this method allows one to evaluate error bars on the energies including systematic errors. The framework employed is Bayesian

probability theory and more specifically the maximum entropy (MaxEnt) method. Maximum entropy has been used in a wide variety of image reconstruction problems encountered in such different fields as astronomy, magnetic resonance imaging, neutron scattering, etc.² MaxEnt is a general and powerful technique for reconstructing positive images from noisy and incomplete data. Recently, several groups have applied this technique to extract dynamical information from imaginary-time quantum Monte Carlo Green's functions of lattice models,³⁻⁵ e.g., a single-impurity Anderson model.

Here, we propose to apply this method to data from electronic systems, calculated by zero-temperature quantum Monte Carlo. Although we shall also be concerned with extracting a spectral overlap, our main purpose is to estimate the ground-state energy. As explained before, our ultimate goal is to avoid the sign problem appearing at large times while still calculating converged results, both for the ground state of Fermion systems and for quantum excited states.

Let us briefly outline our approach. Quantum Monte Carlo can estimate imaginary-time correlation functions of the form

$$h(t) = \langle \Psi_T | e^{-tH} | \Psi_T \rangle, \quad (1)$$

where Ψ_T is a known antisymmetric trial function. This correlation function is related by a Laplace transform

$$h(t) = \int_{-\infty}^{+\infty} dE c(E) e^{-tE} \quad (2)$$

to the spectral overlap

$$c(E) = \sum_i \delta(E - E_i) | \langle \Psi_T | \Phi_i \rangle |^2, \quad (3)$$

^aOn leave from: Laboratoire Dynamique des Interactions Moléculaires, Université Paris VI, 75252 Paris Cedex 05, France.

where $\{E_p, \Phi_i\}$ are the i th exact eigenvalue and eigenfunction of H . In contrast to the usual spectral density, $c(E)$ includes the squared overlap between the trial function and the exact excited states. The use of a good trial function leads to very accurate estimates of the ground-state energy. Essentially, one is doing Monte Carlo only on the errors of the trial function.

The usual method of calculating the ground-state energy from $h(t)$ is to find its rate of decay at large time. Let the transient estimate energy be defined as

$$E_{TE}(t) = -\frac{d \ln[h(t)]}{dt} \quad (4)$$

Then

$$\lim_{t \rightarrow \infty} E_{TE}(t) = E_0. \quad (5)$$

It is this transient estimate which has an exponentially increasing signal-to-noise ratio at large time for a Fermion ground state.

The approach considered here is to regard Eq. (2) as an ill-conditioned inversion problem and ask what spectral overlaps are consistent with the noisy estimates of $h(t)$. Using Bayes' theorem, we postulate that the probability distribution of a given spectral overlap is

$$P(c|h, c^*) \propto P(h|c)P(c|c^*), \quad (6)$$

where the likelihood function $P(h|c)$ is the distribution of Monte Carlo errors given a spectral overlap and $P(c|c^*)$ is the prior probability of a given spectral overlap and may depend on an assumed model spectral function c^* . We will use an entropic form for this prior probability.

The proposed approach includes two steps. First, we maximize $P(c|h, c^*)$ with respect to c and thus determine the most likely overlap. This we will call the MaxEnt step. Then, to obtain a reliable estimate of the statistical errors, we sample possible overlaps with probability $P(c|h, c^*)$. This we will call the AvEnt step.

The organization of this paper is as follows: In Sec. II, the quantum Monte Carlo methods used in this work are discussed briefly. Section III is concerned with the general presentation of the proposed approach. In Sec. IV, the main ideas of the method and details of implementation are presented for a harmonic oscillator and in Sec. V, for the LiH molecule. Finally, some concluding remarks are made in Sec. VI.

II. THE QUANTUM MONTE CARLO METHODS

In this paper, we are concerned with quantum systems described by a Hamiltonian of the form

$$H = -\frac{1}{2} \sum_{i=1}^N \nabla_i^2 + V(\mathbf{r}_1, \dots, \mathbf{r}_N), \quad (7)$$

where \mathbf{r}_i is the position of the i th particle and $V(R)$ is the potential energy. Our analysis is based on the following three imaginary-time correlation functions:

$$h^{(k)}(t) = \langle \Psi_T | H^k O(t) | \Psi_T \rangle \quad (8)$$

where $k = \{0, 1, 2\}$, Ψ_T is the trial function, generally the best available computable approximate wave function known for the system under consideration, and the operator $O(t)$ is an evolution operator. Two forms for $O(t)$ are used for continuous systems; they define the two following algorithms:

(i) Diffusion Monte Carlo (DMC)

$$O(n\tau) = \exp[-n\tau(H - E_T)]; \quad (9)$$

(ii) Green's function Monte Carlo (GFMC)

$$O(n\tau) = [1 + \tau(\hat{H} - \hat{E}_T)]^{-n}. \quad (10)$$

Here E_T is the reference energy and τ is the time step.

In both approaches, time-correlation functions of Eq. (8) may be computed as averages over an ensemble of configurations (walkers) evolving in the $3N$ -dimensional configuration space according to some appropriate probabilistic rules. Since both methods will be used to compute the time-correlation functions $h^{(k)}(t)$, we shall give a brief description of each of them. For the complete description of the basic aspects of QMC techniques, the reader is referred to the original works.

A. Diffusion Monte Carlo (DMC)

In DMC, configurations advance according to three elementary processes—diffusion, drift, and branching. In fact, branching is not a necessary step in DMC since it may be taken into account by introducing weights in the correlation functions defined along the stochastic trajectories generated by diffusion and drift. In this case, the number of walkers remains constant and the notion of trajectory is identical with that used in a classical molecular dynamics simulation. In this "pure" DMC, the configurations advance from t to $t + \tau$ according to

$$f(\mathbf{R}', t + \tau) = \int d\mathbf{R} p(\mathbf{R} \rightarrow \mathbf{R}', \tau) f(\mathbf{R}, t), \quad (11)$$

where $f(\mathbf{R}, t)$ represents the density of configurations (walkers) at time t and $p(\mathbf{R} \rightarrow \mathbf{R}', \tau)$ is the transition probability density describing the drifted diffusion. In the short-time approximation, it has the form

$$p(\mathbf{R} \rightarrow \mathbf{R}', \tau) = \left(\frac{1}{2\pi\tau}\right)^{3N/2} \exp\{-[\mathbf{R}' - \mathbf{R} - \mathbf{b}(\mathbf{R})\tau]^2/2\tau\}, \quad (12)$$

where the drift is

$$\mathbf{b}(\mathbf{R}) = \nabla \ln(\Psi_G) \quad (13)$$

and Ψ_G a strictly positive function is a guiding (or importance) function used to increase the efficiency of the simulation by keeping the walk in important regions of phase space.

It is possible to show by iterating the relation (11), and by introducing at each iteration the weight factor $e^{-\tau E_L^G}$, where $E_L^G(\mathbf{R}) \equiv H\Psi_G(\mathbf{R})/\Psi_G$ is the local energy associated with Ψ_G , $h^{(k)}(t)$ may be estimated as

$$h^{(0)}(t) = I \left\langle w(0)w(t) \exp\left[-\int_0^t E_L^G(s) ds\right] \right\rangle_{\text{DRW}},$$

$$h^{(1)}(t) = I \left\langle w(0)w(t) \frac{1}{2} [E_L^T(0) + E_L^T(t)] \right. \\ \left. \times \exp \left[- \int_0^t E_L^G(s) ds \right] \right\rangle_{\text{DRW}},$$

and

$$h^{(2)}(t) = I \langle w(0)w(t) E_L^T(0) E_L^T(t) \rangle \\ \times \exp \left[- \int_0^t E_L^G(s) ds \right]_{\text{DRW}}, \quad (14)$$

where $w(R) \equiv \Psi_T / \Psi_G$ is a weight, $E_L^T(R) \equiv H\Psi_T / \Psi_T$ is the local energy associated with the trial function, $\langle \dots \rangle_{\text{DRW}}$ refers to the average over drifting random walks generated by Eqs. (11)–(13), and $I \equiv \int \Psi_G^2$ is a normalization constant which will eventually drop out. The practical evaluation of time-correlation functions from Eq. (14) is rather simple; for more details, the interested reader is referred to Ref. 6.

Note that when Ψ_G is chosen to be $|\Psi_T|$, drifting random walks generated via Eqs. (11)–(13) are trapped in subdomains of the configuration space delimited by the $(3N-1)$ -dimensional nodes of the trial wave function Ψ_T and no change of sign of the weight factors w occurs. This approach is called fixed-node approximation since the nodes are in general approximate. When Ψ_G is chosen to be strictly positive everywhere, no approximation is made, but the weights have no longer a definite sign for fermions. This exact, but unstable method will be referred to in the following as the transient method. More details about both approaches may be found elsewhere.^{6–9}

B. Green's function Monte Carlo (GFMC)

The Green's function Monte Carlo method is similar to the DMC method, but it does not have the time-step error inherent to DMC approaches. We will see that it is important to remove all systematic errors before using the Bayesian statistical analysis since otherwise these errors could be amplified. There exist different variants of GFMC; we shall use the formalism developed by Ceperley⁸ which is particularly convenient for particles interacting via a Coulombic force. Precise rules for diffusion, drift, and branching are described in the Ref. 8.

To compute the time correlation functions let us assume that \mathbf{R}_0 is a configuration distributed according to $\Psi_G^2(\mathbf{R}_0)/I$. Then assume that the set of configurations $\{\mathbf{R}_n^j\}$, with $1 \leq j \leq M(\mathbf{R}_0, n)$, are produced after n generations (applications of the evolution operator). Then

$$h^{(0)}(n\tau) = I \left\langle w(\mathbf{R}_0) \sum_{j=1}^{M(\mathbf{R}_0, n)} w(\mathbf{R}_n^j) \right\rangle. \quad (15)$$

The other correlation functions $h^{(1)}(t)$ and $h^{(2)}(t)$ are computed in a similar way.

The situation with respect to Fermi statistics is identical in GFMC and DMC. The fixed-node approximation is obtained when Ψ_G is chosen to be $|\Psi_T|$, and a transient approach corresponds to the use of a positive guiding function.

Here, we shall consider an additional exact approach, the released-node method,⁸ where the basic GFMC algorithm is used with an important difference. The initial configuration (denoted above as \mathbf{R}_0) comes from the output of a fixed-node calculation instead of a variational one. It should be emphasized that by so doing, slightly different matrix elements of the evolution operator are obtained, namely,

$$h^{(0)}(t) = \left\langle \Psi_T \left| \left[\frac{1}{1 + \tau(H - E_T)} \right]^n \right| \Phi_{\text{FN}} \right\rangle$$

and

$$h^{(1)}(t) = \left\langle \Psi_T \left| H \left[\frac{1}{1 + \tau(H - E_T)} \right]^n \right| \Phi_{\text{FN}} \right\rangle, \quad (16)$$

where Φ_{FN} stands for the “exact” fixed-node wave function. It is difficult to compute $h^{(2)}(t)$, since the analytical form for the result of the action of H on the fixed-node wave function is not known.

III. MAXIMUM ENTROPY ANALYSIS

In order not to repeat almost identical formulas for both DMC and GFMC data, we shall present the method only with DMC evolution [Eq. (9)], the extension to GFMC evolution [Eq. (10)] being straightforward.

The first step consists of realizing that the data $h^{(i)}(t)$ are related to the spectral overlap $c(E)$ via a linear transformation

$$h^{(k)}(t) = \int_{-\infty}^{+\infty} dE E^k c(E) e^{-t(E - E_T)}, \quad k=0,1,2, \quad (17)$$

where $c(E)$ has already been defined in Eq. (3). Now $c(E)$ exhibits a very sharp maximum at $E = E_0$ since Ψ_T is chosen as close as possible to the ground-state wave function Φ_0 . The “zero-variance” principle of (zero-temperature) quantum Monte Carlo states that as the trial function approaches an exact eigenfunction, the statistical variance vanishes. It is important to preserve this property in the MaxEnt analysis. This we do by requiring that the reconstruction fit both $h^{(0)}(t)$ and $h^{(1)}(t)$.

Now, our problem is the following: Having computed with QMC a set of data $\{h^{(0)}, h^{(1)}, h^{(2)}\}$ at different times t_k : $1 \leq k \leq M$ and estimated (via statistically independent calculations) the statistical errors of this data, we would like to find the “best” and the “average” spectral overlap $c(E)$ compatible—in a sense to be specified below—with our incomplete and noisy data. This problem is often encountered in image processing where noisy data are related to the quantity of interest—the image—by a linear transformation. A robust and coherent way of tackling this difficult problem is the maximum entropy method based on Bayesian logic. The essence of this approach is to look for the most probable function $c(E)$ compatible with the data and with any prior knowledge about $c(E)$.

For simplicity, we shall represent the data by using a single vector $h(t)$ as follows:

$$h(t_k) = h^{(0)}(t_k), \quad h(t_{k+M}) = h^{(1)}(t_k),$$

$$h(t_{k+2M}) = h^{(2)}(t_k) \quad (18)$$

and use a subscript C and F to distinguish between computed (QMC) data $h_C(t_k)$ and their corresponding fitted values $h_F(t_k)$ obtained via a representation of Eq. (17) in terms of a large (but finite) number of real exponentials

$$h_F^{(k)}(t) = \sum_{l=0}^P c_l E_l^k e^{-t(E_l - E_T)}, \quad (19)$$

where P is typically of the order of 200. The number of components and the spacing in energy are chosen to have a good representation of the integral in Eq. (17).

Now consider the first of the two probability functions in Bayes' theorem [Eq. (6)], the likelihood function. According to the central limit theorem [assuming that the variances of $w(R)$ and $w(R)E_L(R)$ exist] for sufficiently large simulation times, the probability of finding of a given QMC correlation function $h_C(t)$ will have a Gaussian distribution about its exact value $h_F(t)$;

$$P(h_C|c) \propto \exp(-\chi^2/2), \quad (20)$$

where

$$\chi^2 = \sum_{ij}^{3M} [h_F(t_i) - h_C(t_i)] C_{ij}^{-1} [h_F(t_j) - h_C(t_j)]. \quad (21)$$

Here C_{ij} is the covariance matrix defined by

$$C_{ij} = \langle h_C(t_i) h_C(t_j) \rangle - \langle h_C(t_i) \rangle \langle h_C(t_j) \rangle, \quad (22)$$

where the averages are over a set of statistically independent calculations. We have checked systematically that our QMC-calculated correlation functions obey Gaussian statistics.

Any image $c(E)$ [in practice, the finite number of coefficients c_l in Eq. (19)] with a χ^2 significantly greater than the number $3M$ of data points is improbable. The set of feasible images is defined as the set of images verifying

$$\chi^2 \sim \text{number of data points}. \quad (23)$$

Clearly, when the chi squared is significantly smaller than the number of data points, we are overfitting the data, and the resulting fit, which is essentially determined by the noise, should be excluded from the set of feasible images.

Now we need a criterion to pick up among all these feasible images. Many of the feasible images are physically impossible or improbable, e.g., those with a negative spectral overlap $C(E) < 0$. The role of the prior probability $P(c|c^*)$ is to filter out from all feasible images those that are very different from a default model containing any prior knowledge we have about the exact solution. It can be argued by using very general probabilistic concepts that for positive and additive images, there is a natural measure for that probability—the entropic form¹⁰

$$P(c|c^*) \propto \exp[\alpha S(c|c^*)], \quad (24)$$

where the entropy is

$$S = \sum_{l=0}^P c(E_l) - c^*(E_l) - c(E_l) \ln \frac{c(E_l)}{c^*(E_l)} \quad (25)$$

and $c^*(E)$ is a default spectral overlap which encapsulates all exact knowledge about the spectral overlap before adding in the information from QMC. One may question whether this entropic function is appropriate for the spectral overlap function of a small molecule, where the discreteness of the energy levels may be important. Two of its features are significant—it only allows overlaps with $c(E) > 0$ and it has a maximum at $c=c^*$.

The maximum entropy image is then defined as the image having a $\chi^2 \sim$ number of data and maximizing the entropy. Since both the χ^2 function and the entropy are convex functions, this image is defined uniquely. The parameter α controls the competition between S and χ^2 .

Since our goal is to have an accurate evaluation of the ground state energy E_0 , it is included in the set of fitting parameters. In practice, this means that we shall define our max entropy solution is the set $\{E_0, c_0, \dots, c_P\}$ maximizing S with the constraint that $\chi^2 \sim 3M$. In the Bayesian framework, the parameter α becomes an additional variable with its own prior distribution. Following standard practice,¹⁰ we use a probability distribution uniform in $\log(\alpha)$ and the MaxEnt optimization and AvEnt averages evaluated with $P(c|h, c^*)P(\alpha)$, where $P(\alpha) \propto 1/\alpha$ over some "sensible" range.

Once the MaxEnt spectral function has been determined, it is important to estimate the statistical and systematic error. For that, we look at a typical set of feasible images, sampled from $P(c|h, c^*)$ as defined from Eqs. (6), (21), and (24). Then the error on any component of the spectral density, say the ground-state energy, is

$$\delta E_0 = \sqrt{\langle (E_0 - \langle E_0 \rangle)^2 \rangle}, \quad (26)$$

where the averages are over $P(c|h, c^*)$. A similar formula may be written for the error of any coefficient c_l . This approach, which consists of integrating the fluctuations around the MaxEnt solution in the functional space of all possible images, is the average maximum entropy method.¹¹ The multidimensional integrals involved can be computed using the Metropolis algorithm.

The reader may be wondering why we have chosen to fit the three functions $h^{(k)}(t)$ rather than simply $h^{(0)}(t)$, since analytically $h^{(0)}(t)$ is equivalent. There are several reasons. In the pure DMC approach, if the trial function equals the guiding function, it is true that one could numerically differentiate $h^{(0)}(t)$ to obtain $h^{(1)}(t)$ and $h^{(2)}(t)$. In practice, this introduces systematic errors which cause the statistical analysis to become unreliable. In the more important case where the guiding function is not equal to the trial function, statistical fluctuations in the time derivative of $h^{(0)}(t)$ are different from those where $h^{(1)}(t)$ is computed directly. In fact, it is the very strong correlation between the fluctuations of $h^{(0)}(t)$ and $h^{(1)}(t)$ which lead to the zero variance property of QMC. It is clearly important to use both $h^{(0)}$ and $h^{(1)}$ in doing the statistical analysis, since it is in the correlation between these two functions that gives a low variance energy estimate.

Knowledge of all three correlation functions implies that the feasible images have values of the ground-state energy bounded from both above and below. The upper bound is given by the transient estimate energy and a lower bound by the Temple bound¹²

$$E_{\text{TE}}(t) - \frac{[h^{(2)}(t) - E_{\text{TE}}(t)]^2}{E_{\text{gap}}} < E_0 < E_{\text{TE}}(t), \quad (27)$$

where E_{gap} is the gap to the next state of the same symmetry. Note that these upper and lower bounds squeeze in the exact energy exponentially fast in t because the energy E_{TE} of the projected trial function $e^{-iH/2}\Psi_T$ converges exponentially fast to the ground state. Now the spread in ground-state energies for feasible images will be smaller than the bounds in the above inequalities because we are asking that the spectral overlap and energy fit the Monte Carlo data at many times simultaneously. For example, the results of the Lanczós method, described below, give tighter upper bounds than the transient estimate energy using the same functions $h^{(0)}(t)$ and $h^{(1)}(t)$.

The fact that the fitting gives tighter energy bounds is only one of the reasons to use this approach. It is perhaps more important that the information in the correlation functions is combined in a statistically robust way. The error bars on the correlation functions are all exponentially increasing in time. Thus it is important to strongly weight the small time data. Bayesian statistics provides a systematic framework for balancing the statistically accurate, but biased data at short times with the noisy, but more converged data at large times.

IV. APPLICATION TO THE HARMONIC OSCILLATOR

In this section, we apply our approach to the Hamiltonian

$$H = -\frac{1}{2} \frac{d^2}{dx^2} + \frac{1}{2} x^2 + \gamma x, \quad (28)$$

where γ is some constant defining the magnitude of the linear perturbation. By using the Green's function Monte Carlo method presented in Sec. II B, we calculate the time-correlation functions with a trial wave function Ψ_T chosen to be the ground-state wave function of the unperturbed ($\gamma=0$) harmonic oscillator

$$\Psi_T \sim e^{-x^2/2} \quad (29)$$

and $\Psi_G = \Psi_T$. Then one can show

$$h^{(i)}(n\tau) = e^{-\gamma^2/2} \sum_{k=0}^{\infty} \frac{1}{k} \left(\frac{\gamma^2}{2}\right)^k (k + E_0)^i \left(\frac{1}{1+k\tau}\right)^n \quad (30)$$

when the reference energy is equal to the ground-state energy $E_T = (1/2) - (\gamma^2/2)$. We have performed a GFMC calculation using the time-dependent Green's function of the unperturbed harmonic oscillator as trial Green's function.

The upper curve of Fig. 1 shows the transient energy $E_{\text{TE}}(t)$. The open circles are the QMC results, to be compared with the solid line representing the analytical results

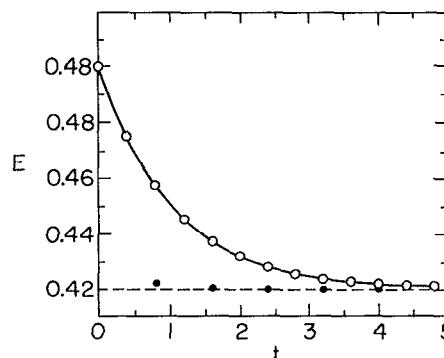


FIG. 1. Energy as a function of the projecting time for the harmonic oscillator. The solid line is the exact transient estimate energy from Eq. (30); the open circles are $E_{\text{TE}}(t)$ from QMC. Results obtained from a Lanczós-type analysis are shown by the filled circles and t labels the amount of data used in the analysis. The dashed line shows the exact ground-state energy.

obtained from Eq. (30). The agreement between exact and computed values is excellent.

The lower curve gives the result of a Lanczós-type analysis using the *same* data. The Lanczós algorithm used here has been presented elsewhere¹ and may be summarized as follows: Consider the following projected trial wave function at some given time $t_p = p\tau$:

$$\tilde{\Psi}_T(t_p) = \left[\frac{1}{1 + \tau(H - E_T)} \right]^p \Psi_T. \quad (31)$$

The overlap and Hamiltonian matrix elements between any two such states, say, at times t_p and t_q may be expressed in terms of the time-correlation functions $h^{(0)}$ and $h^{(1)}$. We have

$$\begin{aligned} \langle \tilde{\Psi}_T(t_p) | \tilde{\Psi}_T(t_q) \rangle &= h^{(0)}(t_p + t_q), \\ \langle \tilde{\Psi}_T(t_p) | H | \tilde{\Psi}_T(t_q) \rangle &= h^{(1)}(t_p + t_q). \end{aligned} \quad (32)$$

Having computed all the time-correlation functions $h^{(i)}$ up to a given maximum time t , we consider the generalized eigenvalue problem defined in the basis set consisting of all of the projected trial wave functions defined at different times with $t_i \leq t/2$. By doing this, tighter upper bounds are obtained from the QMC data than from the transient estimate energy since more variational freedom is introduced. One is constructing the best linear combination of the projected trial wave function defined at different times $\sum_k c_k \tilde{\Psi}_T(t_k)$. One sees from Fig. 1 that the exact result is obtained almost immediately from the “short-time” information. However, this procedure, based on a nonlinear relation between QMC correlation functions and the energy, is unstable with respect to statistical errors.

Because of the discrete nature of the energy levels of the oscillator, we represent the spectral overlap by a sum of delta functions

$$c^*(E) = \sum_{i=0}^{P-1} \delta(E - E_i) c_i^*. \quad (33)$$

TABLE I. Maximum entropy analysis for the harmonic oscillator.

	$c^*(E)$	Most probable $c(E)$	Average $c(E)$	Exact $c(E)$
E_0	0.500	0.419 8	0.419 9(2)	0.420 00
c_0	0.900	0.923 21	0.923 2(2)	0.923 12
c_1	0.025	0.073 78	0.073 8(1)	0.073 85
c_2	0.025	0.003 13	0.003 10(5)	0.002 95
c_3	0.025	0	0	7.8×10^{-5}
c_4	0.025	0	0	1.5×10^{-6}

The coefficient representing the ground state is by far the largest since the overlap between the trial wave function and the ground state has been optimized. The energies E_i for $i > 1$ could be incorporated into the fitting procedure, but for simplicity in this model, we only optimized the location of the main peak corresponding to the ground-state energy E_0 . The other energies were fixed at their exact value. In applications to many-electron systems with a quasicontinuum of excited states, the assumption of a uniform grid in energy is more appropriate.

We assumed a "flat" default model, i.e., a model in which a uniform weight is used for the excited peaks. It is essential to introduce in the default model the fact that there is a very dominant peak close to the variational energy, but its precise magnitude does not matter. Once the magnitude of this peak has been chosen (we have taken 0.9), the common magnitude of the other peaks is chosen uniformly

$$\sum_{i=0}^{P-1} c_i^* = h^{(0)}(0) = 1. \quad (34)$$

In our numerical applications, we have chosen $P=5$ and therefore $c_i^* = 0.025$ (for $i > 0$). We have then used the GFMC method to calculate the values of $h^{(0)}(t)$, $h^{(1)}(t)$, and $h^{(2)}(t)$ at the 13 times shown in Fig. 1.

A very important point to notice is that the transient estimate of the ground-state energy is a relatively smooth function of time despite the stochastic nature of its evaluation. This is due to the fact that we use a common set of random walks to compute the correlation functions at different times. In other words, all the QMC data on which we base our analysis are highly correlated. It is essential to include this correlation between the data in calculating the χ^2 . In fact, when we tried to perform the MaxEnt analysis neglecting this correlation, the resulting ground-state energy was systematically biased because of a tendency to fit the noise. Therefore, our first step consists of performing a singular value decomposition of the covariance matrix C_{ij} to determine the degree of correlation between data and to discard those eigenvalues with singular values less than the computer's precision 10^{-16} . For the case shown in Fig. 1, 12 eigenvectors are kept out of 39 original data points.

The maximum entropy solution is given in Table I. It is remarkable that the analysis succeeds in reproducing accurately the magnitude of the first three peaks. The error bars have been obtained by averaging over the probability distribution of feasible images. This simple example illustrates the feasibility of this approach on an exact model.

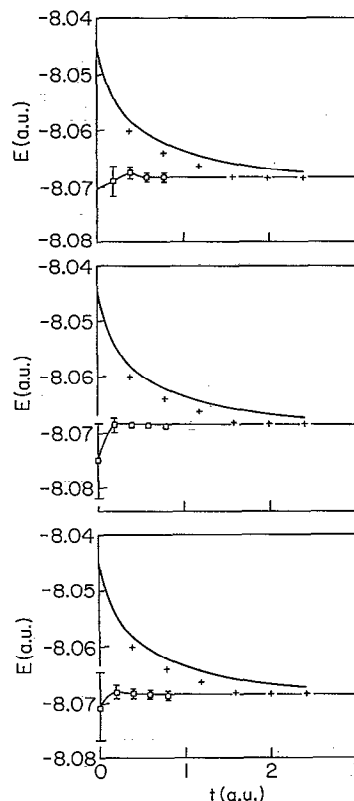


FIG. 2. Fixed node energy as a function of the projecting time t for LiH. The upper curve of the three pictures is $E_{TE}(t)$ and '+'s are the Lanczós results. The lower curve of the first picture represents the average MaxEnt results obtained from the time-correlation function $h^{(0)}(t')$ only using the data $t' < t$. The second picture gives the result obtained with $h^{(0)}$ and $h^{(1)}$ and the third with $h^{(0)}$, $h^{(1)}$, and $h^{(2)}$. The solid horizontal line indicates the fixed-node energy.

V. A REALISTIC APPLICATION: THE LIH MOLECULE

Let us now apply the maximum entropy ideas to the determination of the ground-state energy of the LiH molecule. We begin with the fixed-node, pure DMC method of Sec. II A. In the calculations below, the Li and H ions were fixed with a bond length of 3.015 bohr, the trial wave function was Ψ_{II} of Ref. 13, and the guiding function from Ref. 8. The exact electronic energy, corrected from zero-point and relativistic effects, is estimated at -8.07023 hartrees. This number is computed by adding together the nonrelativistic energies of Li and H atoms,¹⁴ subtracting the experimental binding energy of the molecule,¹⁵ and the zero point energy of LiH. This experimental number is lower than a modern configuration interaction (CI) calculation¹⁶ (which obtained an energy of -8.06904 hartrees) by 1.2 mhartrees.

A. Fixed node approach

The Monte Carlo data input to the Bayesian analysis consist of a set of 13 values for each correlation function $h^{(i)}(t)$ ($i=0,1,2$) starting at $t=0$ and uniformly distributed with a spacing of $\delta t=0.2$ a.u. The upper curve of Fig. 2(a) [upper curves of Figs. 2(a)–2(c) are all identical] shows the transient energy $E_{TE}(t)$. Because the fixed-node

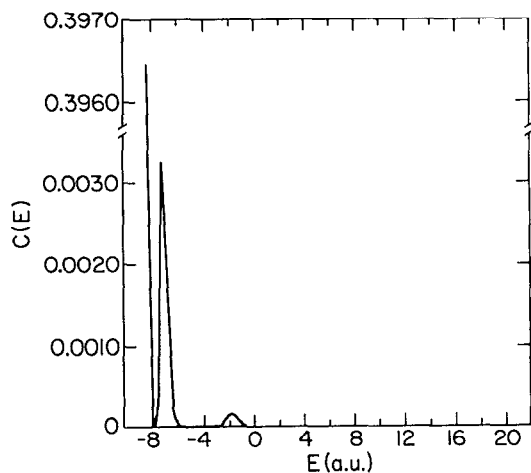


FIG. 3. Fixed node spectral overlap for LiH using all the Monte Carlo data.

method is stable, one can extend this curve until the transient energy has converged. This occurs for times on the order of 3–4 a.u., where it reaches the value of $-8.0680(6)$ (represented by the horizontal solid line). This is higher than the exact energy because the assumed nodes of the trial function are not correct. We also show the Lanczós results [Figs. 2(a)–2(c), “+”s] obtained by using a two-dimensional basis set consisting of $\Psi_T(0)$ and $\Psi_T(n\tau)$ with $n=1, \dots, 6$. The convergence of the Lanczós energy is faster than that of the transient energy.

We have used a flat model for the spectral overlap, but in order to represent the continuum of states present, it was necessary to use a large number of fixed energies. P in Eq. (19) was on the order of a few hundreds. The spacing between these peaks needed to describe the details of the spectral overlap was found to be 0.1 a.u. In order to get a good fit to the data, energies up to 20 a.u. were included. Only the ground-state energy was varied in the analysis; the other energies (but not the spectral overlaps) were fixed. We note that one can prove by considering the existence of the integrals $\int \Psi_T H_m \Psi_T = \int dE E^m c(E)$ that the spectral overlap for a trial function of a Coulombic interaction will decay as $O(E^{-k})$ at large energies where the exponent k depends on whether the trial function has the correct two-particle cusp condition. We have chosen not to use this additional analytic prior information in our analysis. Indeed, our results are insensitive to the default model.

Figure 3 presents the maximum entropy spectral overlap obtained when all the data available [$h^{(0)}(t_i)$, $h^{(1)}(t_i)$, and $h^{(2)}(t_i)$ for $i=1-13$] are used. We see clearly besides the very dominant peak associated with the ground state, a structure for the excited states. More precisely, a second peak is seen ~ -7 a.u. as well as a smaller peak ~ -2 a.u. Note that the location of the first peak is in agreement with the estimate of the gap in energy which can be obtained from the exponential decay of the transient estimate curve of Fig. 2(a). This gap does not represent the first excited state, which is much smaller, but represents the lowest

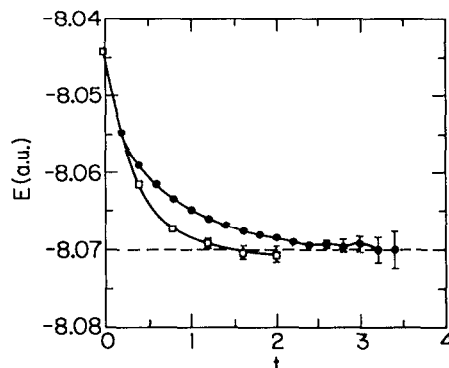


FIG. 4. Transient estimate energy (filled circles) and Lanczós energies (open squares) for LiH. The dashed line indicates the exact energy.

excited state having a large overlap with the trial wave function. The small peak at an energy of -2 a.u., which is always present in our analysis, represents a nontrivial feature of $c(E)$.

The lower curves of Figs. 2 (squares with error bars) show the dependence of the estimated ground-state energy on the quantity of information available. For example, at $t=0.2$ [Fig. 2(a)], we use only $h^{(0)}(0.2)$, perform the fit, and calculate errors. Obviously, the quantity of information is very limited and the error bar obtained on the energy is therefore large. Nonetheless, the error bars overlap with the exact result. Then, we incorporate the next value $h^{(0)}(2\tau)$, etc. The convergence is very rapid. Figures 2(b) and 2(c) show how the information contained in $h^{(1)}$ and $h^{(2)}$ affects the estimated energy and errors. The convergence is much enhanced, particularly at the very short times for which any additional information improves our knowledge of the ground-state energy substantially. However, we also see when convergence is reached, at approximately 1 a.u., introducing more data does not significantly reduce the error bars since little additional information is contained in the correlation functions. The only way of decreasing this error bar would be to decrease the statistical errors on the data by making a much longer Monte Carlo run.

In this example, the trial function was chosen equal to the guiding function which implies that the information in $h^{(1)}$ and $h^{(2)}$ is essentially present in $h^{(0)}$. Hence there is not a rapid decrease in errors bars as $h^{(1)}$ and $h^{(2)}$ are added to the analysis.

B. Transient method

We have computed the correlation functions using a strictly positive guiding function, thus removing the fixed-node restriction. The results in this section were done with the pure diffusion Monte Carlo scheme presented in Sec. II A. The upper curve of Fig. 4 reproduces the convergence of the transient estimate energy $E_{TE}(t)$. The sign problem is evident for $t \approx 2.0$ a.u. The lower curve shows the results obtained by using the Lanczós algorithm for these data. In contrast to the fixed-node case for which the MaxEnt analysis was successful, we encountered some se-

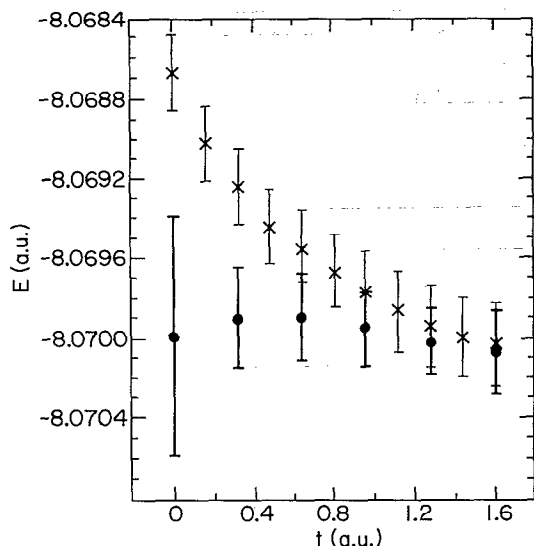


FIG. 5. Released-node energy as a function of the projecting time for LiH. The upper curve (X) is E_{TE} . The average MaxEnt results are given by filled circles. Note the expanded scale.

rious problems in doing the analysis for the transient data. Indeed, we found that the analysis is very sensitive to systematic time-step errors in the data. Very small time steps are required to obtain a time step-independent image. Unfortunately, in that case, the corresponding total simulation time (roughly, the number of MC steps multiplied by the time step) is too short to give reliable QMC data.

C. Nodal-release approach

To avoid the time-step errors and to speed up the convergence in imaginary time, we used the GFMC method with released node where one starts from the fixed-node output $\Psi_T\Psi_{FN}$ as initial population instead of the transient method which starts from Ψ_T^2 . This means that we compute slightly different matrix elements of the evolution operator and that

$$c(E) = \sum_i \delta(E - E_i) \langle \Psi_T | \Phi_i \rangle \langle \Phi_i | \Phi_{FN} \rangle \quad (35)$$

is not necessarily positive. However, since the trial wave function Ψ_T is chosen quite close to the fixed-node solution, it is likely that significant values of $c(E)$ are positive and we continued to use the entropic prior function. We are currently investigating a more rigorous prior function which will be needed to extend this analysis to excited state energies.

The transient energy is shown as the upper curve (X) of Fig. 5. The Bayesian results are given by filled circles. Since there is no simple way of computing the correlation function $h^{(2)}(t)$, the fit only includes $h^{(0)}$ and $h^{(1)}$. We see that the convergence of the MaxEnt solution is very rapid and leads to a stable solution without going to large projecting times. We get a very accurate value of -8.0700 ± 0.0002 for the ground-state energy. In contrast to previous calculations, our errors include both statistical errors

and systematic errors. The only uncontrolled systematic error arises from the assumption of the prior probability. Our result is 0.23 ± 0.2 mhartree above the experimental result.

VI. CONCLUSIONS

In this paper, we have presented an application of Bayesian statistics to the determination of the ground-state energy of quantum systems. We analyze time-correlation functions obtained from zero-temperature quantum Monte Carlo calculations (projector methods) to obtain the spectral overlap function of a given trial function. This spectral overlap contains a dominant peak at the ground state and small components at higher energies. It has been found that the default model appearing in the prior probability does not play a role as important as in other applications, so a flat model for the density of excited states is sufficient. In order to calculate the ground-state energy, we considered the location of the main peak as a parameter to be optimized. By using a chi-squared likelihood function and an entropic prior function, we have computed the average and the dispersion of the estimator of the energy (average maximum entropy) with the Metropolis method. In that way, a reliable estimate of the errors is obtained. Our numerical applications have demonstrated the efficiency of this approach for simple problems, e.g., the LiH molecule treated with the fixed-node method. However, the situation is a little more difficult when real Fermion data (data exhibiting the sign problem) are analyzed. In particular, we found that the maximum entropy analysis for LiH was very sensitive to systematic errors such as the finite time-step error. By using a GFMC scheme free of systematic error and a released-node approach starting from an initial fixed-node population, we demonstrated feasibility of the method on the four-electron LiH molecule. It is not yet clear how this method will scale with the number of Fermions, but this way of analyzing the correlation functions is guaranteed to be better than the transient estimate method, simply because all information generated in the QMC is used.

The Bayesian approach also appears to provide a way of calculating excited state properties with quantum Monte Carlo. Our previous work¹⁷ has used a generalization of the transient estimate method and was bedeviled with instabilities coming from statistical fluctuations. The approach considered here is the most general way of treating systematic and statistical errors and uses all information in the correlation functions. At present, we are testing various choices for the nonpositive prior functions needed for excited states. Applications to these more difficult problems will determine the usefulness and generality of this type of analysis.

ACKNOWLEDGMENTS

This work was supported by the National Science Foundation through grant number NSF DMR88-08126 by the Department of Physics at the University of Illinois, by the National Center for Supercomputing Applications, by

NATO, and by the CNRS. The computational aspects of this work used the CRAY-YMP at the National Center for Supercomputing Applications.

- ¹M. Caffarel, F. X. Gadea, and D. M. Ceperley, *Europhys. Lett.* **16**, 249 (1991).
- ²S. F. Gull and J. Skilling, *IEEE Proc.* **131**, 646 (1984).
- ³R. N. Silver, D. S. Sivia, and J. E. Gubernatis, *Phys. Rev. B* **41**, 2380 (1990).
- ⁴R. N. Silver, J. E. Gubernatis, D. S. Sivia, and M. Jarrell, in *Condensed Matter Theories 6*, edited by S. Fantoni and A. Fabrocini (Plenum, New York, 1991), pp. 189–202.
- ⁵J. E. Gubernatis, M. Jarrell, R. N. Silver, and D. S. Sivia, *Phys. Rev. B* **44**, 6011 (1991).
- ⁶M. Caffarel and P. Claverie, *J. Stat. Phys.* **43**, 797 (1986); *J. Chem. Phys.* **88**, 1088 (1988); **88**, 1100 (1988).
- ⁷M. H. Kalos, in *Monte Carlo Methods in Quantum Problems, NATO ASI Series C* (Reidel, Dordrecht, 1982).
- ⁸D. M. Ceperley, *J. Comp. Phys.* **51**, 404 (1983), D. M. Ceperley and B. J. Alder, *J. Chem. Phys.* **64**, 5833 (1984).
- ⁹K. E. Schmidt and M. H. Kalos in *Monte Carlo Methods in Statistical Physics*, edited by K. Binder (Springer, Berlin, 1984).
- ¹⁰J. Skilling and S. F. Gull, MaxEnt Conference SAMS-SIAM, 1988.
- ¹¹S. R. White (unpublished).
- ¹²G. Temple, *Proc. R. Soc. London, Ser. A* **119**, 22 (1928).
- ¹³P. J. Reynolds, D. M. Ceperley, B. J. Alder, and W. A. Lester, *J. Chem. Phys.* **77**, 5593 (1982).
- ¹⁴C. F. Bunge, *Phys. Rev. A* **16**, 2496 (1977).
- ¹⁵K. Huber and G. Herzberg, *Constants of Diatomic Molecules* (Van Nostrand, New York, 1979).
- ¹⁶N. C. Handy, R. J. Harrison, P. J. Knowles, and H. F. Schaefer III, *J. Phys. Chem.* **88**, 4852 (1984). We have corrected the estimate of the experimental LiH energy by the exact energy of an isolated H atom, $-0.499\,73$ a.u.
- ¹⁷D. M. Ceperley and B. Bernu, *J. Chem. Phys.* **89**, 6316 (1988); B. Bernu, D. M. Ceperley, and W. A. Lester, *ibid.* **93**, 552 (1990).

J. M. Caffarel, M. Rérat, and C. Pouchan, “Evaluating Dynamic Multipole Polarizabilities and van Der Waals Dispersion Coefficients of two-electron Systems with a Quantum Monte Carlo Calculation: A Comparison with some *Ab Initio* Calculations”, *Phys. Rev. A* 47, 3704 (1993)

Evaluating dynamic multipole polarizabilities and van der Waals dispersion coefficients of two-electron systems with a quantum Monte Carlo calculation: A comparison with some *ab initio* calculations

Michel Caffarel

*Laboratoire Dynamique des Interactions Moléculaires, Université Paris VI,
Tour 22, 4 place Jussieu, 75252 Paris CEDEX 05, France*

Michel Rérat and Claude Pouchan

Laboratoire de Chimie Structurale, Université de Pau, 64000 Pau, France

(Received 14 September 1992)

We present some systematic calculations of dynamic multipole polarizabilities and van der Waals dispersion coefficients for the helium atom and H_2 molecule with a quantum Monte Carlo calculation. Using an original method based on a gauge-invariant formalism we also report some *ab initio* results of the same quantities. In light of the results we discuss the advantages and drawbacks of both approaches in comparison to prior theoretical results.

PACS number(s): 31.20.Di, 31.90.+s

I. INTRODUCTION

Dynamic multipole polarizabilities determine a number of properties of systems interacting with external electric fields. In particular, they can be closely related to the van der Waals dispersion coefficients that describe the long-range interaction of atoms and molecules. It is well known that such quantities which formally involve all the excited states of the system (both the discrete and continuous part of the spectrum) are very difficult to evaluate with accuracy. To illustrate this, it is quite instructive to point out that, for the rather elementary case of the helium atom, it is only in 1976 that Glover and Weinhold [1] were able to determine some high-quality upper and lower bounds of the dynamic dipole polarizabilities; more interestingly, these bounds were tight enough to rule out the majority of previous theoretical and experimental predictions.

A number of approaches based on *ab initio* methods has been devised to obtain dynamic polarizabilities. Among the numerous *ab initio* models currently in use (corresponding to various levels of accuracy) we may cite the self-consistent-field configuration-interaction (SCF-CI) and the full-configuration-interaction (FCI) methods [2–4], the multiconfigurational time-dependent Hartree-Fock or multiconfigurational linear response (MCTDHF and MCLR) [5, 6], the random phase approximation (RPA) [7], or the more elaborate second-order polarization propagator approximation (SOPPA) [8, 9], and a time-dependent gauge-invariant (TDGI) method introducing a dipole-moment factor in the SCF-CI approximation [10–13].

Very recently, Caffarel and Hess have presented a method of computing response properties with quantum Monte Carlo (QMC) [14]. Basically, this scheme relies on the possibility of connecting the imaginary-time-dependent dynamics of the unperturbed system (the

time-dependent Green's function closely related to quantum response properties) with the transition probability density of a diffusion process. As a consequence, the usual perturbational components of the Rayleigh-Schrödinger perturbation theory may be expressed in a natural way in terms of stochastic correlation functions of the perturbing potential. These correlation functions are then computed from random walks in configuration space generated using the transition probability density (Langevin techniques). The salient features of this approach will be presented with some detail in Sec. II. It is interesting to note that such a scheme is formally very similar to that of standard molecular dynamics, except that Newtonian trajectories are replaced here by Brownian trajectories (mimicking the "diffuse" character of quantum mechanics).

The chief advantage of the QMC approach with respect to *ab initio* schemes is that no basis expansion nor explicit summation over a large, but necessarily incomplete, set of basis functions are introduced. It is, of course, a fundamental property of QMC, considering the importance of such aspects in *ab initio* schemes. Other original features include the possibility of computing several response properties (e.g., dipole, quadrupole, octopole, etc., components) in *one single* Monte Carlo run; the possibility of having a rigorous estimation of the error bars on results (a difficult task for *ab initio* methods); the very favorable computational aspects of QMC (memory requirements are perfectly bounded—no calculation and storage of huge numbers of bielectronic integrals; the computer codes are short, simple and very well suited for vector and parallel computing), etc. All these aspects will be illustrated in this paper.

The quantum Monte Carlo perturbation formalism has been first applied to the problem of the interaction of two helium atoms at short distances [14]. Some preliminary calculations concerning the dynamic dipole polar-

izability of helium have also been reported [15]. In this paper we are concerned with the presentation of some more systematic calculations of dynamic multipole polarizabilities and van der Waals dispersion coefficients for the helium atom and H₂ molecule. These results are presented together with some *ab initio* calculations of the same quantities we performed by using an original formalism based on a TDGI method [12] derived in the spirit of the variation-perturbation approach [16, 17] later used by Karplus and Kölker [18] for the time-dependent interaction. The very different features of QMC and *ab initio* approaches are emphasized and the advantages and drawbacks of each of them are discussed in comparison with the most accurate theoretical results available [1, 19–41].

Just before completing this work we received a paper from Huiszoon and Briels in which the static dipole polarizabilities of helium and H₂ (at equilibrium geometry) are computed using a differential-diffusion Monte Carlo method [42]. In fact, their approach is very similar to ours as presented in Refs. [14] and [15], and in the present work, except that a branching process is used in their simulations (like in most QMC methods designed so far to compute total energies).

The organization of this paper is as follows. In Sec. II, the quantum Monte Carlo method for computing response properties of two-electron systems is presented. We also give a brief presentation of the TDGI *ab initio* method we shall use for making some comparisons (in particular, when no *ab initio* data are available). Section III presents calculations of dynamic multipole polarizabilities (both in real and imaginary frequencies) for He and H₂. In Sec. IV we present some results concerning van der Waals dispersion coefficients. Finally, some concluding remarks are presented in Sec. V.

II. METHODS

A. Quantum Monte Carlo

Dynamic multipole polarizability components of an N -electron system at frequency ω are given by

$$\alpha_l^{uv}(\omega) = \alpha_l^{uv+}(\omega) + \alpha_l^{uv-}(\omega) \quad (1)$$

with

$$\alpha_l^{uv\pm}(\omega) = \sum_{i (\neq 0)} \frac{\langle \phi_0 | Q_l^u | \phi_i \rangle \langle \phi_i | Q_l^v | \phi_0 \rangle}{E_i - E_0 \pm \omega}, \quad (2)$$

where Q_l^u stands for the multipole operator:

$$Q_l^u = \left(\frac{4\pi}{2l+1} \right)^{1/2} \sum_i |r_i|^l Y_l^u(\theta_i, \phi_i), \quad u = -l, \dots, +l$$

and ϕ_i are the eigenfunctions of H (the Hamiltonian describing the isolated atomic or molecular system) with the corresponding energies E_i . It is easy to see that

$$\begin{aligned} \bar{C}_{Q_l^u Q_l^v}(\tau) &= \langle [Q_l^u(\mathbf{R}(0)) - \bar{Q}_l^u] [Q_l^v(\mathbf{R}(\tau)) - \bar{Q}_l^v] \rangle \\ &= \int d\mathbf{R}_0 d\mathbf{R}_1 [Q_l^u(\mathbf{R}_0) - \bar{Q}_l^u] p(\mathbf{R}_0) p(\mathbf{R}_0 \rightarrow \mathbf{R}_1, \tau) [Q_l^v(\mathbf{R}_1) - \bar{Q}_l^v], \end{aligned} \quad (10)$$

$\alpha_l^{uv\pm}(\omega)$ may be rewritten in terms of the Laplace transform of the following centered two- (imaginary) time correlation function:

$$\alpha_l^{uv\mp}(\omega) = - \int_0^{+\infty} d\tau e^{\pm\tau\omega} \bar{C}_{Q_l^u Q_l^v}(\tau), \quad (3)$$

where

$$\bar{C}_{Q_l^u Q_l^v}(\tau) \equiv \langle \phi_0 | (Q_l^u - \bar{Q}_l^u) e^{-\tau(H-E_0)} (Q_l^v - \bar{Q}_l^v) | \phi_0 \rangle, \quad (4)$$

and

$$\bar{Q}_l^w \equiv \langle \phi_0 | Q_l^w | \phi_0 \rangle, \quad w = u, v. \quad (5)$$

The important point is that such correlation functions may be computed by using simulation techniques based on diffusion processes. To do that, we introduce a Markovian diffusion process in configuration space whose transition probability density is closely related to the imaginary-time-dependent Green's function associated with H . More precisely, the transition probability density employed here is

$$p(\mathbf{R} \rightarrow \mathbf{R}', t) = \frac{\phi_0(\mathbf{R}')}{\phi_0(\mathbf{R})} \sum_i \phi_i(\mathbf{R}) \phi_i(\mathbf{R}') e^{-t(E_i - E_0)}, \quad (6)$$

where \mathbf{R} is a compact notation for representing a point in the $3N$ -dimensional configuration space, that is $\mathbf{R} = (\mathbf{r}_1, \dots, \mathbf{r}_N)$, where N is the number of particles of the system. It should be noted that the stationary density, $p(\mathbf{R})$, of the diffusion process (obtained by letting t go to infinity in the preceding formula) is nothing but the usual quantum-mechanical probability density associated with the ground-state wave function

$$p(\mathbf{R}) = \phi_0^2. \quad (7)$$

In practice, a Gaussian short-time version of the transition probability density (6) is used to generate stochastic trajectories of the diffusion process:

$$p(\mathbf{R} \rightarrow \mathbf{R}', \Delta t) = \left(\frac{1}{2\pi\Delta t} \right)^{3N/2} e^{-[\mathbf{R}' - \mathbf{R} - \mathbf{b}(\mathbf{R})\Delta t]^2 / 2\Delta t}, \quad (8)$$

where the so-called drift vector \mathbf{b} responsible for importance sampling is given by

$$\mathbf{b}(\mathbf{R}) = \frac{\nabla \phi_0}{\phi_0}. \quad (9)$$

The effect of drifting the mean value of the Gaussian function (8) is to increase the efficiency of the simulation by keeping the configurations in important regions of phase space. The two-time correlation functions are formally defined in terms of the stationary and transition probability densities as follows:

where $\langle \rangle$ denotes the average with respect to stochastic trajectories. The validity of Eq. (10) is easily checked by inserting expressions (6) and (7) into (10) and comparing with (4). In practice, such averages may be calculated from random walks generated from Eqs. (8)–(9) and by averaging the two-time product of Q 's along them. However, at this point this scheme is rather formal since the ground-state wave function of H [whose expression is needed to construct the drift vector (9)] is generally not known. In fact, it is possible to avoid this problem by introducing a new diffusion process defined from a known trial wave function ψ_T instead of the exact one [43]. In order to compute the very same correlation functions, it is possible to show that one just has to introduce a suitable weight factor in the preceding averages (for a detailed presentation, see [14] and [43]). For example, the two-time correlation functions in which we are interested here are expressed as

$$\langle [Q_i^u(\mathbf{R}(0)) - \bar{Q}_i^u][Q_i^v(\mathbf{R}(\tau)) - \bar{Q}_i^v] \rangle = \lim_{t \rightarrow +\infty} \frac{\langle [Q_i^u(\mathbf{R}(0)) - \bar{Q}_i^u][Q_i^v(\mathbf{R}(\tau)) - \bar{Q}_i^v] e^{-\int_{-t/2}^{t/2} E_L(\mathbf{R}(s)) ds} \rangle_{\psi_T}}{\langle e^{-\int_{-t/2}^{t/2} E_L(\mathbf{R}(s)) ds} \rangle_{\psi_T}}, \quad (11)$$

where averages of the right-hand side of the equation are defined with respect to the diffusion process built from a trial wave function ψ_T . In fact, formula (11) is nothing but a generalization of the well-known Feynman-Kac formula [43]. The quantity E_L appearing in the weight (Feynman-Kac) factor is defined as

$$E_L = H\Psi_T/\Psi_T \quad (12)$$

and is usually referred to as the local energy.

As discussed in length in [14] it is important to emphasize that the formalism presented here is effective for systems having no more than two electrons (no antisymmetry constraints from the Pauli principle). In theory bigger systems could be treated by introducing some projecting weights with appropriate antisymmetry. In practice, doing this introduces a dramatic sign problem at large times which renders the simulation very delicate to perform. Note that the commonly used fixed-node approximation cannot be employed for computing multi-time correlation functions (even if the exact nodes of the ground state were known, see [14]). Some proposals to control this difficulty have been very recently proposed by one of us [44, 45]. However, the situation is not yet fully satisfactory.

B. *Ab initio* TDGI method

Since this original *ab initio* method has been described in detail in Ref. [12], only its main features will be given here. The dynamic polarizability components [Eqs. (1)–(2)] may be obtained from a time-dependent variation-perturbation approach [18] using the following expressions:

$$\alpha_i^{uv}(\omega) = - \sum_{\pm} \langle \phi_0 | Q_i^u - \bar{Q}_i^u | 1^{v\pm} \rangle$$

with

$$(H - E_0 \pm \omega) | 1^{v\pm} \rangle = -(Q_i^v - \bar{Q}_i^v) | \phi_0 \rangle \quad (13)$$

where H is the Hamiltonian of the unperturbed (isolated system), ϕ_0 is its ground-state wave function, E_0 the corresponding energy, and $| 1^{v\pm} \rangle$ the first-order perturba-

tional wave function.

We have shown elsewhere [12] that the use of a first-order wave function which combines a polynomial function $\hat{g}(\mathbf{r})$ and both true spectral states ϕ_n and quasi-spectral states ψ_m allows us to reach accurate values for static and dynamic polarizability components. For the case of dipole polarizabilities ($Q_i^u = u$) the expression of this first-order wave function is

$$| 1^{v\pm} \rangle = \hat{g}^{v\pm}(\mathbf{r}) | \phi_0 \rangle + \sum_{n (>0)} c_n^{v\pm} | \phi_n \rangle + \sum_m c_m^{v\pm} | \psi_m \rangle, \quad (14)$$

where $\hat{g}(\mathbf{r})$ is a first degree polynomial function of the electronic coordinate:

$$\hat{g}^{v\pm}(\mathbf{r}) = \sum_u a_u^{v\pm} u \quad \text{with } u, v = x, y, z$$

when the electric field lies in the v direction. ϕ_n are the true spectral states built from Slater determinants

$$\phi_n = \sum_m C_m^n \psi_m,$$

and ψ_m is a quasispectral series determined by Slater determinants selected using the following threshold:

$$s = \left| \frac{q \langle \phi_0 | v | \psi_m \rangle}{H_{mm} - E_0} \right|$$

with $H_{mm} = \langle \psi_m | H | \psi_m \rangle$.

The computation of the dynamic polarizability requires the calculations of $a_u^{v\pm}$, $c_n^{v\pm}$, and $c_m^{v\pm}$ factors obtained by projecting Eqs. (13) (for $+\omega$ and $-\omega$) on $v | \phi_0 \rangle$, $|\phi_n\rangle$, and $|\psi_m\rangle$. This leads to a system of two linear sets of equations to be solved.

When the origin is fixed at the electronic centroid, the dynamic dipole polarizability components are given in atomic units by

$$\alpha_{l=1}^{uv}(\omega) = \sum_{\pm, w} a_w^{v\pm} \langle wu \rangle + \sum_{\pm, n} c_n^{v\pm} \langle \phi_0 | u | \phi_n \rangle + \sum_{\pm, m} c_m^{v\pm} \langle \phi_0 | u | \psi_m \rangle \quad (15)$$

with $u, v, w = x, y, z$ and $\langle wu \rangle = \langle \phi_0 | \sum_{i,j}^{n_e} w_i u_j | \phi_0 \rangle$ (n_e being the number of electrons).

We have reformulated the TDGI expressions for the imaginary frequency-dependent dipole polarizability $\alpha(i\omega)$ in order to calculate the dispersion coefficients via the Casimir-Polder formula [46]. The two systems of linear equations become identical but twice greater than for real frequencies. The resolution is made as described by Koch and Harrison [47].

Quadrupole polarizability components are obtained in the same way by replacing the dipole moment operator by the quadrupole moment but the polynomial function $\hat{g}(\mathbf{r})$ has not been used in this case.

III. DYNAMIC MULTIPOLE POLARIZABILITIES FOR HE AND H₂

A. He

Tables I–IV present the dynamic dipole, quadrupole, and octopole polarizabilities of helium as calculated by QMC and TDGI (present work), and various *ab initio* methods for comparison. The most commonly used method for evaluating dynamic polarizabilities is certainly the time-dependent Hartree-Fock method (TDHF). TDHF results may be largely improved by using a MCSCF wave function as reference (MCTDHF) instead of a single one [25]. However, for a simple two-electron system such as He nearly exact results may be

obtained using full CI (FCI) calculations or explicitly correlated wave functions [1, 24, 37]. Note also that, in the case of He, Glover and Weinhold [1] have used a method for calculating rigorous upper and lower bounds to dynamic dipole polarizabilities using explicitly correlated wave functions. To study the reliability of QMC and TDGI methods, our values are to be compared to these almost exact results when possible.

Let us first discuss the QMC results. As emphasized in Sec. II A a central role is played by the trial wave function used. The closer the exact solution of the trial wave function is, the smaller the fluctuations of the local energy (12) are, and the better the simulation for a given amount of computer time is. In practice, one of the best trial wave functions available for the system under consideration is generally chosen. The wave function may have a rather arbitrary form since only its first (drift vector) and second derivatives (local energy) are to be calculated (no integrals to perform). Highly and explicitly correlated trial wave functions (i.e., including the interelectronic distance) are generally used. Here, we have chosen a rather simple form

$$\Psi_T = |1s(r_1)\rangle |1s(r_2)\rangle \exp\left(\frac{ar_{12}}{1+br_{12}}\right) \quad (16)$$

with

$$|1s(r)\rangle = \sum_{i=1}^3 c_i \exp(-\lambda_i r),$$

where parameters a , b , λ_i , and c_i have been optimized to minimize the energy. With our optimized trial wave function ($a = 0.5$; $b = 0.51571$; $c_1 = 0.00698$; $c_2 = 0.36714$; $c_3 = 0.53762$; $\lambda_1 = 4.462$; $\lambda_2 = 2.8955$; $\lambda_3 = 1.5689$) we re-

TABLE I. Dynamic dipole polarizabilities $\alpha(\omega)$ (in a.u.) of He for real frequencies (in a.u.). GW stands for Glover and Weinhold [1], QMC for quantum Monte Carlo, and TDGI, TDHF [25], MCTDHF or MCLR [25], SOPPA [27], and FCI [26] for the corresponding *ab initio* methods. Statistical errors on the last digit of QMC results are indicated in parentheses.

Frequency ω	$\alpha(\omega)$						
	QMC	TDGI	GW	TDHF	MCLR	SOPPA	FCI
0.00	1.382(16) ^a	1.3827	1.3834(8)	1.3214	1.3821	1.3674	1.3846
0.05	1.386(17)		1.3872(8)			1.3712	1.3885
0.10	1.398(17)	1.3984	1.3990(8)	1.3354	1.3976	1.3826	1.4003
0.15	1.418(19)		1.4191(8)			1.4022	
0.20	1.449(22)	1.4478	1.4485(8)	1.3797	1.4467	1.4307	1.4500
0.25	1.490(25)		1.4885(9)			1.4695	
0.30	1.546(31)	1.5404	1.5412(9)	1.4619	1.5385	1.5205	1.5431
0.35	1.618(39)		1.6096(10)			1.5866	
0.40	1.715(52)	1.6974	1.6983(11)	1.5995	1.6938	1.6722	1.7009
0.45	1.846(73)		1.8145(13)			1.7840	
0.50	2.031(111)	1.9696	1.9705(15)	1.8327	1.9621	1.9334	1.9746
0.55	2.318(188)		2.1875(18)		2.1753	2.1402	
0.60	2.858(399)	2.5091	2.5091(23)	2.2741	2.4897	2.4441	
0.65			3.0391(34)			2.9380	
0.70		4.1308	4.1184(73)	3.4320	4.0339	3.9173	4.1527
0.75			8.1640(761)				

^aReference [42]: $\alpha(0) = 1.38(1)$.

cover 89% of the correlation energy. Stochastic trajectories in the six-dimensional configuration space are generated using the Gaussian transition probability density (8) with

$$\mathbf{b}(\mathbf{R}) = \frac{\nabla \Psi_T}{\Psi_T}. \quad (17)$$

As usual when using a step-wise procedure to generate trajectories, a finite time-step error is introduced (the “short-time error”). In order to reduce it significantly we have used the acceptance-rejection procedure presented in Refs. [14] and [48], essentially a standard Metropolis algorithm based on a Langevin move. To keep the short-time error under control, we have repeated our simulations for different time steps of decreasing magnitude up to some value for which the time-step error is significantly smaller than the statistical one. A typical value of the time step for the simulations presented here is 0.01 a.u. The following autocorrelation functions have been calculated:

$$C_l(\tau) = \langle (Q_l - \bar{Q}_l)(0)(Q_l - \bar{Q}_l)(\tau) \rangle, \quad l = 1, 2, 3 \quad (18)$$

TABLE II. Dynamic dipole polarizabilities $\alpha(\omega)$ (in a.u.) of He for imaginary frequencies (in a.u.). GW stands for Glover and Weinhold [20], QMC for quantum Monte Carlo, and TDGI for the *ab initio* method. Statistical errors on the last digit of QMC results are indicated in parentheses.

Frequency ω	$\alpha(i\omega)$		
	QMC	TDGI	GW
0.00	1.382(16) ^a	1.3827	1.3834(8)
0.05	1.378(16)		
0.10	1.366(15)	1.3675	1.370(10)
0.15	1.347(14)		
0.20	1.322(12)	1.3242	1.322(7)
0.25	1.291(11)		
0.30	1.256(9)	1.2587	1.257(5)
0.35	1.217(7)		
0.40	1.175(6)	1.1788	1.178(4)
0.45	1.132(5)		
0.50	1.088(4)	1.0918	1.090(3)
0.55	1.044(4)		
0.60	1.001(4)	1.0035	1.002(2)
0.65	0.958(4)		
0.70	0.916(4)	0.9180	0.917(2)
0.75	0.875(4)		
0.80	0.836(4)	0.8377	0.836(2)
0.85	0.799(4)		
0.90	0.763(4)	0.7637	0.762(2)
0.95	0.729(4)		
1.00	0.696(3)	0.6964	0.695(2)
1.10	0.635(3)	0.6358	
1.20	0.581(3)	0.5813	0.580(1)
1.30	0.532(2)	0.5326	
1.40	0.488(2)	0.4891	
1.50	0.449(1)	0.4501	0.449(1)
2.00	0.305(1)	0.3075	0.3069(9)
3.00	0.1647(7)	0.1659	
4.00	0.1016(3)		
5.00	0.0686(1.5)		

^aReference [42]: $\alpha(0)=1.38(1)$.

where the Q_l 's are the dipole ($l = 1$), quadrupole ($l = 2$), and octopole ($l = 3$) operators given by (only one component for each multipole moment has been considered because of spherical symmetry)

$$Q_1 = x_1 + x_2,$$

$$Q_2 = \frac{3}{2}(x_1^2 + x_2^2) - \frac{1}{2}(r_1^2 + r_2^2),$$

$$Q_3 = x_1^3 + x_2^3 - \frac{3}{2}x_1(y_1^2 + z_1^2) - \frac{3}{2}x_2(y_2^2 + z_2^2),$$

where x_i, y_i, z_i denotes the position of electron i . A very important feature of this type of approach is that the different correlation functions are computed from a *common* set of random walks. Only integrands change when computing different averages. It should be noted that within the framework of *ab initio* methods computing polarizabilities corresponding to different multipole moments requires in theory as many calculations as different operators. In practice, this is not strictly true (the perturbation-independent part of the calculation is evaluated only once; it is possible to take advantage of efficient algorithms for solving simultaneous equations, etc.), but the cost remains larger. Figure 1(a) (upper curve) presents the dipole correlation function C_1 versus τ as calculated for several statistically independent sets of random walks (here, only eight curves have been drawn). The location of the different curves gives a visual representation of the dispersion of QMC results. The number of independent calculations done for any result presented in this paper is always of the order of 100, the error bars given in the tables being estimated from these statistically independent sets of trajectories. As usual when computing correlation functions it is important to realize that the long-time regime may be difficult to reproduce. The reason for that is the exponential decay of the function, together with the presence of an error bar more or less constant as a function of time. We illustrate this difficulty by showing the logarithm of $C(\tau)$ in Fig. 1(b) (lower curve). The theoretical expression (4) indicates that $\ln C$ should become linear for sufficiently large times (the slope representing the gap in energy of the system). In practice, this is what happens for large enough times (here, around $\tau \approx 2$ a.u.); however, at too large times (here, around $\tau > 3$ a.u.) the noise dominates. To compute polarizabilities and van der Waals force constants [Eqs. (3) and (22)] the correlation function must be integrated over the entire time domain. Therefore, we must pay special attention to the long-time domain. The strategy employed here is simple. We determine at large times a range of time values where the correlation function decays as a single exponential and for which the noise is still small. On this interval a fit of the correlation function as a single exponential is performed. This representation for $C(\tau)$ is used for ulterior times. In the short-time regime, the data are represented analytically via a spline interpolation procedure. Accordingly, the integrations involved in (3) and (22) are expressed as a finite sum (the number of QMC points) of Laplace transforms of a third-order polynomial (spline part) plus a trivial residue corresponding to large times. Here also, as in the case of evaluating properties related to different multipole op-

erators, it is important to stress that we do not need to do two separate calculations when both imaginary- and real-frequency polarizabilities are needed. Indeed, once the multipole correlation function has been computed as a function of time over a sufficiently large range of time values, evaluating multipole polarizabilities at zero or arbitrary frequencies (real or imaginary) and even van der Waals dispersion coefficients is just a matter of performing a few trivial analytical integrations. Let us now have a closer look at our QMC results. A first observation is that the results obtained are good since in all cases (Tables I–IV) they are compatible with the estimated exact values. This is, of course, expected since QMC results are supposed to be exact and free of any systematic error (such as the choice of the basis set in *ab initio* methods). The only relevant quantity here is the magnitude of the error bar defining the accuracy of the QMC simulation. According to the central-limit theorem, the error bar behaves as c/\sqrt{T} , where T is the computer CPU time which is directly related to the total number of Monte Carlo steps performed. c is a constant depending on different factors such as the quality of the trial wave function used and the amount of statistical correlation between successive configurations generated and the nature of the operators involved in the averages. Since in the present work

a common set of trajectories has been used to compute all the quantities presented, differences in statistical errors are mainly due to the nature of operators. In particular, it is worth noting that the statistical error on polarizabilities increases when multipole operators corresponding to increasing l are considered. To explain this we first notice that errors on polarizabilities and correlation functions are expected to be roughly proportional due to the linear relation between them. On the other hand, a rough estimate of the error on correlation functions may be obtained by evaluating this error at the initial time, which is essentially given by the dispersion of the squared multipole operator. We have

$$\frac{\delta\alpha_l}{\alpha_l} \sim \frac{\delta C(0)}{C(0)} \sim \frac{\sqrt{\langle\phi_0 | \delta Q_l^4 | \phi_0\rangle - \langle\phi_0 | \delta Q_l^2 | \phi_0\rangle^2}}{\langle\phi_0 | \delta Q_l^2 | \phi_0\rangle}, \quad (19)$$

where

$$\delta Q_l \equiv Q_l - \bar{Q}_l.$$

A crude estimate of these errors may be obtained by com-

TABLE III. Dynamic quadrupole polarizabilities (in a.u.) of He for both real and imaginary frequencies (in a.u.). BL stands for Bishop and Lam [24]. Statistical errors on the last digit of QMC results are indicated in parentheses.

Frequency ω	$C(\omega)_{\text{QMC}}$	$C(\omega)_{\text{TDMI}}$	$C(\omega)_{\text{BL}}$	$C(i\omega)_{\text{QMC}}$	$C(i\omega)_{\text{TDMI}}$
0.00	0.800(16)	0.8022	0.8146	0.800(16)	0.8022
0.05	0.802(16)		0.8161	0.799(16)	
0.10	0.807(16)	0.8085	0.8208	0.794(15)	0.7960
0.15	0.815(17)		0.8289	0.787(15)	
0.20	0.827(17)	0.8280	0.8404	0.776(15)	0.7781
0.25	0.843(18)		0.8559	0.763(14)	
0.30	0.864(20)	0.8633	0.8757	0.749(13)	0.7504
0.35	0.891(22)		0.9007	0.732(13)	
0.40	0.926(26)	0.9192	0.9318	0.714(12)	0.7153
0.45	0.972(31)		0.9705	0.695(11)	
0.50	1.034(40)	1.0058	1.0189	0.675(10)	0.6754
0.55	1.125(57)		1.0802	0.655(10)	
0.60	1.287(104)	1.1449	1.1596	0.634(9)	0.6331
0.65			1.2661	0.613(9)	
0.70		1.3965	1.4172	0.593(8)	0.5903
0.75			1.6541	0.572(8)	
0.80		2.0946		0.552(7)	0.5485
0.85				0.533(7)	
0.90				0.513(6)	0.5086
0.95				0.495(6)	
1.00				0.477(6)	0.4712
1.10				0.442(5)	0.4364
1.20				0.410(5)	0.4043
1.30				0.381(4)	0.3750
1.40				0.353(4)	0.3482
1.50				0.329(4)	0.3237
2.00				0.233(2)	0.2301
3.00				0.129(1)	0.1296
4.00				0.0803(3)	
5.00				0.0545(2)	

puting the averages in (19) using the approximate trial wave function instead of the exact one. Resorting to a standard Metropolis algorithm to compute integrals we obtain

$$\frac{\delta\alpha_2}{\alpha_2} \bigg/ \frac{\delta\alpha_1}{\alpha_1} \sim 2.5,$$

$$\frac{\delta\alpha_3}{\alpha_3} \bigg/ \frac{\delta\alpha_1}{\alpha_1} \sim 6.8.$$

These ratios agree quite well with ratios of QMC errors presented in Tables I–IV. For the case of the dipole results, our values are compatible with the narrow range of possible values resulting from the very tight rigorous upper and lower bounds of Glover and Weinhold [1, 20] obtained by using correlated Hylleraas-type wave functions or, for the static case, with the experimental value of 1.383 79(7) obtained by Guban and Michel [49] [after correcting for the motion of the nucleus we get 1.383 23(7), in agreement with the best *ab initio* value (1.383 192) given by Bishop and Lam [24]].

This is true for both real and imaginary frequencies. Concerning quadrupole polarizabilities our results are compatible with our TDGI results and the results obtained by Bishop and Lam [24] (note that we have di-

vided our results by a factor 3 to match their convention). Table IV presents dynamic octopole polarizabilities of He. They are compared with the *ab initio* results of Luyckx, Coulon, and Lekkerkerker [38] obtained by a simple variation method. The latter ones agree quite well with our QMC results within statistical errors. Another feature which deserves to be commented on is the increase of the statistical error with real frequency. This behavior arises from the fact that high real frequencies require an accurate evaluation of the correlation function for increasing times [the Laplace kernel $\exp(\omega\tau)$ in (3) explodes for large frequencies], and the small statistical errors on the tail of the correlation function are then exponentially magnified by the Laplace transform. Note that this problem does not exist in the case of imaginary frequencies.

In order to make some comparisons, a number of *ab initio* calculations are also presented in Tables I–IV. Our *ab initio* calculations were performed using the TDGI approach [12, 13] briefly presented in Sec. II B. For He, the basis set employed consists of 13*s*, 7*p*, and 6*d* primitive Gaussian orbitals based on the van Duijneveldt (10*s*) primitive set [50, 51] and an even tempered (7*p*, 6*d*) polarization set augmented by adding 3*s* diffuse function.

TABLE IV. Dynamic octopole polarizabilities (in a.u.) of He for both real and imaginary frequencies (in a.u.). *Ab initio* results are taken from Ref. [38]. Statistical errors on the last digit of QMC results are indicated in parentheses.

Frequency ω	$\alpha_3(\omega)_{\text{QMC}}$	$\alpha_3(\omega)_{\text{ab initio}}$	$\alpha_3(i\omega)_{\text{QMC}}$	$\alpha_3(i\omega)_{\text{ab initio}}$
0.00	10.36(69)	10.48 ^a	10.36(69)	10.48 ^a
0.05	10.38(70)	10.49	10.33(69)	10.46
0.10	10.45(71)	10.54	10.26(68)	10.42
0.15	10.57(72)	10.63	10.15(66)	10.34
0.20	10.75(75)	10.74	10.01(64)	10.23
0.25	11.00(80)	10.90	9.83(62)	10.10
0.30	11.33(86)	11.10	9.62(59)	9.94
0.35	11.77(96)	11.34	9.40(57)	9.76
0.40	12.35(113)	11.64	9.16(54)	9.56
0.45	13.14(144)	12.01	8.91(51)	9.35
0.50	14.26(212)	12.45	8.66(49)	9.12
0.55			8.41(46)	8.89
0.60			8.17(44)	8.65
0.65			7.92(41)	8.40
0.70			7.69(39)	8.15
0.75			7.46(36)	7.90
0.80			7.23(34)	7.66
0.85			7.02(32)	7.41
0.90			6.81(30)	7.17
0.95			6.61(28)	6.93
1.00			6.41(26)	6.70
2.00			3.51(9)	3.42
3.00			1.92(2)	1.93
4.00			1.198(9)	1.217
5.00			0.820(11)	0.828
6.00			0.591(8)	0.597
7.00			0.452(4)	0.449
8.00			0.350(3)	0.350
9.00			0.276(3)	0.280
10.0			0.225(2)	0.228

^aReference [37]: $\alpha_3(0) = 10.6144$.

Exponents of the $3s$ orbitals are, respectively, 0.049 069, 0.022 304, and 0.010 138. SCF and CI calculations within this basis set give an atomic energy of $-2.861\,67$ a.u. and $-2.902\,52$ a.u., respectively. Dynamic dipole polarizabilities of He for real frequencies computed with TDGI are listed in Table I together with some TDHF [25], MCLR [25], SOPPA [27], and FCI [26] results and the very accurate rigorous upper and lower bounds obtained by Glover and Weinhold [19, 20]. A first point to emphasize is that our *ab initio* TDGI results for the static polarizability (1.3827 a.u.) is in excellent agreement with the one obtained by Glover and Weinhold [1.3834(8)] and with the very accurate value (1.383 192) given by Bishop and Lam [24] using explicitly electron-correlated wave functions.

MCTDHF and FCI methods give quite accurate results; an error of approximately 1% is found with SOPPA. The main differences between various calculations appear at frequencies close to the first excitation energy of He. Table I shows that, for frequencies up to

0.7 a.u., the TDGI results, close to the accurate results of Glover and Weinhold [1], are the most accurate ones among *ab initio* calculations. The main explanation is that the excitation energy corresponding to the transition $1s \rightarrow 2p$ is very well reproduced in our calculations, namely, 21.193 eV, to be compared with the experimental value of 21.22 eV. As already explained above QMC results have a statistical error which increases very rapidly with the frequency. Calculating polarizabilities for real frequencies close to the excitation energy is not an easy task for the QMC approach. For the case of imaginary frequencies where this problem does not exist, we obtain a very good agreement between QMC and TDGI results (Table II). Concerning the dynamic quadrupole polarizabilities (Table III) our results are compared with those obtained by Bishop and Lam [24] which have to be considered as reference values. Between 0.0 and 0.6 a.u. our *ab initio* values have a similar behavior as Bishop and Lam results. However, it seems that our results are too

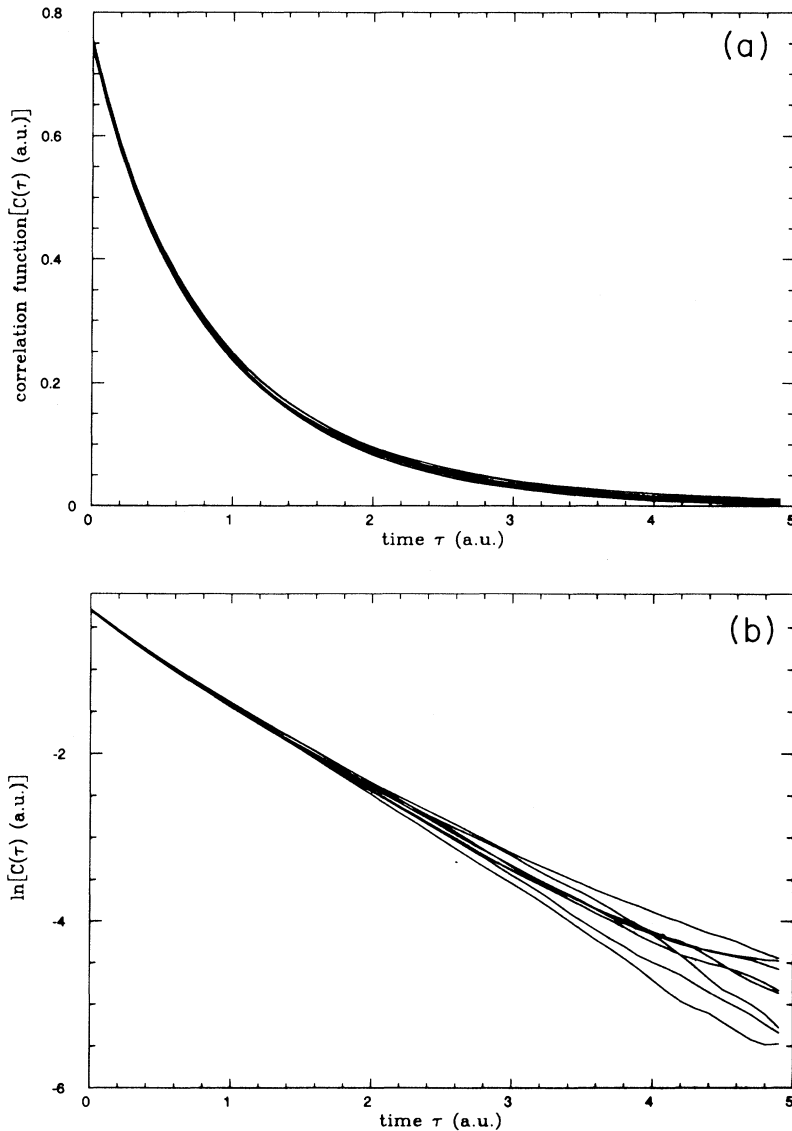


FIG. 1. (a) Dipole correlation function of He vs τ as calculated in eight independent runs. (b) Logarithm of $C(\tau)$. Note the effect of the noise in the large-time domain.

small with an error of approximately 1.5%. QMC results within the statistical errors are in good agreement with both sets of results.

B. H₂

Calculating response properties for a molecular system such as H₂ using QMC does not introduce any additional difficulties with respect to an atomic system such as He. As usual choosing a good approximate trial wave function is the crucial step. Since calculations at both intermediate and large internuclear separations, R_{H-H} , are considered here it is important to choose a wave function capable of describing both the equilibrium region (covalent regime) and the large R_{H-H} region (valence-bond regime). This could be realized with one single wave function with some parameters connecting both cases. For simplicity we have chosen here to use two different wave functions

For large distances

$$\Psi_T = \exp\left(\frac{ar_{12}}{1+br_{12}}\right) [\Phi_A(1)\Phi_B(2) + \Phi_A(2)\Phi_B(1)] \quad (20)$$

with

$$\Phi_M(i) = \exp(-\lambda_1 r_{iM}) + c \exp(-\lambda_2 r_{iM}), \quad M = A, B,$$

where r_{iM} denotes the distance between electron i and nucleus M ($M = A, B$).

For intermediate distances

$$\Psi_T = \exp\left(\frac{ar_{12}}{1+br_{12}}\right) \Phi(1)\Phi(2), \quad (21)$$

where the molecular orbital is given by

$$\Phi(i) = \exp(-\lambda r_{iA}) + \exp(-\lambda r_{iB}).$$

Concerning our *ab initio* TDGI calculations, we have chosen for each hydrogen atom a contracted basis [6s, 6p, 3d] issued from the basis [4s, 3p, 1d] proposed by Siegbahn and Liu [52] in their study of the potential energy surface of H₃. The two additional *s* functions

TABLE V. Dynamic dipole polarizabilities (in a.u.) of H₂ at $R = 1.4$ for real and imaginary frequencies (in a.u.). QMC stands for quantum Monte Carlo and TDGI, Rych [28] and SOPPA [27] stand for the corresponding *ab initio* methods. Statistical errors on the last digit of QMC results are indicated in parentheses.

Frequencies	$\alpha_{\parallel}^{\text{QMC}}$	$\alpha_{\parallel}^{\text{TDGI}}$	$\alpha_{\parallel}^{\text{Rych}}$	$\alpha_{\parallel}^{\text{SOPPA}}$	$\alpha_{\perp}^{\text{QMC}}$	$\alpha_{\perp}^{\text{TDGI}}$	$\alpha_{\perp}^{\text{Rych}}$	$\alpha_{\perp}^{\text{SOPPA}}$
Real								
0.0000	6.42(8) ^a	6.4310	6.3873	6.4495	4.53(7) ^a	4.5944	4.5786	4.5676
0.0720	6.55(9)	6.5617	6.5164	6.5812	4.60(7)	4.6725	4.6562	4.6445
0.0834	6.59(9)	6.6077	6.5618	6.6276	4.62(7)	4.6999	4.6834	4.6715
0.1045	6.69(9)	6.7132	6.6659	6.7338	4.68(9)	4.7626	4.7457	4.7331
0.1363	6.90(10)	6.9278	6.8776	6.9501	4.79(9)	4.8892	4.8715	4.8576
0.1535	7.04(10)	7.0756	7.0235	7.0990	4.87(10)	4.9758	4.9576	4.9427
0.1979	7.52(13)	7.5865	7.5256	7.6136	5.13(13)	5.2713	5.2503	5.2328
0.2354	8.09(15)	8.2125	8.1412	8.2437	5.43(18)	5.6257	5.6017	5.5800
0.2500	8.37(17)	8.5226	8.4481	8.5568	5.57(22)	5.7982	5.7738	5.7493
0.3000	9.68(34)	10.0190	9.9160	10.0649		6.6041	6.5713	6.5367
0.3500		12.7855	12.6126	12.8558		7.9877	7.9320	7.8834
0.3748		15.2223	14.9610	15.3084		9.1058	9.0182	8.9633
0.4000		19.4440	18.9847	19.5639		10.8521	10.6930	10.6421
0.4500		61.6664	54.3276	62.0977		20.9387	19.4400	20.0551
Imaginary								
0.0000	6.42(8) ^a	6.4310			4.53(7) ^a	4.5944		
0.1000	6.19(7)	6.1939			4.40(7)	4.4517		
0.2000	5.59(6)	5.5834			4.05(5)	4.0777		
0.3000	4.82(4)	4.8082			3.58(4)	3.5888		
0.4000	4.05(3)	4.0395			3.09(3)	3.0870		
0.5000	3.36(2)	3.3624			2.63(2)	2.6294		
0.8000	1.96(1)	1.9746			1.63(1)	1.6367		
1.0000	1.423(7)	1.4396			1.220(8)	1.2290		
1.2000	1.073(5)	1.0848			0.942(4)	0.9481		
1.5000	0.743(4)	0.7484			0.670(3)	0.6718		
1.8000	0.542(3)	0.5437			0.499(2)	0.4978		
2.0000	0.448(2)	0.4496			0.417(2)	0.4160		

^aReference [42]: $\alpha_{\parallel}(0) = 6.38(5)$; $\alpha_{\perp}(0) = 4.60(3)$.

and three p functions have an exponent of (0.028 773 9, 0.012 510 3) and (0.101 818, 0.037 025, 0.013 463 5), respectively. The three exponents of the d functions are 1.202 52, 0.463 925, and 0.081 240 6. Even if this basis set is far from being complete, the introduction of the polynomial in the determination of polarizabilities improves the convergence. Performing a full CI calculation within this basis set leads to an energy of $-1.173 485$ a.u. at $R=1.401$ a.u. A most important point when determining the dynamical properties of H_2 is to correctly describe the vertical transition $X^1\Sigma_g^+ \rightarrow B^1\Sigma_u^+$ and $X^1\Sigma_g^+ \rightarrow C^1\Pi_u$. Our results for the corresponding excitation energies are 12.73 eV and 13.21 eV, respectively, in excellent agreement with the exact values of 12.76 and 13.22 eV.

Table V presents dynamic dipole polarizabilities of H_2 at the equilibrium geometry for both real and imaginary frequencies as computed with QMC and TDGI. Results for real frequencies are compared with the reference calculations by Rychlewski [28] based on a variation-perturbation method using explicitly correlated wave functions and some recent SOPPA results by Sauer, Dierksen, and Oddershede [27].

QMC results for real frequencies are compatible with

Rychlewski's values within statistical error bars. Concerning *ab initio* (TDGI) results, it is noted that the static components $\alpha_{zz}(0)$ and $\alpha_{xx}(0)$ overestimate Rychlewski results by a factor of 0.7% and 0.3%, respectively. This overestimation is true for all frequencies. At frequency 0.4 a.u., close to the resonance, our values are too large by a factor of 2.4% and 1.5%, respectively. It should be emphasized that our TDGI results, obtained using a much smaller basis set than Sauer, Dierksen, and Oddershede [27] with SOPPA are of comparable quality. Although the parallel component is better reproduced with TDGI than with SOPPA, this is no longer true for the perpendicular one much more sensitive to the angular correlation. In the case of imaginary frequencies, only our QMC and TDGI results can be compared. Both sets of results appear to be compatible.

Table VI presents dynamic quadrupole polarizabilities of H_2 at the equilibrium geometry for both real and imaginary frequencies for the three independent components denoted as $C_{zz,zz}$, $C_{xz,xz}$, and $C_{xx,xx}$ (z is the internuclear axis), as computed by QMC and TDGI. Our static components and values at real frequency $\omega=0.0720$ a.u. are compatible with those available in the literature [33, 34]. TDGI results are in good agreement with QMC

TABLE VI. Dynamic quadrupole polarizabilities (in a.u.) of H_2 at $R = 1.4$ a.u. for real and imaginary frequencies (in a.u.). QMC and TDGI stand for quantum Monte Carlo and *ab initio*, respectively. Statistical errors on the last digit of QMC results are indicated in parentheses.

Frequencies	$C_{zz,zz}^{\text{QMC}}$	$C_{zz,zz}^{\text{TDGI}}$	$C_{xz,xz}^{\text{QMC}}$	$C_{xz,xz}^{\text{TDGI}}$	$C_{xx,xx}^{\text{QMC}}$	$C_{xx,xx}^{\text{TDGI}}$
Real						
0.0000 ^a	6.10(35)	5.9914	4.30(36)	4.1976	4.93(24)	4.7929
0.0720 ^b	6.17(36)	6.0645	4.35(37)	4.2440	4.99(25)	4.8465
0.0834	6.19(38)	6.0879	4.37(38)	4.2601	5.01(26)	4.8651
0.1045	6.25(39)	6.1410	4.40(40)	4.2968	5.05(27)	4.9074
0.1363	6.36(44)	6.2466	4.47(45)	4.3696	5.14(30)	4.9914
0.1535	6.43(47)	6.3177	4.52(49)	4.4186	5.20(32)	5.0478
0.1979	6.66(62)	6.5530	4.68(65)	4.5806	5.41(41)	5.2340
0.2354	6.93(80)	6.8209	4.87(83)	4.7650	5.64(54)	5.4451
0.2500	7.06(90)	6.9461	4.96(93)	4.8511	5.75(62)	5.5433
0.3000		7.4885		5.2236	6.23(115)	5.9652
0.3500		8.2798		5.7656		6.5684
0.3748		8.8137		6.1304		6.9660
0.4000		9.5016		6.5989		7.4656
0.4500		11.6312		8.0344		8.9104
Imaginary						
0.0000	6.10(35)	5.9914	4.30(36)	4.1976	4.93(24)	4.7929
0.1000	5.98(31)	5.8662	4.21(30)	4.1113	4.82(21)	4.6929
0.2000	5.64(25)	5.5243	3.99(27)	3.8750	4.53(15)	4.4191
0.3000	5.16(18)	5.0444	3.66(19)	3.5428	4.13(11)	4.0336
0.4000	4.63(14)	4.5098	3.29(16)	3.1720	3.69(9)	3.6035
0.5000	4.10(12)	3.9815	2.92(13)	2.8047	3.26(8)	3.1789
0.8000	2.80(9)	2.6840	2.01(9)	1.8986	2.23(5)	2.1454
1.0000	2.18(6)	2.0839	1.59(6)	1.4774	1.75(3)	1.6734
1.2000	1.73(4)	1.6455	1.28(5)	1.1687	1.39(3)	1.3302
1.5000	1.25(2)	1.1935	0.92(2)	0.8495	1.01(1)	0.9760
1.8000	0.921(8)	0.8975	0.680(9)	0.6399	0.768(6)	0.7421
2.0000	0.775(6)	0.7553	0.570(7)	0.5389	0.653(4)	0.6286

^aReference [34]: $C_{zz,zz} = 5.983$; $C_{xz,xz} = 4.180$; $C_{xx,xx} = 4.927$.

^bReference [34]: $C_{zz,zz} = 6.050$, $C_{xz,xz} = 4.226$, $C_{xx,xx} = 4.981$.

TABLE VII. Dipole static polarizabilities (in a.u.) of H₂ at selected internuclear distances R (in a.u.). Rych stands for Rychlewski [29], BL stands for Bishop and Lam [31], QMC stands for quantum Monte Carlo, and TDGI stands for *ab initio*. Statistical errors on the last digit of QMC results are indicated in parentheses.

Distance R	$\alpha_{\perp}^{\text{QMC}}$	$\alpha_{\perp}^{\text{TDGI}}$	$\alpha_{\perp}^{\text{Rych}}$	$\alpha_{\perp}^{\text{BL}}$	$\alpha_{\parallel}^{\text{QMC}}$	$\alpha_{\parallel}^{\text{TDGI}}$	$\alpha_{\parallel}^{\text{Rych}}$	$\alpha_{\parallel}^{\text{BL}}$
1.4	4.53(7) ^a	4.5944	4.57856	4.5785	6.42(8) ^a	6.4310	6.38732	6.3875
2.4	7.61(14)	7.6697	7.66049	7.6592	14.57(57)	14.2932	14.26621	14.2691
3.0	8.76(20)	8.8494	8.85806	8.8555	17.60(79)	17.8692	17.79965	17.9990
3.4	9.01(26)	9.2238	9.22883		18.35(90)	18.3724	18.28339	
3.8	9.13(18)	9.3003	9.30201		17.41(53)	17.3388	17.30680	
4.4	9.10(17)	9.2143			14.59(28)	14.7043		
6.0	8.98(13)	8.9371	8.92719		10.17(17)	10.2007	10.19754	

^aReference [42]: $\alpha_{\parallel}(0) = 6.38(5)$; $\alpha_{\perp}(0) = 4.60(3)$.

ones, except at large imaginary frequencies where TDGI seems to give too small values.

The dependence of static dipole polarizabilities on the internuclear distance H-H is presented in Table VII. For all distances the TDGI results are in excellent agreement with the reference values obtained by Rychlewski [29]. The same remark is valid for QMC results.

IV. van der WAALS COEFFICIENTS FOR He AND H₂

The multipole dispersion force coefficients between two systems a and b may be expressed in terms of the dynamic polarizabilities as follows (see, e.g., Ref. [53])

$$C^{ab}(l_a, l_b) = \frac{(2l_a + 2l_b)!}{2\pi(2l_a)!(2l_b)!} \int_0^{+\infty} d\omega \alpha_a^a(i\omega) \alpha_b^b(i\omega), \quad (22)$$

usual van der Waals constants being related to these coefficients in the following way:

$$C_6^{ab} = C^{ab}(1, 1),$$

$$C_8^{ab} = C^{ab}(1, 2) + C^{ab}(2, 1), \quad (23)$$

$$C_{10}^{ab} = C^{ab}(1, 3) + C^{ab}(2, 2) + C^{ab}(3, 1).$$

A. c_6 - c_8 and c_{10} for He

As already pointed out a remarkable feature of QMC is that no additional calculations are needed to compute van der Waals constants once the polarizabilities have been evaluated. Indeed, when computing polarizabilities we built an analytical representation of the correlation function of each multipole operator. Obtaining van der Waals coefficients is then a simple matter of performing the analytic integrations involved in formula (22). Our results for c_6 , c_8 , and c_{10} are presented in Table VIII together with some other results found in literature [20,27,35–40]. QMC results appear to be quite good.

Our TDGI results are obtained from the values of the polarizabilities at imaginary frequencies using the

TABLE VIII. van der Waals dispersion coefficients (in a.u.) of He. Statistical errors on the last digit are indicated in parentheses.

Method	c_6	c_8	c_{10}
Glover and Weinhold ^a	1.460(6)		
Maeder and Kutzelnigg ^b	1.457	13.90	177.24
Meyer ^c	1.456	13.90	175.4
Thakkar ^d	1.4608	14.1118	183.6
Luyckx, Coulon, and Lekkerkerker ^e	1.458	14.06	182.2
Buckingham and Hibbard ^f	1.4638	14.094	183.47
SOPPA ^g	1.4394		
MCTDHF ^h	1.4608		
Present work:			
QMC	1.454(14)	13.88(22)	177.9(69)
TDGI	1.4593	13.883	

^aReference [20].

^bReference [35].

^cReference [36].

^dReference [37].

^eReference [38].

^fReference [39].

^gReference [27].

^hReference [40].

TABLE IX. c_6 dispersion force constant (in a.u.) for He-H₂ as a function of the interhydrogen distance R (in a.u.) with quantum Monte Carlo (QMC) and *ab initio* (TDGI) methods. Comparison with the semiempirical results of Matias and Varandas [41], see text.

Method \ R	1.4	2.4	3.0	3.4	3.8	4.4	6.0
Parallel							
QMC	4.61(4)	7.81(15)	8.75(22)	8.88(29)	8.30(12)	7.46(11)	5.99(5)
TDGI	4.6267	7.8405	8.8621	8.8602	8.4148	7.4756	6.04
Max. Matias	4.6	7.5		8.6	8.4	7.8	6.6
Min. Matias	4.2	6.8		7.6	7.3	6.7	5.7
Perpendicular							
QMC	3.53(4)	5.05(6)	5.52(8)	5.64(9)	5.68(9)	5.67(8)	5.59(8)
TDGI	3.5579	5.0702	5.5774	5.7275	5.7563	5.7198	5.61
Max. Matias	4.	6.1		6.9	6.9	6.6	6.4
Min. Matias	3.2	5.8		5.4	5.3	5.2	5.0

Casimir-Polder formalism. More precisely, we first solve Eq. (13) in order to get $\alpha(i\omega)$ for a number of imaginary frequencies. Then, we perform a fit of the resulting curve using the oscillator strengths and transition frequencies as fitting parameters. Finally, the coefficient c_6 is obtained from the following expression:

$$c_6 = \frac{3}{2} \sum_{\nu,\mu} \frac{f_\nu^A f_\mu^B}{\omega_\nu^A \omega_\mu^B (\omega_\nu^A + \omega_\mu^B)}$$

using the optimized parameters. Note that the values of the oscillator strengths (f_ν^A, f_μ^B) and transition frequencies ($\omega_\nu^A, \omega_\mu^B$) calculated at the CI level for the two systems A and B are used as a starting point of our optimization.

The evaluation of the coefficient c_{10} which requires some additional calculations has not been performed. The values obtained for c_6 and c_8 are in excellent agreement with those obtained by QMC and preceding calculations.

B. c_6 for He-H₂

Table IX presents calculations of the c_6 dispersion force constants (both parallel and perpendicular) for the system He-H₂ as a function of the interhydrogen distance $R_{\text{H-H}}$ with quantum Monte Carlo and *ab initio* (TDGI) methods. To our knowledge this is the first from-first-principles calculation of this quantity. We have compared our results with the recent results of Matias and Varandas ([41]) obtained from a number of more or less crude semiempirical approximations. It is very satisfactory to note that our QMC and TDGI results are compatible (within statistical error bars) for any distance. We have given the upper and lower bounds obtained from calculations by Matias and Varandas (denoted as Min and Max). We see that for a number of distances our evaluations are

in complete disagreement with their results. This illustrates how semiempirical evaluations can be significantly poor.

V. DISCUSSION

The purpose of this work was to present some systematic calculations of dynamic multipole polarizabilities and van der Waals dispersion coefficients of two-electron systems (He and H₂) with quantum Monte Carlo results. A detailed presentation of the practical implementation of this new approach has been given. We compared our results with a number of previous theoretical results obtained by using various *ab initio* methods. In all cases QMC results are in good agreement with estimated “exact” values within statistical error bars. The typical statistical error on QMC results is of the order of a few percent. This should be considered as satisfactory, even if for simple systems such as He and H₂ more accurate results have been obtained by using explicitly correlated wave functions (particularly for static quantities). However, it should be noted that the accuracy on QMC results could be increased by making longer Monte Carlo runs (that was not the purpose of this work).

We also reported some results obtained using an original *ab initio* method based on a gauge-invariant formalism (TDGI method). It has been illustrated that TDGI results are of comparable quality with the best *ab initio* values, although the size of our basis sets was significantly smaller. This is essentially due to the fact that, besides giving a good description of the ground-state wave function, in TDGI we also give a very good description of the first excited state, an essential step to correctly reproduce the dynamical properties of the system. Having, at our disposal, this accurate *ab initio* method appeared to be essential in checking our QMC calculations in the interesting cases where QMC results entered in conflict with existing theoretical results. That was, in particular,

the case when calculating the c_6 dispersion coefficient for He-H₂, a quantity for which only semiempirical results were known. In addition, presenting QMC results together with *ab initio* results helps us to emphasize the very different features of both approaches.

QMC does not require any expansion on a basis set. Most of the correlation energy is taken into account via the high-quality trial wave function used. The remaining part is recovered using an appropriate weight factor (Feynman-Kac factor) when computing averages. Such a property is remarkable. In some very rough sense, we may view the various *ab initio* methods referred to in the tables as different clever ways of trying to tackle the problem of basis-set convergence. In particular, as emphasized above, our TDGI method is another original way of getting accurate results from a relatively modest basis set. In addition, it should be emphasized that no error bars appear in tables for *ab initio* results. Indeed, computing errors resulting from an incomplete basis set with a given *ab initio* method is by no way an easy task. In sharp contrast, QMC gives a natural and viable estimate (nonbiased statistical estimator) of the error made for a given amount of numerical effort.

Using our QMC framework based on two-time correlation functions enables us to compute during a same run all the response properties corresponding to different multipole operators (real and imaginary polarizabilities for $l=1,2,\dots$, van der Waals dispersion coefficients). This is particularly convenient. Within the framework of an *ab initio* calculation, in theory, a calculation is required for each separate quantity (although in practice it is possible to reduce a non-negligible part of the cost). In particular, that was the reason why we did not compute dynamic octopole polarizabilities with TDGI (even if, of course, this is possible).

The computational aspects of QMC are remarkably favorable: the memory requirements are very small (no calculation and storage of bielectronic integrals); the codes are short, simple, and very well suited for vector and parallel processing.

Finally, we would like to end with some of the limitations of QMC. First, as pointed out above, the method is not suitable for computing real dynamic polarizabilities at a frequency close to a resonance. Big error bars in the frequency region close to 0.7 a.u. in Tables I and III-VI illustrate this point. However, this does not occur for imaginary frequencies which are used for computing van der Waals constants. However, the most important limitation of QMC is that the formalism used in this work is limited in practice to two-electron systems (see discussion at the end of Sec II A), systems for which accurate *ab initio* calculations may be performed using explicitly electron-correlated wave functions. Accordingly, it will be possible to consider QMC as a viable alternative to the use of full CI methods only when efficient methods of computing multitime correlation functions for many-electron systems will be available. This will require some more methodological developments.

ACKNOWLEDGMENTS

We would like to thank the "Centre National de la Recherche Scientifique" (CNRS), the "Ministère de l'Éducation Nationale" (MEN), and the C3NI of the Centre National Universitaire Sud de Calcul (CNUSC) for their support. Laboratoire Dynamique des Interactions Moléculaires is "Unité de Recherche Propre du CNRS No. 271" and Laboratoire de Chimie Structurale is "Unité de Recherche Associée au CNRS No. 474."

-
- [1] R.M. Glover and F. Weinhold, *J. Chem. Phys.* **65**, 4913 (1976).
 - [2] E.N. Svendsen and T. Stroyer-Hansen, *Theoret. Chim. Acta* **45**, 33 (1977).
 - [3] H.F. Hameka and E.N. Svendsen, *Int. J. Quantum Chem.* **11**, 129 (1977).
 - [4] J. Olsen, A.M. Sanchez de Meras, H.J. Aa Jensen, and P. Jorgensen, *Chem. Phys. Lett.* **154**, 380 (1989).
 - [5] J. Olsen and P. Jorgensen, *J. Chem. Phys.* **82**, 3235 (1985).
 - [6] P. Jorgensen, H.J. Aa Jensen, and J. Olsen, *J. Chem. Phys.* **89**, 3654 (1988).
 - [7] H.J. Aa Jensen, H. Koch, P. Jorgensen, and J. Olsen, *Chem. Phys.* **119**, 297 (1988).
 - [8] J. Oddershede and E.N. Svendsen, *Chem. Phys.* **64**, 359 (1982).
 - [9] J. Oddershede, P. Jorgensen, and D.L. Yeager, *Comput. Phys. Rep.* **2**, 33 (1984).
 - [10] M. Rérat, *Int. J. Quantum Chem.* **36**, 169 (1989).
 - [11] M. Rérat, C. Pouchan, M. Tadjeddine, J.P. Flament, H.P. Gervais, and G. Berthier, *Phys. Rev. A* **43**, 5832 (1991).
 - [12] M. Rérat, M. Mérawa, and C. Pouchan, *Phys. Rev. A* **45**, 6263 (1992).
 - [13] M. Rérat, M. Mérawa, and C. Pouchan, *Phys. Rev. A* **46**, 5471 (1992).
 - [14] M. Caffarel and O. Hess, *Phys. Rev. A* **43**, 2139 (1991).
 - [15] M. Caffarel and O. Hess, in *Advances in Biomolecular Simulations*, AIP Conf. Proc. No. 239 (AIP, New York, 1991), pp. 20-32.
 - [16] F. Dupont, J. Tillieu, and J. Guy, *J. Phys. Rad.* **22**, 9 (1961).
 - [17] H.F. Hameka, *Rev. Mod. Phys.* **34**, 87 (1962).
 - [18] M. Karplus and H.J. Kölker, *J. Chem. Phys.* **38**, 1263 (1963).
 - [19] R.M. Glover and F. Weinhold, *J. Chem. Phys.* **66**, 185 (1977).
 - [20] R.M. Glover and F. Weinhold, *J. Chem. Phys.* **66**, 191 (1977).
 - [21] M. Jaszunski and R. McWeeny, *Mol. Phys.* **46**, 863 (1982).
 - [22] E.A. Reinsch, *J. Chem. Phys.* **83**, 5784 (1985).
 - [23] D.M. Bishop and B. Lam, *Phys. Rev. A* **37**, 464 (1988), and references therein.
 - [24] D.M. Bishop and B. Lam, *J. Chem. Phys.* **88**, 3398

- (1988).
- [25] N.K. Rahman, A. Rizzo, and D.L. Yeager, *Chem. Phys. Lett.* **166**, 565 (1990).
- [26] M. Jaszunski and B.O. Roos, *Mol. Phys.* **52**, 1209 (1984).
- [27] S.P.A. Sauer, G.H.F. Dierksen, and J. Oddershede, *Int. J. Quantum Chem.* **39**, 667 (1991).
- [28] J. Rychlewski, *Mol. Phys.* **41**, 833 (1980).
- [29] J. Rychlewski, *Chem. Phys. Lett.* **73**, 135 (1980).
- [30] D.M. Bishop and J. Pipin, *Phys. Rev. A* **36**, 2171 (1987).
- [31] D.M. Bishop and B. Lam, *J. Chem. Phys.* **89**, 1571 (1988).
- [32] D.M. Bishop and J. Pipin, *J. Chem. Phys.* **94**, 6073 (1991).
- [33] D.M. Bishop, J. Pipin, and M. Rérat, *J. Chem. Phys.* **92**, 1902 (1990).
- [34] D.M. Bishop, J. Pipin, and S.M. Cybulski, *Phys. Rev. A* **43**, 4845 (1991).
- [35] F. Maeder and W. Kutzelnigg, *Chem. Phys. Lett.* **37**, 285 (1976).
- [36] W. Meyer, *Chem. Phys.* **17**, 27 (1976).
- [37] A.J. Thakkar, *J. Chem. Phys.* **75**, 4496 (1981).
- [38] R. Luyckx, P. Coulon, and H.N.W. Lekkerkerker, *Chem. Phys. Lett.* **48**, 187 (1977).
- [39] A.D. Buckingham and P.G. Hibbard, *Symp. Faraday Soc.* **2**, 41 (1968).
- [40] P.W. Fowler, P. Jorgensen, and J. Olsen, *J. Chem. Phys.* **93**, 7256 (1990).
- [41] M.A. Matias and J.C. Varandas, *Mol. Phys.* **70**, 623 (1990).
- [42] C. Huiszoon and W.J. Briels (unpublished).
- [43] M. Caffarel and P. Claverie, *J. Chem. Phys.* **88**, 1088 (1988); **88**, 1100 (1988).
- [44] M. Caffarel, X. Gadea, and D.M. Ceperley, *Europhys. Lett.* **16**, 249 (1991).
- [45] M. Caffarel and D.M. Ceperley, *J. Chem. Phys.* **97**, 8415 (1992).
- [46] H.B.G. Casimir and D. Polder, *Phys. Rev.* **73**, 360 (1948).
- [47] H. Koch and R.J. Harrison, *J. Chem. Phys.* **95**, 7479 (1991).
- [48] E.L. Pollock and D.M. Ceperley, *Phys. Rev. B* **30**, 2555 (1984).
- [49] D. Guban and G.W. Michel, *Mol. Phys.* **39**, 783 (1980).
- [50] F.B. Van Duijneveldt, IBM Technical Report No. RJ945 (1971) (unpublished).
- [51] G. Chalasinski, S. Van Smaalen, and F.B. van Duijneveldt, *Mol. Phys.* **45**, 1113 (1982).
- [52] P. Siegbahn and B. Liu, *J. Chem. Phys.* **68**, 2457 (1978).
- [53] G. Lamm and A. Szabo, *J. Chem. Phys.* **72**, 3354 (1980).

K. M. Rérat, M. Caffarel, and C. Pouchan, “Dynamic Polarizabilities and van der Waals Coefficients of the 2^1S and 2^3S Metastable States of Helium”, *Phys. Rev A* **48**, 161 (1993)

Dynamic polarizabilities and van der Waals coefficients of the 2^1S and 2^3S metastable states of helium

Michel Rérat

Laboratoire de Chimie Structurale, Université de Pau, 64000 Pau, France

Michel Caffarel*

IRSAMC, Laboratoire de Physique quantique, Université Paul Sabatier, 118 route de Narbonne, 31062 Toulouse, France

Claude Pouchan

Laboratoire de Chimie Structurale, Université de Pau, 64000 Pau, France

(Received 21 January 1993)

Dynamic dipole and quadrupole polarizabilities of the 2^1S and 2^3S metastable states of He are calculated using our time-dependent gauge-invariant method and compared with previous theoretical results. Dispersion coefficients for the He(2^1S)-H₂ and He(2^3S)-H₂ systems, and their dependence on the intramolecular H—H distance are reported.

PACS number(s): 31.20.Di, 31.50.+w, 31.90.+s, 35.10.Di

I. INTRODUCTION

Collision processes involving excited atoms play an important role in many fields of physics including gas-laser physics, plasma physics, and upper-atmosphere physics [1]. Among these processes, an important one—which has been extensively studied—is the Penning-ionization process involving metastable helium. For the systems He(2^1S and 2^3S)-H₂, experimental data in the thermal [2–6] and superthermal [7] energy range have been reported. Qualitatively good agreement between experimental results and quantum-mechanical calculations based on an optical-potential model [8] and classical trajectory calculations [9,10] has shown that the dipole-dipole interaction is the major contribution to the autoionization process at large interatomic distances [11]. However, although reliable values for the dipole-dipole (C_6) dispersion coefficients are available for a large number of rare-gas diatomic systems in which atoms are in their ground state [12–15], very little is known for excited atoms. On the other hand, it is well known that dispersion coefficients may be obtained from the knowledge of frequency-dependent polarizabilities. Then, to be capable of calculating frequency-dependent polarizabilities for the low-lying excited states of rare gas is of importance.

The purpose of this paper is first to present accurate calculations of the dynamic (both real and imaginary frequencies) dipole and quadrupole polarizabilities for the two low-lying metastable states (2^1S and 2^3S) of He using our time-dependent gauge-invariant (TDGI) method [16–18]. When possible, our values are compared with the nearly exact results obtained by Glover and Weinhold [19,20] using explicitly correlated wave functions. Then, the frequency-dependent polarizabilities are used to compute the two-body dispersion coefficients corresponding to 1^1S , 2^1S , and 2^3S states, and by combining the present results with those obtained in a previous work [18], to ob-

tain the C_6 dispersion coefficients and their dependence on the intramolecular coordinate of H₂ for the He(2^1S and 2^3S)-H₂ systems.

Some methodological and computational details are given in Sec. II. Results are presented and discussed in Sec. III. Atomic units are used throughout the paper.

II. METHODOLOGICAL AND COMPUTATIONAL DETAILS

Our calculations are done by using a recently presented method based on a TDGI formalism for calculating static as well as dynamic linear and nonlinear polarizabilities [16,17]. This method, which has been first applied to systems in their ground state, is extended here to calculate polarizabilities of the 2^1S and 2^3S metastable excited states of He at frequencies below and above the first excitation threshold. Many of the theoretical details are similar to those described in Refs. [16,17] and [21], and therefore need not be repeated here. The fundamental ingredient to obtain accurate values of dynamic polarizabilities is to generate wave functions leading to accurate energies for the ground 1^1S and excited 2^1S , 2^3S , 2^1P , and 2^3P states, as well as accurate dipole-transition moments.

TABLE I. Comparison between calculated and experimental transition energies (ΔE), oscillator strengths (f_{ik}), and transition probability (A_{ki}) involving 2^1S , 2^1P , 2^3S , and 2^3P states of He. Experimental values (see Ref. [29]) are in parentheses.

Transition	ΔE (a.u.)	f_{ik}	A_{ki} (10^9 s ⁻¹)
$1^1S \rightarrow 2^1P$	0.778 879	0.2723	1.769
$1s^2 \ 1s2p$	(0.779 751)	(0.2762)	(1.799)
$2^1S \rightarrow 2^1P$	0.022 251	0.3801	0.002 015
$1s2s \ 1s2p$	(0.022 130)	(0.3764)	(0.001 976)
$2^3S \rightarrow 2^3P$	0.042 143	0.5408	0.010 28
$1s2s \ 1s2p$	(0.042 060)	(0.5391)	(0.010 22)

For He, the basis set used consists of $13s$, $7p$, and $6d$ primitive Gaussian orbitals based on the van Duijneveldt ($10s$) primitive set [22,23] augmented by an even-tempered ($7p,6d$) polarization set and $3s$ diffuse functions. Exponents of the $3s$ orbitals are 0.049 069, 0.022 304, and 0.010 138, respectively. Using this basis set, full configuration-interaction (CI) calculations were carried out to obtain the ground and the low-lying excited states by means of the multireference second-order many-body perturbation through the CIPSI algorithm [24,25]. A comparison of our energies with the “exact” nonrelativistic values [26–28] illustrates how good our wave functions are: 2^1S : $-2.145\,916$ (exact: $-2.145\,974$), 2^3S : $-2.175\,229$ (exact: $-2.175\,229$), 2^1P : $-2.123\,666$ (exact: $-2.123\,843$), and 2^3P : $-2.133\,086$ (exact: $-2.133\,163$). As an additional test of the accuracy and the completeness of our wave functions, we calculated the absorption oscillator strengths

TABLE II. Dynamic dipole polarizability $\alpha_1(\omega)$ of the 2^1S state of He. Comparison with the rigorous bounds results of Glover and Weinhold [19,20]. We think there must be a typing error on this value marked with an asterisk. All results are in a.u.

$\hbar\omega$	TDGI results	Rigorous bounds [19,20]
0	803.25	803.31±6.61
0.001	804.84	804.90±6.63
0.002	809.66	809.68±6.68
0.003	817.81	817.81±6.76
0.004	829.51	829.46±6.87
0.005	845.07	844.96±7.03
0.006	864.93	864.74±7.22
0.007	889.69	889.38±7.47
0.008	920.14	919.68±7.77
0.009	957.38	956.71±8.14
0.010	1002.85	1011.91*±8.60
0.011	1058.59	1057.28±9.15
0.012	1127.45	1125.63±9.84
0.013	1213.58	1211.02±10.71
0.014	1323.18	1319.56±11.81
0.015	1466.01	1460.78±13.26
0.016	1658.27	1650.45±15.22
0.017	1928.94	1916.66±17.99
0.018	2335.48	2314.75±22.18
0.019	3010.05	2970.69±29.21
0.020	4339.60	4246.89±43.32
0.021	8149.49	7785.88±85.30
0.025	-2700.55	-2707.52±93.61
0.030	-877.88	-881.51±22.42
0.035	-474.98	-477.48±13.19
0.040	-301.61	-303.61±10.09
0.045	-206.30	-208.08±8.77
0.050	-146.21	-147.95±8.30
0.055	-104.49	-106.35±8.39
0.060	-73.05	-72.23±9.04
0.065	-47.24	-50.04±10.41
0.070	-23.65	-27.60±12.97
0.075	1.46	-4.78±17.98
0.080	35.23	24.01±29.18
0.085	103.15	78.79±64.32
0.090	529.0	631.0±591.0

f_{ik} for the dipole transitions between lower (i) and upper (k) states as well as the Einstein spontaneous-transition probability A_{ki} .

As can be seen in Table I, there is an excellent agreement between our theoretical values for ΔE , f_{ik} , and A_{ki} for the $2^1S \rightarrow 2^1P$ and $2^3S \rightarrow 2^3P$ transitions and the experimental ones [29]. Such an agreement is important since the more these properties are accurately described the more the results on computed dynamic dipole polarizabilities are expected to be good. In order to obtain realistic potential surfaces for triatomic van der Waals systems consisting of a metastable atom and a stable diatom, the knowledge of the dependence of the atom-diatom dispersion coefficients on the diatomic internal distance is needed [18,30–33]. For the He(2^1S and 2^3S)-H₂ systems, calculations of the dispersion coefficients are based on the so-called Casimir-Polder [34] formula which expresses dispersion coefficients in terms of imaginary-frequency integrals of the dynamic polarizabilities for the noninteracting systems. Note that by us-

TABLE III. Dynamic dipole polarizability $\alpha_1(\omega)$ of the 2^3S state of He. Comparison with the rigorous bounds results of Glover and Weinhold [19,20]. All results are in a.u.

$\hbar\omega$	TDGI results	Rigorous bounds [19,20]
0	315.92	316.24±0.78
0.0025	317.00	317.33±0.78
0.0050	320.31	320.63±0.79
0.0075	325.97	326.30±0.80
0.0100	334.25	334.59±0.83
0.0125	345.56	345.90±0.86
0.0150	360.50	360.75±0.90
0.0175	379.96	380.32±0.96
0.0200	405.28	405.65±1.03
0.0225	438.51	438.89±1.13
0.0250	482.95	483.34±1.25
0.0275	544.17	544.57±1.43
0.0300	632.41	632.82±1.70
0.0325	768.67	769.05±2.10
0.0350	1003.68	1003.93±2.82
0.0375	1499.53	1499.16±4.39
0.0400	3205.28	3199.13±10.27
0.0450	-2097.0	-8388.0±6339.0
0.0500	-726.27	-724.20±5.89
0.0550	-417.20	-416.44±3.05
0.0600	-281.78	-281.32±2.14
0.0650	-206.21	-205.84±1.74
0.0700	-158.17	-157.82±1.56
0.0750	-124.94	-124.58±1.51
0.0800	-100.49	-100.11±1.55
0.0850	-81.55	-81.15±1.71
0.0900	-66.11	-65.71±2.03
0.0950	-52.74	-52.38±2.63
0.1000	-40.07	-39.91±3.79
0.1050	-26.03	-26.50±6.40
0.1090	-10.17	-11.93±11.88
0.1095	-7.49	-9.82±12.77
0.1125	16.98	10.98±25.63
0.1150	74.32	61.24±67.87
0.1170	450.0	1193.0±1192.0

TABLE IV. Dynamic quadrupole polarizability of the 2^1S and 2^3S states of He. All results are in a.u. $C_{zz,zz}$ is defined [49] as $C_{zz,zz} = 2/3\hbar \sum_{m \neq g} |\langle g | \hat{\theta}_{zz} | m \rangle|^2 / \omega_{mg} = 1/3\alpha_2$.

$\hbar\omega$	$C_{zz,zz}$ (2^1S)	$C_{zz,zz}$ (2^3S)
0	2290.3	887.34
0.005	2296.9	888.97
0.010	2317.0	893.07
0.015	2351.1	900.14
0.020	2400.9	910.51
0.025	2468.1	923.80
0.030	2555.6	940.91
0.035	2667.7	961.92
0.040	2810.0	987.40
0.045	2991.6	1018.1
0.050	3225.6	1054.8
0.055	3531.8	1098.5
0.060	3944.5	1151.2
0.065	4522.8	1214.4
0.070	5383.5	1292.1
0.075	6785.9	1387.5
0.080	9460.5	1507.5
0.085	16 548.0	1662.6
0.090	90 882.0	1868.1
0.095	-22 973.0	2153.9
0.100	-9525.4	2577.6
0.105	-5639.2	3267.9

ing our TDGI method the dispersion coefficients for seven specific H—H bond distances varying from 1.4 to 6.0 a.u. have already been calculated in a previous work [18].

III. RESULTS AND DISCUSSION

There is a vast amount of theoretical [19,20,35–45] and experimental data [46] for the static dipole polarizabilities α_1 of the 2^1S and 2^3S metastable states of helium. To our knowledge, none are so accurate and so reliable as the rigorous upper- and lower-bound results obtained by Glover and Weinhold [19,20]. They also give the rigorous bounds for dynamic dipole polarizability at real $[\alpha_1(\omega)]$ and at imaginary frequencies $[\alpha_1(i\omega)]$ for a wide

range of energies. We shall use these rigorous bounds as a criterion to estimate the quality of our TDGI results (Tables II and III). A first point to emphasize is that our results for the static polarizabilities (803.25 and 315.92 a.u. for 2^1S and 2^3S , respectively) are in excellent agreement with the rigorous bounds of Glover and Weinhold [19,20] (803.31 ± 6.61 and 316.24 ± 0.78 a.u.), and also agree with the experimental values (728.8 ± 87.7 and 301 ± 20 a.u.) determined by the electric-deflection time-of-flight method [26]. For the dynamic polarizabilities at frequencies up to the second excitation threshold, TDGI results are always compatible with the rigorous bounds, except for the 2^1S metastable state near the resonance within the range 0.019–0.021 a.u.

In contrast to the dipole polarizabilities very little is known about quadrupole polarizabilities ($\alpha_2 = 3C_{zz,zz}$) of excited states of He. For the 2^3S state, earlier theoretical values for the static quadrupole polarizability component $C_{zz,zz}$ range from 887.7 to 947.6 a.u. [47] in the extended Coulomb approximation (ECA) and quantum-defect orbital (QDO) methods, while multiconfiguration self-consistent-field (MCSCF) calculations done by Konowalow and Lengsfeld [48] give a value of 914.4 a.u. (note that we have divided their results by a factor 3 to adopt Bishop's convention [49]).

For the 2^1S state, the values obtained by Lamm and Szabo [47] are 2346 and 2425 a.u. depending on the approximation used. Calculated dynamic quadrupole polarizabilities are given in Table IV. Our static $C_{zz,zz}$ values (2290.3 a.u. for 2^1S and 887.34 a.u. for 2^3S) agree within 2% with the ECA value of Lamm and Szabo [47]. For the dynamic values we found no published data to compare with [50].

The multipole expansion of the second-order interaction energy between a pair of neutral S -state atoms is given by

$$\Delta E = -C_6 R^{-6} - C_8 R^{-8} - C_{10} R^{-10} \dots,$$

where the C_n 's are the van der Waals or dispersion coefficients. The C_6 and C_8 dispersion coefficients for the interaction between the ground (1^1S) and excited states

TABLE V. van der Waals C_6 and C_8 coefficients (in a.u.) for He in the 1^1S , 2^1S , and 2^3S states. The rigorous bounds results are given in parentheses for C_6 .

C_6	1^1S	2^1S	2^3S
1^1S	1.4593 (1.4597 \pm 0.0055)	42.12 (41.47 \pm 1.70)	29.19 (29.00 \pm 0.51)
2^1S		1.136×10^4 ($[1.133 \pm 0.063] \times 10^4$)	5.866×10^3 ($[5.767 \pm 0.339] \times 10^3$)
2^3S			3.279×10^3 ($[3.289 \pm 0.090] \times 10^3$)
C_8	1^1S	2^1S	2^3S
1^1S	13.883	3263	1689
2^1S		8.125×10^5	4.068×10^5
2^3S			2.086×10^5

TABLE VI. Calculated C_6 dispersion coefficients for $\text{He}(2^1S)\text{-H}_2$ and $\text{He}(2^3S)\text{-H}_2$ as a function of the interhydrogen distance R .

R	1.4	2.4	3.0	3.4	3.8	4.4	6.0
$\text{He}(2^1S)\text{-H}_2$							
C_6^{\parallel}	188.7	406.7	501.5	513.4	484.4	412.9	292.1
C_6^{\perp}	135.8	222.8	255.7	266.0	268.2	265.7	258.0
C_6	153.4	284.1	337.6	348.5	340.3	314.8	269.4
$\text{He}(2^3S)\text{-H}_2$							
C_6^{\parallel}	129.1	274.4	336.6	343.8	324.4	277.1	197.5
C_6^{\perp}	93.0	151.6	173.8	180.7	182.0	180.5	175.3
C_6	105.0	192.5	228.1	235.1	229.5	212.7	182.7

(2^1S and 2^3S) of He were calculated by combining our $\alpha_1(i\omega)$ and $\alpha_2(i\omega)$ TDGI values through a simple numerical integration using (see [51] and Table IV),

$$C_6 = \frac{3\hbar}{\pi} \int_0^{\infty} \alpha_1^A(i\omega) \alpha_1^B(i\omega) d\omega,$$

$$C_8 = \frac{15\hbar}{\pi} \int_0^{\infty} [\alpha_2^A(i\omega) \alpha_1^B(i\omega) + \alpha_1^A(i\omega) \alpha_2^B(i\omega)] d\omega.$$

For the ground and low-lying S states of He, C_6 and C_8 values are given in Table V. For C_6 our values are compatible with the very tight error bounds obtained by Glover and Weinhold [20]. Our best estimate of C_6 for (1^1S-1^1S), (2^1S-2^1S), and (2^3S-2^3S) are different from rigorous calculations by 0.03%, 0.26%, and 0.3%, while our (2^1S-2^3S) result is too high by 1.7% with respect to the rigorous bounds mean value of [20]. For C_8 the largest difference between the values in Table V and the results given by Proctor and Stwalley [52] is 2.7%. As expected, in all cases the results obtained for systems consisting of excited atoms are fairly large with respect to those obtained with atoms in their ground state since excited rare-gas atoms lose their “closed-shell” character.

Table VI presents TDGI calculations of the C_6 dispersion coefficients (both parallel and perpendicular) for the

systems $\text{He}(2^1S)\text{-H}_2$ and $\text{He}(2^3S)\text{-H}_2$ as a function of the interhydrogen $R_{\text{H-H}}$ distance. This is a calculation from first principles of this quantity involving low-lying metastable states of He. C_6 dispersion coefficients for both systems are obtained using accurate dipole polarizabilities at seven H—H distances ranging from 1.4 to 6.0 a.u. calculated in [18]. A maximum for the C_6 coefficients occurs at values of R similar to those at which the polarizabilities of H_2 reach their maximum value. It should be noted that for all distances the C_6 [$\text{He}(2^1S)\text{-H}_2$] coefficient is roughly 50% higher than the C_6 [$\text{He}(2^3S)\text{-H}_2$] value. These R -dependent coefficients may be used for representing model potential functions.

ACKNOWLEDGMENTS

We would like to thank the “Centre National de la Recherche Scientifique” (CNRS), the “Ministère de l’Education Nationale” (MEN), and the C3NI of the Center National Universitaire Sud de Calcul (CNUSC) for their support. Laboratoire de Physique Quantique is “Unité de Recherche Associé du CNRS No. 505” and Laboratoire de Chimie Structurale is “Unité de Recherche Associée au CNRS No. 474.”

*Permanent address: Laboratoire Dynamique des Interactions Moléculaires, Université Paris VI, Tour 22, 4 place Jussieu, 75252 Paris Cédex 05, France.

- [1] A. Hitachi, M. Ukai, and Y. Hatano, *CRC Handbook of Radiation Chemistry*, edited by Y. Tabata, Y. Ito, and S. Tagawa (CRC, Boca Raton, 1991), Chap. IV, p. 223.
- [2] J. Fort, T. Bolzinger, D. Corno, T. Ebding, and A. Pesnelle, *Phys. Rev. A* **18**, 2075 (1978).
- [3] A. Munzer and A. Niehaus, *J. Electron. Spectrosc.* **23**, 367 (1981).
- [4] D. W. Martin, D. Bernfeld, and P. E. Siska, *Chem. Phys. Lett.* **110**, 298 (1984).
- [5] D. W. Martin, C. Weiser, R. F. Sperlein, D. L. Bernfeld, and P. E. Siska, *J. Chem. Phys.* **90**, 1564 (1989).
- [6] T. Bregel, A. J. Yench, H. W. Ruf, H. Waibel, and H. Hotop, *Z. Phys. D* **13**, 51 (1989).
- [7] H. Ferkel, *Chem. Phys. Lett.* **192**, 327 (1992).
- [8] Y. Mirishima, M. Ukai, N. Kouchi, and Y. Hatano, *J. Chem. Phys.* **96**, 8187 (1992), and references therein.
- [9] T. Watanabe and K. Katsuura, *J. Chem. Phys.* **47**, 800 (1967).
- [10] M. Kohmoto and T. Watanabe, *J. Phys. B* **10**, 1875 (1977).
- [11] M. Ukai, H. Yoshida, Y. Morishima, H. Nakazawa, K. Shinsaka, and Y. Hatano, *J. Chem. Phys.* **90**, 4865 (1989).
- [12] G. C. Maitland, M. Rigby, E. B. Smith, and W. A. Wakeham, *Intermolecular Forces: Their Origin and Determination* (Clarendon, Oxford, 1981), Chap. 9.
- [13] R. A. Aziz, *Inert Gases: Potentials Dynamics and Energy Transfer in Doped Crystals*, edited by M. L. Klein (Springer Verlag, Berlin, 1984), Chap. 2.
- [14] J. M. Hutson, *Annu. Rev. Phys. Chem.* **41**, 123 (1990) and references therein.
- [15] A. J. Thakkar, H. Hettema, and P. E. S. Wormer, *J. Chem. Phys.* **97**, 3252 (1992) and references therein.
- [16] M. Rérat, M. Mérawa, and C. Pouchan, *Phys. Rev. A* **45**, 6263 (1992).
- [17] M. Rérat, M. Mérawa, and C. Pouchan, *Phys. Rev. A* **46**, 5471 (1992).

- [18] M. Caffarel, M. Rérat, and C. Pouchan, *Phys. Rev. A* **47**, 3704 (1993).
- [19] R. M. Glover and F. Weinhold, *J. Chem. Phys.* **66**, 185 (1977).
- [20] R. M. Glover and F. Weinhold, *J. Chem. Phys.* **66**, 191 (1977).
- [21] M. Rérat, C. Pouchan, M. Tadjeddine, J. P. Flament, H. P. Gervais, and G. Berthier, *Phys. Rev. A* **43**, 5832 (1991).
- [22] F. B. Van Duijneveldt, IBM Technical Report No. RJ945, 1971.
- [23] G. Chalasinski, S. Van Smaalen, and F. B. Van Duijneveldt, *Mol. Phys.* **45**, 1113 (1982).
- [24] B. Huron, P. Rancurel, and J. P. Malrieu, *J. Chem. Phys.* **58**, 5745 (1973).
- [25] E. Evangelisti, J. P. Daudey, and J. P. Malrieu, *Chem. Phys.* **75**, 91 (1983).
- [26] Y. Accad, C. L. Pekeris, and B. Schiff, *Phys. Rev. A* **4**, 516 (1971).
- [27] K. Frankowski and C. L. Pekeris, *Phys. Rev.* **146**, 46 (1966).
- [28] A. J. Thakkar and V. H. Smith, Jr., *Phys. Rev. A* **15**, 16 (1977).
- [29] W. L. Wiese, M. W. Smith, and B. M. Glennon, *Atomic Transition Probabilities*, Natl. Bur. Stand. Ref. Data Ser., Natl. Bur. Stand. (U.S.) Circ. No. 4 (U.S. GPO, Washington, D. C., 1966), Vol. I, pp. 11–15.
- [30] K. T. Tang and J. P. Toennies, *J. Chem. Phys.* **68**, 5501 (1978).
- [31] K. T. Tang and J. P. Toennies, *J. Chem. Phys.* **74**, 1148 (1981).
- [32] W. R. Rodwell and G. Scoles, *J. Phys. Chem.* **86**, 1053 (1982).
- [33] M. A. Matias and A. J. C. Varandas, *Mol. Phys.* **70**, 623 (1990).
- [34] H. B. G. Casimir and D. Polder, *Phys. Rev.* **73**, 360 (1948).
- [35] K. T. Chung and R. P. Hurst, *Phys. Rev.* **152**, 35 (1966).
- [36] G. A. Victor, A. Dalgarno, and A. J. Taylor, *J. Phys. B* **1**, 13 (1968).
- [37] A. Dalgarno and G. A. Victor, *J. Chem. Phys.* **49**, 1982 (1968).
- [38] G. W. F. Drake, *Can. J. Phys.* **50**, 1896 (1972).
- [39] S. A. Adleman and A. Szabo, *Phys. Rev. Lett.* **28**, 1427 (1972).
- [40] A. Dalgarno and R. M. Pengelly, *Proc. Phys. Soc. London* **89**, 503 (1966).
- [41] A. L. Stewart, *J. Phys. B* **2**, 1309 (1969).
- [42] A. Dalgarno and A. E. Kingston, *Proc. Phys. Soc. London* **72**, 1053 (1958).
- [43] G. W. F. Drake and M. Cohen, *J. Chem. Phys.* **48**, 1168 (1968).
- [44] V. Jacobs, *Phys. Rev.* **3**, 289 (1971).
- [45] R. C. Sklarew and J. Callaway, *Phys. Rev.* **175**, 103 (1968).
- [46] D. A. Crosby and J. C. Zorn, *Phys. Rev. A* **16**, 488 (1977).
- [47] G. Lamm and A. Szabo, *J. Chem. Phys.* **72**, 3354 (1980).
- [48] D. D. Konowalow and B. H. Lengsfeld III, *J. Chem. Phys.* **87**, 4000 (1987).
- [49] D. M. Bishop, *Rev. Mod. Phys.* **62**, 343 (1990).
- [50] Upon completion of this work we have received from Bishop and Pipin some of their not yet published results for the dynamic dipole and quadrupole polarizabilities of the triplet states of He. While our dipole values are in perfect agreement with their values, our quadrupole results differ from their results by about 1%.
- [51] J. E. Bohr and K. L. C. Hunt, *J. Chem. Phys.* **86**, 5441 (1987).
- [52] T. R. Proctor and W. C. Stwalley, *J. Chem. Phys.* **68**, 5292 (1978).

L. M. Caffarel and W. Krauth, "Exact Diagonalization Approach to Correlated Fermions in Infinite Dimensions: Mott Transition and Superconductivity", *Phys. Rev. Lett.* **72**, 1545 (1994)

Exact Diagonalization Approach to Correlated Fermions in Infinite Dimensions: Mott Transition and Superconductivity

Michel Caffarel^{1,*,\dagger} and Werner Krauth^{2,\ddagger}

¹Centre Nationale de la Recherche Scientifique-Laboratoire de Physique Quantique, Institut de Recherche sur les Systèmes Atomiques et Moléculaires Complexes, Université Paul Sabatier, 118, route de Narbonne, F-31062 Toulouse Cedex, France

²Centre Nationale de la Recherche Scientifique-Laboratoire de Physique Statistique de l'École Normale Supérieure, 24, rue Lhomond, 75231 Paris Cedex 05, France

(Received 21 June 1993)

We present a powerful method for calculating the thermodynamic properties of infinite-dimensional Hubbard-type models using an exact diagonalization of an Anderson model with a finite number of sites. The resolution obtained for Green's functions is far superior to that of quantum Monte Carlo calculations. We apply the method to the half-filled Hubbard model for a discussion of the metal-insulator transition, and to the two-band Hubbard model where we find direct evidence for the existence of a superconducting instability at low temperatures.

PACS numbers: 75.10.Lp, 71.10.+x, 71.45.Lr, 75.30.Fv

Following the pioneering work of Metzner and Vollhardt [1], the limit of large dimensions for models of strongly correlated fermions has received much attention. In this limit, the highly intricate quantum many-body problem simplifies considerably and leads to a nontrivial mean-field theory [2]. Remarkably, this limit captures many features of the physics in finite dimensions and gives a very successful description of quantum fluctuations.

In spite of the considerable simplification obtained in taking the large D limit, the mean-field equations still have to be solved numerically. Up to now, all calculations [3–5] have relied on the Hirsch-Fye quantum Monte Carlo (QMC) algorithm [6]. A major limitation of this scheme is the difficulty of accessing low temperatures, where statistical and finite time-step discretization errors of the QMC algorithm become very important.

In this paper, we present a powerful exact diagonalization method for solving these mean-field equations. We find that the resolution obtained for thermodynamic Green's functions is far superior to that of QMC calculations and that essentially the exact solution of the model is obtained, except at very small frequencies. Having at our disposal such a unique method, we investigate two important physical issues for which no definite answers have been given so far. *First*, we consider the metal-insulator transition in the half-filled Hubbard model, where our numerical results are indicative of a second-order transition at zero temperature. *Second*, we establish the instability of the normal state of the two-band Hubbard model [7] with respect to singlet superconductivity at large U and small doping (the regime of relevance for high- T_c superconductors) and also an instability towards triplet superconductivity in the large doping regime $n \sim 2$.

For concreteness, we explain the method in the single-band Hubbard model on a Bethe lattice of infinite con-

nectivity $z \rightarrow \infty$. The Hamiltonian is written as

$$H = - \sum_{(ij)\sigma} \frac{1}{\sqrt{2z}} c_{i\sigma}^\dagger c_{j\sigma} + \text{H.c.} + U \sum_i n_{i\uparrow} n_{i\downarrow}. \quad (1)$$

The calculation of the single-site properties of the Hubbard model in this limit reduces to the self-consistent determination of the on-site Green's function $G(i\omega)$ of the Hubbard model and of a bath Green's function $G_0(i\omega)$, which describes the interaction on the single site with the external environment. $G(i\omega)$ and $G_0(i\omega)$ are related by a self-consistency condition which (in the paramagnetic normal state, on the Bethe lattice) reads

$$G_0^{-1}(i\omega) = i\omega + \mu - G(i\omega)/2. \quad (2)$$

As is well known [8], the on-site Green's function of the Hubbard model may be interpreted as the Green's function of an Anderson model

$$H_{\text{And}} = \epsilon_d \sum_{\sigma} d_{\sigma}^\dagger d_{\sigma} + \sum_{\sigma, l=2}^{n_s} \epsilon_l a_{l\sigma}^\dagger a_{l\sigma} + U n_{d\uparrow} n_{d\downarrow} + \sum_{\sigma, l=2}^{n_s} (V_l a_{l\sigma}^\dagger d_{\sigma} + \text{H.c.}), \quad (3)$$

the function $G_0(i\omega_n)$ being given by the $U = 0$ Green's function of the impurity

$$G_0(i\omega_n) = G_0^{\text{And}}(i\omega_n) = \left(i\omega_n - \epsilon_d - \mu - \sum_{l=2}^{n_s} \frac{V_l^2}{i\omega_n - \epsilon_l} \right)^{-1}. \quad (4)$$

Given the infinite number of degrees of freedom of the models defined in Eq. (1) and Eq. (3), it is evident that strict self-consistency can only be obtained with a continuous Anderson model, i.e., with $n_s = \infty$. Our algorithm is based on the observation that a *systematic* approximation (i.e., fit) of $G_0(i\omega)$ with a finite- n_s Anderson model

gives extremely good results. We stress from the beginning that we perform a fit of the imaginary-frequency Green's functions only.

In practice, we approximate any $G_0^{-1}(i\omega)$ by a function $G_0^{-1 \text{ And}}(i\omega)$ with a finite number n_s of sites. This can be cast into a minimization problem in the variables ϵ_l and V_l . In this work, we choose the following cost function:

$$\chi^2 = \frac{1}{n_{\max} + 1} \sum_{n=0}^{n_{\max}} |G_0^{-1}(i\omega_n) - G_0^{-1 \text{ And}}(i\omega_n)|^2, \quad (5)$$

where n_{\max} is chosen sufficiently large [$\omega_{n_{\max}} \gg \max_l(\epsilon_l)$] [9]. We search for the parameters ϵ_l and V_l minimizing the χ^2 in Eq. (5) with a standard conjugate gradient method.

For a small number of sites, $n_s \leq 6$, the Green's function $G(i\omega_n)$ can be obtained exactly from the complete set of eigenvectors and eigenvalues of the Anderson Hamiltonian equation (3). The procedure

$$G_0^{-1}(i\omega) \xrightarrow{\text{Eq. (5)}} G_0^{-1 \text{ And}}(i\omega) \xrightarrow{\text{Eq. (3)}} G(i\omega) \xrightarrow{\text{Eq. (2)}} G_0^{-1}(i\omega) \quad (6)$$

is then iterated to convergence.

Beyond $n_s = 6$, the size of the Hilbert space becomes too large for an explicit diagonalization of the Anderson Hamiltonian. However, the calculation of *zero-temperature* Green's functions is still possible by means of the Lanczòs algorithm [10], which allows us to easily calculate $G(i\omega)$ and $G_0(i\omega)$ up to $n_s \sim 10$ on a work station. The fit with the Anderson model is performed as before. We simply replace the Matsubara frequencies by a fine grid of imaginary frequencies, which correspond to a "fictitious" inverse temperature $\tilde{\beta}$ ($\omega_n = (2n+1)\pi/\tilde{\beta}$). $\tilde{\beta}$ introduces a low-frequency cutoff in an obvious way.

The following observations are made:

(1) We notice in general very small differences between $G_0^{-1}(i\omega)$ and $G_0^{-1 \text{ And}}(i\omega)$ as expressed by small minimal values of χ^2 in Eq. (5). χ^2 decreases by approximately a constant factor each time we add one more site. This means that *exponential* convergence in n_s is observed.

(2) The extensive comparisons with QMC [5] which we have undertaken indicate that, even at finite temperature, exact diagonalization is by far the superior method for this problem. Using exact diagonalization at $n_s = 3, \dots, 6$, very precise values of the Green's function $G(\tau)$ can be obtained in a few minutes on a work station, which it has taken us days to check by QMC [11].

(3) Using the Lanczòs algorithm at $T = 0$ we can go higher in n_s , and the quality of fit can be ameliorated by another 2 orders of magnitude. To illustrate, we display in Fig. 1(a) the low-frequency part of $G_0^{-1}(i\omega)$ and $G_0^{-1 \text{ And}}(i\omega)$ for $U = 2$ at $\tilde{\beta} = 200$ [see also Fig. 3(a) for the two-band Hubbard case]. Notice the *systematic* amelioration of the fit. Furthermore, the bath Green's function G_0^{-1} [the Green's function obtained from Eq. (2), once $G(i\omega)$ has been computed] is extremely independent of n_s , especially at high frequency. Already at $\omega = 0.11$, e.g., G_0^{-1} varies by less than 0.0001 between

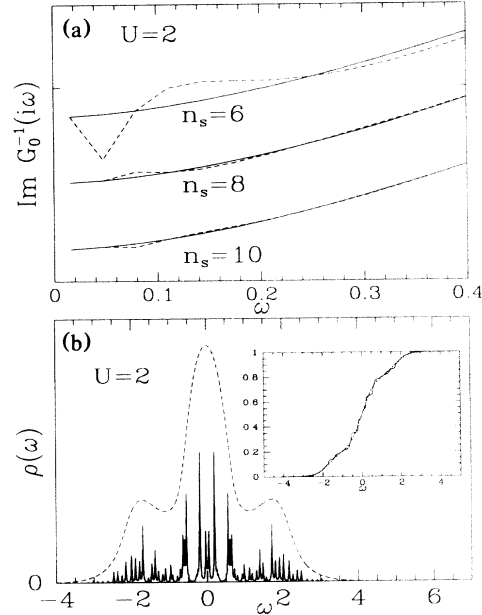


FIG. 1. (a) $G_0(i\omega)^{-1}$ and $G_0^{-1 \text{ And}}$ in the Hubbard model at $U = 2$ at small frequency for $n_s = 6, 8, 10$. Note the systematic improvement of the solution. The maximal misfit between the two functions is 0.082 for $n_s = 6$. (b) Density of states $\rho(\omega)$ for $U = 2$ ($\epsilon = 0.01$). We compare with the IPT density of states [12]. Inset: Comparison of the integrated densities of states between exact diagonalization and IPT.

$n_s = 6, 8$, and 10. The same convergence is observed for the physical Green's function $G(i\omega)$ in which we are ultimately interested.

(4) Even though the method has been geared exclusively at the calculation of thermodynamic Green's quantities, it is very interesting to consider the dynamic properties, e.g., the one-particle spectral densities $\rho(\omega) = -\text{Im}G(\omega + i\epsilon)/\pi$. We have computed $\rho(\omega)$ ($n_s=10$) for different values of U . In the Fermi-liquid regime at moderate U , the excitation spectrum of our finite-size Anderson model consists of a large number of peaks, which are grouped into three well-separated structures: a central quasiparticle peak and two broad high-energy satellite features, corresponding to the formation of the upper and lower Hubbard bands. At sufficiently large U a Mott insulator gap is observed, and far fewer peaks contribute to the spectrum. Figure 1(b) gives the spectral density as obtained at $U = 2$. The dashed line represents the results given by the iterated perturbation theory (IPT) approximation. This method is based essentially on the use of a weak coupling calculation to second order in U of Σ which gives an interpolation between the small and large U limits (exclusively at half filling and in the paramagnetic phase) [8,12,13]. We also present the *integrated* density of states corresponding to Lanczòs and IPT. The agreement between both curves is seen to be excellent, provided we average over a small frequency interval. This indicates that the spectral density, as calculated by our

method, contains coarse-grained information about the exact solution, and can be very useful in cases in which IPT cannot be applied.

Let us now give a more quantitative discussion of the metal-insulator transition. Figure 2 presents some results for the quasiparticle spectral weight Z calculated from the slope of the self-energy $\Sigma = G_0^{-1} - G^{-1}$. In the inset of Fig. 2 we present the data for $\text{Im}\Sigma(i\omega)$ at small frequencies from which the spectral weight is extracted [$\text{Im}\Sigma(i\omega) \sim (1 - 1/Z)\omega + \dots$]. To get a truly stabilized slope of Σ we have found it necessary to reach very large values of $\tilde{\beta}$. The main plot compares the results at $n_s = 10$ with IPT. On a few points we give in addition the results at $n_s = 6$ and $n_s = 8$. Given the extremely good agreement between the values of Z calculated with $n_s = 8$ and 10, we are very confident of the numerical values presented.

As discussed in Ref. [12], the IPT approximation leads to a first-order Mott-Hubbard transition (cf. Fig. 2), and the quasiparticle weight Z jumps discontinuously at $U \sim 3.6$. We have only found limited evidence for such a scenario within the present approach. At $n_s = 6$, we are unable to stabilize two solutions at the same values of the physical parameters (the coexistence of two solutions is indicative of a first-order phase transition). At $n_s = 8$, and using a fictitious temperature of $\tilde{\beta} = 120$, we find a coexistence region within a very small interval of U : $4.45 \leq U \leq 4.60$ [14]. Even though the question of the order of the transition will have to await a more detailed investigation, it seems to us to be difficult to reconcile our numerical results with an abrupt zero-temperature transition anywhere close to $U = 3.6$. Let us reiterate the fact that the results presented in Fig. 2 are at zero temperature and that $\tilde{\beta}$ only serves as a frequency cutoff.

We now consider the very important issue of supercon-

ductivity in Hubbard-type models in infinite D . We have looked for it in the single-band model defined above, and in the two-band Hubbard model defined by the Hamiltonian [7]

$$\mathcal{H} = - \sum_{i \in D, j \in P, \sigma} t_{ij} d_{i\sigma}^\dagger p_{j\sigma} + \text{H.c.} + \epsilon_p \sum_{j \in P, \sigma} p_{j\sigma}^\dagger p_{j\sigma} + \epsilon_d \sum_{i \in D, \sigma} d_{i\sigma}^\dagger d_{i\sigma} + U_d \sum_{i \in D} n_{i\uparrow}^d n_{i\downarrow}^d, \quad (7)$$

where the hopping is scaled as $t_{ij} \sim 1/\sqrt{2z}$. In Eq. (7) (d_σ, p_σ) represent two atomic orbitals on different sublattices (D, P) of a bipartite lattice with $z \rightarrow \infty$ which, as before, is taken to be the infinitely connected Bethe lattice.

In the standard Nambu notation, $\Psi_d^\dagger \equiv (d_\uparrow^\dagger, d_\downarrow)$ (equivalently for Ψ_p) the d -orbital Green's function can be written as a 2×2 matrix

$$\mathbf{D}(\omega) \equiv -T \langle \Psi_d(\omega) \Psi_d^\dagger(\omega) \rangle = \begin{pmatrix} G_d(\omega) & F_d(\omega) \\ F_d(\omega)^* & -G_d(-\omega) \end{pmatrix} \quad (8)$$

and the self-consistency equations for the Green's functions are given by [7]

$$\begin{aligned} \mathbf{D}_0^{-1}(i\omega_n) &= i\omega_n + (\mu - \epsilon_d)\sigma_3 - t_{pd}^2 \sigma_3 \mathbf{P}(i\omega_n) \sigma_3, \\ \mathbf{P}^{-1}(i\omega_n) &= i\omega_n + (\mu - \epsilon_p)\sigma_3 - t_{pd}^2 \sigma_3 \mathbf{D}(i\omega_n) \sigma_3 \end{aligned} \quad (9)$$

(note that \mathbf{D}_0 and \mathbf{D} are 2×2 matrices and that \mathbf{D}_0^{-1} denotes the matrix inverse).

In the presence of superconducting order, the Green's functions $D(i\omega_n)$ and $D_0(i\omega_n)$ may be viewed as impurity Green's functions of an effective Anderson model in a superconducting medium, which we fit by a generalization of Eq. (4), modified by an explicit pairing between all the sites [11].

We are interested in the normal state exclusively as a starting point for a linear stability analysis and investigate the regime close to the normal solution. An example of the excellent quality of the normal state solution [15] is presented in Fig. 3(a). Here, $\text{Re}[G_{d0}(i\omega)]$ and $\text{Re}[G_{d0}^{\text{And}}(i\omega)]$ are displayed. The "fictitious" temperature is $\tilde{\beta} = 250$, $U_d = 8$, $\epsilon_p - \epsilon_d = 4$, $\mu = 3.5$, and the density corresponds to the lightly doped regime of the two-band model ($n \sim 1.3$). We now consider the stability analysis of the normal state solution. A possible way of studying this stability is to calculate the pairing susceptibility. An alternative way used here is to establish the stability properties of the solution by introducing small superconducting terms in the Anderson Hamiltonian, and following the evolution under subsequent iterations [7]. Under such conditions, the normal state solutions very quickly acquire nonzero values of $F(\omega)$, which indicate a superconducting instability. More rigorously, and in order to study quantitatively the effects of increasing n_s , we may calculate the largest eigenvalue, and the corresponding eigenvector of the matrix $\partial F(i\omega)^{n+1} / \partial F(i\omega)^n$ close to the normal state, where the

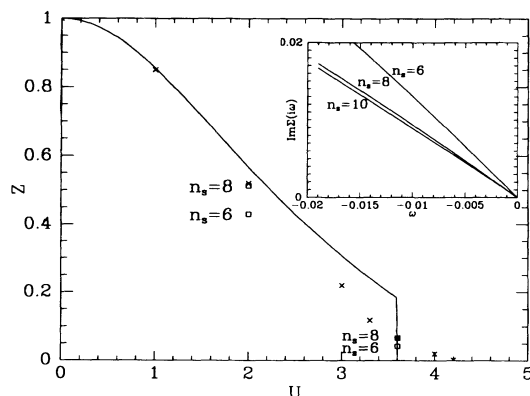


FIG. 2. Quasiparticle weight Z as a function of U for the half-filled Hubbard model. The curve gives the IPT approximation, which predicts a first-order transition. The crosses give the results for $n_s = 10$, with the corresponding results for $n_s = 6, 8$ at two points. The inset shows the small- ω behavior of $\text{Im}\Sigma(i\omega)$ for $n_s = 6, 8, 10$ from which the quasiparticle weight is calculated. Note the excellent convergence with n_s .

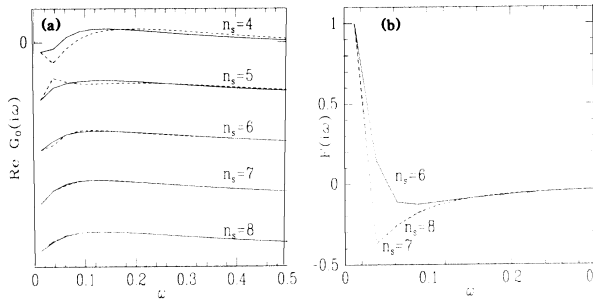


FIG. 3. (a) Real part of $G_d^{\text{And}}(i\omega)$ and $G_{d0}(i\omega)$ for $n_s = 4, \dots, 8$ (two-band model: $U_d = 8, \mu = 3.5, \epsilon_p - \epsilon_d = 4$). (b) Largest eigenvector of the matrix $\partial F(i\omega)^{n+1}/\partial F(i\omega)^n$ close to the normal state solution for $n_s = 6, 7$, and 8 (singlet sector). The corresponding eigenvalues are $\lambda_{\text{max}} \sim 2$ in all three cases.

superscripts on the F 's indicate two subsequent iterations of the self-consistency loop. We have done such calculations, which correspond to the well-known procedure of extracting the largest eigenvalue and eigenvector of a matrix with the "power method." We are able to identify a linear regime at small $F(i\omega)$, with the largest eigenvalue always of the order $\lambda_{\text{max}} \sim 2$. The corresponding (rescaled) eigenvectors for $n_s = 6, 7, 8$ are plotted in Fig. 3(b). Clearly, the agreement between these completely independent curves is excellent. We have checked this result in a variety of ways [by changing $\tilde{\beta}$, the precise form of the function used in Eq. (5), and the doping]. This leads us to the conviction that the normal state solution of the $d = \infty$ model at small doping is indeed unstable with respect to singlet superconductivity. We have performed a completely analogous stability analysis for the lightly doped ($n \sim 1.2$ and $n \sim 1.4$) regime of the corresponding one-band Hubbard model for a number of values of the interaction ($U = 2, 4, 6, 8$). In sharp contrast to the two-band Hubbard model, we have found no indication of a superconducting instability in that case.

We have also studied the point investigated previously [7], i.e., values of the physical parameters corresponding to a total density of $n \sim 2$, where the Hubbard interaction is just large enough to create a large overlap between the upper Hubbard band of the d -level and the p -level band. There our evidence for singlet superconductivity is very limited (at least for frequencies larger than $\sim 1/200$). However, we have on that point found very clear evidence for superconductivity in the triplet sector. Following the procedure outlined above (at $T = 0$), we find consistently that any small superconducting term, in addition to the normal state solution, blows up at a rate which corresponds to a largest eigenvalue of ~ 1.8 of the matrix $\partial F(i\omega)^{n+1}/\partial F(i\omega)^n$ [16] (typical values of parameters are $U_d = 4.5, \mu = \epsilon_p - \epsilon_d = 4, \tilde{\beta} = 200$). Superconducting order of this kind has been first proposed by Berezinskii [17] in the context of ^3He , and, very recently by Coleman, Miranda, and Tsvelik [18] for heavy-

fermion superconductors.

We acknowledge helpful discussions with J. Bellissard, A. Georges, G. Kotliar, D. Poilblanc, and T. Ziman. This work was supported by DRET Contract No. 921479.

* Permanent address: Laboratoire CNRS-Dynamique des Interactions Moléculaires, Tour 22 Université Paris VI, 4 place Jussieu F-75252 Paris Cedex 05, France. Electronic address: mc@dim.jussieu.fr

† Electronic address: mc@tolosa.ups-tlse.fr

‡ Electronic address: krauth@physique.ens.fr

- [1] W. Metzner and D. Vollhardt, Phys. Rev. Lett. **62**, 324 (1989).
- [2] For a recent review and references, see, e.g., D. Vollhardt, in "Correlated Electron Systems," Proceedings of the Jerusalem Winter School of Theoretical Physics, edited by V. J. Emery (World Scientific, Singapore, to be published) (Report No. RWTH/ITP-C 6/92).
- [3] M. Jarrell, Phys. Rev. Lett. **69**, 168 (1992).
- [4] M. Rozenberg, X. Y. Zhang, and G. Kotliar, Phys. Rev. Lett. **69**, 1236 (1992).
- [5] A. Georges and W. Krauth, Phys. Rev. Lett. **69**, 1240 (1992).
- [6] J. E. Hirsch and R. M. Fye, Phys. Rev. Lett. **56**, 2521 (1986).
- [7] A. Georges, G. Kotliar, and W. Krauth, Z. Phys. B **92**, 313 (1993).
- [8] A. Georges and G. Kotliar, Phys. Rev. B **45**, 6479 (1992).
- [9] The precise form of the function which is minimized plays no role, as it should be. Practically the same results can be obtained by fitting G_0 and G_0^{And} instead of their inverses or by putting in ω -dependent factors.
- [10] R. Haydock, V. Heine, and M. J. Kelly, J. Phys. C **8**, 2591 (1975).
- [11] A longer version of this paper containing more technical details can be obtained directly from the authors (unpublished).
- [12] A. Georges and W. Krauth, Phys. Rev. B **48**, 7167 (1993).
- [13] X. Y. Zhang, M. Rozenberg, and G. Kotliar, Phys. Rev. Lett. **70**, 1666 (1993).
- [14] Convergence is very slow in the transition region. There it may take several hundred iterations to destroy an apparently stable Fermi-liquid or Mott insulating phase. However, we always end up with a fully stabilized solution. Such a situation is almost impossible to handle correctly in expensive QMC calculations at low temperatures.
- [15] This means that the anomalous Green's function is forced to be 0 and that a self-consistent solution for $G_d(i\omega_n)$ is searched for. $F_d = 0$ is always a possible solution of the self-consistency equation (9).
- [16] In the triplet case we have very good convergence of the eigenvalues as a function of n_s , but the eigenvectors—although qualitatively the same—show some quantitative differences at small frequencies. Larger simulations are probably called for in order to settle this point.
- [17] V. L. Berezinskii, JETP Lett. **20**, 287 (1974).
- [18] P. Coleman, E. Miranda, and A. Tsvelik, Phys. Rev. Lett. **70**, 2960 (1993); (to be published).

M. M. Caffarel, P. Azaria, B. Delamotte, and D. Mouhanna, “Monte Carlo Calculation of the Spin-stiffness of the two-dimensional Heisenberg Model”, *Europhys. Lett.* **26**, 493 (1994)

Monte Carlo Calculation of the Spin Stiffness of the Two-Dimensional Heisenberg Model

This article has been downloaded from IOPscience. Please scroll down to see the full text article.

1994 Europhys. Lett. 26 493

(<http://iopscience.iop.org/0295-5075/26/7/003>)

View [the table of contents for this issue](#), or go to the [journal homepage](#) for more

Download details:

IP Address: 86.221.86.45

The article was downloaded on 24/09/2010 at 18:03

Please note that [terms and conditions apply](#).

Europhys. Lett., **26** (7), pp. 493-498 (1994)

Monte Carlo Calculation of the Spin Stiffness of the Two-Dimensional Heisenberg Model.

M. CAFFAREL (*)^(§), P. AZARIA (**)^(§§)

B. DELAMOTTE (***)^(§§§) and D. MOUHANNA (***)^(§§§)

(*) *CNRS-Laboratoire de Dynamique des Interactions Moléculaires
Université Paris VI - 4 Place Jussieu, 75252 Paris Cedex 05, France*

(**) *Laboratoire de Physique Théorique des Liquides, Université Paris VI
4 Place Jussieu, 75230 Paris Cedex 05, France*

(***) *Laboratoire de Physique Théorique et Hautes Energies, Université Paris VII
2 Place Jussieu, 75251 Paris Cedex 05, France*

(received 19 October 1993; accepted in final form 26 April 1994)

PACS. 11.10G – Field theory: Renormalization.

PACS. 75.10H – Ising and other classical spin models.

PACS. 75.30F – Spin-density waves.

Abstract. – Using a collective-mode Monte Carlo method (the Wolff-Swendsen-Wang algorithm), we compute the spin stiffness of the two-dimensional classical Heisenberg model. We show that it is the relevant physical quantity to investigate the behaviour of the model in the very low-temperature range inaccessible to previous studies based on correlation length and susceptibility calculations.

As well known, the long-distance, low-energy physics of two-dimensional spin systems is expected to be obtained from a low-temperature perturbative expansion of a suitable non-linear sigma ($NL\sigma$) model. In order to have a non-perturbative control of this low-temperature expansion, one can take advantage of Monte Carlo simulations. Up to now, calculations have been mainly concerned with correlation lengths and susceptibilities [1]. Unfortunately, because of their exponential behaviour as a function of $\beta = 1/kT$ and the computationally accessible lattice sizes, studying the very low-temperature regime is very demanding, or even impossible. The aim of this paper is: 1) to show that the relevant physical quantity allowing to reach this regime for accessible sizes in the spin stiffness ρ_s , a measure of the free-energy increment under twisting of the boundary conditions [2, 3]; 2) to argue that it is essential to use a *non-local* Monte Carlo algorithm to get truly converged values of the spin stiffness in the very low-temperature regime; 3) to exhibit in the case of the two-dimensional classical Heisenberg model the quasi-perfect agreement between the Monte

^(§) E-mail: mc@dim.jussieu.fr.

^(§§) E-mail: aza@lptl.jussieu.fr.

^(§§§) E-mail: delamotte@lpthe.jussieu.fr and mouhanna@lpthe.jussieu.fr.

Carlo simulation of the spin model and the predictions of the corresponding non-linear sigma (NL σ) model; applications to more involved systems will be presented in a forthcoming work.

To our knowledge, two previous works have attempted to compute the spin stiffness of the Heisenberg model. However, they are either based on a wrong formula [4], or on the use of a local Monte Carlo scheme [4, 5] not suited at all to the problem as discussed in the following. In our opinion, we present here the first unambiguous numerical calculation validating the precise finite-size behaviour of the spin stiffness of the two-dimensional classical Heisenberg model.

The Hamiltonian of the Heisenberg model is

$$H = -J \sum_{\langle ij \rangle} \mathbf{S}_i \cdot \mathbf{S}_j, \quad (1)$$

where $\langle ij \rangle$ denotes the summation over nearest neighbours of a finite square lattice of size L . In (1), \mathbf{S}_i are three-component unit length classical vectors and J is positive. Each site i of the lattice is indexed by two coordinates x_i and y_i .

We impose a twist in the \mathbf{x} -direction, by coupling the system with two walls of spins: $\mathbf{S}(\mathbf{x} = 0) = \mathbf{S}_1$, $\mathbf{S}(\mathbf{x} = L) = \mathbf{S}_2$, \mathbf{S}_2 being deduced from \mathbf{S}_1 by a rotation of angle θ around a direction \mathbf{e} . The spin stiffness ρ_s is defined as

$$\rho_s(L) = \left. \frac{\partial^2 F(\theta)}{\partial \theta^2} \right|_{\theta=0}, \quad (2)$$

where F is the free energy.

In terms of the spins it writes

$$\rho_s(L) = \frac{J}{L^2} \left\langle \sum_{\langle ij \rangle} (\mathbf{S}_i \cdot \mathbf{S}_j - \mathbf{S}_i \cdot \mathbf{e} \mathbf{S}_j \cdot \mathbf{e})(x_i - x_j)^2 \right\rangle - \frac{J^2}{TL^2} \left\langle \left(\sum_{\langle ij \rangle} (\mathbf{S}_i \wedge \mathbf{S}_j) \cdot \mathbf{e}(x_i - x_j) \right)^2 \right\rangle, \quad (3)$$

where T is the temperature and Boltzmann averages are performed with two walls of parallel spins fixed at boundaries in the \mathbf{x} -direction.

The finite-size behaviour of $\rho_s(L)$, when L is much larger than the lattice spacing a but much smaller than the correlation length ξ , has been calculated at one- and two-loop order with use of the $O(3)/O(2)$ NL σ model [2, 6]:

$$\frac{\rho_s}{T} \sim \frac{1}{2\pi} \ln \frac{\xi}{L} + \frac{1}{2\pi} \ln \ln \frac{\xi}{L}, \quad (4)$$

where the common coefficient $1/2\pi$ in front of the leading and subleading logarithmic terms is a universal number which is not modified by higher orders in the low-temperature expansion.

The crucial point in measuring ρ_s is that its predicted size dependence given by (4) is all the more valid since $L \ll \xi$. Therefore, in the very low-temperature regime we can hope to test formula (4) by using a large range of relatively small lattice sizes. In contrast, measuring the temperature dependence of ξ requires $\xi \leq L$ and, therefore, relatively high temperatures for accessible sizes [1], a regime where the validity of the perturbation theory becomes less controlled. A most important point to notice is that at the very low temperatures considered here the physics of the model is entirely controlled by collective excitations—spin waves—and therefore *we must take great care of these large-scale moves in any simulation of the model* («beating» the critical slowing-down).

The purpose of this paper is to present a Monte Carlo study of the spin stiffness for the

finite two-dimensional classical Heisenberg model free of critical slowing-down and then to investigate prediction (4) numerically. To summarize what has been obtained, our Monte Carlo calculations confirm the existence of a leading logarithmic contribution with the universal amplitude $1/2\pi$. In addition, an extra-contribution to the spin stiffness consistent with the subleading term of (4) has also been clearly identified. The Monte Carlo results presented have been obtained using the Wolff-Swendsen-Wang method [7] of updating large clusters of spins simultaneously. At the low temperatures considered here, using a *collective* Monte Carlo algorithm appeared to be essential to get a well-converged estimate of the slope of the spin stiffness as a function of the lattice size. In particular, our preliminary attempts making use of a Monte Carlo algorithm based on *local* spin updates failed due to the severe critical slowing-down.

At this point, it seems important to discuss in more detail the previous attempts of calculating the spin stiffness of the Heisenberg model. Apart from the paper of Mon [4] in which a wrong formula for ρ_s has been used (he has mistakenly used the spin stiffness formula of the XY case), another calculation by Ritchey [5] done with the correct formula and using a local Metropolis algorithm has been performed. We have redone entirely his calculations with the very same conditions (same lattice sizes, same temperatures, same number of Monte Carlo steps). As already emphasized, we realized soon that such calculations are hampered by a severe critical slowing-down. Instead of getting a slope of approximately -0.16 (*i.e.* $1/2\pi$) Ritchey obtained a value of approximately -0.12 . At the lowest temperature he treated, the difference between both figures results in fact from the non-convergence of his estimate of the slope (very slow convergence, independent configurations are too scarce). It is interesting to note that this difference has been boldly interpreted elsewhere as taking its origin from cubic corrections to the scaling [8], corrections which in fact are negligible at the lowest temperature presented by Ritchey. In this paper, highly converged estimates of the slope of the spin-stiffness are presented. Cubic corrections to the β -function (*i.e.* $\ln \ln$ corrections in formula (4)) showing up at sufficiently high temperatures are also put into evidence (see fig. 2).

Results. – The Wolff-Swendsen-Wang (WSW) algorithm has been implemented to simulate the Heisenberg model on an $L \times L$ square lattice. In the y -direction periodic boundary conditions have been chosen. In the x -direction, fixed boundary conditions are to be used. However, for simplicity we have also chosen periodic boundary conditions in the x -direction. This introduces an error in the spin stiffness exponentially small in $\ln L$. By using a very recently proposed interpretation of Wolff-type algorithms as algorithms based on an embedding of Ising spins into continuous spins [9] it can be seen that fixed boundary conditions can be implemented by introducing a suitable external magnetic field in the underlying Ising model. We have implemented this idea and found that the errors in the calculated spin stiffness are indeed exponentially small (less than 0.5% relative error for lattice sizes with $L > 8$). No difference on the resulting slopes have been observed within statistical fluctuations.

One of the major results of this paper is that relatively moderate sizes L are in fact sufficient to validate formula (4). Lattices of sizes $L = 4, 8, 12, \dots, 32$ have been simulated. We have performed our simulations at four different temperatures: $T/J = 0.1, 0.15, 0.3$, and 0.395 . In each case we are at a sufficiently low temperature to be in the regime of validity of formula (4) ($L \ll \xi$).

Figure 1 presents the complete set of results obtained for the spin stiffness at different sizes and temperatures. At the scale of fig. 1, all curves appear to be very rapidly linear as a function of $\ln L$. In order to determine accurately the corresponding slope, a closer look is necessary. Figure 2 presents a blow-up of data of fig. 1 for the lowest (upper figure) and

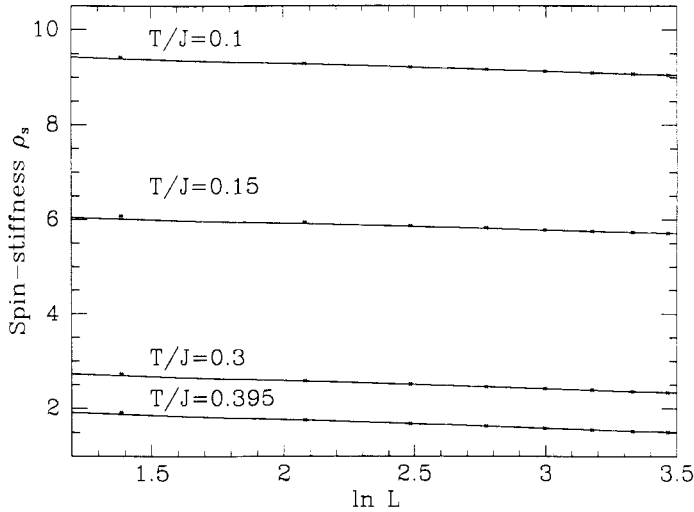


Fig. 1. – Spin stiffness for different sizes and temperatures. Statistical fluctuations smaller than the size of crosses.

highest (lower figure) temperatures treated, $T/J = 0.1$ and $T/J = 0.395$, respectively. A first point to notice is that a very high accuracy on our data has been achieved. Such a level of accuracy is absolutely necessary to put into evidence the linear regime of the spin stiffness as well as to get a truly converged estimate of the slope. We emphasize that only when resorting to a collective Monte Carlo scheme we have been able to fulfil both requirements. A first important remark concerning fig.2 is how fast we enter the linear regime: at all temperatures considered it is reached at $L \sim 16$. By using data for $L = 16, 20, 24, 28,$ and 32 an estimate of the slope can be extracted, we get: $-0.162(4), -0.166(5), -0.171(5),$ and $-0.184(7)$ at $T/J = 0.1, 0.15, 0.3,$ and 0.395 , respectively. At the very low temperature $T/J = 0.1$ we recover within statistical fluctuations the theoretical result $1/2\pi = 0.1592\dots$ predicted by formula (4)⁽¹⁾. At higher temperatures non-negligible higher-order

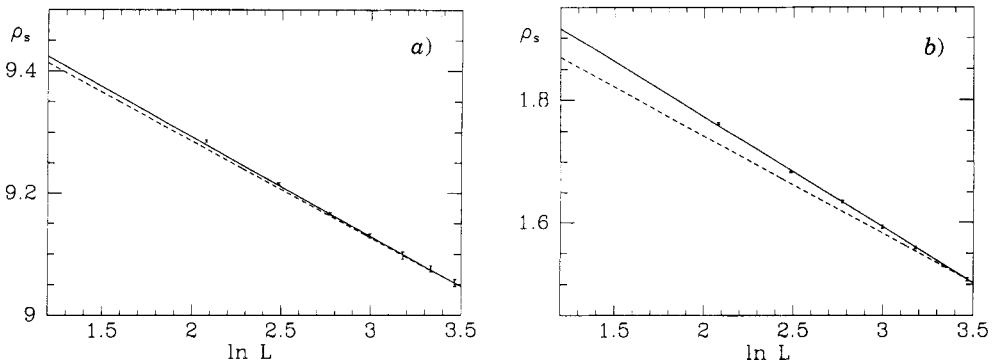


Fig. 2. – Blow-up of fig. 1 for $T/J = 0.1$ (a) and $T/J = 0.395$ (b). The solid line is the best fit using eq. (4), the dashed line the first-order prediction (no renormalization of the slope).

⁽¹⁾ In fact, at this temperature the slope is very slightly renormalized. Using eqs. (4), (5) we get -0.162 instead of the bare value of $-0.1592\dots$. However, both values are not distinguishable within statistical fluctuations.

contributions in the spin stiffness show up. To put this on a more quantitative basis, we have performed a fit of the data using the full expression (4). The resulting curve is represented by a solid line in fig. 2. The only free parameter entering the fit is the correlation length ξ , the arbitrary reference value for the spin stiffness being chosen so as to reproduce exactly the last data ($L = 32$). The dashed line is the linear curve obtained when resorting to the leading logarithmic behaviour (no $\ln \ln$ corrections, no renormalization of the $1/2\pi$ slope) using the very same correlation length as determined in the fit. At $T/J = 0.1$, both curves almost coincide in the linear regime, illustrating the correctness of the leading log prediction and the smallness of the higher-order corrections at this temperature. At the higher temperatures considered, we clearly see the necessity of going beyond leading order. In addition, it is striking to see how good representation (4) is in reproducing our Monte Carlo data. Of course, due to the accuracy determined by statistical fluctuations and to the narrow range of lattice sizes used, it is not realistic to hope to resolve the precise analytical $\ln \ln$ behaviour of the second-order theoretical expression. However, our data are perfectly consistent with the «renormalized slope» predicted by (4), $s^* = \partial(\rho_s/T)/\partial \ln L = -1/2\pi(1 + 1/\ln(\xi/L))$.

In fig. 3 we have plotted the correlation length ξ issued from the fit using formula (4). We also present the curve obtained from the formula proposed by Shenker and Tobochnik [10] (obtained by matching high- and low-temperature calculations):

$$\xi \approx 0.01 \frac{\exp[2\pi J/T]}{1 + 2\pi J/T} . \tag{5}$$

It is very satisfactory to see that our rough estimates of ξ are in good agreement with this completely independent calculation of the correlation length.

In this paper, we have shown that for the case of the two-dimensional classical Heisenberg model it is possible to get a quasi-perfect agreement between the Monte Carlo simulation of the spin model and the predictions of the corresponding low-temperature non-linear sigma ($NL\sigma$) model. We have overemphasized that the essential point to obtain such a nice agreement is the use of an appropriate non-local Monte Carlo algorithm. The study of the spin stiffness of more involved 2D systems such as frustrated Heisenberg spin models could be

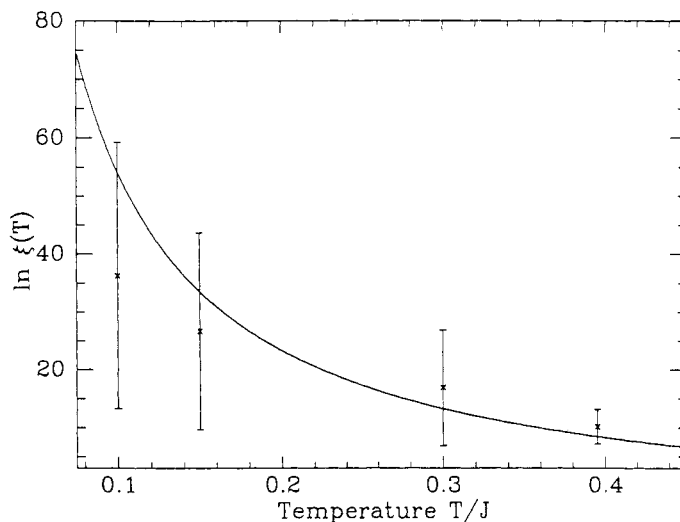


Fig. 3. – Correlation length ξ . The solid line is obtained from eq. (5), the values indicated by crosses from the fit of our data using eq. (4).

a very efficient test of the validity of the low-temperature perturbative expansion of the corresponding more general non-linear sigma models [11], an expansion which can be questioned due to the presence of non-trivial topological excitations [12]⁽²⁾. However, the implementation of a non-local Monte Carlo scheme for such models is a highly non-trivial task; work in that direction is in progress.

⁽²⁾ Note that after completion of this work an interesting study of the spin stiffness for the case of a classical antiferromagnet on a triangular lattice using a local Monte Carlo scheme has been published [13].

REFERENCES

- [1] EDWARDS R. G., FERREIRA S. J., GOODMAN J. and SOKAL A. D., *Nucl. Phys. B*, **380** (1992) 621 and references therein.
- [2] CHAKRAVARTY S., *Phys. Rev. Lett.*, **66** (1991) 318.
- [3] AZARIA P., DELAMOTTE B., JOLICOEUR T. and MOUHANNA D., *Phys. Rev. B*, **45** (1992) 12612.
- [4] MON K. K., *Phys. Rev. B*, **44** (1991) 6809.
- [5] RITCHEY L., Trinity College Fellowship Dissertation (1991).
- [6] BRÉZIN E., KORUTCHEVA E., JOLICOEUR T. and ZINN-JUSTIN J., *J. Stat. Phys.*, **70** (1993) 583.
- [7] SWENDSEN R. H. and WANG J. S., *Phys. Rev. Lett.*, **58** (1987) 86; WOLFF U., *Phys. Rev. Lett.*, **62** (1989) 361.
- [8] CHANDRA P. and COLEMAN P., in *Proceedings of the 1991 Les Houches Summer School Lectures* (1993).
- [9] CARACCILO S., EDWARDS R. G., PELISSETTO A. and SOKAL A. D., *Nucl. Phys. B*, **403** (1993) 475.
- [10] SHENKER S. H. and TOBOCHNIK J., *Phys. Rev. B*, **22** (1980) 4462.
- [11] AZARIA P., DELAMOTTE B. and JOLICOEUR T., *Phys. Rev. Lett.*, **64** (1990) 3175; AZARIA P., DELAMOTTE B., DELDUC F. and JOLICOEUR T., to be published in *Nucl. Phys.*
- [12] KAWAMURA H. and MIYASHITA S., *J. Phys. Soc. Jpn.*, **53** (1984) 38.
- [13] SOUTHERN B. W. and YOUNG A. P., *Phys. Rev. B*, **48** (1993) 13170.

N. J. Langlet, J. Caillet, and M. Caffarel, "A Perturbational Study of some Hydrogen-Bonded Dimers", *J. Chem. Phys.* 103, 8043 (1995)

A perturbational study of some hydrogen-bonded dimers

Jacqueline Langlet,^{a)} Jacqueline Caillet,^{b)} and Michel Caffarel^{c)}
CNRS-Laboratoire de Dynamique des Interactions Moléculaires, Université Paris VI,
Tour 22 4 Place Jussieu 75252 Paris Cedex 05, France

(Received 31 January 1995; accepted 31 July 1995)

We present a detailed study of several hydrogen-bonded dimers consisting of H₂O, NH₃, and HF molecules using the Symmetry Adapted Perturbation Theory (SAPT) at different levels of approximations. The relative importance of each individual perturbational components and the quality of the total interaction energies obtained are discussed. The dependence of the results on the relative orientation of the molecules of the dimers and on the intermonomer distance is also investigated. © 1995 American Institute of Physics.

I. INTRODUCTION

It is well-known that evaluating intermolecular interaction energies with the level of accuracy required by the physics and chemistry of complex molecular systems is very difficult. There are two basic reasons for that. First, the interaction energy (defined as the difference between the total energy of the complex and the sum of the total energies of the individual noninteracting species) is really a tiny fraction of the total energies involved. Typically, this fraction can vary from about 10⁻⁷ (weakly interacting van der Waals complexes) to about 10⁻⁴ (strong hydrogen-bonded systems). Second, there is no *exact* method to compute *directly* this very small difference. In absence of such a procedure, two different theoretical strategies are usually employed. A first natural strategy consists in computing the total energy of each species separately (the complex and the individual molecules) and then to subtract out these energies according to the very definition of the interaction energy (the so-called *supermolecular* method). To do that is difficult due to the very high level of control required on the different sources of approximation of the particular method used to compute the total energies. Without entering into the technical details (choice of the basis set functions, finite-basis-set error, basis set superposition error (BSSE), etc...) it is fair to say that current state-of-the-art *ab initio* calculations are not able to reach the necessary level of accuracy, except of course for very small interacting species. A second quite natural approach is to consider that the interaction energy is the result of a very small physical perturbation of the isolated monomers and thus to employ some kind of perturbational method. This line of research has been intensively followed during the last decades and has led to the so-called Symmetry Adapted Perturbation Theories (SAPT) (see e.g., Refs. 1, 2, or 3), a variety of methods based on the usual Rayleigh–Schrödinger perturbation theory supplemented by some technique to force the change of antisymmetry property of the wave function between the monomers and the interacting complex (as known there is not a unique way to do that and, then, various schemes have been proposed, see references in Ref. 1). It is this constraint which is at the origin of the strong repulsion at short distances (exchange contributions).

In order to take account of the continuum contribution present in the infinite sums involved in the perturbational components (except, of course, for the first-order), a variation-perturbation scheme is usually employed (it can be shown that this can be reduced to a calculation in a suitable dimer basis set).^{4,5} In their pioneering work on the use of SAPT Jeziorski and van Hemert (JvH)⁴ have proposed to compute the interaction energy using the following minimal representation:

$$\Delta E_{int} \sim E_{RS}^{(1)} + E_{exch}^{(1)} + E_{ind}^{(2)} + E_{disp}^{(2)}, \quad (1)$$

where all quantities are computed using the wave functions issued from a SCF calculation of the monomers. $E_{RS}^{(1)}$ is the standard Rayleigh–Schrödinger first-order component (physically, the classical electrostatic interaction of the unperturbed charge distributions in the monomers), $E_{exch}^{(1)}$ is the first-order exchange part resulting from the change of the antisymmetry property of the wave function (physically, the dominant part of the repulsive interaction at short distances) and where $E_{ind}^{(2)}$ and $E_{disp}^{(2)}$ are the second-order Rayleigh–Schrödinger induction and dispersion energy, respectively (physically, the energy of interaction of one monomer within the electric field of the other, and the major attractive contribution to the interaction energy for neutral systems, respectively). It is important to emphasize that Eq. (1) describes the main physical facts of the intermolecular interaction (electrostatic interaction, repulsive force, induction and dispersive forces). However, a number of corrections are neglected when using Eq. (1). The numerical experience shows that their importance is very system-dependent. It is therefore very important to compute them if a reliable (although approximate) answer for any interacting system and not just for a specific class of systems is wanted. Three types of corrections may be distinguished:

- (i) corrections to the exchange part due to effects beyond the first-order,
- (ii) corrections due to higher-order perturbational Rayleigh–Schrödinger components ($E_{RS}^{(n)}$ with $n > 2$),
- (iii) corrections due to the intramolecular correlation effects.

A great deal of activity has been devoted to the calculation of these corrections. First of all, it has been very soon realized that the first-order exchange contribution was not sufficient to give a proper description of the repulsive part at

^{a)}E-mail: jl@dim.jussieu.fr

^{b)}E-mail: jc@dim.jussieu.fr

^{c)}E-mail: mc@dim.jussieu.fr

intermediate distances and different methods have been proposed to evaluate the second-order exchange contributions.^{5–12} Note that at much shorter distances no satisfactory approach seems to exist.¹³ Incorporating these important contributions we arrive at the following decomposition

$$\Delta E_{int}^{SAPT} \sim E_{RS}^{(1)} + E_{exch}^{(1)} + E_{ind}^{(2)} + E_{exch-ind}^{(2)} + E_{disp}^{(2)} + E_{exch-disp}^{(2)}, \quad (2)$$

which we shall refer to in the following as the SAPT decomposition. An alternative way of going beyond Eq. (1) is to combine both perturbational and supermolecular worlds as follows:

$$\Delta E_{int}^{hybrid} \sim \Delta E_{SCF} + E_{disp}^{(2)} + E_{exch-disp}^{(2)}, \quad (3)$$

where ΔE_{SCF} is the SCF binding energy computed with the supermolecular method (corrected for the BSSE). Such a procedure is attractive since the SCF interaction energy is supposed to contain most of the second-order exchange-induction energy, some induction part of third- and higher-order perturbational terms and even some intramolecular correlation contribution introduced when doing a SCF supermolecular calculation,¹⁴ contributions which are all neglected when using Eq. (1). In the following we shall refer to it as the *hybrid* method. However, when resorting to Eq. (3) it is important to realize that mixing both approaches renders difficult the control on the errors made. How much of the higher-order perturbational contributions, what part of the exchange-induction energy, etc... is gotten with a SCF supermolecular calculation is not easy to estimate. Note that it can be argued that a pure perturbational treatment where individual errors are in a better control may be preferable. In the same idea of incorporating nonperturbational effects it has been proposed to include the so-called apparent correlation or self-consistency effects into the second-order induction energy, $E_{ind}^{(2)}$.^{15–18} In short, it consists in resorting to a coupled Hartree-Fock (CHF) which implicitly sums up to infinity certain diagrams appearing in the many-body expansion of the induction energy. This is expected to give a better approximation of the total induction energy. Note that this can also be done for the exchange-induction part.¹⁹ Concerning the explicit calculation of higher-order perturbational components very little is found in the literature (see, references in Refs. 1,20,21). Finally, let us note that very recently a great deal of attention has been focused on the calculation of intramolecular correlation contributions to the interaction energy.^{11,13,20,22–28} The monomer Hamiltonians are decomposed as a sum of the Fock operator and some residual intramonomer correlation operator (Møller-Plesset partitioning). Using a many-body expansion framework a double perturbation theory (in the correlation operators of each monomer) may be written down for any of the interaction components. Some calculations of the leading corrections to the first- and second-order perturbational components have been presented (see previous references). Note also that quantum Monte Carlo (QMC) techniques can be used to compute *exactly* perturbational quantities (in particular, the intramonomer correlation effects can be fully taken into ac-

count, see application to the He–He interaction in Refs. 21,29). However, it should be noted that the method is in practice limited to the case of two-electron systems because of the celebrated fermionic “sign problem” (see, e.g., Refs. 30,31).

The purpose of this paper is to present a detailed study of several hydrogen-bonded dimers (ranging from weak to rather strong bonded-systems) using the perturbational formalism with different levels of description (two different pure perturbational approaches and the hybrid method). More precisely, using the original formalism presented by Hess *et al.*¹² a few years ago we investigate the dependence of the different perturbational contributions on the geometry of the dimer (both the intermonomer distance and the relative orientation) for five different hydrogen-bonded dimers (consisting of H₂O, NH₃, and HF). We discuss in detail the validity of the different representations for the interaction energy presented above and investigate the peculiar role of the second-order exchange-induction energy.

The organization of the present paper is as follows. In section II we give a rapid summary of the formalism used in this work. In particular we give the rather unfamiliar expressions for the exchange-induction and -dispersion energies derived within SAPT theories by Hess *et al.*¹² Section III contains the computational details. In section IV, we present our numerical results for the different contributions of the intermolecular interaction energy and a comparison between the interaction energies obtained with the different approaches. Finally, some conclusions are presented in section V.

II. METHOD

In this section we give a rapid overview of the formalism used in this work; for a very detailed and self-contained presentation the reader is referred to the original work of Hess *et al.*¹² In the perturbation theory of interactions the total Hamiltonian is decomposed as $H = H_0 + V^{AB}$ where H_0 denotes the sum of the non-interacting Hamiltonians of the two monomers *A* and *B* (we shall consider here only dimers, formulas can be trivially generalized to an arbitrary number of monomers) and V^{AB} is the intermolecular interaction potential.

Following standard Symmetry Adapted Perturbation Theories (SAPT) (see, e.g., Refs. 1–3) and using standard notations, the complete first- and second-order interaction energies are written in the form:

$$E^{(1)} = \frac{\langle \Psi_0^A \Psi_0^B | V^{AB} \mathbf{A} | \Psi_0^A \Psi_0^B \rangle}{\langle \Psi_0^A \Psi_0^B | \mathbf{A} | \Psi_0^A \Psi_0^B \rangle}, \quad (4)$$

$$E^{(2)} = - \frac{\langle \Psi_0^A \Psi_0^B | V^{AB} R_0 \mathbf{A} (V^{AB} - E^{(1)}) | \Psi_0^A \Psi_0^B \rangle}{\langle \Psi_0^A \Psi_0^B | \mathbf{A} | \Psi_0^A \Psi_0^B \rangle}, \quad (5)$$

where R_0 denotes the reduced resolvent of H_0 given by

$$R_0 = \sum'_{ij} \frac{|\Psi_i^A \Psi_j^B\rangle \langle \Psi_i^A \Psi_j^B|}{(E_i^A + E_j^B) - (E_0^A + E_0^B)} \quad (6)$$

(the prime in \sum' means as usual that the term corresponding to $i=0$ and $j=0$ is excluded from the summation) and \mathbf{A} is the intersystem antisymmetrizer:

A. Exchange–induction energy

By using Eqs. (11) and (12), $E_{exch-ind}^{(2)}(A \rightarrow B)$ is written as

$$E_{exch-ind}^{(2)}(A \rightarrow B) = -\langle \Psi_0^A \Psi_0^B | (V^{AB} - \langle V^{AB} \rangle) \times (P_{(1)} - \langle P_{(1)} \rangle) | \Psi_0^A \Phi_{ind}^B \rangle, \quad (17)$$

with a similar formula for $E_{exch-ind}^{(2)}(B \rightarrow A)$. A first point is that it is possible to rewrite Φ_{ind}^B in the form:

$$\Phi_{ind}^B = \sum_{k \in B} \Psi_0^B \begin{pmatrix} f_k^B \\ b_k \end{pmatrix}, \quad (18)$$

where the summation runs over all occupied spin orbitals b_k of monomer B and where the so-called “induction functions” f_k^B 's are some well-defined linear combinations of the virtual spin orbitals of B (one associated with each occupied orbital). Using Eq. (18) it is not difficult to show that the exchange induction energy may be now written

$$E_{exch-ind}^{(2)}(A \rightarrow B) = -\sum_{k \in B} ([V^{AB} P_{(1)}]_k - \langle V^{AB} \rangle [P_{(1)}]_k - \langle P_{(1)} \rangle [V^{AB}]_k), \quad (19)$$

with the notation

$$[O]_k \equiv \left\langle \Psi_0^A \Psi_0^B \left| O \right| \Psi_0^A \Psi_0^B \begin{pmatrix} f_k^B \\ b_k \end{pmatrix} \right\rangle, \quad (20)$$

where O stands for an arbitrary operator. Now, by using the fact that the action of the permutation operator $P_{(1)}$ on a product of two determinants Ψ_A and Ψ_B may be expressed as a linear combination of simple products of determinants corresponding to subsystems A and B and by using the Longuet-Higgins representation of the interaction operator V^{AB} (Eqs. (15),(16)) it is possible to show that the three basic contributions in (19) may be written as some specific combinations of electrostatic interactions between some generalized intermolecular charge densities. For example, we obtain for the major contribution¹²

$$[V^{AB} P_{(1)}]_k = \sum_{i \in A} \sum_{\substack{j \in B \\ j \neq k}} \int \int \frac{f_{00}^A \begin{pmatrix} b_j \\ a_i \end{pmatrix} f_{00}^B \begin{pmatrix} f_k^B a_i \\ b_k b_j \end{pmatrix}}{|\mathbf{r}^A - \mathbf{r}^B|} d\mathbf{r}^A d\mathbf{r}^B + \sum_{i \in A} \int \int \frac{f_{00}^A \begin{pmatrix} f_k^B \\ a_i \end{pmatrix} f_{00}^B \begin{pmatrix} a_i \\ b_k \end{pmatrix}}{|\mathbf{r}^A - \mathbf{r}^B|} d\mathbf{r}^A d\mathbf{r}^B, \quad (21)$$

where

$$f_{00}^A \begin{pmatrix} b_j \\ a_i \end{pmatrix} \equiv \left\langle \Psi_0^A \left| \rho^A(\mathbf{r}^A) \right| \Psi_0^A \begin{pmatrix} b_j \\ a_i \end{pmatrix} \right\rangle,$$

with similar definitions for the other generalized charge distributions involved in Eq. (21). Finally, explicit expressions for the generalized charge distributions in terms of mono- and bi-electronic integrals involving spin orbitals a_i, b_j , and f_k^B may be easily obtained.

B. Exchange-dispersion energy

A similar route to that followed for the exchange-induction energy can be used for the exchange-dispersion component. Writing Φ_{disp}^{AB} (see, Eq. (12)) as:

$$\Phi_{disp}^{AB} = \sum_{k \in A} \sum_{l \in B} \sum_{r \in A} \sum_{s \in B} c_{kl}^{rs} \Psi_0^A \begin{pmatrix} a_r \\ a_k \end{pmatrix} \Psi_0^B \begin{pmatrix} b_s \\ b_l \end{pmatrix}, \quad (22)$$

where indices k and l are associated with summations over the corresponding set of *occupied* spin orbitals while s and l refer to summations over the corresponding set of *virtual* spin orbitals and where c_{kl}^{rs} are some coefficients analogous to the linear coefficients of the “induction functions” introduced above, we can express $E_{exch-disp}^{(2)}$ in a form very similar to Eq. (19):

$$E_{exch-disp}^{(2)} = -\sum_{k \in A} \sum_{l \in B} \sum_{r \in A} \sum_{s \in B} c_{kl}^{rs} ([V^{AB} P_{(1)}]_{kl}^{rs} - \langle V^{AB} \rangle [P_{(1)}]_{kl}^{rs} - \langle P_{(1)} \rangle [V^{AB}]_{kl}^{rs}), \quad (23)$$

with the notation

$$[O]_{kl}^{rs} \equiv \left\langle \Psi_0^A \Psi_0^B \left| O \right| \Psi_0^A \begin{pmatrix} a_r \\ a_k \end{pmatrix} \Psi_0^B \begin{pmatrix} b_s \\ b_l \end{pmatrix} \right\rangle. \quad (24)$$

Exactly in the same way as before it is possible to write the elementary contributions of $E_{exch-disp}^{(2)}$ as a combination of some electrostatic interactions between generalized charge distributions which are ultimately written in terms of mono- and bi-electronic integrals. As an example, the major contribution to $E_{exch-disp}^{(2)}$ writes:

$$[V^{AB} P_{(1)}]_{kl}^{rs} = \sum_{\substack{i \in A \\ i \neq k}} \sum_{\substack{j \in B \\ j \neq l}} \int \int \frac{f_{00}^A \begin{pmatrix} a_r b_j \\ a_k a_i \end{pmatrix} f_{00}^B \begin{pmatrix} b_s a_j \\ b_l b_j \end{pmatrix}}{|\mathbf{r}^A - \mathbf{r}^B|} d\mathbf{r}^A d\mathbf{r}^B + \sum_{\substack{i \in A \\ i \neq k}} \int \int \frac{f_{00}^A \begin{pmatrix} a_r b_s \\ a_k a_i \end{pmatrix} f_{00}^B \begin{pmatrix} a_i \\ b_l \end{pmatrix}}{|\mathbf{r}^A - \mathbf{r}^B|} d\mathbf{r}^A d\mathbf{r}^B + \sum_{\substack{j \in B \\ j \neq l}} \int \int \frac{f_{00}^A \begin{pmatrix} b_j \\ a_k \end{pmatrix} f_{00}^B \begin{pmatrix} b_s a_r \\ b_l b_j \end{pmatrix}}{|\mathbf{r}^A - \mathbf{r}^B|} d\mathbf{r}^A d\mathbf{r}^B + \int \int \frac{f_{00}^A \begin{pmatrix} b_s \\ a_k \end{pmatrix} f_{00}^B \begin{pmatrix} a_r \\ b_l \end{pmatrix}}{|\mathbf{r}^A - \mathbf{r}^B|} d\mathbf{r}^A d\mathbf{r}^B, \quad (25)$$

and similar formulas for the other contributions.

III. COMPUTATIONAL DETAILS

A. Dimers

We have studied five different hydrogen-bonded dimers made of the molecules H_2O , NH_3 , and HF . The intramolecular geometry of the monomers has been taken to be the experimental geometry for isolated monomers (water molecule: $R_{OH} = 1.8088$ bohr, $\theta_{HOH} = 104.87^\circ$; ammonia molecule: $R_{NH} = 1.9219$ bohr, $\theta_{HNH} = 107.81^\circ$; HF molecule:

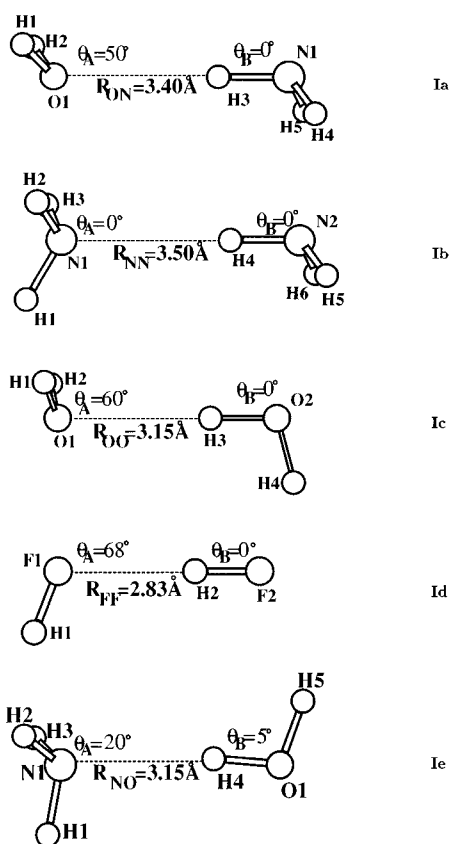


FIG. 1. The five hydrogen-bonded dimers studied. For a definition of the angles θ_A and θ_B , see text.

$R_{\text{HF}} = 1.71362$ bohr). In Figure 1, we present the different dimers in their equilibrium geometry as obtained by the pure perturbational treatment (SAPT, see Eq. (2)), note that slightly different geometries can be obtained with other theoretical schemes, see discussion in the next section. In this work, we shall denote A the proton acceptor molecule and B the proton donor molecule. The dimer geometries will be described by the quantities θ_A , θ_B , and R_{AB} where:

- θ_A defines the angle between the principal axes of the proton acceptor molecule (bisector in H_2O , C_v axis in NH_3 , and bond axis in HF) and the axis $A \cdots B$ connecting the two heavy atoms A and B .
- θ_B is the angle between the B-H bond axis of the proton donor and the axis $A \cdots B$.
- R_{AB} is the (intermolecular) distance between the two heavy atoms A and B of the two monomers. The values of these different quantities at the SAPT equilibrium geometry are given in Figure 1.

The five different dimers have been chosen from very weak to rather strong hydrogen-bonded dimers. The less bounded system is the dimer $\text{H}_2\text{O} \cdots \text{HNH}_2$. In fact, there is no experimental evidence of its existence. It is well-known that NH_3 acts as a proton acceptor when it is involved in a H-bonded system.^{32,33} For example, this is the case for $\text{H}_3\text{N} \cdots \text{HF}$,³⁴ $\text{NCH} \cdots \text{NH}_3$,³⁵ and $\text{HCCH} \cdots \text{NH}_3$.³⁶ There is so far no known example of systems in the gas phase where the

ammonia molecule acts as a proton donor. Here, the $\text{H}_2\text{O} \cdots \text{HNH}_2$ dimer has been studied as a prototype of a H-bonded dimer with NH_3 as a proton donor. A stronger but still weak example of H-bonded dimer is $(\text{NH}_3)_2$. Since the ammonia molecule exhibits no tendency to proton donation, the $(\text{NH}_3)_2$ complex is expected to be a case of H-bonded dimer not easy to treat. In this work a linear H-bonded structure has been chosen for the dimer. Earlier *ab initio* calculations have predicted such a structure.^{37,38} However, this picture is not supported by microwave experiments,^{39,40} which predict a cyclic structure. More recent theoretical (*ab initio*) calculations⁴¹ indicate that cyclic and linear complexes are almost degenerate in energy and that which one is found to be the most stable is extremely sensitive to details of the basis set as well as to the amount of correlation effects included. In fact, three kinds of tunneling motions exist for the ammonia dimer: interchange of the *donor* and *acceptor* roles of the monomers, internal rotation of the monomers about their C_3 symmetry group and *umbrella* inversion tunneling.⁴² A computational exploration of the six-dimensional vibration-rotation-tunneling dynamics of $(\text{NH}_3)_2$ by van Bladel *et al.*⁴³ has concluded that the $(\text{NH}_3)_2$ structure can be obtained from the *ab initio* equilibrium structure by vibrational averaging. Here, the radial evolution of the intermolecular interaction (and its components) of $(\text{NH}_3)_2$ has been mainly studied in order to compare the ammonia dimer with the dimer $\text{HOH} \cdots \text{NH}_3$. The dimers $(\text{H}_2\text{O})_2$ and $(\text{HF})_2$ can be considered as good examples of intermediate H-bonded dimers. Finally, we treat the $\text{H}_3\text{N} \cdots \text{HOH}$ dimer as an example of a rather strong H-bonded system.

B. Basis set

Our calculations for the different dimers have been performed with a very large basis set $(13s \ 8p \ 3d)/(7s \ 2p)$ contracted into $(8s \ 5p \ 3d)/(4s \ 2p)$ (the first set of basis functions corresponds to the heavy atom N, O, or F, the second to the hydrogen atoms). The basis set used has been taken from Voisin⁴⁴ and has been built as follows. First, based on atomic calculations the sets of primitives optimized by van Duijnveltdt $(12s \ 7p)/(6s)$,⁴⁵ have been contracted into some reduced set $(7s \ 4p)/(3s)$. Then, a set of diffuse functions s and p has been added. Their exponents have been obtained according to the averaging procedure presented in Ref. 46. Finally, to better describe the heavy atoms (N, O, and F), three polarization functions d have been added according to the rules proposed by Werner and Meyer.⁴⁷ The two orbitals p of hydrogen are those given by Christiansen and McCullough.⁴⁸ In order to evaluate the quality of our basis set we have performed a number of checks.

1. Basis-set quality: Some monomer properties

The SCF energy and dipole moment have been compared to the some recently estimated Hartree-Fock limits for the three molecules (Table I). Our values for the SCF energies appear to be quite close to the nearly-infinite-basis-set results. The values of the dipole moments are also quite good. It is important to emphasize that reproducing correctly

TABLE I. SCF energies and dipole moments obtained with the basis set used in this work. Comparison with the corresponding near Hartree–Fock limits. All energies in a.u. Dipole moments in Debye.

Molecule	E_{SCF}	$E_{\text{near HF limit}}$	μ_{SCF}	$\mu_{\text{near HF limit}}$
H ₂ O	-76.0606	-76.0673 ^a	1.98	1.98 ^{a,b}
NH ₃	-56.2179	-56.2246 ^a	1.56	1.62 ^a
HF	-100.064	-100.0706 ^a	1.93	1.92 ^a

^aReference 49.

^bReference 53.

the permanent dipole moments is crucial since the interaction energy of hydrogen-bonded systems is dominated by the electrostatic interaction.

2. Basis-set quality: Some dimer properties

a. Complementary exchange energy. A very useful quantity to evaluate the quality of a given finite basis set for computing intermolecular interactions is the so-called “complementary exchange energy.” A very detailed presentation of this quantity can be found in references.^{1,50} However, since the use of this quantity is not very common, let us first give a short presentation of it. The complementary exchange energy, $\epsilon_{\text{compl-exch}}$, is defined via the following formula

$$E_0 \equiv \frac{\langle \Psi_0^A \Psi_0^B | H \mathbf{A} | \Psi_0^A \Psi_0^B \rangle}{\langle \Psi_0^A \Psi_0^B | \mathbf{A} | \Psi_0^A \Psi_0^B \rangle} = \bar{E}_0^0 + \epsilon_{\text{compl-exch}} + \frac{\langle \Psi_0^A \Psi_0^B | V^{AB} \mathbf{A} | \Psi_0^A \Psi_0^B \rangle}{\langle \Psi_0^A \Psi_0^B | \mathbf{A} | \Psi_0^A \Psi_0^B \rangle} \quad (26)$$

where

$$\epsilon_{\text{compl-exch}} = \frac{\langle \Psi_0^A \Psi_0^B | (\bar{E}_0^0 - H_0) \mathbf{A}' | \Psi_0^A \Psi_0^B \rangle}{\langle \Psi_0^A \Psi_0^B | \mathbf{A} | \Psi_0^A \Psi_0^B \rangle}. \quad (27)$$

In Eq. (26) E_0 denotes the total Heitler–London energy and \bar{E}_0^0 the total energy corresponding to the approximate wave function $|\Psi_0^A \Psi_0^B\rangle$ for the unperturbed Hamiltonian H_0 . When Ψ_0^M ($M=A, B$) are chosen to be the exact (ground-state) wave functions of the monomers the complementary exchange energy vanishes and the Heitler–London interaction energy (defined as $E_0 - \bar{E}_0^0$) coincides with the complete first-order interaction energy. Note that, due to the presence of the operator \mathbf{A}' at the numerator, $\epsilon_{\text{compl-exch}}$ decreases exponentially as a function of the distance. This is the reason

why this quantity, which may be viewed as a correction to the ordinary exchange energy, is called “complementary exchange energy.” Now, the important property we shall use is that *within the one-exchange approximation* the complementary exchange energy vanishes if and only if the approximate functions used for the unperturbed monomers are the exact Hartree–Fock solutions. Since for not too small intermonomer distances the exact and one-exchange complementary exchange energies are almost identical $\epsilon_{\text{compl-exch}}$ is a good indicator of how far an approximate SCF wave function built from some given basis set is from the Hartree–Fock limit. Of course, for very small values of $\epsilon_{\text{compl-exch}}$ it would be necessary to consider the true one-exchange complementary energy instead of $\epsilon_{\text{compl-exch}}$. In Table II we present for the different dimers treated the values obtained for $\epsilon_{\text{compl-exch}}$ at a few representative distances R_{AB} . To compare with, we also report the values of the Heitler–London exchange energy defined as

$$E_{\text{exch-HL}}^{(1)} = E_{\text{exch}}^{(1)} + \epsilon_{\text{compl-exch}}. \quad (28)$$

The values obtained for $\epsilon_{\text{compl-exch}}$ are found to be rather small when compared with typical values (see, e.g., Refs. 1 or 51). This illustrates the good quality of the basis sets used in this work.

b. Counterpoise correction at the SCF level. In a supermolecular calculation of a complex the better the basis set used for describing each monomer is, the smaller the basis-set-superposition error (BSSE) is. We have computed this error by using the standard counterpoise method of Boys and Bernardi,⁵² some of our results are displayed in Table III. As a general rule, we get a very small counterpoise correction.

c. Second-order dispersion energy. Szalewicz *et al.*⁵³ pointed out that the use of f functions improved considerably the dispersion energy. Their estimate of the exact value was -2.0 kcal/mol for the water dimer near the equilibrium distance ($R_{O\dots O} = 3. \text{ \AA}$). In a recent work, Rybak *et al.*²⁰ have obtained a value of -1.90 kcal/mol by using a very large basis set. Here, although no f functions are present in our calculations, our 122 atomic-orbital dimer basis set leads, for the water dimer, to a value of -1.89 kcal/mol which is almost identical to the value obtained by Rybak *et al.* and quite close to the exact one estimated by Szalewicz *et al.*

TABLE II. Complementary exchange energy $\epsilon_{\text{compl-exch}}$ and first-order Heitler–London exchange energy $E_{\text{exch-HL}}^{(1)}$ for some representative values of the distance R_{AB} between the heavy atoms. Energies in kcal/mol, distances in Å.

R_{AB}		H ₂ O...HNH ₂	H ₃ N...HNH ₂	H ₂ O...HOH	HF...HF	H ₃ N...HOH
2.75	$\epsilon_{\text{compl-exch}}$	-0.05	0.43	-0.22	-0.30	0.03
	$E_{\text{exch-HL}}^{(1)}$	19.70	30.49	12.80	4.91	19.84
3.00	$\epsilon_{\text{compl-exch}}$	-0.16	-0.10	-0.15	-0.26	-0.10
	$E_{\text{exch-HL}}^{(1)}$	8.12	13.69	5.18	1.78	8.72
3.70	$\epsilon_{\text{compl-exch}}$	0.00	0.01	0.02	-0.02	0.00
	$E_{\text{exch-HL}}^{(1)}$	0.64	1.40	0.40	0.09	0.85

TABLE III. Counterpoise-corrected SCF interaction energy, ΔE_{CP}^{SCF} , and counterpoise correction, ϵ_{CP} for some representative distances. Energies in kcal/mol. Distances in Å.

R_{AB}		H ₂ O...HNH ₂	H ₃ N...HNH ₂	H ₂ O...HOH	HF...HF	H ₃ N...HOH
2.75	ΔE_{CP}^{SCF}	3.84	5.84	-2.46	-3.64	-2.78
	ϵ_{CP}	0.09	0.10	0.10	0.20	0.10
3.00	ΔE_{CP}^{SCF}	-0.01	0.60	-3.65	-3.48	-4.54
	ϵ_{CP}	0.05	0.06	0.06	0.16	0.06
3.70	ΔE_{CP}^{SCF}	-1.38	-1.73	-2.50	-1.90	-3.29
	ϵ_{CP}	0.02	0.03	0.02	0.11	0.02

IV. PERTURBATIONAL RESULTS

A. Total interaction energies at equilibrium geometries

In Table IV we present the total interaction energies obtained for the different dimers studied. We also present the optimized geometries, R_{AB} , θ_A , and θ_B . We have used three different approaches:

- (i) The pure perturbational approach, SAPT, including all perturbational components up to the second-order

$$\Delta E_{int}^{SAPT} = E_{RS}^{(1)} + E_{exch}^{(1)} + E_{ind}^{(2)} + E_{exch-ind}^{(2)} + E_{disp}^{(2)} + E_{exch-disp}^{(2)}. \quad (29)$$

- (ii) A truncated approach we shall refer to in the following as SAPT_{trunc} in which the exchange part of the induction is neglected (this method will play an important role in the discussion to follow)

$$\Delta E_{int}^{SAPT_{trunc}} = E_{RS}^{(1)} + E_{exch}^{(1)} + E_{ind}^{(2)} + E_{disp}^{(2)} + E_{exch-disp}^{(2)}. \quad (30)$$

- (iii) The hybrid approach mixing the SCF interaction en-

ergy (counterpoise-corrected) and the complete dispersion contribution calculated with SAPT:

$$\Delta E_{int}^{hybrid} = \Delta E_{int}^{SCF} + E_{disp}^{(2)} + E_{exch-disp}^{(2)}. \quad (31)$$

For the three different approaches the geometries have been optimized by varying the angles θ_I ($I=A$ and B) and the distance R_{AB} around the estimated equilibrium geometry (θ_I within -30° and $+30^\circ$ around θ_I^{exp} using $\pm 5^\circ$ steps, R_{AB} within -0.40 Å and 0.4 Å around R_{AB}^{exp} with 0.03 Å steps).

From a qualitative point of view, both SAPT, SAPT_{trunc}, and the hybrid methods lead essentially to the same results. The force of the hydrogen bond (importance of the total interaction energy) for the dimers we have studied may be classified as follows: H₂O...HNH₂ < H₃N...HNH₂ < H₂O...HOH ~ HF...HF < H₃N...HOH, where the notation $X < Y$ means that the dimer X is less bounded than the dimer Y . We verify the well-known result that NH₃ acts preferentially as a proton acceptor rather than a proton donor since here H₃N...HOH is much more stable than H₂O...HNH₂. Note also that NH₃ acts as a better acceptor than H₂O since

TABLE IV. Intermolecular interaction energy, ΔE_{int} , obtained from different methods (see text) at the corresponding equilibrium geometry. The values of θ_A , θ_B , and R_{AB} are given together with the known experimental values. Energies in kcal/mol, distances in bohr.

	H ₂ O...HNH ₂	H ₃ N...HNH ₂	H ₂ O...HOH	HF...HF	H ₃ N...HOH
ΔE_{int}^{SAPT}	-2.09	-2.50	-4.22	-3.75	-5.19
$\Delta E_{int}^{SAPT_{trunc}}$	-2.50	-3.15	-5.45	-5.82	-7.55
ΔE_{int}^{hybrid}	-2.49	-3.13	-5.31	-4.89	-6.76
ΔE_{int}^{exp}	^a	^b	-5.4 ± 0.7^c	-4.9 ± 0.1^d	$\sim 6^e$
R_{eq}^{SAPT}	3.40	3.50	3.15	2.83	3.15
$R_{eq}^{SAPT_{trunc}}$	3.20	3.20	2.68	2.48	2.70
R_{eq}^{hybrid}	3.25	3.30	2.91	2.68	2.93
R_{eq}^{exp}	^a	^b	2.98 ^f	2.68 ^g	2.99 ^h
θ_A	50°	0°	60°	68°	20°
θ_A^{exp}	^a	^b	60° ^f	62° ^g	11° < θ_A < 23° ^h
θ_B	0°	0°	0°	0°	5°
θ_B^{exp}	^a	^b	0° ^f	11° ^g	$\approx 13^{\circ h}$

^aUnphysical molecule, see text.

^bLinear H-bonded structure, no experimental values, see text.

^cReference 55.

^dReference 20.

^eTo our knowledge no experimental value available. The value quoted is an *ab initio* estimate given by Latajka and Scheiner (Ref. 56).

^fReference 57.

^gReference 58.

^hReference 59.

$\text{H}_3\text{N}\dots\text{HOH}$ is more stable than $\text{H}_2\text{O}\dots\text{HOH}$. Concerning the geometrical parameters it appears that the value of the angle θ_A defining the angle between the axes $A\dots B$ (A and B being the heavy atoms of the complex) and the principal axis of the proton acceptor depends strongly on the chemical nature of the acceptor. A value of about 60° has been obtained when the proton acceptor is H_2O or HF . A smaller value is obtained when the proton acceptor is NH_3 . The value of the angle θ_B characterizing the position of the bond $A\text{-H}$ (A being N , O , or F) of the proton acceptor is always very close to 0° . The smallest distance $R_{A\dots B}$ between the two heavy atoms at the equilibrium geometry has been obtained for the HF dimer. We get the following series: $R_{\text{F}\dots\text{F}}(\text{HF})_2 < R_{\text{O}\dots\text{O}}(\text{H}_2\text{O})_2 < R_{\text{N}\dots\text{N}}(\text{NH}_3)_2$. The equilibrium distance $R_{A\dots B}$ calculated for the heterodimer involving NH_3 and H_2O increases from the most stable dimer ($\text{H}_3\text{N}\dots\text{HOH}$) to the less stable one ($\text{H}_2\text{O}\dots\text{HNH}_2$).

From a more quantitative point of view, the first important point to note is that values of the interaction energy, ΔE_{inter} , depend appreciably on the method used and/or the dimer considered. First, it is clear that $\Delta E_{\text{int}}^{\text{SAPT}}$ is always smaller in magnitude than $\Delta E_{\text{int}}^{\text{hybrid}}$ or $\Delta E_{\text{int}}^{\text{SAPT}_{\text{trunc}}}$. The systematic difference is about 20%. The comparison between $\Delta E_{\text{int}}^{\text{SAPT}_{\text{trunc}}}$ and $\Delta E_{\text{int}}^{\text{hybrid}}$ depends on the dimer. We can distinguish three different cases:

(i) the weak H-bonded dimers case (including $\text{H}_2\text{O}\dots\text{HNH}_2$ and $(\text{NH}_3)_2$) for which $\Delta E_{\text{int}}^{\text{SAPT}_{\text{trunc}}}$ and $\Delta E_{\text{int}}^{\text{hybrid}}$ almost coincide.

(ii) the intermediate case of medium H-bonded dimers ($(\text{H}_2\text{O})_2$ and $(\text{HF})_2$) for which we obtain two different results. For the $(\text{H}_2\text{O})_2$ dimer the total interaction energy calculated with $\text{SAPT}_{\text{trunc}}$ and the hybrid methods are almost identical (the difference is less than 3%). This is a result which has already been obtained by Refs. 4, 12, and 20. However, this is no longer true for the $(\text{HF})_2$ dimer for which $\Delta E_{\text{int}}^{\text{SAPT}_{\text{trunc}}}$ and $\Delta E_{\text{int}}^{\text{hybrid}}$ are off by about 20%, therefore, the equality of these two quantities cannot be considered as a general rule. We shall return to this important point later after having presented the individual components of the interaction energy (sec. C below).

(iii) the rather strong H-bonded dimer, $\text{H}_3\text{N}\dots\text{HOH}$, for which an important difference between the truncated and hybrids results is observed.

Regarding the equilibrium distance R_{eq} we find that the SAPT results are systematically larger than those obtained with the two other methods. Once again, the situation is not so clear when we compare the values obtained with $\text{SAPT}_{\text{trunc}}$ and the hybrid methods. Almost identical results have been obtained for the case of weakly bonded dimers while shorter distances have been calculated with the $\text{SAPT}_{\text{trunc}}$ approach for the other dimers. If we compare with the known experimental values it is clear that the hybrid method is the method which gives the most plausible results. Now, regarding the calculated angular parameters (θ_A and θ_B) defining the relative position of the two molecules within the H-bonded dimer we have systematically obtained almost the same values with the three different procedures. We have also found that not only the equilibrium angles are

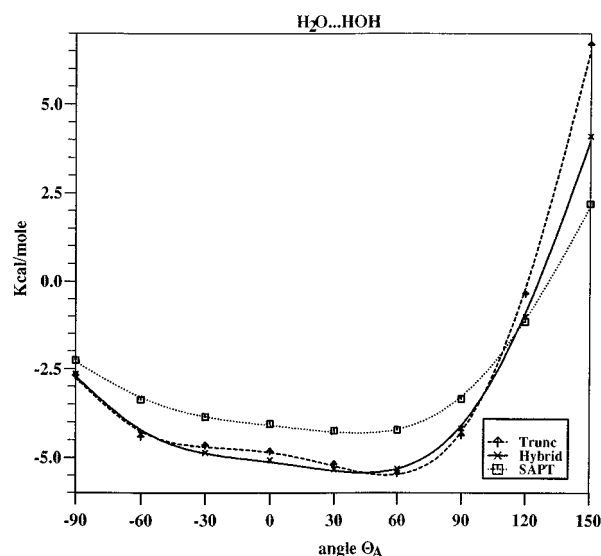


FIG. 2. Interaction energy curves, ΔE_{int} , as a function of θ_A (see text) for the water dimer as calculated by SAPT, $\text{SAPT}_{\text{trunc}}$, and the hybrid methods.

very similar but also the general shape of the interaction energy curves with respect to the relative angles for all dimers presented here. To illustrate this point we present in Figure 2 the energy curve obtained for the water dimer as a function of the angle θ_A . Clearly, there exists some important radial dependence of the interaction energy on the procedure used but a much smaller one for the relative position of the molecules. In what follows we study in more detail this radial dependence.

B. Radial dependence of the perturbational contributions

Keeping the angular parameters θ_A and θ_B of each dimer fixed at their optimized values, we have investigated the radial dependence of the intermolecular interaction energy perturbational components.

Our main purpose is to study which contributions to the interaction energy are actually dominant in stabilizing the five studied complexes. We are also interested to trace back to its origin the poor stability of the dimer $(\text{NH}_3)_2$ and also the very short $\text{F}\dots\text{F}$ distance in the $(\text{HF})_2$ dimer.

In the next few tables we present the radial dependence of the following contributions:

- (i) $E_{\text{RS}}^{(1)}$, $E_{\text{exch}}^{(1)}$ and the complete first-order, $E^{(1)\text{SAPT}}$ (Table V);
- (ii) the second-order induction energy $E_{\text{ind}}^{(2)}$, its exchange part $E_{\text{exch-ind}}^{(2)}$, and the complete induction energy $E_{\text{ind}}^{(2)\text{SAPT}}$ (Table VI);
- (iii) the second-order dispersion energy $E_{\text{disp}}^{(2)}$, its exchange part $E_{\text{exch-disp}}^{(2)}$, and the complete dispersion energy $E_{\text{disp}}^{(2)\text{SAPT}}$ (Table VII).

We make the following comments on the results presented in Tables V–VII:

- (i) All contributions of the Rayleigh–Schrödinger (RS) treatment (no exchange terms), namely $E_{\text{RS}}^{(1)}$, $E_{\text{ind}}^{(2)}$, and

TABLE V. First-order Rayleigh–Schrödinger energy, $E_{RS}^{(1)}$, first-order exchange energy, $E_{exch}^{(1)}$, and complete first-order, $E_{SAPT}^{(1)} = E_{RS}^{(1)} + E_{exch}^{(1)}$ for different values of R_{AB} . Energies in kcal/mol and distances in Å.

R_{AB}		H ₂ O...HNH ₂	H ₃ N...HNH ₂	H ₂ O...HOH	HF...HF	H ₃ N...HOH
2.75	$E_{RS}^{(1)}$	-11.28	-17.00	-11.51	-6.63	-16.36
	$E_{exch}^{(1)}$	19.75	30.07	13.10	5.21	19.87
	$E_{SAPT}^{(1)}$	8.48	13.08	1.59	-1.42	3.44
2.90	$E_{RS}^{(1)}$	-7.62	-12.00	-8.40	-5.16	-12.30
	$E_{exch}^{(1)}$	11.40	18.90	7.40	2.98	12.23
	$E_{SAPT}^{(1)}$	3.78	6.90	-1.00	-2.18	-0.07
3.00	$E_{RS}^{(1)}$	-6.20	-9.60	-7.15	-4.42	-10.27
	$E_{exch}^{(1)}$	8.32	13.80	5.33	2.04	8.83
	$E_{SAPT}^{(1)}$	2.12	4.20	-1.82	-2.38	-1.44
3.17	$E_{RS}^{(1)}$	-4.32	-6.71	-5.39	-3.47	-7.72
	$E_{exch}^{(1)}$	4.54	8.02	2.84	1.06	5.03
	$E_{SAPT}^{(1)}$	0.22	1.31	-2.55	-2.41	-2.70
4.00	$E_{RS}^{(1)}$	-1.24	-1.76	-1.94	-1.39	-2.61
	$E_{exch}^{(1)}$	0.21	0.52	0.12	0.03	0.31
	$E_{SAPT}^{(1)}$	-1.03	-1.24	-1.82	-1.36	-2.30

$E_{disp}^{(2)}$, have a stabilizing effect. Of course, the major contribution is the electrostatic interaction energy which represents between 55 and 70 % of the total RS contribution. When we compare the relative force of the RS interaction energy for the different H-bonded dimers we get the following order: $(\text{NH}_3)_2 \approx \text{H}_3\text{N}\dots\text{HOH} < \text{H}_2\text{O}\dots\text{HNH}_2 \approx (\text{H}_2\text{O})_2 < (\text{HF})_2$. For an average distance of $R_{AB} = 3$ Å, it appears that for the dimers $(\text{H}_2\text{O})_2$ and $(\text{HF})_2$ the electrostatic energy represents 75% and 50% of the value obtained for $(\text{NH}_3)_2$; for the dimers $(\text{H}_2\text{O})_2$ and $(\text{HF})_2$, $E_{ind}^{(2)}$ represents 75% and 40% of the value obtained for $(\text{NH}_3)_2$, respectively; and for $(\text{H}_2\text{O})_2$ and $(\text{HF})_2$ $E_{disp}^{(2)}$ represents, 50% and 20% of $E_{disp}^{(2)}$ of $(\text{NH}_3)_2$, respectively.

(ii) The total first- and total second-order exchange contributions (including both induction and dispersion contributions) reduce the stabilizing effect of the Rayleigh–Schrödinger terms just discussed. As expected, the major exchange contribution results from the first-order exchange term which represents 80% of the total exchange contribu-

tion at intermediate distances, while the second-order induction and dispersion exchange components have been obtained to represent 14% and 6% of the total exchange, respectively. Regarding the total exchange contribution we obtain the following order: $(\text{NH}_3)_2 > (\text{H}_2\text{O}\dots\text{HNH}_2) \approx (\text{H}_3\text{N}\dots\text{HOH}) > (\text{H}_2\text{O})_2 > (\text{HF})_2$. We have investigated the behavior of each individual exchange component as a function of the distance R_{AB} . We have found that for distances greater than 3 Å the exchange contribution may be very well represented via a single exponential function, $Ce^{-\alpha(R-R_0)}$. The set of parameters obtained for the different dimers and for the different components of the exchange part using the results for $R_{AB} = 3.00, 3.17, 3.70,$ and 4.00 Å are given in Table VIII (note that R_0 has been chosen to be fixed at 3 Å). The values of the parameters depend essentially on the nature of the exchange contribution (first-order, exchange-induction or exchange-dispersion) and on the chemical nature of the molecules involved in the complex.

TABLE VI. Second-order induction energy, $E_{ind}^{(2)}$, second-order exchange induction energy, $E_{ind-exch}^{(2)}$, and complete second-order induction, $E_{ind}^{(2)SAPT} = E_{ind}^{(2)} + E_{ind-exch}^{(2)}$ for different values of R_{AB} . Energies in kcal/mol and distances in Å.

R_{AB}		H ₂ O...HNH ₂	H ₃ N...HNH ₂	H ₂ O...HOH	HF...HF	H ₃ N...HOH
2.75	$E_{ind}^{(2)}$	-6.10	-9.59	-4.55	-2.39	-7.58
	$E_{ind-exch}^{(2)}$	4.27	6.30	2.81	1.36	4.70
	$E_{ind}^{(2)SAPT}$	-1.83	-3.29	-1.74	-1.03	-2.88
2.90	$E_{ind}^{(2)}$	-3.26	-5.69	-2.49	-1.38	-4.63
	$E_{ind-exch}^{(2)}$	2.17	3.61	1.40	0.70	2.74
	$E_{ind}^{(2)SAPT}$	-1.09	-2.08	-1.00	-0.68	-1.89
3.00	$E_{ind}^{(2)}$	-2.30	-4.04	-1.80	-0.96	-3.36
	$E_{ind-exch}^{(2)}$	1.48	2.49	0.95	0.45	1.91
	$E_{ind}^{(2)SAPT}$	-0.82	-1.55	-0.85	-0.51	-1.45
3.17	$E_{ind}^{(2)}$	-1.22	-2.30	-1.00	-0.54	-1.99
	$E_{ind-exch}^{(2)}$	0.71	1.32	0.45	0.20	1.04
	$E_{ind}^{(2)SAPT}$	-0.51	-0.98	-0.55	-0.34	-0.95
4.00	$E_{ind}^{(2)}$	-0.10	-0.21	-0.10	-0.06	-0.21
	$E_{ind-exch}^{(2)}$	0.02	0.07	0.02	0.01	0.06
	$E_{ind}^{(2)SAPT}$	-0.08	-0.14	-0.08	-0.05	-0.15

TABLE VII. Second-order dispersion energy, $E_{disp}^{(2)}$, second-order exchange dispersion energy, $E_{disp-exch}^{(2)}$, and complete second-order dispersion energy, $E_{disp}^{(2)SAPT} = E_{disp}^{(2)} + E_{disp-exch}^{(2)}$ for different values of R_{AB} . Energies in kcal/mol and distances in Å.

R_{AB}		H ₂ O...HNNH ₂	H ₃ N...HNNH ₂	H ₂ O...HOH	HF...HF	H ₃ ...HOH
2.75	$E_{disp}^{(2)}$	-4.63	-6.78	-3.38	-1.46	-4.82
	$E_{disp-exch}^{(2)}$	1.28	2.28	0.82	0.24	1.35
	$E_{disp}^{(2)SAPT}$	-3.35	-4.50	-2.56	-1.22	-3.47
2.90	$E_{disp}^{(2)}$	-3.19	-4.88	-2.32	-1.00	-3.45
	$E_{disp-exch}^{(2)}$	0.77	1.45	0.48	0.14	0.88
	$E_{disp}^{(2)SAPT}$	-2.42	-3.43	-1.84	-0.86	-2.57
3.00	$E_{disp}^{(2)}$	-2.59	-3.93	-1.89	-0.79	-2.77
	$E_{disp-exch}^{(2)}$	0.57	1.07	0.34	0.09	0.64
	$E_{disp}^{(2)SAPT}$	-2.02	-2.86	-1.55	-0.70	-2.13
3.17	$E_{disp}^{(2)}$	-1.79	-2.74	-1.31	-0.53	-1.93
	$E_{disp-exch}^{(2)}$	0.33	0.64	0.19	0.05	0.38
	$E_{disp}^{(2)SAPT}$	-1.46	-2.10	-1.13	-0.48	-0.92
4.00	$E_{disp}^{(2)}$	-0.34	-0.54	-0.24	-0.10	-0.38
	$E_{disp-exch}^{(2)}$	0.02	0.05	0.01	0.00	0.03
	$E_{disp}^{(2)SAPT}$	-0.32	-0.49	-0.23	-0.10	-0.35

(iii) Clearly, at very short distances the repulsive exchange part of the first-order dominates the attractive RS contribution. However, at sufficiently large distances the exchange part vanishes and only the electrostatic term survives (it behaves as $1/R_{AB}^3$). Accordingly, the total first-order energy displays a minimum. The location of the minimum depends very much on the system studied. Looking at results of Table V we see that the weak H-bonded dimer (NH₃)₂ has a shallow minimum at a relatively large distance (-1.30 kcal/mol with $R_{eq} \approx 3.8$ Å). In contrast, the stronger-bonded dimers (H₂O)₂ and (HF)₂ have a larger total first-order interaction energy (about -2.50 kcal/mol). The minimum region of (HF)₂ is found to be quite broad within a range of values between 2.9 Å and 3.3 Å.

(iv) The positive (repulsive) exchange contributions, $E_{exch-ind}^{(2)}$ and $E_{exch-disp}^{(2)}$ terms never dominate their Rayleigh-Schrödinger counterparts, $E_{ind}^{(2)}$ and $E_{disp}^{(2)}$. In fact, the second-order RS terms tend to decrease the intermolecular interaction energy and to push the equilibrium distance R_{AB} towards shorter distances, this effect is slightly reduced by the second-order exchange terms whose main effect is to bring back R_{AB} to more reasonable values. The effect of the

second-order exchange contributions is more important for (NH₃)₂ than for the (HF)₂ dimer (see Tables IV, VI, and VII). In conclusion, the relative stability between the different H-bonded dimers results from a subtle balance between Rayleigh-Schrödinger and total exchange contributions.

C. Radial dependence of the total interaction energy: A comparison between the different approaches

In Table IX we present the total interaction energy as calculated within SAPT, SAPT_{trunc} and the hybrid methods (Eqs. (29), (30), and (31)) as a function of R_{AB} . We also present in Figures 3 and 4 the complete interaction energy curves for two representative examples: the NH₃ and HF dimers. A number of remarks are in order. First, it is clear that at very large distances the three approaches give the same results for the total interaction energy and thus, the same dissociative behavior. The results obtained by the different methods at small and intermediate distances may be quite different depending on the force of the hydrogen bond. For the two weak H-bonded cases (H₂O...HNNH₂ and (NH₃)₂) the agreement between the truncated and hybrid

TABLE VIII. Parameters of the representation $Ce^{-\alpha(R-R_0)}$ ($R_0=3$ Å) for: (a) the first-order exchange energy, (b) the second-order exchange induction energy, (c) the second-order exchange dispersion energy. Parameters C in kcal/mol and α in Å⁻¹.

	H ₂ O...HNNH ₂	H ₃ N...HNNH ₂	H ₂ O...HOH	HF...HF	H ₃ N...HOH
$E_{exch}^{(1)}$					
α	3.685	3.280	3.777	4.205	3.351
C	8.404	13.910	5.397	2.121	8.860
$E_{exch-ind}^{(2)}$					
α	4.317	3.585	3.906	5.489	3.450
C	1.473	2.444	0.893	0.474	1.893
$E_{exch-disp}^{(2)}$					
α	3.392	3.053	3.518	3.115	3.085
C	0.572	1.077	0.344	0.088	0.636

TABLE IX. Total interaction energy calculated with SAPT, SAPT_{trunc} and the hybrid methods, see text. Energies in kcal/mol and distances in Å.

R_{AB}		H ₂ O...HNH ₂	H ₃ N...HNH ₂	H ₂ O...HOH	HF...HF	H ₃ N...HOH
2.54	ΔE_{int}^{SAPT}	11.29	15.31	1.60	-2.41	2.79
	$\Delta E_{int}^{SAPT_{trunc}}$	1.31	2.04	-5.11	-5.73	-7.14
	ΔE_{int}^{hybrid}	6.63	9.15	-2.51	-4.45	-2.84
2.75	ΔE_{int}^{SAPT}	3.31	5.26	-2.71	-3.67	-2.90
	$\Delta E_{int}^{SAPT_{trunc}}$	-0.96	-1.00	-5.51	-5.03	-7.60
	ΔE_{int}^{hybrid}	0.50	1.35	-5.02	-4.86	-6.26
2.90	ΔE_{int}^{SAPT}	0.27	1.39	-3.94	-3.72	-4.53
	$\Delta E_{int}^{SAPT_{trunc}}$	-1.90	-2.22	-5.34	-4.42	-7.27
	ΔE_{int}^{hybrid}	-1.48	-1.29	-5.31	-4.51	-6.74
3.00	ΔE_{int}^{SAPT}	-0.72	-0.21	-4.20	-3.59	-5.02
	$\Delta E_{int}^{SAPT_{trunc}}$	-2.19	-2.70	-5.10	-4.03	-6.93
	ΔE_{int}^{hybrid}	-2.03	-2.25	-5.19	-4.18	-6.68
3.17	ΔE_{int}^{SAPT}	-1.76	-1.75	-4.22	-3.23	-5.19
	$\Delta E_{int}^{SAPT_{trunc}}$	-2.46	-2.97	-4.68	-3.42	-5.57
	ΔE_{int}^{hybrid}	-2.47	-2.98	-4.73	-3.57	-6.15
3.70	ΔE_{int}^{SAPT}	-1.83	-2.27	-2.84	-2.01	-3.72
	$\Delta E_{int}^{SAPT_{trunc}}$	-1.90	-2.52	-2.89	-2.02	-3.88
	ΔE_{int}^{hybrid}	-1.92	-2.53	-2.90	-2.07	-3.88
4.00	ΔE_{int}^{SAPT}	-1.43	-1.87	-2.13	-1.51	-2.82
	$\Delta E_{int}^{SAPT_{trunc}}$	-1.45	-1.93	-2.14	-1.51	-2.86
	ΔE_{int}^{hybrid}	-1.46	-1.96	-2.16	-1.53	-2.88

results is very good except at small distances (see Figure 3). For the rather strong dimers (HF)₂ and H₂O...HOH the truncated and hybrid curves appear to differ quite substantially by about 20%. The water dimer appears as an intermediate species for which both methods are in reasonable agreement, a result which has been already obtained by Refs. 4, 12, and 20. It should be noticed that for strong enough dimers the equilibrium distance obtained with the truncated method is systematically smaller than with the hybrid method. Regarding the SAPT results it is clear that ΔE_{int}^{SAPT} is always smaller in magnitude than ΔE_{int}^{hybrid} or $\Delta E_{int}^{SAPT_{trunc}}$. The systematic difference for all dimers is about 20%. Note also that the equilibrium distance obtained by the pure perturbational method is also systematically greater than with the two other methods. In order to discuss further these results it is impor-

tant to point out that the equality of the results obtained with the truncated and hybrid methods should result from the following equality:

$$\Delta E_{int}^{SCF} \sim E^{(1)} + E_{ind}^{(2)}, \quad (32)$$

where $E^{(1)}$ is the complete first-order (electrostatic and exchange terms) and $E_{ind}^{(2)}$ is the Rayleigh–Schrödinger part of the induction energy. It has been argued that this equality should result from a fortunate cancellation between the exchange part of the induction energy and some part of the higher-order perturbational contributions which are implicitly included in a SCF supermolecular calculation of the interaction energy.⁴ Despite the fact that it is roughly true for the water dimer, our results clearly demonstrate that it is wrong for the (HF)₂ and H₃N...HOH dimers. To illustrate

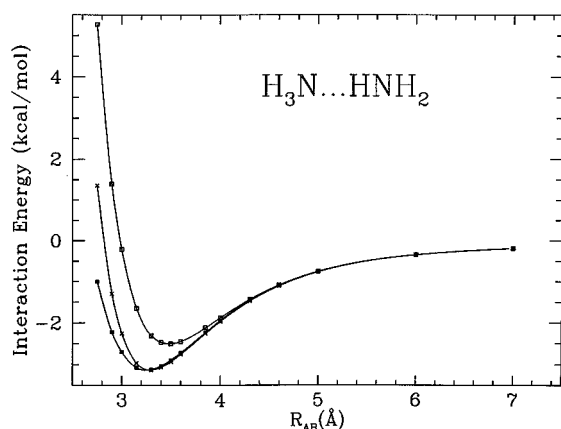


FIG. 3. Interaction energy curves, ΔE_{int} , as a function of R_{AB} for the (NH₃)₂ dimer as calculated by SAPT (curve with open squares), SAPT_{trunc} (solid squares), and the hybrid methods (crosses).

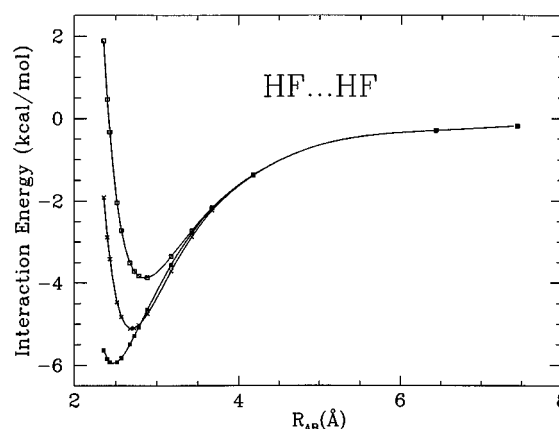


FIG. 4. Interaction energy curves, ΔE_{int} , as a function of R_{AB} for the (HF)₂ dimer as calculated by SAPT (curve with open squares), SAPT_{trunc} (solid squares), and the hybrid methods (crosses).

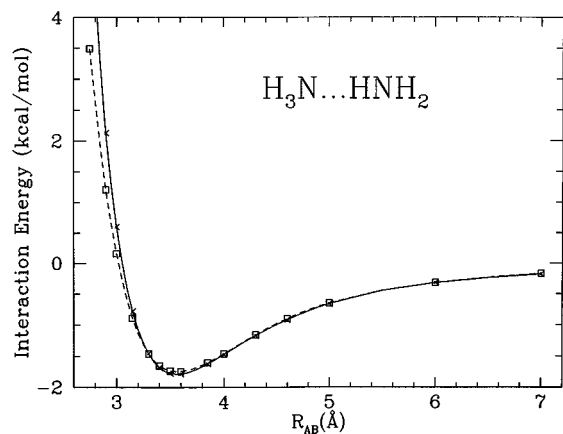


FIG. 5. Comparison between the SCF interaction energy curve (solid line with crosses) and the curve representing the perturbational sum $E^{(1)} + E_{ind}^{(2)}$ (dashed line with open squares) for the $(\text{NH}_3)_2$ dimer.

this point we present in Figures 5 and 6 a comparison between the SCF interaction energy curve and the curve representing the perturbational sum $E^{(1)} + E_{ind}^{(2)}$ for the $(\text{NH}_3)_2$ and $(\text{HF})_2$ dimers, respectively. For the NH_3 dimer the overall agreement between the two curves is strikingly good. In contrast, for the $(\text{HF})_2$ dimer there is a clear disagreement, the main feature being an important difference in the location of the minimum. Although the difference of minimum energies is small (about 0.2 kcal/mol) this difference at the new corresponding minima is magnified when the total dispersion energy is added to lead to the complete interaction energy. Following the Morokuma decomposition (see e.g., Ref. 54) the SCF interaction energy may be written as:

$$\Delta E_{int}^{SCF} = E_{elec} + E_{exch-HL} + E_{ind}^{SCF}, \quad (33)$$

where E_{elec} is the electrostatic energy (identical to $E_{RS}^{(1)}$) as calculated here with SAPT, $E_{exch-HL}$ is the Heitler–London exchange energy which reduces almost to $E_{exch}^{(1)SAPT}$ when a very large basis set is used (see discussion on the complementary exchange in Sec. III.B) and E_{ind}^{SCF} is by definition the

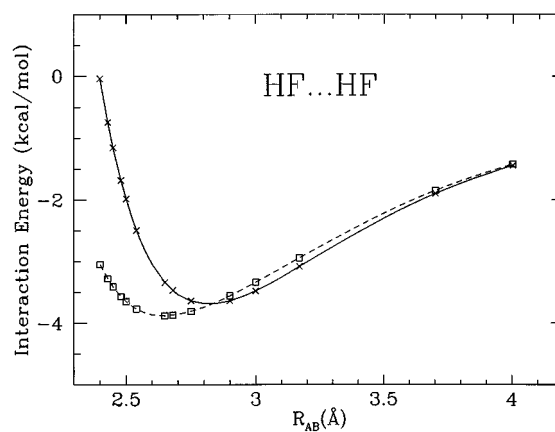


FIG. 6. Comparison between the SCF interaction energy (solid line with crosses) and the curve representing the perturbational sum $E^{(1)} + E_{ind}^{(2)}$ (dashed line with open squares) for the $(\text{HF})_2$ dimer.

induction part of the SCF interaction energy. In order to discuss the status of the SAPT induction energy (including or not the exchange contribution) with respect to the SCF induction energy, we have presented in Table X the SCF induction energy, the difference between the SCF induction energy and the total SAPT induction energy (including exchange effects) and the same difference without the exchange terms, all quantities being given as a function of the distance R_{AB} . It immediately appears that at short and intermediate distances, the three calculated values of the induction energy are different. The nice agreement obtained for the water dimer at $R_{O\dots O} = 3 \text{ \AA}$ between E_{ind}^{SCF} and $E_{ind}^{(2)}$ is actually fortuitous. In fact, E_{ind}^{SCF} should not be compared to $E_{ind}^{(2)}$ because the so-called *apparent correlation* or self-consistency effects are included in the supermolecular Hartree–Fock interaction energy but not in our computation of $E_{ind}^{(2)}$.¹⁵ As emphasized by Sadlej¹⁵ the second-order RS induction energy calculated within SAPT methodology by using the first-order perturbed wave function is equivalent to that computed within a UnCoupled Hartree–Fock (UCHF)

TABLE X. Comparison between the SCF induction energy and the perturbational induction energy. Energies in kcal/mol and distances in Å.

R_{AB}		$\text{H}_2\text{O}\dots\text{H}_2\text{O}$	$\text{H}_3\text{N}\dots\text{H}_2\text{N}$	$\text{H}_2\text{O}\dots\text{HOH}$	$\text{HF}\dots\text{HF}$	$\text{H}_3\text{N}\dots\text{HOH}$
2.75	E_{ind}^{SCF}	-4.57	-7.66	-3.84	-1.92	-6.26
	$E_{ind-tot}^{(2)} - E_{ind}^{SCF}$	2.74	4.37	2.10	0.89	3.39
	$E_{ind}^{(2)} - E_{ind}^{SCF}$	-1.53	-1.93	-0.71	-0.47	-1.32
2.90	E_{ind}^{SCF}	-2.61	-4.75	-2.25	-1.15	-4.00
	$E_{ind-tot}^{(2)} - E_{ind}^{SCF}$	1.52	2.67	1.25	0.47	2.11
	$E_{ind}^{(2)} - E_{ind}^{SCF}$	-0.65	-0.94	-0.24	-0.23	-0.63
3.00	E_{ind}^{SCF}	-1.93	-3.49	-1.68	-0.84	-3.00
	$E_{ind-tot}^{(2)} - E_{ind}^{SCF}$	1.11	1.94	0.83	0.33	1.55
	$E_{ind}^{(2)} - E_{ind}^{SCF}$	-0.37	0.55	-0.12	-0.12	-0.36
3.17	E_{ind}^{SCF}	-1.10	-2.00	-0.99	-0.50	-1.85
	$E_{ind-tot}^{(2)} - E_{ind}^{SCF}$	0.59	1.02	0.44	0.16	0.90
	$E_{ind}^{(2)} - E_{ind}^{SCF}$	-0.12	-0.30	-0.01	-0.04	-0.14
3.70	E_{ind}^{SCF}	-0.23	-0.48	-0.23	-0.13	-0.46
	$E_{ind-tot}^{(2)} - E_{ind}^{SCF}$	0.08	0.20	0.07	0.03	0.18
	$E_{ind}^{(2)} - E_{ind}^{SCF}$	0.01	0.01	0.02	0.02	0.01

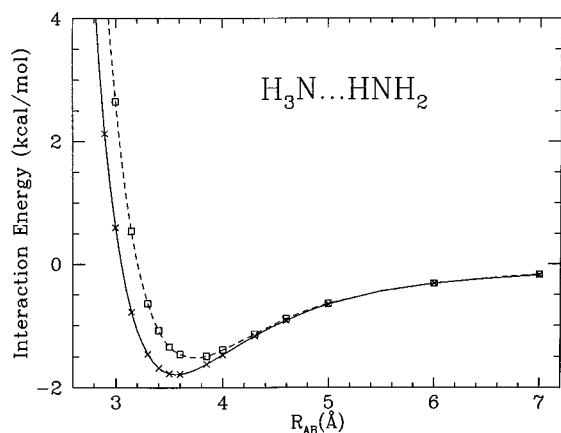


FIG. 7. Comparison between the SCF interaction energy curve (solid line with crosses) and the curve representing the perturbational sum $E^{(1)} + E_{ind}^{(2)} + E_{exch-ind}^{(2)}$ (dashed line with open squares) for the $(\text{NH}_3)_2$ dimer.

perturbation scheme. In particular, the perturbation-induced modification of the Hartree–Fock (HF) potential is not taken into account. In a UCHF scheme, the results obtained for $E_{ind}^{(2)}$ are underestimated. Sadlej emphasizes that if both unperturbed and perturbed many-electron systems are described in the HF approximation, then the appropriate perturbation theory is the Coupled Hartree–Fock (CHF) scheme. The induction computed at the CHF level is usually denoted as $E_{ind,resp}^{(2)}$, it sums up to infinity certain linear diagrams without rings and then fully accounts for the self-consistency effects. The CHF scheme corrects the HF potential of the unperturbed systems but no correlation corrections are introduced. The total exchange-induction contributions are also present in the SCF induction energy. However, at the SCF level, once again because of the self-consistency effects we get $E_{exch-ind,resp}^{(2)}$ instead of $E_{exch-ind}^{(2)}$. Finally, the SCF induction contribution is written as:

$$\Delta E_{ind}^{SCF} = E_{ind,resp}^{(2)} + E_{exch-ind,resp}^{(2)} + \delta E_{mixt}, \quad (34)$$

where δE_{mixt} gathers all higher perturbational terms. A number of calculations of $E_{ind,resp}^{(2)}$ and $E_{exch-ind,resp}^{(2)}$ have been presented (see references in Ref. 28).

Although results obtained with the hybrid approach are good it is important to realize that escaping from a pure perturbational treatment has some drawbacks. How much of the higher-order perturbational contributions, what part of the exchange-induction energy, etc... is recovered from a SCF supermolecular calculation is not easy to estimate. It may be argued that the good results obtained with the hybrid approach could result from a subtle balance between neglected contributions very different in nature. It is not clear whether that balance will still hold when higher-order contributions will be evaluated. Of course, a similar problem is present in a pure perturbational scheme but it is important to emphasize that the neglected quantities not taken into account are much more clearly identified. Accordingly, in our opinion it is still important to study the pure perturbational treatments. From Tables IV and IX (in particular the comparisons with experimental values) it appears that the complete pure perturbational treatment (SAPT) is the approach

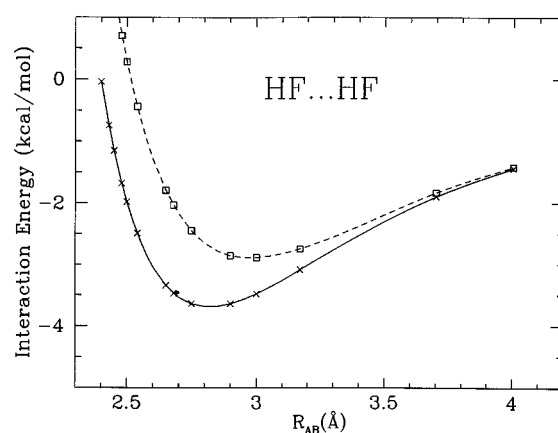


FIG. 8. Comparison between the SCF interaction energy curve (solid line with crosses) and the curve representing the perturbational sum $E^{(1)} + E_{ind}^{(2)} + E_{exch-ind}^{(2)}$ (dashed line with open squares) for the $(\text{HF})_2$ dimer.

which gives the less plausible results. Results from the truncated approach demonstrate that the main part of the disagreement between ΔE_{int}^{SAPT} on one hand, and $\Delta E_{int}^{SAPT, trunc}$ and ΔE_{int}^{hybrid} on the other hand, comes from the second-order exchange-induction energy which destroys the overall quality of the results. To illustrate this point Figures 7 and 8 display a comparison between the ΔE_{int}^{SCF} curve and the curve representing the perturbational sum $E^{(1)} + E_{ind}^{(2)} + E_{exch-ind}^{(2)}$ for the dimers $\text{H}_3\text{N}\dots\text{HNH}_2$ and $(\text{HF})_2$ (same curves as in Figures 5 and 6, except that the exchange-induction energy has been added). In Figure 7 it is seen that the very good agreement found in Figure 5 is destroyed. This result shows that the calculated values for $E_{exch-ind}^{(2)}$ are overestimated since for a weak dimer such as $\text{H}_3\text{N}\dots\text{HNH}_2$ the perturbational contributions beyond the second-order should be small and a perturbational description should be adequate. For stronger dimers like $(\text{HF})_2$ the clear disagreement between the two curves does not necessarily mean that we are in trouble (higher-order terms certainly play a role) but there is no reason not to believe that, in that case also, the exchange-induction term has been overestimated. Let us have a closer look to our estimate of the exchange-induction energy. Within the one-exchange approximation used in this work $E_{exch-ind}^{(2)}$ is calculated as a sum of three terms (see Sec. II, Eq. (19)). The analysis of our results has shown that the first term is positive and represents the major part of $E_{exch-ind}^{(2)}$ while the sum of the second and third terms is negative and essentially reduces $E_{exch-ind}^{(2)}$ by a quantity which depends on R_{AB} . For instance, for the $\text{H}_3\text{N}\dots\text{HOH}$ dimer this quantity has been calculated to be 24%, 15% and 11% for $R_{AB} = 2.54 \text{ \AA}$, 2.75 \AA , and 2.93 \AA , respectively. Quite similar results have been obtained with the other dimers. The sum of the two last terms entering into $E_{exch-ind}^{(2)}$ (see Eq. (19)) may be rewritten as

$$E_{RS}^{(1)} \sum_k \left[\sum_{i \in A} S_{ij}^{AB} S_{ik}^{AB} + \sum_{j \in B} S_{jk}^{AB} S_{jk}^{AB} \right] + E_{ind}^{(2)} \sum_{i \in A} \sum_{j \in B} |S_{ij}^{AB}|^2. \quad (35)$$

From Eq. (35) we see that an underestimation of the last term related to the induction part leads to an overestimation of the

exchange-induction energy. If, as emphasized by Sadlej,¹⁵ the induction part is underestimated within the SAPT treatment, then, it is plausible that there exists some reducing effect for the exchange-induction energy related to the induction part. In other words, higher-order terms (related to the apparent correlation effects) would contribute significantly to the total exchange-induction energy. Besides this effect, we can also argue that the one-exchange approximation is only valid for intermediate and large intermolecular distances and some bias could be introduced by neglecting multiple exchanges. The neat effect of the neglect of multiple exchange terms is not easy to estimate.

Finally, we would like to end with some remarks about the intramonomer correlation effects on the results presented here. Quite recently a number of studies have addressed the problem of evaluating the intramonomer correlations contributions to the interaction energy.^{11,13,20,22–28} Although a complete knowledge of all contributions is not at our disposal, the calculations made so far show clearly the importance of such effects. Of course, this is expected for the electrostatic energy of hydrogen-bonded systems which depends essentially on the magnitude of the permanent dipoles of the molecules known to be overestimated at the SCF level. However, it is more surprising to get even stronger corrections for the exchange contribution to the first-order.¹³ Some important effects (about 0.5 kcal/mol) have also been obtained for the dispersion and induction part (-0.42 kcal/mol for $E_{disp}^{(22)}$ and -0.60 kcal/mol for $E_{ind}^{(22)}$ in the case of the water dimer,²⁰ the second superscript indicating the perturbational order in the Møller-Plesset expansion). These results are of particular importance for the discussion just presented on the exchange-induction. As mentioned above, an underestimation of the induction energy leads to an overestimation of the exchange-induction. Accordingly, the neat effect of the intramonomer correlation could be a reduction of the exchange-induction energy. However, it should be noted that there is an opposite trend for the electrostatic energy, although this effect is probably less pronounced. This discussion illustrates the fact that there is still much room left to fully understand the intricate balance between the different contributions to the interaction energy.

V. CONCLUSIONS

In this work we have presented a detailed perturbational study of several hydrogen-bonded dimers consisting of H₂O, NH₃, and HF molecules. Three different approaches have been used to compute the interaction energy: a pure perturbational approach, ΔE_{int}^{SAPT} , including all perturbational components up to the second-order calculated at the SCF level, a so-called truncated approach, $\Delta E_{int}^{SAPT_{trunc}}$, in which the exchange part of the induction is not considered, and the hybrid approach, ΔE_{int}^{hybrid} , in which the supermolecular SCF interaction energy (counterpoise-corrected) is supplemented by the complete dispersion contribution calculated with SAPT (both Rayleigh-Schrödinger and exchange contributions). The quality of the large basis sets used has been checked by computing a number of properties for both the monomers and the corresponding dimers (SCF monomer

energies, dipole moments, complementary exchange energies, etc...). From a qualitative point of view, the physical results obtained with the three approaches are essentially similar. The relative force of the different hydrogen bonds are in agreement with experimental results and, in particular, the acceptor or donor properties are correctly reproduced. From a quantitative point of view, a number of differences emerge when using the different approaches. These quantitative differences are particularly important for the radial properties, much less for the angular ones. A general result already emphasized by some authors is that, at the level of approximation employed here (SCF level, perturbational components up to the second-order only, etc.), the hybrid approach seems to be the most reliable approach (see Table IV). The pure perturbational approach including the main contributions up to the second-order (calculated at the SCF level) gives the less plausible results. Clearly, some of the neglected contributions must be introduced to get better results. In particular, the second-order exchange-induction energy is certainly overestimated. We have argued that this quantity is very probably reduced by some intramonomer correlation contribution. However, it is important to emphasize that the error on the known experimental quantities is in general of the same order of magnitude as the dispersion of the results obtained using the different approaches. Accordingly, there is still no clearcut conclusion on which method is the best at the present time. To analyze further the importance of each perturbational components is therefore essential if we want to reach in a controlled way the asymptotic regime of the perturbational expansion of the intermolecular interaction energy.

ACKNOWLEDGMENT

The authors are grateful to the “Institut du Développement et des Ressources en Informatique Scientifique” (IDRIS) for providing them with computer time.

¹P. Arrighini, in *Intermolecular Forces and their Evaluation by Perturbation Theory*, Lectures Notes in Chemistry (Springer-Verlag, Berlin, 1981).

²B. Jeziorski and W. Kolos, in *Molecular Interactions*, edited by H. Ratajczak and W. J. Orville-Thomas (Wiley, New York, 1982), Vol. 3.

³I. G. Kaplan, in *Theory of Molecular Interactions* (Elsevier, Amsterdam, 1986), Vol. 42.

⁴B. Jeziorski and M. van Hemert, *Mol. Phys.* **31**, 713 (1976).

⁵G. Chalasiniski, *Mol. Phys.* **49**, 1353 (1983).

⁶G. Chalasiniski and B. Jeziorski, *Mol. Phys.* **32**, 81 (1976).

⁷G. Chalasiniski and B. Jeziorski, *Theor. Chim. Acta* **46**, 277 (1977).

⁸G. Chalasiniski, *Chem. Phys.* **82**, 207 (1983).

⁹G. Chalasiniski, *Chem. Phys. Lett.* **86**, 165 (1982).

¹⁰S. Rybak, Ph.D. thesis, University of Warsaw, Warsaw, 1988.

¹¹B. Jeziorski, R. Moszynski, S. Rybak, and K. Szalewicz, in *Proceedings of the Symposium on Many-Body Methods, Tel-Aviv, Israel, 1988*, edited by U. Kaldor (Springer-Verlag, Berlin, 1989).

¹²O. Hess, M. Caffarel, C. Huiszoon, and P. Claverie, *J. Chem. Phys.* **92**, 6049 (1990).

¹³R. Moszynski, B. Jeziorski, and K. Szalewicz, *J. Chem. Phys.* **100**, 1312 (1994).

¹⁴G. Chalasiniski and B. Jeziorski, *Int. J. Quantum Chem.* **7**, 63 (1973).

¹⁵A. J. Sadlej, *Mol. Phys.* **39**, 1249 (1980).

¹⁶R. Moszynski, S. M. Cybulski, and G. Chalasiniski, *J. Chem. Phys.* **100**, 4998 (1994).

¹⁷S. M. Cybulski, *J. Chem. Phys.* **96**, 8225 (1992).

¹⁸S. M. Cybulski, *J. Chem. Phys.* **97**, 7545 (1992).

¹⁹M. Jaszunski, *Mol. Phys.* **39**, 777 (1980).

- O. C. Huiszoon and M. Caffarel, "A quantum Monte Carlo perturbational study of the He-He interaction", *J. Chem. Phys.* 104, 4621 (1996)

A quantum Monte Carlo perturbational study of the He–He interaction

Cornelis Huiszoon^{a)}

Center for Theoretical Physics, Department of Applied Physics, Twente University, P.O. Box 217, Enschede 7500 AE, The Netherlands

Michel Caffarel^{b)}

CNRS-Laboratoire de Dynamique des Interactions Moléculaires, Université Paris VI, Tour 22-23, 4 Place Jussieu, 75252 Paris Cedex 05, France

(Received 3 October 1995; accepted 5 December 1995)

Using a recently proposed quantum Monte Carlo method the *exact* first-, second-, and third-order Rayleigh–Schrödinger interaction energies of the He–He interaction have been calculated for internuclear distances in the range 1.5- to 7.0 bohr. Putting together these new data with the best *ab initio* results available, the relative importance of the different contributions appearing in the perturbational expansion of the He–He interaction energy is discussed. In particular, the results show that the third-order Rayleigh–Schrödinger term and the intra-atomic correlation contribution to the second-order component play a significant role. For intermediate and large distances (including the equilibrium distance), it is found that the perturbational expansion limited to the complete first- and second-order, plus the third-order Rayleigh–Schrödinger energy agrees with the best known values of the total interaction energy of the helium dimer. © 1996 American Institute of Physics. [S0021-9606(96)02610-X]

I. INTRODUCTION

The determination of the intermolecular potential between chemically nonbonding atoms and molecules is a problem of fundamental importance in the field of molecular physics. However, even in the case of the interaction between two helium atoms—the simplest inert gas pair—the problem is known to be difficult and has been the subject of numerous papers spanning a period from the late twenties to the present time (see, e.g., Ref. 1 for a historical review).

Two mainstreams in the methods of calculation can be distinguished: the supermolecular and the perturbational methods. In the supermolecular method the energy of interaction is obtained by subtracting from the total energy of the interacting molecules (the supermolecule) the sum of the energies of each monomer. Since the energies involved cannot be evaluated exactly one is confronted with the difficulty of obtaining a very small number as the difference of two huge numbers, both being known only approximately. As has been stated by van Lenthe *et al.*,² for an accurate evaluation of the interaction energy using *ab initio* techniques three requirements should be fulfilled: saturation of the basis set, saturation of the configuration set, and effective elimination of the basis set superposition error. In practice, it turns out to be hard to meet these requirements, even for a relatively small system such as the helium dimer. Nevertheless, according to Liu and McLean,³ “... one seems to have come close to writing the end of the chapter on helium dimer potentials.” Aziz and Slaman⁴ have fitted model potentials to the supermolecular *ab initio* energies of interaction calculated by Vos *et al.*⁵ and by Liu and McLean.³ With these potentials the prediction of a variety of accurate experimental data such as the

second virial coefficient, viscosity and thermal conductivity was attempted. The agreement with experiment can be considered excellent,¹ although, as has been stated by Aziz and Slaman,⁴ “... small failures nevertheless remain.” In this context it is important to keep in mind the remark made by Anderson *et al.*,¹ regarding a result given by Liu and McLean,³ “... that one should be a little nervous about the estimated uncertainty of ± 0.03 K in the interaction potential when the calculated total energy is 1200 K above the exact total energy.” Finally, van Mourik and van Lenthe⁶ very recently presented the results of full configuration interaction calculations for the helium dimer employing large basis sets, which contain up to *h*-type basis functions, including bond functions. Their results probably are the best at present for the He₂ interaction energy. At the equilibrium distance, $R=5.6$ bohr, the interaction energy was calculated to be $-34.67 \mu\text{hartree}$ with an error of $\pm 0.03 \mu\text{hartree}$.

Quantum Monte Carlo (QMC) methods also can be used to compute molecular energies. Lowther and Coldwell,⁷ using a variational QMC approach have calculated the energy of interaction for internuclear distances ranging from 4.5- to 15 bohr using a 189-term Hylleraas-type atomic wave function from which a fully correlated dimer wave function was constructed. They found a very good energy of interaction at the minimum of the potential of $-35.5 \pm 1.5 \mu\text{hartree}$ which agrees well with the more recent values of $-34.64 \mu\text{hartree}$ (Liu and McLean³), $-34.42 \mu\text{hartree}$ (Vos *et al.*⁵), and $-34.67 \mu\text{hartree}$ (van Mourik and van Lenthe⁶). Exact QMC supermolecular calculations have been done by Ceperley and Partridge,⁸ for the small internuclear distances, ranging from 1.0–3.0 bohr, and by Anderson *et al.*¹ for distances greater than 3 bohr. The results obtained by Anderson¹ fully agree with those of Liu and McLean,³ Vos *et al.*,⁵ and van Lenthe.⁶ It should be emphasized that the difficult problems connected with the use of a basis set in *ab initio* calculations are

^{a)}e-mail: c.huiszoon@thn.tn.utwente.nl

^{b)}e-mail: mc@lct.jussieu.fr

absent in exact QMC calculations. The only input is the so-called trial wave function. It is important to realize that, although the statistical error is directly related to the quality of the trial wave function, the statistical estimate of the energy is not biased by a particular choice of the input trial wave function.

A very natural alternative approach to supermolecular methods is to consider the interaction energy as the result of a very small physical perturbation of the isolated monomers and thus to employ some kind of perturbational method. At this point, it is worthwhile to recall that, at the equilibrium distance of the helium dimer in which we are interested here, the interaction energy represents only approximately 6×10^{-6} of the total dimer energy. Such a tiny fraction clearly justifies the use of perturbational methods. This line of research has been intensively followed during the last decades and has led to the so-called symmetry adapted perturbation theories (SAPT) for intermolecular interactions (see, e.g., Refs. 9, 10 or 11). Within this framework the intermolecular Coulomb potential is treated as a perturbation, and the interaction energy is directly given as a sum of perturbational components. This type of approach does not involve the typical difficulties of the supermolecular method mentioned above. Each perturbational component can be split into an exchange and a Rayleigh–Schrödinger (RS) or polarization contribution. A number of methods have been designed to calculate these contributions. A general feature is that exchange contributions are more difficult to obtain than the RS contributions since they require a wave function of good quality also in the outer region of the system, a region which is not necessarily very well described by wave functions obtained from a variational principle on the energy. Note that a quite complete review of the perturbation approach to van der Waals complexes has recently been published by Jeziorski, Moszynski, and Szalewicz.¹² Unfortunately, the use of perturbational approaches is limited because the computation of the perturbational components is not easy to do. Even in the case of the helium dimer, only the first- and second-order contributions have been considered in practice.^{13,14} Of these two, the first-order term has been evaluated accurately since the wave function for the dimer is a simple product of the ground state monomer wave functions and these functions can be chosen to approximate the exact result very closely.¹³ Contrary to the first-order energy of interaction, the higher-order terms are given in sum-over-states representations and the excited-states must be known (explicitly or implicitly) to evaluate the sums. Accordingly, accurate evaluations of these terms are much more difficult to perform. In Sec. IV we will discuss this point in detail.

In this paper we present exact calculations of the first-, second-, and third-order RS interaction energies of the He–He interaction for internuclear distances ranging from 1.5- to 7.0 bohr. In order to do that, we resort to a recently proposed QMC method to compute perturbational quantities,^{15,16} In this approach the perturbational quantities are expressed as multitime integrals of some well-defined autocorrelation functions of the perturbing potential. The correlation functions are defined along the stochastic trajec-

tories of some generalized diffusion process associated with the unperturbed system.^{17,18} In practice, to construct these trajectories only a good approximate trial wave function for the unperturbed Hamiltonian is required. It is important to emphasize that the results obtained are essentially exact within their statistical errors. In particular, the complete intramonomer correlation contribution is included. The QMC perturbational approach has been applied to the helium dimer in the original work of Caffarel and Hess.¹⁵ However, the numerical results presented in their work were obtained only for very short distances (1.5- to 2.0 bohr), and only for the first- and second-order interaction energies. Here, we make a much more systematic study including the short, intermediate, and large distances. In particular, we focus our attention on the region of the potential well which is the region of physical interest. The third-order RS term is also computed here and is found to play a significant role. As has been already stated above when discussing *ab initio* SAPT techniques, exchange contributions responsible for the repulsive part of the potential energy curve, are in general difficult to evaluate. This is particularly true for QMC. In fact, the results of the calculations presented here show that it is not realistic to expect quantitative results for the longer distances. In order to illustrate this we will report some calculations of the first-order exchange interaction energy using a high-quality approximate formula. The results are compared with accurate *ab initio* values and are found to agree within large statistical errors. In principle, it is possible to write exact expressions for the exchange components¹⁹ but, due to these large statistical fluctuations, they will be of no practical use and, therefore, will not be considered further.

By using the exact QMC data presented here for the second- and third-order RS interaction energies, and the best *ab initio* values for the complete first-order and second-order exchange contributions we discuss the relative importance of the different perturbational contributions making up the total interaction energy of the helium dimer: The RS contributions of different orders, the intraatomic electron–electron correlation, the exchange effects. To our knowledge, this is the first example of an intermolecular interaction whose perturbational description is fully understood. Besides its own interest, it is clearly of general interest for the theory of intermolecular forces and their evaluation by perturbation theory.

The organization of the paper is as follows. Section II presents the basic equations of the QMC-perturbational approach used here. Section III contains the computational details. Finally, Sec. IV presents and discusses the numerical results for the perturbational components of the He–He interaction.

II. BASIC EQUATIONS

A. Rayleigh–Schrödinger interaction energies

Let us first consider the calculation of the first-, second-, and third-order RS interaction energies. The formulas presented here are some particular cases of a general n th order formula derived by Caffarel and Hess.^{15,16} Since the formalism presented in Refs. 15 and 16 is very general and not

commonly used, we have chosen to rederive the perturbational expressions using a more pedestrian approach. It is emphasized that the equations are valid for any perturbational problem and are, therefore, not limited to intermolecular forces.

In any perturbational treatment the full Hamiltonian, H , is written as the sum of a reference Hamiltonian, $H^{(0)}$, and a perturbing potential V

$$H = H^{(0)} + V. \quad (1)$$

In the present application, H is the Hamiltonian of the interacting helium dimer, $H^{(0)}$ is the Hamiltonian of the noninteracting dimer: $H^{(0)} = H^A + H^B$, where H^M represents the Hamiltonian of the isolated helium atom ($M = A, B$). V is the interatomic interaction operator

$$V = \frac{1}{r_{13}} + \frac{1}{r_{23}} + \frac{1}{r_{14}} + \frac{1}{r_{24}} - \frac{2}{r_{1B}} - \frac{2}{r_{2B}} - \frac{2}{r_{3A}} - \frac{2}{r_{4A}} + \frac{4}{R_{AB}}, \quad (2)$$

where the indices 1 and 2 refer to the electrons of atom A and indices 3 and 4 to those of atom B , r_{ij} is the distance between electrons i and j , and R_{iM} the distance between electron i and nucleus M ($M = A, B$).

We are interested in computing the change in the ground state energy of the dimer due to the presence of the perturbing operator V . Within the framework of perturbational treatments this change in energy is expressed as an infinite perturbation series

$$\Delta E_{\text{RS}} \equiv E_0 - E_0^{(0)} = \sum_{n=1}^{+\infty} E_{\text{RS}}^{(n)}, \quad (3)$$

where E_0 denotes the exact ground state energy of H but calculated with the complete neglect of the interatomic exchange of electrons, $E_0^{(0)}$ is the ground state energy of the reference Hamiltonian: $E_0^{(0)} = E_0^A + E_0^B$ with E_0^M ($M = A, B$) is the energy of the isolated atoms. ΔE_{RS} is the so-called Rayleigh–Schrödinger (RS) interaction energy, and $E_{\text{RS}}^{(n)}$ represents the n th order RS component. In the literature this quantity is also often called the n th order polarization component. At this point, it is important to emphasize that the ground state energy of the interacting dimer obtained by Eq. (3) is *not* the true physical ground state energy of the actual interacting dimer. Indeed, the change of symmetry of the wave function with respect to the exchange of electrons between the noninteracting and interacting dimers must also be taken into account. Physically, this leads to the repulsive interaction at short distances. In practice, this important physical effect is described by introducing in the perturbational series the so-called exchange terms. We shall discuss the exchange contribution later.

Now, Caffarel and Hess¹⁵ have shown that the n th order RS contribution can be written in terms of a multitime integral of the n -point autocorrelation function of the perturbing potential along the stochastic trajectories of some diffusion process built from the reference Hamiltonian $H^{(0)}$. Let us denote by $\phi_i^{(0)}$ the eigenfunctions of the reference Hamiltonian with energies $E_i^{(0)}$

$$H^{(0)} \phi_i^{(0)} = E_i^{(0)} \phi_i^{(0)}. \quad (4)$$

The diffusion process associated with $H^{(0)}$ is entirely defined by its transition probability density

$$p(x \rightarrow y, t) = \frac{\phi_0^{(0)}(y)}{\phi_0^{(0)}(x)} \sum_i \phi_i^{(0)}(x) \phi_i^{(0)}(y) \times \exp[-t(E_i^{(0)} - E_0^{(0)})], \quad (5)$$

where x and y represent two points in the configuration space ($x = (\mathbf{r}_1, \mathbf{r}_2, \mathbf{r}_3, \mathbf{r}_4)$ in the present application), and t is the time parameter. In other words, the transition probability density is, up to some factor involving the ground state wave function, connected to the imaginary time-dependent Green's function of $H^{(0)}$

$$p(x \rightarrow y, t) = \frac{\phi_0^{(0)}(y)}{\phi_0^{(0)}(x)} \langle y | \exp[-t(H^{(0)} - E_0^{(0)})] | x \rangle. \quad (6)$$

Note that expressions Eqs. (5) and (6) are identical only if all the eigenfunctions are real. This condition is satisfied since only real Hamiltonians will be considered (for such Hamiltonians a complete set of real eigenfunctions can always be constructed). As a consequence, no conjugation sign will appear in the formulas that follow. Eq. (5) defines a diffusion process consisting of a standard free diffusion part in configuration space plus a deterministic part corresponding to a drifted move with a drift vector given by

$$b = \frac{\nabla \phi_0^{(0)}}{\phi_0^{(0)}}. \quad (7)$$

It can be verified by substitution that the previous transition probability density, Eq. (5), is the solution of the following (forward Fokker–Planck) diffusion equation

$$\frac{\partial p}{\partial t} = \frac{1}{2} \nabla_y^2 p - \nabla_y [b(y)p] \quad (8)$$

with the initial condition, $p(x \rightarrow y, 0) = \delta(x - y)$ (for a general presentation of diffusion processes, see, e.g., Refs. 19 and 20). In practice, stochastic trajectories of the diffusion process are generated using a discretized version of the Langevin equation

$$\Delta x(t + \Delta t) = b(x(t)) \Delta t + \eta \sqrt{\Delta t}, \quad (9)$$

where η is a random vector whose independent components are drawn from a Gaussian distribution with zero mean and unit variance (free diffusion process in a multidimensional space).

Next the different perturbational components can be written in terms of averages of the diffusion process just presented. The first order is given by the usual formula ($\phi_0^{(0)}$ is supposed to be normalized)

$$E^{(1)} = \langle \phi_0^{(0)} | V | \phi_0^{(0)} \rangle, \quad (10)$$

which can be written as

$$E^{(1)} = \int dx p(x) V(x), \quad (11)$$

where $p(x)$ is given by

$$p(x) = [\phi_0^{(0)}(x)]^2. \quad (12)$$

In this formula, $p(x)$ is the quantum-mechanical probability density associated with the ground state wave function of the reference Hamiltonian. In fact, $p(x)$ is also the stationary density of the diffusion process. This property is easily checked by looking at the long-time behavior of the transition probability density, Eq. (5), or by verifying that p is the stationary solution of Eq. (8). Denoting by $\langle \dots \rangle$ the stochastic average along any trajectory or group of trajectories generated using the Langevin equation (these two methods of averaging are equivalent due to the ergodicity of the diffusion process, see Ref. 15), the first order is simply given by

$$E^{(1)} = \langle V \rangle. \quad (13)$$

The derivation of the second order is more involved and explicitly makes use of the dynamics of the diffusion process. In what follows, we will use the reduced resolvent of $H^{(0)}$ defined by

$$R_0 \equiv \sum_{i \neq 0} \frac{1}{E_0^{(0)} - E_i^{(0)}} |\phi_i^{(0)}\rangle \langle \phi_i^{(0)}|. \quad (14)$$

The usual expression for the second order is

$$E^{(2)} = \sum_{i \neq 0} \frac{\langle \phi_0^{(0)} | V | \phi_i^{(0)} \rangle \langle \phi_i^{(0)} | V | \phi_0^{(0)} \rangle}{E_0^{(0)} - E_i^{(0)}}, \quad (15)$$

which can be written in the compact form

$$E^{(2)} = \langle \phi_0^{(0)} | V R_0 V | \phi_0^{(0)} \rangle. \quad (16)$$

Now, from the basic relation, Eq. (6), we can express the reduced resolvent, Eq. (14), in terms of the transition probability density in the following way:

$$\int_0^{+\infty} dt [p(x \rightarrow y, t) - p(y)] = - \frac{\phi_0^{(0)}(y)}{\phi_0^{(0)}(x)} \langle y | R_0 | x \rangle. \quad (17)$$

Using Eqs. (16) and (17) we get

$$E^{(2)} = - \int_0^{+\infty} dt \left\{ \int dx dy p(x) V(x) p(x \rightarrow y, t) V(y) - \left[\int dx p(x) V(x) \right]^2 \right\}, \quad (18)$$

which can be viewed as the integral of the two time-centered autocorrelation function of the perturbing potential

$$E^{(2)} = - \int_0^{+\infty} dt C_{\bar{v}\bar{v}}(t), \quad (19)$$

where the autocorrelation function $C_{\bar{v}\bar{v}}(t)$ is given by

$$\begin{aligned} C_{\bar{v}\bar{v}}(t) &\equiv \langle (V(0) - \langle V \rangle)(V(t) - \langle V \rangle) \rangle \\ &= \langle V(0)V(t) \rangle - \langle V \rangle^2. \end{aligned} \quad (20)$$

This is the final formula for the second-order interaction energy. Note that $C_{\bar{v}\bar{v}}$ appears as a second-order cumulant of the perturbing potential. A similar formula can be obtained

for the third-order RS component by starting from the usual expression of the third-order component in terms of the reduced resolvent

$$E^{(3)} = \langle \phi_0^{(0)} | V R_0 (V - E^{(1)}) R_0 V | \phi_0^{(0)} \rangle, \quad (21)$$

which can be written in the form

$$\begin{aligned} E^{(3)} &= \int_0^{+\infty} \int_0^{+\infty} dt_1 dt_2 \int \int \int dx dy dz p(x) V(x) \\ &\quad \times [p(x \rightarrow y, t_1) - p(y)] (V(y) - \langle V \rangle) \\ &\quad \times [p(y \rightarrow z, t_2) - p(z)] V(z). \end{aligned} \quad (22)$$

After some algebra, this formula can be rewritten as

$$\begin{aligned} E^{(3)} &= \int_0^{+\infty} \int_0^{+\infty} dt_1 dt_2 \{ \langle V(0)V(t_1)V(t_2) \rangle \\ &\quad - \langle V \rangle \langle V(0)V(t_1) \rangle - \langle V \rangle \langle V(t_1)V(t_2) \rangle \\ &\quad - \langle V \rangle \langle V(0)V(t_2) \rangle + 2 \langle V \rangle^3 \}, \end{aligned} \quad (23)$$

which can be used for practical Monte Carlo calculations. Note that, now, it is a third-order cumulant of the perturbing potential which appears in the formula. Quite naturally, the general formula for the general n th order in perturbation involves the n th order cumulant of the potential (see Ref. 15).

At this point, we have shown that, for a general Hamiltonian, it is possible to express any perturbational component as an integral of a stochastic autocorrelation function of the external potential. To compute this correlation function, only the ground state wave function has to be known. From this wave function the drift vector can be computed and, then, the stochastic trajectories can be generated using the Langevin equation, Eq. (9). In general, except for very simple cases, the ground state wave function is not known and stochastic trajectories corresponding to the true reference problem cannot be constructed. This problem is easily solved by making use of a slightly different diffusion process constructed from a very good approximation of the unknown ground state wave function. Of course, in that case, it is also necessary to change in some suitable way the integrands in the stochastic averages so that the perturbational expressions remain exact. Let us denote by ψ_T (T for trial wave function) this new approximate wave function. It is important to emphasize that, once a trial wave function is given, the diffusion process is entirely determined via the Fokker-Planck equation Eq. (8) and the drift vector Eq. (7) that is built from it. Doing this corresponds to choosing a new transition probability density whose expression is given by

$$p_T(x \rightarrow y, t) = \frac{\psi_T(y)}{\psi_T(x)} \langle y | \exp[-t(H_T^{(0)} - E_T^{(0)})] | x \rangle, \quad (24)$$

where $H_T^{(0)}$ is the Hamiltonian which has ψ_T as its ground state wave function, or

$$H_T^{(0)} \psi_T = E_T^{(0)} \psi_T. \quad (25)$$

The important point is that this new approximate Hamiltonian is explicitly known

$$H_T^{(0)} = H^{(0)} - (E_L(x) - E_T^{(0)}), \quad (26)$$

where E_L is the so-called local energy corresponding to the trial wave function

$$E_L(x) = H^{(0)} \psi_T / \psi_T. \quad (27)$$

When the approximate wave function reduces to the exact one, the local energy reduces to the exact energy and the difference between $H_T^{(0)}$ and $H^{(0)}$ vanishes. Accordingly, the smoothness of the local energy is a measure for the quality of the trial wave function.

In the short time limit a relation between the exact and trial transition probability density can be found. Using Eqs. (6), (24), (26), and keeping the leading contribution in time, we get

$$p(x \rightarrow y, \tau) \sim_{\tau \rightarrow 0} p_T(x \rightarrow y, \tau) \exp[-\tau(E_L(x) - E_T^{(0)})]. \quad (28)$$

Essentially there are two different ways to take into account the additional exponential weight factor. A first method considers this factor as a simple weight and carries it along the stochastic trajectories. This method, which is usually referred to as the pure diffusion Monte Carlo (PDMC) method, is the method we shall employ here. The different aspects of this method have been presented elsewhere^{15–18} and will not be repeated here. The general expression used for the multi-time correlation functions is

$$\langle V[x(u_1)] \cdots V[x(u_k)] \rangle = \lim_{t \rightarrow \infty} \frac{\langle V[x(u_1)] \cdots V[x(u_k)] \exp[-\int_{-t/2}^{t/2} ds (E_L(x(s)) - E_T^{(0)})] \rangle}{\langle \exp[-\int_{-t/2}^{t/2} ds (E_L(x(s)) - E_T^{(0)})] \rangle}, \quad (29)$$

where the u_i 's are some fixed time values in the interval $(-t/2, t/2)$. Note that the total exponential weight appearing in this formula is usually referred to as the Feynman–Kac weight.^{17,18}

A second possible approach is to simulate the exponential term using a birth–death process or branching process. In contrast with the pure diffusion method, the number of walkers varies during the simulation with some rate related to the magnitude of the exponential factor. This method is referred to as the diffusion Monte Carlo (DMC) method (see, e.g., Ref. 21 for a detailed presentation). Note that this method could be used here for computing correlation functions. However, its implementation is not straightforward because of the varying number of walkers. In order to compute the different multitime correlation functions we have to keep trace of all the death and birth events during a given period of time. This is a nontrivial accounting problem that is avoided here by using a PDMC approach.

B. Exchange terms

As mentioned in Sec. I, this paper does not focus on the evaluation of the different exchange energy components with QMC. Indeed, large statistical fluctuations associated with very small exchange overlaps prevent accurate results being obtained. Let us just present the approximate formula of the first-order exchange contribution employed here.

The exact first-order energy of interaction is defined as

$$E^{(1)} = \frac{\langle \phi_0^{(0)} | V \mathcal{A} | \phi_0^{(0)} \rangle}{\langle \phi_0^{(0)} | \mathcal{A} | \phi_0^{(0)} \rangle}, \quad (30)$$

where $\phi_0^{(0)}$ is the exact ground state wave function of the Hamiltonian $H^A + H^B$. The operator \mathcal{A} denotes the antisym-

metrizer for all electrons. The first-order energy can be split into two contributions: the first-order RS energy of interaction and the first-order exchange interaction

$$E^{(1)} = E_{\text{RS}}^{(1)} + E_{\text{exch}}^{(1)}. \quad (31)$$

The first-order Rayleigh–Schrödinger has already been considered in the previous section. It is given by

$$E_{\text{RS}}^{(1)} = \frac{\langle \phi_0^{(0)} | V | \phi_0^{(0)} \rangle}{\langle \phi_0^{(0)} | \phi_0^{(0)} \rangle}. \quad (32)$$

After integration over the spin coordinates, it is not difficult to obtain the following expression for the first-order exchange component:

$$E_{\text{exch}}^{(1)} = \frac{\langle \mathcal{P} \rangle \langle V \rangle - \langle V \mathcal{P} \rangle}{1 - \langle \mathcal{P} \rangle} \quad (33)$$

with $\mathcal{P} = \frac{1}{2}(P_{13} + P_{14} + P_{23} + P_{24}) - P_{13}P_{24}$, P_{ij} denoting the transposition of electrons i and j . The brackets indicate the stochastic average along stochastic trajectories of the diffusion process constructed from $\phi_0^{(0)}$. In practice, our approximate expression for this quantity is obtained by using the stochastic trajectories of the approximate diffusion process built from the high-quality trial wave function ψ_T . The present definition for the first-order energy exchange is in accordance with Rybak *et al.*¹³ and Caffarel and Hess¹⁵ but differs from that given by Conway and Murrell,²² as these authors split the total first-order energy in a different way into two components. The differences are, however, completely negligible for regions of small overlap.

III. SOME COMPUTATIONAL DETAILS

The trial wave function ψ_T used to describe the noninteracting dimer is constructed from a high-quality wave function for the helium atom

TABLE I. Optimized 6-term Hylleraas wave function for the helium atom (atomic units).^a

ζ	1.858 924 275 683 8
c_1	3.887 171 410 750 7×10^{-1}
c_2	1.457 928 455 588 9×10^{-1}
c_3	-6.957 678 799 139 1×10^{-2}
c_4	2.581 677 920 603 8×10^{-2}
c_5	-2.123 795 845 962 8×10^{-3}
Energy	-2.903 452 763 436 1
Correlation energy ^b	99.35%
Best literature value for the energy ^c	-2.903 724 377 034
Hartree–Fock energy ^d	-2.861 679 995 6

^aNot all figures displayed are significant. Some are displayed only to avoid round-off errors.

^bDefined as the difference between the exact nonrelativistic energy and the Hartree–Fock energy.

^cReference 24.

^dReference 25.

$$\psi_T(\mathbf{r}_1, \mathbf{r}_2, \mathbf{r}_3, \mathbf{r}_4) = \psi_K^A(\mathbf{r}_1, \mathbf{r}_2) \psi_K^B(\mathbf{r}_3, \mathbf{r}_4). \quad (34)$$

The helium atom wave function ψ_K^M ($M = A, B$) is a six-term Hylleraas-type wave function optimized and parameterized by Koga²³ and written as

$$\psi_K^M = \exp(-\zeta s)(1 + c_1 u + c_2 t^2 + c_3 u^2 + c_4 s^2 u + c_5 s^3 u), \quad (35)$$

where s , t , and u are the Hylleraas coordinates defined by

$$s = r_i + r_j, t = r_i - r_j, u = r_{ij}, \quad (36)$$

and where the exponent ζ and the coefficients c_i are variational parameters. r_i is the distance of electron i to nucleus M ($M = A, B$), r_{ij} is the distance between the two electrons. The values of the parameters are listed in Table I. This atomic trial wave function gives an accurate total energy corresponding to 99.35% of the correlation energy. In addition, its very compact form is quite attractive since the calculation of its first (drift vector) and second derivatives (Laplacian appearing in the local energy) is not too time consuming, an important point since this calculation must be performed at each Monte Carlo step.

Besides the statistical error inherent to any statistical method, the only source of error is the use of a finite time step when integrating the Langevin equation, Eq. (9) (short-time approximation). In order to reduce this short-time error we have imposed the detailed balance property during the simulation. Detailed balancing is introduced via an acceptance/rejection step at each Langevin move in a way similar to what is done in the usual Metropolis algorithm. Such a procedure is presented in detail in Ref. 15. It is important to note that the time step used in this work has been chosen small enough so that short-time errors are smaller than the statistical fluctuations.

The total local energy associated with the trial wave function appears in the different formulas used to compute the exact correlation functions of the interatomic potential. Using Eqs. (27) and (34) we get

$$E_L = H^A \psi_K^A / \psi_K^A + H^B \psi_K^B / \psi_K^B. \quad (37)$$

The total local energy is the sum of two monomer local energies. In fact, the two terms of the sum are statistically independent. Each monomer local energy depends only on its own actual configuration but not on the internuclear distance or on the relative orientation with respect to the other monomer. This property was used to accelerate the calculations. The local energy of an atom, in a particular configuration, does not change if one of the operations of the full octahedral point group, O_h , the symmetry group of the cube, is applied to the configuration. The point group contains 48 symmetry operations. Application of these operations to each monomer leads to 48×48 different configurations all having the same total local energy. Of these configurations there are 6×48 configurations leading to different values for the interatomic potential. These have been used in the calculations. No bias in the results is caused due to the application of the symmetry operations. In practice, the reduction in computation time achieved by considering these new configurations was approximately a factor of 10.

Let us now consider the practical computation of the correlation functions. Rewriting the one-point correlation function of the interatomic potential, Eq. (29), as an average along an arbitrary stochastic trajectory (this is possible because of ergodicity, see Refs. 15, 17, 18 for all details), the first-order is written as

$$E_{\text{RS}}^{(1)} = \lim_{t \rightarrow \infty} \lim_{T \rightarrow \infty} \frac{\int_0^T d\tau V[x(\tau)] \exp(-\int_{\tau-t/2}^{\tau+t/2} ds E_L[x(s)])}{\int_0^T d\tau \exp(-\int_{\tau-t/2}^{\tau+t/2} ds E_L[x(s)])}. \quad (38)$$

Here, T is related to the total time considered along the trajectory (actually, the total time is $T+t$) and $x(\tau)$ is an arbitrary stochastic trajectory generated with the Langevin equation. The typical time step used in this work is $\Delta t = 0.03$ a.u. and $T = 3000\Delta t$. The projection time t appearing in the Feynman–Kac weight is taken to be $t = 449\Delta t$. This relatively large value of t is in fact not required for the calculation of the first-order RS energy (a much smaller value would be sufficient). However, this value is needed for the evaluation of the time correlation functions. The two- and three-point correlation functions from which the second- and third-order RS interaction energies are calculated, are

$$C_{VV}(u) = \lim_{t \rightarrow \infty} \lim_{T \rightarrow \infty} \frac{\int_0^T d\tau V[x(\tau)] V[x(\tau+u)] \exp(-\int_{\tau-t/2}^{\tau+t/2} ds E_L[x(s)])}{\int_0^T d\tau \exp(-\int_{\tau-t/2}^{\tau+t/2} ds E_L[x(s)])} \quad (39)$$

and

$$C_{VVV}(u,v) = \lim_{t \rightarrow \infty} \lim_{T \rightarrow \infty} \frac{\int_0^T V[x(\tau)]V[x(\tau+u)]V[x(\tau+u+v)] \exp(-\int_{\tau-t/2}^{\tau+t/2} ds E_L[x(s)])}{\int_0^T d\tau \exp(-\int_{\tau-t/2}^{\tau+t/2} ds E_L[x(s)])}, \quad (40)$$

respectively. Note that, because of the stationarity property of the diffusion process, C_{VV} depends only on one time interval u and C_{VVV} on two time intervals, u and v . Figure 1 gives a typical example of the time-correlation function, $C_{\bar{V}\bar{V}}$, as a function of the time interval u [$C_{\bar{V}\bar{V}}$ is the centered time correlation function defined according to Eq. (20)]. In order not to bias the final result it is important to take large enough values of u and thus of the projecting time t . To get the second-order term the correlation function, Eq. (39), has to be integrated (in fact, the centered version of it). The integration has been done using Bode's rule.²⁶ Figure 2 shows the negative of the integral of the time correlation function as a function of the total integration time, also for $R=5.6$ bohr. By taking sufficiently large values of the correlation time, we can reach a regime where the integral has converged within statistical error bars.

Finally, in order to estimate the statistical error in each of the energy components, each calculation was split into a number of independent blocks. The final result was obtained as the mean value of the results obtained for the independent blocks, the error being obtained as the standard deviation of the mean. For R ranging from 3- to 7 bohr, we have used 38 blocks, each of them containing 50 trajectories. Taking into account the configurations generated with the symmetry as discussed above our statistics is based on approximately 1.6×10^9 Monte Carlo events for each perturbational component and distance. For the shorter distances we have used 14 blocks.

IV. RESULTS AND DISCUSSION

A. First-order energy

In contrast with higher-order terms, the first-order perturbational energy depends only on the ground state wave functions of the constituent monomers. A high accuracy can then be achieved by expanding these wave functions over a

sufficiently large set of basis functions. Table II reports the very accurate results obtained by Rybak *et al.*¹³ for both the RS part, denoted as $E_{RS-ab}^{(1)}$, and the exchange part, $E_{exch-ab}^{(1)}$. These results have been obtained using a 75-term GTG (Gaussian-type geminal) basis which reproduces 99.9976% of the helium correlation energy and properly represents the behavior of the electron density in the outer region of the helium atom. The error, in the interaction energy, is approximately $0.1 \mu\text{hartree}$.¹³ Note that, even for the first-order terms, the convergence of the calculations with the size of the basis set, is not easy to achieve. As an illustrative example consider the very recent results of Tachikawa *et al.*¹⁴ Using quite a large basis set these authors obtained RS contributions being very similar to those given by Rybak *et al.*¹³ However, the first-order exchange contributions differ noticeably from those reported by Rybak *et al.*¹³ For example, at $R=5.6$ bohr, the values of the polarization (RS) components almost equal (-5.35 - and $-5.37 \mu\text{hartree}$), but the exchange contributions differ by approximately $1 \mu\text{hartree}$ (38.95 - and $37.92 \mu\text{hartree}$). To illustrate the effect of the intra-atomic correlation on the first-order energies, the SCF values, $E_{RS}^{(10)}$ and $E_{exch}^{(10)}$ as given by Tachikawa *et al.*¹⁴ also have been listed in Table II (as usual, the second superscript 0 indicates that the quantities are evaluated at the SCF level). When we regard the exponentially small first-order RS part (there are no permanent multipoles and this contribution results only from the penetration of the atomic wave functions) the contribution of the correlation energy is between 5% to 8%, except at the largest distance ($R=7$ bohr) where it seems to be larger (however, care must be taken with the quality of the SCF value at such a large distance). The first-order exchange contribution is much more important and the effect of the intra-atomic correlation energy is a little stronger: between 6% to 12%. As for the RS component, the effect increases with the distance, showing that the tail of the atomic wave function seems to be sensitive to a

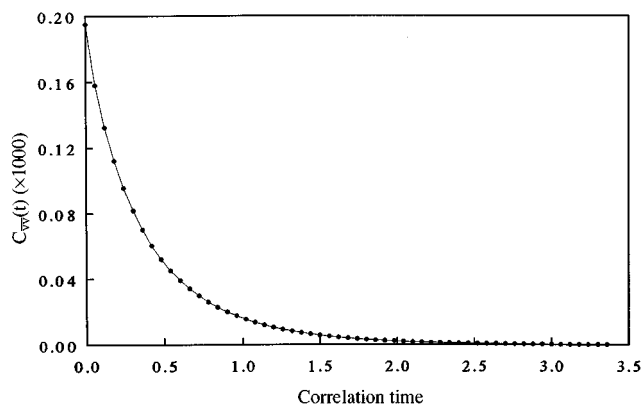


FIG. 1. The time correlation function, $C_{\bar{V}\bar{V}}(u)$ (a.u.), $R=5.6$ bohr.

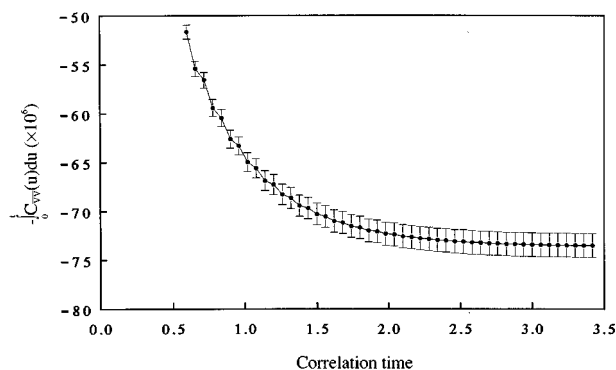


FIG. 2. The negative of the integral of $C_{\bar{V}\bar{V}}(u)$ (a.u.) as a function of the total integration time, $R=5.6$ bohr.

TABLE II. Quantum Monte Carlo and *ab initio* perturbational components at various interatomic distance R . Statistical errors on the last digit in QMC results are indicated in parentheses. Energies in μ hartree, distances in bohr.

R	3.0	4.0	5.0	5.6	6.0	7.0
$E_{RS}^{(10)a}$		−283.09	−22.79	−4.94	−1.78	−0.138
$E_{RS-ab\ initio}^{(1)b}$		−298.24	−24.56	−5.35	−1.90	−0.09
$E_{RS-QMC}^{(1)}$	−3355(56)	−283(13)	−25(6)	−6(1)	−3(2)	−0.3(3)
$E_{exch}^{(10)a}$		1752.71	155.85	35.52	13.11	1.040
$E_{exch-ab\ initio}^{(1)b}$		1854.16	168.14	38.95	14.55	1.18
$E_{exch-QMC}^{(1)c}$	16932(604)	1381(313)	449(339)	300(269)	62(43)	1(1)
$E_{RS}^{(20)}$		−520.11 ^a	−114.38 ^a	−55.27 ^d	−33.25 ^a	−11.97 ^a
$E_{RS-ab\ initio}^{(2)}$		−639.21 ^a	−143.62 ^a	−68.89 ^d	−42.14 ^a	−15.20 ^a
$E_{RS-QMC}^{(2)}$	−4421(68)	−703(17)	−161(10)	−74(1)	−45(2)	−15.9(4)
$E_{exch}^{(20)a}$		96.05	8.13	1.894	0.723	0.067
$E_{exch-ab\ initio}^{(2)a}$		135.96	11.38	2.65	1.01	0.09
$E_{RS-QMC}^{(3)}$	−1186(96)	−46(22)	−6(11)	2.2(2)	0.3(7)	0.13(3)

^aReference 14.^bReference 13.^cApproximate QMC first-order exchange energy, Eq. (33) with trial wave function Eq. (34).^dReference 27.

proper description of the intra-atomic correlation. We also present our QMC evaluation of the first-order components, $E_{RS-QMC}^{(1)}$ and $E_{exch-QMC}^{(1)}$. The first-order RS energy has been computed using the exact expression Eq. (38), whereas the first-order exchange energy has been calculated using the approximate expression Eq. (33). The first-order QMC results are given to show that they are in rough agreement with the much more accurate *ab initio* results. For the RS component the statistical fluctuations are 5% for $R=4$ bohr, 17% at the equilibrium distance, $R=5.6$ bohr, and essentially 100% at the largest distance, $R=7$ bohr, where the first-order RS component is very small. As has been mentioned already, the situation for the first-order exchange energy is even worse. Statistical fluctuations range from 23% to 100%. For the shorter distances the situation is more favorable. Table III lists the results. It is seen that, in this region, accuracies of, say, 1% to 2% are obtained. Hence, in what follows we shall use the accurate *ab initio* values, for the longer distances, as reference values for the first-order energy. As we discuss below, QMC results for the higher orders are much more interesting.

B. Second- and third-order interaction energies

Perturbational components beyond the first-order have been obtained, so far, by using *ab initio* frameworks where the monomer wave functions (ground and excited states) are expanded over a more or less extended set of basis functions. As is well known, a number of difficulties are present in such

calculations. First, in order to perform the infinite summations, present in the perturbational expressions, the entire set of the *exact* eigenfunctions of the monomers is needed. These functions are in general not known and approximate wave functions have to be used. In general, these functions are issued from a self-consistent-field (SCF) calculation in which the intra-atomic electron correlation is neglected. Very recently, a great deal of attention has been focused on the calculation of intramonomer correlation contributions to the interaction energy components.^{14,27–35} The usual approach consists in decomposing the monomer Hamiltonians as a sum of the Fock operator and some residual intramonomer correlation operators (Møller–Plesset partitioning) and, then, to resort to a double perturbation theory (in the correlation operators of each monomer) using a many-body expansion framework. However, such calculations are not so easy to do and are limited, in practice, to the calculation of some leading corrections (e.g., up to second order in the internal correlation) and/or to some partial infinite-order summation corresponding to specific classes of diagrams (see, e.g., Ref. 36). Second, there is the problem of efficiently evaluating the infinite sums present in the perturbational expressions. In particular, the summations corresponding to the continuous part of the spectrum are in practice almost inexecutable integrations (see, Ref. 37). To solve this problem, variation-perturbation schemes have been proposed in which the perturbed wave function is interpreted as the solution of a variational problem (Hylleraas variational procedure). Then,

TABLE III. Quantum Monte Carlo perturbational components at short internuclear distances R . Statistical errors on the last digit are indicated in parentheses. Energies in hartree, distances in bohr.

R	1.5	1.6	1.7	1.8	1.9	2.0
$E_{RS-QMC}^{(1)}$	−0.0813(6)	−0.0694(6)	−0.0583(6)	−0.0484(5)	−0.0398(5)	−0.0323(5)
$E_{exch-QMC}^{(1)}$	0.576(7)	0.462(6)	0.370(6)	0.297(6)	0.239(5)	0.191(5)
$E_{RS-QMC}^{(2)}$	−0.125(1)	−0.099(1)	−0.0781(9)	−0.0620(8)	−0.0495(8)	−0.0390(7)
$E_{RS-QMC}^{(3)}$	−0.077(2)	−0.059(2)	−0.045(1)	−0.035(1)	−0.028(1)	−0.021(1)

TABLE IV. Intraatomic correlation contributions to the second-order interaction energy. The first superscript gives the order in the interatomic perturbation, the second superscript indicates the perturbational order in the Møller–Plesset expansion with respect to the intraatomic electron correlation operator. Energies in $\mu\text{hartree}$, $R=5.6$ bohr.

$E_{\text{ind}}^{(20)\text{a}}$	−0.73
$E_{\text{disp}}^{(20)\text{a}}$	−54.53
$E_{\text{RS}}^{(20)} = E_{\text{ind}}^{(20)} + E_{\text{disp}}^{(20)}$	−55.27
$E_{\text{RS}}^{(20)} + E_{\text{disp}}^{(21)\text{a}}$	−65.10
$E_{\text{RS}}^{(20)} + E_{\text{disp}}^{(21)} + E_{\text{disp}}^{(22)\text{a}}$	−68.89
$E_{\text{RS-QMC}}^{(2)}$	−74(1)
$E_{\text{exch}}^{(20)\text{b}}$	1.894
$E_{\text{exch}}^{(20)} + E_{\text{exch}}^{(21)\text{b}}$	2.37
$E_{\text{exch}}^{(20)} + E_{\text{exch}}^{(21)} + E_{\text{exch}}^{(22)\text{b}}$	2.65

^aReference 27.

^bReference 14.

standard sets of basis functions can be used to describe the variational space. Finally, as in any *ab initio* framework, one still has the important problem of achieving a sufficiently complete basis set. This is particularly important here, since perturbational quantities are very sensitive to the basis set used.

In Table II we show the *ab initio* second-order RS interaction energies obtained very recently by Tachikawa *et al.*¹⁴ and by Jeziorski *et al.*²⁷ To our knowledge, these values are the best *ab initio* values calculated so far. It is worth remarking that, for $R=5.6$ bohr, both SCF and correlated values of $E_{\text{RS}}^{(2)}$ differ by approximately $2 \mu\text{hartree}$ between the two sets of results (the values given by Tachikawa *et al.*¹⁴ are $-52.93 \mu\text{hartree}$, at the SCF level, and $-66.91 \mu\text{hartree}$ at the correlated level, to compare with the better results of Jeziorski *et al.*²⁷ presented here). These large differences illustrate the difficulties in obtaining converged values with *ab initio* techniques.

In order to discuss the role of the intra-atomic electron correlation Table IV shows some of its perturbational contributions to the second-order components for $R=5.6$ bohr. The differences between RS and *ab initio* values on one hand, and QMC values on the other, are due to the intra-atomic electron correlation effects. In Table IV the first superscript gives the order in the interatomic perturbation, while the second superscript indicates the perturbational order in the Møller–Plesset expansion with respect to the intraatomic electron correlation operator. Note also that the second-order energy is decomposed as usual into an induction and dispersion part (see, e.g., Ref. 9). It may be clear that this distinction is specific to SCF and *ab initio* calculations but is meaningless within our QMC framework. For $R=5.6$ bohr, the exact QMC value is $-74 \mu\text{hartree}$ with a statistical error of only $1 \mu\text{hartree}$ or approximately 1%. The SCF second-order RS energy, $E_{\text{RS}}^{(20)}$, is quite different from our exact value, $E_{\text{RS-QMC}}^{(2)}$. This shows that the intra-atomic effect is strong. It is interesting to compare this result with the Møller–Plesset perturbational estimates of the same contribution presented by Jeziorski *et al.*²⁷ Note that the induction contribution to the total second order is very small [penetration contribution behaving as $\sim\exp(-aR)$] and only the contribution of the

correlation effect to the dispersion part has been considered. At the first-order level 53% of the correlation contribution is recovered. The second-order gives some additional 21% so that the total contribution recovered is 74%. The remaining correlation contribution represents 14% of the total interaction energy. This illustrates the fact that any accurate evaluation of the intramonomer correlation effects must incorporate contributions beyond second-order. Note that the error in the QMC result is small enough (only 5% of this correlation effect) to validate this conclusion.

As noticed in previous works (e.g., Refs. 27 and 39) the second-order exchange effects in intermolecular interactions are in general not negligible. Here, this contribution is 8% of the total interaction energy. The correlation contribution to the second-order exchange part is small but significant (2% of the total interaction energy).

We have computed the exact second-order RS energy for various internuclear distances. The relative statistical error grows slowly with the distance (see Tables II and III). Even for the largest distance the error is only 3%, which is a satisfactory result. For the large distances the QMC results for $E_{\text{RS}}^{(2)}$ are compatible with a behavior as c_6/R^6 as it should be for a van der Waals dimer. Note that a QMC evaluation of the van der Waals coefficient, c_6 , has been presented elsewhere.³⁸

The results for the third-order interaction energy are presented in Tables II and III. To the best of our knowledge there are no quantitative estimates of these values published so far. At the small distances this contribution is found to be negative, while at larger distances it corresponds to a repulsive contribution. It changes sign between $R=5-$ and 5.6 bohr. At the equilibrium distance, we find a repulsive contribution of $2.2 \mu\text{hartree}$ with a statistical error of 10%. This contribution is clearly significant since it represents 6% of the total interaction energy. In particular, it gives a contribution almost equal to the second-order exchange energy.

C. Total interaction energy

We are now in position to summarize the previous results and to discuss the relative importance of each perturbational component making up the complete interaction energy of the helium dimer. Within the framework of perturbational treatments (symmetry adapted perturbation theories (SAPT), the total interaction energy can be written as

$$\Delta E_{\text{int}} = E_{\text{RS}}^{(1)} + E_{\text{exch}}^{(1)} + E_{\text{RS}}^{(2)} + E_{\text{exch}}^{(2)} + E_{\text{RS}}^{(3)}. \quad (41)$$

In this expansion *all* contributions occurring at first- and second-order in perturbation are taken into account. The neglected contributions are the third-order exchange effects and all contributions beyond the third-order. Putting together all these contributions according to Eq. (41) we get the values for the perturbational sum as listed in Table V. At the minimum of the potential the value of $-35.0 \pm 1.2 \mu\text{hartree}$ for the total interaction energy of the helium dimer is found. This result is in good agreement with the very recent full CI interaction energy of van Mourik and van Lenthe⁶ which was calculated to be $-34.68 \pm 0.03 \mu\text{hartree}$. It is also in accor-

TABLE V. Sum of perturbational contributions to the total interaction energy at various internuclear distances R . Statistical errors on the last digit in QMC results are indicated in parentheses. Energies in $\mu\text{hartree}$, distances in bohr.

R	4.0	5.0	5.6	6.0	7.0
$E^{(1)} = E_{\text{RS}}^{(1)} + E_{\text{exch}}^{(1)}$ ^a	1555.92	143.58	33.60	12.65	1.08
$E_{\text{RS-QMC}}^{(2)}$	-703(17)	-161(10)	-74(1)	-45(2)	-15.9(4)
$E_{\text{exch}}^{(2)}$ ^b	135.96	11.38	2.65	1.01	0.09
$E_{\text{RS-QMC}}^{(3)}$	-46(22)	-6(11)	2.2(2)	0.3(7)	0.13(3)
Perturbational sum	942(39)	-12(21)	-35(1)	-31(2)	-14.5(4)
Full CI ^c	933.88	-0.709	-34.67	-30.60	
VVVVR ^d	934.5	-0.507	-34.58	-30.56	-14.62
LM2M2 ^e	927.7	-1.23	-34.73	-30.63	-14.54
Supermolecular QMC ^f		-1.3(25)	-34.9(3)		

^aReference 13, *ab initio* calculations.

^bReference 14, *ab initio* calculations.

^cReference 6.

^dReferences 4 and 3.

^eReferences 4 and 40.

^fReference 1.

dance with the so-called VVVVR^{4,5} and LM2M2^{4,40} potentials, and with the supermolecular QMC calculation of Anderson *et al.*¹ Note that we have found a similar agreement for the other distances considered. At this point, it is important to remark that the statistical error in the total interaction energy is rather large. At the equilibrium distance it is about three times larger than the supermolecular QMC error of Anderson *et al.*,¹ which is itself an order of magnitude greater than the error in the very recent highly accurate result of van Mourik and van Lenthe.⁶ To obtain more accurate QMC results for the second- and third-order Rayleigh–Schrödinger terms is certainly possible but would require quite significant amounts of computer time. However, to achieve the 0.03 $\mu\text{hartree}$ accuracy of the full CI calculation is certainly out of reach at the present time. In any case, at this level of accuracy, the contributions neglected in Eq. (41) would have to be considered. In fact, a major result of this work is that the perturbational expansion Eq. (41) gives a complete description of the total interaction energy for distances equal and larger than the equilibrium distance. Statistical errors on the QMC results presented here, although large with respect to the best accuracy obtained so far for the total interaction energy, are sufficiently small to lead to the most accurate values that have been calculated for the second- and third-order RS interaction energies. From our results, we can conclude the following:

- (i) The intraatomic correlation contribution to the second-order RS component is large and higher-order contributions beyond the second-order in a Møller–Plesset-like expansion must absolutely be taken into account. A nonperturbative value of the total intraatomic correlation contribution has been exactly evaluated in this work (with a relative error of only 5%).
- (ii) The third-order RS part is significant and is as large as the second-order exchange contributions at intermediate and large distances.
- (iii) The perturbational expansion limited to the complete first- and second-order, plus the Rayleigh–Schrödinger third-order energy is sufficient to repro-

duce the total interaction energy of the helium dimer at intermediate and large distances.

Beyond this particular application it is clear that these conclusions are also important for the general theory of intermolecular forces and their evaluation by perturbation theory.

ACKNOWLEDGMENTS

The authors are grateful to Professor Koga for providing them with the parameters of the wave function not published in his paper.²³ We would like to thank the “Institut du Développement et des Ressources en Informatique Scientifique” (IDRIS) for providing us with computer time.

¹J. B. Anderson, C. A. Traynor, and B. M. Boghosian, *J. Chem. Phys.* **99**, 345 (1993).

²J. H. van Lenthe, R. J. Vos, J. G. C. M. van Duijneveldt-van de Rijdt, and F. B. van Duijneveldt, *Chem. Phys. Lett.* **143**, 435 (1988).

³B. Liu and A. D. McLean, *J. Chem. Phys.* **91**, 2348 (1989).

⁴R. A. Aziz and M. J. Slaman, *J. Chem. Phys.* **94**, 8047 (1991).

⁵R. J. Vos, J. H. van Lenthe, and F. B. van Duijneveldt, *J. Chem. Phys.* **93**, 643 (1990).

⁶T. van Mourik and J. H. van Lenthe, *J. Chem. Phys.* **102**, 7479 (1995).

⁷R. E. Lowther and R. L. Coldwell, *Phys. Rev. A* **22**, 14 (1980).

⁸D. M. Ceperley and H. Partridge, *J. Chem. Phys.* **84**, 820 (1986).

⁹P. Arrighini, in *Intermolecular Forces and their Evaluation by Perturbation Theory*, Lectures Notes in Chemistry (Springer, Berlin, 1981).

¹⁰B. Jeziorski and W. Kolos, in *Molecular Interactions*, edited by H. Ratajczak and W. J. Orville-Thomas (Wiley, New York, 1982), Vol. 3.

¹¹I. G. Kaplan, in *Theory of Molecular Interactions* (Elsevier, Amsterdam, 1986), Vol. 42.

¹²B. Jeziorski, R. Moszynski, and K. Szalewicz, *Chem. Rev.* **94**, 1887 (1994)

¹³S. Rybak, K. Szalewicz, and B. Jeziorski, *J. Chem. Phys.* **91**, 4779 (1989).

¹⁴M. Tachikawa, K. Suzuki, K. Iguchi, and T. Miyazaki, *J. Chem. Phys.* **100**, 1995 (1994).

¹⁵M. Caffarel and O. Hess, *Phys. Rev. A* **43**, 2139 (1991).

¹⁶M. Caffarel and O. Hess, in *AIP Conference Proceedings No 239, Advances in Biomolecular Simulations, Obernai, France 1991* (AIP, New York, 1991), pp. 20–32.

¹⁷M. Caffarel and P. Claverie, *J. Chem. Phys.* **88**, 1088 (1988).

¹⁸M. Caffarel and P. Claverie, *J. Chem. Phys.* **88**, 1100 (1988).

¹⁹D. M. Ceperley (private communication).

²⁰C. W. Gardiner, *Handbook of Stochastic Methods* (Springer, Berlin, 1983).

²¹H. Risken, *The Fokker–Planck Equation* (Springer, Berlin, 1984).

²²B. L. Hammond, W. A. Lester, Jr., and P. J. Reynolds, *Monte Carlo Methods in Ab Initio Quantum Chemistry*, World Scientific Lecture and Course

- Notes in Chemistry, Vol. 1 (World Scientific, Singapore, 1994).
- ²² A. Conway and J. N. Murrell, *Mol. Phys.* **23**, 1143 (1972).
- ²³ T. Koga, *J. Chem. Phys.* **96**, 1276 (1992).
- ²⁴ D. E. Freund, B. D. Huxtable, and J. D. Morgan III, *Phys. Rev. A* **29**, 980 (1984).
- ²⁵ K. Szalewicz, H. J. Monkhorst, *J. Chem. Phys.* **75**, 5785 (1981).
- ²⁶ W. H. Press, B. P. Flannery, S. A. Teukolsky, and W. T. Vetterling, *1200 Numerical Recipes in Fortran* (Cambridge University, London, 1992).
- ²⁷ B. Jeziorski, R. Moszynski, A. Ratkiewicz, S. Rybak, K. Szalewicz, and H. L. Williams, in *Methods and Techniques in Computational Chemistry*, Vol. B, Medium Size Systems, edited by E. Clementi (STEF, Cagliari, 1993), p. 79.
- ²⁸ B. Jeziorski, R. Moszynski, S. Rybak, and K. Szalewicz, in *Proceedings of the Symposium on Many-Body Methods, Tel-Aviv, Israel, 1988* edited by U. Kaldor (Springer, Berlin, 1989).
- ²⁹ R. Moszynski, B. Jeziorski, and K. Szalewicz, *J. Chem. Phys.* **100**, 1312 (1994).
- ³⁰ S. Rybak, B. Jeziorski, and K. Szalewicz, *J. Chem. Phys.* **95**, 6576 (1991).
- ³¹ P. Jankowski, B. Jeziorski, S. Rybak, and K. Szalewicz, *J. Chem. Phys.* **92**, 7441 (1990).
- ³² R. Moszynski, B. Jeziorski, A. Ratkiewicz, and S. Rybak, *J. Chem. Phys.* **99**, 8856 (1993).
- ³³ R. Moszynski, S. M. Cybulski, and G. Chalasinski, *J. Chem. Phys.* **100**, 4998 (1994).
- ³⁴ R. Moszynski, B. Jeziorski, S. Rybak, K. Szalewicz, and H. L. Williams, *J. Chem. Phys.* **100**, 5080 (1994).
- ³⁵ H. L. Williams, K. Szalewicz, B. Jeziorski, R. Moszynski, and S. Rybak, *J. Chem. Phys.* **98**, 1279 (1993).
- ³⁶ B. Jeziorski, R. Moszynski, S. Rybak, and K. Szalewicz, *Lect. Notes Chem.* **52**, 65 (1989).
- ³⁷ B. Jeziorski and M. van Hemert, *Mol. Phys.* **31**, 713 (1976).
- ³⁸ M. Caffarel, M. Rérat, and C. Pouchan, *Phys. Rev. A* **47**, 3704 (1993).
- ³⁹ O. Hess, M. Caffarel, C. Huiszoon, and P. Claverie, *J. Chem. Phys.* **92**, 6049 (1990).
- ⁴⁰ R. A. Aziz, F. R. W. McCourt, and C. C. K. Wong, *Mol. Phys.* **61**, 1487 (1987).

P. M. van den Bossche and M. Caffarel, "One-dimensional pair-hopping and attractive Hubbard models: A comparative study", *Phys. Rev. B* 54, 17414 (1996)

One-dimensional pair hopping and attractive Hubbard models: A comparative study

Mathias van den Bossche*

Laboratoire CNRS-Physique Théorique des Liquides, Tour 16, 4 place Jussieu, 75252 Paris Cedex 05, France

Michel Caffarel†

Laboratoire CNRS-Chimie Théorique, Tour 22-23, 4 place Jussieu, 75252 Paris Cedex 05, France

(Received 25 April 1996)

The low-energy physics of the one-dimensional pair hopping (PH) and attractive Hubbard models are expected to be similar. Based on numerical calculations on small chains, several authors have recently challenged this idea and predicted the existence of a phase transition at half filling and finite positive coupling for the pair-hopping model. We reexamine the controversy by making systematic comparisons between numerical results obtained for the PH and attractive Hubbard models. To do so, we have calculated the Luttinger parameters (spin and charge velocities, stiffnesses, etc.) of the two models using both the density matrix renormalization-group method for large systems and Lanczós calculations with twisted boundary conditions for smaller systems. Although most of our results confirm that both models are very similar we have found some important differences in the spin properties for the small sizes considered by previous numerical studies (6–12 sites). However, we show that these differences disappear at larger sizes (14–42 sites) when sufficiently accurate eigenstates are considered. Accordingly, our results strongly suggest that the ground-state phase transition previously found for small systems is a finite size artifact. Interpreting our results within the framework of the Luttinger liquid theory, we discuss the origin of the apparent contradiction between the predictions of the perturbative renormalization-group approach and numerical calculations at small sizes. [S0163-1829(96)05047-3]

I. INTRODUCTION

In this paper we are concerned with the pair-hopping (PH) model described by the Hamiltonian

$$H = -t \sum_{\langle i,j \rangle \sigma} [c_{i\sigma}^\dagger c_{j\sigma} + \text{H.c.}] - V \sum_{\langle i,j \rangle} [c_{i\uparrow}^\dagger c_{i\downarrow}^\dagger c_{j\downarrow} c_{j\uparrow} + \text{H.c.}], \quad (1.1)$$

where $c_{i\sigma}^\dagger$ ($c_{i,\sigma}$) creates (destroys) a fermion of spin σ ($\sigma = \uparrow, \downarrow$) at lattice site i . The first term is the usual kinetic energy term (tight-binding approximation), the V term allows spin-singlet pairs of electrons to hop from site to site. In what follows, we shall restrict our study to the case $V > 0$.¹

There are a number of reasons that make this model interesting to study. First, the pair-hopping model can be viewed as a phenomenological model to describe the dynamics of small size Cooper pairs. Since high- T_c superconductors are known to display such pairs, to study this model can be important to capture some of the physics of these materials. Of course, when working with such a model nothing is said about the nature of the underlying mechanism responsible for the tight binding of the pairs. Second, it can be shown that the pair-hopping term arises from Coulomb interaction at large negative U in the Hubbard model.^{2,3} Accordingly, the competition between the usual one-electron hopping and pair hopping is related to the physics of the Hubbard model at strong coupling. Finally, understanding the physics resulting from all possible unusual interactions in one-dimensional (1D) strongly correlated models is clearly a problem of central importance in solid-state physics.

Very recently this model has led to some contradictory results. Using exact diagonalization calculations on small 1D chains (up to $L=10$ sites, with periodic boundary conditions), Penson and Kolb claimed⁴ that a phase transition should occur at some finite critical value of the hopping parameter V with $V_c/t \sim 1.4$. More precisely, they showed that a gap in the single-particle spectrum of the half-filled system opens up at that value. They have also observed that the second derivative of the ground-state energy with respect to V (a quantity similar to a specific heat) has a local maximum at the transition, which seems not to diverge. This would indicate a phase transition with an essential singularity. Very soon after, Affleck and Marston,⁵ making a renormalization-group analysis with bosonization methods of the PH model, showed that, in the continuum limit (low-energy, long-distance physics), this model is essentially equivalent, up to some irrelevant terms, to the negative- U Hubbard model, the only important difference lying in the bare coupling constants. Accordingly, they predicted that the transition in the pair-hopping model must occur at $V=0$ just as in the Hubbard model, the finite value observed in the numerical calculations for very small chains being attributed to a finite-size artifact. A few years later, Hui and Doniach⁶ presented some numerical calculations analyzed with more sensitive tools than the standard finite-size scaling analysis based on very small samples. Using an eigenprojection decomposition of the different order parameter operators involved and also some calculations of the helicity modulus, they found that the data seemed indeed to be compatible with the existence of a phase transition at a finite value of V , thus in contradiction with the weak-coupling renormalization-group results. They also presented some arguments as to why the predic-

tions of the renormalization-group analysis of Affleck and Marston could be not valid. Very recently, Bhattacharyya and Roy⁷ have investigated the PH model using a real-space renormalization-group method. At small positive V they also found the existence of a gapless phase (identified as a quasi-metallic phase dominated by short-range superconducting correlations), which disappears at some finite value of the coupling. Finally, Sikkema and Affleck⁸ have presented some numerical results for the one-particle gap as a function of V using the density matrix renormalization-group (DMRG) method with open boundary conditions. Using samples up to $L=60$, they concluded that there is no spin-gap transition at a nonzero positive value of V and that the standard low-energy picture given by the perturbative renormalization-group approach is valid. Although we reach in this work essentially the same conclusions, we shall follow here a quite different route. In particular, our DMRG calculations are done with periodic boundary conditions (PBC) instead of open BC. This will allow us to study in detail the very peculiar behavior of the pair hopping at small couplings (large correlation lengths). This point is discussed in Sec. IV.

At the heart of the controversy is the question of knowing whether the long-distance, low-energy physics of the pair-hopping model is different from that of the usual attractive Hubbard model. As we shall see in the next section all standard approaches lead to the same conclusion: the low-energy sector of both Hamiltonians should be similar under the trivial correspondence $U = -2V$. At half filling it is known (an exact result) that no phase transition at a nonzero value of U exists for the attractive Hubbard model. How can the PH model exhibit a different behavior? This should result from a highly nontrivial process involving nontrivial excitations. Note also that the exotic gapless phase is supposed to exist at an arbitrary small value of the hopping parameter, a domain where the high-energy degrees of freedom are not expected to play an important role. In order to settle down the controversy we propose to make a systematic comparison of the physics of the pair-hopping and attractive Hubbard models at low energy. To do so, we have calculated the spin and charge velocities of the two models using both the density matrix renormalization-group method with periodic boundary conditions for large systems and Lanczós calculations with twisted boundary conditions for smaller systems. Our results show that there are some important differences in the finite-size behavior of the two models. Using the framework of the Luttinger liquid we propose an interpretation of the origin of the controversy between the perturbative RG prediction and the numerical results for small chains presented up to now.

The paper is structured in the following way. In Sec. II, we briefly present the results of a number of approaches illustrating the very close similarity between the attractive Hubbard model and the pair-hopping model. In Sec. III, we present our numerical results using the Luttinger liquid theory and the twisted boundary conditions method on both models for chains up to $L=12$ sites. Then, using the DMRG method we generalize the results presented for small chains at some larger chains up to $L=42$ sites. In Sec. V, we discuss the results and comment on what we believe to be the origin of the controversy. We conclude that (1) both models are indeed equivalent at low energy in the thermodynamic limit and that there is no phase transition at finite V and half filling in the PH model and (2) for small systems there exists

a transient regime specific to the PH model and responsible for the unconventional behavior of this model.

II. PAIR-HOPPING AND ATTRACTIVE HUBBARD MODELS

The Hamiltonian (1.1) for the pair-hopping model describes a competition between the usual kinetic term (t term) corresponding to single-electron hopping and a V term corresponding to the hopping of spin-singlet pairs, the range of both types of hopping being limited to nearest neighbors. When V/t is large ($V > 0$), the pair-hopping term dominates and the model becomes equivalent to spinless fermions (for an even number of electrons). The ground state is massively paired and there is a gap of order V in the one-particle spectrum (binding energy of the pairs). In the opposite limit, $V/t \ll 1$, the one-particle hopping dominates and the pairs tend to be destroyed. This type of competition is very similar to that encountered in the attractive Hubbard model described by the Hamiltonian

$$H = -t \sum_{\langle i,j \rangle \sigma} [c_{i\sigma}^\dagger c_{j\sigma} + \text{H.c.}] + U \sum_i n_{i\uparrow} n_{i\downarrow}. \quad (2.1)$$

Here also we have a competition between a one-electron hopping and the formation of spin-singlet pairs. However, in contrast with the PH model, pairs have no intrinsic mobility (uncorrelated mobility via the t term). The physics of the attractive Hubbard model is well understood since this model admits an exact solution via the Bethe ansatz technique. In particular, it is known that the effect of the on-site interaction is rather drastic: a gap in the one-particle spectrum opens up for any nonzero value of the interaction U (negative or positive) at half filling. It is usually thought that a similar situation should occur in the PH model. This opinion is supported by the fact that standard approximate approaches applied to both Hamiltonians lead quite systematically to the same physics at low energy under the trivial correspondence $U \leftrightarrow -2V$. However, as already emphasized, this idea has been recently challenged. The purpose of the next few sections is to shed some light on this controversy. Here, we would like to briefly illustrate, by applying some standard methods, why the correspondence between both models is usually taken for granted.

A first approach to consider is the mean-field approximation. Defining the superconducting order parameter by $\Pi = \langle gnd | c_{i\downarrow} c_{i\uparrow} | gnd \rangle$, where $|gnd\rangle$ denotes the BCS-type ground state, we consider the quantum fluctuations around this value and construct the approximate mean-field Hamiltonian by keeping only the terms that are of first order with respect to the fluctuations. The following Hamiltonian is obtained:

$$H_{\text{MF}} = \sum_{\mathbf{k}, \sigma} \varepsilon(\mathbf{k}) c_{\mathbf{k}, \sigma}^\dagger c_{\mathbf{k}, \sigma} - 4V\Pi D \sum_{\mathbf{k}} [c_{\mathbf{k}, \uparrow}^\dagger c_{-\mathbf{k}, \downarrow}^\dagger + c_{\mathbf{k}, \downarrow} c_{-\mathbf{k}, \uparrow}] + 4V\Pi^2 D L^D, \quad (2.2)$$

where $\varepsilon(\mathbf{k}) = -4t \sum_{\mu=1}^D \cos(\mathbf{k} \cdot \mathbf{e}_\mu)$, \mathbf{e}_μ being the unit vector in direction μ , and D the dimension of space. The main observation is that this Hamiltonian is identical to that obtained in the case of the Hubbard model⁹ with the substitu-

tion $U = -2V$. Introducing the elementary excitations in the usual way, we can compute the dependence of the gap Δ in energy of the system, we get

$\Delta \sim te^{-ct/|V|}$ for $V \rightarrow 0$, where c is a positive constant and

$$\Delta \sim V \text{ for } V \rightarrow \infty. \quad (2.3)$$

Clearly, in this approach both models are equivalent and the gap opens up at $V/t=0$ with a standard behavior.

We have also considered the large-dimension limit of the pair-hopping model. This recent approach can be seen as a sort of dynamical mean-field theory. Although this limit may seem rather academic, practical calculations have illustrated the fact that a great part of the physics of low-dimensional systems is captured.^{10,11} Once again, in that approximation we have found that the equations reduce to those of the corresponding attractive Hubbard model with $U = -2V$. In fact, this is not really surprising since, because of the structure of the Fermi hypersurface in the limit of large dimensions, the effects of the high-energy excitations that could be responsible for nontrivial processes are strongly suppressed.

As we shall see in Sec. V the renormalization-group (RG) flows in the weak-coupling limit are also identical for the two models [Eq. (5.1)] with, here also, the same correspondence between couplings. Only the initial values of the coupling constants, are model dependent.

Finally, one can try to find out whether the PH model has an exact solution via the Bethe ansatz. The essential step is to compute the two-particle S matrix from the Schrödinger equation and then to verify whether the S matrix satisfies the Yang-Baxter condition. Denoting by $A_{\sigma_1, \sigma_2}(p_1, p_2)$ the amplitude of the two-particle wave function written in terms of a combination of plane waves, defining as usual the two-particle S matrix as

$$A_{\sigma_2, \sigma_1}(p_2, p_1) = \sum_{\sigma'_1, \sigma'_2} S_{\sigma_2, \sigma_2}^{\sigma_1, \sigma'_1}(p_1, p_2) A_{\sigma'_1, \sigma'_2}(p_1, p_2), \quad (2.4)$$

forcing the wave function to obey the Schrödinger equation, and imposing the continuity condition of the wave function, we get the following expression for the S matrix:

$$\begin{aligned} S_{\sigma_2, \sigma_2}^{\sigma_1, \sigma'_1}(p_1, p_2) &= \frac{\sin ap_1 - \sin ap_2}{\sin ap_1 - \sin ap_2 - iV \cos[a(p_1 + p_2)]} \\ &\quad \times \delta_{\sigma_1, \sigma'_1} \delta_{\sigma_2, \sigma'_2} \\ &\quad - \frac{iV \cos[a(p_1 + p_2)]}{\sin ap_1 - \sin ap_2 - iV \cos[a(p_1 + p_2)]} \\ &\quad \times \delta_{\sigma_1, \sigma'_2} \delta_{\sigma_2, \sigma'_1}. \end{aligned} \quad (2.5)$$

It is easy to verify that the S matrix just given does not satisfy the Yang-Baxter condition.¹² Now, the important point is that the S matrix (2.5) is identical to that of the Hubbard model with the substitution $U \rightarrow -2V \cos[a(p_1 + p_2)]$. The lattice spacing a gives a natural high-energy cutoff, $1/a$, in the problem. In the low-energy regime, i.e.,

$p_i \ll 1/a$, both approaches lead to the same equations and the two models related by $U = -2V$ should be equivalent.

To summarize, mean-field approximation, large- D limit, weak-coupling renormalization-group, and Bethe ansatz approaches indicate that the PH model and the $U = -2V$ attractive Hubbard model should be equivalent in the low-energy regime.

III. LUTTINGER LIQUID BEHAVIOR: AN EXACT DIAGONALIZATION STUDY ON SMALL SYSTEMS

In this part we are interested in evaluating the Luttinger liquid parameters for both the pair-hopping and attractive Hubbard models. As is well known the long distance behavior of one-dimensional gapless fermion systems can be studied by making use of the concept of ‘‘Luttinger liquid.’’ Within the framework of this theory the low-energy properties are given by an effective Luttinger model describing collective spin and charge density oscillations. The general form of the effective Hamiltonian can be obtained by writing the 1D fermion model in momentum space, restricting excitations and interactions to lie close to the Fermi surface, and looking for the important processes. As is well known only four processes survive (in the renormalization-group sense): one describing backward scattering of oppositely moving electrons with coupling g_1 , one describing forward scattering of oppositely moving electrons with coupling g_2 , one describing umklapp scattering with coupling g_3 , and, finally, one describing forward scattering of electrons moving in the same direction with coupling g_4 . (Notations are those of Refs. 13 and 14.) Taking the continuum limit of the fermion Hamiltonian and, then, bosonizing the Fermi fields, one gets

$$H_b = H_\rho + H_\sigma + H_1 + H_3, \quad (3.1)$$

where H_ν ($\nu = \rho, \sigma$) are two free Bose Hamiltonians describing the spin ($\nu = \sigma$) and charge ($\nu = \rho$) collective excitations:

$$H_\nu = \int dX \left[\frac{u_\nu}{2\pi K_\nu} (\partial_X \phi_\nu)^2 + \frac{u_\nu \pi K_\nu}{2} \Pi_\nu^2 \right] \quad (3.2)$$

and H_1 and H_3 are the terms corresponding to the backward and umklapp scattering contributions, respectively,

$$H_1 = \frac{2g_1}{(2\pi\alpha)^2} \int dX \cos(\sqrt{8}\phi_\sigma) \quad (3.3)$$

and

$$H_3 = \frac{2g_3}{(2\pi\alpha)^2} \int dX \cos(\sqrt{8}\phi_\rho). \quad (3.4)$$

Here, ϕ_ρ (ϕ_σ) is the Bose field describing the charge (spin) excitations, and Π_ρ (Π_σ) is its canonical conjugated field. The coefficients u_ρ (u_σ) are the charge (spin) excitation velocities, and the parameters K_ρ and K_σ are some constants that can be shown to be related to the (nonuniversal) exponents of the power-law behavior of the correlation functions. In Eqs. (3.3) and (3.4) α is a short-distance cutoff.¹⁴

In the free-fermion case, $K_\rho = K_\sigma = 1$ and $u_\rho = u_\sigma = v_F = 2t \sin[(\pi/2)n]$, where $n = N/L$ is the electron density. When interactions are switched on, the u and the K param-

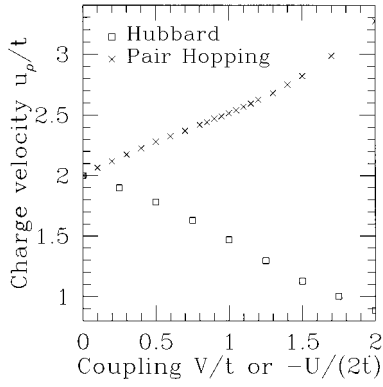


FIG. 1. Charge velocity u_ρ as a function of the coupling. Crosses, pair-hopping model, squares, Hubbard model. Lanczós calculations with twisted boundary conditions. Chains of sizes up to 12 sites.

eters are renormalized. In particular, the two velocities become different, charge and spin excitations do not propagate at the same speed. This phenomenon is known as the spin-charge separation in one-dimensional systems. All the details concerning the Luttinger liquid theory can be found, e.g., in Refs. 14 and 13 and references therein.

In order to compute numerically the Luttinger coefficients, we have used their expressions in terms of spin and charge compressibilities and stiffnesses of the system. More precisely, for the charge degrees of freedom we have

$$\frac{1}{\kappa} = \frac{\pi}{2} \frac{u_\rho}{K_\rho}, \quad D_\rho = 2u_\rho K_\rho, \quad (3.5)$$

where κ is the compressibility of the system and D_ρ is the charge stiffness, and for the spin degrees:

$$\frac{1}{\chi} = \frac{\pi}{2} \frac{u_\sigma}{K_\sigma}, \quad D_\sigma = 2u_\sigma K_\sigma, \quad (3.6)$$

where χ is the spin susceptibility of the system and D_σ the spin stiffness. These quantities can be computed from the spectrum of the system by using the relation¹⁵

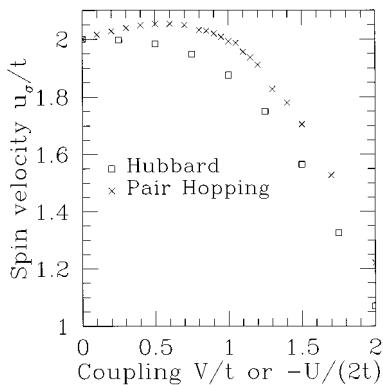


FIG. 2. Spin velocity u_σ as a function of the coupling. Crosses, pair-hopping model; squares, Hubbard model. Lanczós calculations with twisted boundary conditions. Chains of sizes up to 12 sites.

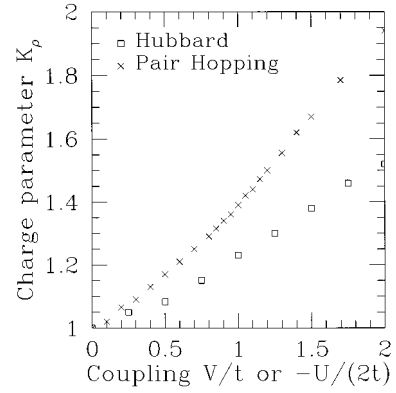


FIG. 3. Charge parameter K_ρ as a function of the coupling. Crosses, pair-hopping model; squares, Hubbard model. Lanczós calculations with twisted boundary conditions. Chains of sizes up to 12 sites.

$$D_\nu = \pi \left. \frac{\partial^2 E_0}{\partial \varphi_\nu^2} \right|_{\varphi_\nu=0}, \quad (3.7)$$

where φ_ρ is a charge twist in the system [i.e., the system has twisted boundary conditions such as $c_{j+L,\sigma}^\dagger = \exp(i\varphi_\rho)c_{j,\sigma}^\dagger$], and φ_σ is a spin twist in the system [i.e., $c_{j+L,\sigma}^\dagger = \exp(i\sigma\varphi_\sigma)c_{j,\sigma}^\dagger$], and

$$\frac{1}{\kappa} = \frac{1}{2L} \frac{\partial^2 E_0}{\partial n^2}, \quad \frac{1}{\chi} = \frac{1}{2L} \frac{\partial^2 E_0}{\partial s_z^2}, \quad (3.8)$$

with $n = (N_\uparrow + N_\downarrow)/L$ and $s_z = (N_\uparrow - N_\downarrow)/L$. By computing these quantities for different values of the interaction, we can deduce the behavior of the Luttinger parameters u_ν and K_ν as a function of the coupling strength.

We have applied this approach to systems of sizes ranging from $L=4$ to $L=12$. The ground-state energies have been calculated using a standard Lanczós procedure. The results are presented in Figs. 1–5. Each figure shows the variation of the corresponding Luttinger coefficient as a function of the interaction, both for the attractive Hubbard model (squares) and for the pair-hopping model (crosses). Figure 1 gives the variation of the charge velocity, u_ρ , as a function of U or V . At small coupling both curves are linear with a

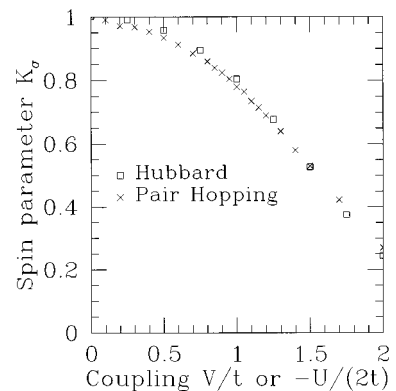


FIG. 4. Spin exponent K_σ as a function of the coupling. Crosses, pair-hopping model; squares, Hubbard model. Lanczós calculations with twisted boundary conditions. Chains of sizes up to 12 sites.

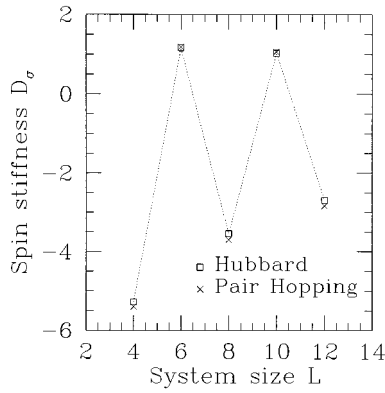


FIG. 5. Spin stiffness D_σ as a function of the coupling. Crosses, pair-hopping model, squares, Hubbard model. Lanczós calculations with twisted boundary conditions. Chains of sizes up to 12 sites. The dotted line is just a guide to the eye.

very good accuracy. More precisely, we find $u_\rho \sim 2 + V/2$ and $u_\rho \sim 2 + U/4$, for the pair-hopping and Hubbard models, respectively. For stronger couplings, small corrections to linearity show up. Both behaviors are typical of a regime with no charge gap. As we shall see later, these results are in perfect quantitative agreement with the prediction of the Luttinger liquid theory [Eqs. (5.2) and (5.3)]. Data for the spin velocities are rather different. As can be seen in Fig. 2 two distinct behaviors for the spin velocity are obtained. In the case of the attractive Hubbard model u_σ decreases uniformly from the free fermion value to zero at large coupling. In contrast, a maximum around $V = 0.55t$ is found for the pair-hopping model. Both models recover a similar behavior between approximately $V = 1$ and $V = 1.5$. Note that the transition value observed in Refs. 4 and 6 lies within this interval. We shall discuss further this important difference of behavior for u_σ in Sec. V. Figures 3 and 4 demonstrate that the constants K_ρ and K_σ behave essentially the same way in both models. As already mentioned, in the Luttinger liquid theory these constants are related to the exponents of the power-law behavior of correlation functions. Accordingly, this common behavior would suggest that both models have the same phases. In Fig. 5, the behavior of the spin stiffness of the pair-hopping model as a function of the size is displayed. A very interesting feature is that this quantity can be exactly computed for the Hubbard model. The formula is¹⁶

$$D_\sigma(L) = (-1)^{L/2+1} L^{1/2} D(U) e^{-L/\xi_\sigma(U)}$$

with

$$\xi_\sigma^{-1}(U) = \frac{4}{U} \int_1^\infty dy \frac{\ln(y + \sqrt{y^2 - 1})}{\cosh(2\pi y/U)}$$

and

$$D(U) \sim \begin{cases} \sqrt{(2/\pi)\xi_\sigma} & \text{for } U \rightarrow 0 \\ 0.147376U & \text{for } U \rightarrow \infty \end{cases} \quad (3.9)$$

This function is plotted in Fig. 5, for $U/t = -2$, with the corresponding quantity for the pair-hopping model, at $V/t = 1$. The similarity between the two curves is striking. In the case of the Hubbard model, the oscillations around zero

are related to the existence of a gap in the spin spectrum. In the case of a gapless mode, the corresponding curve is smooth and never changes sign. Accordingly, we have here strong evidence in favor of the existence of a spin gap in the pair-hopping model.

At this point, our results are contradictory. On one hand, most of the results indicate that both models are quite similar (behavior of u_ρ , K_ν , and spin stiffnesses). On the other hand, the spin velocities at small sizes for both models display a different behavior. A closer look at spin degrees of freedom at larger sizes is therefore necessary.

IV. LUTTINGER LIQUID BEHAVIOR: A DMRG STUDY FOR LARGER SYSTEMS

Conformal field theory (CFT) is a powerful theory to describe the physics of 1D quantum (or 2D statistical) critical systems. Once conformal invariance is supposed, CFT provides a general framework relating finite-size scaling of physical quantities to thermodynamic properties.^{17–19} In this work we shall essentially compare our data for excitation gaps with the predictions of CFT. This will allow us to check whether or not our data are compatible with the existence of a critical regime for the pair-hopping model. Denoting ν the gapless excitation under consideration and u_ν the velocity of the corresponding critical mode, the finite-size scaling expression of the excitation gap Δ_ν predicted by CFT is

$$\Delta_\nu = \frac{2\pi u_\nu}{L}, \quad (4.1)$$

where L is the system size. For a finite system at a given filling, the spin gap is defined as

$$\Delta_\sigma = E_0(N_\uparrow + 1, N_\downarrow - 1) - E_0(N_\uparrow, N_\downarrow),$$

where N_σ is the number of σ -spin electrons. Physically, it gives the change in ground-state energy produced when flipping one spin, the charge number being kept fixed.

In order to calculate the spin gaps we have used the density matrix renormalization-group method.²⁰ DMRG is a powerful technique to compute low-energy properties of quantum lattice systems. This method has been applied with success to several problems including the spin-1/2 Heisenberg chains,²⁰ the spin-1 chains,²¹ the one-dimensional Kondo insulator,²² the two-chain Hubbard model,²³ etc. The results obtained are very accurate and the method allows one to treat systems of sizes a few times larger than those accessible with exact diagonalization techniques. Essentially, DMRG is a real-space numerical renormalization-group procedure. It differs from standard approaches in the way that states of individual blocks are chosen. Instead of keeping the lowest eigenstates of the block considered as isolated from the outside world, the kept states are the most probable eigenstates of the density matrix associated with the block considered as a part of the whole system. It is easy to show that doing this is equivalent to constructing the most accurate representation of the complete state of the system: block plus the rest of the system. For a detailed and very clear presentation of the method the reader is referred to Ref. 20. There exist different ways of choosing the configuration of blocks used for the density matrix calculations. In particular, this

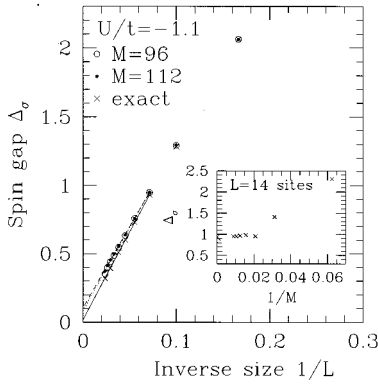


FIG. 6. Spin gap vs inverse of the system size for the attractive Hubbard model at $U/t = -1.1$ using DMRG with periodic boundary conditions for different values of M (see text). Inset shows the convergence of the spin gap as a function of M at $L = 14$ sites. The value at $1/M = 0$ is the exact value calculated by solving the Lieb-Wu equations.

choice will depend on the type of boundary conditions used. Here, all calculations have been done by using periodic boundary conditions (PBC). We have chosen the superblock configuration $B_l \bullet B_l^R \bullet$ with $B_{l+1}^R = B_l \bullet$ as proposed in Ref. 20 for PBC. B_l represents a block consisting of l sites, B_l^R is the reflected block (right interchanged with left), and \bullet represents a single site. All notations are those of Ref. 20. In what follows we shall denote by M the number of eigenstates of the density matrix that are kept.

Very recently, Sikkema and Affleck have presented DMRG calculations for the pair-hopping model.⁸ Their calculations have been performed using open boundary conditions (OBC). When the correlation length is finite and calculations with $L \gg \xi$ are possible using OBC is usually preferable (calculations with OBC are less demanding than with PBC, the convergence as a function of M being much more rapid). In the regime of small ξ , Sikkema and Affleck have shown that their data are consistent with the prediction of the standard perturbative RG flow. In this work we shall use PBC in a regime where the correlation lengths are large (small values of V). As we shall see now, this will allow us to study the very peculiar behavior of the pair-hopping model at small couplings.

To begin with we present some DMRG calculations for the attractive Hubbard model. The value of the Coulomb interaction, $U = -1.1$, has been chosen to correspond to $V = -U/2 = 0.55$, the value for which the spin velocity of the PH model is maximum; see Fig. 2. Since the Hubbard model admits an exact solution our results can be compared to the exact values obtained by solving the Lieb-Wu equations.²⁴ The inset of Fig. 6 shows how the DMRG spin gap Δ_σ converges to the exact value $\Delta_\sigma = 0.9297$ for a chain of 14 sites as a function of M , the number of states kept. Here, M ranges from $M = 16$ to $M = 112$. Clearly, the convergence of the DMRG values is quite good. In addition, this curve provides a useful check of the validity of our code. The main plot displays the variation of the spin gap as a function of $1/L$. The studied sizes are ranging from $L = 6$ to $L = 42$. We

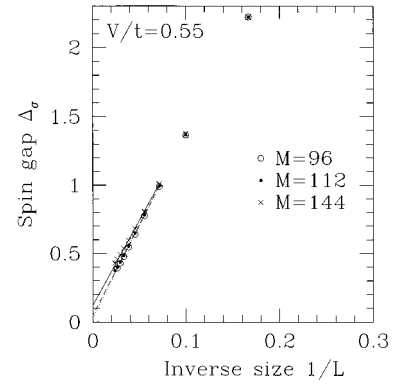


FIG. 7. Spin gap vs inverse of the system size for the pair-hopping model at $V/t = 0.55$ using DMRG with periodic boundary conditions for different values of M (see text).

did not consider the system sizes corresponding to a multiple of 4 since, in this case, the ground state is degenerate, thus causing a strong boundary frustration effect (which, of course, disappears in the $L \rightarrow \infty$ limit). For each size, we plot the value of the DMRG spin gap for a number of kept states $M = 96$, $M = 112$, and $M = \infty$ (exact Lieb-Wu value). Let us first consider the exact solution. Looking at the $L \rightarrow \infty$ limit, we observed a very small gap as expected. In this regime the systems considered ($L = 6-42$) are in an effective quasicritical regime with a spectrum structure remaining close to the conformal tower structure. This allows us to write the following ansatz:

$$\Delta_\sigma(L) = \Delta_\sigma^\infty + \frac{2\pi u_\sigma}{L}, \quad (4.2)$$

valid in the regime $a \ll L \ll \xi$, and where u_σ should be considered as an effective spin velocity. The results obtained are in excellent agreement with the behavior predicted by formula (4.2) with a spin velocity very close to the free value. In addition, for small systems ($L = 6, 10$) the spin velocity obtained from the slope of the spin gap is in very good agreement with the value obtained in the preceding section (within 1.5%) based on a completely independent evaluation.

Let us now consider the DMRG results. We have observed that, for large enough values of M , the linear behavior of the spin gap as a function of $1/L$ is recovered. In Fig. 6 we show typical results for $M = 96$ and $M = 112$. The value of the spin velocity obtained from different M are displayed in Fig. 8 and are slightly smaller than the free value of 2. These results are consistent with a convergence to the exact value at large M . However, it is not possible from DMRG results to get an accurate estimate of the value of the gap itself. Indeed, although we have a good convergence of the results for a given size as a function of M (see inset of Fig. 6), the extrapolated value of the gap using different sizes is a very sensitive quantity. In fact, it is not reasonable to discriminate between a small but finite gap and a strictly vanishing gap. We clearly see in Fig. 6 that the extrapolated gap is not at all converged as a function of M . In order to get converged values we would need much larger values of M , which are clearly beyond of reach of present computers.

In Fig. 7 we present DMRG calculations for the pair-hopping model at $V = 0.55$. Results of the spin gap as a func-

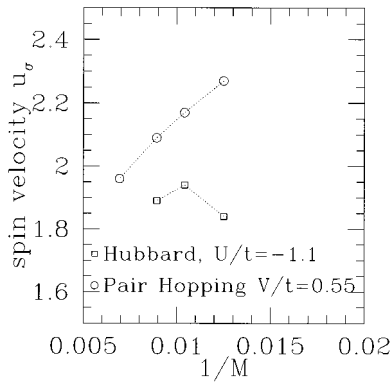


FIG. 8. Spin velocity u_σ computed from DMRG data as a function of $1/M$.

tion of $1/L$ are presented for $M=96, 112$, and 144 . Here again we clearly see a quasicritical regime very well described by formula (4.2). As already emphasized for the attractive Hubbard model, the accessible values of M do not allow a direct conclusion on the existence or not of a finite spin gap. However, the data provide an estimate of the effective spin velocity via the slope of the curves. The spin velocities obtained are plotted for $M=84, 96, 112$, and 144 in Fig. 8. It is remarkable that the results are rather different for both models. As already noticed, for the Hubbard model the values of u_σ are slowly varying and always smaller than the free fermion value. In contrast, for the PH model u_σ is quite important for small values of M and decreases uniformly for increasing M . Only when large enough values of M are used, spin velocities of both models become comparable. We shall comment more on this point in the next section.

V. DISCUSSION

Let us summarize the results obtained. For small sizes ($L=4-12$) we have computed the Luttinger parameters $u_\rho, u_\sigma, K_\rho, K_\sigma, D_\rho$, and D_σ as a function of the interaction for both the attractive Hubbard and pair-hopping models. Regarding charge degrees of freedom all results for both models are consistent with the existence of a vanishing charge gap for arbitrary values of the interaction and with the fact that the low-energy charge sectors of both models are very similar. These results are in agreement with the conclusions of previous works.

Now, regarding spin degrees of freedom the situation is not so clear. For small sizes our results show that parameters K_σ and D_σ for both models are almost identical (see Figs. 4 and 5). In particular, in the case of the PH model we clearly see the oscillations of D_σ around zero as a function of the size L , a behavior that is usually interpreted as resulting from the existence of a gap. However, data for the spin velocity of the PH model do not display the expected behavior of a system with a gap. In contrast with the case of the attractive Hubbard model for which u_σ decreases uniformly from the free fermion value to zero at large coupling (a typical behavior for a finite system with a finite gap in the thermodynamic limit), we have observed a clear enhancement of u_σ when the pair-hopping term is switched on. At $V \sim 0.55t$ the spin ve-

locity of the PH model reaches a maximum and then decreases to zero. A similar behavior is recovered for both models at approximately $V > 1.5$. In order to understand whether this surprising result has something to do with the existence of a gapless phase we have computed the spin gaps for larger systems using a DMRG approach with periodic boundary conditions. Extracting from the spin gaps some effective spin velocity (meaningful only when correlation lengths are much larger than lattice sizes) we have, here also, systematically obtained larger spin velocities for the PH model. In contrast, in the case of the Hubbard model the spin velocities are rather constant and are close to the free fermion value at small coupling. However, a remarkable result is that the abnormally large values of u_σ for the PH model tend to disappear when sufficiently accurate representations of the ground state of the system are considered (large number of states kept for the density matrix). Accordingly, our results are consistent with the fact that the unconventional behavior of spin excitations of the PH model is a transient effect specific to this model.

Now, it is quite interesting to discuss our results within the renormalization-group framework. As discussed very recently by Sikkema and Affleck, contradictory results have been reported from the RG analyses of the phase diagram of the PH model. Using standard notations (see Ref. 13), to cubic order, the RG equations for the four coupling constants of the continuum-limit Hamiltonian are

$$\begin{aligned}
 -\frac{dg_s}{dl} &= g_s^2 + \frac{1}{2}(g_s + g_4)g_s^2, \\
 -\frac{dg_\rho}{dl} &= g_3^2 + \frac{1}{2}(g_\rho - g_4)g_3^2, \\
 -\frac{dg_3}{dl} &= g_\rho g_3 + \frac{1}{4}(g_\rho^2 + g_3^2 - 2g_\rho g_4)g_3, \\
 -\frac{dg_4}{dl} &= \frac{3}{4}(g_\rho g_3^2 - g_s^3),
 \end{aligned} \tag{5.1}$$

where $l = -\ln \Lambda$, Λ being the ultraviolet cutoff. It is important to emphasize that these equations are identical for both models. The only difference lies in the initial values of the coupling constants. To the lowest-order weak-coupling limit the initial values are

$$\begin{aligned}
 v_F = 2tg_\rho = -g_s = g_3 = g_4 \\
 = 2V/\pi v_F \quad (\text{pair-hopping model})
 \end{aligned} \tag{5.2}$$

$$v_F = 2tg_s = -g_\rho = g_3 = g_4 = U/\pi v_F \quad (\text{Hubbard model}).$$

$O(V^2)$ corrections are given in Refs. 5 and 6. When solving the RG equations, a standard approach consists in considering that g_4 simply shifts the spin and charge velocities according to

$$u_\rho = v_F(1 + g_4/2), \tag{5.3}$$

$$u_\sigma = v_F(1 - g_4/2) \tag{5.4}$$

and then can be dropped from the RG equations. Doing this and using the initial conditions Affleck and Marston have

remarked that $g_s=0$ is not a stable fixed point and that starting with $g_s<0$ ($V>0$) then g_s flows to strong coupling, thus indicating the opening of a gap in the spin excitations. In contrast, Hui and Doniach have kept the g_4 constant in the RG equations and integrated them using the initial condition at order $O(V^2)$. By doing this they obtained that $g_s=0$ becomes a stable fixed point provided that $g_4<-2$. For $0<V/t<1$ the fixed point was obtained with $g_4\sim-2.5$. This new phase was interpreted as having no gap for single particles and spin excitations. For a full discussion of the controversy the reader is referred to Ref. 8. However, whether or not we keep the coupling constant g_4 in the RG equations, it is clear that it is difficult to draw firm conclusions using weak-coupling RG equations in a strong-coupling regime (fixed point with $g_4\sim-2.5$). Nonperturbative results are essential to support any reasonable scenario. Let us discuss our numerical results from that point of view. Figure 1 shows very clearly that the charge velocity for both models follows exactly the behavior predicted by Eqs. (5.2) and (5.3) with the correct slope. The charge degrees of freedom are gapless and the effect of the coupling constant g_4 is to renormalize the charge velocity. Figure 2 for u_σ for small sizes is consistent with the fact that a spin gap exists for the attractive Hubbard model. The behavior of u_σ is not linear at small U as would be the case for a critical system. In addition, u_σ decreases uniformly as a function of U . In contrast, as already pointed out we have found a different behavior for the PH model. At small sizes ($L=6-10$) and small coupling, u_σ is larger than the free fermion value. This is also true for larger systems ($L=14-42$) when approximate ground-state

wave functions are considered. From Eqs. (5.4) we can view this regime as corresponding to a situation where the effective constant g_4 starts to renormalize to negative values. In this situation the system appears to be attracted by a fixed point similar to the one discussed by Hui and Doniach. However, as discussed before this is only a transient regime. When the low-lying eigenstates are sufficiently well described (large number of kept states in DMRG) the high-energy components responsible for this unconventional behavior are removed and the standard low-energy behavior is recovered. We believe that this very specific behavior of the PH model is at the origin of the unconventional results obtained for sizes $L=4,12$ in previous numerical works (Refs. 4, 6, and 7).

Note added in proof. Recently we became aware of a paper by A. Belkasri and F. D. Buzatu, Phys. Rev. B **53**, 7171 (1996). In this work these authors reach essentially the same conclusions as those presented here using a different method based on an approximate Bethe-Salpeter equation.

ACKNOWLEDGMENTS

The authors are grateful to Professor I. Affleck for an important remark related to this subject. We also want to acknowledge helpful discussions with P. Azaria, B. Douçot, T. Giamarchi, P. Lecheminant, C. Lhuillier, K.A. Penson, and C. Sire. Part of the computations have been done using an allocation of computer time from the ‘‘Institut du Développement et des Ressources en Informatique Scientifique’’ (IDRIS, Orsay).

*Electronic address: vdb@lptl.jussieu.fr

†Electronic address: mc@lct.jussieu.fr

¹The pair-hopping model has been mainly studied in the case $V>0$. For the case $V<0$, see Refs. 5 and 8, and G. Bouzerar and G.I Japaridze (unpublished).

²V. J. Emery, in *Highly Conducting One-Dimensional Solids*, edited by J. T. Devreese, R. P. Evrard, and V. E. Van Doren (Plenum, New York, 1979), p. 327.

³P. Nozières and S. Schmitt-Rink, J. Low Temp. Phys. **59**, 195 (1985).

⁴K. A. Penson and M. Kolb, Phys. Rev. B **33**, 1663 (1986); M. Kolb, K. A. Penson, J. Stat. Phys. **44**, 129 (1986).

⁵I. Affleck and J. B. Marston, J. Phys. C **21**, 2511 (1988).

⁶A. Hui and S. Doniach, Phys. Rev. B **48**, 2063 (1993).

⁷B. Bhattacharyya and G. K. Roy, J. Phys. C **7**, 5537 (1995).

⁸A. Sikkema and I. Affleck, Phys. Rev. B **52**, 10 207 (1995).

⁹M. Ma and P. A. Lee, Phys. Rev. B **32**, 5658 (1985).

¹⁰W. Metzner and D. Vollhardt, Phys. Rev. Lett. **62**, 324 (1989).

¹¹A. Georges, G. Kotliar, W. Krauth, and M. J. Rozenberg, Rev. Mod. Phys. **68**, 13 (1996).

¹²Yu. A. Izyumov and Yu. N. Skryabin, *Statistical Mechanics of Magnetically Ordered Systems* (Consultants Bureau, New York 1988).

¹³J. Sólyom, Adv. Phys. **28**, 201 (1979).

¹⁴J. Voit (unpublished).

¹⁵E. B. Stechel, A. Sudbø, T. Giamarchi, and C. M. Varma, Phys. Rev. B **51**, 553 (1995).

¹⁶C. A. Stafford and A. J. Millis, Phys. Rev. B **48**, 1409 (1993).

¹⁷J.L. Cardy, 1988, *Fields, Strings and Critical Phenomena*, edited by E. Brezin and J. Zinn-Justin, Les Houches Session XLIX (Elsevier Science Publishers, Amsterdam, 1990).

¹⁸F. Woynarovich, J. Phys. A **22**, 4243 (1989).

¹⁹H. Frahm and V. E. Korepin, Int. J. Mod. Phys. B **8**, 57 (1994).

²⁰S. R. White, Phys. Rev. B **48**, 10 345 (1993).

²¹S. R. White and D. Huse, Phys. Rev. B **48**, 3844 (1993); E.S. Sorensen and I. Affleck, Phys. Rev. Lett. **71**, 1633 (1993).

²²C. C. Yu and S. White, Phys. Rev. Lett. **71**, 3866 (1993).

²³R. M. Noack, S. R. White, and D. J. Scalapino, Phys. Rev. Lett. **73**, 882 (1994).

²⁴E. H. Lieb and F. Y. Wu, Phys. Rev. Lett. **20**, 1445 (1968).

Q. M. Caffarel and R. Mosseri, “Hubbard model on d-dimensional hypercubes: Exact solution for the two-electron case”, *Phys. Rev. B* , 12651 (1998)

Hubbard model on d -dimensional hypercubes: Exact solution for the two-electron case

Michel Caffarel*

CNRS-Laboratoire de Chimie Théorique, Université Pierre et Marie Curie, Tour 22-23, 4 place Jussieu, 75252 Paris Cedex 05, France

Rémy Mosseri†

CNRS-Groupe de Physique des Solides, Université Paris 6 et Paris 7, 2 place Jussieu, 75251 Paris Cedex 05, France

(Received 13 March 1998)

The Hubbard model is exactly solved for two particles on d -dimensional hypercubes. It is shown that the spectrum can be separated into two parts: a trivial (U -independent) part resulting from symmetries of hypercubes and a nontrivial part expressed as a single-impurity problem on a set of finite chains of size $d' + 1$ ($d' \leq d$). The exact expression for the one-particle Green's function is given. Finally, we discuss the extension of these results to standard hypercubic lattices with periodic boundary conditions. [S0163-1829(98)51520-2]

One of the most widely used models to describe strongly correlated fermion systems is the Hubbard model and its various extensions. Unfortunately, only limited *exact* information about its physical properties is available. For the one-dimensional lattice the celebrated solution of Lieb and Wu¹ provides the exact eigenspectrum of the model. In the opposite limit of large dimensions investigated very recently,² some almost exact results have also been obtained. However, for intermediate dimensions, and particularly for the very important two-dimensional case believed to be relevant to high- T_c superconductivity, very little, is at our disposal. Most of the results reported so far have been obtained either from numerical solutions on very small clusters (subject to important finite-size effects) or by using a variety of approximate analytical methods (with domains of validity and/or systematic errors difficult to evaluate).³

In this paper we present an exact solution for the Hubbard model with first-neighbor hopping term t and on-site interaction energy U

$$H = -t \sum_{(ij)\sigma} c_{i\sigma}^\dagger c_{j\sigma} + U \sum_i c_{i\uparrow}^\dagger c_{i\uparrow} c_{i\downarrow}^\dagger c_{i\downarrow} \\ = T(t) + V(U), \quad (1)$$

for two particles with opposite spins ($S_z=0$) on a d -dimensional hypercube γ_d defined as the set of $N=2^d$ sites whose d coordinates are either 0 or 1. Although our solution is yet limited to the two-electron case, to exhibit exact results for a truly interacting system in a dimension greater than 1 is clearly of primary interest. This is particularly true since hypercubes are related to the usual cubic lattices with periodic boundary conditions: γ_{2d} is topologically equivalent to a d -dimensional hypercubic lattice of linear size equal to 4 with periodic boundary conditions, noted Z_4^d (i.e., γ_2 is equivalent to the four-site ring, γ_4 is equivalent to the two-dimensional 4×4 cluster with periodic conditions,^{4,5} etc.). To solve the above Hamiltonian we first use an Abelian subgroup of the full γ_d point group, to block diagonalize the initial matrix of size 2^{2d} into 2^d blocks of size 2^d . Quite interestingly, these smaller submatrices correspond to a simple family of effective one-electron Hamilto-

nians defined on $\gamma_{d'}$ ($d' \leq d$), some of which have a single-impurity site. In a second step, we show how to further reduce these matrices into smaller blocks of size $d' + 1$ (instead of 2^d), corresponding to finite chains of size $d' + 1$ with one impurity site at one end and new specific hopping terms. Using a standard approach for impurity problems we provide a closed expression sum rule for the eigenspectrum. We also derive the exact expression for the one-particle Green's function. Finally, the extension of these results to hypercubic lattices with periodic boundary conditions is briefly discussed.

Let us define Λ_d , an Abelian subgroup of the full γ_d point group, generated by the d reflections π_i into perpendicular $(d-1)$ -dimensional planes meeting at the γ_d center. It is easy to show that Λ_d has 2^d elements (owing to the commutativity between the mirror operations), and that the orbit of a generic point under Λ_d is a hypercube γ_d . Let us number the Λ_d elements L by integers between 0 and $2^d - 1$, in the following way: L being a product of mirrors π_i , let L be the number, written in base two, whose corresponding i th digits are equal to 1 (π_1 is $L=1$, $\pi_1\pi_2\pi_3$ is $L=7$, etc.). Let us also locate the sites according to their numbering in base two: The i th coordinate is equal to the i th digit. Now, the action of the symmetry operation L , onto a site s , noted as the "special product" $L \bullet s$, translates into the following digit operation: each time a digit equals 1 in L , it switches the corresponding digit in s . For example, in three dimensions, $7 \bullet 1 = 6$, with corresponds in coordinates to $\pi_1\pi_2\pi_3(0,0,1) = (1,1,0)$. To construct the irreducible representations (irreps) and the character table of Λ_d , it is useful to remark that this group is isomorphic to d times the tensorial product with itself of the two-element group $Z_2 = \{E, \pi_1\} = \Lambda_1$.⁶ The Λ_d irreps (unidimensional since Λ_d is Abelian) are easily obtained as tensor products of the two irreps Γ_0 and Γ_1 of Z_2 . Now, the N irreps can be labeled by integers M , through their base-two decomposition, by ordering the different occurrences of Z_2 in the tensorial product, and fixing the corresponding digit to 0 or 1, whether the irreps Γ_0 and Γ_1 occur.

Let us first consider the one-electron tight-binding spectrum with hopping term t . Each eigenstate belongs to a given irrep of Λ_d , and reads

$$|M\rangle = \frac{1}{\sqrt{2^d}} \sum_{R \in \Lambda_d} \chi_R^M R(|0\rangle) = \frac{1}{\sqrt{2^d}} \sum_{r=0}^{N-1} (-1)^{m_{M,r}} |r \bullet 0\rangle, \quad (2)$$

where $m_{M,r}$ is the number of digits equal to 1 simultaneously in M and r (we have used the above defined special product \bullet to denote the action of the symmetry operation R onto the basis kets). Since all the sites are equivalent, it is sufficient to consider the interaction of the site number 0 with its d first neighbors that have exactly one digit equal to 1 and belong to the set $V_d = \{v_j = 2^j, j=0, \dots, d-1\}$. As a result, one finds that the eigenenergies read

$$E_M = \sum_{j=0}^{d-1} \chi_{v_j}^M = -t(d - 2N_M), \quad (3)$$

where N_M is the number of digits equal to 1 in M . Since M runs from 0 to $2^d - 1$, the γ_d spectrum consists of $d+1$ levels, from $-dt$ to dt , with equal spacing $2t$ (the degeneracy of a E_M level being given by a standard binomial coefficient).

Let us now consider the two-electron case ($S_z=0$). The full Hamiltonian matrix, of size 2^{2d} , is readily block diagonalized into 2^d blocks of size 2^d , associated with each representation M . For a given M , one constructs a basis with 2^d kets $|M, l\rangle$

$$\begin{aligned} |M, l\rangle &= \frac{1}{\sqrt{2^d}} \sum_{R \in \Lambda_d} \chi_R^M R(|0 \uparrow, l \downarrow\rangle) \\ &= \frac{1}{\sqrt{2^d}} \sum_{r=0}^{N-1} \chi_r^M |(r \bullet 0) \uparrow, (r \bullet l) \downarrow\rangle, \end{aligned} \quad (4)$$

where $|i \uparrow, j \downarrow\rangle$ represents a configuration with electron \uparrow at site i and electron \downarrow at site j . Depending on the parity of the number of digits equal to 1 and common to integers M and l , it can be shown that $|M, l\rangle$ is either symmetric (even number) or antisymmetric (odd number) with respect to the exchange of position of electrons. Accordingly, $|M, l\rangle$ corresponds either to a singlet or a triplet state. It is clear that U only occurs in $\langle M, 0 | V(U) | M, 0 \rangle$, while the kinetic part reads

$$\begin{aligned} \langle M, l | T | M, l' \rangle &= \frac{1}{2^d} \sum_{r=0}^{N-1} \sum_{r'=0}^{N-1} \chi_r^M \chi_{r'}^M \\ &\quad \times \langle (r \bullet 0) \uparrow, (r \bullet l) \downarrow | T | (r' \bullet 0) \uparrow, (r' \bullet l') \downarrow \rangle \\ &= \frac{1}{2^d} \sum_{r=0}^{N-1} \left[\chi_r^M \chi_r^M \langle (r \bullet 0) \uparrow, (r \bullet l) \downarrow | T | (r \bullet 0) \uparrow, (r \bullet l') \downarrow \rangle \right. \\ &\quad \left. + \sum_{j=0}^{d-1} \chi_r^M \chi_{v_j \bullet r}^M \right. \\ &\quad \left. \times \langle (r \bullet 0) \uparrow, (r \bullet l) \downarrow | T | (v_j \bullet r \bullet 0) \uparrow, (v_j \bullet r \bullet l') \downarrow \rangle \right]. \end{aligned} \quad (5)$$

In the latter expression, we have decoupled the terms where the \downarrow spin jumps (first part) from those where the \uparrow spin jumps. In the latter part (sum over j) the only nonvanishing term corresponds to $r \bullet l = v_j \bullet r \bullet l' \rightarrow l' = v_j \bullet l$, which means l and l' neighbors (recall that the group is Abelian and its elements are their own inverse). One finally gets that the nonvanishing kinetic terms read

$$\langle M, l | T | M, v_j \bullet l \rangle = -\frac{t}{2^d} \sum_{r=0}^{N-1} (1 + \chi_r^M \chi_{v_j \bullet r}^M), \quad (6)$$

The block matrix associated with the irrep M corresponds therefore to an effective one-electron tight-binding Hamiltonian, with sites labeled by l , kets $|M, l\rangle$, and hopping terms given by the above expression (6). A simple case is provided by the identity irrep $M=0$, for which $\chi_r^M=1$ for any r . The effective Hamiltonian $H^{(0)}$ corresponds to a hypercube γ_d , with one ‘‘impurity’’ site (with diagonal term U) and a constant hopping term $-2t$. We now show that the other irreps correspond to the effective Hamiltonian $H^{(M)}$ on

hypercubes $\gamma_{d'}$ with $d' < d$. One has to evaluate the right-hand part of Eq. (6). By definition of the v_j (mirrors that connect a site to one of its first neighbors), r and $v_j \bullet r$ differ by one digit, which depends on j , not on r . If this digit takes the value 1 in the base-two decomposition of M , then $\chi_r^M \chi_{v_j \bullet r}^M = -1$ for any r , and the corresponding $H^{(M)}$ matrix element vanishes. $H^{(M)}$ therefore corresponds to a γ_d in which families of parallel edges have been cut (those orthogonal to the mirrors labeled by the digits 1 in the decomposition of M). Figure 1 displays graphically this general result for $d=2$ and $d=3$.

So, at this step, the spectrum is solved in terms of one-electron tight-binding models on hypercubes of dimension lower or equal to d . The only nontrivial contributions correspond to those parts, in the hypercube decomposition, which contain the impurity site.⁷ We now show how to further greatly reduce their complexity.

To do that it is convenient to reexpress the effective Hamiltonian H [hereafter we will drop the superscript (0)]

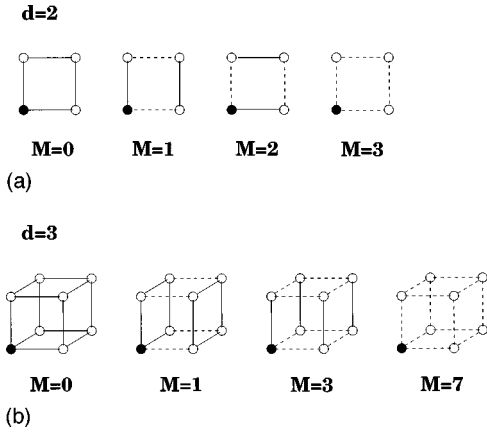


FIG. 1. Graphical illustration of the effective Hamiltonian $H^{(M)}$ associated with the irrep M . Full circles correspond to impurity sites with a diagonal term U , full edges to hopping terms equal to $-2t$, and dotted lines to the edges that are cut in the given irrep. (a) $d=2$, the four irreps are depicted. (b) $d=3$, only four irreps among the eight are shown.

since only the $M=0$ case has finally to be considered] in the one-electron basis, Eq. (2). It is easy to verify that H can be written in the form

$$H = \text{Diag}(\epsilon) + \frac{U}{N} I_N, \quad (7)$$

where $\text{Diag}(\epsilon)$ is a diagonal matrix whose entries are the 2^d free electron solutions of the hypercube with hopping $2t$ (solution at $U=0$) and I_N is the $N \times N$ matrix with unit entries for all i and j . The latter part is nothing but a projection operator on the eigenstate $|v_0\rangle$ with energy U , and H can be rewritten

$$H = \text{Diag}(\epsilon) + U|v_0\rangle\langle v_0|, \quad (8)$$

with $(v_0)_i = (1/\sqrt{N})$ $i=1, \dots, N$.

To proceed further we define for each subspace corresponding to a given value ϵ_i (there are $d+1$ such subspaces of degeneracy g_i , the binomial coefficient) a basis consisting of the normalized vectors $v_1^{(i)} = (1/\sqrt{g_i})(1, \dots, 1)$ and a set of vectors $\{v_k^{(i)}, k \neq 1\}$ spanning the subspace orthogonal to $v_1^{(i)}$. In this new basis only the $(d+1)$ vectors v_1 have a nonzero overlap with $|v_0\rangle$, and H , of dimension 2^d , decomposes into a diagonal matrix having $2^d - (d+1)$ trivial solutions ϵ_i , and a residual U -dependent part, noted \mathcal{H} , given by the matrix of linear size $(d+1)$ written in the form

$$\mathcal{H} = \text{Diag}(\epsilon) + U|v\rangle\langle v| \equiv \mathcal{H}_0 + \mathcal{V}, \quad (9)$$

where $|v\rangle$ has components $v_i = \sqrt{g_i/N}$ and the ϵ 's represent now the $(d+1)$ distinct free-electron energies:

$$\epsilon_i = -2t(d-2i) \quad i=0, \dots, d. \quad (10)$$

An alternative representation consists of going back to the basis where the potential operator \mathcal{V} is diagonal. H is then found to be tridiagonal (one-dimensional tight-binding model) with off-diagonal hopping term given by $t_{i,i+1} = 2t\sqrt{(d-i)(i+1)}$, $i=0$ to $d-1$ and a diagonal U contribution at the initial site (here numbered 0). In other words,

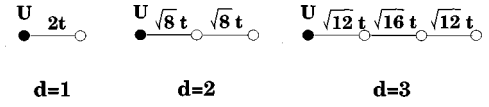


FIG. 2. Graphical illustration of the single-impurity one-electron problems associated with the nontrivial part of the spectrum (the general formula is given in the text).

the problem is mapped onto a single-impurity problem on a finite chain of linear size $(d+1)$. Figure 2 illustrates this result for $d \leq 3$.

It is known that the eigenspectrum of single-impurity problems can be expressed under the form of a sum rule expression using the Koster-Slater approach.⁸ This result can be briefly reobtained as follows. First, the following operator identity is invoked:

$$(\mathcal{H} - z)^{-1} = (\mathcal{H}_0 - z)^{-1} - \frac{U}{1 + U G_{vv}^{(0)}(z)} \times \frac{1}{(\mathcal{H}_0 - z)} |v\rangle\langle v| \frac{1}{(\mathcal{H}_0 - z)}, \quad (11)$$

where z is an arbitrary complex number and $G_{vv}^{(0)}$ is the unperturbed Green's function given by $G_{vv}^{(0)} = \langle v | (\mathcal{H}_0 - z)^{-1} | v \rangle$. Then, using this identity, the fully interacting Green's function $G_{vv}(z)$ can be written as

$$G_{vv}(z) = \frac{G_{vv}^{(0)}(z)}{1 + U G_{vv}^{(0)}(z)}. \quad (12)$$

Searching for poles of $G_{vv}(z)$ we get

$$\frac{1}{N} \sum_{i=0}^d \frac{g_i}{E - \epsilon_i} = \frac{1}{U}. \quad (13)$$

Equation (13) is the final closed expression determining the nontrivial part of the spectrum. It is easily shown that this equation admits $(d+1)$ distinct solutions, which we shall denote as $\text{Spect}^{(d)}(U)$.

To summarize, the set of 2^{2d} eigenvalues of the hypercube γ_d consists of a U -dependent part given by the collection of the nontrivial spectra at dimensions lower or equal to d :

$$\bigoplus_{i=0}^d \binom{d}{i} \text{Spect}^{(i)}(U), \quad (14)$$

(note that here the binomial coefficient counts the number of occurrences of γ_i hypercubes with an impurity site in the decomposition of the initial γ_d , see Fig. 1) and a trivial U -independent part given by $E_l = 2tl$, $l = -d, \dots, d$ with degeneracy:

$$g_l = \sum_{i=|l|}^d \left[2^{d-i} \binom{i}{l+i} - 1 \right] \binom{d}{i}, \quad (15)$$

the prime in Σ' indicating that the summation over i is done with an increment of 2. Formula (15) can be obtained by tracing back the contributions due to the different irreps and those issued from the internal symmetry of hypercubes

[trivial solutions extracted when passing from Eq. (8) to Eq. (9)]. Eigenenergies correspond either to singlet or triplet states. Since U only connects basis states $|M, l\rangle$ with $l=0$ (see above), triplet states are not sensitive to U and only singlet states belong to the U -dependent part of the spectrum. The ground-state energy is not degenerate and corresponds to the lowest solution in $\text{Spect}^{(d)}(U)$. Note also that in the limit of large dimensions, and after proper renormalization of the parameters of the Hamiltonian, an infinite-dimensional model can be defined, as done recently for a number of correlated fermions models, see Ref. 2.

Let us now consider dynamical properties. We are interested in evaluating the one-particle Green's function defined by

$$G_k^{(d)}(z, U) \equiv \langle \psi_0 | a_k \frac{1}{H-z} a_k^\dagger | \psi_0 \rangle, \quad (16)$$

where $|\psi_0\rangle$ denotes the one-particle ground state consisting of one electron of given spin and a_k^\dagger creates one electron of opposite spin in a one-particle state, noted k . Hereafter, k varies from 0 to d and labels one of the $(d+1)$ degenerate subspaces of the one-electron problem, the ground state corresponding to $k=0$. Now, note that vector $a_k^\dagger|\psi_0\rangle$ belongs to the subspace corresponding to the decomposition on hypercubes of dimension $(d-k)$. There exist 2^k different families of hypercubes having such a dimension (see Fig. 1) among which only one has the U -impurity site. Accordingly, we get the following result:

$$G_k^{(d)}(z, U) = \frac{1}{2^k} G_0^{(d-k)}(z, U) + \left(1 - \frac{1}{2^k}\right) G_0^{(d-k)}(z, U=0). \quad (17)$$

Now, we need to evaluate the fundamental quantity $G_0^{(d')}(z, U)$ with Hamiltonian (9), the dimension d' ranging from 0 to d . For that we note that the ket $|0\rangle \equiv a_0^\dagger|\psi_0\rangle$ represents the (first) basis element corresponding to the diagonal energy ϵ_0 in representation (9). Projecting out identity (11) onto vector $|0\rangle$ and expressing the different quantities in terms of the noninteracting spectrum we get

$$G_0^{(d')}(z, U) = \frac{1}{\epsilon_0^{(d')} - z} - \frac{U}{2^{d'} (\epsilon_0^{(d')} - z)^2 \left(1 + \frac{U}{2^{d'}} \sum_{i=0}^{d'} \frac{g_i}{\epsilon_i^{(d')} - z}\right)}. \quad (18)$$

This equation together with Eqs. (10) and (17) give the exact one-particle Green's function of the problem.

Generalization of this approach to higher fillings is presently under investigation. We have already found that the existence of large fractions of U -independent eigenvalues is still valid for some specific fillings. However, the underlying structure for the U -dependent part of the spectrum is more difficult to elucidate.

Returning to the two-electron case, we would like to mention that by using rotations instead of reflections, a similar calculation can be done for standard d -dimensional hypercubic lattices of linear size L and periodic boundary conditions (Z_L^d). We have found that the problem can still be mapped onto a family of L^d single-impurity one-electron effective problems defined on the very same lattice Z_L^d . Each irrep corresponds to a value of a d -dimensional integer vector \mathbf{M} ($M_i=0, \dots, L-1$), or more physically, to a value for the total momentum $\mathbf{K}=(2\pi/L)\mathbf{M}$. The only difference between irreps lies in the value of the hopping term that depends explicitly on \mathbf{M} . More precisely, for each irrep labeled by \mathbf{K} , Eq. (13) now reads

$$\frac{1}{L^d} \sum_{n_1=0}^{L-1} \cdots \sum_{n_d=0}^{L-1} \frac{1}{E - \epsilon_{\mathbf{n}}^{(\mathbf{K})}} = \frac{1}{U}, \quad (19)$$

where the noninteracting energies $\epsilon^{(\mathbf{K})}$ are given by

$$\epsilon_{\mathbf{n}}^{(\mathbf{K})} = -4t \sum_{i=1}^d \cos(K_i/2) \cos(k_i + K_i/2), \quad (20)$$

with $\mathbf{K}=(2\pi/L)\mathbf{M}$ and $\mathbf{k}=(2\pi/L)\mathbf{n}$. In contrast with hypercubes, the sum in Eq. (19) runs over L^d values and cannot be further reduced. Note that, since the effective hopping term varies with the irrep (and can even vanish), both localized and resonant states (irreps by irreps) may be present. Finally, it is worth noticing that in the $d=1$ case the Bethe ansatz equations for two particles¹

$$\tan \frac{k_1 L}{2} = \frac{U}{2t(\sin k_1 - \sin k_2)}, \quad (21)$$

with $E = -2t(\cos k_1 + \cos k_2)$ and $k_1 + k_2 = (2\pi/L)M$ ($M=0, \dots, L-1$), can be recovered from Eq. (19) after simple but tedious algebra.

This work was supported by the ‘‘Contre National de la Recherche Scientifique.’’

*Electronic address: mc@lct.jussieu.fr

†Electronic address: mosseri@gps.jussieu.fr

¹E. H. Lieb and F. Y. Wu, Phys. Rev. Lett. **20**, 1445 (1968).

²See, e.g., A. Georges, G. Kotliar, W. Krauth, and M. J. Rozenberg, Rev. Mod. Phys. **68**, 13 (1996).

³See, e.g., E. Dagotto, Rev. Mod. Phys. **66**, 763 (1994).

⁴R. Mosseri, D. P. DiVincenzo, J. F. Sadoc, and M. H. Brodsky,

Phys. Rev. B **32**, 3974 (1985).

⁵H. Bruus and J. C. Anglès d'Auriac, Phys. Rev. B **55**, 9142 (1997).

⁶For $d=4$, Λ_4 coincides with the group \mathcal{A} used in Ref. 5.

⁷The occurrence of a large fraction of trivial states was noted for $d=2$ (Ref. 5). Our results put a light on this topic for general d .

⁸G. F. Koster and J. C. Slater, Phys. Rev. **95**, 1167 (1954).

R. R. Assaraf, P. Azaria, M. Caffarel, and P. Lecheminant, “ Metal-insulator transition in the one-dimensional $SU(N)$ Hubbard model”, Phys. Rev. B 60, 2299 (1999)

Metal-insulator transition in the one-dimensional $SU(N)$ Hubbard model

Roland Assaraf

CNRS-Laboratoire de Chimie Théorique, Université Pierre et Marie Curie, 4 Place Jussieu, 75252 Paris, France

Patrick Azaria

CNRS-Laboratoire de Physique Théorique des Liquides, Université Pierre et Marie Curie, 4 Place Jussieu, 75252 Paris, France

Michel Caffarel

CNRS-Laboratoire de Chimie Théorique, Université Pierre et Marie Curie, 4 Place Jussieu, 75252 Paris, France

Philippe Lecheminant

*Laboratoire de Physique Théorique et Modélisation, Université de Cergy-Pontoise, Site de Saint Martin,
2 avenue Adolphe Chauvin, 95302 Cergy-Pontoise Cedex, France*

(Received 3 March 1999)

We investigate the metal-insulator transition of the one-dimensional $SU(N)$ Hubbard model for repulsive interaction. Using the bosonization approach a Mott transition in the charge sector at half filling ($k_F = \pi/Na_0$) is conjectured for $N > 2$. Expressions for the charge and spin velocities as well as for the Luttinger-liquid parameters and some correlation functions are given. The theoretical predictions are compared with numerical results obtained with an improved zero-temperature quantum Monte Carlo approach. The method used is a generalized Green's function Monte Carlo scheme in which the stochastic time evolution is partially integrated out. Very accurate results for the gaps, velocities, and Luttinger-liquid parameters as a function of the Coulomb interaction U are given for the cases $N=3$ and $N=4$. Our results strongly support the existence of a Mott-Hubbard transition at a *nonzero* value of the Coulomb interaction. We find $U_c \sim 2.2$ for $N=3$ and $U_c \sim 2.8$ for $N=4$. [S0163-1829(99)00728-6]

I. INTRODUCTION

Although the metal-insulator transition has certainly been one of the most studied phenomenon in condensed-matter physics, it is only in recent years that important progress has been achieved. This is mainly due to careful experimental and numerical studies but also to the improvement of the theoretical tools.¹⁻³ It has been proved extremely difficult to investigate the effect of strong correlations in dimensions greater than 1, and it is only quite recently that, thanks to a new dynamical mean field, our understanding has substantially progressed.⁴ For one-dimensional systems, the situation is rather different: There exist powerful analytical and numerical approaches at our disposal. Moreover, from the experimental point of view, the Mott-transition can be realized in organic conductors⁵ and quantum wires.⁶ Therefore, one may expect to gain a lot of information on the physics of the metal-insulator transition.

In one dimension, it has been recognized very rapidly that umklapp processes are at the heart of the problem. In the Abelian bosonization formalism, one can draw a general and consistent picture of the Mott transition. Indeed, the charge properties are expected to be described, in the absence of umklapp contributions, by a Luttinger liquid with only two independent parameters: The charge velocity u_c and the charge exponent K_c that controls the decay of correlation functions. These quantities, which are nonuniversal, completely characterize the low-energy properties of a one-dimensional system.^{7,8} Within this framework, the effect of umklapp processes are investigated in perturbation theory,

and one can write down an effective theory that describes the Mott transition as well as a full description of the transport properties for any commensurate filling.^{9,10} The only parameter that controls the transition is the (in general unknown) Luttinger charge exponent K_c and the transition is predicted to be universal of the Kosterlitz-Thouless (KT) type.

Most of the theoretical work in $d=1$ focused on the properties of the standard $SU(2)$ Hubbard model which is known to be a Mott insulator at half filling from its exact solution.¹¹ An extension of this model was considered by introducing long-range hopping or finite-range interaction (nearest-neighbor interaction, for instance).² In the present work, we study a most natural generalization of the usual Hubbard model: Instead of considering fermions with a two-valued spin index [with $SU(2)$ symmetry] we generalize to the case of an arbitrary $SU(N)$ spin index. Apart from the theoretical interest it is important to emphasize that these additional degrees of freedom are realized physically through orbital degeneracy as, for example, in Mn oxides.³ In this paper, we shall study the phase diagram of the one-dimensional $SU(N)$ Hubbard model for repulsive interaction and at half filling corresponding to one "electron" per site. The Hamiltonian on a finite chain with L sites that we shall consider reads

$$\mathcal{H} = -t \sum_{i=1}^L \sum_{a=1}^N (c_{ia}^\dagger c_{i+1a} + \text{H.c.}) + \frac{U}{2} \sum_{i=1}^L \left(\sum_{a=1}^N n_{ia} \right)^2, \quad (1)$$

where the fermion annihilation operator of spin index $a = 1, \dots, N$ at site i is denoted by c_{ia} and satisfies the canonical anticommutation relation

$$\{c_{ia}, c_{jb}^\dagger\} = \delta_{ab} \delta_{ij}. \quad (2)$$

The density of species a at the i th site is defined by $n_{ia} = c_{ia}^\dagger c_{ia}$. In the following, we shall consider that the nearest-neighbor hopping (t) and the on-site interaction (U) are positive.

The Hamiltonian (1) is not exactly solvable by the Bethe ansatz for $N > 2$ and arbitrary U . It is, however, possible to solve the generalization of the Lieb-Wu Bethe ansatz equations for fermions carrying a $SU(N)$ spin index.^{12,13} The result is that for any $N > 2$, there exists a Mott-Hubbard transition from a metallic phase to an antiferromagnetic insulating phase at a *finite* value of the coupling U . The transition is found to be of *first* order in contrast with the accepted view that the metal-insulator transition in one-dimensional systems should be of the KT type. The point is that a projection onto the subspace of states having at most two electrons at each site is crucial for the use of the Bethe ansatz approach. The other configurations are automatically excluded by the Pauli principle in the $SU(2)$ Hubbard model whereas for $N > 2$ it is no longer the case. As a consequence, it is believed that the lattice model associated with the $SU(N)$ generalization of Lieb-Wu Bethe ansatz equations should coincide with an integrable *nonlocal* version of the $SU(N)$ Hubbard model (1).^{12,13} Although one naturally expects that the true $SU(N)$ Hubbard model will share some properties with its nonlocal partner, in particular the existence of a metallic phase at small enough U , the first-order character of the transition could take its origin in the nonlocality of the interaction. In any case, in order to study Eq. (1) one must abandon the exact Bethe ansatz approaches and resort to two powerful techniques available in one dimension: the bosonization and numerical approaches. As we shall show, none of these techniques is by itself sufficient to demonstrate the existence of the Mott transition. Regarding bosonization, the mere existence of the metal-insulator transition—even in the simplest scenario of a KT phase transition—relies on the knowledge of U dependence of the Luttinger parameter K_c , a nonuniversal quantity which can only be computed in a perturbative expansion in U . In other words, bosonization cannot tell us *whether* a given lattice model will undergo a Mott- U transition. However, it defines a rich theoretical framework in which many qualitative and quantitative predictions are obtained. This provides an essential guide for the numerical investigation of a particular lattice model. Regarding numerical investigations the situation is also not fully satisfactory. Beyond the evident problem of memory and CPU time limitations, it is well known that it is very difficult to characterize a KT phase transition. As we shall emphasize later, it is almost impossible to discriminate between the opening of a charge gap at $U=0$ and at a finite positive U , even when very accurate numerical data are at our disposal. The strategy employed in this work will consist in combining both approaches. Very strong evidence will be given in favor of a metal-insulator transition occurring at a finite positive value of the interaction U for $N > 2$.

Various numerical methods can be used to study the ground-state properties of Hamiltonian (1). In exact diagonalization methods¹⁴ the exact ground-state eigenvector is calculated. Unfortunately, the rapid increase of the size of the Hilbert space restricts severely the attainable system

sizes. In order to treat bigger systems two types of approach are at our disposal: The density matrix renormalization group (DMRG) method and the stochastic approaches.

Since its discovery a few years ago the DMRG method has been extensively used for studying various one-dimensional systems and coupled chain problems (for a review, see Ref. 15, for a detailed presentation of the method, see Refs. 16,17). DMRG is a very efficient real-space numerical renormalization-group (RG) approach. The fundamental point which makes the method successful is the way that “important” degrees of freedom are chosen at each RG iteration. Instead of keeping the lowest eigenstates of the RG block considered as isolated from the outside world (as it was usually done in previous approaches), the states which are selected are the most probable eigenstates of the density matrix associated with the block considered as a part of the whole system. The main error of DMRG is related to the finite number of states kept at each iteration of the algorithm. In order to get the exact property the extrapolation to an infinite number of states has to be performed. At least for 1D and quasi-1D problems, and for systems having a small number of states per site, the errors obtained are small. Note also that DMRG works especially well when open boundary conditions are used. For periodic boundary conditions, errors are significantly larger.

In this paper we use an alternative approach based on a stochastic sampling of the configuration space. Such approaches are referred to as quantum Monte Carlo (QMC) methods. There exists a large variety of QMC approaches. A first set of methods is defined within a finite-temperature framework (path-integral Monte Carlo, world-line Monte Carlo, etc., see, e.g., Ref. 18). In these approaches, the main systematic error is the high-temperature approximation associated with the Trotter break-up¹⁹ (Trotter or short-time error). When interested in obtaining the zero-temperature properties the number of “time slices” to consider must be taken large and the computational effort becomes important. Practical calculations have shown that the method is much less accurate than DMRG, at least for one-dimensional systems. In the second type of approaches used here, the stochastic sampling is directly defined within a zero-temperature framework. These methods are usually referred to as a Green’s function Monte Carlo (GFMC) or projector Monte Carlo. For systems having a nodeless ground-state wave function as it is the case here, the GFMC method can be extremely powerful. The basic idea is to extract from a known trial wave function ψ_T its exact ground-state component ψ_0 . To do that an operator $G(\mathcal{H})$ acting as a filter is introduced. Statistical rules are defined in order to calculate stochastically the action of the operator G on a given function. Apart from statistical fluctuations, the GFMC method is an exact method. It does not require an extrapolation to zero temperature as in finite-temperature schemes. In addition, there exists a so-called zero-variance property for the energy: The better the trial wave function ψ_T is, the smaller the statistical fluctuations are. In the limit of an exact wave function, the statistical fluctuations entirely disappear (zero-variance property). As an important consequence, by choosing a good enough trial wave function very accurate calculations can be performed (see, for example, Ref. 19). Note that, in contrast with DMRG, the efficiency of GFMC does not depend on the

specific type of boundary conditions chosen and that the number of states per site is not a critical parameter of the simulation. Here, it is an important point since the $SU(N)$ model displays 2^N states per site [for the $SU(4)$ case treated here it gives 16 states per site].

In order to improve further the accuracy of the approach we present a generalized version of the GFMC method in which the dynamics of the Monte Carlo process is partially integrated out. More precisely, we generalize an idea introduced by Trivedi and Ceperley in their GFMC study of the $S=1/2$ Heisenberg quantum antiferromagnet.¹⁹ In the GFMC method the probability that the random walk remains a certain number of times in the same configuration is described by a Poisson distribution. It is then possible to sample the corresponding ‘‘trapping time’’ from this distribution and to weight the expectations values according to it. As remarked by Trivedi and Ceperley, doing this can lead to a considerable improvement in the simulation. This is particularly true when the wave function is localized (large U regime for our model, systems with deep potential wells, etc.). Here, we show that the method can be improved further by integrating out exactly the time evolution associated with this trapping phenomenon. Once this is done we are left with a random walk defined by an ‘‘escape transition probability’’ connecting nonidentical configurations (the system never remains in the same configuration) and a modified branching term resulting from the time integration. Note that introducing trapping times in averages helps a lot when optimizing the parameters of the trial wave function. Finally, we present an original method for computing the Luttinger-liquid parameters within a QMC scheme. We show that these parameters can be obtained from a series of ground-state calculations of total energies of *real*—but not necessarily Hermitian—Hamiltonians. In this way we escape from the difficulty of calculating with QMC ground-state energies of the *complex* Hamiltonians resulting from the definition of the charge and spin stiffnesses. Although it is difficult to compare the efficiency of our generalized GFMC approach with DMRG (since the quality of GFMC simulations is too much dependent on the quality of the trial wave function used) we believe that the accuracy of our results is comparable or even better to what can be done with DMRG. In any case, our data are sufficiently accurate to conclude to the existence of a metal-insulator phase transition in the model studied.

Very recently, Beccaria *et al.*²⁰ have proposed a QMC algorithm based on the use of Poisson processes. Their approach contains similar ideas. However, in contrast with the present approach no importance sampling is used and no integration of the Poisson dynamics is performed. It should also be noted that the use of Poisson processes for describing the time evolution of systems trapped in some configuration is not restricted to quantum systems. Krauth and collaborators have proposed related ideas within the context of classical Monte Carlo simulations.^{21,22}

The organization of the paper is as follows. In Sec. II, a bosonization approach of the $SU(N)$ Hubbard model will be given. Some of the results have already been obtained by Affleck²³ whereas additional new ones will also be useful to compare with the numerical simulations. The purpose of Sec. III is to give a presentation of the GFMC method together with our generalization based on the partial integration of the

dynamics. The practical implementations of the GFMC approach for the Hamiltonian (1) will be discussed in Sec. IV and the numerical results for $N=2,3,4$ will be presented in Sec. V. Finally, Sec. VI gives a summary of the work together with a comparison between the physical results obtained for the $SU(N)$ Hubbard model and those corresponding to its nonlocal integrable version. In the Appendix we give some details of computation occurring in Sec. II.

II. THE $SU(N)$ HUBBARD MODEL

In this section, we shall use a bosonization approach (for recent reviews see Refs. 8,24) to study the $SU(N)$ Hubbard model. Before doing that, let us first discuss the symmetries of the model.

The Hamiltonian (1) has a $U(1) \otimes SU(N)$ symmetry:

$$\begin{aligned} c_{ia} &\rightarrow e^{i\theta} c_{ia}, \\ c_{ia} &\rightarrow U_{ab} c_{ib}, \end{aligned} \quad (3)$$

where the matrix U belongs to $SU(N)$. These symmetries express the conservation of the charge and spin invariance under a $SU(N)$ rotation. The associated generators are given by the following operators:

$$\begin{aligned} \mathcal{N} &= \sum_{i,a} n_{ia}, \\ \mathcal{S}^A &= \sum_i \mathcal{S}_i^A, \end{aligned} \quad (4)$$

with

$$\mathcal{S}_i^A = c_{ia}^\dagger \mathcal{T}_{ab}^A c_{ib}, \quad (5)$$

where the summation over repeated indexes (except for lattice indexes) is assumed in the following. In the latter equation, the N^2-1 matrices \mathcal{T}^A are the generators of the Lie algebra of $SU(N)$ in the fundamental representation. They satisfy the commutation relation

$$[\mathcal{T}^A, \mathcal{T}^B] = i f^{ABC} \mathcal{T}^C, \quad (6)$$

f^{ABC} being the structure constants of the Lie algebra and the generators are normalized according to $\text{Tr}(\mathcal{T}^A \mathcal{T}^B) = \delta^{AB}/2$. The conservation law associated with the $U(1)$ symmetry allows to study the Hamiltonian (1) for a fixed density n . The Coulomb interaction can thus be rewritten, up to a constant, in terms of the $SU(N)$ spin operator:

$$\frac{U}{2} \left(\sum_{a=1}^N n_{ia} \right)^2 = -\frac{UN}{N+1} \mathcal{S}_i^A \mathcal{S}_i^A, \quad (7)$$

where we have used the identity

$$\mathcal{T}_{ab}^A \mathcal{T}_{de}^A = \frac{1}{2} \left(\delta_{ae} \delta_{bd} - \frac{1}{N} \delta_{ab} \delta_{de} \right). \quad (8)$$

The relation (7) makes explicit the $SU(N)$ invariance of the model.

The Hamiltonian (1) is not exactly solvable by the Bethe ansatz for $N>2$ and arbitrary U , even if, as already emphasized, some integrable nonlocal extension of Eq. (1) with a

$SU(N)$ symmetry can be considered. The situation is simpler in the limit $U \rightarrow \infty$ and at half filling (one ‘‘electron’’ per site), i.e., when $k_F = \pi/Na_0$ (a_0 being the lattice spacing). In that case, it can be shown that Eq. (1) reduces to the $SU(N)$ Heisenberg antiferromagnetic chain for which an exact solution is available. As shown by Sutherland,²⁵ this latter model is critical with $N-1$ massless bosonic modes with the same velocity. In the conformal field theory (CFT) language, the central charge of the model in the infrared (IR) limit is $c = N-1$ and using a non-Abelian bosonization of Eq. (1), Affleck²³ identifies the nature of the critical theory in the spin sector as the $SU(N)_1$ Wess-Zumino-Novikov-Witten (WZNW) model. In the following, we shall present both non-Abelian and Abelian bosonization approaches of the $SU(N)$ Hubbard model (1) at half filling and give a number of results that will be essential for discussing the numerical data presented in Sec. V.

A. Continuum limit

In the continuum limit, the spectrum around the two Fermi points $\pm k_F$ is linearized and gives rise to left-moving fermions ψ_{aL} and right-moving fermions ψ_{aR} . In this low-energy procedure, the lattice fermion operators c_{ia} are expressed in terms of these left-right moving fermions as

$$\frac{c_{ia}}{\sqrt{a_0}} \rightarrow \psi_a(x) \sim \psi_{aR}(x) e^{ik_F x} + \psi_{aL}(x) e^{-ik_F x}, \quad (9)$$

where $x = ia_0$. In this continuum limit, the noninteracting part of the Hamiltonian (1) corresponds to the Hamiltonian density of N free relativistic fermions

$$\mathcal{H}_0 = -i v_F (: \psi_{aR}^\dagger \partial_x \psi_{aR} : - : \psi_{aL}^\dagger \partial_x \psi_{aL} :), \quad (10)$$

where the normal ordering $::$ with respect of the Fermi sea is assumed and the Fermi velocity v_F is given by

$$v_F = 2ta_0 \sin \frac{\pi}{N}. \quad (11)$$

In the continuum limit, the $SU(N)$ spin operator (5) decomposes into a uniform and a $2k_F$ contribution

$$\frac{S_i^A}{a_0} \rightarrow S^A(x) \simeq \mathcal{J}^A(x) + [e^{2ik_F x} \mathcal{N}^A(x) + \text{H.c.}], \quad (12)$$

where the $2k_F$ contribution is given by

$$\mathcal{N}^A = \psi_{aL}^\dagger \mathcal{T}_{ab}^A \psi_{bR}, \quad (13)$$

whereas the uniform part reads $\mathcal{J}^A = \mathcal{J}_R^A + \mathcal{J}_L^A$ with

$$\mathcal{J}_{R(L)}^A = : \psi_{aR(L)}^\dagger \mathcal{T}_{ab}^A \psi_{bR(L)} :. \quad (14)$$

These left-right $SU(N)$ spin currents obey the following operator product expansion (OPE) (see the Appendix):

$$\lim_{x \rightarrow y} \mathcal{J}_{R(L)}^A(x) \mathcal{J}_{R(L)}^B(y) \sim \frac{-\delta^{AB}}{8\pi^2(x-y)^2} \mp \frac{f^{ABC}}{2\pi(x-y)} \mathcal{J}_{R(L)}^C(y) \quad (15)$$

which shows that they satisfy the $SU(N)_1$ Kac-Moody (KM) algebra.^{24,26} In the same way, the total charge density $\sum_a n_{ia}$ reads in the continuum limit

$$\sum_a n_{ia} \rightarrow a_0^{1/2} \{ \mathcal{J}^0(x) + [e^{-2ik_F x} \psi_{aR}^\dagger(x) \psi_{aL}(x) + \text{H.c.}] \}, \quad (16)$$

where $\mathcal{J}^0 = \mathcal{J}_R^0 + \mathcal{J}_L^0$ and

$$\mathcal{J}_{R(L)}^0 = : \psi_{aR(L)}^\dagger \psi_{aR(L)} : \quad (17)$$

are the U(1) right and left charge currents. These currents satisfy the OPE

$$\lim_{x \rightarrow y} \mathcal{J}_{R(L)}^0(x) \mathcal{J}_{R(L)}^0(y) \sim - \frac{N}{4\pi^2(x-y)^2} \quad (18)$$

and $\mathcal{J}_{R(L)}^0$ belongs to the $U(1)_N$ KM algebra.

With these identifications, it is not difficult to show (see the Appendix) that the free part of the Hamiltonian (10) can be expressed only in terms of spin and charge currents (the so-called Sugawara form):

$$\mathcal{H}_0 = \mathcal{H}_{0s} + \mathcal{H}_{0c} \quad (19)$$

with

$$\mathcal{H}_{0s} = \frac{2\pi v_F}{N+1} (: \mathcal{J}_R^A \mathcal{J}_R^A : + : \mathcal{J}_L^A \mathcal{J}_L^A :), \quad (20)$$

and

$$\mathcal{H}_{0c} = \frac{\pi v_F}{N} (: \mathcal{J}_R^0 \mathcal{J}_R^0 : + : \mathcal{J}_L^0 \mathcal{J}_L^0 :). \quad (21)$$

At the level of the free theory, spin and charge degrees of freedom decouple. The symmetry of the free Hamiltonian \mathcal{H}_0 in the continuum limit is therefore enlarged to give $U(1)_L \otimes SU(N)_L \otimes U(1)_R \otimes SU(N)_R$. The Hamiltonian \mathcal{H}_{0s} is nothing but the Sugawara form of the $SU(N)_1$ WZNW model.^{24,26} It is a conformally invariant theory with central charge $c = N-1$ ($N-1$ massless bosons). The contribution \mathcal{H}_{0c} describes the U(1) charge degrees of freedom and has central charge $c = 1$ (1 massless boson).

The nontrivial part of the problem stems from the Coulomb interaction (7). At sufficiently small $U \ll t$, from Eq. (7), we see that its contribution will be given by the OPE

$$\mathcal{V}(x) = -U a_0 \frac{N}{N+1} \lim_{\epsilon \rightarrow 0} S^A(x+\epsilon) S^A(x). \quad (22)$$

From Eq. (12), there are three contributions to \mathcal{V} :

$$\mathcal{V} = \mathcal{V}_0 + \mathcal{V}_{2k_F} + \mathcal{V}_{4k_F}. \quad (23)$$

The first term is the uniform $k=0$ component while the others contain oscillating factors $e^{\pm 2ik_F x}$ and $e^{\pm 4ik_F x}$. Neglecting all oscillatory contributions, we are thus left with the uniform part \mathcal{V}_0 . Performing the necessary OPE's (see the Appendix), one finds that the total effective low energy Hamiltonian density separates into two commuting charge and spin parts

$$\mathcal{H} = \mathcal{H}_c + \mathcal{H}_s \quad (24)$$

with

$$\mathcal{H}_c = \frac{\pi v_c}{N} (: \mathcal{J}_R^0 \mathcal{J}_R^0 : + : \mathcal{J}_L^0 \mathcal{J}_L^0 :) + G_c \mathcal{J}_R^0 \mathcal{J}_L^0 \quad (25)$$

and

$$\mathcal{H}_s = \frac{2\pi v_s}{N+1} (: \mathcal{J}_R^A \mathcal{J}_R^A : + : \mathcal{J}_L^A \mathcal{J}_L^A :) + G_s \mathcal{J}_R^A \mathcal{J}_L^A, \quad (26)$$

where the renormalized velocities are

$$v_s = v_F - \frac{U a_0}{2\pi},$$

$$v_c = v_F + (N-1) \frac{U a_0}{2\pi} \quad (27)$$

and the current-current couplings in the charge and the spin sectors are given by

$$G_c = \frac{N-1}{N} U a_0,$$

$$G_s = -2U a_0. \quad (28)$$

Apart from a velocity renormalization, the effect of the Coulomb interaction is exhausted in the two marginal interactions in both charge and spin sectors. When $U > 0$, the spin current-current interaction is marginal irrelevant. At the IR fixed point $G_s^* = 0$ the Hamiltonian in the spin sector is that of the $SU(N)_1$ WZNW model. On the other hand, the current-current interaction in the charge sector is exactly marginal since one can diagonalize \mathcal{H}_c with a Bogolioubov transformation to recover the Tomonaga-Luttinger Hamiltonian. Therefore, \mathcal{H}_c describes the line of fixed points of the Luttinger liquid.

From the above analysis we conclude that the $SU(N)$ Hubbard model at half filling is massless for small $U > 0$. The spin sector is described by the $SU(N)_1$ WZNW model while the charge sector is a Luttinger liquid with continuously varying exponents. The main point in the above analysis is the absence of umklapp terms which, when $N=2$, opens a gap in the charge sector for an infinitesimal value of the interaction. At this point it is worth recalling that the main approximation made in the above analysis is the omission of the oscillating contributions \mathcal{V}_{2k_F} and \mathcal{V}_{4k_F} . This is a reasonable assumption as far as U is not too large. However one expects, on general grounds, that umklapp processes should contribute at sufficiently large U and that a Mott transition to an insulating phase should occur at a finite U_c . Indeed, in the $U \rightarrow \infty$ limit, we have an insulating phase where the spin degrees of freedom are described by the $SU(N)$ Heisenberg antiferromagnet. We shall return to this point later. For now let us concentrate on the properties of the metallic phase.

B. The metallic phase

At this point, we introduce N chiral bosonic fields $\phi_{aR(L)}$, $a = (1, \dots, N)$, using the Abelian bosonization of Dirac fermions²⁴

$$\psi_{aR(L)} = \frac{\kappa_a}{\sqrt{2\pi}} : \exp(\pm i \sqrt{4\pi} \phi_{aR(L)}) :, \quad (29)$$

where the bosonic fields satisfy the commutation relation $[\phi_{aR}, \phi_{bL}] = (i/4) \delta_{ab}$. The anticommutation between fermions with different spin indexes is realized through the presence of Klein factors (here Majorana fermions) κ_a with the following anticommutation rule: $\{\kappa_a, \kappa_b\} = 2\delta_{ab}$. As in the $N=2$ case, it is suitable to switch to a basis where the charge and spin degrees of freedom single out. To this end, let us introduce a charge bosonic field $\Phi_{cR(L)}$ and $N-1$ spin bosonic fields $\Phi_{msR(L)}$, $m = (1, \dots, N-1)$ as follows:

$$\Phi_{cR(L)} = \frac{1}{\sqrt{N}} (\phi_1 + \dots + \phi_N)_{R(L)},$$

$$\Phi_{msR(L)} = \frac{1}{\sqrt{m(m+1)}} (\phi_1 + \dots + \phi_m - m\phi_{m+1})_{R(L)}. \quad (30)$$

The transformation (30) is canonical and preserves the bosonic commutation relations. The inverse transformation is easily found to be

$$\phi_{1R(L)} = \frac{1}{\sqrt{N}} \Phi_{cR(L)} + \sum_{l=1}^{N-1} \frac{\Phi_{lsR(L)}}{\sqrt{l(l+1)}},$$

$$\phi_{aR(L)} = \frac{1}{\sqrt{N}} \Phi_{cR(L)} - \sqrt{\frac{a-1}{a}} \Phi_{(a-1)sR(L)} + \sum_{l=a}^{N-1} \frac{\Phi_{lsR(L)}}{\sqrt{l(l+1)}}, \quad a = 2, \dots, N-1,$$

$$\phi_{NR(L)} = \frac{1}{\sqrt{N}} \Phi_{cR(L)} - \sqrt{\frac{N-1}{N}} \Phi_{(N-1)sR(L)}. \quad (31)$$

In this new basis, the Hamiltonian density in the spin sector at the $SU(N)_1$ fixed point reads

$$\mathcal{H}_s^* = \frac{u_s}{2} \sum_{m=1}^{N-1} [: (\partial_x \Phi_{ms})^2 : + : (\partial_x \Theta_{ms})^2 :], \quad (32)$$

where u_s is the spin velocity at the fixed point and

$$\Phi_{ms} = \Phi_{msL} + \Phi_{msR},$$

$$\Theta_{ms} = \Phi_{msL} - \Phi_{msR}. \quad (33)$$

This representation makes clear the fact that the central charge in the spin sector is indeed $c = N-1$.

Let us now concentrate on the charge sector. It is not difficult to show, using Eqs. (17), (29), and (30) that the charge current expresses as

$$\mathcal{J}_{R(L)}^0 = \sqrt{\frac{N}{\pi}} \partial_x \Phi_{cR(L)}. \quad (34)$$

Therefore, the Hamiltonian density (25) in the charge sector reads

$$\begin{aligned} \mathcal{H}_c = & \frac{v_c}{2} [:(\partial_x \Phi_c)^2: + :(\partial_x \Theta_c)^2:] \\ & + (N-1) \frac{Ua_0}{\pi} \partial_x \Phi_{cL} \partial_x \Phi_{cR}, \end{aligned} \quad (35)$$

where we have introduced the total charge bosonic field $\Phi_c = \Phi_{cR} + \Phi_{cL}$ and its dual $\Theta_c = \Phi_{cL} - \Phi_{cR}$. The Hamiltonian (35) can be written in the Luttinger-liquid form

$$\mathcal{H}_c = \frac{u_c}{2} \left(\frac{1}{K_c} :(\partial_x \Phi_c)^2: + K_c :(\partial_x \Theta_c)^2: \right), \quad (36)$$

where the charge exponent K_c and the renormalized charge velocity u_c are given by

$$\begin{aligned} K_c &= \frac{1}{\sqrt{1 + (N-1)Ua_0/\pi v_F}}, \\ u_c &= v_F \sqrt{1 + (N-1)Ua_0/\pi v_F}. \end{aligned} \quad (37)$$

The U dependence of the Luttinger parameters K_c and u_c given in the above expressions should not be taken too seriously. Indeed, the continuum limit approach is strictly speaking valid only provided $U/t \ll 1$. In this regime one has

$$\begin{aligned} K_c &\sim 1 - (N-1) \frac{Ua_0}{2\pi v_F}, \\ u_c &\sim v_F + (N-1) \frac{Ua_0}{2\pi}. \end{aligned} \quad (38)$$

The physically relevant question is now what happens for higher values of the interaction U . In the absence of umklapp terms, the accepted view is that the effect of interaction corresponds to a renormalization of the Luttinger parameters K_c and u_c as well as the spin velocity u_s which have therefore to be thought as phenomenological parameters as the Landau coefficients in the Fermi-liquid theory.^{7,8} These parameters completely characterize the low energy properties of the metallic phase as we shall see now. Let us first discuss the electronic Green's function defined by

$$G_{ab}(x, \tau) = \langle \psi_a^\dagger(x, \tau) \psi_b(0, 0) \rangle, \quad (39)$$

τ being the imaginary time. This correlation function can be computed using Eqs. (9), (29), and (31). After some calculations, one finds

$$\begin{aligned} G_{ab}(x, \tau) \sim & \frac{\delta_{ab}}{2\pi} \left[\frac{1}{x^2 + u_c^2 \tau^2} \right]^{\alpha/2} \left[\frac{\exp(ik_F x)}{(ix + u_c \tau)^{1/N} (ix + u_s \tau)^{1-1/N}} \right. \\ & \left. + \frac{\exp(-ik_F x)}{(-ix + u_c \tau)^{1/N} (-ix + u_s \tau)^{1-1/N}} \right], \end{aligned} \quad (40)$$

where the exponent α is given by

$$\alpha = \frac{1}{2NK_c} (1 - K_c)^2. \quad (41)$$

This allows us to give an estimate of the single particle density of states which is related to the electronic Green's function at $x=0$:

$$\rho(\omega) \sim |\omega|^\alpha. \quad (42)$$

Similarly, K_c determines the singularity of the momentum distribution $n_a(k)$ around the Fermi point k_F :

$$n_a(k) = n_a(k_F) + \text{Cte} \operatorname{sgn}(k - k_F) |k - k_F|^\alpha \quad (43)$$

and the momentum distribution function has a power law singularity at the Fermi level unlike a standard Fermi liquid. This anomalous power law behavior for any finite value of N is inherent of a Luttinger liquid.

The computation of the $SU(N)$ spin-spin correlation function

$$\Delta^{AB}(x, \tau) = \langle \mathcal{S}^A(x, \tau) \mathcal{S}^B(0, 0) \rangle \quad (44)$$

is more involved. It can be shown that the leading asymptotics of this correlation function is given by the $2k_F$ part

$$\Delta^{AB}(x, \tau) \sim \delta^{AB} \frac{\cos(2k_F x)}{(x^2 + u_c^2 \tau^2)^{K_c/N} (x^2 + u_s^2 \tau^2)^{1-1/N}}. \quad (45)$$

We deduce from the above correlation function the low temperature dependence of the NMR relaxation rate T_1

$$\frac{1}{T_1 T} \sim T^{2/N + 2K_c/N - 2}. \quad (46)$$

As seen, once the U dependence of the Luttinger parameters u_c , K_c , and u_s is known, the low energy properties of the metallic phase are entirely determined. These parameters are nonuniversal and cannot be obtained for arbitrary U by the continuum limit approach. Although $K_c < 1$ when $U > 0$, one does not know its minimum value. It is only in the $N=2$ case, that the Luttinger parameters can be extracted from the exact solution.²⁷⁻²⁹ When $N > 2$ no exact solution is available and one has to use numerical computations to estimate these parameters. This will be done for the two cases $N=3$ and $N=4$ in Sec. V. Before doing that, let us discuss the Mott transition that should occur in the problem for a finite critical value of the repulsion U for $N > 2$.

C. The Mott transition

The very difference between the $N=2$ and $N > 2$ cases lies in the fact that there is no umklapp term at half filling in the bare Hamiltonian in the continuum limit. The reason for this is that these terms came with oscillating factors and were omitted for small value of the repulsion. However, in the RG strategy one has to look at the stability of the Luttinger fixed line and any operator that is compatible with the symmetry of the problem should be taken into account: they will be generated during the renormalization process. In our problem, the important symmetries are the $SU(N)$ spin rotation invariance, chiral invariance and translation invariance.

From Eqs. (9), (29), and (30), one easily finds that under a translation by one lattice site, the charge field Φ_c is shifted according to

$$\Phi_c \rightarrow \Phi_c + \sqrt{\frac{\pi}{N}}. \quad (47)$$

Therefore one can add any operator in the charge sector that is invariant under the transformation (47) and will be necessarily generated by higher order in perturbation theory. The operator with the smallest scaling dimension that is invariant under Eq. (47) is

$$\mathcal{H}_{\text{umklapp}} = -G_u : \cos(\sqrt{4\pi N}\Phi_c) :. \quad (48)$$

Other operators, with higher scaling dimensions, that couple spin and charge degrees of freedom may also be included. This is the reason why one cannot exclude the possibility of a charge density wave (CDW) instability. For instance, such processes are present in the extended SU(2) Hubbard model at half filling.³⁰ Although it requires some formal proof, we expect that, due to the fact that in the present model the interaction is local in the density, the leading umklapp contribution should only affect the charge sector. We have checked that this is indeed true for the particular cases, $N=3$ and $N=4$.³¹ We have shown indeed by perturbation theory that the oscillating contributions \mathcal{V}_{2k_F} and \mathcal{V}_{4k_F} generate $6k_F$ and $4k_F$ processes for $N=3$ and $N=4$, respectively. Up to irrelevant operators, the only contribution we found is precisely Eq. (48) with $N=3$ and $N=4$. In any case in what follows, we shall thus make the hypothesis, first made by Affleck,²³ that all the effects of high energy processes are exhausted by Eq. (48) for the general SU(N) case. Consequently, the effective Hamiltonian density in the spin sector is still given by the SU(N)₁ WZNW model and the effective Hamiltonian in the charge sector is now

$$\begin{aligned} \mathcal{H}_c = & \frac{u_c}{2} \left(\frac{1}{K_c} : (\partial_x \Phi_c)^2 : + K_c : (\partial_x \Theta_c)^2 : \right) \\ & - G_u : \cos(\sqrt{4\pi N}\Phi_c) :. \end{aligned} \quad (49)$$

Rescaling the fields as $\Phi_c \rightarrow \Phi_c \sqrt{K_c}$ and $\Theta_c \rightarrow \Theta_c / \sqrt{K_c}$, the Hamiltonian (49) in the charge sector becomes the Hamiltonian of the sine-Gordon model

$$\mathcal{H}_c = \frac{u_c}{2} [: (\partial_x \Phi_c)^2 : + : (\partial_x \Theta_c)^2 :] - G_u : \cos(\sqrt{4\pi N K_c} \Phi_c) :. \quad (50)$$

Since the scaling dimension of the cosine term in Eq. (50) is $\Delta_u = NK_c$, we deduce that a gap opens in the charge sector when

$$K_c = \frac{2}{N}. \quad (51)$$

On the other hand, when $K_c < 2/N$, the umklapp term is irrelevant and the system remains in the metallic phase described in the preceding subsection. Therefore, as U increases, K_c will decrease from 1 at $U=0$ to $K_c=2/N$ at a critical value of the interaction U_c where a Mott transition to an insulating phase occurs. Within this scheme, the phase

transition is expected to be of the KT type. Of course when $U > U_c$, K_c vanishes so that the jump is $1 - 2/N$ and is universal. The present approach cannot give an accurate value of U_c . However, one can get a rough estimate of U_c using Eqs. (11), (37), and (51):

$$\frac{U_c}{t} = \frac{\pi}{2} \frac{N^2 - 4}{N - 1} \sin \frac{\pi}{N}. \quad (52)$$

In the insulating phase, the charge field Φ_c is locked in a special well of the sine-Gordon model (50) and the leading asymptotics of the SU(N) spin-spin correlation functions is now

$$\Delta^{AB}(x, \tau) \sim \lambda_1 \delta^{AB} \frac{\cos(2k_F x)}{(x^2 + u_s^2 \tau^2)^{1-1/N}}, \quad (53)$$

where λ_1 is a nonuniversal constant stemming from the charge degrees of freedom. One recovers the result previously derived by Affleck.²³ The NMR relaxation rate behaves now as $1/(T_1 T) \sim T^{2/N-2}$. Finally, let us note that there are other harmonics $4k_F, 6k_F, \dots$, in the SU(N) spin density (12) that will be generated by higher orders in perturbation theory. Together with the uniform contribution with scaling dimension 1, these terms will give subleading power law contributions in the SU(N) spin-spin correlation function (53). These operators correspond to the primary fields of SU(N)₁ WZNW transforming to another representation of SU(N) than the fundamental one. One should recall that for the SU(N)₁ WZNW, there are $N-1$ primary fields.²⁶ A primary field $\tilde{\phi}_a$ ($a=1, \dots, N-1$) of SU(N)₁ transforms according to the a th basic representation of SU(N) (Young tableau with a boxes and a single column) and has scaling dimension $\Delta_a = a(N-a)/N$. We thus expect the following asymptotics for Δ^{AB} with some nonuniversal constants (λ_a):

$$\begin{aligned} \Delta^{AB}(x, \tau) \sim & - \frac{\delta^{AB}}{8\pi^2} \left(\frac{1}{(u_s \tau - ix)^2} + \frac{1}{(u_s \tau + ix)^2} \right) \\ & + \delta^{AB} \sum_{a=1}^{N-1} \lambda_a \frac{\cos(2ak_F x)}{(x^2 + u_s^2 \tau^2)^{a-a^2/N}} \end{aligned} \quad (54)$$

up to logarithmic contributions originating from the marginal irrelevant current-current interaction in the spin sector.³²

We end this subsection by giving the low-temperature expression of the uniform susceptibility χ and the specific heat of the SU(N) Hubbard model in the insulating antiferromagnetic phase. The continuum density that describes the behavior of the SU(N) spins degrees of freedom in a uniform magnetic field H is given by

$$\mathcal{H}_H = \frac{u_s}{2} \sum_{m=1}^{N-1} [: (\partial_x \Phi_{ms})^2 : + : (\partial_x \Theta_{ms})^2 :] - H \sum_{m=1}^{N-1} \mathcal{J}^m, \quad (55)$$

where we have neglected the marginally irrelevant current-current interaction. In Eq. (55), we have considered a uniform magnetic field along the diagonal \mathcal{T}^m ($m=1, \dots, N-1$) generators of SU(N) that span the Cartan subalgebra of SU(N). According to our normalization convention, they can be written in $N \times N$ diagonal matrices as follows:

$$T^m = \frac{1}{\sqrt{2m(m+1)}} \text{diag}(1, 1, \dots, -m, 0, \dots, 0) \quad (56)$$

with $m = 1, \dots, N-1$ and $-m$ is located on the $m+1$ element of the diagonal. Using the bosonization correspondence (29) and the canonical transformation (31), the total density Hamiltonian (55) in a magnetic field can be written as

$$\begin{aligned} \mathcal{H}_H = & \frac{u_s}{2} \sum_{m=1}^{N-1} [:(\partial_x \Phi_{ms})^2: + :(\partial_x \Theta_{ms})^2:] \\ & - \frac{H}{\sqrt{2\pi}} \sum_{m=1}^{N-1} \partial_x \Phi_{ms}. \end{aligned} \quad (57)$$

Doing the substitution

$$\partial_x \Phi_{ms} \rightarrow \partial_x \Phi_{ms} + \frac{H}{\sqrt{2\pi}u_s}, \quad (58)$$

we obtain the expression of the uniform susceptibility of the $SU(N)$ Heisenberg antiferromagnet

$$\chi = \frac{N-1}{2\pi u_s} \quad (59)$$

which is nothing but $N-1$ times the uniform susceptibility of the $SU(2)$ Heisenberg antiferromagnet. This result is easy to understand since the critical theory in the spin sector corresponds to $N-1$ decoupled massless bosonic modes. Finally, using the general formula of the specific heat at low temperatures for a conformally invariant theory,³³ one has for the $SU(N)$ Heisenberg antiferromagnet

$$C_V = \frac{\pi(N-1)}{3u_s} T. \quad (60)$$

Before closing this section, it is important to emphasize that the Mott transition expected in the bosonization approach relies on the full expression of $K_c(U)$ as function of the interaction. However, one should stress that this parameter cannot be obtained for arbitrary U within this approach and only in the weak coupling limit $U \ll t$ where the model is in its metallic phase. To conclude in favor of the existence of a Mott transition for a finite value of the Coulomb interaction, one has thus to compute $K_c(U)$ of the lattice model by an independent approach. Since the $SU(N)$ Hubbard model with $N > 2$ is not exactly soluble, one cannot determine the expression $K_c(U)$ by the Bethe ansatz as for the standard Hubbard model.²⁷⁻²⁹ We shall thus compute the value $K_c(U)$ of the lattice model using very accurate numerical calculations based on QMC methods described in the next section. In Sec. V, we shall then compare the numerical results with the predictions of the bosonization approach given in this section to conclude on the existence of a Mott transition in the model.

III. THE NUMERICAL APPROACH

In this section we present our improved zero-temperature Green's function Monte Carlo method used for computing ground-state properties. In the first part a sketchy but self-

contained presentation of the basic GFMC method is given. In addition to introducing our notations for the next part, this section will enable the interested reader to understand all the practical aspects of the method. The second part is devoted to the presentation of the generalized GFMC method itself.

A. Green's function Monte Carlo

As already noticed in the Introduction the basic idea of the GFMC method is to extract from a known trial wave function $|\psi_T\rangle$ the exact ground-state component $|\psi_0\rangle$. To do that an operator $G(\mathcal{H})$ acting as a filter is introduced. For continuum problems standard choices are $G(\mathcal{H}) = \exp(-\tau\mathcal{H})$ (diffusion Monte Carlo) or $G(\mathcal{H}) = 1/[1 + \tau(E - \mathcal{H})]$ (Green's function Monte Carlo). For a lattice problem or any model with a finite number of states (finite matrix) a natural choice to consider is

$$G(\mathcal{H}) \equiv 1 - \tau(\mathcal{H} - E_T), \quad (61)$$

where τ plays the role of a timestep (a positive constant) and E_T is some reference energy. If τ is chosen sufficiently small and $|\psi_T\rangle$ has a nonzero overlap with the ground state, the exact ground state is filtered out as follows:

$$\lim_{P \rightarrow \infty} G(\mathcal{H})^P |\psi_T\rangle \sim |\psi_0\rangle. \quad (62)$$

This result is easily obtained by expanding $|\psi_T\rangle$ within the complete set of eigenstates of \mathcal{H} .

In Monte Carlo schemes, successive applications of the operator $G(\mathcal{H})$ on $|\psi_T\rangle$ are done using probabilistic rules. These rules are implemented in configuration space where the trial wave function and matrix elements of \mathcal{H} are easily evaluated. In what follows we shall denote by $|i\rangle$ an arbitrary configuration of the system. To give an example, in actual calculations presented below we consider $|i\rangle = |i^{(1)}\rangle \dots |i^{(M)}\rangle$ with $|i^{(a)}\rangle \equiv |n_{1a}, \dots, n_{La}\rangle$ where L is the number of sites, a the $SU(N)$ color index, and n_{ia} the occupation number of site i ($n_{ia} = 0$ or 1) for the species a .

In this work Hamiltonians considered are of the form

$$\mathcal{H} = T + V, \quad (63)$$

where T is the kinetic term (a nondiagonal operator) and V is a (diagonal) potential term. For fermions in one dimension it is known that by choosing a suitable labeling of the sites, nonzero matrix elements of the kinetic term can all be made negative

$$\langle i|T|j\rangle \leq 0 \quad (i \neq j). \quad (64)$$

A most important consequence of this property is that the exact ground state has a constant sign. In other words, simulations presented here are free of the sign problem.

Let us now introduce the following transition probability:

$$P_{i \rightarrow j}(\tau) = \psi_T(j) \langle j|[1 - \tau(\mathcal{H} - E_L)]|i\rangle \frac{1}{\psi_T(i)}, \quad (65)$$

where $\psi_T(i)$ are the components of the vector $|\psi_T\rangle$, $\psi_T(i) \equiv \langle i|\psi_T\rangle$, and E_L is a diagonal operator called the local energy and defined as follows:

$$\langle i|E_L|j\rangle = \delta_{ij} E_L(i)$$

with

$$E_L(i) = \frac{\langle i | \mathcal{H} | \psi_T \rangle}{\langle i | \psi_T \rangle}. \quad (66)$$

Note the important relation associated with the definition of the local energy

$$(\mathcal{H} - E_L) | \psi_T \rangle = 0. \quad (67)$$

To define a transition probability $P_{i \rightarrow j}$ must fulfill the two following conditions. First, the sum over final states $\sum_j P_{i \rightarrow j}$ must be equal to 1. Here, this is true as a direct consequence of Eq. (67). Second, $P_{i \rightarrow j}$ must be positive. To see this and for later use, let us distinguish between the cases $i=j$ and $i \neq j$.

For $i=j$ we have

$$P_{i \rightarrow i}(\tau) = 1 + \tau T_L(i), \quad (68)$$

where $T_L(i) \equiv E_L(i) - H_{ii}$. Using Eq. (63), $T_L(i)$ can be rewritten as

$$T_L(i) = \frac{\langle i | T | \psi_T \rangle}{\langle i | \psi_T \rangle}, \quad (69)$$

$T_L(i)$ is called the local kinetic energy. Because of Eq. (64) it is a negative quantity and the transition probability can be made positive by taking τ sufficiently small. More precisely, the time step must verify

$$0 < \tau < \text{Min}_i[-1/T_L(i)]. \quad (70)$$

Note that the upper bound is a nonzero quantity for a finite system. On the other hand, when $i \neq j$ we have

$$P_{i \rightarrow j}(\tau) = -\tau H_{ij} \frac{\psi_T(j)}{\psi_T(i)} \quad (i \neq j), \quad (71)$$

a positive expression since $\psi_T(i)$ is chosen to be positive and off-diagonal terms H_{ij} are negative [Eq. (64)].

Using expressions (68) and (71) for the transition probability random walks in configuration space can be generated. By averaging over configurations, statistical estimates for various quantities can be defined. A first important example is the calculation of the variational energy associated with $|\psi_T\rangle$ (variational Monte Carlo). The variational energy is defined as

$$E_v(\psi_T) = \frac{\langle \psi_T | \mathcal{H} | \psi_T \rangle}{\langle \psi_T | \psi_T \rangle}. \quad (72)$$

Here, it is rewritten as

$$E_v(\psi_T) = \lim_{K \rightarrow \infty} \frac{1}{K} \sum_{i=1}^K E_L(i) = \langle \langle E_L \rangle \rangle_{(P)}, \quad (73)$$

where $\langle \langle \dots \rangle \rangle_{(P)}$ is the stochastic average over configurations $|i\rangle$ generated using the transition probability P , K being the number of configurations calculated. Equation (73) holds because $\psi_T(i)^2$ is the stationary density of the stochastic process, that is,

$$\sum_i \psi_T(i)^2 P_{i \rightarrow j}(\tau) = \psi_T(j)^2 \quad \forall j. \quad (74)$$

This property is directly verified by using expressions (65) and (67).

As already pointed out, the estimate of the exact energy is based on the stochastic calculation of $[1 - \tau(\mathcal{H} - E_T)]^n | \psi_T \rangle$, Eq. (62). Introducing between each operator in the product the decomposition of the identity over the basis set $1 = \sum_i |i\rangle \langle i|$ and making use of the definition of the transition probability, Eq. (65), we get the following path integral representation:

$$[1 - \tau(\mathcal{H} - E_T)]^P | \psi_T \rangle = \sum_{i_0 \dots i_P} \psi_T(i_0)^2 \prod_{k=0}^{P-1} P_{i_k \rightarrow i_{k+1}} \times \prod_{k=0}^{P-1} w_{i_k i_{k+1}} \frac{1}{\psi_T(i_P)} |i_P\rangle, \quad (75)$$

where the weights w_{ij} are defined as follows:

$$w_{ij} \equiv \frac{\langle i | [1 - \tau(\mathcal{H} - E_T)] | j \rangle}{\langle i | [1 - \tau(\mathcal{H} - E_L)] | j \rangle} \quad (76)$$

or, more explicitly,

$$w_{ij} = 1, \quad i \neq j,$$

$$w_{ii} = \frac{1 - \tau(H_{ii} - E_T)}{1 - \tau[H_{ii} - E_L(i)]}, \quad i = j. \quad (77)$$

From Eq. (62) the exact energy can be obtained as

$$E_0 = \lim_{P \rightarrow \infty} \frac{\langle \psi_T | \mathcal{H} [1 - \tau(\mathcal{H} - E_T)]^P | \psi_T \rangle}{\langle \psi_T | [1 - \tau(\mathcal{H} - E_T)]^P | \psi_T \rangle}, \quad (78)$$

which is rewritten here in terms of stochastic averages as

$$E_0 = \lim_{P \rightarrow \infty} \left\langle \left\langle E_L(i_P) \prod_{k=0}^{P-1} w_{i_k i_{k+1}} \right\rangle \right\rangle_{(P)} / \left\langle \left\langle \prod_{k=0}^{P-1} w_{i_k i_{k+1}} \right\rangle \right\rangle_{(P)}. \quad (79)$$

In order to compute the averages appearing in that expression two strategies can be employed. First, formula (79) can be directly used as it stands: Paths are generated using the transition probability and the local energy at each step is weighted by the quantity $W = \prod_k w_{i_k i_{k+1}}$. This approach where the number of configurations is kept fixed and the weights are carried out along trajectories is usually referred to as the pure diffusion or Green's function Monte Carlo method. For extended systems such as those considered here, this approach is not optimal. Indeed, it is important to sample less frequently regions of configuration space where the total weight is small and to accumulate statistics where it is large. To realize this, a birth-death process (or branching process) associated with the local weight is introduced. In practice, it consists in adding to the standard stochastic move defined by the transition probability, a new step in which the current configuration is destroyed or copied a number of times proportional to the local weight. Denoting m_{ij} the number of copies (multiplicity) of the state j , we take

$$m_{ij} \equiv \text{int}(w_{ij} + \eta), \quad (80)$$

where $\text{int}(x)$ denotes the integer part of x , and η a uniform random number on $(0,1)$. Adding a branching process can be viewed as sampling with a generalized transition probability $P_{i \rightarrow j}^*(\tau)$ defined as

$$\begin{aligned} P_{i \rightarrow j}^*(\tau) &\equiv P_{i \rightarrow j}(\tau) w_{ij} \\ &= \psi_T(j) \langle j | [1 - \tau(\mathcal{H} - E_T)] | i \rangle \frac{1}{\psi_T(i)}. \end{aligned} \quad (81)$$

Of course, the normalization is not constant (the population fluctuates) and P^* is not a genuine transition probability. However, we can still define a stationary density for it. From Eq. (81) we see that the stationary condition is obtained when E_T is chosen to be the exact energy E_0 , and that the density is $\psi_T(i) \psi_0(i)$. Accordingly, by using a stabilized population of configurations the exact energy may be now obtained as

$$E_0 = \langle \langle E_L \rangle \rangle_{(P,w)}. \quad (82)$$

Note the use of an additional subscript w in the average to recall the presence of the branching process.

At this point, we shall not expand further the method. For more details regarding the implementation of GFMC to lattice systems the interested reader is referred to Refs. 19, 34–36. Let us just emphasize on two important aspects. First, there exists a so-called zero-variance property for the energy: The better the trial wave function ψ_T is, the smaller the statistical fluctuations are. In the limit of an exact wave function for which the local energy is a constant, fluctuations entirely disappear (zero variance). From this important remark follows that in any QMC method, it is crucial to optimize as much as possible the trial wave function used. Of course, in practice, a compromise between the complexity of the wave function and the gain in reduction of variance has to be found.

Once a good trial wave function has been chosen, the only room left for improvement is the implementation of the dynamical process itself. In the algorithm presented here the only dynamical parameter which can be adjusted is the time

step τ . In a configuration $|i\rangle$ associated with a small local kinetic energy $T_L(i)$, the system remains in this configuration a relatively large time and a large value of τ is necessary to help the system to escape from it. Unfortunately, because of the constraint (68) ($P_{i \rightarrow j}$ must be positive) configurations with a high local kinetic energy impose a small value of τ . In order to circumvent this difficulty, we propose to integrate out exactly the time evolution of the system when trapped in a given configuration. This idea is developed in the next section.

B. GFMC and Poisson processes

Consider the probability that the system remains in a given configuration i a number of times equal to n . It is given by

$$\begin{aligned} \mathcal{P}_i(n) &\equiv P(i_1 = i, \tau; \dots; i_n = i, \tau; i_{n+1} \neq i, \tau) \\ &= [P_{i \rightarrow i}(\tau)]^n [1 - P_{i \rightarrow i}(\tau)]. \end{aligned} \quad (83)$$

$\mathcal{P}_i(n)$ defines a normalized discrete Poisson distribution. In terms of the local kinetic energy it can be rewritten as

$$\mathcal{P}_i(n) = -\tau T_L(i) \exp\{n \ln[1 + \tau T_L(i)]\}, \quad (84)$$

where the integer n runs from zero to infinity. To describe transitions towards states j different from i we introduce the following escape transition probability:

$$\tilde{P}_{i \rightarrow j} = \frac{P_{i \rightarrow j}(\tau)}{1 - P_{i \rightarrow i}(\tau)}, \quad j \neq i. \quad (85)$$

Using Eqs. (68) and (69) $\tilde{P}_{i \rightarrow j}$ is rewritten in the most explicit form

$$\tilde{P}_{i \rightarrow j} = \frac{H_{ij} \psi_T(j)}{\sum_{k \neq i} H_{ik} \psi_T(k)}, \quad j \neq i. \quad (86)$$

Note that this transition probability is positive, normalized, and independent of the time-step τ . Now, by using both probabilities $\mathcal{P}_i(n)$ and $\tilde{P}_{i \rightarrow j}$, the path integral representation of $G(\mathcal{H})^P | \psi_T \rangle$, formula (75), can be rewritten as

$$\begin{aligned} &[1 - \tau(\mathcal{H} - E_T)]^P | \psi_T \rangle \\ &= \sum_{(i,n) \in \mathcal{C}_P} \psi_T(i_0)^2 \left[\prod_{k=0}^{l-1} \mathcal{P}_{i_k}(n_k) \tilde{P}_{i_k \rightarrow i_{k+1}} \right] \mathcal{P}_{i_l}(n_l) \\ &\quad \times \prod_{k=0}^l w_{i_k}^{n_k} \frac{1}{\psi_T(i_l)} | i_l \rangle, \end{aligned} \quad (87)$$

where the sum is performed over the set of all families of states $(i_0 \dots i_l)$ with multiplicities $(n_0 \dots n_l)$ verifying $\sum_{k=0}^{l-1} (n_k + 1) + n_l = P$. In a given family successive states are different and the variable n_k represents the number of times the system remains in configuration i_k . The set of all families is denoted \mathcal{C}_P and an arbitrary element is written $(i,n) \equiv (i_0 \dots i_l, n_0 \dots n_l)$. Since off-diagonal weights are equal to 1, Eq. (77), a shortened notation for the diagonal weights $w_i \equiv w_{ii}$ has been introduced.

Now, let us remark that the time step τ plays a role in the path integral formula (87) only when the system is trapped

into a given configuration. Indeed, both the escape probability \tilde{P} and the off-diagonal weight w_{ij} are independent of τ . As an important consequence the limit $\tau \rightarrow 0$ and $P \rightarrow \infty$ with $P\tau = t$ can be done exactly. In this limit the discrete Poisson process $\mathcal{P}_i(n)$ defined in Eq. (84) converges to a continuous Poissonian distribution for the variable $\theta = n\tau$

$$\mathcal{P}_i(\theta) = \frac{1}{\bar{\theta}_i} e^{-\theta/\bar{\theta}_i}. \quad (88)$$

In this formula $\bar{\theta}_i$ represents the average time spent in configuration i . In what follows we shall refer to it as the average trapping time, its expression is

$$\bar{\theta}_i = -1/T_L(i). \quad (89)$$

The fact that $\bar{\theta}_i$ is inversely proportional to the local kinetic energy is explained as follows. When the kinetic energy is small the system is almost blocked in its configuration and $\bar{\theta}$ is large. In contrast, when a large kinetic energy is available, the system can escape easily from its current configuration and $\bar{\theta}$ is small. As already remarked the escape transition probability is independent of τ and is therefore not affected by the zero-time-step limit. Finally, after exponentiating the product of weights, the path integral can be rewritten in the form

$$\begin{aligned} & e^{-t(\mathcal{H}-E_T)}|\psi_T\rangle \\ &= \sum_{i_0 \cdots i_l} \int_0^{+\infty} d\theta_0 \cdots \int_0^{+\infty} d\theta_l \psi_T(i_0)^2 \\ & \times \left[\prod_{k=0}^{l-1} \mathcal{P}_{i_k}(\theta_k) \tilde{P}_{i_k \rightarrow i_{k+1}} \right] \mathcal{P}_{i_l}(\theta_l) e^{-\sum_{k=0}^l \theta_k (E_L(i_k) - E_T)} \\ & \times \frac{1}{\psi_T(i_l)} |i_l\rangle \end{aligned} \quad (90)$$

with the constraint that the trapping times verify $\sum_{k=0}^l \theta_k = t$.

In order to compute ground-state properties the limit $t \rightarrow \infty$ must be performed, Eq. (62). In this limit the constraint $\sum_{k=0}^l \theta_k = t$ can be relaxed and, quite remarkably, integrations over the Poisson distributions for the different trapping times can be performed. For large enough time t we obtain

$$\begin{aligned} e^{-t(\mathcal{H}-E_T)}|\psi_T\rangle &\sim_{l \rightarrow \infty} \sum_{i_0 \cdots i_l} \psi_T(i_0)^2 \prod_{k=0}^{l-1} \tilde{P}_{i_k \rightarrow i_{k+1}} \prod_{k=0}^l \tilde{w}_{i_k} \\ &\times \frac{-1}{T_L(i_l)} \frac{1}{\psi_T(i_l)} |i_l\rangle, \end{aligned} \quad (91)$$

where the new integrated weights \tilde{w} are found to be

$$\tilde{w}_i = \frac{T_L(i)}{E_T - H_{ii}}. \quad (92)$$

In the same way as before the exact energy can be obtained as

$$E_0 = \lim_{t \rightarrow \infty} \frac{\langle \psi_T | \mathcal{H} e^{-t(\mathcal{H}-E_T)} | \psi_T \rangle}{\langle \psi_T | e^{-t(\mathcal{H}-E_T)} | \psi_T \rangle}. \quad (93)$$

In terms of stochastic averages it gives

$$E_0 = \lim_{l \rightarrow \infty} \left\langle \left\langle E_L(i_l) \bar{\theta}_i \prod_{k=0}^l \tilde{w}_{i_k} \right\rangle \right\rangle_{(\tilde{P})} / \left\langle \left\langle \bar{\theta}_i \prod_{k=0}^l \tilde{w}_{i_k} \right\rangle \right\rangle_{(\tilde{P})}, \quad (94)$$

where configurations are generated using the escape transition probability \tilde{P} .

As in the standard approach it is preferable to simulate the weights via a branching process. Here also, the reference energy E_T stabilizing the population is given by the exact energy E_0 . The new stationary density is written as

$$\pi(i) \sim \psi_T(i) \psi_0(i) / \bar{\theta}_i \quad (95)$$

up to an immaterial normalization constant. Finally, our estimator for E_0 is

$$E_0 = \frac{\langle \langle \bar{\theta}_i E_L(i) \rangle \rangle_{(\tilde{P}, \tilde{w})}}{\langle \langle \bar{\theta}_i \rangle \rangle_{(\tilde{P}, \tilde{w})}}, \quad (96)$$

where configurations are generated using \tilde{P} and branched with \tilde{w} . Note that the variational energy can be recovered by removing the branching process ($\tilde{w} = 1$)

$$E_v(\psi_T) = \frac{\langle \langle \bar{\theta}_i E_L(i) \rangle \rangle_{(\tilde{P})}}{\langle \langle \bar{\theta}_i \rangle \rangle_{(\tilde{P})}}. \quad (97)$$

IV. COMPUTATIONAL DETAILS

In this section some important aspects of the practical implementation of the GFMC approach to the $SU(N)$ Hubbard model are presented.

A. Hardcore boson Hamiltonian

The Hamiltonian considered here is the one-dimensional $SU(N)$ Hubbard model described by Eq. (1). Simulations are performed for a finite ring of length L . In one dimension the sites can be labeled in such way that the hopping term connects only sites represented by consecutive integers. As a consequence no fermion sign appears, except eventually when a fermion crosses the boundary ($1 \rightarrow L$ or $L \rightarrow 1$). By choosing either periodic or antiperiodic boundary conditions this sign can always be absorbed and our model (1) becomes equivalent to a model made up with hardcore bosons and described by

$$\mathcal{H} = -t \sum_{i=1}^L \sum_{a=1}^N c_{i+1a}^+ c_{ia} + \text{H.c.} + \frac{U}{2} \sum_i \left(\sum_a n_{ia} \right)^2, \quad (98)$$

where c_{ia}^+ creates a hardcore boson of color a on site i , n_{ia} is the occupation number $n_{ia} = c_{ia}^+ c_{ia}$, and $c_{L+ia}^+ \equiv c_{ia}^+$.

B. Trial wave function

As already emphasized a most important aspect of any Monte Carlo scheme is the choice of a good trial wave func-

tion. To guide our choice, let us consider the exact solution at $U=0$. In this case the ground state is obtained by filling N independent Fermi seas consisting of planes waves with momenta $k_n = 2\pi n/L$ ($n=0, \pm 1, \dots$). For a given type of fermion, the ground state can be written as a Vandermonde determinant³⁷ and the following expression for the ground state is obtained:

$$\psi_0^{U=0}(i_1, \dots, i_P) = \prod_{i < i'} \sin \left[\frac{\pi}{L} (i_i - i_{i'}) \right], \quad (99)$$

where i_1, \dots, i_P are the positions of the P fermions on the chain, $i_k = 1, \dots, L$. In terms of occupation numbers the solution can be rewritten as

$$\phi(n_1, \dots, n_L) = e^{t \vec{n} \mathcal{A}_0 \vec{n} / 2}, \quad (100)$$

where the matrix \mathcal{A}_0 of size $(L \times L)$ is given by

$$\mathcal{A}_0(i, i') = \ln \left| \sin \left[\frac{\pi}{L} (i - i') \right] \right|. \quad (101)$$

Note that Eqs. (100) and (101) describe a system of particles interacting via a logarithmic potential (one-dimensional Log gas). The exact ground-state wave function of the complete $SU(N)$ model at $U=0$ is simply obtained by writing the product of the N wave functions (100) associated with each color.

When the Coulomb interaction is switched on, we have chosen to take the same functional form as before for ψ_T

$$\psi_T(\vec{n}) \equiv e^{t \vec{n} A_U \vec{n} / 2}. \quad (102)$$

Here, A_U is an arbitrary matrix of size $(NL \times NL)$. Taking into account the translational and $SU(N)$ symmetries, at most $L+2$ independent variational parameters can be defined. In all GFMC calculations presented in this paper the entire set of parameters has been systematically optimized. To do that, we have generalized the correlated sampling method of Umrigar *et al.*³⁸ along the lines presented in the preceding section. To be more precise, the set of configurations used to calculate the quantities to be minimized (variational energy or variance of \mathcal{H} , see Ref. 38) are generated using the escape transition probability and weighted with the corresponding average trapping times. Doing this, the effective number of configurations is increased and the optimization process is facilitated. We have found that large numbers of parameters can be easily optimized.

C. $O(L)$ algorithm

In the occupation-number representation the numerical effort for calculating the trial wave function $\psi_T(\vec{n})$ is of order $O(L^2)$. To evaluate the local energy the Hamiltonian has to be applied to the vector $|\psi_T\rangle$. Since a given configuration $|\vec{n}\rangle$ is connected by \mathcal{H} to about $O(L)$ states, the total computational cost per Monte Carlo step is about $O(L^3)$. In fact, this cost can be reduced to $O(L)$. To do that, we introduce the following set of $2NL+1$ variables:

$$(\vec{n}, \vec{n}_U, n_0) \equiv \left(\vec{n}, A_U \vec{n}, \frac{t \vec{n} A_U \vec{n}}{2} \right). \quad (103)$$

Using this representation, the wave function is given by e^{n_0} . Configurations connected by the Hamiltonian differ from each other by removing a particle of a given color a on a site i and putting it on a neighboring site j . In the occupation-number language it corresponds to add one to the component ja and remove one to the component ia of vector \vec{n} . For convenience let us introduce the vector $\tilde{\delta}^{(ia)}$ whose components are zero except the component ia which is equal to 1. Using the new variables just defined we have

$$\begin{aligned} (\vec{n}, \vec{n}_U, n_0) \rightarrow & \left(\vec{n} + \tilde{\delta}^{(ja)} - \tilde{\delta}^{(ia)}, \vec{n}_U + A_U \tilde{\delta}^{(ja)} - A_U \tilde{\delta}^{(ia)}, \right. \\ & n_0 + \frac{t(\tilde{\delta}^{(ia)} - \tilde{\delta}^{(ja)}) A_U (\tilde{\delta}^{(ia)} - \tilde{\delta}^{(ja)})}{2} \\ & \left. - t \vec{n}_U (\tilde{\delta}^{(ia)} - \tilde{\delta}^{(ja)}) \right). \end{aligned} \quad (104)$$

In the simulation the set of new variables is stored for each configuration. At each Monte Carlo step they are reactualized using Eq. (104). Finally, the numerical effort is limited to $O(L)$.

V. RESULTS

Let us now present the results for the $SU(2)$, $SU(3)$, and $SU(4)$ Hubbard models. $SU(2)$ results have been obtained by solving numerically the Lieb-Wu equations.¹¹ Other results have been obtained with the GFMC method presented in the previous section. In all calculations we have set $t=1$.

A. Charge gaps

The finite-size charge gap $\Delta_c(N_e, L)$ is defined as

$$\Delta_c(N_e, L) \equiv E_0(N_e + 1, L) + E_0(N_e - 1, L) - 2E_0(N_e, L), \quad (105)$$

where $E_0(N_e, L)$ is the total ground-state energy of a ring of length L with N_e electrons. In this expression $N_e \pm 1$ means that a fermion of an arbitrary color is added to or removed from the system. Denoting N the number of colors, calculations are done for a number of fermions of each color equal to L/N , and therefore for a total density $n \equiv N_e/L$ equal to 1. In order to get the exact charge gap the limit $L \rightarrow \infty$ must be performed. As usual this is done by calculating charge gaps for different sizes and extrapolating to infinity. Here, $SU(3)$ and $SU(4)$ calculations have been done for $L=9, 12, 18, 27$ and $L=8, 16, 24, 32$, respectively. The finite-size gaps have been found to converge almost linearly as a function of the inverse of the size. Accordingly, the limit $L \rightarrow \infty$ of the gap has been obtained from a fit of the data with a linear or quadratic function of $1/L$. Figure 1 presents the charge gaps obtained for $N=2, 3, 4$ as a function of the Coulomb interaction U .

A first important remark concerns the quality of the Monte Carlo simulations. As it can be seen in Fig. 1, the error bars on the different gaps are quite small. A typical value is about 0.001. Errors are small because total energies are calculated with a very high level of accuracy. For example, for the $SU(4)$ model with $L=32$ and $U=0.5$, we get

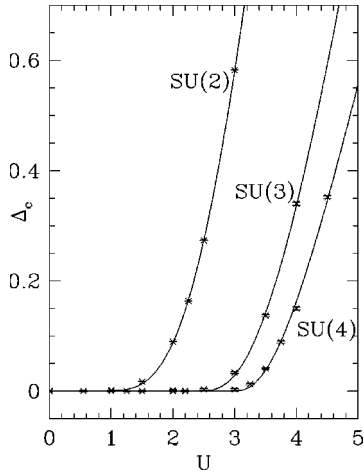


FIG. 1. Charge gaps as a function of the interaction U for the SU(2), SU(3), and SU(4) Hubbard models. The values of the gaps have been extrapolated to $L \rightarrow \infty$ (see text).

$E_0(32,32) = -52.13056(15)$ for a total number of elementary Monte Carlo steps equal to 8×10^7 . Clearly, the relative error of about 3×10^{-6} is very small. In the large U regime where the trial wave function is not expected to be as good as for small U , we still get excellent results. For example, for $U = 4.5$ we get $E_0(32,32) = -23.7118(13)$ (1.6×10^8 MC steps) with a relative error of about 6×10^{-5} . Using the standard GFMC method (presented in Sec. III A) we get, for $U = 0.5$, $E_0(32,32) = -52.13050(40)$ and, for $U = 4.5$, $E_0(32,32) = -23.7210(110)$ [in both cases the maximum time-step allowed has been chosen, see Eq. (70)]. The improvement resulting from the new approach, particularly at large U , is noticeable. Finally, using the approach of Trivedi and Ceperley¹⁹ (introduction of the Poisson process but no integration in time) we get for $U = 0.5$ $E_0(32,32) = -52.13041(22)$ and for $U = 4.5$, $E_0(32,32) = -23.7121(30)$. These results illustrate the improvement resulting from the time integration.

Having at our disposal such accurate results we can try to find out whether or not a gap opens for a nonzero value of U . Considering only continuous transitions, two scenarios are possible. A first possibility is to open a gap for any non-zero value of U . In that case we write the gap versus U as follows:

$$\Delta_c = C \exp(-G/U). \quad (106)$$

A second scenario consists in looking for the existence of a KT-type transition at a finite value U_c of the Coulomb interaction. In that case the gap is written as

$$\Delta_c = C_{\text{KT}} \exp\left(-\frac{G_{\text{KT}}}{\sqrt{U-U_c}}\right) \quad (107)$$

for $U > U_c$ and zero otherwise. The three sets of results have been fitted either using Eqs. (106) or (107). The fitting procedure used is a standard one, based on the minimization of a chi-square type function including statistical errors. Our most important conclusion is that all sets of data can be correctly represented within our small statistical errors either using the gapful representation, Eq. (106), or using a KT scenario, Eq. (107), with a not too large value of U_c . For

example, using Eq. (106) possible representations are ($C = 25.313, G = 11.318$), ($C = 274.634, G = 26.745$), and ($C = 515.649, G = 32.755$), for $N = 2, 3$, and 4 , respectively. Although no clear physical content can be given to the magnitude of coefficients, it is nevertheless satisfactory to verify that in the case of SU(2), the gapful (106) leads to not too large values for the coefficients. This should be contrasted with the SU(3) and SU(4) cases for which the parameters are important. Within a KT scenario all data can also be very well fitted. In the case of SU(2) where we know for sure that no KT transition exists, the ‘‘critical value’’ issued from our fits ranges from 0 to about 0.5. For example, a possible representation is given by ($C_{\text{KT}} = 541.310, G_{\text{KT}} = 11.053$, and $U_c = 0.384$). For the SU(3) model accurate representations can be obtained with a value of U_c ranging from 0 to about 2.3 For $U_c = 2.2$ (the value we shall propose later for the critical value) we get ($C_{\text{KT}} = 45.050, G_{\text{KT}} = 6.567$, and $U_c = 2.2$). For SU(4) the interval is larger. Allowed values range from 0 to about 2.9. For $U_c = 2.8$ (our proposed value, see below) we get ($C_{\text{KT}} = 17.889, G_{\text{KT}} = 5.144$, and $U_c = 2.8$). In contrast with the gapful representation, it should be noted that coefficients are now much larger for the SU(2) model than for the SU(3) and SU(4) models.

In conclusion, using accurate values of the gaps no conclusions can be reasonably drawn about the existence or not of a KT-type transition at a finite value of U . Numerical evidence based on other quantities are therefore called for (see next sections). From the fitting of our data the only conclusion we are allowed to draw is that a KT transition is only possible within the range (0,2.3) for SU(3) and within the range (0,2.9) for SU(4). In addition to this, if such a transition actually occurs in both models, we should expect a difference for the critical values given by $U_c[\text{SU}(4)] - U_c[\text{SU}(3)] \sim 0.5 - 0.6$ (see Fig. 1).

B. Spin gap

The spin gap is defined as the change in ground-state energy produced when destroying a fermion of a given color and creating a fermion of a different color [in the SU(2) case it consists in flipping one spin]. Note that in this process the charge number is kept fixed. For a finite system we have

$$\Delta_s(N_e, L) \equiv E_0(N_e \pm 1, L) - E_0(N_e, L), \quad (108)$$

where $N_e \pm 1$ involves an arbitrary pair of electrons of different colors (one created, one destroyed).

For the SU(2) case the system is known from the exact solution to be gapless for an arbitrary value of the interaction strength U . For a number of colors greater than 2, it is an open question. This is an important point since the existence of a gapful regime would very likely indicate the existence of a coupling between spin and charge degrees of freedom. In all calculations performed for $N = 3$ and 4 , and for a coupling constant U ranging from very small to very large values (up to $U = 10$) no evidence for the existence of such a gap has been found. Thus, it can be quite safely concluded that the spin sector of SU(N) $N = 2, 3, 4$ is gapless for an arbitrary interaction in full agreement with the bosonization prediction. To illustrate this point we present in Fig. 2 a typical behavior for the spin gap of SU(3) as a function of $1/L$ at the relatively large value $U = 4.5$ (at least two times greater than the maximal value expected for U_c in the charge

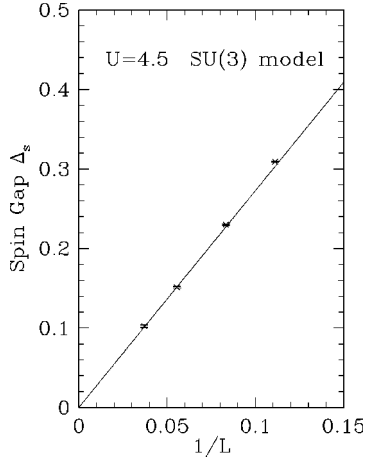


FIG. 2. Spin gap as a function of $1/L$ for the SU(3) Hubbard model at $U=4.5$. The solid line is a linear fit of the data.

sector). The behavior of the gap is essentially linear and extrapolation to the origin leads to a vanishing gap.

C. Luttinger-liquid parameters

In this section we present calculations of the Luttinger liquid parameters u_c and K_c . For that we shall make use of their relations with the compressibility κ and charge stiffness D_c of the system. For a model with N colors [SU(N)] we have the following relations:

$$\frac{\pi u_c}{K_c} \kappa n^2 = \frac{N}{2} \quad (109)$$

and

$$D_c = N u_c K_c, \quad (110)$$

where $n = N_e/L$ (N_e total number of electrons) is the electron density. The compressibility κ is defined as the second derivative of the ground-state energy E_0 with respect to the density of particles

$$\frac{1}{\kappa} = \frac{1}{L} \frac{\partial^2 E_0}{\partial n^2}. \quad (111)$$

A convenient finite-size approximation of the compressibility is

$$\kappa = \frac{L}{N_e^2} \left(\frac{E_0(N_e + N, L) + E_0(N_e - N, L) - 2E_0(N_e, L)}{N^2} \right)^{-1}, \quad (112)$$

where $N_e \pm N$ in E_0 means that N fermions—one of each color—are added to or removed from the system.

The charge stiffness is given by

$$D_c = \frac{\pi}{L} \left. \frac{\partial^2 E_0}{\partial \varphi^2} \right|_{\varphi=0}, \quad (113)$$

where φ is a charge twist in the system. This charge twist is imposed by introducing the following twisted boundary conditions:

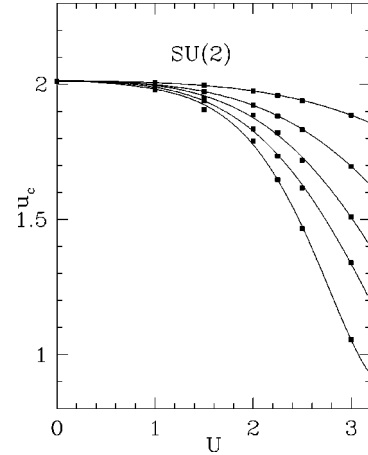


FIG. 3. u_c as a function of U for the SU(2) Hubbard model.

$$c_{i+La}^+ = e^{i\varphi} c_{ia}^+, \quad (114)$$

for an arbitrary site i and color a .

By calculating with GFMC total ground-state energies for different numbers of electrons, formula (112) allows a direct calculation of the compressibility. In contrast, the GFMC calculation of the charge stiffness is more tricky due to the presence of a complex hopping term at the boundary. To circumvent this difficulty we resort to the second-order perturbation-theory expression of the charge stiffness. We have

$$D_c = \frac{\pi}{L} \left(\langle -T \rangle - 2 \sum_{k \neq 0} \frac{|k \langle J | 0 \rangle|^2}{E_k - E_0} \right), \quad (115)$$

where $T = -t \sum (c_{i+1a}^+ c_{ia} + \text{H.c.})$ is the kinetic-energy operator, $J = -it \sum (c_{i+1a}^+ c_{ia} - \text{H.c.})$ is the paramagnetic current operator, $\langle \dots \rangle$ denoting the expectation value in the ground state, all quantities being evaluated at $\varphi=0$. To evaluate the kinetic term we make use of the Hellman-Feynman theorem $\langle T \rangle = E_0 - U(\partial E_0 / \partial U)$. In practice, the following finite-difference expression is used:

$$\langle T \rangle = E_0 - U \left(\frac{E_0(U + \delta U) - E_0(U - \delta U)}{2 \delta U} \right), \quad (116)$$

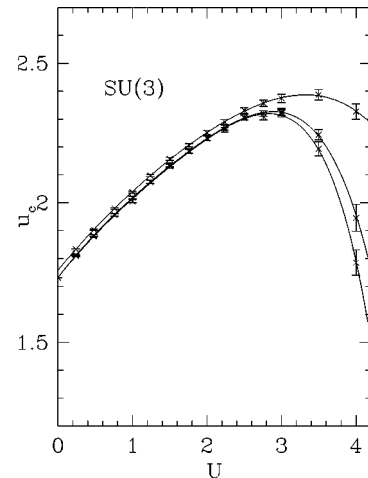
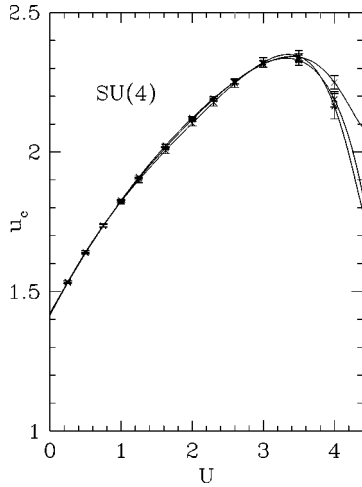


FIG. 4. u_c as a function of U for the SU(3) Hubbard model.

FIG. 5. u_c as a function of U for the SU(4) Hubbard model.

with δU small enough to make higher-order contributions negligible.

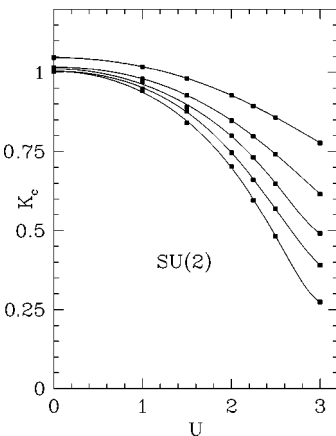
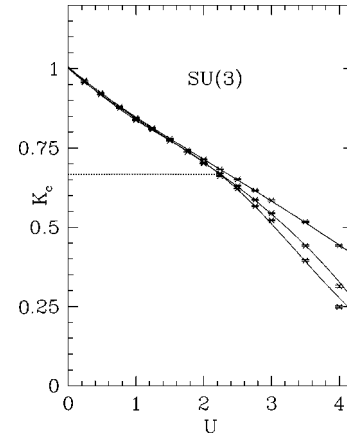
The second-order part of formula (115) can be reinterpreted back as the second-derivative of the total ground-state energy of a new Hamiltonian consisting of the original Hamiltonian plus a perturbation associated with the flux operator J . This leads to the relation

$$\sum_{k \neq 0} \frac{|\langle k|J|0\rangle|^2}{E_0 - E_k} = \frac{1}{2} \frac{\partial^2 \tilde{E}_0(\lambda)}{\partial \lambda^2}, \quad (117)$$

where \tilde{E}_0 is the ground-state energy of the new Hamiltonian defined by

$$\tilde{H} = -(t+\lambda) \sum_{ia} (c_{i+1a}^+ c_{ia}) - (t-\lambda) \sum_{ia} (c_{i-1a}^+ c_{ia}) + V(U) \quad (118)$$

and $V(U)$ is the potential part of the problem. Using formulas (117) and (118) the charge stiffness can now be obtained from a series of GFMC ground-state calculations of total energies of *real* Hamiltonians [more precisely, E_0 , $E_0(\delta U)$, and $E_0(-\delta U)$ for \mathcal{H} , and $\tilde{E}_0(\lambda)$ for \tilde{H} , Eq. (118)]. It should be emphasized that the new Hamiltonian \tilde{H} is real but not symmetric: Left-moving and right-moving electrons do not

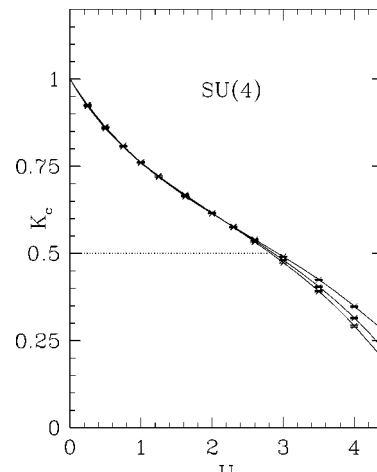
FIG. 6. K_c as a function of U for the SU(2) Hubbard model.FIG. 7. K_c as a function of U for the SU(3) Hubbard model.

have the same velocity. Of course, such a property is easily implemented within a QMC framework.

Figures 3–8 present the Luttinger parameters u_c and K_c for the SU(2), SU(3), and SU(4) Hubbard models as a function of the interaction U and for different sizes L . For the SU(2) model, parameters have been obtained by computing ground-state energies issued from the standard Lieb-Wu equations [computation of the compressibility, formula (112)] and from their generalization to the case of twisted boundary conditions as presented by Shastry and Sutherland³⁹ [computation of the charge stiffness, formula (113)]. For the SU(3) and SU(4) models we have followed the general route just presented above.

A first striking result emerging from the figures is the strong qualitative differences between the general behavior of Luttinger parameters of the SU(2) model on the one hand, and of the SU(3) and SU(4) models, on the other hand. Let us first have a look at the charge velocity u_c .

In the SU(2) case the charge velocity has been calculated for various values of U and for the sizes $L=6, 10, 14, 18,$ and 22 . Results are presented in Fig. 3. The upper curve corresponds to $L=6$, the lower one to the maximum size, $L=22$. In between, the curves are ordered according to the magnitude of L . For a given size L , the charge velocity is found to decrease as a function of U . For a given U , u_c also decreases as a function of the size L . Such a behavior is

FIG. 8. K_c as a function of U for the SU(4) Hubbard model.

quite typical of a gapped system in which collective charge excitations are damped away. In the limit of large sizes, the charge velocity is expected to vanish for a nonzero value of the interaction. The charge velocities of the SU(3) model, Fig. 4, and of the SU(4) model, Fig. 5, display a very similar behavior which is dramatically different from the one observed for SU(2). Starting from their free value at $U=0$ [$u_c=\sqrt{3}$ and $u_c=\sqrt{2}$ for SU(3) and SU(4), respectively], they increase as a function of U with a finite slope at the origin. After some critical value of U both velocities go down quite rapidly. In the first part of the curves (small and intermediate values of U) the charge velocity is found to converge quite rapidly as a function of the size. All curves presented cannot be distinguished within statistical errors. Although the calculations presented here are limited to systems with a maximum size of $L=27$ [SU(3)] or $L=32$ [SU(4)] some preliminary calculations at larger sizes strongly suggest that the values plotted are indeed converged. Such results strongly support the existence of a gapless phase for the SU(3) and SU(4) models. At larger values of U the situation is rather different. The charge velocities decrease quite rapidly both as a function of U and as a function of L . This behavior indicates the existence of a gapped phase. In order to be more quantitative let us have a look at the value of the slope at the origin. The theoretical prediction can be obtained from Eqs. (38). For SU(3) the slope at the origin is found to be 0.32(1), 0.32(1), and 0.33(2) for $L=9, 18,$ and $27,$ respectively. These results are in perfect agreement with the theoretical prediction of $1/\pi \approx 0.318$. For the SU(4) model the slope at the origin is found to be 0.46(1), 0.47(1), and 0.45(2) for $L=16, 24,$ and $32,$ respectively. Here also, the results are in perfect agreement with the theoretical prediction of $3/2\pi \approx 0.477$. Let us now consider our results for K_c . Here also, there exists a common behavior for the cases SU(3) and SU(4), and a different one for SU(2). In the latter case, Fig. 6, K_c decreases either as a function of U or as a function of the size. The slope at the origin, $U=0$, is essentially zero and K_c is expected to vanish at large sizes, except, of course, in the free case. Once again, this behavior is typical of a gapped system. In the two other cases, the situation is rather different. In the same way as for the charge velocity, two regimes can be distinguished, see Figs. 7 and 8. At small and intermediate U , the values of K_c are found to be very well converged within statistical errors as a function of the size L . The curve is smooth with a finite slope at the origin. In the second regime corresponding to larger values of U the curves K_c versus U go down as a function of the size. Clearly, this latter regime corresponds to a gapped phase. Having nearly exact values of K_c up to some critical value U_c for SU(3) and SU(4), the next logical step consists in comparing these values to the predictions of bosonization. A first important prediction was the opening of a gap in the charge sector for a value of K_c equal to $2/N$, Eq. (51). In Fig. 7 corresponding to the SU(3) case, a dashed line has been drawn at the value $K_c=2/3$. The intersection of this line with the curves of K_c appears at about $U_c \sim 2.2$. A most remarkable result is that this value of U is both consistent with the critical value extracted from the calculation of the charge gaps, Fig. 1, but also with the fact that it lies in the domain of U where the values of K_c begin not to converge as a function of the size (a fact usually interpreted as resulting from the

existence of a finite correlation length). A very similar situation is obtained in the SU(4) case. Using the same type of arguments, U_c is found to be around 2.8. When studying charge gaps we had observed a difference of U_c , Fig. 1, between SU(3) and SU(4) of between 0.5 and 0.6. This is in very good agreement with what is found here from independent data on K_c . A second prediction which can be tested is the estimate of the value of U_c itself. Formula (52) gives

$$U_c = \frac{\pi}{2} \frac{N^2 - 4}{N - 1} \sin \frac{\pi}{N}.$$

For $N=3$ and $N=4$ one gets $U_c=3.40$ and $U_c=4.44$, respectively. As already pointed out, these estimates must be considered with caution. However, it should give the correct trend as a function of N . Here, if we look at the ratio $U_c[\text{SU}(4)]/U_c[\text{SU}(3)]$ we get about 1.31 from the theoretical estimate and about 1.27 from our data. The agreement is excellent. Another point which can be checked is the value of the slope at the origin. For the SU(3) case, it is found to be $-0.18(1)$, $-0.19(1)$, and $-0.19(2)$ for $L=9, 18,$ and $27,$ respectively. These results are in very good agreement with the theoretical prediction of $-1/\sqrt{3}\pi \approx -0.183$ given by Eq. (38). For SU(4) we find a slope of $-0.31(1)$, $-0.33(1)$, and $-0.32(2)$ for $L=16, 24,$ and $32,$ respectively. These results are also in total agreement with the theoretical prediction of $-3/2\sqrt{2}\pi \approx -0.337$.

Finally, it can be very useful for interested readers to give some compact and accurate representations of the Luttinger parameters K_c and u_c as a function of U . For both parameters a minimal representation we may think of (see Sec. IIB) is

$$K_c = \frac{1}{\sqrt{1 + k_1 U + k_2 U^2}},$$

$$u_c = v_F \sqrt{1 + u_1 U + u_2 U^2}. \quad (119)$$

For SU(3) we obtain

$$k_1 = 0.33452, k_2 = 0.08789,$$

$$u_1 = 0.37929, u_2 = -0.025509.$$

Note that these values are not too far from the bare values corresponding to Eqs. (37), $k_1^0 = u_1^0 = 2/\pi v_F \approx 0.36755$, $k_2^0 = u_2^0 = 0$.

For SU(4) we obtain

$$k_1 = 0.62065, k_2 = 0.12298,$$

$$u_1 = 0.71486, u_2 = -0.052705$$

to compare to the bare values given by $k_1^0 = u_1^0 = 3/\pi v_F \approx 0.675237$, $k_2^0 = u_2^0 = 0$.

As already discussed we have found no evidences for the opening of a spin gap in the case of the SU(3) and SU(4) models. In other words, the system remains critical with respect to the spin degrees of freedom for any value of the interaction. For these models the slope at the origin is predicted to be equal to $-1/2\pi \approx -0.159$ [Eq. (27)]. Once again, this value has been recovered using our numerical

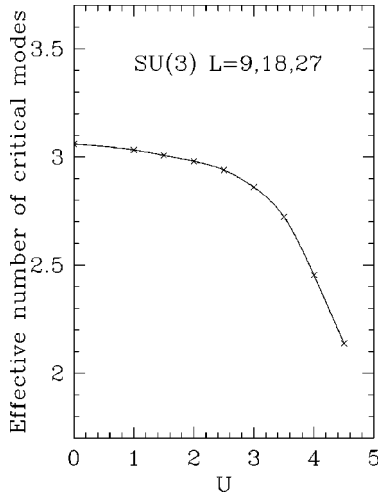


FIG. 9. Effective number of critical modes as a function of U for the SU(3) Hubbard model.

data. To compute the spin velocity we have used the formula expressing the spin gap as a function of the size for a critical system²⁸

$$u_s = \frac{\Delta_s(N_e, L)}{2\pi L}. \quad (120)$$

For SU(3) and SU(4) we get for the slope $-0.18(2)$ and $-0.18(3)$, respectively, in very good agreement with the theoretical prediction.

A final piece of information which can be extracted from our data is related to the way the total ground-state energy converges to its asymptotic value. To be more precise, it is known that the ground-state energy per site $e_0(L)$ of a Luttinger liquid is expected to behave as²⁸

$$e_0(L) \approx e_0(+\infty) - \frac{\pi}{6L^2} \sum_i u_i, \quad (121)$$

where $\sum_i u_i$ denotes the total velocity associated with all critical excitations. In the free case, N degrees of freedom are critical, and the total velocity is equal to Nv_F . When the interaction is turned on, it is possible to follow the evolution of the total velocity as a function of U . This has been done for the SU(3) model. Taking our data for the sizes $L=9, 18$, and 27 the ground-state energy has been fitted with a form adapted to Eq. (121), $e_0 = a - b/L^2$. From this fit an effective number of critical modes can be defined as

$$N_{\text{eff}} = \frac{6b}{\pi v_F}.$$

The result is presented in Fig. 9. Although the transition is not as sharp as for the Luttinger parameters, the loss of one critical mode (passing from 3 to 2) is clearly seen when U varies from zero to infinity. A similar curve may be obtained for the SU(4) case.

VI. CONCLUDING REMARKS

In this work, we have studied the SU(N) generalization of the one-dimensional Hubbard model for repulsive interaction

at half filling. Using a combination of bosonization and QMC results, we have clearly shown that the SU(N) Hubbard model for $N > 2$ behaves very differently from the SU(2) case. Strong numerical and theoretical evidences have been given in favor of a Mott transition, between a metallic and an insulating phase, occurring for a finite value of the Coulomb repulsion $U_c > 0$ for $N > 2$.

The picture emerging from the bosonization approach consists in a spin-charge separation at low energy. The spin degrees of freedom are critical for arbitrary U and described by the SU(N)₁ WZNW model with a central charge $c = N - 1$ ($N - 1$ gapless bosonic modes). The effective theory associated with the charge degrees of freedom corresponds to a sine-Gordon model at $\beta^2 = 4\pi N K_c(U)$. For a small value of the Coulomb interaction U , the interaction is irrelevant. The charge sector is then critical and described by a massless bosonic field. In this weak coupling phase, the system is metallic with anomalous power law behaviors in the physical quantities typical of a Luttinger liquid. For a finite value of the interaction U_c such that $K_c(U_c) = 2/N$, a KT phase transition to an insulating phase is expected in the bosonization approach. In this strong-coupling phase, the charge bosonic field becomes locked and the infinite discrete Z_∞ symmetry related to the periodicity of the potential of the sine-Gordon model is spontaneously broken. The only degrees of freedom that remain critical in this strong coupling phase are the $N - 1$ spin modes and after integrating out the massive charge degrees of freedom, the low-energy theory of the model corresponds to the SU(N) Heisenberg antiferromagnet.

Very accurate numerical simulations based on a generalization of the GFMC method and fully optimized trial wave functions have been performed to obtain the spin and charge gaps, and the Luttinger-liquid parameters as a function of the Coulomb interaction for the SU(2), SU(3), and SU(4) Hubbard models. A metal-insulator phase transition at a finite value U_c is clearly seen for SU(3) ($U_c \sim 2.2$) and SU(4) ($U_c \sim 2.8$) in contrast with the standard SU(2) case. In addition all the results obtained for $N=3$ and $N=4$ are fully consistent with the theoretical framework drawn in Sec. II. This provides an accurate test of the bosonization approach to the SU(N) Hubbard model for small and large values of U . It is therefore natural to expect that the physical picture emerging from the two cases studied here can be extended to *arbitrary* values of N . Thus one may conclude that the occurrence at a finite value of the interaction of a Mott transition of the KT type is *generic* in the SU(N) Hubbard model for $N > 2$ at half filling. In addition, it should be emphasized that the calculations of the Luttinger parameters K_c and u_c presented in Sec. IIB are of very good quality (in particular they are converged as a function of the size) and thus provide an accurate characterization of the low-energy properties of the metallic phase of the SU(3) and SU(4) Hubbard models.

Let us now compare our results with the exact solution of the integrable model based on the SU(N) generalization of the Lieb-Wu Bethe ansatz equations.¹² As discussed in the Introduction, an exact solution of an SU(N) generalization of the Hubbard model is available. Although the underlying lattice Hamiltonian of the model is not known, it involves very likely long-range interactions that dynamically exclude three-electron configurations. The question that naturally arises is whether the physics described by the latter model is

similar, when $N > 2$, to that of the lattice $SU(N)$ Hubbard model that we have studied in this paper. At half filling, the $SU(N)$ integrable model undergoes a *first-order* phase transition, as one varies U , from a metallic to an insulating phase.¹³ This is in disagreement with the KT transition predicted by our analysis. In the metallic phase the integrable model is a Luttinger liquid for every N (Refs. 13,41) with the same physical properties as those obtained by the bosonization approach for the $SU(N)$ Hubbard model. However, the charge stiffness K_c obtained from the Bethe ansatz equations varies between $1/N$ and 1 as U decreases from U_c to 0.^{13,41} The value at the transition ($K_c = 1/N$) is thus two times larger than the value obtained for the $SU(N)$ Hubbard model. This clearly confirms that the integrable model differs from the lattice $SU(N)$ Hubbard model in the charge sector. As already pointed out, this difference should result from the presence of nonlocal interactions in the lattice model associated with the integrable $SU(N)$ model.

Regarding perspectives, it is clearly of interest to further explore the phase diagram of the $SU(N)$ Hubbard model: case of an attractive interaction, dependence on the filling, etc. For an attractive interaction at half filling, bosonization predicts that a phase transition should also occur as $|U|$ varies. For incommensurate fillings, it is easy to see, within the bosonization framework, that the system is a Luttinger liquid for arbitrary N and positive U where the leading asymptotics of the electronic Green's function and spin-spin correlation coincide with those computed in the metallic phase. The situation is less clear for commensurate fillings $k_F = \pi n / (Na_0)$ (N/n being an integer). In the bosonization approach, a gap opens in the charge sector for $K_c = 2n^2/N$. The existence of a Mott transition for commensurate fillings clearly requires the full knowledge of $K_c(U, n)$ of the lattice model. Some preliminary calculations show that there is a very special commensurate filling, $n = N/2$, where no Mott transition exists and for which the charge and spin degrees of freedom are massive for $N > 2$ and arbitrary U .⁴⁰

Let us end by noting a very interesting connection between the metal-insulator transition predicted in the $SU(N)$ Hubbard model and the existence of plateaux in magnetization curves of spin ladders under a strong magnetic field.⁴²⁻⁴⁴ Using the Jordan-Wigner transformation, one can indeed interpret the $SU(N)$ Hubbard model as a N -leg $S = 1/2 XY$ spin ladder in a uniform magnetic field along the z axis and coupled in a symmetric way by Ising interaction. The relation between the Fermi momenta and the magnetization $\langle M \rangle$ (normalized such that the saturation value is ± 1) is $k_F = \pi(1 - \langle M \rangle) / (2a_0)$. The Mott transition found in this work for the $SU(N)$ Hubbard model at half filling corresponds to the appearance of plateaux at $\langle M \rangle = (N-2)/N$ in the magnetization curves of the previous N -leg XY spin ladder. Moreover, the existence of a Mott transition for the $SU(N)$ Hubbard model at commensurate filling will give additional plateaux located at $\langle M \rangle = (N-2n)/N$ in the magnetization curves of the corresponding spin ladder.

ACKNOWLEDGMENTS

We would like to thank A. O. Gogolin and A. A. Nersisyan for valuable discussions and for a related collabora-

tion. This work was supported by the ‘‘Center National de la Recherche Scientifique’’ (CNRS).

APPENDIX

In this appendix, we give some details of computations to establish the separation of spin and charge (24) at the Hamiltonian level in the continuum limit of the $SU(N)$ Hubbard model and fix the expressions of $u_{c,s}$ and $G_{c,s}$ given by Eqs. (27), (28).

1. Sugawara form of the free Hamiltonian

To begin with, we shall recall some basic things on the $SU(N)$ non-Abelian bosonization (for a review see Refs. 23, 24,26). As seen in Sec. II A, the chiral $SU(N)$ spin current $\mathcal{J}_{R,L}^A$ can be expressed in terms of N right-left moving fermions $\psi_{aR,L}$:

$$\mathcal{J}_{R(L)}^A = : \psi_{aR(L)}^\dagger \mathcal{T}_{ab}^A \psi_{bR(L)} : \dots \quad (\text{A1})$$

The left- (right-) moving fermions are holomorphic (antiholomorphic) fields of the complex coordinate ($z = \tau + ix$, τ being the imaginary time): $\psi_{aL}(z), \psi_{aR}(\bar{z})$. These fields are defined by the following OPE's:

$$\begin{aligned} \psi_{aL}^\dagger(z) \psi_{bL}(\omega) &\sim \frac{\delta_{ab}}{2\pi(z-\omega)} + : \psi_{aL}^\dagger \psi_{bL} : (\omega) \\ &\quad + (z-\omega) : \partial \psi_{aL}^\dagger \psi_{bL} : (\omega) + \dots, \\ \psi_{aR}^\dagger(\bar{z}) \psi_{bR}(\bar{\omega}) &\sim \frac{\delta_{ab}}{2\pi(\bar{z}-\bar{\omega})} + : \psi_{aR}^\dagger \psi_{bR} : (\bar{\omega}) \\ &\quad + (\bar{z}-\bar{\omega}) : \bar{\partial} \psi_{aR}^\dagger \psi_{bR} : (\bar{\omega}) + \dots \end{aligned} \quad (\text{A2})$$

with $\partial = \partial_\omega$, $\bar{\partial} = \partial_{\bar{\omega}}$ and there are no singularities in the OPE when one does the fusion of two operators belonging to different sectors.

Let us now consider the OPE between two left $SU(N)$ spin currents, for instance,

$$\begin{aligned} \mathcal{J}_L^A(z) \mathcal{J}_L^B(\omega) &= : \psi_{aL}^\dagger \mathcal{T}_{ab}^A \psi_{bL} : (z) : \psi_{dL}^\dagger \mathcal{T}_{de}^B \psi_{eL} : (\omega) \\ &= \mathcal{T}_{ab}^A \mathcal{T}_{de}^B \psi_{aL}^\dagger(z) \psi_{eL}(\omega) \psi_{bL}(z) \psi_{dL}^\dagger(\omega). \end{aligned} \quad (\text{A3})$$

Using the OPE's (A2), the commutation relation (6), and the normalization of the generators of the $SU(N)$ Lie algebra, one obtains

$$\mathcal{J}_L^A(z) \mathcal{J}_L^B(\omega) \sim \frac{\delta^{AB}}{8\pi^2(z-\omega)^2} + \frac{if^{ABC}}{2\pi(z-\omega)} \mathcal{J}_L^C(\omega). \quad (\text{A4})$$

In the same way, we find for the right spin current

$$\mathcal{J}_R^A(\bar{z}) \mathcal{J}_R^B(\bar{\omega}) \sim \frac{\delta^{AB}}{8\pi^2(\bar{z}-\bar{\omega})^2} + \frac{if^{ABC}}{2\pi(\bar{z}-\bar{\omega})} \mathcal{J}_R^C(\bar{\omega}). \quad (\text{A5})$$

Evaluating these OPE at equal time, one recovers the OPE (15) showing that $\mathcal{J}_{R,L}^A$ are $SU(N)_1$ spin current. With the same procedure, one can compute the OPE between the charge current $\mathcal{J}_{R,L}^0$ using its definition (17) in terms of the underlying fermions

$$\mathcal{J}_L^0(z)\mathcal{J}_L^0(\omega)\sim\frac{N}{4\pi^2(z-\omega)^2},$$

$$\mathcal{J}_R^0(\bar{z})\mathcal{J}_R^0(\bar{\omega})\sim\frac{N}{4\pi^2(\bar{z}-\bar{\omega})^2} \quad (\text{A6})$$

so that the charge current $\mathcal{J}_{R,L}^0$ belongs to the $U(1)_N$ KM algebra.

The next step is to obtain the Sugawara form (20), (21) of the free part of the Hamiltonian (\mathcal{H}_0). Let us consider, for instance, the left sector of the theory since we shall obtain the same result for the right part with the substitution $L \rightarrow R$, $(z, w) \rightarrow (\bar{z}, \bar{w})$ and $\partial \rightarrow \bar{\partial}$. We need now the following OPE for the spin sector:

$$\begin{aligned} \mathcal{J}_L^A(z)\mathcal{J}_L^A(\omega) &:= :\psi_{aL}^\dagger \mathcal{T}_{ab}^A \psi_{bL}:(z) : \psi_{dL}^\dagger \mathcal{T}_{de}^A \psi_{eL}:(\omega) \\ &= \frac{1}{2} \left(\delta_{ae} \delta_{bd} - \frac{1}{N} \delta_{ab} \delta_{de} \right) \\ &\quad \times \psi_{aL}^\dagger(z) \psi_{eL}(\omega) \psi_{bL}(z) \psi_{dL}^\dagger(\omega), \quad (\text{A7}) \end{aligned}$$

where we have used the relation (8). Using Eq. (A2) and keeping also the first regular terms in the fusion, we get

$$\begin{aligned} \mathcal{J}_L^A(z)\mathcal{J}_L^A(\omega) &\sim \frac{N^2-1}{8\pi^2(z-\omega)^2} + \frac{N+1}{2N} : \psi_{aL}^\dagger \psi_{aL} \psi_{bL} \psi_{bL}^\dagger :(\omega) \\ &\quad - \frac{N^2-1}{2\pi N} : \psi_{aL}^\dagger \partial \psi_{aL} :(\omega). \quad (\text{A8}) \end{aligned}$$

Therefore, one obtains

$$:\mathcal{J}_L^A \mathcal{J}_L^A := \frac{N+1}{2N} : \psi_{aL}^\dagger \psi_{aL} \psi_{bL} \psi_{bL}^\dagger : - \frac{N^2-1}{2\pi N} : \psi_{aL}^\dagger \partial \psi_{aL} :. \quad (\text{A9})$$

In the same way, we obtain for the left charge current

$$:\mathcal{J}_L^0 \mathcal{J}_L^0 := - : \psi_{aL}^\dagger \psi_{aL} \psi_{bL} \psi_{bL}^\dagger : - \frac{1}{\pi} : \psi_{aL}^\dagger \partial \psi_{aL} :. \quad (\text{A10})$$

One can eliminate the four fermions terms by considering the following combination:

$$\frac{\pi}{N} : \mathcal{J}_L^0 \mathcal{J}_L^0 : + \frac{2\pi}{N+1} : \mathcal{J}_L^A \mathcal{J}_L^A := - : \psi_{aL}^\dagger \partial \psi_{aL} :. \quad (\text{A11})$$

Since one has $\partial \psi_{aL} = -i \partial_x \psi_{aL}$ within our convention, the identity (A11), the so-called Sugawara form, states that the free Hamiltonian of N relativistic left-moving fermions can be written only as a function of left current-current terms. In the right part, we have also a similar identity

$$\frac{\pi}{N} : \mathcal{J}_R^0 \mathcal{J}_R^0 : + \frac{2\pi}{N+1} : \mathcal{J}_R^A \mathcal{J}_R^A := -i : \psi_{aR}^\dagger \partial_x \psi_{aR} :. \quad (\text{A12})$$

Collecting all terms, we finally obtain the Sugawara form of the free Hamiltonian \mathcal{H}_0 (10):

$$\begin{aligned} &-i(:\psi_{aR}^\dagger \partial_x \psi_{aR}:-:\psi_{aL}^\dagger \partial_x \psi_{aL}:) \\ &= \frac{\pi}{N}(:\mathcal{J}_R^0 \mathcal{J}_R^0 + \mathcal{J}_L^0 \mathcal{J}_L^0:) + \frac{2\pi}{N+1}(:\mathcal{J}_R^A \mathcal{J}_R^A + \mathcal{J}_L^A \mathcal{J}_L^A:). \quad (\text{A13}) \end{aligned}$$

2. Sugawara form of the $SU(N)$ Hubbard Hamiltonian

We shall now investigate the effect of the Hubbard interaction in the continuum limit to fix the expressions (27) and (28) of the velocities ($u_{c,s}$) and the coupling constants ($G_{c,s}$). Using the continuum description of the $SU(N)$ spin density (12), the interacting part (7) is given by dropping all oscillatory contributions:

$$\mathcal{V}_0 = -\frac{Ua_0N}{N+1}(:\mathcal{J}^A :: \mathcal{J}^A : + : \mathcal{N}^A :: \mathcal{N}^{A\dagger} : + : \mathcal{N}^{A\dagger} :: \mathcal{N}^A :). \quad (\text{A14})$$

The OPE between the $2k_F$ parts of the spin density can be computed using Eqs. (13) and (A2) as in the previous subsection. We find up to constant terms

$$\begin{aligned} &:\mathcal{N}^A:(z,\bar{z}) : \mathcal{N}^{A\dagger}:(\omega,\bar{\omega}) + : \mathcal{N}^{A\dagger}:(z,\bar{z}) : \mathcal{N}^A:(\omega,\bar{\omega}) \\ &\sim -\frac{N^2-1}{2\pi N} \frac{z-\omega}{\bar{z}-\bar{\omega}} : \psi_{aL}^\dagger \partial \psi_{aL} :(\omega) \\ &\quad - \frac{N^2-1}{2\pi N} \frac{\bar{z}-\bar{\omega}}{z-\omega} : \psi_{aR}^\dagger \bar{\partial} \psi_{aR} :(\bar{\omega}) \\ &\quad - : \psi_{aL}^\dagger \psi_{aL} \psi_{bR}^\dagger \psi_{bR} :(\omega,\bar{\omega}) \\ &\quad + \frac{1}{N} : \psi_{aL}^\dagger \psi_{bL} \psi_{bR}^\dagger \psi_{aR} :(\omega,\bar{\omega}). \quad (\text{A15}) \end{aligned}$$

Using Eqs. (A9), (A10) and similar equations in the right sector together with the definition of the charge current (17), we end with

$$\begin{aligned} \mathcal{J}^A \mathcal{J}^A + \mathcal{N}^A \mathcal{N}^{A\dagger} + \mathcal{N}^{A\dagger} \mathcal{N}^A &\sim -\frac{N^2-1}{2N^2}(:\mathcal{J}_R^0 \mathcal{J}_R^0 + \mathcal{J}_L^0 \mathcal{J}_L^0:) \\ &\quad + \frac{1}{N}(:\mathcal{J}_R^A \mathcal{J}_R^A + \mathcal{J}_L^A \mathcal{J}_L^A:) \\ &\quad + 2\frac{N+1}{N} \mathcal{J}_R^A \mathcal{J}_L^A \\ &\quad - \frac{N^2-1}{N^2} \mathcal{J}_R^0 \mathcal{J}_L^0. \quad (\text{A16}) \end{aligned}$$

As a consequence, the continuum limit of the $SU(N)$ Hubbard model at half filling exhibits the spin-charge separation

$$\mathcal{H} = \mathcal{H}_c + \mathcal{H}_s \quad (\text{A17})$$

with

$$\mathcal{H}_c = \frac{\pi v_c}{N} (: \mathcal{J}_R^0 \mathcal{J}_R^0 : + : \mathcal{J}_L^0 \mathcal{J}_L^0 :) + G_c \mathcal{J}_R^0 \mathcal{J}_L^0 \quad (\text{A18})$$

and

$$\mathcal{H}_s = \frac{2\pi v_s}{N+1} (: \mathcal{J}_R^A \mathcal{J}_R^A : + : \mathcal{J}_L^A \mathcal{J}_L^A :) + G_s \mathcal{J}_R^A \mathcal{J}_L^A. \quad (\text{A19})$$

The renormalized velocities are given by

$$v_s = v_F - \frac{U a_0}{2\pi},$$

$$v_c = v_F + (N-1) \frac{U a_0}{2\pi}, \quad (\text{A20})$$

whereas the current-current couplings in the charge and the spin sectors are written as

$$G_c = \frac{N-1}{N} U a_0, \quad G_s = -2U a_0. \quad (\text{A21})$$

-
- ¹N. F. Mott, *Metal-Insulator Transitions* (Taylor-Francis, New York, 1990).
- ²F. Gebhard, *The Mott Metal-Insulator Transition* (Springer-Verlag, Berlin, 1997).
- ³M. Imada, A. Fujimori, and Y. Tokura, *Rev. Mod. Phys.* **70**, 1039 (1998).
- ⁴A. Georges, G. Kotliar, W. Krauth, and M. J. Rozenberg, *Rev. Mod. Phys.* **68**, 13 (1996).
- ⁵D. Jérôme and H. J. Schulz, *Adv. Phys.* **31**, 299 (1982).
- ⁶S. Tarucha, T. Saku, Y. Tokura, and Y. Hirayama, *Phys. Rev. B* **47**, 4064 (1993).
- ⁷F. D. M. Haldane, *Phys. Rev. Lett.* **47**, 1840 (1981); *J. Phys. C* **14**, 2585 (1981).
- ⁸For recent reviews, see J. Voit, *Rep. Prog. Phys.* **58**, 977 (1995); H. J. Schulz, G. Cuniberti, and P. Pieri, *cond-mat/9807366* (unpublished).
- ⁹T. Giamarchi, *Phys. Rev. B* **44**, 2905 (1991); T. Giamarchi and A. J. Millis, *ibid.* **46**, 9325 (1992); T. Giamarchi, *Physica B* **230-232**, 975 (1997).
- ¹⁰H. Schulz, in *Strongly Correlated Electronic Materials*, edited by K. S. Bedell *et al.* (Addison-Wesley, New York, 1994), p. 187.
- ¹¹E. H. Lieb and F. Y. Wu, *Phys. Rev. Lett.* **20**, 1445 (1968).
- ¹²P. Schlottmann, *Phys. Rev. B* **45**, 5784 (1992), and references therein.
- ¹³H. Frahm and A. Schadschneider, *J. Phys. A* **26**, 1463 (1993).
- ¹⁴E. Dagotto, *Rev. Mod. Phys.* **66**, 763 (1994).
- ¹⁵*Lectures Notes on "Density-Matrix Renormalization Group,"* Dresden, Germany, 1998, edited by I. Peschel, K. Hallberg, and X. Wang (Springer-Verlag, Berlin, 1999).
- ¹⁶S. R. White, *Phys. Rev. B* **48**, 10 345 (1993).
- ¹⁷S. R. White, *Phys. Rep.* **301**, 187 (1998).
- ¹⁸W. von der Linden, *Phys. Rep.* **220**, 53 (1992).
- ¹⁹Note that some progress has been made recently to eliminate this error for finite quantum systems, see B. B. Beard and U.-J. Wiese, *Phys. Rev. Lett.* **77**, 5130 (1996); N. Trivedi and D. M. Ceperley, *Phys. Rev. B* **41**, 4552 (1990).
- ²⁰M. Beccaria, C. Presillia, G. Fabrizio De Angelis, and G. Jonas-Lasinio, *cond-mat/9810347* (unpublished).
- ²¹W. Krauth and O. Pluchery, *J. Phys. A* **27**, L715 (1994).
- ²²W. Krauth and M. Mézard, *Z. Phys. B* **97**, 127 (1995).
- ²³I. Affleck, *Nucl. Phys. B* **265**, 409 (1986); I. Affleck and F. D. M. Haldane, *Phys. Rev. B* **36**, 5291 (1987); I. Affleck, *Nucl. Phys. B* **305**, 582 (1988).
- ²⁴For a review, see, for instance, A. M. Tsvelik, *Quantum Field Theory in Condensed Matter Physics* (Cambridge University Press, Cambridge, 1995); A. O. Gogolin, A. A. Nersesyan, and A. M. Tsvelik, *Bosonization and Strongly Correlated Systems* (Cambridge University Press, Cambridge, 1998).
- ²⁵B. Sutherland, *Phys. Rev. B* **12**, 3795 (1975).
- ²⁶P. Di Francesco, P. Mathieu, and D. Sénéchal, *Conformal Field Theory* (Springer-Verlag, Berlin, 1997).
- ²⁷H. J. Schulz, *Phys. Rev. Lett.* **65**, 2462 (1990).
- ²⁸H. Frahm and V. E. Korepin, *Phys. Rev. B* **42**, 10 553 (1990).
- ²⁹N. Kawakami and S. K. Yang, *J. Phys.: Condens. Matter* **3**, 5983 (1991).
- ³⁰J. Voit, *Phys. Rev. B* **45**, 4027 (1992).
- ³¹P. Azaria, A. O. Gogolin, P. Lecheminant, and A. A. Nersesyan, *cond-mat/9903047*, *Phys. Rev. Lett.* (to be published).
- ³²C. Itoi and M.-H. Kato, *Phys. Rev. B* **55**, 8295 (1997).
- ³³H. W. J. Blote, J. L. Cardy, and M. P. Nightingale, *Phys. Rev. Lett.* **56**, 742 (1986); I. Affleck, *ibid.* **56**, 746 (1986).
- ³⁴J. Carlson, *Phys. Rev. B* **40**, 846 (1989).
- ³⁵M. Gross, E. Sanchez-Velasco, and E. Siggia, *Phys. Rev. B* **39**, 2484 (1989).
- ³⁶K. J. Runge, *Phys. Rev. B* **45**, 7229 (1992).
- ³⁷M. Ogata and H. Shiba, *Phys. Rev. B* **41**, 2326 (1990).
- ³⁸C. J. Umrigar, K. G. Wilson, and J. W. Wilkins, *Phys. Rev. Lett.* **60**, 1719 (1988).
- ³⁹B. S. Shastry and B. Sutherland, *Phys. Rev. Lett.* **65**, 243 (1990).
- ⁴⁰N. Kawakami, *Phys. Rev. B* **47**, 2928 (1993); T. Fujii, Y. Tsukamoto, and N. Kawakami, *cond-mat/9811189* (unpublished).
- ⁴¹R. Assaraf, P. Azaria, M. Caffarel, and P. Lecheminant (unpublished).
- ⁴²M. Oshikawa, M. Yamanaka, and I. Affleck, *Phys. Rev. Lett.* **78**, 1984 (1997).
- ⁴³K. Totsuka, *Phys. Lett. A* **228**, 103 (1997); *Phys. Rev. B* **57**, 3454 (1998).
- ⁴⁴D. C. Cabra, A. Honecker, and P. Pujol, *Phys. Rev. Lett.* **79**, 5126 (1997); *Phys. Rev. B* **58**, 6241 (1998).

S. R. Assaraf and M. Caffarel, “Zero-variance principle for Monte Carlo algorithms”, *Phys. Rev. Lett.* **83**, 4682 (1999)

Zero-Variance Principle for Monte Carlo Algorithms

Roland Assaraf* and Michel Caffarel†

CNRS-Laboratoire de Chimie Théorique Tour 22-23, Université Pierre et Marie Curie,
4 place Jussieu, 75252 Paris Cedex 05, France

(Received 7 June 1999)

We present a general approach to greatly increase at little cost the efficiency of Monte Carlo algorithms. To each observable to be computed we associate a renormalized observable (improved estimator) having the same average but a different variance. By writing down the zero-variance condition a fundamental equation determining the optimal choice for the renormalized observable is derived (zero-variance principle for each observable separately). We show, with several examples including classical and quantum Monte Carlo calculations, that the method can be very powerful.

PACS numbers: 02.70.Lq, 05.10.Ln, 05.50.+q, 75.40.Mg

Since the pioneering work of Metropolis *et al.* [1] Monte Carlo methods have been widely used in many areas of natural sciences. At the root of Monte Carlo methods lies a very efficient stochastic method for calculating many-dimensional integrals (or sums) written under the general form

$$\langle O \rangle \equiv \frac{\int_S dx \pi(x) O(x)}{\int_S dx \pi(x)}, \quad (1)$$

where $O(x)$ is some arbitrary observable (real-valued function) defined on the configuration space S (continuous or discrete) and $\pi(x)$ some probability distribution. In Monte Carlo methods the integrals are evaluated using a large but finite set of configurations $\{x^{(i)}\}_{i=1,N}$ distributed according to π and generated by a step-by-step stochastic procedure (Markov chain),

$$\langle O \rangle = \frac{1}{N} \sum_{i=1}^N O[x^{(i)}] + \delta O, \quad (2)$$

where δO is the statistical error associated with the finite statistics. For a large enough number N of Monte Carlo steps, standard statistical arguments lead to the following expression of the error:

$$\delta O = K \frac{\sigma(O)}{\sqrt{N}}, \quad (3)$$

where K is some positive constant proportional to the amount of correlation between configurations, and $\sigma(O)$ is a measure of the fluctuations of the observable,

$$\sigma(O) \equiv \sqrt{\langle O^2 \rangle - \langle O \rangle^2}. \quad (4)$$

In this Letter, it is shown that by introducing a suitably renormalized observable $\tilde{O}(x)$ the statistical error can be drastically reduced and even suppressed, thus defining a zero-variance principle for the Monte Carlo calculation of observables. To realize this, a trial operator H and a trial function $\psi(x)$ are introduced (a trial matrix and a trial vector in the discrete case). The operator H is supposed to be Hermitian (in all practical applications, real symmetric) and is chosen such that

$$\int dy H(x, y) \sqrt{\pi(y)} = 0. \quad (5)$$

On the other hand, the trial function $\psi(x)$ is a rather arbitrary function which is simply supposed to be integrable.

Now, the renormalized observable $\tilde{O}(x)$ associated with the observable $O(x)$ is defined as follows:

$$\tilde{O}(x) = O(x) + \frac{\int dy H(x, y) \psi(y)}{\sqrt{\pi(x)}}. \quad (6)$$

As a direct consequence of Eq. (1) and of the very definition of the Hermitian operator H , Eq. (5), we have the important property

$$\langle \tilde{O} \rangle = \langle O \rangle. \quad (7)$$

In other words, both quantities $O(x)$ and $\tilde{O}(x)$ can be used as estimators of the desired average. However, the statistical errors, which are controlled by $\sigma(O)$ and $\sigma(\tilde{O})$, can be very different. The optimal choice for (H, ψ) is obtained by imposing the renormalized function to be constant and equal to the exact average. This leads to the following fundamental equation:

$$\begin{aligned} \int dy H(x, y) \psi(y) &= -[O(x) - \langle O \rangle] \sqrt{\pi(x)} \\ \Leftrightarrow \sigma(\tilde{O}) &= 0. \end{aligned} \quad (8)$$

At this point it should be emphasized that the idea of using renormalized estimators for reducing the variance is not new. A number of applications have been performed using various “improved” estimators having a lower variance (see, e.g., [2,3]). The basic idea is to construct new estimators by integrating out some intermediate degrees of freedom and, therefore, removing the corresponding source of fluctuations. However, to the best of our knowledge, no general and systematic approach based on a zero-variance principle and valid for any type of Monte Carlo methods has been proposed so far.

In this work the following strategy is proposed. First, a Hermitian operator H verifying (5) is chosen. Second, some approximate solution of Eq. (8) is searched for. The various parameters entering ψ are then optimized by minimizing the fluctuations of the renormalized observable over a finite set of points distributed according to π and obtained from a short Monte Carlo calculation. Finally, a standard much longer Monte Carlo simulation is performed using $\tilde{O}(x)$ instead of $O(x)$ as estimator.

Choice of H .—Clearly, a large variety of choices are possible for the trial operator H . For Monte Carlo algorithms satisfying the detailed balance condition (in practice, the vast majority of MC schemes) a very natural choice is at our disposal. Denoting $p(x \rightarrow y)$ the transition probability distribution defining the Monte Carlo dynamics, the detailed balance condition is written as $\pi(x)p(x \rightarrow y) = \pi(y)p(y \rightarrow x)$ for all pairs (x, y) in configuration space. A most natural operator to consider is

$$H(x, y) = \sqrt{\frac{\pi(x)}{\pi(y)}} [p(x \rightarrow y) - \delta(x - y)]. \quad (9)$$

From the detailed balance condition it follows that the operator H is symmetric, $H(x, y) = H(y, x)$. The fundamental property (5) is verified since the sum-over-final states for a transition probability is equal to one. For continuous systems Schrödinger-type Hamiltonians can also be considered

$$H = -\frac{1}{2} \sum_{i=1}^d \frac{\partial^2}{\partial x_i^2} + V(x), \quad (10)$$

where $V(x)$ is some local potential constructed to fulfill condition (5):

$$V(x) = \frac{1}{2\sqrt{\pi(x)}} \sum_{i=1}^d \frac{\partial^2 \sqrt{\pi(x)}}{\partial x_i^2}, \quad (11)$$

where d is the number of degrees of freedom. Note that in Eq. (10), H is written using the standard quantum-mechanical notation for a *local* Hamiltonian in the x -space realization.

Choice of ψ .—Once the operator H has been chosen, the optimal choice for ψ is the exact solution of the fundamental equation. Of course, in practice only approximate solutions are available. What particular form to choose for ψ is very dependent on the problem at hand, on the type of observables considered, and also on the form chosen for the trial operator H . However, a most important point to be stressed is that the global normalization factor associated with ψ is a pertinent parameter of the trial function. Minimizing the fluctuations of the renormalized function $\sigma(\tilde{O})$ with respect to it, we get

$$\sigma(\tilde{O})^2 = \sigma(O)^2 - \frac{\left\langle \frac{O(x) \int dy H(x, y) \psi(y)}{\sqrt{\pi(x)}} \right\rangle^2}{\left\langle \left(\frac{\int dy H(x, y) \psi(y)}{\sqrt{\pi(x)}} \right)^2 \right\rangle}. \quad (12)$$

The correction to $\sigma(O)^2$ being negative, we obtain the important result that, whatever the choice made for the trial function (even the most unphysical one), the optimization of the multiplicative factor always leads to a reduction of the statistical error.

Our first application concerns the Monte Carlo calculation of the internal energy of the standard 2D Ising model at various temperatures and linear sizes $L = 5, 10, 20$, and 25. The observable considered is the en-

ergy function given by $E(S) = -\sum_{\langle i, j \rangle} S_i S_j$ (coupling constant $J = 1$, sum limited to nearest neighbors, and periodic boundary conditions). The probability distribution is $\pi(S) = \exp[-\beta E(S)]$ with $\beta = 1/k_B T$. Here, $S \equiv (S_1, \dots, S_N)$ with $S_i = \pm 1$, and $N = L \times L$ is the total number of spins. Simulations have been performed using a Swendsen-Wang-type algorithm [4] (nonlocal updates of clusters of spins). To construct the trial operator H we have chosen to use the transition probability distribution of Monte Carlo algorithms with local updates (“heat-bath”-type algorithms). The probability of flipping the spin $S_i = \pm 1$ at site i is given by

$$p(S_i \rightarrow \epsilon S_i) = \frac{e^{\beta \epsilon S_i \tilde{S}_i}}{e^{\beta S_i \tilde{S}_i} + e^{-\beta S_i \tilde{S}_i}}, \quad (13)$$

where $\epsilon = 1$ (no flip) or -1 (flip), and \tilde{S}_i is the sum of neighboring spin values. With this choice and using Eq. (9) the fundamental equation (8) can be rewritten under the form

$$\sum_{i=1}^N p(S \rightarrow T_i S) [Q(S) - Q(T_i S)] = E(S) - \langle E \rangle, \quad (14)$$

$$\psi(S) = Q(S) \sqrt{\pi(S)},$$

where the application T_i ($i = 1, \dots, N$) describes a flip at site i , and is defined by $T_i(S_1, \dots, S_i, \dots, S_N) = (S_1, \dots, -S_i, \dots, S_N)$. At $\beta = 0$ ($T = \infty$) the transition probability distribution becomes constant and the exact solution is easily found to be $Q(S) = E(S)/2$. For finite temperatures some approximate solution has to be found. Here we introduce for $Q(S)$ a polynomial expansion up to the fourth order in the variables $X = \sum_{i=1}^N S_i$ (magnetization) and $Y = \sum_{i=1}^N g(S_i \tilde{S}_i)$ [“generalized energy,” the usual energy being recovered for $g(x) = x$]. Precisely, we have chosen the form $Q(S) = e^{-Z} \sum_{n+m \leq 4} c_{nm} X^n Y^m$ where $Z = \sum_{i=1}^N h(S_i \tilde{S}_i)$. The set of variational parameters of ψ consists of all coefficients c_{nm} of the polynomial plus the ten possible values of functions g and h . All coefficients have been optimized by minimizing the fluctuations of the renormalized energy $\sigma(\tilde{E})$ defined by (4) and calculated from 2000 to 5000 different spin configurations $S^{(i)}$ drawn according to π . Finally, the last step consists in performing a long Monte Carlo simulation to compute accurately the various quantities. The number of clusters built varies from 10^6 (for the larger size) to 2×10^8 (for the smaller size). Results are presented in Table I. Three different temperatures have been considered. $T = 3$ corresponds to the low-temperature regime, $T = T_c = 4/\ln(\sqrt{2} + 1)$ is the critical temperature for the infinite lattice, and $T = 8$ is in the high-temperature regime of the model. At $T = 3$, our representation is extremely good whatever the size of the lattice considered. The variance associated with the renormalized energy is drastically reduced with respect to the bare value and the gain in computational effort can be as great as ~ 360 . Here, the gain in computational effort is defined as the ratio of the squared statistical errors $(\delta \tilde{E}/\delta E)^2$. In

TABLE I. Internal energies for the 2D Ising model at different temperatures. N is the number of sites. Statistical uncertainties on the last digit are indicated in parentheses.

Size	5×5	10×10	20×20	25×25	$\infty \times \infty$
$T = 3$					
$\sigma(E)^2/N$	1.789(1)	1.777(2)	1.78(1)	1.79(1)	
$\sigma(\tilde{E})^2/N$	0.012 5(4)	0.006 1(1)	0.006 0(2)	0.006 1(2)	
Ratio of variances	~ 143	~ 291	~ 297	~ 293	
$\langle E/N \rangle$	-3.902 044(31)	-3.902 200(55)	-3.902 17(21.4)	-3.902 42(29)	
$\langle \tilde{E}/N \rangle$	-3.902 020(2.4)	-3.902 229(3)	-3.902 25(1.2)	-3.902 22(1.5)	
Gain in computational effort ^a	~ 167	~ 336	~ 318	~ 360	
$\langle E/N \rangle$ Exact value	-3.902 021 4...				-3.902 233 1... ^b
$T = T_c = 4.538 37 \dots$					
$\sigma(E)^2/N$	18.581(4)	25.97(3)	33.1(2)	35.3(2)	
$\sigma(\tilde{E})^2/N$	0.215(2)	4.85(1)	16.5(1)	16.9(2)	
Ratio of variances	~ 86	~ 5.4	~ 2.0	~ 2.1	
$\langle E/N \rangle$	-3.073 34(13)	-2.952 14(33)	-2.890 2(12)	-2.880 0(14)	
$\langle \tilde{E}/N \rangle$	-3.073 45(1.3)	-2.952 36(13)	-2.890 8(7)	-2.878 8(8)	
Gain in computational effort ^a	~ 100	~ 6.4	~ 3	~ 3.1	
$\langle E/N \rangle$ Exact value	-3.073 439 6...				-2.828 427 1... ^b
$T = 8$					
$\sigma(E)^2/N$	13.17(1)	10.96	11.1(2)	10.9(3)	
$\sigma(\tilde{E})^2/N$	0.041	0.455	0.8(1)	0.9(1)	
Ratio of variances	~ 321.2	~ 24	~ 13.9	~ 12	
$\langle E/N \rangle$	-1.164 40(33)	-1.115 56(48)	-1.115 6(20)	-1.116 5(25.6)	
$\langle \tilde{E}/N \rangle$	-1.163 48(1.6)	-1.115 02(8.2)	-1.114 5(4.4)	-1.114 5(5.6)	
Gain in computational effort ^a	~ 425	~ 34	~ 20.7	~ 20.9	
$\langle E/N \rangle$ Exact value	-1.163 492 6...				-1.114 544 4... ^b

^aSee text for definition.^bReference [5].

other words, according to Eq. (3) it represents the factor by which it would be necessary to increase the number of Monte Carlo steps in the standard approach to get the same accuracy. Note that for $L = 5$ our Monte Carlo value coincides with the exact one (computed by exact numeration of the 2^N configurations) with an accuracy of less than 10^{-6} . Note also that our MC values converge as the size is increased to the exact infinite-lattice value as given by the Onsager solution [5]. At $T = 8$ (high-temperature regime) our representation is not as good, but still very satisfactory. As a function of the size, the gain in computational effort converges and a value of about 20 is gotten. At the infinite-lattice critical value the results are less spectacular but still of interest. A converged value of about 3 for the gain in efficiency is obtained. At this temperature the correlation length for the spin variables diverges and more accurate representations for the solution of Eq. (14) are needed. Starting from our basic equation built from a transition probability corresponding to *local* moves we need to resort to approximate solutions which contain in some way the collective spin excitations. Alternatively, we can change our fundamental equation by resorting to a nonlocal transition probability density, and then to a new operator H . A natural choice is, of course, the transition probability of the Swendsen-Wang

algorithm used here to generate configurations. Preliminary calculations show that statistical fluctuations are indeed strongly decreased. However, to sum up analytically all contributions corresponding to the different Swendsen-Wang clusters (action of H on ψ) is very time consuming, and the advantages of the method can be lost. Some approximate scheme is clearly called for; this is left for future development. Finally, a last important point is that the gain in computational effort is found to be systematically greater (by about 50%) than the corresponding ratio of variances. This result is a direct consequence of the fact that the integrated autocorrelation time known to control the amount of correlation between successive measurements (see, e.g., [3]) has been decreased when passing from the bare observable to the renormalized one. Note that a similar behavior has also been obtained in applications based on improved estimators [2,3]. Without entering into the details, it can be shown that this result is directly related to the fact that the fluctuations of the renormalized observable are much smaller than in the bare case.

The second application illustrates the method in the case of a continuous configuration space (calculation of multi-dimensional integrals). We have calculated a mean energy as it appears in the so-called variational Monte Carlo

TABLE II. Energy of the helium atom. All quantities are given in atomic units. Statistical uncertainties on the last digit are indicated in parentheses.

Variational Monte Carlo	
$\sigma(E_L)^2$	0.040 9(2)
$\sigma(\tilde{E}_L)^2$	0.006 88
Ratio of variances	~ 5.9
$\langle E_L \rangle$	-2.896 71(4.8)
$\langle \tilde{E}_L \rangle$	-2.896 74(1.6)
Gain in computational effort ^a	~ 9
Exact Green's function Monte Carlo ^b	
$\sigma(E_L)^2$	0.041 1(9)
$\sigma(\tilde{E}_L)^2$	0.008 55(8)
Ratio of variances	~ 4.9
$\langle E_L \rangle$	-2.903 745(99)
$\langle \tilde{E}_L \rangle$	-2.903 734(33)
Gain in computational effort ^a	~ 9
Exact energy	-2.903 724 377... ^c

^aSee text for definition.

^bReference [9].

^cReference [10].

(VMC) methods [6]. Starting from a quantum Hamiltonian H_Q (to be distinguished from our trial operator H) and a known trial-wave function ψ_T , our purpose is to compute the variational energy E_v associated with ψ_T . E_v can be easily rewritten as an average over the probability distribution ψ_T^2 , $E_v = \langle E_L \rangle$ where $E_L \equiv H_Q \psi_T / \psi_T$ is called the local energy. Here, we consider the case of the helium atom described by the Hamiltonian $H_Q = -1/2(\vec{\nabla}_1^2 + \vec{\nabla}_2^2) - 2/r_1 - 2/r_2 + 1/r_{12}$ (atomic units) with usual notations. As trial wave function a standard form has been chosen [7],

$$\psi_T(\vec{r}_1, \vec{r}_2) = \exp\left[\frac{ar_{12}}{1 + br_{12}} - c(r_1 + r_2)\right] 1s(r_1)1s(r_2), \quad (15)$$

where $1s(r)$ is the Hartree-Fock orbital as given by Clementi and Roetti [8], and the variational parameters have been chosen to be $a = 0.5$, $b = 0.522$, and $c = 0.0706$. As already remarked, a natural choice for the trial Hamiltonian H is a Schrödinger operator admitting ψ_T as ground state, Eqs. (10) and (11). Regarding ψ we have chosen a form similar to the trial wave function multiplied by some function of the potential energy. Configurations are generated using a standard Metropolis algorithm with local moves constructed using a Langevin equation [7]. Results are presented in Table II. It is seen that the introduction of the renormalized local energy increases the efficiency of the Monte Carlo calculation by about 1 order of magnitude.

In the last application it is shown that the method can even be used in exact (zero-temperature) quantum Monte Carlo (QMC) calculations. In QMC a combination of diffusion and branching process is used to construct a stationary density proportional to $\psi_T \psi_0$, where ψ_0 is the exact unknown ground-state wave function. By averaging the local energy over this distribution, an estimate of the exact energy E_0 is obtained [6]. Although the analytical form of the stationary density is no longer known, a renormalized function whose average is identical to that of the bare local energy can still be defined, $\tilde{E}_L = E_L + (H - E_0)\psi / \psi_T$, where H admits ψ_T as eigenvector, $H\psi_T = 0$. Calculations have been done using the exact Green's function Monte Carlo of Ceperley and Alder [9]. Results are presented in Table II. They are of a quality similar to that obtained in the variational case. About 1 order of magnitude in computer time has been gained.

To conclude, we have presented a simple and powerful method to greatly increase at little cost the efficiency of Monte Carlo calculations. The examples presented have been chosen to illustrate the great versatility of the method (discrete and continuous configuration spaces, classical or quantum Monte Carlo, local or nonlocal Monte Carlo updates). Although our examples have only been concerned with total energies, let us emphasize that the zero-variance principle is valid for any type of observable including important quantities such as local properties other than energy, differences of energies, spatial correlation functions, etc.

*Email address: ra@lct.jussieu.fr

†Email address: mc@lct.jussieu.fr

- [1] N. Metropolis, A. W. Rosenbluth, M. N. Rosenbluth, A. H. Teller, and E. Teller, *J. Chem. Phys.* **21**, 1097 (1953).
- [2] M. Sweeny, *Phys. Rev. B* **27**, 4445 (1983); G. Parisi, R. Petronzio, and F. Rapuano, *Phys. Lett. B* **128**, 418 (1983); U. Wolff, *Nucl. Phys.* **B334**, 581 (1990).
- [3] B. Ammon, H. G. Evertz, N. Kawashima, M. Troyer, and B. Frischmuth, *Phys. Rev. B* **58**, 4304 (1998).
- [4] R. H. Swendsen and J. S. Wang, *Phys. Rev. Lett.* **58**, 86 (1987).
- [5] L. Onsager, *Phys. Rev.* **65**, 117 (1944).
- [6] W. von der Linden, *Phys. Rep.* **220**, 53 (1992).
- [7] K. E. Schmidt and J. W. Moskowitz, *J. Chem. Phys.* **93**, 4172 (1990).
- [8] E. Clementi and C. Roetti, *At. Data Nucl. Data Tables* **14**, 177 (1974).
- [9] D. M. Ceperley and B. J. Alder, *J. Chem. Phys.* **64**, 5833 (1984).
- [10] K. Frankowski and C. L. Pekeris, *Phys. Rev.* **146**, 46 (1966).

T. R. Assaraf, M. Caffarel, and A. Khelif, “ Diffusion Monte Carlo Methods with a fixed-number of walkers”, *Phys. Rev. E.* 61 4566 (2000)

Diffusion Monte Carlo methods with a fixed number of walkers

Roland Assaraf,¹ Michel Caffarel,¹ and Anatole Khelif²

¹CNRS, Laboratoire de Chimie Théorique, Université Pierre et Marie Curie, 4 Place Jussieu, 75252 Paris, France

²CNRS, Laboratoire de Logique Mathématique, Université Denis Diderot, 2 Place Jussieu, 75251 Paris, France

(Received 14 June 1999)

In this paper we discuss various aspects of diffusion Monte Carlo methods using a fixed number of walkers. First, a rigorous proof of the divergence of pure diffusion Monte Carlo (PDMC) methods (DMC without branching in which the weights are carried along trajectories) is given. Second, a bias-free Monte Carlo method combining DMC and PDMC approaches, and based on a minimal stochastic reconfiguration of the population, is discussed. Finally, some illustrative calculations for a system of coupled quantum rotators are presented.

PACS number(s): 02.70.Lq, 75.40.Mg

I. INTRODUCTION

Quantum Monte Carlo (QMC) methods are powerful approaches to compute the ground-state properties of quantum systems. They have been applied with success to a great variety of problems including quantum liquids and solids, nuclear matter, spin systems, the electron gas, the electronic structure of small atoms and molecules, etc. (see, e.g., Refs. [1–4]). The basic idea of QMC is to extract from a known trial vector $|\psi_T\rangle$ its exact ground-state component $|\psi_0\rangle$. This is realized by using an operator $G(\mathcal{H})$ acting as a filter,

$$\lim_{L \rightarrow \infty} G(\mathcal{H})^L |\psi_T\rangle \sim |\psi_0\rangle, \quad (1)$$

where \mathcal{H} is the Hamiltonian operator of the system. For problems defined in a continuous configuration space two forms for $G(\mathcal{H})$ are usually introduced; they define the two following types of approaches.

(i) Diffusion Monte Carlo (DMC) methods

$$G(\mathcal{H}) = e^{-\tau(\mathcal{H} - E_T)}. \quad (2)$$

(ii) Green's function Monte Carlo (GFMC) methods

$$G(\mathcal{H}) = \frac{1}{1 + \tau(\mathcal{H} - E_T)}, \quad (3)$$

where E_T is some reference energy and τ plays the role of a time step. For lattice problems or any problem described by a Hamiltonian matrix in a finite linear space, a most natural choice is

$$G(\mathcal{H}) \equiv 1 - \tau(\mathcal{H} - E_T) \quad (4)$$

and the method is usually referred to as lattice Green's function Monte Carlo. Note that the denomination ‘‘projector Monte Carlo’’ is also found in the literature to refer to any of the previous variants of the method. For simplicity we shall use here the general denomination ‘‘diffusion Monte Carlo’’ for QMC methods based on Eq. (1) and present our results for a *finite* linear space with the choice (4) for the operator $G(\mathcal{H})$. All results presented in this paper can be straightforwardly generalized to continuous models.

In a Monte Carlo scheme, successive applications of $G(\mathcal{H})$ are done using probabilistic rules. In short, it is based on the fact that the quantity

$$P_{i \rightarrow j}^*(\tau) \equiv \psi_T(j) \langle j | [1 - \tau(\mathcal{H} - E_T)] | i \rangle \frac{1}{\psi_T(i)} \quad (5)$$

can be viewed as a ‘‘generalized’’ transition probability and can be used to sample stochastically the action of $G(\mathcal{H})$ on an arbitrary vector. This statement can be made more explicit by rewriting $P_{i \rightarrow j}^*(\tau)$ under the form

$$P_{i \rightarrow j}^*(\tau) \equiv P_{i \rightarrow j}(\tau) w_{ij}, \quad (6)$$

where

$$P_{i \rightarrow j}(\tau) \equiv \psi_T(j) \langle j | [1 - \tau(\mathcal{H} - E_L)] | i \rangle \frac{1}{\psi_T(i)} \quad (7)$$

is now a *genuine* transition probability: $P_{i \rightarrow j}(\tau) \geq 0$ and $\sum_j P_{i \rightarrow j} = 1$ (the latter condition is not fulfilled by $P_{i \rightarrow j}^*$, except when $|\psi_T\rangle$ is the exact ground state) and where the quantity w_{ij} is defined as follows:

$$w_{ij} \equiv \frac{\langle i | [1 - \tau(\mathcal{H} - E_T)] | j \rangle}{\langle i | [1 - \tau(\mathcal{H} - E_L)] | j \rangle}. \quad (8)$$

In both expressions E_L is the so-called local energy which plays an important role in any QMC scheme

$$E_L(i) = \frac{\langle i | \mathcal{H} | \psi_T \rangle}{\langle i | \psi_T \rangle}. \quad (9)$$

In order to apply stochastically $G(\mathcal{H})$, two types of approaches have been considered. A first type of approaches consists in using the transition probability $P_{i \rightarrow j}$ to generate successive states and then introducing at each step the quantity w_{ij} as a weight in the averages (‘‘to carry’’ the weights). In this type of approaches the number of configurations (or ‘‘walkers’’) is constant by the very definition of the stochastic process. These methods are usually referred to as pure (no branching) diffusion Monte Carlo (PDMC) methods. In the second type of approach a birth-death (or branching) process associated with the local weight is introduced. In practice, it

consists in adding to the stochastic move defined by the transition probability, a new step in which the current configuration is destroyed or copied a number of times proportional to the local weight w_{ij} . In these methods—generically referred to as the diffusion Monte Carlo method—the number of configurations is no longer constant. Remark that in theory there is no need to go beyond the pure diffusion Monte Carlo method. In practice, this is not true since the numerical experience has shown that for extended and/or complex systems, the efficiency (computer time needed to achieve a given accuracy) is drastically reduced when configurations are let to go to regions of configuration space where the weights are small. In other words, it is important to sample less frequently regions where the total weight is small and to accumulate statistics where it is large. This is the basic reason which motivates the introduction of the branching process and justifies the widespread use of DMC compared to PDMC methods. Now, since in DMC the number of walkers can fluctuate, some sort of population control is required. Indeed, nothing prevents the total population from exploding or collapsing entirely. Various solutions to this problem have been proposed. The most employed approaches consist either in performing from time to time a random deletion/duplication step or in varying slowly the reference energy to keep the average number of walkers approximately constant. In both cases, a finite bias is introduced by the population control step. In order to minimize this undesirable source of error it is important to control the size of population as rarely as possible and in the most gentle way [1].

Very recently, following an idea introduced by Hetherington [5], Sorella and co-workers [6–8] have reconsidered the use of stochastic reconfiguration in diffusion Monte Carlo. Their motivation is to combine the best of both worlds: efficiency of DMC and absence of bias as in PDMC. Their approach is derived within a PDMC framework (the walkers “carry” some weight) but the population is “reconfigured” using specific rules. The reconfiguration is done in a such way that the number of walkers is kept constant at each step.

In this work we present a number of results regarding diffusion Monte Carlo methods and stochastic reconfiguration strategies. First, we present a rigorous proof that any PDMC method is expected to diverge as the simulation time and the number of iterations L [as defined by Eq. (1)] are let to go to infinity. This result is not surprising and has already been realized by a number of authors. However, to our knowledge no rigorous arguments have been given so far to clarify this point. In general, it is stated in a more or less detailed fashion that the variance of the product of weights w_{ij} explodes as the number of iterations is made large. Quite interestingly, the derivation of the proof of the divergence of PDMC presented here shows that this result is in fact far from being trivial. In particular, the proof of the divergence requires some care from a mathematical point of view. Second, we present a variant of the stochastic reconfiguration method which we consider to be a minimal bias-free QMC method combining efficiently PDMC and DMC ideas. This approach is built such as to minimize as much as possible the fluctuations associated with the reconfiguration step and also to recover the PDMC and DMC methods as two well-defined

limits. Finally, we illustrate and compare the respective qualities and drawbacks of the different approaches on some numerical examples.

The organization of the paper is as follows. In Sec. II we give the basic ingredients of the diffusion Monte Carlo methods. Section III is devoted to the derivation of the proof of the divergence of PDMC approaches. Section IV discusses the construction of a DMC method including a minimal reconfiguration process. In Sec. V some practical calculations for a system of coupled quantum rotators are shown. Calculations are intended to illustrate the important aspects of the various DMC approaches discussed in this work. Finally, a summary of our results is presented in Sec. VI.

II. DIFFUSION MONTE CARLO METHODS

In this section we give a very brief account of the main aspects of diffusion Monte Carlo methods. This part is essentially designed to introduce formulas and notations used in the following sections. It will also enable the nonexpert to understand the major steps of DMC approaches. For more detailed presentations of the implementation of DMC to lattice (finite) systems the reader is referred to Refs. [9–12].

A. Pure diffusion Monte Carlo

As already mentioned in the Introduction the basic idea of QMC approaches is to extract from a known trial vector $|\psi_T\rangle$ its exact ground-state component $|\psi_0\rangle$. Note that such approaches are in a very close relation with power-type methods in which the ground-state eigenvector is obtained by applying a large number of times the matrix on an arbitrary initial vector. Here, the major difference is that the basic step (matrix times a vector) is no longer done exactly (the size of the linear space is too large) but in a probabilistic way using a Markov chain. Once the ground-state eigenvector has been determined, a number of properties can be obtained. As an important example, the energy is given by

$$E_0 = \lim_{L \rightarrow \infty} \frac{\langle \psi_T | \mathcal{H} [1 - \tau(\mathcal{H} - E_T)]^L | \psi_T \rangle}{\langle \psi_T | [1 - \tau(\mathcal{H} - E_T)]^L | \psi_T \rangle}. \quad (10)$$

Using the basic formula relating the matrix elements of the Hamiltonian and the “generalized” transition probability already presented in the Introduction, Eqs. (5)–(8), we easily get

$$E_0 = \lim_{L \rightarrow \infty} \frac{\left\langle \left\langle E_L(i_L) \prod_{k=0}^{L-1} w_{i_k i_{k+1}} \right\rangle \right\rangle}{\left\langle \left\langle \prod_{k=0}^{L-1} w_{i_k i_{k+1}} \right\rangle \right\rangle}. \quad (11)$$

In this formula the symbol $\langle \langle \dots \rangle \rangle$ denotes the stochastic average over all realizations of the Markov chain described by $P_{i \rightarrow j}$, Eq. (7). It is easily checked that the stationary density of the process verifying

$$\sum_i \Pi_i P_{i \rightarrow j}(\tau) = \Pi_j \quad (12)$$

is given by

$$\Pi_i = \psi_T(i)^2. \quad (13)$$

The probability of a given realization of the chain corresponding to L steps and a total time of $t = L\tau$ is

$$P[i_0 \rightarrow i_1 \rightarrow \dots \rightarrow i_{L-1} \rightarrow i_L] = \Pi_{i_0} P_{i_0 \rightarrow i_1}(\tau) \cdots P_{i_{L-1} \rightarrow i_L}(\tau). \quad (14)$$

Remark that in the limit $P \rightarrow \infty$ and $\tau \rightarrow 0$ with $t = L\tau$ fixed, this probability defines a functional measure on the set of all ‘‘trajectories’’ of time-length t . View from that point, formula (11) is nothing but a generalized version of the well-known Feynman-Kac formula [13–15]. Using the ergodic (recurrent) property of the Markov chain, the sum-over-all trajectories restricted to a finite time interval can be rewritten as a sum along *one single* arbitrary infinite realization of the chain

$$E_0 = \lim_{L \rightarrow \infty} \frac{\frac{1}{L} \sum_{j=1}^L E_L(j) \prod_{k=0}^{j-1} w_{kk+1}}{1/L \sum_{j=1}^L \prod_{k=0}^{j-1} w_{kk+1}}, \quad (15)$$

where different states are denoted for simplicity as $[0, 1, 2, \dots, L]$. In practice, numerical calculations are based on this formula which is particular simple to implement on a computer. Now, for later use, let us remark that the basic equation (11) can be rewritten as a simple sum-over states under the form

$$E_0 = \sum_i E_L(i) P_i / \sum_i P_i, \quad (16)$$

where the probability P_i associated with a given state i is given by

$$P_i \equiv \lim_{L \rightarrow \infty} \sum_{i_0, i_1, \dots, i_{L-1}} P[i_0 \rightarrow i_1 \rightarrow \dots \rightarrow i_{L-1} \rightarrow i_L] \prod_{k=0}^{L-1} w_{i_k i_{k+1}}, \quad (17)$$

where, for simplicity of notation, state i is identified to state i_L . By using Eqs. (7), (8), (13), and (14) it can be verified that P_i is given by

$$P_i = \psi_T(i) \psi_0(i) \quad (18)$$

up to an immaterial normalization constant. Note that when the weights are all taken to be equal to one, P_i reduces to the stationary density Π_i of the Markov chain as it should be.

B. Diffusion Monte Carlo

In the pure DMC method just described the number of configurations is kept fixed and the weights are carried out along random sequences of states. In DMC approaches the weight is introduced directly into the stochastic process via a birth-death or branching process. In practice, it consists of adding to the standard stochastic move of the PDMC method a new step in which the current configuration is destroyed or copied a number of times proportional to the local weight. Denoting m_{ij} the number of copies (multiplicity) of the state j , we take

$$m_{ij} \equiv \text{int}(w_{ij} + \eta), \quad (19)$$

where $\text{int}(x)$ denotes the integer part of x , and η a uniform random number on $(0, 1)$. In theory, such a process is properly defined only for an infinite number of walkers. Of course, in practice only a large but finite number of walkers (a population) is considered. Adding a branching process can be viewed as sampling directly with the generalized transition probability $P_{i \rightarrow j}^*(\tau)$ defined above, Eq. (5). The fact that its normalization is not constant is responsible for the fluctuations of population. However, a stationary density for this modified process can still be defined. By writing the stationary condition

$$\sum_i P_i P_{i \rightarrow j}^*(\tau) = P_j \quad (20)$$

we see from Eq. (5) that this relation is fulfilled if E_T is chosen to be the exact energy E_0 and for the following stationary density:

$$P_i = \psi_T(i) \psi_0(i). \quad (21)$$

By using a stabilized population of configurations the exact energy may be obtained as

$$E_0 = \langle \langle E_L \rangle \rangle_w. \quad (22)$$

Note the use of an additional subscript w in the average to recall the presence of the branching process. Formally, expressions (16) and (22) for the estimate of the exact energy in PDMC and DMC methods, respectively, are identical. The same for the expressions of the probability P_i of a given state i in both approaches, Eqs. (18), (21). However, there is an essential difference which distinguishes both methods. This is the way that this probability is realized stochastically. In PDMC, the stationary density of the Markov chain is $\Pi = \Psi_T^2$ and P_i represents some effective probability obtained from averaging the weights along trajectories of infinite time-length, formula (17). In DMC, the probability P_i is realized by the stochastic process itself. There is no need to introduce additional weights in averages [see formula (22)]. As a consequence, the DMC approach is a much more stable method from a numerical point of view. The price to pay for that is the introduction of a bias resulting from the population control (done either by random deletion/duplication or smooth variation of the reference energy, see discussion in the Introduction). In contrast, with PDMC there is no need for population control. However, as we shall see in the next section, the method is intrinsically unstable.

III. DIVERGENCE OF THE PDMC

In this section it is shown that the estimate of the effective probability P_i associated with a given state i as defined in PDMC, Eq. (17), does not converge to a finite deterministic value. Let us define $\lambda_n(i)$ ($n \geq 1$) the product of weights between the $(n-1)$ th and n th occurrences of state i in the Markov sequence:

$$\lambda_n(i) \equiv \prod_{l=N_{n-1}}^{N_n-1} w_{i_l i_{l+1}}, \quad (23)$$

where N_k denotes the time index of the Markov chain. Let us denote $X_n(i)$ the total weight associated with all states occurring between time N_{n-1} and time N_n

$$X_n(i) \equiv \sum_{k=N_{n-1}}^{N_n} \prod_{l=N_{n-1}}^{k-1} w_{i_l i_{l+1}}. \quad (24)$$

As an important consequence of the Markov property all pairs of random variables $[X_n(i), \lambda_n(i)]$ are independent and equidistributed (same law). Only random variables X and λ corresponding to the same index n and same state i are dependent. Using the ergodic property of the chain and previous definitions, expression (17) for P_i can be rewritten as

$$P_i(n) \equiv \frac{\lambda_1(i) + \lambda_1(i)\lambda_2(i) + \cdots + \lambda_1(i)\lambda_2(i) \cdots \lambda_n(i)}{X_1(i) + \lambda_1(i)X_2(i) + \cdots + \lambda_1(i)\lambda_2(i) \cdots \lambda_{n-1}(i)X_n(i)} \quad (25)$$

when the number n of occurrences of state i becomes large. Now, our problem is to determine whether or not this quantity has a well-defined limit as n goes to infinity. For reasons we shall understand later, two different cases must be distinguished. Denoting $E[\ln(\lambda)]$ the finite expectation value of the random variable λ we consider separately the two cases $|E[\ln(\lambda)]| > 0$ and $E[\ln(\lambda)] = 0$. Note that the time or state indices are not specified since all random variables λ are independent and of the same law.

A. $|E[\ln \lambda]| > 0$

Let us first consider the case $E[\ln \lambda] > 0$. After some elementary manipulations the inverse of $P_i(n)$ as expressed by Eq.(25) can be rewritten in the equivalent form (same law)

$$\frac{1}{P_i} = \frac{X_1(i) + \frac{X_2(i)}{\lambda_2(i)} + \frac{X_3(i)}{\lambda_2(i)\lambda_3(i)} + \cdots + \frac{X_n(i)}{\lambda_2(i) \cdots \lambda_n(i)}}{\lambda_1(i) + 1 + \frac{1}{\lambda_2(i)} + \frac{1}{\lambda_2(i)\lambda_3(i)} + \cdots + \frac{1}{\lambda_2(i) \cdots \lambda_n(i)}}. \quad (26)$$

Note that, while deriving this expression, subscripts of random variables have been interchanged. Such a manipulation is allowed since random variables are independent and equidistributed. To proceed further we define the following quantities:

$$Y_n \equiv \frac{X_2(i)}{\lambda_2(i)} + \frac{X_3(i)}{\lambda_2(i)\lambda_3(i)} + \cdots + \frac{X_n(i)}{\lambda_2(i) \cdots \lambda_n(i)}$$

and

$$Z_n \equiv 1 + \frac{1}{\lambda_2(i)} + \frac{1}{\lambda_2(i)\lambda_3(i)} + \cdots + \frac{1}{\lambda_2(i) \cdots \lambda_n(i)}. \quad (27)$$

We then have

$$\frac{1}{P_i} = \frac{X_1 + Y_n}{\lambda_1 + Z_n} \quad (28)$$

and

$$\frac{Y_n}{Z_n} = \frac{X_2 + Y_{n-1}}{\lambda_2 + Z_{n-1}}. \quad (29)$$

Let us now suppose that $1/P_i$ converges to a constant. Then it follows that in the limit of large n , the random variables Y_n/Z_n and $(X_1 + Y_n)/(\lambda_1 + Z_n)$ converge to the same constant. Now, since (Y_n, Z_n) are independent of (X_1, λ_1) [and the same for (Y_{n-1}, Z_{n-1}) and (X_2, λ_2)] it follows that the random variables (X_1, λ_1) must reduce to some constants, and the same for all (X_i, λ_i) . This result shows that, except in the trivial case where the weights are equal to one (no branching), P_i cannot converge to a well-defined limit as n goes to infinity. Note that similar arguments can be given in the case $E(\ln \lambda) < 0$, after the transformation $\lambda_i \rightarrow 1/\lambda_i$.

Now, the important remark is that all these arguments are valid only if the random variable Z_n converges to a finite distribution. For our purposes, the convergence of Y_n has not to be considered here since the two conditions (Z_n converges and P_i finite and different from zero) implies the convergence of Y_n . In the case $E[\ln \lambda] > 0$ the convergence of Z_n is a consequence of the law of large numbers. Indeed, according to this theorem, for a given realization of the Markov chain there exist two constants $C > 0$ and $\beta > 1$ such that

$$\lambda_1(i) \cdots \lambda_n(i) \geq C\beta^n \quad (30)$$

for n large enough. As a consequence Z_n converges to a positive and *finite* distribution almost surely. In the case $E[\ln \lambda] = 0$ this is no longer true: Z_n tends to infinity for large n and no direct constraint on the law of random variables X_i or λ_i can be drawn. As a consequence, this case must be treated separately. Before doing that, let us emphasize that this case is in fact general. Indeed, the expectation value of $\ln \lambda$ does not depend on the particular state (as a result of the Markov property) and by multiplying all weights by a suitable constant we can always impose $E(\ln \lambda) = 0$.

B. $E(\ln \lambda) = 0$

To treat this case we try to depart as less as possible from the previous case. For that we introduce some new quantities $\gamma_n(i)$ which will play a role similar to that played by quantities $\lambda_n(i)$, except that by their very definition $\gamma_n(i) \geq C$ where C is some constant strictly greater than 1. As a direct consequence $E(\ln \gamma) > 0$ and arguments similar to those employed previously will be invoked.

Let us define $\gamma_n(i)$ as the product of weights $w_{i_k i_{k+1}}$ between two occurrences of state i such that the ratio of the total product of weights at the two occurrences is greater than the

constant $C > 1$. $\gamma_n(i)$ can be written as

$$\gamma_n(i) = \prod_{l=N_{\phi(n-1)}}^{N_{\phi(n)}-1} w_{i_i l_{l+1}}, \tag{31}$$

where $\phi(n)$ denotes the $\phi(n)$ th occurrence of state i verifying the condition associated with the threshold C . More precisely, $\phi(n)$ is defined as

$$\phi(n) = \inf_{(k > \phi(n-1)+1)} \left\{ \prod_{l=N_{\phi(n-1)+1}}^{N_k} w_{i_i l_{l+1}} > C \right\}. \tag{32}$$

Note that the function $\phi(n)$ is well defined [successive values of $\phi(n)$ are finite] because we have

$$P_i(n) \equiv \frac{U_1(i) + \gamma_1(i)U_2(i) + \dots + \gamma_1(i)\gamma_2(i) \dots \gamma_{n-1}(i)U_n(i)}{V_1(i) + \gamma_1(i)V_2(i) + \dots + \gamma_1(i)\gamma_2(i) \dots \gamma_{n-1}(i)V_n(i)}, \tag{34}$$

where $U_n(i)$ represents the sum of the products of $\lambda(i)$ between the occurrences $\phi(n-1)$ and $\phi(n)$

$$U_n(i) \equiv \sum_{k=N_{\phi(n-1)}}^{N_{\phi(n)}} \prod_{l=N_{\phi(n-1)}}^k \lambda_l(i) \tag{35}$$

and V_n the sum of all weights between the two occurrences

$$V_n(i) \equiv \sum_{k=N_{\phi(n-1)}}^{N_{\phi(n)}} \left[\prod_{l=N_{\phi(n-1)}}^k \lambda_l(i) \right] \frac{X_k(i)}{\lambda_k(i)}. \tag{36}$$

The triplets (U_n, V_n, γ_n) are independent and equidistributed. After some elementary manipulations the inverse of P_i as expressed by Eq. (34) can be rewritten in the equivalent form (same law)

$$\frac{1}{P_i} = \frac{V_1 + T_n}{U_1 + W_n} \tag{37}$$

and

$$\frac{T_n}{W_n} = \frac{V_2 + T_{n-1}}{U_2 + W_{n-1}} \tag{38}$$

with the following definitions:

$$T_n \equiv \frac{V_2(i)}{\gamma_2(i)} + \frac{V_3(i)}{\gamma_2(i)\gamma_3(i)} + \dots + \frac{V_n(i)}{\gamma_2(i) \dots \gamma_n(i)}$$

and

$$W_n \equiv \frac{U_2(i)}{\gamma_2(i)} + \frac{U_3(i)}{\gamma_2(i)\gamma_3(i)} + \dots + \frac{U_n(i)}{\gamma_2(i) \dots \gamma_n(i)}. \tag{39}$$

In order to complete the proof we need to show that the series associated with W_n converges to some finite distribution (as already discussed in the preceding section, the deri-

$$\sup_{1 \leq k \leq n} \sum_{l=1}^k \ln \lambda_l(i) \rightarrow +\infty \tag{33}$$

as $n \rightarrow +\infty$ for a given realization.

This property is a consequence of the theorem (40) which will be presented later. Roughly speaking, what is done here is to extract from the full set of occurrences of state i a subset of occurrences (labeled by the function ϕ) corresponding to a series of ‘‘stopping times’’ along the random sequence. Once more, as a result of the Markov property the random variables $\gamma_n(i)$ are independent and equidistributed. In addition, from their very definition $\gamma_n(i) \geq C > 1$. Using previous definitions we can rewrite P_i as

vation of the convergence of T_n is not necessary). If Z_n converges we can conclude (same arguments as before) that P_i converges to a finite (deterministic) value only if the ratio V_n/U_n is a constant, which is not the case. To do that let us first introduce the following theorem.

Theorem. Let X_l be a family of independent, equidistributed and centered (zero mean) random variables. If all moments of the random variables are finite we have

$$\frac{\sup_{1 \leq k \leq n} \sum_{l=1}^k X_l}{n^\alpha} \rightarrow +\infty \quad \text{as } n \rightarrow +\infty \quad \forall \alpha < \frac{1}{2}. \tag{40}$$

This theorem is a consequence of the central-limit theorem. Using rough arguments we can say that the sum of the independent variables in the numerator converges to some Gaussian distribution with a variance proportional to n and that the greatest value is expected to behave as the square root of the variance \sqrt{n} . As a consequence, the ratio of the numerator and denominator must diverge as soon as $\alpha > 1/2$. Although these arguments are correct, a rigorous derivation is actually not so simple. It requires some mathematical care which is beyond the scope of this work. The derivation will be presented elsewhere [20]. Now, the important point is that the random variables $\ln \lambda_l(i)$ verify the hypotheses of the theorem. They are independent, equidistributed (with zero mean), and as a consequence of the finite variation of the weights and ‘‘stopping times’’ [as defined by the function $\phi(n)$] all their moments are finite. Using the fact that $\phi(n)$ is a series extracted from the full series of occurrences of state i we obtain the following property:

$$\frac{\sup_{1 \leq k \leq \phi(n)} \left[\sum_{l=1}^k \ln \lambda_l(i) \right]}{\phi(n)^\alpha} \rightarrow +\infty \quad \text{as } n \rightarrow +\infty \quad \forall \alpha < \frac{1}{2} \tag{41}$$

or, equivalently,

$$\frac{\sum_{l=1}^n \ln \gamma_l(i)}{\phi(n)^\alpha} \rightarrow +\infty \quad \text{as } n \rightarrow +\infty \quad \forall \alpha < \frac{1}{2}. \quad (42)$$

Note that, in the particular case $\alpha=0$, we recover the property (33), a result which guarantees that the function $\phi(n)$ is well defined. From its definition (35) the series $U_n(i)$ is a sum of at most (but not equal) $\phi(n)$ terms all smaller than the constant C except the last one which is $\gamma_n(i)$. Therefore, we have

$$0 \leq U_n(i) \leq C\phi(n) + \gamma_n(i). \quad (43)$$

From this relation we can write

$$0 \leq \frac{U_n(i)}{\gamma_2(i) \cdots \gamma_n(i)} \leq \frac{C\phi(n)}{\gamma_2(i) \cdots \gamma_n(i)} + \frac{1}{\gamma_2(i) \cdots \gamma_n(i)}. \quad (44)$$

The series of general term $1/\gamma_2(i) \cdots \gamma_n(i)$ is convergent since all $\gamma_n(i)$ are greater or equal to $C > 1$. Regarding the other term $A_n \equiv C\phi(n)/\gamma_2(i) \cdots \gamma_n(i)$ we can write as a result of Eq. (42) that there exists a constant $M(\alpha)$ such that

$$\phi(n) \leq M \left[\sum_{l=1}^n \ln \gamma_l(i) \right]^{1/\alpha} \quad \text{for } 0 < \alpha < \frac{1}{2}. \quad (45)$$

Therefore, we have

$$\frac{C\phi(n)}{\gamma_2(i) \cdots \gamma_n(i)} \leq CM \gamma_1(i) \frac{\left[\ln \prod_{l=1}^n \gamma_l(i) \right]^{1/\alpha}}{\prod_{l=1}^n \gamma_l(i)}. \quad (46)$$

From the fact that the function $[\ln x]^{1/\alpha}/x$ decreases for x large enough and that $\gamma_l > C$ it follows that A_n is bounded from above by $CM \gamma_1(i) [n \ln C]^{1/\alpha}/C^n$, the general term of a convergent series. Finally, we can conclude that the series W_n converges to some finite positive distribution. This result completes our proof of the nonconvergence of the PDMC estimate of the effective probability P_i .

IV. DMC WITH MINIMAL STOCHASTIC RECONFIGURATION

As seen in the previous section PDMC is intrinsically unstable. As already remarked, the basic reason for that is the increase of variance of the products of weights as a function of the number of iterations (or projecting time). However, as illustrated by a number of applications performed using this type of approaches (e.g., Refs. [15,11,16–19]) the method has proven to be very useful. This is the case when the trial wave function is accurate enough to allow the convergence of the various averages before large fluctuations associated with large projecting times arise. When convergence is achieved no finite bias due to a population control process is introduced. In order to make PDMC approaches effective the fluctuations of the weights must be decreased in some way.

Before considering this point, let us determine the dependence of the error as a function of the computational effort in a PDMC scheme. The fluctuations of the weight from iteration n to iteration $n+1$ will be described by the variance β^2 defined as

$$\beta^2 = \frac{\left\langle \left(\frac{w^{(n+1)}}{w^{(n)}} \right)^2 \right\rangle}{\left\langle \frac{w^{(n+1)}}{w^{(n)}} \right\rangle^2}. \quad (47)$$

By definition β is greater or equal to one. The equality is obtained in the optimal case corresponding to constant weights (no branching). Let N be the total number of Monte Carlo steps of the simulation (the computational effort is proportional to N). The systematic error due to a finite projecting time T (number of iterations $L=T/\tau$) is of order $\exp(-T\Delta)$ where Δ is the gap in energy of the model ($\Delta = E_1 - E_0$, where E_0 is the ground-state energy and E_1 the energy of the lowest state having a nonzero overlap with the trial wave function). The statistical error due to the finite statistics on some quantity evaluated at some fixed projecting time T is given by $\beta^T/\sqrt{N}/T$. By equating both errors an estimate of the relation between the computational effort (via N) and a given accuracy ϵ can be obtained. In the large- N limit the relation is easily found to be

$$\epsilon \sim \frac{1}{N^{\gamma/2}}$$

with

$$\gamma = \frac{\Delta}{\ln \beta + \Delta}. \quad (48)$$

When $\beta=1$ (no fluctuations of the weights) $\gamma=1$ and the efficiency of the simulation is optimal: the standard $1/\sqrt{N}$ law of diffusion processes is recovered. As β is increased the efficiency of the simulations can decrease quite rapidly. Accordingly, to enhance the efficiency of PDMC the fluctuations of the weights must be decreased. An elegant solution to this problem has been introduced more than ten years ago by Hetherington [5]. The idea consists in carrying many walkers simultaneously and introducing a global weight associated with the entire population instead of a local weight for each walker. The global weight W is chosen to be the average of the local weights w_{i_l}

$$W_{i_1 \cdots i_M} \equiv \frac{1}{M} \sum_{l=1}^M w_{i_l}, \quad (49)$$

where M is the number of walkers considered (to avoid confusion between various indices only one subscript has been used for individual weights). By increasing the number M of walkers the fluctuations of the global weight is reduced and β as defined in Eq. (47) is decreased. It is easy to check that the quantity $\ln \beta$ decreases as the inverse of the number of walkers. As a consequence of Eq. (48) the gain in computational efficiency can be very important. Now, the method consists in defining a PDMC scheme in the enlarged linear

space defined by the tensorial product (M times) of the initial linear space. In this new space the full transition probability is defined as the tensorial product of individual transition probabilities. Note that no correlation between the stochastic moves of different walkers is introduced at this level. Second, and this is the important point, each individual weight carried by a walker is rewritten as a function of the global weight

$$w_{i_l} = \tilde{w}_{i_l}(i_1 \cdots i_M) W_{i_1 \cdots i_M}$$

with

$$\tilde{w}_{i_l}(i_1 \cdots i_M) = \frac{w_{i_l}}{W_{i_1 \cdots i_M}}. \quad (50)$$

This rewriting allows us to introduce the global weight as a weight common to all walkers and thus to define a standard PDMC scheme in the tensorial product of spaces. To take into account the new weight \tilde{w}_{i_l} a so-called reconfiguration process is introduced. At each step the total population of M walkers is ‘‘reconfigured’’ by selecting with probability proportional to \tilde{w} the same number M of walkers. Note that, at this point, some correlation between different walkers is introduced. Now, let us discuss the two important limits of the algorithm, namely, the case of an infinite number of walkers, $M \rightarrow \infty$ and the case of constant weights, $w_i \rightarrow 1$. When $M \rightarrow \infty$ the global weight converges to its stationary exact value. As a consequence, the different weights \tilde{w} associated with each walker [as given by Eq. (50)] become independent from each other and the reconfiguration process reduces to the usual branching process (19) without population control and systematic bias since the population is infinite. In the limit $w_i \rightarrow 1$ the method does not reduce to the standard PDMC approach. Indeed, the reconfiguration step ‘‘reconfigures’’ the entire population whatever the values of the weights. In order to improve the efficiency of such methods this undesirable source of fluctuations must be reduced and the limit of the exact PDMC should be implemented in the method. For that we divide the population of walkers into two different sets. A first set of walkers corresponds to all walkers verifying $\tilde{w} \geq 1$. These walkers can be potentially duplicated and will be called ‘‘positive’’ walkers. The other walkers verify $0 \leq \tilde{w} < 1$, they can be potentially destroyed and will be called ‘‘negative walkers.’’ The number of reconfigurations is defined as

$$N_{\text{Reconf}} = \sum_{i_+} |\tilde{w}_{i_+} - 1| = \sum_{i_-} |\tilde{w}_{i_-} - 1|, \quad (51)$$

where Σ_{i_+} (Σ_{i_-}) indicates that the summation is done over the set of positive (negative) walkers. The equality in Eq. (51) is a simple consequence of the definition of positive and negative walkers. In practice, an integer number of reconfigurations is obtained by considering $\text{int}(N_{\text{reconf}} + \eta)$, where η is a uniform random number on the interval $(0,1)$. Once the number of reconfigurations has been drawn, N_{reconf} walkers are added to or removed from the current population by drawing separately N_{reconf} walkers among the lists of positive and negative walkers. It is easily verified that by doing this

no source of systematic error has been introduced and that it is equivalent to the original reconfiguration process of Hetherington. However, in contrast with the latter the average number of reconfigurations is kept minimal and, consequently, the efficiency of the simulation is significantly enhanced. In addition, the average number of reconfigurations vanishes as the weights become constant. In other words, the reconfiguration method reduces in this limit to the standard PDMC method. In their recent work Calandra-Buonaura and Sorella [7] (CBS) have proposed to use a reconfiguration process which is essentially identical to that of Hetherington, except that the reconfiguration step is not necessarily done at each iteration. Besides reducing the finite bias on the stationary density they have shown that their approach allows to calculate efficiently ground-state correlation functions within a forward walking approach. Here, our reconfiguration process is built in order to minimize as much as possible the fluctuations of the weights at each step. As a consequence, the finite bias on the stationary density is also reduced as much as possible. In particular, and in contrast with the CBS scheme, our algorithm is found to be optimal when the reconfiguration process is applied at each iteration.

V. AN ILLUSTRATIVE EXAMPLE

In this section we present some calculations illustrating the various aspects of DMC approaches discussed in the preceding sections. The system considered is a chain of N_s coupled quantum rotators (one per site). In the angular representation the Hamiltonian is written

$$H = - \sum_{i=1}^{N_s} \frac{\partial^2}{\partial \theta_i^2} - \frac{x}{2} \sum_{i=1}^{N_s} \cos(\theta_{i+1} - \theta_i), \quad (52)$$

where $(\theta_1 \cdots \theta_{N_s})$ are angular variables $\theta_i \in \mathbb{R}/2\pi\mathbb{Z}$ and periodic boundary conditions are used ($\theta_{N_s+1} = \theta_1$). In this formula x is a parameter defining the relative weight of the potential and kinetic terms. It can be shown that the model described by this Hamiltonian has the same critical properties as the two-dimensional XY spin model [21]. The finite-temperature Kosterlitz-Thouless (KT) classical phase transition of the spin model is equivalent to a zero-temperature quantum phase transition in the rotator model occurring at some critical value for the parameter x . Monte Carlo simulations have been done in the angular momentum representation. In this representation H is expressed in the discrete basis, $|l_1 \cdots l_{N_s}\rangle$ ($l_i \in \mathbb{Z}$), consisting of the eigenvectors of the angular momentum operators at different sites. We have

$$H = \sum_{i=1}^{N_s} \hat{J}_i^2 - \frac{x}{2} \sum_{i=1}^{N_s} (\phi_{i+1}^+ \phi_i + \text{H.c.}), \quad (53)$$

where the operators $(\phi_i^+, \phi_i, \hat{J}_i)$ are defined as follows [Lie-algebra of $O(2)$]:

$$\begin{aligned} \phi_i^+ |l_1 \cdots l_i \cdots\rangle &= |l_1 \cdots l_i + 1 \cdots\rangle, \\ \phi_i |l_1 \cdots l_i \cdots\rangle &= |l_1 \cdots l_i - 1 \cdots\rangle, \\ \hat{J}_i |l_1 \cdots l_i \cdots\rangle &= l_i |l_1 \cdots l_i \cdots\rangle. \end{aligned} \quad (54)$$

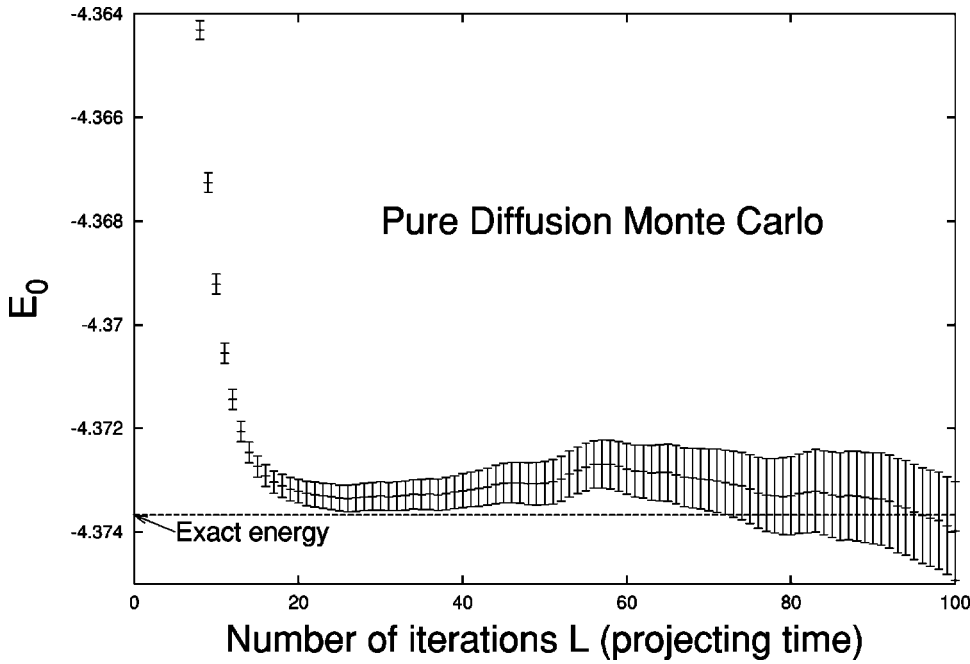


FIG. 1. PDMC calculation of the energy as a function of the projecting time. E_0 is in units of \hat{J}^2 , Eqs. (53),(54).

Here we are interested in calculating the ground-state energy of the model. Note that the ground state belongs to the fundamental representation of $O(2)$ corresponding to a total momentum equal to zero $\sum_{i=1}^{N_s} l_i = 0$. In what follows the parameter x is taken to be 1.8, a value expected to be very close to the exact critical value (see, Hamer *et al.* [21]). In actual calculations we have taken $N_s = 6$. By using exact diagonalization methods (Lanczòs algorithm) and after extrapolation to an infinite basis set ($l_i \rightarrow \infty$) we get $E_0 = -4.37367626$ (all digits converged) for parameters ($x = 1.8, N_s = 6$).

In Fig. 1 a PDMC calculation of the exact energy is presented. The trial wave function used is given by

$$\psi_T = e^{-k \sum_{i=1}^{N_s} l_i^2}, \quad (55)$$

where k is some positive parameter.

The unstable character of PDMC at large times is clearly illustrated. At zero-projecting time the variational energy associated with the trial wave function is recovered with small fluctuations, $E_v = -4.10284(25)$. The fact that this value is quite different from the exact one illustrates the poor quality of the trial wave function. Now, when the projecting time is increased the estimate of the energy converges to the exact value (number of iterations of about 25). For larger times the estimate of the energy begins to wander and no stabilization is observed.

In Fig. 2 we present some DMC calculations performed by using the standard branching process associated with w_{ij} [Eq. (19)] and a population control step to keep the number of walkers under control. The population control has been done by adjusting the reference energy to the fluctuations of population by using a formula of the type

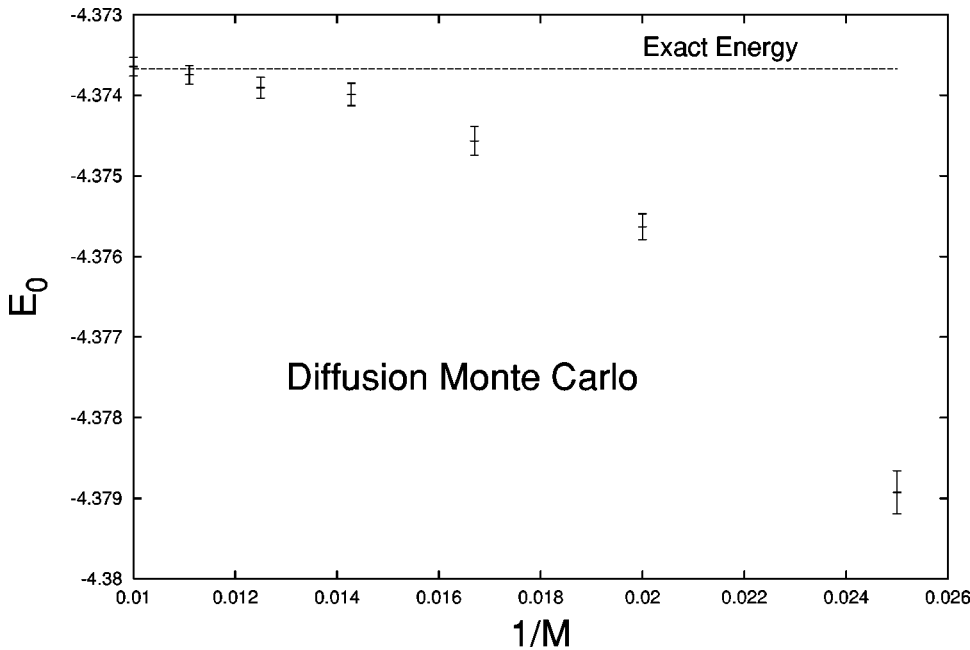


FIG. 2. DMC calculation of the exact energy as a function of the size of the population. E_0 is in units of \hat{J}^2 , Eqs. (53),(54).

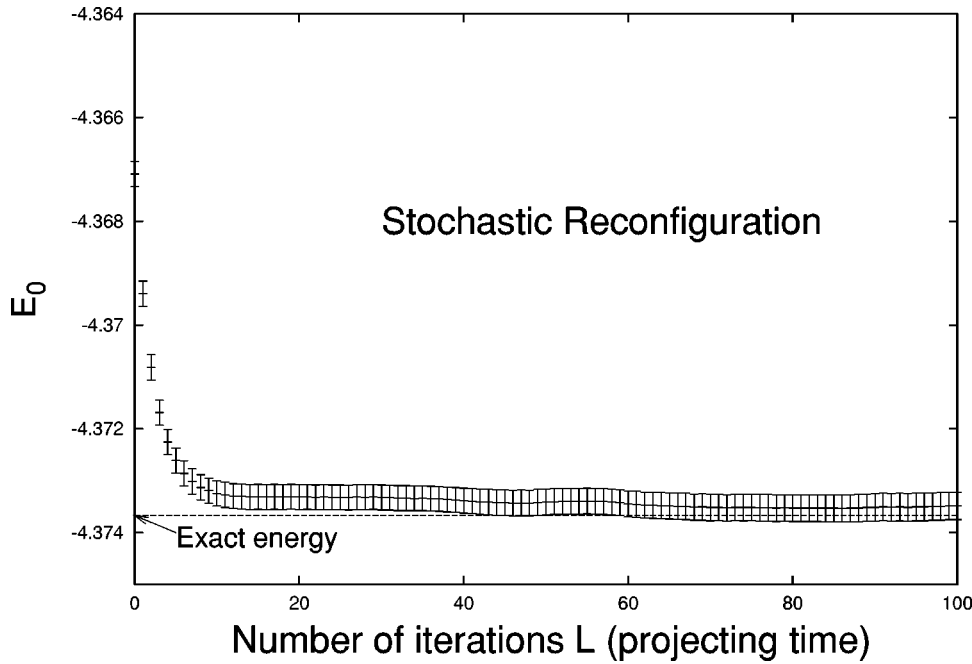


FIG. 3. PDMC with stochastic reconfiguration method. E_0 is in units of J^2 , Eqs. (53),(54).

$$E_T(t+\tau) = E_T(t) + K/\tau \ln[M(t)/M(t+\tau)], \quad (56)$$

where $M(t)$ is the total number of walkers at time t and K is some positive constant. When $M(t+\tau) > M(t)$ the reference energy is reduced and more walkers are killed at the next step. In the opposite case E_T is raised and more walkers are duplicated.

Calculations have been done with populations of different sizes ranging from $M=40$ to $M=100$. At $M=40$ the bias is small (systematic error of about $1/1000$) but much greater than the statistical error. The error is seen to decrease as the size of the population is increased. For $M=100$ it is smaller than the statistical error. It should be emphasized that the magnitude of the systematic error is very dependent on the quality of the trial wave function. Here a quite simple trial

wave function has been used. With more sophisticated and fully optimized forms the error would be much smaller.

In Fig. 3 we present a PDMC calculation with the original reconfiguration process of Hetherington. The number of walkers used is $M=50$. When compared to the PDMC calculation of Fig. 1 (same range for the projecting time) the stabilization in time resulting from the use of the global weight and the reconfiguration process is clearly seen. A chaotic behavior similar to that observed in Fig. 1 at large times is also expected but for much larger projecting times.

In the next figure, Fig. 4, we present our improved version for the stochastic reconfiguration process. The convergence as a function of time of the energy is very satisfactory and the fluctuations are reduced. Note that the value of the energy at the origin (no projection) $E_0 = -4.37115(16)$ is

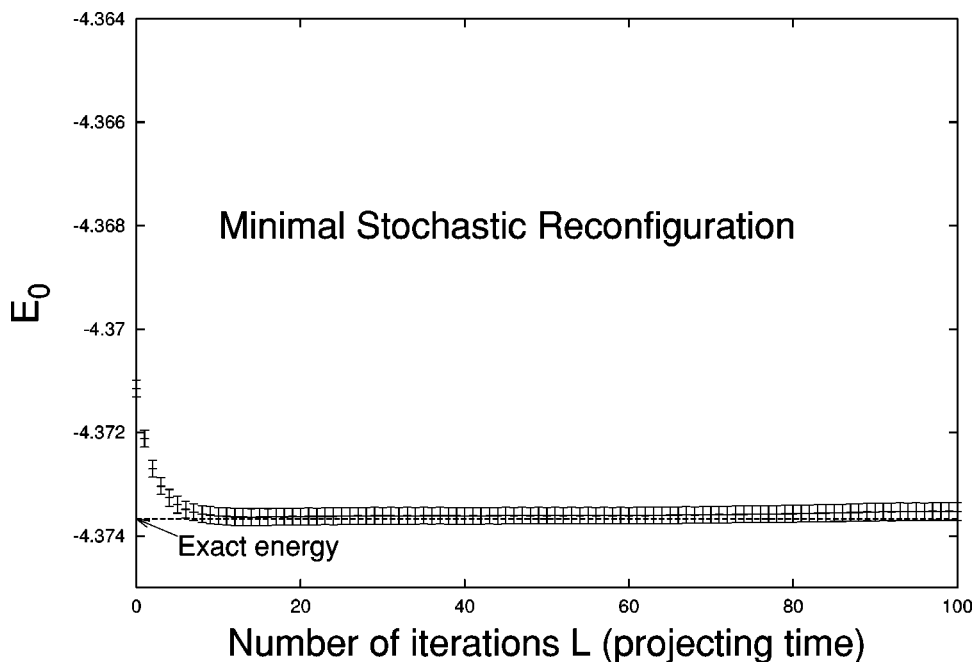


FIG. 4. PDMC with minimal stochastic reconfiguration. E_0 is in units of J^2 , Eqs. (53),(54).

much closer to the exact result ($E_0 = -4.37367 \dots$) than in the standard case (Fig. 3) $E_0 = -4.36708(24)$. This result is a direct consequence of the fact that the average number of reconfigurations with our minimal scheme is much smaller than in the previous case. In other words, the effective number of walkers has been increased and, then, the finite bias on the stationary density has been reduced. Note that in the limit of an infinite number of walkers the finite error on the energy would entirely disappear.

VI. SUMMARY

In this paper we have discussed various aspects of diffusion Monte Carlo methods at fixed number of walkers. First, we have concentrated our attention on the so-called pure diffusion Monte Carlo (PDMC) methods in which no branching process is introduced (the weights are carried) and for which the number of configurations is kept fixed at any level of the algorithm. As already remarked by a number of authors, PDMC methods are powerful, but they suffer from a severe problem at large projecting times (rapid increase of the variance). In this paper this statement has been made much more precise by showing that the statistical estimate of the effective

probability associated with a given state as calculated in a PDMC scheme does not converge to a finite deterministic value. This is in sharp contrast with what happens in DMC where a different —but biased— estimate is used for the same quantity. Quite interestingly, the derivation of the proof turns out to be far from being trivial. In particular, it was necessary to deal in detail with a difficult case [$E(\ln \lambda) = 0$ with our notations] from which a convergent variant of PDMC could have emerged. Second, based on an original estimate of the PDMC error [formula (48)] we have discussed the most natural generalization of PDMC which can make the method effective for problems associated with large fluctuations of the weights. By introducing stochastic reconfiguration processes as proposed by Hetherington and very recently reconsidered by Sorella and co-workers we have proposed an alternative approach to realize what can be called a minimal stochastic reconfiguration DMC approach. The method has been designed to reduce as much as possible the statistical fluctuations associated with the reconfiguration process and also to recover both PDMC and DMC limits. The numerical calculations presented have illustrated the validity of such an approach.

-
- [1] D.M. Ceperley and M.H. Kalos, in *Monte Carlo Method in Statistical Physics*, edited by K. Binder (Springer-Verlag, Heidelberg, 1992).
- [2] D.M. Ceperley, *Rev. Mod. Phys.* **67**, 279 (1995).
- [3] W. von der Linden, *Phys. Rep.* **220**, 53 (1992).
- [4] B.L. Hammond, W.A. Lester, Jr., and P.J. Reynolds, in *Monte Carlo Methods in Ab Initio Quantum Chemistry*, Vol. 1 of *World Scientific Lecture and Course Notes in Chemistry* (World Scientific, Singapore, 1994).
- [5] J.H. Hetherington, *Phys. Rev. A* **30**, 2713 (1984).
- [6] S. Sorella, *Phys. Rev. Lett.* **80**, 4558 (1998).
- [7] M. Calandra Buonaura and S. Sorella, *Phys. Rev. B* **57**, 11 446 (1998).
- [8] S. Sorella and L. Capriotti, *Phys. Rev. B* **61**, 2599 (2000).
- [9] J. Carlson, *Phys. Rev. B* **40**, 846 (1989).
- [10] N. Trivedi and D.M. Ceperley, *Phys. Rev. B* **41**, 4552 (1990).
- [11] K.J. Runge, *Phys. Rev. B* **45**, 7229 (1992).
- [12] R. Assaraf, P. Azaria, M. Caffarel, and P. Lecheminant, *Phys. Rev. B* **60**, 2299 (1999).
- [13] J. Glimm and A. Jaffé, *Quantum Physics. A Functional Integral Point of View* (Springer, New York, 1981).
- [14] M. Caffarel and P. Claverie, *J. Chem. Phys.* **88**, 1088 (1988).
- [15] M. Caffarel and P. Claverie *J. Chem. Phys.* **88**, 1100 (1988).
- [16] D.M. Ceperley and B. Bernu, *J. Chem. Phys.* **89**, 6316 (1988).
- [17] B. Bernu, D.M. Ceperley, and W.A. Lester, Jr., *J. Chem. Phys.* **93**, 552 (1990).
- [18] M. Caffarel, M. Rérat, and C. Pouchan, *Phys. Rev. A* **47**, 3704 (1993).
- [19] F. Schautz and H.-J. Flad, *J. Chem. Phys.* **110**, 11 700 (1999).
- [20] A. Khelif, R. Assaraf, and M. Caffarel (unpublished).
- [21] C.J. Hamer, J.B. Kogut, and L. Susskind, *Phys. Rev. D* **19**, 3091 (1979).

U. R. Assaraf and M. Caffarel “Computing forces with quantum Monte Carlo” *J. Chem. Phys.* 113 4028 (2000)

Computing forces with quantum Monte Carlo

Roland Assaraf^{a)}

Scuola Internazionale Superiore di Studi Avanzati (SISSA), and Istituto Nazionale Fisica della Materia (INFN), Via Beirut 4, I-32013 Trieste, Italy

Michel Caffarel^{b)}

CNRS-Laboratoire de Chimie Théorique Tour 22-23, Université Pierre et Marie Curie, 4 place Jussieu, 75252 Paris Cedex 05, France

(Received 12 April 2000; accepted 11 May 2000)

We present a simple and stable quantum Monte Carlo approach for computing forces between atoms in a molecule. In this approach we propose to use as Monte Carlo estimator of the force the standard Hellmann–Feynman expression (local force expressed as the derivative of the total potential energy with respect to the internuclear coordinates). Invoking a recently introduced zero-variance principle it is shown how the infinite variance associated with the Hellmann–Feynman estimator can be made finite by introducing some suitably renormalized expression for the force. Practical calculations for the molecules H_2 , Li_2 , LiH , and C_2 illustrate the efficiency of the method. © 2000 American Institute of Physics. [S0021-9606(00)31330-7]

I. INTRODUCTION

Over the recent years quantum Monte Carlo (QMC) methods have become more and more successful in computing ground-state properties of atomic and molecular systems (see, e.g., Refs. 1–3). However, the vast majority of applications has been limited to the calculation of the ground-state total energy. Although this is clearly a most important quantity, other properties (dipole moments, forces, polarizabilities, etc.) are also of primary interest. In theory, there is no difficulty for computing such quantities within a QMC framework. However, in practice, the convergence of the Monte Carlo calculations is much more slower and, therefore, much more computationally demanding than the case of the energy. Thus, only a limited number of calculations of properties can be found in the literature. The fundamental point allowing very efficient and accurate calculations of the energy (compared to other properties) is the existence of a so-called “zero-variance” property for this special observable. To understand this point, let us first briefly recall how the energy is computed with QMC. In short, the energy is expressed as a simple average over some suitably chosen distribution

$$E_0 = \langle E_L \rangle, \quad (1)$$

where the brackets $\langle \dots \rangle$ denote the statistical average and E_L is a local function defined as

$$E_L(x) = H\psi_T / \psi_T, \quad (2)$$

and usually referred to as the local energy. Here, H denotes the Hamiltonian under consideration and ψ_T a trial wave function. The distribution for the average defines the type of quantum Monte Carlo calculation performed. In variational Monte Carlo (VMC) schemes, the distribution is constructed

to be proportional to ψ_T^2 and Eq. (1) is nothing but an estimate of the standard quantum-mechanical variational energy associated with the trial wave function. In diffusion Monte Carlo (DMC) schemes, the stochastic rules employed to generate configurations are essentially similar to those of VMC, except that a new step—a branching process—is added to pass from the VMC distribution to the so-called “mixed” distribution given by $\phi_0\psi_T$, where ϕ_0 denotes the exact ground-state wave function. In that case, Eq. (1) realizes an exact estimate of the energy. From expression (1) it is clear that the statistical error on the energy is directly related to the magnitude of the fluctuations of the local energy. In turn, such fluctuations depend on the “quality” of the trial wave function. The closer the trial wave function is to the exact one, the smaller these fluctuations are. In the limit of an exact trial wave function the local energy becomes strictly constant and the statistical error vanishes completely. This is the result which is known as the “zero-variance” property. In practice, this property is of great importance: very accurate calculations can be performed with a reasonable amount of computer time only if accurate enough trial wave functions are at our disposal. When no particular trial wave function is used [$\psi_T=1$ in the preceding formula, (1)] the local energy reduces to the total potential energy. In this case the statistical error on the energy is very important since the bare potential fluctuates enormously. Introducing a trial wave function can be viewed as defining a “renormalizing procedure” applied to the bare potential in order to reduce its fluctuations. Of course, such a process is allowed only because both the bare potential (the total potential energy) and the renormalized one (the local energy) have the same average.

Very recently, we have generalized this zero-variance property to any observable defined on the configuration space.⁴ Denoting O some rather arbitrary observable we have shown that it is possible to construct *in a systematic way* a renormalized observable \tilde{O} verifying:

^{a)}Electronic mail: assaraf@sisssa.it

^{b)}Electronic mail: mc@lct.jussieu.fr

$$\langle \tilde{O} \rangle = \langle O \rangle \quad (3)$$

and

$$\sigma^2(\tilde{O}) < \sigma^2(O) \quad (4)$$

where $\sigma^2(A)$ represents the variance of operator A

$$\sigma^2(A) \equiv \langle (A - \langle A \rangle)^2 \rangle. \quad (5)$$

When using \tilde{O} instead of O as estimator of the observable, the convergence of the calculations can be improved since the statistical error on a finite Monte Carlo sample is directly proportional to the variance of the quantity to be averaged. As we shall see later, the renormalized observable depends on two auxiliary quantities, \tilde{H} and $\tilde{\psi}$ which play a role similar to that played by H and ψ_T in the renormalized version of the bare potential, Eq. (2). Some preliminary classical and quantum Monte Carlo calculations on simple systems have shown that very important reduction of the computational effort can be achieved by using this general zero-variance principle.⁴ In the present paper we apply this idea to the problem of calculating forces between atoms in molecules. The calculation of forces is known to be a very difficult task for QMC methods.³ Some calculations limited to very small molecules (typically H_2 and LiH) have been reported.^{5,6} However, their extension to bigger systems is essentially not realistic. Note that very recently Filippi and Umrigar have presented a new method for computing forces.⁷ Their method is based on a special transformation coordinates and a correlated sampling approach. Here, we follow a quite different route. It is shown that forces can be computed in a very natural way by using the standard Hellmann–Feynman (HF) theorem. More precisely, the force is computed as the average of the local force, a quantity defined as the gradient of the potential energy with respect to the internuclear coordinates. In previous works (see, e.g., discussion in Ref. 3) such a possibility was excluded because of the uncontrolled statistical fluctuations associated with the bare force (infinite variance). Here, it will be shown that with the help of the generalized zero-variance principle, the pathological part of the force responsible for the infinite variance can be removed exactly in a simple and general way. Once this is achieved, it is possible to perform stable calculations of the forces by using standard variational and diffusion Monte Carlo methods. The first applications presented here illustrate the accuracy and efficiency of the method.

II. METHOD

To compute forces between atoms in a molecule we take advantage of the Hellmann–Feynman theorem. According to this theorem the average force defined as

$$\langle F_q \rangle \equiv -\nabla_q E_0(\mathbf{q}) \quad (6)$$

is given by the expectation value of the gradient of the potential (local force)

$$\langle F_q \rangle = \frac{\int d\mathbf{x} \phi_0^2(\mathbf{x}, \mathbf{q}) F_q(\mathbf{x}, \mathbf{q})}{\int d\mathbf{x} \phi_0^2(\mathbf{x}, \mathbf{q})}, \quad (7)$$

with

$$F_q(\mathbf{x}) \equiv -\nabla_q V(\mathbf{x}, \mathbf{q}). \quad (8)$$

In these formulas \mathbf{q} represents the set of the $3N_{\text{nuc}}$ nuclear coordinates (N_{nuc} being the number of nuclei), V the total potential energy operator of the problem, $E_0(\mathbf{q})$ the total ground-state energy for a given molecular geometry, and ϕ_0 the corresponding ground-state wave function.

As remarked by a number of authors, one of the major difficulties in computing forces by QMC via formulas (7) and (8) is the presence of uncontrolled statistical fluctuations (see, e.g., Ref. 3). Indeed, the variance of the Hellmann–Feynman estimator of the force is infinite. This is a simple consequence of the fact that at short electron-nucleus distances r , the local force behaves as $F \sim 1/r^2$, so that $\langle F^2 \rangle = \infty$. Various solutions to this problem have been proposed. A common idea consists in introducing some sort of cutoff when the electrons approach the nuclei.⁶ However, by doing this a systematic error is introduced. In addition, to control this error is a very tricky problem since any extrapolation procedure (cutoff going to zero) is ill-defined.

To escape from this difficulty we propose to replace the standard expression of the local force $F_q(\mathbf{x})$ by a ‘renormalized’ expression, $\tilde{F}_q(\mathbf{x})$, having the same average but smaller fluctuations. It should be emphasized that the decrease in fluctuations will be dramatic here since, in contrast with the bare expression, the renormalized version will have now *finite* fluctuations. Let us give the explicit expressions for the renormalized quantities. We shall consider two different cases. The first case corresponds to variational Monte Carlo (VMC) calculations. The distribution of walkers in configuration space, $\pi(\mathbf{x})$ is given by

$$\pi_{\text{VMC}}(\mathbf{x}) \sim \psi_T^2(\mathbf{x}). \quad (9)$$

The second case corresponds to calculations within the diffusion Monte Carlo (DMC) approach. In that case the distribution employed is the so-called mixed distribution given by

$$\pi_{\text{DMC}}(\mathbf{x}) \sim \psi_T(\mathbf{x}) \phi_0(\mathbf{x}). \quad (10)$$

In the variational case and for a particular component q we consider the following renormalized expression:

$$\tilde{F}_q(\mathbf{x}) = F_q(\mathbf{x}) + \left[\frac{\tilde{H}\tilde{\psi}}{\tilde{\psi}} - \frac{\tilde{H}\psi_T}{\psi_T} \right] \frac{\tilde{\psi}}{\psi_T}, \quad (11)$$

where \tilde{H} is some rather arbitrary auxiliary Hermitian operator and $\tilde{\psi}$ an arbitrary auxiliary function (supposed to be square-integrable). Note that the choice of the auxiliary quantities depends on the particular component q considered. Because \tilde{H} is Hermitian we have $\langle \psi_T | \tilde{H} | \tilde{\psi} \rangle = \langle \tilde{\psi} | \tilde{H} | \psi_T \rangle$ and it is an elementary exercise to check that the average value of the bare and renormalized expressions over the VMC distribution (9) are identical

$$\langle \tilde{F}_q \rangle = \langle F_q \rangle. \quad (12)$$

Note that this result requires that both the trial function and its first derivatives are continuous over the whole configuration space. These conditions are fulfilled by the trial wave functions used in VMC schemes. Now, regarding the variances we have the following expression:

$$\begin{aligned}\sigma^2(\tilde{F}_q) &\equiv \langle (\tilde{F}_q - \langle \tilde{F}_q \rangle)^2 \rangle \\ &= \sigma^2(F_q) + 2\langle F_q \Delta H w \rangle + \langle \Delta H^2 w^2 \rangle,\end{aligned}\quad (13)$$

where, for the sake of simplicity, we have used the following notations:

$$\Delta H \equiv \left[\frac{\tilde{H}\tilde{\psi}}{\tilde{\psi}} - \frac{\tilde{H}\psi_T}{\psi_T} \right] \quad (14)$$

and

$$w \equiv \frac{\tilde{\psi}}{\psi_T} \quad (15)$$

Now, let us show that, from an arbitrary auxiliary function $\tilde{\psi}$, we can always construct a renormalized expression having a smaller variance. For that we consider the multiplicative constant of $\tilde{\psi}$, denoted here α , as a variational parameter. Minimizing the variance $\sigma^2(\tilde{F}, \alpha)$ with respect to α we get the following optimal value:

$$\alpha_{\text{opt}} = -\langle F_q \Delta H w \rangle / \langle \Delta H^2 w^2 \rangle \quad (16)$$

and, therefore,

$$\sigma^2(\tilde{F}, \alpha_{\text{opt}}) = \sigma^2(F) - \langle F \Delta H w \rangle^2 / \langle \Delta H^2 w^2 \rangle, \quad (17)$$

In general, the quantity $\langle F \Delta H w \rangle$ will not be equal to zero. As a consequence, equation (17) shows that, whatever the quality of the auxiliary function $\tilde{\psi}$ chosen, the use of the optimized prefactor (16) always leads to a decrease of the statistical fluctuations. Clearly, this gain in variance can be small but let us emphasize that it is a systematic gain. Of course, this is only by choosing appropriate auxiliary functions that large gains can be expected.

In the case of a diffusion Monte Carlo scheme the stationary distribution, Eq. (10), is no longer known analytically since it involves the unknown exact wave function which is stochastically sampled, and our general procedure which supposes the knowledge of the distribution cannot be readily applied to. However, in the particular case of the mixed distribution, a renormalized expression can still be defined.⁴ A natural choice is

$$\tilde{F}_q(\mathbf{x}) = F_q(\mathbf{x}) + \left[\frac{H\tilde{\psi}}{\tilde{\psi}} - E_0 \right] \frac{\tilde{\psi}}{\psi_T}, \quad (18)$$

where E_0 is some unbiased estimator of the exact ground-state energy. In this case also, it is quite easy to verify that the averages of the bare and renormalized estimators over the mixed distribution (10) are equal

$$\langle \tilde{F}_q \rangle = \langle F_q \rangle. \quad (19)$$

It should be emphasized that this result is valid only if the wave function ϕ_0 and its first derivatives are continuous everywhere. This is true for the exact solution of the problem. However, in general it will not be the case for the approximate solution obtained with a fixed-node diffusion Monte Carlo calculation. We shall return to this important point in the next section.

To make the connection with the variational case, remark that the latter expression can be rewritten as

$$\tilde{F}_q(\mathbf{x}) = \tilde{F}_q^{\text{VMC}}(\mathbf{x}) + [E_L - E_0]w, \quad (20)$$

where E_L represents the local energy function associated with the trial wave function ψ_T , Eq. (2), and $\tilde{F}_q^{\text{VMC}}(\mathbf{x})$ is the variational Monte Carlo expression of the renormalized force, Eq. (11). Note that the correction between the VMC and DMC estimators in formula (20) consists of a product of two quantities, namely $E_L - E_0$ and w . The quantity $E_L - E_0$ has a vanishing average and its statistical fluctuations are in general much smaller than those of w . Accordingly, it is quite efficient to introduce a centered version of the variable w . Indeed, it can be easily shown that the fluctuations of the product are in this way greatly reduced. Our final version of the DMC force used in our calculations is therefore

$$\tilde{F}_q(\mathbf{x}) = \tilde{F}_q^{\text{VMC}}(\mathbf{x}) + [E_L - \langle E_L \rangle][w - \langle w \rangle]. \quad (21)$$

Finally, it should be noted that the force calculated according to the preceding formulas are not exact since the DMC distribution is the mixed distribution instead of the exact one. This point is discussed later.

Now, in order to illustrate the method we consider the case of a diatomic molecule AB consisting of an atom A (nucleus charge Z_A) located at $(R, 0, 0)$ and an atom B (nucleus charge Z_B) located at the origin. Note that the general case corresponding to an arbitrary number of nuclei does not involve particular difficulties. It can be obtained by straightforward generalization of what is presented below. For a diatomic molecule we have the following expression of the force: $\mathbf{F} = (F, 0, 0)$, with

$$F(\mathbf{x}) = \frac{Z_A Z_B}{R^2} - Z_A \sum_{i=1}^{N_{\text{elect}}} \frac{(x_i - R)}{|\mathbf{r}_i - \mathbf{R}|^3}, \quad (22)$$

where N_{elect} is the total number of electrons and \mathbf{r}_i represents the position of electron i . The second term on the right-hand side of Eq. (22) is responsible for the infinite variance contribution. Let us now show that this contribution can be exactly removed. In what follows we shall write the auxiliary function as

$$\tilde{\psi}(\mathbf{x}) = Q \psi_T, \quad (23)$$

where Q is some arbitrary function. Using this form it can be verified that the simplest form for Q canceling the pathological part of the bare force is the following:

$$Q = Z_A \sum_{i=1}^{N_{\text{elect}}} \frac{(x_i - R)}{|\mathbf{r}_i - \mathbf{R}|^3}. \quad (24)$$

Finally, we get for the renormalized force in the variational case [Eq (11)]:

$$\tilde{F}(\mathbf{x}) = \frac{Z_A Z_B}{R^2} - \nabla Q \cdot \nabla \psi_T / \psi_T, \quad (25)$$

with a similar expression in the DMC case [see Eqs. (18) and (20)]. It can be checked that this latter expression has now a finite variance.

As already mentioned the QMC calculations presented here are done at two different levels of approximation. First, we present variational Monte Carlo calculations of the force. The average of the force is then obtained as

$$\langle \mathcal{F} \rangle_{\text{VMC}} = \frac{\int d\mathbf{x} \psi_T^2(\mathbf{x}) \mathcal{F}(\mathbf{x})}{\int d\mathbf{x} \psi_T^2(\mathbf{x})}, \quad (26)$$

where ψ_T is the trial wave function, and \mathcal{F} represents here either the bare force, $\mathcal{F} = F$, Eq. (7), or the renormalized one, $\mathcal{F} = \tilde{F}$, Eq. (11). We also consider averages over the mixed distribution as obtained in a diffusion Monte Carlo scheme:

$$\langle \mathcal{F} \rangle_{\text{mixed}} = \frac{\int d\mathbf{x} \phi_0(\mathbf{x}) \psi_T(\mathbf{x}) \mathcal{F}(\mathbf{x})}{\int d\mathbf{x} \phi_0(\mathbf{x}) \psi_T(\mathbf{x})}, \quad (27)$$

where ϕ_0 is the exact wave function. Here, \mathcal{F} is given either by Eq. (7) or by Eq. (18). In order to get a more accurate approximation of the unbiased exact force, corresponding to the density ϕ_0^2 , we shall also have recourse to the following ‘hybrid’ formula:

$$\langle \mathcal{F} \rangle \approx 2\langle \mathcal{F} \rangle_{\text{mixed}} - \langle \mathcal{F} \rangle_{\text{VMC}}. \quad (28)$$

This formula is constructed so that the first-order contributions in the difference $\phi_0(\mathbf{x}) - \psi_T(\mathbf{x})$ for the quantities $\langle \mathcal{F} \rangle_{\text{mixed}}$ and $\langle \mathcal{F} \rangle_{\text{VMC}}$ compensate exactly (see, e.g., Ref. 3). From a practical point of view, expression (28) is particularly interesting. Both quantities involved can be straightforwardly computed in routine DMC and VMC calculations. Note that in principle it is also possible to get an exact estimate of $\langle \mathcal{F} \rangle$ but it requires some more elaborate scheme involving some kind of forward-walking.^{3,8} We shall not consider here such calculations, but let them for future publication.

III. A FEW REMARKS REGARDING THE PRACTICAL IMPLEMENTATION

As seen in the preceding section we use both VMC and DMC approaches in our actual computations. Regarding variational Monte Carlo no particular difficulties arise. In practice, the main weakness of the VMC approach lies in the fact that the average force obtained according to Eq. (26) is quite dependent on the trial wave function used. This is particularly true since ψ_T is optimized in order to improve the total electronic energy but not its derivatives with respect to the internuclear coordinates. However, as illustrated by the practical calculations presented below (see Table II), combining DMC and VMC calculations of the force according to the hybrid formula, Eq. (28), seems to represent a simple but accurate solution to this problem.

Let us now consider the specific difficulties associated with DMC calculations. In order to avoid the famous ‘sign problem’ for fermions⁹ all calculations presented here are done using the stable but approximate fixed-node (FN) method. In this approach the Schrödinger equation is solved *separately* in each nodal domain (or ‘pocket’) where ψ_T has a definite sign. When the trial wave function satisfies the tiling property^{10,11} all nodal domains are equivalent and related by the permutational symmetry. When this is not the case, energies associated with each nodal domain can be dif-

ferent and the FN solution corresponds to the eigensolution defined in the domain corresponding to the lowest energy. Without entering more into the details of the fixed-node approach (for that, see, e.g., Refs. 12 and 3) we just remark that a most important point with FN calculations is that the sampled fixed-node solution displays in general some discontinuous derivatives at the nodes (zeroes of ψ_T). Because of that, some mathematical care is necessary when integrating quantities (energy, derivatives of the energy, etc.) that are defined over the entire configuration space; in other words, the various nodal domains must be properly connected. A first example illustrating this remark is the problem of the validity of the Hellmann–Feynman (HF) theorem in fixed node QMC calculations, a point which has raised some discussion very recently.^{13–15} Due to the presence of the discontinuity at nodes the HF theorem is not true in general in that case. It can be shown that the theorem is valid only when the derivative of the total fixed-node energy with respect to the coordinate q is done without changing the nodes of the trial wave function when varying q .¹⁴ However, since in the present work no finite difference expressions for the fixed-node energy are used, this point is in fact of no practical importance. Let us just mention that the average force obtained in our fixed-node DMC calculations corresponds to the Hellmann–Feynman force we would obtain by performing such finite differences fixed-node calculations with the nodes kept fixed.

A second example of difficulties, which is here of fundamental importance, concerns the validity of the equality between the bare and renormalized expressions, Eq. (19). To clarify this point let us have a closer look at the condition we would like to fulfill. Using expression (18) the condition can be written as

$$\langle \tilde{F} \rangle - \langle F \rangle = \langle \phi_0^{\text{FN}} | \frac{(H - E_0^{\text{FN}}) \tilde{\psi}}{\psi_T} | \psi_T \rangle = 0, \quad (29)$$

where E_0^{FN} is the fixed-node energy. Denoting Ω a nodal domain of the fixed-node solution we can write

$$\langle \tilde{F} \rangle - \langle F \rangle = \int_{\Omega} d\mathbf{x} \phi_0^{\text{FN}} (H - E_0^{\text{FN}}) \tilde{\psi}. \quad (30)$$

Now, decomposing H under its kinetic and potential parts and invoking Green’s formula this quantity can be rewritten as an integral over the nodal hypersurface

$$\langle \tilde{F} \rangle - \langle F \rangle = -\frac{1}{2} \int_{\partial\Omega} (\phi_0^{\text{FN}} \vec{\nabla} \tilde{\psi} - \tilde{\psi} \vec{\nabla} \phi_0^{\text{FN}}) \vec{d}S. \quad (31)$$

From this expression it is seen that a nonzero bias may indeed appear in a fixed-node calculation of the renormalized force. Clearly, a simple way of removing this bias is to use auxiliary functions $\tilde{\psi}$ having the same nodes as ψ_T and, therefore, the same nodes as ϕ_0^{FN} . The actual simulations presented below fulfill this condition.

Finally, let us end this section with some words about the nature of the errors introduced. Since the exact nodes are not known there is some difference between the exact and fixed-node functions

TABLE I. Total energies in variational Monte Carlo [$E_0(\text{VMC})$] and diffusion Monte Carlo [$E_0(\text{DMC})$] with the trial wave functions employed here. $E_c^{\text{VMC}}(\%)$ and $E_c^{\text{DMC}}(\%)$ are the percentages of correlation energy recovered in VMC and DMC. $\sigma^2(\text{VMC})$ is the variance of the local energy in VMC. Bond lengths are in Bohrs and energies in Hartree atomic units. Statistical uncertainties on the last digit are indicated in parentheses.

Molecule	$E_0(\text{HF})$	E_0	$E_0(\text{VMC})$	$\sigma^2(\text{VMC})$	$E_c^{\text{VMC}}(\%)$	$E_0(\text{DMC})$	$E_c^{\text{DMC}}(\%)$
H_2 ($R=1.4$)	-1.133 63	-1.174 475	-1.172 80(7.7)	0.0050(1)	95.8(2)	-1.174 45(6.7)	99.9(2)
LiH ($R=3.015$)	-7.987	-8.070 21	-8.055 54(26)	0.070(2)	82.37(3)	-8.067 57(70)	96.8(8)
Li_2 ($R=5.051$)	-14.871 52	-14.9954	-14.9429(46)	0.196(1.2)	57.6(4)	-14.9910(3.7)	96.4(3)
C_2 ($R=2.3481$)	-75.4062	-75.923(5)	-75.581(2.9)	1.088(6)	33.8(6)	-75.854(5.2)	87(1)

^aFrom experimental data analysis.

$$\delta\phi \equiv \phi_0^{\text{FN}} - \phi_0, \quad (32)$$

where ϕ_0 and ϕ_0^{FN} are the normalized exact and fixed-node solutions. The fixed-node bias can be evaluated as

$$\langle \phi_0^{\text{FN}} | \mathcal{F} | \phi_0^{\text{FN}} \rangle - \langle \phi_0 | \mathcal{F} | \phi_0 \rangle = 2 \langle \delta\phi | \mathcal{F} | \phi_0 \rangle + O(\delta\phi^2). \quad (33)$$

In other words, the fixed-node bias for \mathcal{F} is of order 1 in $\delta\phi$ in contrast with the FN bias on the energy which is of order 2 in the same quantity. Finally, it is easy to see that the bias on the mixed average, Eq. (27), is of order $O(\psi_T - \phi_0^{\text{FN}}) + O(\delta\phi)$ while the bias on the ‘hybrid’ estimator, Eq. (28), is of order $O[(\psi_T - \phi_0^{\text{FN}})^2] + O(\delta\phi)$.

IV. RESULTS AND DISCUSSION

We present a number of variational Monte Carlo (VMC) and diffusion Monte Carlo (DMC) calculations for the diatomic molecules H_2 , LiH , Li_2 , and C_2 . Standard implementations of the VMC and DMC methods have been used and will not be detailed here. For some general presentation of these approaches the interested reader is referred for example to Refs. 1, 3, and 16. As already indicated in the preceding section all DMC calculations have been done within the fixed-node approach. Numerical experience shows that the fixed-node error on the energy resulting from the approximate location of the trial nodes is rather small when good enough trial wave functions are used. As we shall see later, this will also turn out to be true when calculating forces. In order to remove the short-time error all DMC calculations have been systematically performed with different time-steps and extrapolated to zero time-step. Regarding the trial wave function we have chosen a standard form consisting of a determinant of single-particle orbitals multiplied by a Jastrow factor

$$\psi_T = D^\dagger D^\downarrow \exp \sum_\alpha \sum_{\langle i,j \rangle} U(r_{i\alpha}, r_{j\alpha}, r_{ij}), \quad (34)$$

where the sum over α denotes a sum over the nuclei and $\sum_{\langle i,j \rangle}$ a sum over the pair of electrons. Here, the function U is chosen to be

$$U(r_{i\alpha}, r_{j\alpha}, r_{ij}) = s(x_{ij}) + p^{(\alpha)}(x_{i\alpha}) + c_1 x_{i\alpha}^2 x_{j\alpha}^2 + c_2 (x_{i\alpha}^2 + x_{j\alpha}^2) x_{ij}^2 + c_3 x_{ij}^2 \quad (35)$$

with

$$x_{ij} = \frac{r_{ij}}{1 + b_\sigma r_{ij}}, \quad x_{i\alpha} = \frac{r_{i\alpha}}{1 + b_\alpha r_{i\alpha}},$$

$$s(x) = s_1 x + s_2 x^2 + s_3 x^3 + s_4 x^4,$$

$$p^{(\alpha)}(x) = p_1^{(\alpha)} x + p_2^{(\alpha)} x^2 + p_3^{(\alpha)} x^3 + p_4^{(\alpha)} x^4.$$

b_σ can take two different values depending on the spin of the pairs of electrons considered. The different parameters of the trial wave function have been optimized using the correlated sampling method of Umrigar *et al.*¹⁷ The total energies obtained at the variational and DMC levels are presented in Table I.

The calculations have been done at the experimental bond lengths. The quality of our trial wave functions is good since a non-negligible part of the correlation energy is recovered at the variational level. Note that more sophisticated trial wave functions could be used (see, e.g., Ref. 18).

At the heart of the zero-variance principle employed here is the choice of the auxiliary quantities \tilde{H} and $\tilde{\psi}$. Exactly in the same way as for the total energy we need to construct some optimal choice guided by a zero-variance equation. In the case of the energy the zero-variance equation is nothing but the usual Schrödinger equation

$$E_L(x) = H \psi_T / \psi_T = \langle E_L \rangle, \quad (36)$$

and the optimal choice (zero-variance) for ψ_T is $\psi_T = \phi_0$. Here, the ideal zero-variance condition is written as

$$\tilde{F}_q(\mathbf{x}) = \langle F_q \rangle. \quad (37)$$

In the variational case, using expression (11) this equation can be written as

$$\left[\tilde{H} - \frac{\tilde{H} \psi_T}{\psi_T} \right] \tilde{\psi} = -[\tilde{F}_q(\mathbf{x}) - \langle \tilde{F}_q \rangle] \psi_T. \quad (38)$$

In the DMC case, we have

$$[H - E_0] \tilde{\psi} = -[\tilde{F}_q(\mathbf{x}) - \langle \tilde{F}_q \rangle] \psi_T. \quad (39)$$

In this latter case we just need to construct an ‘‘accurate’’ solution of this equation. In the variational case we have more freedom since the auxiliary operator \tilde{H} is also to be chosen. Here, in order to demonstrate the feasibility and the simplicity of the approach we will consider the simplest choice possible for the auxiliary quantities. Regarding the auxiliary operator we will just choose $\tilde{H} = H$. Regarding $\tilde{\psi}$ we choose the minimal form required to get a finite variance of the force, namely Q as given by (24). Note that using such forms for the auxiliary quantities there are no free parameters left. Our results are presented in Table II. Before discussing these results let us first look at the convergence of the vari-

TABLE II. Forces at the experimental bond lengths (atomic units) for the four diatomic molecules considered. $\langle F \rangle_{\text{VMC}}$ and $\langle F \rangle_{\text{mixed}}$ are the standard forces obtained with VMC and DMC. $\langle \tilde{F} \rangle_{\text{VMC,mixed}}$ are the same quantities obtained with the “renormalized” expression of the force, Eq. (18). $\langle \tilde{F} \rangle$ is the “hybrid” estimator combining the VMC and DMC results, Eq. (28). Statistical uncertainties on the last digit are indicated in parentheses.

Molecule	$\langle F \rangle_{\text{VMC}}$	$\langle \tilde{F} \rangle_{\text{VMC}}$	$\langle F \rangle_{\text{mixed}}$	$\langle \tilde{F} \rangle_{\text{mixed}}$	$\langle \tilde{F} \rangle$
H ₂ ($R=1.4$)	0.06(7)	-0.0047(1.5)	-0.0034(10)	-0.0041(3.6)	-0.0035(5)
LiH ($R=3.015$)	-0.037(12)	-0.0263(2)	-0.03(2)	-0.0125(9)	-0.0013(11)
Li ₂ ($R=5.051$)	-0.8(4)	-0.196(1.8)	-0.2(2)	-0.096(2.5)	-0.004(4)
C ₂ ($R=2.3481$)	2(3)	-0.101(22)	1.(4)	-0.05(2)	-0.00(4)

ous estimators. Typical behaviors are shown in Figs. 1 and 2. Calculations are VMC calculations of the force (at experimental length) for the two larger molecules treated here, namely Li₂ and C₂.

Both figures show the convergence of the estimators of the bare and renormalized forces, respectively, as a function of the simulation time (a quantity proportional to the number of Monte Carlo steps). In both cases the difference between the two curves obtained is striking. In the case of the bare force the estimator of the force converges with a lot of difficulty. The fluctuations are very large and at some places “jumps” in the curves are observed. These jumps correspond in the simulation to some configurations where an electron approaches a nucleus. Their location and their magnitude are very dependent on the sequence of random numbers and initial conditions used. In fact, there is no hope to obtain a converged value of the bare force in a finite simulation time (whatever its length be). This behavior is of course related to the infinite variance of the estimator. The second curve associated with the renormalized force, Eq. (11), has an entirely different behavior. In sharp contrast with the bare case the convergence is now reached very easily. At the scale of the figure the fluctuations of the curve have almost disappeared.

Table II summarizes the various calculations we have performed. All calculations have been done at the experimental bond lengths, the expectation values of the force are therefore expected to be very close to zero.

The bare VMC and DMC values presented are reported as given by the output of our program. However, as just remarked they have to be considered with a lot of caution. Indeed, the values are not and cannot be converged due to the infinite variance. Consequently, the values quoted just give a very rough estimate. Their actual values depends strongly on the initial conditions and on the series of random numbers used. In contrast, the renormalized value are perfectly well-defined and the estimate of the average and of the statistical error are converged. At the variational level the average values of the renormalized forces are significantly different from zero. These values depend on the choice of the trial wave function. The mixed estimators are less dependent. In our calculations the results display a systematic error about 2 times smaller than the variational ones. Combining both sets of values and using formula (28) to remove as much as possible the dependence on the trial function we obtain very accurate estimates of the forces (column $\langle \tilde{F} \rangle$). Except for the molecule H₂ for which very small statistical

errors have been obtained, our estimates of the force are essentially exact (≈ 0) within error bars. Note that in the three cases where a fixed-node error on the result is expected (LiH, Li₂, and C₂) no significant bias on the results is observed. As already remarked in the introduction there are very few results to compare with in the literature. Regarding H₂ we can cite the work by Reynolds *et al.*⁵ At the equilibrium distance, they obtained for the force a value of 0.0009(24). Note that within statistical errors our (slightly biased) result is compatible with this value. However, our statistical error is about 5 times smaller. In the case of LiH we get a much more accurate value than the one given by Vrbik and Rothstein,⁶ namely $F=0.12(16)$. Quite remarkably, our statistical error is about two orders of magnitude smaller. Comparisons with the very recent results obtained by Filippi and Umrigar⁷ are not easy because the quantities calculated are different. In their work the authors present the error in the bond lengths obtained in their correlated DMC calculations and not the force like in the present work. In order to make some quantitative comparisons it is necessary to compute the dependence of our results on the distance and

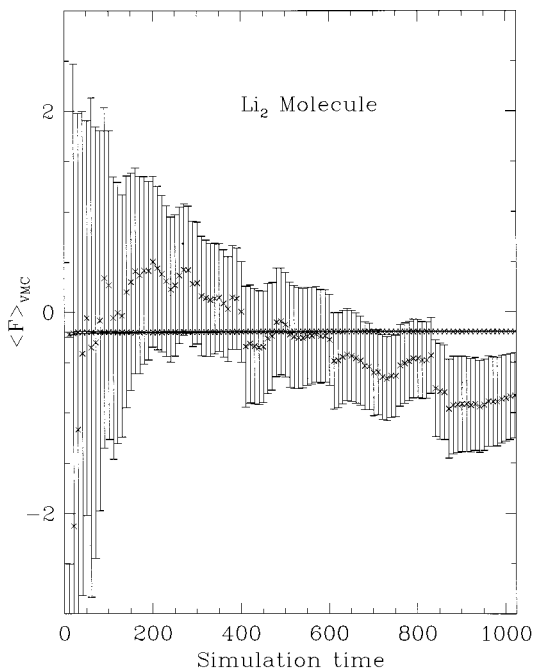


FIG. 1. Convergence of $\langle F \rangle_{\text{VMC}}$ and $\langle \tilde{F} \rangle_{\text{VMC}}$ as a function of the simulation time (proportional to the number of Monte Carlo steps) for the Li₂ molecule at the equilibrium geometry, $R=3.015$.

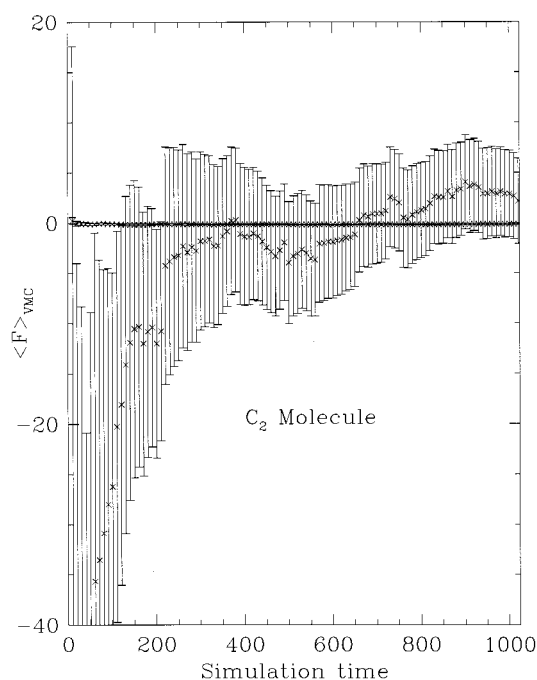


FIG. 2. Convergence of $\langle F \rangle_{\text{VMC}}$ and $\langle \bar{F} \rangle_{\text{VMC}}$ as a function of the simulation time (proportional to the number of Monte Carlo steps) for the C_2 molecule at the equilibrium geometry, $R=5.051$.

define some estimate of the equilibrium distance. Such a study is out of purpose here and is left for future investigation. Finally, let us emphasize that the auxiliary function used here is the simplest form allowing the reduction of the variance of the local force to a finite value. Clearly, more general and sophisticated forms for the auxiliary function can be introduced and optimized. There is no doubt that significantly smaller errors on the computed forces can be achieved.

In summary, we have presented a simple and stable approach for computing forces within a QMC scheme. To do that, we propose to use the Hellmann–Feynman theorem to re-express the force as a standard local average of the gradient of the potential. The force is computed approximately using standard variational Monte Carlo and fixed-node diffusion Monte Carlo approaches. To remove as much as possible the dependence of the results on the trial wave functions we resort to the commonly used “hybrid” estimator combining both VMC and DMC results. In order to suppress the unbounded statistical fluctuations associated with the lo-

cal force we apply to this observable a generalized zero-variance property. In practice, this idea is implemented by replacing the bare local force by some renormalized expression depending on some auxiliary quantities. A simple procedure to construct the renormalized force (choice of auxiliary quantities) is presented. As emphasized, it is a general procedure: It can be performed without practical difficulty for an arbitrary molecular system. Introducing the simplest form possible for the renormalized force (minimal form, no free parameters) and using standard forms for the trial functions we get very satisfactory results for some simple diatomic molecules. Applications to bigger systems and calculations away from the equilibrium geometry are now under investigation.

ACKNOWLEDGMENTS

We thank C. Filippi and C. Umrigar for useful discussions and P. Reinhardt for some useful comments on the manuscript. This work was supported by the “Centre National de la Recherche Scientifique” (CNRS). Part of the work has been done by R. Assaraf at SISSA under EU sponsorship, TMR Network FULPROP.

- ¹J. B. Anderson, in *Reviews in Computational Chemistry*, Vol. 13, edited by K. B. Lipkowitz and D. B. Boyd (Wiley, New York, 1999).
- ²See contributions, in *Recent Advances in Computational Chemistry*, Vol. 2, edited by W. A. Lester, Jr. (World Scientific, Singapore, 1997).
- ³B. L. Hammond, W. A. Lester, Jr., and P. J. Reynolds, in *Monte Carlo Methods in Ab Initio Quantum Chemistry*, World Scientific Lecture and course notes in chemistry, Vol. 1 (World Scientific, Singapore, 1994).
- ⁴R. Assaraf and M. Caffarel, *Phys. Rev. Lett.* **83**, 4682 (1999).
- ⁵P. J. Reynolds, R. N. Barnett, B. L. Hammond, R. Grimes, and W. A. Lester, Jr., *Int. J. Quantum Chem.* **29**, 589 (1986).
- ⁶J. Vrbik and S. M. Rothstein, *J. Chem. Phys.* **96**, 2071 (1992).
- ⁷C. Filippi and C. J. Umrigar, *cond-mat/9911326* (1999).
- ⁸M. Caffarel and P. Claverie, *J. Chem. Phys.* **88**, 1088 (1988).
- ⁹J. B. Anderson, in *Understanding Chemical Reactivity*, edited by S. R. Langhoff (Kluwer, Berlin, 1995).
- ¹⁰D. M. Ceperley, *J. Stat. Phys.* **63**, 1237 (1991).
- ¹¹W. M. C. Foulkes, R. Q. Hood, and R. J. Needs, *Phys. Rev. B* **60**, 4558 (1999).
- ¹²P. J. Reynolds, D. M. Ceperley, B. J. Alder, and W. A. Lester, Jr., *J. Chem. Phys.* **77**, 5593 (1982).
- ¹³F. Schautz and H.-J. Flad, *J. Chem. Phys.* **110**, 11700 (1999).
- ¹⁴K. C. Huang, R. J. Needs, and G. Rajagopal, Comment on Ref. 13, *cond-mat/9912243*.
- ¹⁵F. Schautz and H.-J. Flad, Reply to Comment (Ref. 14) *cond-mat/9912277*.
- ¹⁶D. M. Ceperley and M. H. Kalos, in *Monte Carlo Method in Statistical Physics*, edited by K. Binder (Springer-Verlag, Heidelberg, 1992).
- ¹⁷C. J. Umrigar, K. G. Wilson, and J. W. Wilkins, *Phys. Rev. Lett.* **60**, 1719 (1988).
- ¹⁸C. Filippi and C. J. Umrigar, *J. Chem. Phys.* **105**, 213 (1996).